PROTECTING RIVERS: VALIDATION AND EXTRACTION OF PESTICIDES IN A BIOBED SYSTEM'S WATER AND BIOMIXTURE FRACTIONS USING UHPLC-MS/MS

by

T. Phoenix Nakagawa

A thesis, submitted to the Faculty of Graduate Studies of The University of Manitoba, in partial fulfillment of the degree requirements of

MASTER OF SCIENCE

Department of Soil Science

University of Manitoba

Winnipeg, Manitoba

Copyright © 2025 T. Phoenix Nakagawa

ABSTRACT

Nakagawa, T. Phoenix. M.Sc., The University of Manitoba, October, 2025. Protecting Rivers: Validation and Extraction of Pesticides in a Biobed System's Water and Biomixture Fractions using UHPLC-MS/MS. Major Professor; Dr. Annemieke Farenhorst.

This research developed rapid analytical methods to quantify up to eighty-five current-use pesticide active ingredients in spray tank rinsate, effluents, and biomatrices of biobed systems designed to capture and degrade pesticide residues. AMPs (*aminophosphonates*) method focused on two hydrophilic herbicides (glyphosate and glufosinate) and AMPA (2-amino-3-(3-hydroxy-5-methyl-isoxazol-4-yl) propanoic acid), the primary metabolite of glyphosate. The Broad-Spectrum Method examined eight herbicides, 53 insecticides, 22 fungicides, and one adjuvant. Using UHPLC-MS/MS, pesticide concentrations were determined in 2022 and 2023 from a dual-cell biobed in Carman, Manitoba, Canada. Limits of detection (LODs) and quantification (LOQs) were in the parts per trillion for the AMPs method and in the parts per billion for all other compounds. Detected in the biobed system was glyphosate, glufosinate, AMPA, and twelve other pesticide active ingredients. Atrazine, bentazon, clopyralid, imazethapyr, and metolachlor were detected in all twenty-seven samples collected in 2023. The concentrations for most pesticides significantly or numerically decreased in order of rinsate > primary effluent > final effluent. AMPA, dicamba, imazamox, and chlorantraniliprole were only periodically detected in final effluent. 2,4-D, boscalid, tebuconazole, and pyraclostrobin were never detected in the final effluent. Data suggest that biobeds are effective tools at reducing rinsate pesticide concentrations; however, bentazon and clopyralid were consistently quantified in final effluent. This is the first study in Canada to also closely monitor for pesticide persistence within biomixtures of dual-cell biobeds. Some herbicides (imazethapyr) appeared to accumulate within the biomixture, whereas other herbicides (2,4-D, imazamox) were never detected, confirming rapid dissipation. The remaining eight pesticides had higher concentrations within cell one than two while seven pesticides had greater concentrations

in 2023 than 2022, suggesting accumulation over time; in contrast, boscalid concentrations were greatest in 2022 then dissipated over the 2023 field season. Glyphosate showed rapid degradation as AMPA biomatrix concentrations were larger than that of glyphosate. Methods developed can be used to monitor biobed systems in Canada and support additional work to improve on the efficiency and longevity of biobeds in processing rinsate into clean water.

Keywords: Pesticides; Biobeds; Rinsate; Effluent; Biomixture; UHPLC-MS/MS; Method Validation; Crop Protection Products; Prairies; Glyphosate; AMPA.

FOREWORD

This thesis has been written in adherence to the thesis guidelines established by the University of Manitoba's Department of Soil Science (see below), with the exceptions of:

- *Appendices* are formatted numerically with roman numerals within the text of the chapter due to the inability of Microsoft® Word to simultaneously number with roman and arabic numerals. *Appendix I* is a singular chapter (5) while *Appendix II* was split into five chapters (6, 7, 8, 9, and 10) due to the number of tables and figures (>500 individual figures and tables);
- *List of Figure* and *List of Tables* are formatted with *Figure* or *Table* listed with each individual caption instead of column headings; this is due to the inability of < Microsoft® Word to format column headings for *List of Figures* and *Tables*, and;
- Both an *Acknowledgement* and *Dedication* chapter are included to refer to funding, individuals, and laboratories and those who have passed, respectively.

This thesis is comprised of four chapters: an introduction (Chapter 1), two standalone research manuscripts (Chapters 2 and 3) and a conclusion chapter (Chapter 4). Versions of chapters 2 and 3 will be submitted for publication in the future in the format and style towards their respective journals.

Thesis Guidelines: *A guide to thesis preparation for graduate students in the Department fof Soil Science. [As] Approved by Departmental Council January 10, 2018.* Available from: https://umanitoba.ca/agricultural-food-sciences/sites/agricultural-food-sciences/files/2020-07/thesisguidelinesjan2018_final.pdf

CONTRIBUTION OF AUTHORS

The thesis is organized as a grouped-manuscript thesis with chapters 2 and 3 containing material that are to be submitted and published. Following are the relevant chapters of the thesis, tentative manuscript titles, and primary author contributions:

Chapter 2 includes content that will be submitted to a relevant journal manuscript titled "Analytical method for testing biobed system efficacy: quantifying glufosinate, glyphosate, and AMPA in rinsate, effluent, and biomatrix samples."

Author contributions:

T. Phoenix Nakagawa (*Thesis Author*): Conceptualization, Validation, Methodology, Statistical Analysis, Writing - original draft.

Annemieke Farenhorst (*Advisor*): Conceptualization, Supervision, Writing - review & editing.

Chapter 3 includes content that will be submitted to a relevant journal manuscript titled "Analytical method for testing biobed system efficacy: a method for quantifying 84 pesticide analytes in rinsate, effluent, and biomatrix samples."

Author contributions:

T. Phoenix Nakagawa (*Thesis Author*): Conceptualization, Validation, Methodology, Statistical Analysis, Writing - original draft.

Annemieke Farenhorst (*Advisor*): Conceptualization, Supervision, Writing - review & editing.

ACKNOWLEDGMENTS

Firstly, I would like to acknowledge the land that this work was conducted on of Treaty 1 territory, specifically in the regions currently named Carman and Winnipeg; the University of Manitoba's Ian N. Morrison Research Farms, MASS Laboratories, and Department of Soil Science are located on the traditional lands of the Anishinaabeg, Ininiwak, Dakota Oyate, Dene, and Inuit as well as the homeland of the Red River Métis. In addition, I would like to acknowledge the lands of my educational soujourns: the traditional territory of the Anishinaabeg and homeland of the Red River Métis of Treaty 3 territory and Charrúa, Guarani, and Guenoa people of the unceded and unconquered territories of Uruguay. Finally, I would like to acknowledge African Canadians and African Urugyuans, Indigenous peoples who were taken from their lands and enslaved under chattel slavery systems that still persist today. Thank you for allowing me to work, learn, and live on the lands of your ancestors; I will continue to do the work of anti-colonialism, genocide and enslavement recognition, and freedom for all.

I would like to thank the funders of my M.Sc. Program*:* National Sciences and Engineering Research Council (*NSERC*) *Canada Graduate Scholarships (CGS) – Masters* [2022-2023], *NSERC CGS – M Micheal Smith Foreign Studies Supplement* [2022], University of Manitoba's (*UM*) *First-Year Stipend for NSERC CGS-M Students* [2022-2023], *UM's Tri-Agency Masters Supplement Award* [2023-2024], *Orval G. Caldell and H. Ruth Gardner Fellowship in Sustainable Agriculture* [2023-2024, 2024-2025], and *Manitoba Zero-Tillage Research Association Soil Conservation Fellowship* [2023-2024]. In addition, I would like to thank travel funds from the

UM's Faculty of Graduate Studies Travel Award and *Graduate Students Association Conference Grant* for travel to conferences.

I would like to thank my advisor, Dr. Annemieke Farenhorst, who guided me through this research and whose lab this research was conducted in. Dr. Farenhorst has been an advisor in life as well as research. I would also like to thank my committee members, Drs. Mark Hanson and Francis Zvomuya, who both took time out of their busy schedules as department heads to be on my committee and answer my multitude of questions; thank you both for your service and advice. I would like to thank my entire committee for their willingness to have our committee meetings anywhere, including shovelling biomixture into the biobed for the new operation year. To my research sojourn advisors for the *NSERC CGS-M MSFSS*, Drs. Veronica Cesio and Horacio Heinzen, at the Universidad de la República de Uruguay, thank you both for accepting me into your labs in 2022 for me to grow as an analytical chemist and all the help provided; muchas gracias, ahora sé dónde está la acetona.

Thank you to the University of Manitoba's Ian N. Morrison Research Farm's facilities as well as the farm manager, Justice Zhanda, employees Sheldon Beitcher, John Rosset, and Terry Anseeuw, and former manager Alvin Iverson for help in managing, maintaining, and advising on the Carman biobed operations. From the Department of Soil Science (DSS) staff, thank you to the facilities and personnel Katie Webb, Shannon Mustard, Rob Ellis, Fernando Esposito, Lynda Whitlam, Flor Toribio, and Trevor Fraser for their help in transport, safety, and support given through my studies. To the DSS faculty, thank you to Drs. Inoka Amarakoon, Xiaopeng Gao, David Lobb, Brian Amiro, Afua Mante, Joanne Thiessen Martins, Paul Bullock, and Mario Tenuta for the encouragement throughout both my B.Sc. and M.Sc. and the conversations that continue to this day. Thank you to the facilities of the Richardson Center for Food Technology and Research

and personnel Jasmine Arnold, Finn Makila, and John Bachu for troubleshooting keycard access and chemical disposal. Finally, I would like to give thanks to the Department of Entomology, with special thanks to Drs. Kateryn Rochon, Kyle Bobiwash, Jason Gibbs, and Mr. Jordan Bannerman, for their continuous inclusion of me in "Middle Thursday", multitude of reference letters, and conversations about my future and worries; I owe you all a debt of gratitude.

I would like to thank my friend and now-director of the MASS Laboratories and Assistant Professor, Dr. Alistair K. Brown, for his support and kind words throughout this thesis process; his "dad" energy helped take-down and set-up of the biobed on multiple occasions and troubleshoot that bloody machine known as the LC. Thank you to Sarah Johnson, Jade Wish, Tori Maxwell, Céline Chevrefils, Ifeoluwa Omotade, and Kayla Talabis for our journeys to the biobed and troubleshooting the LC. I would like to thank the members of the Grupo de Análisis de Compuestos Traza (GACT; Facultad de Química, Centro Universitario Regional Litoral Norte, Universidad de la República) Natalia Gerez García, Ignacio (Nacho) Migues, Ignacio Machado, Sofia Raffaelli, Lucia Cavallo, Luisina Rodriguez, Santí Fernández, Martín Torino, and Pilar Jorcín as well as at the Paysandú Research Station's Sofía Rezende, Noel Alonzo, and Natalia Besil.

Thank you to my dear friends Andrej Kao, Kyler Clement-Couzens, Yanko Kalem, Justine Gillert, Rianne Boekhorst, Riley Smith, Laird Brown, Alyssa Coopland, Emily van Gorp, Jade Tanner, and Jaclyn Victor; thank you for the check-ins and dragging me out of bed. Finally, I would like to thank my family, my grandmother Chiemi Nakagawa, grandfather Alex Kouritzin and his partner Linda Federspiel, my parents Drs. Sandie Kouritzin and Satoru Nakagawa, and my sister, Ph.D. candidate Hanika Nakagawa; this M.Sc. is yours.

DEDICATION

To the Ancestors of Tokunoshima and Yenisei,

I hope I am you, even if nisei.

To Toku Masu, who's sisters had peaceful nights,

And Jean Kouritzin, who always liked my "spice".

For Yoshi Nakagawa, who knew who I was,

With Betty Johns, who loved, even when I fuss,

Toshiko Hisaeda, who held together family, no matter the cost,

Kouzou Nakagawa, who plowed the fields, even when lost.

From sweet desires of sugar hell,

To the lost of fathers by the Japanese weld.

And from the grand minerals by the river,

To the red army, who murdered for silver,

I know the ancestors shall guide me home.

Even when I am all alone.

And when I bleed, a lesson was learned,

never concede, even if burned.

TABLE OF CONTENTS

Page

ABSTRACT I

FOREWORD III

CONTRIBUTION OF AUTHORS IV

ACKNOWLEDGMENTS V

DEDICATION VIII

TABLE OF CONTENTS IX

LIST OF TABLES XII

LIST OF FIGURES XX

1. INTRODUCTION 1

1.1 Pesticide Usage and Management 1
1.2 Rinsate Management Using Bioreactors: Biobeds 4
1.3 Pesticide Fate Processes in Biomatrix Materials 5
1.4 Canadian Contexts of Biobeds Operation and Application 7
1.5 The Biobed System in Carman, Manitoba 9
1.6 Validation, UHPLC-MS/MS, and Pesticide Quantification 13
1.7 Research Objectives and Thesis Outline 17
1.8 References 18

2. ANALYTICAL METHOD FOR TESTING BIOBED SYSTEM EFFICACY: QUANTIFYING GLUFOSINATE, GLYPHOSATE AND AMPA IN RINSATE, EFFLUENT, AND BIOMATRIX SAMPLES 24

2.1 Abstract 24
2.2 Introduction 25
2.3 Material and Methods 29
2.3.1 Chemicals 29
2.3.2 Description of the Dual-Cell Biobed System. 29
2.3.3 Analytical Method Validation. 32
2.3.4 Collection and Extraction of Rinsate, Effluent and Biomatrix Samples. 33
2.3.5 Separations and Quantifications by UHPLC-MS-MS 35
2.3.6 Statistical Analyses 36
2.4 Results and Discussion 38
2.4.1 Analytical Method Validation 38

2.4.2 Biobed Efficacy: Rinsate versus Effluent 41
2.4.3 Analyte Persistence in Biobed Cell One and Two 48
2.6 Conclusion 55
2.7 References 57

3. ANALYTICAL METHOD FOR TESTING BIOBED SYSTEM EFFICACY: A METHOD FOR QUANTIFYING 84 PESTICIDE ANALYTES IN RINSATE, EFFLUENT, AND BIOMATRIX SAMPLES 63

3.1 Abstract 63
3.2 Introduction 64
3.3 Materials and Methods 67
3.3.1 Analytes and Analyses 67
3.3.2 Validation Experiments 69
3.3.3 Research Site and Biobed System 72
3.3.4 Samples Collected. 72
3.3.5 Analyte Extractions and Quantifications. 73
3.3.6 Statistical Analysis 75
3.4 Results and Discussion 77
3.4.1 Validations 77
3.4.1.1 Rinsate and Effluent. 78
3.4.1.2 Biomatrix. 79
3.4.2 Biobed Performance 81
3.4.2.1 Rinsate and Effluent. 81
3.3.2.2 Biomatrix. 86
3.5 Conclusions 100
3.6 References 101

4. OVERALL CONCLUSIONS 106

4.1 Summary of Research 106
4.2 Practical Implications of the Research 112
4.3 Limitations of the Research and Recommendations for Future Studies. 117
4.4 References 122

5. APPENDIX I: CHAPTER TWO VALIDATION AND SUPPLEMENTARY MATERIALS 126

5.1 Eurachem Method Validation Calculations 126
5.2 Supplementary Materials for Chapter Two 129

6. APPENDIX II: CHAPTER THREE VALIDATION OVERVIEW LC-MS/MS PARAMETERS 144

6.1 Eurachem Method Validation Calculations 144

6.2 Supplementary Materials for Chapter Three: Instrument Chromatograms, Mass Spectrometric and Chromatographic Conditions, and Chemical Characteristics 146
6.2.1 Chromatograms for Pesticides 146
6.2.2 Compounds, Solubility, Fragments, Energies, and Other Parameters for Pesticides Selectivity 171

7. APPENDIX II: CHAPTER THREE VALIDATION OF WATER FRACTIONS 187

7.1 Chapter 3 Water Fraction Method Limits of Detection/Quantification, Accuracy, and Precision Validation for Biobeds 187
7.2 Chapter 3 Water Fraction Method Matrix Effect Validation for Biobeds 195

8. APPENDIX II: CHAPTER THREE VALIDATION OF QUECHERS EXTRACTION .. 222

8.1 Chapter 3 QuEChERS Method Limits of Detection/Quantification, Accuracy, Precision, and Matrix Effect Validation for Biobeds 222
8.2 Chapter 3 QuEChERS Internal Standard Loss for Biobeds 246

9. APPENDIX II: CHAPTER THREE VALIDATION OF QUPPE EXTRACTION 267

9.1 Chapter 3 QuPPe Method Limits of Detection/Quantification, Accuracy, Precision, and Matrix Effects Validation for Biobeds 267
9.2 Chapter 3 QuPPe Internal Standard Losses for Biobeds 285

10. APPENDIX II: CHAPTER THREE IN-SITU DATA FOR 2022 (BIOMIXUTRE) AND 2023 (WATER AND BIOMIXUTRE) 302

10.1 Chapter 3 Water Statistical Analysis 302
10.2 Chapter 3 Biomixture Statistical Analysis 303

LIST OF TABLES

Page

Table 1.1 Overview of Magnusson and Örnemark's (2014) *EURACHEM* validation parameters, purpose of the parameter, and determination method used in this thesis. 14

Table 2.1 2D chemical structures and physico-chemical properties of herbicide glyphosate and its primary metabolite AMPA, as well as the herbicide glufosinate. 26

Table 2.2 Linearity (R^2), working range (WR), limits of detection (LOD) and limits of quantification (LOQ), method limits of detection (MLD) and method limits of quantification (MLQ), accuracy [as percent recovery (% Rec)], and intra- and interday (Intra/Inter) precision [as percent coefficient of variation (% CV)] for AMPA, glufosinate, and glyphosate for biobed effluent, rinsate, and biomixture. *NQ* = not quantifiable. 42

Table 2.3 Comparison of instrument and effluent mean of replicates, standard error of the mean, and limits of quantifications (ng mL^{-1}) for AMPA, glufosinate, and glyphosate across ten replicates samples used to determine quantification limits. 43

Table 3.1 Selected properties determined for the biomatrix in the dual-cell biobed system. 72

Table 3.2 Water solubility (Water sol.), $LogK_{ow}$ (Log_{10} octanol-water partitioning coefficient), pKa (Log_{10} acid-dissociation constant), half-lives in days (DT_{50}) in lab soil (L), field soil (F), and water-phase only (W), K_{oc} (soil organic carbon-water partitioning coefficient), and GUS (Groundwater Ubiquity Score) of compounds as described in Lewis et al. (2016). 84

Table 3.3 Overview of compounds with two-way interactions. Mean concentrations are indicated in case of significant two-way interactions and all numbers are in mg kg^{-1}. *Cell:time* had no significance, so was not included. *Italics* indicate significantly different interactions but yields no additional information about compound fate. PO = Post, PR = Pre, '22 = 2022, '23 = 2023, C1 = Cell 1, C2 = Cell 2. 94

Table 3.4 An overview of general trends for compounds in the case of three-way significant interactions; mean concentrations are not statistical tests but general trends seen within the data for simpler interpretation. All values within parantheses are mg kg^{-1}. PO = Post, PR = Pre, '22 = 2022, '23 = 2023, C1 = Cell 1, C2 = Cell 2. 96

Table 3.5 An overview of general trends for boscalid, which had a significant four-way interaction; mean concentrations are not statistical tests but general trends seen within the data for simpler interpretation. PO = Post, PR = Pre, '22 = 2022, '23 = 2023, C1 = Cell 1, C2 = Cell 2. 97

Table 4.1 Pesticide active ingredient and one metabolite detected in one sample in rinsate, effluent, or biomixture analysed for in this study, and their physicochemical properties. 109

Table 4.2 General overview of the cells required for the dissipation of pesticide active ingredients and metabolite AMPA from rinsate applied to the operational biobed in Carman, Manitoba. Compounds of concern are also highlighted. 110

Table 4.3 Summary of extractable compounds with QuEChERS and QuPPe. Dashed lines indicate the inability to extract while yes indicates extractable. The 46 compounds that were extractable in both QuEChERS and QuPPe are omitted. 115

Table 5.1 The method retention time (Rt), electrospray ionization (ESI), precsuor ion, product ions [both the quantitative (Q) and qualitative (q) product ions], fragmentation voltage (FV), and collision energy (CE). 132

Table 5.2 Assumptions of ANOVA tested for the water matrix effects. Homogeneity of variance was tested with Bartlett's Test while normality was assessed with Shapiro-Wilk's Test. DI = Deionized Water, EF = Effluent Mimic, RN = Rinsate Mimic. Parenthesis indicate dilution level. 133

Table 5.3 ANOVA tests and values for compound response within water matrix effects with a follow-up Dunnett's Post-Hoc Test if significant. - = reduced response; 0 = no response change, and; NA = Not Applicable. 133

Table 5.4 Assumptions of ANOVA tested for the biomixture matrix effects. Homogeneity of variance was tested with Bartlett's Test while normality was assessed with Shapiro-Wilk's Test. DI = Deionized Water, KOH = Potassium Hydroxide Extractant. Parenthesis indicate dilution level. 133

Table 5.5 ANOVA tests and values for compound response within biomatrix matrix effects with a follow-up Dunnett's Post-Hoc Test if significant. - = reduced response; 0 = no response change, and; NA = Not Applicable. 134

Table 5.6 Assumptions of ANOVA tested for the internal standard losses of biomixture extractions. Homogeneity of variance was tested with Bartlett's Test while normality was assessed with Shapiro-Wilk's Test. FD = freeze-drying, SPE = solid-phase extraction. ... 134

Table 5.7 ANOVA tests for internal standard losses of compounds followed up by Tukey's post-hoc test if significant. From preceding to succeeding step, - = reduced response; 0 = no change; + = increased response; and; NA = Not Applicable. 134

Table 5.8 Welch's ANOVA table for glufosinate, glyphosate, and AMPA for water concentrations across all three matrices as well as the Games-Howell Post-Hoc comparisons. Data transformation and Shapiro-wilk Test for Normality also shown for Welch's ANOVA assumptions. 135

Table 5.9 ANOVA tables for glufosinate (GLU), glyphosate (GLY), and AMPA for biomixture analyses. Acronyms for parameters are: SS_n = Sum of Squares (numerator), SS_d = Sum of Squares (denominator), F = F-Statistic, and p = p-value. Acronyms for factors are: (I) = Model Intercept, C = Cell, Y = Year, T = Time, and D = Depth. Orange highlighted cells are significant factors; bolded values are significant p-values. Fact = Factor, df = degrees of freedom. 135

Table 5.10 Results from the Shapiro-Wilk's Test for normality for glufosinate, glyphosate, and AMPA for biomixture analyses. Acronyms for parameters are: C_Y = Cell_Year, T = Time, D = Depth, W = W-statistic, and p = p-value. Orange highlighted cells are significant factors that, when viewed with boxplots, were visually normally distributed. 137

Table 5.11 Results from the Mauchly's Test for sphericity for glufosinate, glyphosate, and AMPA for biomixture analyses. Acronyms for parameters are: W = W-statistic, and p = p-value. Factor Acronyms are the same as Table 5.9. 138

Table 5.12 Results from Levene's Test for homogeneity of variance for glufosinate, glyphosate, and AMPA for biomixture analyses. Acronyms for parameters are: W = W-statistic, and p = p-value. Factor Acronyms are the same as Table 5.9. 138

Table 5.13 Pairwise comparisons for glyphosate tested using the Benjamini-Hochberg correction for the significant Cell*Depth*Time interaction. White "=" values were insignificant, magenta ">" values indicate column value was greater than the row value, and yellow "<" values indicate column value was lesser than the row value. C1 = Cell 1, C2 = Cell 2, Pre = Pre-operation, Pos = Post-operation, 0-5 = 0-5 cm, 5-15 = 5-15 cm, and 15-30 = 15-30 cm. 139

Table 5.14 Pairwise comparisons for glyphosate tested using the Benjamini-Hochberg correction for the significant Cell*Year*Depth interaction. White "=" values were insignificant, magenta ">" values indicate column value was greater than the row value, and yellow "<" values indicate column value was lesser than the row value. C1 = Cell 1, C2 = Cell 2, '22 = 2022, '23 = 2023, 0-5 = 0-5 cm, 5-15 = 5-15 cm, and 15-30 = 15-30 cm. 140

Table 5.15 Pairwise comparisons for AMPA tested using the Benjamini-Hochberg correction for the significant Cell*Year*Depth interaction. White "=" values were insignificant, magenta ">" values indicate column value was greater than the row value, and yellow "<" values indicate column value was lesser than the row value. C1 = Cell 1, C2 = Cell 2, '22 = 2022, '23 = 2023, 0-5 = 0-5 cm, 5-15 = 5-15 cm, and 15-30 = 15-30 cm. 141

Table 5.16 Pairwise comparisons for glufosinate tested using the Benjamini-Hochberg Correction for the significant Depth*Time interaction. White "=" values were insignificant, magenta ">" values indicate column value was greater than the row value, and yellow "<" values indicate column value was lesser than the row value. Pre = Pre-operation, Pos = Post-operation, 0-5 = 0-5 cm, 5-15 = 5-15 cm, and 15-30 = 15-30 cm. 142

Table 5.17 Pairwise comparisons for glufosinate tested using the Benjamini-Hochberg correction for the significant Year*Time interaction. White "=" values were insignificant, magenta ">" values indicate column value was greater than the row value, and yellow "<" values indicate column value was lesser than the row value. '22 = 2022, '23 = 2023, Pre = Pre-operation, Pos = Post-operation. 142

Table 5.18 Pairwise comparisons for glufosinate tested using the Benjamini-Hochberg correction for the significant Year*Depth interaction. White "=" values were insignificant, magenta ">" values indicate column value was greater than the row value, and yellow "<" values indicate column value was lesser than the row value. '22 = 2022, '23 = 2023, 0-5 = 0-5 cm, 5-15 = 5-15 cm, and 15-30 = 15-30 cm. 143

Table 6.1 List of pesticides analyzed in the analytical method with LogP and pKa values as well as acetone, dichloromethane, ethyl acetate, methanol, toluene, and water solubilites. **Bolded** pesticides are independent of the Agilent 96 pesticides Canadian Cannabis Mixture. *Italicized* pesticides have deuterated or ^{13}C labelled internal standards. Pesticides written with ~~strikethroughs~~ were removed from the final chromatography since they are analyzed by GC-MS/MS. All values were retrieved from Lewis et al. (2016). 171

Table 6.2 Pesticide analytical method's retention time (Rt), retention window (ΔRt), electrospray ionization mode (ESI: + = positive; - = negative), parent ions, product ions [both quantitative

(Q) or qualitative (l) product ions], fragmentation voltage (frag), and collision energies (CE). 175

Table 6.3 Method linearity (R^2) and working range (WR) in each of the solvents used for each extraction, associated internal standards (IS), and machine limits of detection and quantification (LOD/LOQ)..... 182

Table 7.1 Method limits of detection and quantification (MLD/MLQ) and accuracy at four spike levels for effluent and rinsate water fractions. *Italicized* values represent recoveries below <70%, **bolded** values represent values >130%, and – represents no response detected..... 187

Table 7.2 Intra- and interday percent coefficient of variation (CV) at four spike levels for both effluent and rinsate water fractions. *Italicized* values represent CV's that exceed 20% while **bolded** values represent CV's that exceed 30%..... 191

Table 7.3 Table of ANOVA "Matrix" significance for the water factions and associated *p-values* (*P*) and responses (R) from Dunnett's Post Hoc Test. + = increased molecule response, - = decreased molecule response, and 0 = no molecule response change. Green highlights indicate two seperate ANOVA's to meet assumptions; blue highlights represent a significant matrix effect *but* no differences in Dunnett's test; yellow highlights represent a removal of rn10dil due to a lack of machine response, and; orange highlights represents the removal of rn10dil *and* undiluted effluent due to no machine responses. 198

Table 7.4 Transformation method, Shapiro-Wilk's Test for normality and Breusch-Pagan's Test for homoscedascity on model residuals and slope homogeneity assumption ANOVA test p-values and notes regarding issues in analysis for water matrix effects ANCOVA's for each compound. *Italicized* values had no response below 20 ppb, so were run as an ANOVA and are found in Table 7.5. NA = not applicable; green highlighted rows were separated into two analyses due to strength of matrix effects causing non-homogenous slopes with transformations..... 203

Table 7.5 Transformation method, Shapiro-Wilk Test for normality for each matrix, Bartlett's Test for homogeneity of variance, and notes regarding issues in analysis for water matrix effects ANOVA's for compounds only detected at 20 ppb..... 206

Table 8.1 Method detection and quantification limits (MLD/MLQ), intra- and interday precision, and accuracy for QuEChERS extraction method. **Bolded** values represent recoveries greater than 130%, *italicized* values represent recoveries below 70%, and – represent non-extractable pesticides with the method. 222

Table 8.2 Table of ANOVA "Matrix" significance as well as the *p-values* (*P*) and responses (R) from Dunnett's Post Hoc Test for QuEChERS. + = increased molecule response, - = decreased molecule response, and 0 = molecule response did not change. Green highlights mean that the matrices had to be separated to meet ANOVA assumptions; blue highlights represent a significant matrix effect *but* no significant differences found in Dunnett's test. 226

Table 8.3 Transformation method, Shapiro-Wilk'a Test for normality, and Bresuch-Pagan Test for homoscedascity, and addition vs. interaction model ANOVA on model residuals; notes for all compounds extractable with the QuEChERS extraction method. Blue highlights represents a need to separate matrices for analysis due to non-normality of residuals. *Italicized* values only had detects at 20 ppb, so were proceeded with an ANOVA model in Table 8.4. NA = Not Applicable. 229

Table 8.4 Transformation method, Shapiro-Wilk Test for normality, and Bartlett's Test for homogeneity of variance for compounds extractable with the QuEChERS extraction method detected at 20 ppb only. 233

Table 8.5 Table of internal standard loss ANOVA p-values as well as the p-values from the Tukey's Post Hoc Test for QuEChERS. *Italicized* values represent square-root transformation. 246

Table 8.6 Table of Shaprio-Wilk Test and Bartlett's Test results for ANOVA assumptions of QuEChERS internal standard loss. *Italicized* values represent square-root transformation. **Bold** values were significantly different from normal, but boxplots demonstrated normal distribution. 248

Table 9.1 Method detection and quantification limits (MLD/MLQ), intra- and interday precision, and accuracy for QuPPe extraction method. **Bolded** values represent recoveries greater than 130%, *italicized* values represent recoveries below 70%, and – represent non-extractable pesticides with the method. 267

Table 9.2 Table of ANOVA "Matrix" significance and *p*-values (*P*) and responses (R) from Dunnett's Post Hoc Test for QuPPe. + = increased molecule response, - = decreased molecule response, and 0 = molecule response did not change. Green highlights represent a significant matrix effect in the ANOVA *but* no significant differences found in Dunnett's test. 271

Table 9.3 Transformation method, Shapiro-Wilk Test for normality, Bresuch-Pagan Test for homoscedascity, and addition vs. interaction model ANOVA test on model residuals; notes for all compounds extractable with the QuPPe extraction method. Blue highlights represent a need to separate matrices due to non-normality of residuals. *Italicized* values only had detects at 20 ppb, so were proceeded with an ANOVA model in Table. 9.4. NA = not applicable. 273

Table 9.4 Transformation method, Shapiro-Wilk Test for normality, and Bartlett's Test for homogeneity of variance for compounds extractable with the QuPPe extraction method and detected at 20 ppb only. 275

Table 9.5 Table of internal standard loss ANOVA *p*-values (*P*) and *p*-values from the Tukey's Post Hoc Test for QuPPe. 285

Table 9.6 Table of Shaprio-Wilk Test and Bartlett's Test Results for ANOVA assumptions of QuPPe internal standard loss. **Bold** values were significantly different from normal, but boxplots demonstrated a normal distribution. 287

Table 10.1 Results from the Shapiro-Wilk Test for normality, Welch's ANOVA, and Games-Howell Post-Hoc Tests for biobed water data in 2023. Bold values represent non-normal distribution. 302

Table 10.2 Repeated Measures ANOVA Table for all compounds detected within biomixtures for both 2022 and 2023. Acronyms for compounds are as follows: IMZ = Imazethapyr, DIC = Dicamba, ATR = Atrazine, BEN = Bentazon, CHL = Chlorantraniliprole, MET = Metolachlor, CLP = Clopyralid, PYR = Pyraclostrobin, TEB = Tebuconazole, and BOS = Boscalid. Factor acronyms are as follows: (I) = Model Intercept, Y = Year of Operation, C = Biobed Cell, D = Depth Sampled, and T = Time of Sampling. Other Acronyms as follows: DF_n = Degrees of Freedom (Numerator), DF_d = Degrees of Freedom (Denominator), SS_n =

Sum of Squares (Numerator), SS_d = Sum of Squares (Denominator), F = F-statistic, and p = p-value. 303

Table 10.3 Testing of sphericity assumption for each RM ANOVA run; acronyms same as Table 10.2. Bolded values indicate Greenhouse-Geisser adjustment due to violation of sphericity. 305

Table 10.4 Summary of Levene's Test for homogeneity of variance across cell years grouped into depth and time categories. Acronyms are the same as Table 10.2. 307

Table 10.5 Summary of Shapiro-Wilk tests for normality of each grouping of cell, year, depth, and time. Acronyms for compounds and factors (bolded) same as Table 10.2. Additional acronyms are: 1_22 = Cell One, 2022; 1_23 = Cell One, 2023; 2_22 = Cell Two, 2022; 2_23 = Cell Two, 2023; T = Top 0-5 cm; M = Middle 5-15 cm; O = Bottom 15-30 cm; B = Pre-Operation; A = After Operation; W = Wilks Statistics, and; p = p-value. 308

Table 10.6 Pairwise comparisons for the significant Depth*Time interaction for bentazon from Table 10.2. White "=" values were insignificant, magenta ">" values indicate column value was greater than the row value, and yellow "<" values indicate column value was lesser than the row value. Pre = Pre-operation, Pos = Post-operation, 0-5 = 0-5 cm, 5-15 = 5-15 cm, and 15-30 = 15-30 cm. 310

Table 10.7 Pairwise comparisons for the significant Year*Time interaction for bentazon from Table 10.2. White "=" values were insignificant, magenta ">" values indicate column value was greater than the row value, and yellow "<" values indicate column value was lesser than the row value. '22 = 2022, '23 = 2023, Pre = Pre-operation, Pos = Post-operation. 310

Table 10.8 Pairwise comparisons for the significant Depth*Time interaction for clopyralid from Table 10.2. White "=" values were insignificant, magenta ">" values indicate column value was greater than the row value, and yellow "<" values indicate column value was lesser than the row value. Pre = Pre-operation, Pos = Post-operation, 0-5 = 0-5 cm, 5-15 = 5-15 cm, and 15-30 = 15-30 cm. 311

Table 10.9 Pairwise comparisons for the significant Year*Time interaction for clopyralid from Table 10.2. White "=" values were insignificant, magenta ">" values indicate column value was greater than the row value, and yellow "<" values indicate column value was lesser than the row value.'22 = 2022, '23 = 2023, Pre = Pre-operation, Pos = Post-operation. 311

Table 10.10 Pairwise comparisons for the significant Depth*Time interaction for tebuconazole from Table 10.2. White "=" values were insignificant, magenta ">" values indicate column value was greater than the row value, and yellow "<" values indicate column value was lesser than the row value. Pre = Pre-operation, Pos = Post-operation, 0-5 = 0-5 cm, 5-15 = 5-15 cm, and 15-30 = 15-30 cm. 312

Table 10.11 Pairwise comparisons for the significant Cell*Depth interaction for tebuconazole from Table 10.2. White "=" values were insignificant, magenta ">" values indicate column value was greater than the row value, and yellow "<" values indicate column value was lesser than the row value. C1 = Cell 1, C2 = Cell 2, 0-5 = 0-5 cm, 5-15 = 5-15 cm, and 15-30 = 15-30 cm. 312

Table 10.12 Pairwise comparisons for the significant Year*Depth interaction for tebuconazole from Table 10.2. White "=" values were insignificant, magenta ">" values indicate column

value was greater than the row value, and yellow "<" values indicate column value was lesser than the row value. '22 = 2022, '23 = 2023, 0-5 = 0-5 cm, 5-15 = 5-15 cm, and 15-30 = 15-30 cm. 313

Table 10.13 Pairwise comparisons for the significant Cell*Year interaction for tebuconazole from Table 10.2. White "=" values were insignificant, magenta ">" values indicate column value was greater than the row value, and yellow "<" values indicate column value was lesser than the row value. C1 = Cell 1, C2 = Cell 2, '22 = 2022, '23 = 2023,. 313

Table 10.14 Pairwise comparisons for the significant Year*Depth interaction for pyraclostrobin from Table 10.2. White "=" values were insignificant, magenta ">" values indicate column value was greater than the row value, and yellow "<" values indicate column value was lesser than the row value.'22 = 2022, '23 = 2023, 0-5 = 0-5 cm, 5-15 = 5-15 cm, and 15-30 = 15-30 cm. 314

Table 10.15 Pairwise comparisons for the significant Depth*Time interaction for pyraclostrobin from Table 10.2. White "=" values were insignificant, magenta ">" values indicate column value was greater than the row value, and yellow "<" values indicate column value was lesser than the row value. Pre = Pre-operation, Pos = Post-operation, 0-5 = 0-5 cm, 5-15 = 5-15 cm, and 15-30 = 15-30 cm. 314

Table 10.16 Pairwise comparisons for the significant Year*Time interaction for pyraclostrobin from Table 10.2. White "=" values were insignificant, magenta ">" values indicate column value was greater than the row value, and yellow "<" values indicate column value was lesser than the row value.'22 = 2022, '23 = 2023, Pre = Pre-operation, Pos = Post-operation. ... 315

Table 10.17 Pairwise comparisons for the significant Cell*Depth interaction for dicamba from Table 10.2. White "=" values were insignificant, magenta ">" values indicate column value was greater than the row value, and yellow "<" values indicate column value was lesser than the row value. C1 = Cell 1, C2 = Cell 2, 0-5 = 0-5 cm, 5-15 = 5-15 cm, and 15-30 = 15-30 cm. 315

Table 10.18 Pairwise comparisons for the significant Year*Depth interaction for dicamba from Table 10.2. White "=" values were insignificant, magenta ">" values indicate column value was greater than the row value, and yellow "<" values indicate column value was lesser than the row value.'22 = 2022, '23 = 2023, 0-5 = 0-5 cm, 5-15 = 5-15 cm, and 15-30 = 15-30 cm. 316

Table 10.19 Pairwise comparisons for the significant Depth*Time interaction for dicamba from Table 10.2. White "=" values were insignificant, magenta ">" values indicate column value was greater than the row value, and yellow "<" values indicate column value was lesser than the row value. Pre = Pre-operation, Pos = Post-operation, 0-5 = 0-5 cm, 5-15 = 5-15 cm, and 15-30 = 15-30 cm. 316

Table 10.20 Pairwise comparisons for the significant Cell*Year*Time interaction for imazethapyr from Table 10.2 White "=" values were insignificant, magenta ">" values indicate column value was greater than the row value, and yellow "<" values indicate column value was lesser than the row value. C1 = Cell 1, C2 = Cell 2, '22 = 2022, '23 = 2023, Pre = Pre-operation, Pos = Post-operation..... 317

Table 10.21 Pairwise comparisons for the significant Year*Depth*Time interaction for imazethapyr from Table 10.2. White "=" values were insignificant, magenta ">" values

indicate column value was greater than the row value, and yellow "<" values indicate column value was lesser than the row value.'22 = 2022, '23 = 2023, Pre = Pre-operation, Pos = Post-operation, 0-5 = 0-5 cm, 5-15 = 5-15 cm, and 15-30 = 15-30 cm..... 318

Table 10.22 Pairwise comparisons for the significant Cell*Year*Depth interaction for metolachlor from Table 10.2. White "=" values were insignificant, magenta ">" values indicate column value was greater than the row value, and yellow "<" values indicate column value was lesser than the row value. C1 = Cell 1, C2 = Cell 2, '22 = 2022, '23 = 2023, 0-5 = 0-5 cm, 5-15 = 5-15 cm, and 15-30 = 15-30 cm. 319

Table 10.23 Pairwise comparisons for the significant Cell*Year*Depth interaction for chlorantraniliprole from Table 10.2. White "=" values were insignificant, magenta ">" values indicate column value was greater than the row value, and yellow "<" values indicate column value was lesser than the row value. C1 = Cell 1, C2 = Cell 2, '22 = 2022, '23 = 2023, 0-5 = 0-5 cm, 5-15 = 5-15 cm, and 15-30 = 15-30 cm. 320

Table 10.24 Pairwise comparisons for the significant Year*Depth*Time interaction for atrazine from Table 10.2. White "=" values were insignificant, magenta ">" values indicate column value was greater than the row value, and yellow "<" values indicate column value was lesser than the row value.'22 = 2022, '23 = 2023, Pre = Pre-operation, Pos = Post-operation, 0-5 = 0-5 cm, 5-15 = 5-15 cm, and 15-30 = 15-30 cm. 321

Table 10.25 Pairwise comparisons for the significant Cell*Year*Depth*Time interaction for boscalid from Table 10.2. Due to its size, the table is split into multiple parts, in order of: within cell one, 2022; within cell two, 2022; within cell one, 2023; within cell two, 2023; between cell comparisons, 2022; between cell comparisons, 2023; between year comparisons, cell one; between years comparisons, cell two; cell one, 2022 compared with cell two, 2023, and; cell one, 2023 compared with cell two, 2022. White "=" values were insignificant, magenta ">" values indicate column value was greater than the row value, and yellow "<" values indicate column value was lesser than the row value. C1 = Cell 1, C2 = Cell 2, '22 = 2022, '23 = 2023, Pre = Pre-operation, Pos = Post-operation, 0-5 = 0-5 cm, 5-15 = 5-15 cm, and 15-30 = 15-30 cm. 322

LIST OF FIGURES

Page

Figure 1.1 The Ian. N. Morrsion Research Farm two-cell biobed located in Carman, MB, showing a) the collection trough and rinsate storage tanks, and b) the roofed, dual-cell biobed filled with biomixture. 9

Figure 1.2 Overview of biobed cell set up with black arrows representing the dimensions of the cell and white labels indicating layer composition within the cell..... 10

Figure 1.3 The biomixture utilized in the biobed at the Morrsion Research Farm, developed from a 1:1:2 volume ratio of soil, peat, and wheat stubble. 11

Figure 1.4 Technical diagram of the biobed layout. The left hand side represent the flow sequence and corresponds to colour on the right hand side. White arrows of the right hand side represent pump-operated flows while orange represent gravity mediated flows..... 12

Figure 1.5 Pumps and flow meters installed at the Ian N. Morrison Research Farm biobed for biobed cell one (bottom) and biobed cell two (top). 12

Figure 2.1 Visual overview photos of the biobed system in Carman, MB,with a) rinsate collection area (white trough – bending is an optical illusion due to panoramic photo) with a black, 1,000 L rinsate storage vessel, b) biobed cells that processes rinsate (foreground cell) and primary effluent (background cell), c) close-up of cell two with the drip-emitter manifold that irrigates the cell, and d) close-up of drip emitters that applies of rinsate (cell one) or effluent (cell two) onto biomatrix surfaces. 31

Figure 2.2 Matrix effects on compound responses (*m/z* units) in rinsate and effluent (top) and biomixture fractions (bottom) for AMPA, glufosinate, and glyphosate at 100 ng mL^{-1} in-vial. Error bars represent standard error; note y-axis for each facet are different scales. Paranthesis indicate dilution level. 44

Figure 2.3 Recoveries from internal standard spikes before freeze-drying (Pre-FD), after freeze-drying (Post-FD), and final solid-phase extraction clean-up (SPE) steps for AMPA (red), glufosinate (green), and glyphosate (blue). Dotted line represents the in-vial spiked concentration of 200 ng mL^{-1}. 45

Figure 2.4 Water concentrations of glyphosate, glufosinate, and AMPA within the collection areas of rinsate, primary effluent, and final effluent for the 2023 growing season. Values below boxplots represent number of samples >MLQ. 46

Figure 2.5 Total, AMPA, glyphosate, and glufosinate biomixture concentrations quantified across cells and years (one, 2022; two, 2022; one 2023, and; two 2023) at sampling times (Pre and Post) and depths (0-5, 5-15, and 15-30 cm). “Pre” represents pre-season operation of biobed while “Post” represents post-season operation of biobed. 50

Figure 3.1 Photo of rinsate (left glass cylinder), primary effluent (middle) and final effluent (right) during sample collection in 2023. Rinsate solution is cloudy from adjuvants in formulation while effluents are yellow-brown from humic substances leached from biomixtures..... 71

Figure 3.2 Ordered in decreasing rinsate concentration, concentrations of metolachlor, bentazon, clopyralid, tebuconazole, dicamba, chlorantraniliprole, atrazine, imazethapyr, boscalid, 2,4-

D, imazamox, and pyraclostrobin quantified in the 2023 operation season for the rinsate, primary effluent, and final effluent. Figure includes imputed <MLQ values for visual clarity. 85

Figure 3.3 Concentrations of bentazon, atrazine, clopyralid, glufosinate (from Chapter 2), imazethapyr, and metolachlor within rinsate, primary effluent, and final effluent across julian days. GUS values are included for posterity. 86

Figure 3.4 Pesticide concentrations quantified within cell one in 2022 and 2023 (including imputed values for visual clarity). Depth* Time factors are highlighted with boxplot colours. “Pre” prefix indicates pre-season operation, “Post” indicate post-season operation; the suffix “0-5”, “5-15”, and “15-30” indicate respective biobed sampling depths in cm. 89

Figure 3.5 Pesticide concentrations quantified within cell two in 2022 and 2023 (including imputed values for visual clarity). Depth* Time factors are highlighted with boxplot colours. “Pre” prefix indicates pre-season operation, “Post” indicate post-season operation; the suffix “0-5”, “5-15”, and “15-30” indicate respective biobed sampling depths in cm. 90

Figure 5.1 Chromatograms for AMPA (top two) and AMPA$^{13}C,^{15}N$ (bottom two) and quantifiers (top, third) and qualifiers (second, bottom). 129

Figure 5.2 Chromatograms for glufosinate (top two) and glufosinate-d_3 (bottom two) and quantifiers (top, third) and qualifiers (second, bottom). 130

Figure 5.3 Chromatograms for glyphosate (top two) and glyphosate-$^{13}C_2,^{15}N$ (bottom two) and quantifiers (top, third) and qualifiers (second, bottom). 131

Figure 6.1 Total ion chromatogram for the method. 146

Figure 6.2 2,4-D chromatograms for the quantifier (top) and qualifier (bottom). 147

Figure 6.3 2,4-D-$^{13}C_6$ chromatograms for the quantifier (top) and qualifier (bottom). 147

Figure 6.4 Acephate chromatograms for the quantifier (top) and qualifier (bottom). 147

Figure 6.5 Acequinocyl chromatograms for the quantifier (top) and both qualifier (bottom). . 147

Figure 6.6 Acetamiprid chromatograms for the quantifier (top) and qualifier (bottom). 148

Figure 6.7 Acetamiprid chromatograms for the quantifier (top) and qualifier (bottom). 148

Figure 6.8 Allethrin chromatograms for the quantifier (top) and qualifiers (middle and bottom). 148

Figure 6.9 Atrazine chromatograms for the quantifier (top) and qualifier (bottom). 148

Figure 6.10 Azoxystrobin chromatograms for the quantifier (top) and qualifier (bottom). 149

Figure 6.11 Bentazon chromatograms for the quantifier (top) and qualifier (bottom). 149

Figure 6.12 Bentazon-d_7 chromatograms for the quantifier (top) and qualifier (bottom). 149

Figure 6.13 Benzovindiflupyr chromatograms for the quantifier (top) and qualifiers (bottom). 149

Figure 6.14 Bifenthrin chromatograms for the quantifier (top) and qualifier (bottom). 150

Figure 6.15 Boscalid chromatograms for the quantifier (top) and qualifier (bottom). 150

Figure 6.16 Buprofezin chromatograms for the quantifier (top) and qualifier (bottom). 150
Figure 6.17 Carbaryl chromatograms for the quantifier (top) and qualifier (bottom). 150
Figure 6.18 Carbofuran chromatograms for the quantifier (top) and qualifier (bottom). 151
Figure 6.19 Chlorantraniliprole chromatograms for the quantifier (top) and qualifier (bottom). 151
Figure 6.20 Chlorpyrifos chromatograms for the quantifier (top) and qualifier (bottom)..... 151
Figure 6.21 Clofentezine chromatograms for the quantifier (top) and qualifier (bottom)..... 151
Figure 6.22 Clopyralid chromatogram for the quantifier..... 151
Figure 6.23 Clothianidin chromatograms for the quantifier (top) and qualifier (bottom). 152
Figure 6.24 Coumaphos chromatograms for the quantifier (top) and qualifier (bottom). 152
Figure 6.25 Cyantraniliprole chromatograms for the quantifier (top) and qualifier (bottom)... 152
Figure 6.26 Cyprodinil chromatograms for the quantifier (top) and qualifier (bottom)..... 152
Figure 6.27 Diazinon chromatograms for the quantifier (top) and qualifier (bottom). 153
Figure 6.28 Dicamba chromatograms for the quantifier (top) and qualifier (bottom)..... 153
Figure 6.29 Dimethomorph I (right peak) chromatograms for the quantifier (top) and qualifier (bottom). 153
Figure 6.30 Dimethomorph II (left peak) chromatograms for the quantifier (top) and qualifier (bottom). 153
Figure 6.31 Dimethoate chromatograms for the quantifier (top) and qualifier (bottom). 154
Figure 6.32 Dinotefuran chromatograms for the quantifier (top) and qualifiers (mid-up, mid-bottom, and bottom). 154
Figure 6.33 Dodemorph chromatograms for the quantifier (top) and qualifier (bottom). 155
Figure 6.34 Ethoprophos chromatograms for the quantifier (top) and qualifier (bottom)..... 155
Figure 6.35 Etofenprox chromatograms for the quantifier (top) and qualifier (bottom). 155
Figure 6.36 Etoxazole chromatograms for the quantifier (top) and qualifier (bottom). 155
Figure 6.37 Fenhexamid chromatograms for the quantifier (top) and qualifier (bottom). 156
Figure 6.38 Fenoxycarb chromatograms for the quantifier (top) and qualifier (bottom). 156
Figure 6.39 Fenpyroximate chromatograms for the quantifier (top) and qualifier (bottom)..... 156
Figure 6.40 Fensulfothion chromatogram for the quantifier (top) and qualifiers (bottom)..... 156
Figure 6.41 Fipronil chromatograms for the quantifier (top) and qualifiers (middle and bottom). 157
Figure 6.42 Flonicamid chromatogram for the quantifier (top) and qualifiers (bottom)..... 157
Figure 6.43 Fludioxinil chromatograms for the quantifier (top) and qualifier (bottom). 157
Figure 6.44 Fluopyram chromatogram for the quantifier (top) and qualifiers (bottom). 157

Figure 6.45 Hexythiazox chromatograms for the quantifier (top) and qualifier (bottom)..... 158
Figure 6.46 Imazalil chromatograms for the quantifier (top) and qualifier (bottom). 158
Figure 6.47 Imazamox chromatogram for the quantifier. 158
Figure 6.48 Imazethapyr chromatograms for the quantifier (top) and qualifiers (middle and bottom). 158
Figure 6.49 Imidacloprid chromatograms for the quantifier (top) and qualifier (bottom). 159
Figure 6.50 Kresoxim-methyl chromatograms for the quantifier (top) and qualifier (bottom). 159
Figure 6.51 Malathion chromatograms for the quantifier (top) and qualifier (bottom)..... 159
Figure 6.52 Metalaxyl chromatograms for the quantifier (top) and qualifier (bottom). 159
Figure 6.53 Methomyl chromatograms for the quantifier (top) and qualifier (bottom). 160
Figure 6.54 Metolachlor chromatograms for the quantifier (top) and qualifier (bottom). 160
Figure 6.55 Metolachlor-d_6 chromatograms for the quantifier (top) and qualifier (bottom).... 160
Figure 6.56 Mevinphos chromatograms for the quantifier (top) and qualifier (bottom). 160
Figure 6.57 MGK-264 chromatograms for the quantifier (top) and qualifier (bottom). 161
Figure 6.58 Myclobutanil chromatograms for the quantifier (top) and qualifier (bottom). 161
Figure 6.59 Oxamyl chromatograms for the quantifier (top) and qualifier (bottom). 161
Figure 6.60 Paclobutrazol chromatograms for the quantifier (top) and qualifier (bottom). 161
Figure 6.61 Permethrin [$NH4^+$] chromatograms for the quantifier (top) and qualifier (bottom). 162
Figure 6.62 Phosmet chromatograms for the quantifier (top) and qualifier (bottom). 162
Figure 6.63 Piperonyl Butoxide chromatograms for the quantifier (top) and qualifier (bottom). 162
Figure 6.64 Pirimicarb chromatograms for the quantifier (top) and qualifier (bottom). 162
Figure 6.65 Prallethrin chromatograms for the quantifier (top) and qualifier (bottom). 163
Figure 6.66 Propiconazole chromatograms for the quantifier (top) and qualifier (bottom). 163
Figure 6.67 Propoxur chromatograms for the quantifier (top) and qualifiers (mid-top, mid-bottom, and bottom). 163
Figure 6.68 Pyraclostrobin chromatograms for the quantifier (top) and qualifier (bottom)..... 164
Figure 6.69 Pyrethrin I chromatograms for the quantifier (top) and qualifiers (middle and bottom). 164
Figure 6.70 Pyrethrin II chromatograms for the quantifier (top) and qualifiers (middle and bottom). 164
Figure 6.71 Pyridaben chromatograms for the quantifier (top) and qualifiers (middle and bottom). 165
Figure 6.72 Resmethrin chromatograms for the quantifier (top) and qualifier (bottom)..... 165

Figure 6.73 Spinetoram J chromatograms for the quantifier (top) and qualifier (bottom). 165
Figure 6.74 Spinosyn A chromatograms for the quantifier (top) and qualifier (bottom). 165
Figure 6.75 Spinosyn D chromatograms for the quantifier (top) and qualifier (bottom). 166
Figure 6.76 Spirodiclofen chromatograms for the quantifier (top) and qualifier (bottom). 166
Figure 6.77 Spiromesifen chromatograms for the quantifier (top) and qualifier (bottom)..... 166
Figure 6.78 Spirotetramat chromatograms for the quantifier (top) and qualifiers (middle and bottom). 166
Figure 6.79 Spiroxamine chromatograms for the quantifier (top) and qualifier (bottom)..... 167
Figure 6.80 Tebuconazole chromatograms for the quantifier (top) and qualifier (bottom)..... 167
Figure 6.81 Tebuconazole-d_9 chromatograms for the quantifier (top) and qualifier (bottom).. 167
Figure 6.82 Tebufenozide chromatograms for the quantifier (top) and qualifier (bottom). 167
Figure 6.83 Teflubenzuron chromatograms for the quantifier (top) and qualifier (bottom). 168
Figure 6.84 Tetrachlorvinphos chromatograms for the quantifier (top) and qualifiers (middle and bottom). 168
Figure 6.85 Tetramethrin chromatograms for the quantifier (top) and qualifiers (mid-top, mid-bottom, and bottom). 168
Figure 6.86 Thiacloprid chromatograms for the quantifier (top) and qualifier (bottom). 169
Figure 6.87 Thiamethoxam chromatograms for the quantifier (top) and qualifier (bottom)..... 169
Figure 6.88 Thiamethoxam-d_4 chromatograms for the quantifier (top) and qualifier (bottom). 169
Figure 6.89 Thiophanate-Methyl chromatograms for the quantifier (top) and qualifier (bottom). 169
Figure 6.90 Trifloxystrobin chromatograms for the quantifier (top) and qualifier (bottom)..... 170
Figure 7.1 ANCOVA's conducted that were found to have a significant matrix effect (yes) vs. no effect (no). 195
Figure 7.2 Summary of molecule responses from matrix effect found to be significant in an ANOVA and analyzed through Dunnett's test (control vs. matrices) for effluent..... 196
Figure 7.3 Summary of molecule responses from matrix effect found to be significant in an ANOVA and analyzed through Dunnett's test (control vs. matrices) for rinsate. 197
Figure 7.4 Acephate response across concentration in a pure water matrix vs effluents and rinsates. 208
Figure 7.5 Dinotefuran response across concentration in a pure water matrix vs effluents and rinsates. 208
Figure 7.6 Oxamyl response across concentration in a pure water matrix vs effluents and rinsates. 208
Figure 7.7 Clopyralid response across concentration in a pure water matrix vs effluents and rinsates. 208

Figure 7.8 Methomyl response across concentration in a pure water matrix vs effluents and rinsates. 208
Figure 7.9 Thiamethoxam response across concentration in a pure water matrix vs effluents and rinsates. 208
Figure 7.10 Flonicamid response across concentration in a pure water matrix vs effluents and rinsates. 209
Figure 7.11 Clothianidin response across concentration in a pure water matrix vs effluents and rinsates. 209
Figure 7.12 Dimethoate response across concentration in a pure water matrix vs effluents and rinsates. 209
Figure 7.13 Pirimicarb response across concentration in a pure water matrix vs effluents and rinsates. 209
Figure 7.14 Mevinphos response across concentration in a pure water matrix vs effluents and rinsates. 209
Figure 7.15 Imidacloprid response across concentration in a pure water matrix vs effluents and rinsates. 209
Figure 7.16 Acetamiprid response across concentration in a pure water matrix vs effluents and rinsates. 210
Figure 7.17 Imazethapyr response across concentration in a pure water matrix vs effluents and rinsates. 210
Figure 7.18 Aldicarb response across concentration in a pure water matrix vs effluents and rinsates. 210
Figure 7.19 Thiacloprid response across concentration in a pure water matrix vs effluents and rinsates. 210
Figure 7.20 Dicamba response across concentration in a pure water matrix vs effluents and rinsates. 210
Figure 7.21 Propoxur response across concentration in a pure water matrix vs effluents and rinsates. 210
Figure 7.22 Imazalil response across concentration in a pure water matrix vs effluents and rinsates. 211
Figure 7.23 Thiophanate-Methyl response at 20 ppb in a pure water matrix vs effluents and rinsates. 211
Figure 7.24 Carbofuran response across concentration in a pure water matrix vs effluents and rinsates. 211
Figure 7.25 Bentazon response across concentration in a pure water matrix vs effluents and rinsates. 211
Figure 7.26 Atrazine response across concentration in a pure water matrix vs effluents and rinsates. 211

Figure 7.27 Carbaryl response across concentration in a pure water matrix vs effluents and rinsates. 211
Figure 7.28 Metalaxyl response across concentration in a pure water matrix vs effluents and rinsates. 212
Figure 7.29 Dodemorph response across concentration in a pure water matrix vs effluents and rinsates. 212
Figure 7.30 2,4-D response across concentration in a pure water matrix vs effluents and rinsates. 212
Figure 7.31 Spiroxamine response across concentration in a pure water matrix vs effluents and rinsates. 212
Figure 7.32 Fensulfothion response at 20 ppb in a pure water matrix vs effluents and rinsates. 212
Figure 7.33 Cyantraniliprole response across concentration in a pure water matrix vs effluents and rinsates. 212
Figure 7.34 Cyprodinil response across concentration in a pure water matrix vs effluents and rinsates. 213
Figure 7.35 Paclobutrazol response across concentration in a pure water matrix vs effluents and rinsates. 213
Figure 7.36 Chlorantraniliprole response across concentration in a pure water matrix vs effluents and rinsates. 213
Figure 7.37 Dimethomorph II response at 20 ppb in a pure water matrix vs effluents and rinsates. 213
Figure 7.38 Fludioxinil response at 20 ppb in a pure water matrix vs effluents and rinsates.... 213
Figure 7.39 Spinosyn A response at 20 ppb in a pure water matrix vs effluents and rinsates... 213
Figure 7.40 Spirotetramat response across concentration in a pure water matrix vs effluents and rinsates. 214
Figure 7.41 Dimethomorph I response across concentration in a pure water matrix vs effluents and rinsates. 214
Figure 7.42 Fenhexamid response across concentration in a pure water matrix vs effluents and rinsates. 214
Figure 7.43 Ethoprophos response across concentration in a pure water matrix vs effluents and rinsates. 214
Figure 7.44 Myclobutanil response across concentration in a pure water matrix vs effluents and rinsates. 214
Figure 7.45 Spinosyn D response at 20 ppb in a pure water matrix vs effluents and rinsates... 214
Figure 7.46 Phosmet response at 20 ppb in a pure water matrix vs effluents and rinsates..... 215
Figure 7.47 Tebuconazole response across concentration in a pure water matrix vs effluents and rinsates. 215

Figure 7.48 Spinetoram J response at 20 ppb in a pure water matrix vs effluents and rinsates. 215
Figure 7.49 Azoxystrobin response across concentration in a pure water matrix vs effluents and rinsates. 215
Figure 7.50 Fluopyram response across concentration in a pure water matrix vs effluents and rinsates. 215
Figure 7.51 Boscalid response across concentration in a pure water matrix vs effluents and rinsates. 215
Figure 7.52 Metolachlor response across concentration in a pure water matrix vs effluents and rinsates. 216
Figure 7.53 Malathion response across concentration in a pure water matrix vs effluents and rinsates. 216
Figure 7.54 Fenoxycarb response across concentration in a pure water matrix vs effluents and rinsates. 216
Figure 7.55 Tebufenozide response across concentration in a pure water matrix vs effluents and rinsates. 216
Figure 7.56 Fipronil response across concentration in a pure water matrix vs effluents and rinsates. 216
Figure 7.57 Tetrachlorvinphos response across concentration in a pure water matrix vs effluents and rinsates. 216
Figure 7.58 Propiconazole response across concentration in a pure water matrix vs effluents and rinsates. 217
Figure 7.59 Imazamox response across concentration in a pure water matrix vs effluents and rinsates. 217
Figure 7.60 Buprofezin response across concentration in a pure water matrix vs effluents and rinsates. 217
Figure 7.61 Kresoxim-Methyl response across concentration in a pure water matrix vs effluents and rinsates. 217
Figure 7.62 Diazinon response across concentration in a pure water matrix vs effluents and rinsates. 217
Figure 7.63 Benzodiflupyr response across concentration in a pure water matrix vs effluents and rinsates. 217
Figure 7.64 Prallethrin response across concentration in a pure water matrix vs effluents and rinsates. 218
Figure 7.65 Pyrethrin II response across concentration in a pure water matrix vs effluents and rinsates. 218
Figure 7.66 Pyraclostrobin response across concentration in a pure water matrix vs effluents and rinsates. 218

Figure 7.67 Clofentazine response across concentration in a pure water matrix vs effluents and rinsates. 218
Figure 7.68 MGK 264 response across concentration in a pure water matrix vs effluents and rinsates. 218
Figure 7.69 Coumaphos response across concentration in a pure water matrix vs effluents and rinsates. 218
Figure 7.70 Teflubenzuron response across concentration in a pure water matrix vs effluents and rinsates. 219
Figure 7.71 Trifloxystrobin response across concentration in a pure water matrix vs effluents and rinsates. 219
Figure 7.72 Piperonyl Butoxide response across concentration in a pure water matrix vs effluents and rinsates. 219
Figure 7.73 Allethrin response across concentration in a pure water matrix vs effluents and rinsates. 219
Figure 7.74 Fenpyroximate response at 20 ppb in a pure water matrix vs effluents and rinsates. 219
Figure 7.75 Tetramethrin response across concentration in a pure water matrix vs effluents and rinsates. 219
Figure 7.76 Etoxazole response across concentration in a pure water matrix vs effluents and rinsates. 220
Figure 7.77 Pyrethrin I response at 20 ppb in a pure water matrix vs effluents and rinsates. ... 220
Figure 7.78 Chlorpyrifos response across concentration in a pure water matrix vs effluents and rinsates. 220
Figure 7.79 Spiromesifen response at 20 ppb in a pure water matrix vs effluents and rinsates. 220
Figure 7.80 Hexythiazox response across concentration in a pure water matrix vs effluents and rinsates. 220
Figure 7.81 Spirodiclofen response across concentration in a pure water matrix vs effluents and rinsates. 220
Figure 7.82 Pyridaben response at 20 ppb in a pure water matrix vs effluents and rinsates. 221
Figure 7.83 Resmethrin response at 20 ppb in a pure water matrix vs effluents and rinsates. .. 221
Figure 7.84 Permethrin response at 20 ppb in a pure water matrix vs effluents and rinsates.... 221
Figure 7.85 Etofenprox response at 20 ppb in a pure water matrix vs effluents and rinsates. .. 221
Figure 7.86 Bifenthrin response at 20 ppb in a pure water matrix vs effluents and rinsates. 221
Figure 7.87 Acequinocyl response at 20 ppb in a pure water matrix vs effluents and rinsates. 221
Figure 8.1 ANOVA's conducted that were found to have a significant matrix effect vs. no effect. 225

Figure 8.2 Summary of molecule responses from matrix effect found to be significant in an ANOVA and analyzed through Dunnett's test (control vs. matrices) for QuEChERS..... 225

Figure 8.3 Acephate response across concentrations in a pure acetonitrile matrix vs QuEChERS extracts. 234

Figure 8.4 Dinotefuran r response across concentrations in a pure acetonitrile matrix vs QuEChERS extracts. 234

Figure 8.5 Oxamyl response across concentrations in a pure acetonitrile matrix vs QuEChERS extracts. 234

Figure 8.6 Thiamethoxam response across concentrations in a pure acetonitrile matrix vs QuEChERS extracts. 234

Figure 8.7 Flonicamid response across concentrations in a pure acetonitrile matrix vs QuEChERS extracts. 234

Figure 8.8 Clothianidin response across concentrations in a pure acetonitrile matrix vs QuEChERS extracts. 234

Figure 8.9 Dimethoate response across concentrations in a pure acetonitrile matrix vs QuEChERS extracts. 235

Figure 8.10 Mevinphos response across concentrations in a pure acetonitrile matrix vs QuEChERS extracts. 235

Figure 8.11 Imidacloprid response across concentrations in a pure acetonitrile matrix vs QuEChERS extracts. 235

Figure 8.12 Acetamiprid response across concentrations in a pure acetonitrile matrix vs QuEChERS extracts. 235

Figure 8.13 Imazethapyr response across concentrations in a pure acetonitrile matrix vs QuEChERS extracts. 235

Figure 8.14 Aldicarb response across concentrations in a pure acetonitrile matrix vs QuEChERS extracts. 235

Figure 8.15 Thiacloprid response across concentrations in a pure acetonitrile matrix vs QuEChERS extracts. 236

Figure 8.16 Dicamba response across concentrations in a pure acetonitrile matrix vs QuEChERS extracts. 236

Figure 8.17 Propoxur response across concentrations in a pure acetonitrile matrix vs QuEChERS extracts. 236

Figure 8.18 Imazalil response across concentrations in a pure acetonitrile matrix vs QuEChERS extracts. 236

Figure 8.19 Thiophanate-Methyl response across concentrations in a pure acetonitrile matrix vs QuEChERS extracts. 236

Figure 8.20 Carbofuran response across concentrations in a pure acetonitrile matrix vs QuEChERS extracts. 236

Figure 8.21 Bentazon response across concentrations in a pure acetonitrile matrix vs QuEChERS extracts. 237
Figure 8.22 Atrazine response across concentrations in a pure acetonitrile matrix vs QuEChERS extracts. 237
Figure 8.23 Carbaryl response across concentrations in a pure acetonitrile matrix vs QuEChERS extracts. 237
Figure 8.24 Metalaxyl response across concentrations in a pure acetonitrile matrix vs QuEChERS extracts. 237
Figure 8.25 Dodemorph response across concentrations in a pure acetonitrile matrix vs QuEChERS extracts. 237
Figure 8.26 2,4-D response across concentrations in a pure acetonitrile matrix vs QuEChERS extracts. 237
Figure 8.27 Spiroxamine response across concentrations in a pure acetonitrile matrix vs QuEChERS extracts. 238
Figure 8.28 Cyprodinil response across concentrations in a pure acetonitrile matrix vs QuEChERS extracts. 238
Figure 8.29 Paclobutrazol response across concentrations in a pure acetonitrile matrix vs QuEChERS extracts. 238
Figure 8.30 Chlorantraniliprole response across concentrations in a pure acetonitrile matrix vs QuEChERS extracts. 238
Figure 8.31 Dimethomorph II response across concentrations in a pure acetonitrile matrix vs QuEChERS extracts. 238
Figure 8.32 Spirotetramat response across concentrations in a pure acetonitrile matrix vs QuEChERS extracts. 239
Figure 8.33 Dimethomorph I response across concentrations in a pure acetonitrile matrix vs QuEChERS extracts. 239
Figure 8.34 Fenhexamid response across concentrations in a pure acetonitrile matrix vs QuEChERS extracts. 239
Figure 8.35 Ethoprophos response at 20 ppb in a pure acetonitrile matrix vs QuEChERS extracts. 239
Figure 8.36 Myclobutanil response across concentrations in a pure acetonitrile matrix vs QuEChERS extracts. 239
Figure 8.37 Tebuconazole response across concentrations in a pure acetonitrile matrix vs QuEChERS extracts. 239
Figure 8.38 Spinetoram J response across concentrations in a pure acetonitrile matrix vs QuEChERS extracts. 240
Figure 8.39 Azoxystrobin response across concentrations in a pure acetonitrile matrix vs QuEChERS extracts. 240

Figure 8.40 Fluopyram response across concentrations in a pure acetonitrile matrix vs QuEChERS extracts. 240
Figure 8.41 Boscalid response at 20 ppb in a pure acetonitrile matrix vs QuEChERS extracts. 240
Figure 8.42 Metolachlor response across concentrations in a pure acetonitrile matrix vs QuEChERS extracts. 240
Figure 8.43 Malathion response across concentrations in a pure acetonitrile matrix vs QuEChERS extracts. 240
Figure 8.44 Fenoxycarb response across concentrations in a pure acetonitrile matrix vs QuEChERS extracts. 241
Figure 8.45 Tebufenozide response across concentrations in a pure acetonitrile matrix vs QuEChERS extracts. 241
Figure 8.46 Fipronil response across concentrations in a pure acetonitrile matrix vs QuEChERS extracts. 241
Figure 8.47 Tetrachlorvinphos response across concentrations in a pure acetonitrile matrix vs QuEChERS extracts. 241
Figure 8.48 Propiconazole response across concentrations in a pure acetonitrile matrix vs QuEChERS extracts. 241
Figure 8.49 Imazamox response across concentrations in a pure acetonitrile matrix vs QuEChERS extracts. 241
Figure 8.50 Buprofezin response across concentrations in a pure acetonitrile matrix vs QuEChERS extracts. 242
Figure 8.51 Kresoxim-Methyl response across concentrations in a pure acetonitrile matrix vs QuEChERS extracts. 242
Figure 8.52 Diazinon response across concentrations in a pure acetonitrile matrix vs QuEChERS extracts. 242
Figure 8.53 Benzovindiflupyr response at 20 ppb in a pure acetonitrile matrix vs QuEChERS extracts. 242
Figure 8.54 Prallethrin response across concentrations in a pure acetonitrile matrix vs QuEChERS extracts. 242
Figure 8.55 Pyrethrin II response at 20 ppb in a pure acetonitrile matrix vs QuEChERS extracts. 242
Figure 8.56 Pyraclostrobin response across concentrations in a pure acetonitrile matrix vs QuEChERS extracts. 243
Figure 8.57 Clofentazine response at 20 ppb in a pure acetonitrile matrix vs QuEChERS extracts. 243
Figure 8.58 MGK 264 response across concentrations in a pure acetonitrile matrix vs QuEChERS extracts. 243

Figure 8.59 Coumaphos response across concentrations in a pure acetonitrile matrix vs QuEChERS extracts. 243

Figure 8.60 Teflubenzuron response across concentrations in a pure acetonitrile matrix vs QuEChERS extracts. 243

Figure 8.61 Allethrin response across concentrations in a pure acetonitrile matrix vs QuEChERS extracts.. 243

Figure 8.62 Tetramethrin response across concentrations in a pure acetonitrile matrix vs QuEChERS extracts. 244

Figure 8.63 Etoxazole response across concentrations in a pure acetonitrile matrix vs QuEChERS extracts. 244

Figure 8.64 Pyrethrin I response across concentrations in a pure acetonitrile matrix vs QuEChERS extracts. 244

Figure 8.65 Chlorpyrifos response at 20 ppb in a pure acetonitrile matrix vs QuEChERS extracts. 244

Figure 8.66 Spiromesifen response across concentrations in a pure acetonitrile matrix vs QuEChERS extracts. 244

Figure 8.67 Hexythiazox response at 20 ppb in a pure acetonitrile matrix vs QuEChERS extracts. 244

Figure 8.68 Spirodiclofen response across concentrations in a pure acetonitrile matrix vs QuEChERS extracts. 245

Figure 8.69 Pyridaben response across concentrations in a pure acetonitrile matrix vs QuEChERS extracts. 245

Figure 8.70 Quick Summary of freeze-drying losses detected by an ANOVA for QuEChERS. 246

Figure 8.71 Acephate internal standard recovery before freeze-drying (BFD), after freeze-drying (AFD), and filter (FIL) stage of extractions. Bars are standard error, dashed line are amount spiked. 250

Figure 8.72 Dinotefuran internal standard recovery before freeze-drying (BFD), after freeze-drying (AFD), and filter (FIL) stage of extractions. Bars are standard error, dashed line are amount spiked. 250

Figure 8.73 Oxamyl internal standard recovery before freeze-drying (BFD), after freeze-drying (AFD), and filter (FIL) stage of extractions. Bars are standard error, dashed line are amount spiked. 250

Figure 8.74 Thiamethoxam internal standard recovery before freeze-drying (BFD), after freeze-drying (AFD), and filter (FIL) stage of extractions. Bars are standard error, dashed line are amount spiked. 250

Figure 8.75 Flonicamid internal standard recovery before freeze-drying (BFD), after freeze-drying (AFD), and filter (FIL) stage of extractions. Bars are standard error, dashed line are amount spiked. 251

Figure 8.76 Clothianidin internal standard recovery before freeze-drying (BFD), after freeze-drying (AFD), and filter (FIL) stage of extractions. Bars are standard error, dashed line are amount spiked. 251

Figure 8.77 Dimethoate internal standard recovery before freeze-drying (BFD), after freeze-drying (AFD), and filter (FIL) stage of extractions. Bars are standard error, dashed line are amount spiked. 251

Figure 8.78 Mevinphos internal standard recovery before freeze-drying (BFD), after freeze-drying (AFD), and filter (FIL) stage of extractions. Bars are standard error, dashed line are amount spiked. 251

Figure 8.79 Imidacloprid internal standard recovery before freeze-drying (BFD), after freeze-drying (AFD), and filter (FIL) stage of extractions. Bars are standard error, dashed line are amount spiked. 252

Figure 8.80 Acetamiprid internal standard recovery before freeze-drying (BFD), after freeze-drying (AFD), and filter (FIL) stage of extractions. Bars are standard error, dashed line are amount spiked. 252

Figure 8.81 Imazethapyr internal standard recovery before freeze-drying (BFD), after freeze-drying (AFD), and filter (FIL) stage of extractions. Bars are standard error, dashed line are amount spiked. 252

Figure 8.82 Aldicarb internal standard recovery before freeze-drying (BFD), after freeze-drying (AFD), and filter (FIL) stage of extractions. Bars are standard error, dashed line are amount spiked. 252

Figure 8.83 Thiacloprid internal standard recovery before freeze-drying (BFD), after freeze-drying (AFD), and filter (FIL) stage of extractions. Bars are standard error, dashed line are amount spiked. 253

Figure 8.84 Dicamba internal standard recovery before freeze-drying (BFD), after freeze-drying (AFD), and filter (FIL) stage of extractions. Bars are standard error, dashed line are amount spiked. 253

Figure 8.85 Propoxur internal standard recovery before freeze-drying (BFD), after freeze-drying (AFD), and filter (FIL) stage of extractions. Bars are standard error, dashed line are amount spiked. 253

Figure 8.86 Imazalil internal standard recovery before freeze-drying (BFD), after freeze-drying (AFD), and filter (FIL) stage of extractions. Bars are standard error, dashed line are amount spiked. 253

Figure 8.87 Thiophanate-Methyl internal standard recovery before freeze-drying (BFD), after freeze-drying (AFD), and filter (FIL) stage of extractions. Bars are standard error, dashed line are amount spiked. 254

Figure 8.88 Carbofuran internal standard recovery before freeze-drying (BFD), after freeze-drying (AFD), and filter (FIL) stage of extractions. Bars are standard error, dashed line are amount spiked. 254

Figure 8.89 Bentazon internal standard recovery before freeze-drying (BFD), after freeze-drying (AFD), and filter (FIL) stage of extractions. Bars are standard error, dashed line are amount spiked. 254

Figure 8.90 Atrazine internal standard recovery before freeze-drying (BFD), after freeze-drying (AFD), and filter (FIL) stage of extractions. Bars are standard error, dashed line are amount spiked. 254

Figure 8.91 Carbaryl internal standard recovery before freeze-drying (BFD), after freeze-drying (AFD), and filter (FIL) stage of extractions. Bars are standard error, dashed line are amount spiked. 255

Figure 8.92 Metalaxyl internal standard recovery before freeze-drying (BFD), after freeze-drying (AFD), and filter (FIL) stage of extractions. Bars are standard error, dashed line are amount spiked. 255

Figure 8.93 Dodemorph internal standard recovery before freeze-drying (BFD), after freeze-drying (AFD), and filter (FIL) stage of extractions. Bars are standard error, dashed line are amount spiked. 255

Figure 8.94 2,4-D internal internal standard recovery before freeze-drying (BFD), after freeze-drying (AFD), and filter (FIL) stage of extractions. Bars are standard error, dashed line are amount spiked. 255

Figure 8.95 Cyprodinil internal standard recovery before freeze-drying (BFD), after freeze-drying (AFD), and filter (FIL) stage of extractions. Bars are standard error, dashed line are amount spiked. 256

Figure 8.96 Paclobutrazol internal standard recovery before freeze-drying (BFD), after freeze-drying (AFD), and filter (FIL) stage of extractions. Bars are standard error, dashed line are amount spiked. 256

Figure 8.97 Chlorantraniliprole internal standard recovery before freeze-drying (BFD), after freeze-drying (AFD), and filter (FIL) stage of extractions. Bars are standard error, dashed line are amount spiked. 256

Figure 8.98 Dimethomorph II internal standard recovery before freeze-drying (BFD), after freeze-drying (AFD), and filter (FIL) stage of extractions. Bars are standard error, dashed line are amount spiked. 256

Figure 8.99 Spirotetramat internal standard recovery before freeze-drying (BFD), after freeze-drying (AFD), and filter (FIL) stage of extractions. Bars are standard error, dashed line are amount spiked. 257

Figure 8.100 Dimethomorph I internal standard recovery before freeze-drying (BFD), after freeze-drying (AFD), and filter (FIL) stage of extractions. Bars are standard error, dashed line are amount spiked. 257

Figure 8.101 Fenhexamid internal standard recovery before freeze-drying (BFD), after freeze-drying (AFD), and filter (FIL) stage of extractions. Bars are standard error, dashed line are amount spiked. 257

Figure 8.102 Ethoprophos internal standard recovery before freeze-drying (BFD), after freeze-drying (AFD), and filter (FIL) stage of extractions. Bars are standard error, dashed line are amount spiked. 257

Figure 8.103 Myclobutanil internal standard recovery before freeze-drying (BFD), after freeze-drying (AFD), and filter (FIL) stage of extractions. Bars are standard error, dashed line are amount spiked. 258

Figure 8.104 Phosmet internal standard recovery before freeze-drying (BFD), after freeze-drying (AFD), and filter (FIL) stage of extractions. Bars are standard error, dashed line are amount spiked. 258

Figure 8.105 Tebuconazole internal standard recovery before freeze-drying (BFD), after freeze-drying (AFD), and filter (FIL) stage of extractions. Bars are standard error, dashed line are amount spiked. 258

Figure 8.106 Spinetoram J internal standard recovery before freeze-drying (BFD), after freeze-drying (AFD), and filter (FIL) stage of extractions. Bars are standard error, dashed line are amount spiked. 258

Figure 8.107 Azoxystrobin internal standard recovery before freeze-drying (BFD), after freeze-drying (AFD), and filter (FIL) stage of extractions. Bars are standard error, dashed line are amount spiked. 259

Figure 8.108 Fluopyram internal standard recovery before freeze-drying (BFD), after freeze-drying (AFD), and filter (FIL) stage of extractions. Bars are standard error, dashed line are amount spiked. 259

Figure 8.109 Boscalid internal standard recovery before freeze-drying (BFD), after freeze-drying (AFD), and filter (FIL) stage of extractions. Bars are standard error, dashed line are amount spiked. 259

Figure 8.110 Metolachlor internal standard recovery before freeze-drying (BFD), after freeze-drying (AFD), and filter (FIL) stage of extractions. Bars are standard error, dashed line are amount spiked. 259

Figure 8.111 Malathion internal standard recovery before freeze-drying (BFD), after freeze-drying (AFD), and filter (FIL) stage of extractions. Bars are standard error, dashed line are amount spiked. 260

Figure 8.112 Fenoxycarb internal standard recovery before freeze-drying (BFD), after freeze-drying (AFD), and filter (FIL) stage of extractions. Bars are standard error, dashed line are amount spiked. 260

Figure 8.113 Tebufenozide internal standard recovery before freeze-drying (BFD), after freeze-drying (AFD), and filter (FIL) stage of extractions. Bars are standard error, dashed line are amount spiked. 260

Figure 8.114 Fipronil internal standard recovery before freeze-drying (BFD), after freeze-drying (AFD), and filter (FIL) stage of extractions. Bars are standard error, dashed line are amount spiked. 260

Figure 8.115 Tetrachlorvinphos internal standard recovery before freeze-drying (BFD), after freeze-drying (AFD), and filter (FIL) stage of extractions. Bars are standard error, dashed line are amount spiked. 261

Figure 8.116 Propiconazole internal standard recovery before freeze-drying (BFD), after freeze-drying (AFD), and filter (FIL) stage of extractions. Bars are standard error, dashed line are amount spiked. 261

Figure 8.117 Imazamox internal standard recovery before freeze-drying (BFD), after freeze-drying (AFD), and filter (FIL) stage of extractions. Bars are standard error, dashed line are amount spiked. 261

Figure 8.118 Buprofezin internal standard recovery before freeze-drying (BFD), after freeze-drying (AFD), and filter (FIL) stage of extractions. Bars are standard error, dashed line are amount spiked. 261

Figure 8.119 Kresoxim-Methyl internal standard recovery before freeze-drying (BFD), after freeze-drying (AFD), and filter (FIL) stage of extractions. Bars are standard error, dashed line are amount spiked. 262

Figure 8.120 Diazinon internal standard recovery before freeze-drying (BFD), after freeze-drying (AFD), and filter (FIL) stage of extractions. Bars are standard error, dashed line are amount spiked. 262

Figure 8.121 Benzodiflupyr internal standard recovery before freeze-drying (BFD), after freeze-drying (AFD), and filter (FIL) stage of extractions. Bars are standard error, dashed line are amount spiked. 262

Figure 8.122 Prallethrin internal standard recovery before freeze-drying (BFD), after freeze-drying (AFD), and filter (FIL) stage of extractions. Bars are standard error, dashed line are amount spiked. 262

Figure 8.123 Pyrethrin II internal standard recovery before freeze-drying (BFD), after freeze-drying (AFD), and filter (FIL) stage of extractions. Bars are standard error, dashed line are amount spiked. 263

Figure 8.124 Pyraclostrobin internal standard recovery before freeze-drying (BFD), after freeze-drying (AFD), and filter (FIL) stage of extractions. Bars are standard error, dashed line are amount spiked. 263

Figure 8.125 Clofentazine internal standard recovery before freeze-drying (BFD), after freeze-drying (AFD), and filter (FIL) stage of extractions. Bars are standard error, dashed line are amount spiked. 263

Figure 8.126 MGK 264 internal standard recovery before freeze-drying (BFD), after freeze-drying (AFD), and filter (FIL) stage of extractions. Bars are standard error, dashed line are amount spiked. 263

Figure 8.127 Coumaphos internal standard recovery before freeze-drying (BFD), after freeze-drying (AFD), and filter (FIL) stage of extractions. Bars are standard error, dashed line are amount spiked. 264

Figure 8.128 Teflubenzuron internal standard recovery before freeze-drying (BFD), after freeze-drying (AFD), and filter (FIL) stage of extractions. Bars are standard error, dashed line are amount spiked. 264

Figure 8.129 Allethrin internal standard recovery before freeze-drying (BFD), after freeze-drying (AFD), and filter (FIL) stage of extractions. Bars are standard error, dashed line are amount spiked. 264

Figure 8.130 Tetramethrin internal standard recovery before freeze-drying (BFD), after freeze-drying (AFD), and filter (FIL) stage of extractions. Bars are standard error, dashed line are amount spiked. 264

Figure 8.131 Etoxazole internal standard recovery before freeze-drying (BFD), after freeze-drying (AFD), and filter (FIL) stage of extractions. Bars are standard error, dashed line are amount spiked. 265

Figure 8.132 Pyrethrin I internal standard recovery before freeze-drying (BFD), after freeze-drying (AFD), and filter (FIL) stage of extractions. Bars are standard error, dashed line are amount spiked. 265

Figure 8.133 Chlorpyrifos internal standard recovery before freeze-drying (BFD), after freeze-drying (AFD), and filter (FIL) stage of extractions. Bars are standard error, dashed line are amount spiked. 265

Figure 8.134 Spiromesifen internal standard recovery before freeze-drying (BFD), after freeze-drying (AFD), and filter (FIL) stage of extractions. Bars are standard error, dashed line are amount spiked. 265

Figure 8.135 Hexythiazox internal standard recovery before freeze-drying (BFD), after freeze-drying (AFD), and filter (FIL) stage of extractions. Bars are standard error, dashed line are amount spiked. 266

Figure 8.136 Spirodiclofen internal standard recovery before freeze-drying (BFD), after freeze-drying (AFD), and filter (FIL) stage of extractions. Bars are standard error, dashed line are amount spiked. 266

Figure 8.137 Pyridaben internal standard recovery before freeze-drying (BFD), after freeze-drying (AFD), and filter (FIL) stage of extractions. Bars are standard error, dashed line are amount spiked. 266

Figure 9.1 ANCOVA's conducted that were found to have a significant matrix effect vs. no effect. 270

Figure 9.2 Summary of molecule responses from matrix effect found to be significant in an ANOVA and analyzed through Dunnett's test (control vs. matrix) for QuPPe. 270

Figure 9.3 Dinotefuran response across concentrations in a 1:1 methanol/water vs QuPPe extracts. 276

Figure 9.4 Oxamyl response across concentrations in a 1:1 methanol/water vs QuPPe extracts. 276

Figure 9.5 Clopyralid response across concentrations in a 1:1 methanol/water vs QuPPe extracts. 276

Figure 9.6 Thiamethoxam response across concentrations in a 1:1 methanol/water vs QuPPe extracts. 276
Figure 9.7 Flonicamid response across concentrations in a 1:1 methanol/water vs QuPPe extracts. 276
Figure 9.8 Clothianidin response across concentrations in a 1:1 methanol/water vs QuPPe extracts. 276
Figure 9.9 Dimethoate response across concentrations in a 1:1 methanol/water vs QuPPe extracts. 277
Figure 9.10 Imidacloprid response across concentrations in a 1:1 methanol/water vs QuPPe extracts. 277
Figure 9.11 Mevinphos response across concentrations in a 1:1 methanol/water vs QuPPe extracts. 277
Figure 9.12 Acetamiprid response across concentrations in a 1:1 methanol/water vs QuPPe extracts. 277
Figure 9.13 Imazethapyr response across concentrations in a 1:1 methanol/water vs QuPPe extracts. 277
Figure 9.14 Aldicarb response across concentrations in a 1:1 methanol/water vs QuPPe extracts. 277
Figure 9.15 Thiacloprid response across concentrations in a 1:1 methanol/water vs QuPPe extracts. 278
Figure 9.16 Dicamba response across concentrations in a 1:1 methanol/water vs QuPPe extracts. 278
Figure 9.17 Propoxur response across concentrations in a 1:1 methanol/water vs QuPPe extracts. 278
Figure 9.18 Carbofuran response across concentrations in a 1:1 methanol/water vs QuPPe extracts. 278
Figure 9.19 Bentazon response across concentrations in a 1:1 methanol/water vs QuPPe extracts. 278
Figure 9.20 Atrazine response across concentrations in a 1:1 methanol/water vs QuPPe extracts. 278
Figure 9.21 Carbaryl response across concentrations in a 1:1 methanol/water vs QuPPe extracts. 279
Figure 9.22 Metalaxyl response across concentrations in a 1:1 methanol/water vs QuPPe extracts. 279
Figure 9.23 2,4-D response across concentrations in a 1:1 methanol/water vs QuPPe extracts.279
Figure 9.24 Paclobutrazol response across concentrations in a 1:1 methanol/water vs QuPPe extracts. 279

Figure 9.25 Chlorantraniliprole response across concentrations in a 1:1 methanol/water vs QuPPe extracts. 279
Figure 9.26 Dimethomorph II response across concentrations in a 1:1 methanol/water vs QuPPe extracts. 279
Figure 9.27 Spirotetramat response across concentrations in a 1:1 methanol/water vs QuPPe extracts. 280
Figure 9.28 Dimethomorph I response across concentrations in a 1:1 methanol/water vs QuPPe extracts. 280
Figure 9.29 Fenhexamid response across concentrations in a 1:1 methanol/water vs QuPPe extracts. 280
Figure 9.30 Ethoprophos response across concentrations in a 1:1 methanol/water vs QuPPe extracts. 280
Figure 9.31 Myclobutanil response across concentrations in a 1:1 methanol/water vs QuPPe extracts. 280
Figure 9.32 Tebuconazole response across concentrations in a 1:1 methanol/water vs QuPPe extracts. 280
Figure 9.33 Azoxystrobin response across concentrations in a 1:1 methanol/water vs QuPPe extracts. 281
Figure 9.34 Fluopyram response across concentrations in a 1:1 methanol/water vs QuPPe extracts. 281
Figure 9.35 Boscalid response across concentrations in a 1:1 methanol/water vs QuPPe extracts. 281
Figure 9.36 Metolachlor response across concentrations in a 1:1 methanol/water vs QuPPe extracts. 281
Figure 9.37 Malathion response across concentrations in a 1:1 methanol/water vs QuPPe extracts. 281
Figure 9.38 Fenoxycarb response across concentrations in a 1:1 methanol/water vs QuPPe extracts. 281
Figure 9.39 Tebufenozide response across concentrations in a 1:1 methanol/water vs QuPPe extracts. 282
Figure 9.40 Fipronil response across concentrations in a 1:1 methanol/water vs QuPPe extracts. 282
Figure 9.41 Tetrachlorvinphos response across concentrations in a 1:1 methanol/water vs QuPPe extracts. 282
Figure 9.42 Propiconazole response across concentrations in a 1:1 methanol/water vs QuPPe extracts. 282
Figure 9.43 Kresoxim-Methyl response at 20 ppb in a 1:1 methanol/water vs QuPPe extracts.282

Figure 9.44 Diazinon response across concentrations in a 1:1 methanol/water vs QuPPe extracts. 282
Figure 9.45 Benzovindiflupyr response across concentrations in a 1:1 methanol/water vs QuPPe extracts. 283
Figure 9.46 Prallethrin response across concentrations in a 1:1 methanol/water vs QuPPe extracts. 283
Figure 9.47 Pyraclostrobin response across concentrations in a 1:1 methanol/water vs QuPPe extracts. 283
Figure 9.48 MGK 264 response across concentrations in a 1:1 methanol/water vs QuPPe extracts. 283
Figure 9.49 Allethrin response across concentrations in a 1:1 methanol/water vs QuPPe extracts. 283
Figure 9.50 Tetramethrin response across concentrations in a 1:1 methanol/water vs QuPPe extracts. 283
Figure 9.51 Spiromesifen response across concentrations in a 1:1 methanol/water vs QuPPe extracts. 284
Figure 9.52 Hexythiazox response across concentrations in a 1:1 methanol/water vs QuPPe extracts. 284
Figure 9.53 Spirodiclofen response across concentrations in a 1:1 methanol/water vs QuPPe extracts. 284
Figure 9.54 Quick Summary of freeze-drying losses detected by an ANOVA for QuPPe. 285
Figure 9.55 Dinotefuran internal standard recovery before freeze-drying (BFD), after freeze-drying (AFD), and filter (FIL) stage of extractions. Bars are standard error, dashed line are amount spiked. 289
Figure 9.56 Oxamyl internal standard recovery before freeze-drying (BFD), after freeze-drying (AFD), and filter (FIL) stage of extractions. Bars are standard error, dashed line are amount spiked. 289
Figure 9.57 Clopyralid internal standard recovery before freeze-drying (BFD), after freeze-drying (AFD), and filter (FIL) stage of extractions. Bars are standard error, dashed line are amount spiked. 289
Figure 9.58 Thiamethoxam internal standard recovery before freeze-drying (BFD), after freeze-drying (AFD), and filter (FIL) stage of extractions. Bars are standard error, dashed line are amount spiked. 289
Figure 9.59 Flonicamid internal standard recovery before freeze-drying (BFD), after freeze-drying (AFD), and filter (FIL) stage of extractions. Bars are standard error, dashed line are amount spiked. 290
Figure 9.60 Clothianidin internal standard recovery before freeze-drying (BFD), after freeze-drying (AFD), and filter (FIL) stage of extractions. Bars are standard error, dashed line are amount spiked. 290

Figure 9.61 Dimethoate internal standard recovery before freeze-drying (BFD), after freeze-drying (AFD), and filter (FIL) stage of extractions. Bars are standard error, dashed line are amount spiked. 290

Figure 9.62 Mevinphos internal standard recovery before freeze-drying (BFD), after freeze-drying (AFD), and filter (FIL) stage of extractions. Bars are standard error, dashed line are amount spiked. 290

Figure 9.63 Imidacloprid internal standard recovery before freeze-drying (BFD), after freeze-drying (AFD), and filter (FIL) stage of extractions. Bars are standard error, dashed line are amount spiked. 291

Figure 9.64 Acetamiprid internal standard recovery before freeze-drying (BFD), after freeze-drying (AFD), and filter (FIL) stage of extractions. Bars are standard error, dashed line are amount spiked. 291

Figure 9.65 Imazethapyr internal standard recovery before freeze-drying (BFD), after freeze-drying (AFD), and filter (FIL) stage of extractions. Bars are standard error, dashed line are amount spiked. 291

Figure 9.66 Aldicarb internal standard recovery before freeze-drying (BFD), after freeze-drying (AFD), and filter (FIL) stage of extractions. Bars are standard error, dashed line are amount spiked. 291

Figure 9.67 Thiacloprid internal standard recovery before freeze-drying (BFD), after freeze-drying (AFD), and filter (FIL) stage of extractions. Bars are standard error, dashed line are amount spiked. 292

Figure 9.68 Dicamba internal standard recovery before freeze-drying (BFD), after freeze-drying (AFD), and filter (FIL) stage of extractions. Bars are standard error, dashed line are amount spiked. 292

Figure 9.69 Propoxur internal standard recovery before freeze-drying (BFD), after freeze-drying (AFD), and filter (FIL) stage of extractions. Bars are standard error, dashed line are amount spiked. 292

Figure 9.70 Carbofuran internal standard recovery before freeze-drying (BFD), after freeze-drying (AFD), and filter (FIL) stage of extractions. Bars are standard error, dashed line are amount spiked. 292

Figure 9.71 Bentazon internal standard recovery before freeze-drying (BFD), after freeze-drying (AFD), and filter (FIL) stage of extractions. Bars are standard error, dashed line are amount spiked. 293

Figure 9.72 Atrazine internal standard recovery before freeze-drying (BFD), after freeze-drying (AFD), and filter (FIL) stage of extractions. Bars are standard error, dashed line are amount spiked. 293

Figure 9.73 Carbaryl internal standard recovery before freeze-drying (BFD), after freeze-drying (AFD), and filter (FIL) stage of extractions. Bars are standard error, dashed line are amount spiked. 293

Figure 9.74 Metalaxyl internal standard recovery before freeze-drying (BFD), after freeze-drying (AFD), and filter (FIL) stage of extractions. Bars are standard error, dashed line are amount spiked. 293

Figure 9.75 2,4-D internal internal standard recovery before freeze-drying (BFD), after freeze-drying (AFD), and filter (FIL) stage of extractions. Bars are standard error, dashed line are amount spiked. 294

Figure 9.76 Paclobutrazol internal standard recovery before freeze-drying (BFD), after freeze-drying (AFD), and filter (FIL) stage of extractions. Bars are standard error, dashed line are amount spiked. 294

Figure 9.77 Chlorantraniliprole internal standard recovery before freeze-drying (BFD), after freeze-drying (AFD), and filter (FIL) stage of extractions. Bars are standard error, dashed line are amount spiked. 294

Figure 9.78 Dimethomorph II internal standard recovery before freeze-drying (BFD), after freeze-drying (AFD), and filter (FIL) stage of extractions. Bars are standard error, dashed line are amount spiked. 294

Figure 9.79 Spirotetramat internal standard recovery before freeze-drying (BFD), after freeze-drying (AFD), and filter (FIL) stage of extractions. Bars are standard error, dashed line are amount spiked. 295

Figure 9.80 Dimethomorph I internal standard recovery before freeze-drying (BFD), after freeze-drying (AFD), and filter (FIL) stage of extractions. Bars are standard error, dashed line are amount spiked. 295

Figure 9.81 Fenhexamid internal standard recovery before freeze-drying (BFD), after freeze-drying (AFD), and filter (FIL) stage of extractions. Bars are standard error, dashed line are amount spiked. 295

Figure 9.82 Ethoprophos internal standard recovery before freeze-drying (BFD), after freeze-drying (AFD), and filter (FIL) stage of extractions. Bars are standard error, dashed line are amount spiked. 295

Figure 9.83 Myclobutanil internal standard recovery before freeze-drying (BFD), after freeze-drying (AFD), and filter (FIL) stage of extractions. Bars are standard error, dashed line are amount spiked. 296

Figure 9.84 Tebuconazole internal standard recovery before freeze-drying (BFD), after freeze-drying (AFD), and filter (FIL) stage of extractions. Bars are standard error, dashed line are amount spiked. 296

Figure 9.85 Azoxystrobin internal standard recovery before freeze-drying (BFD), after freeze-drying (AFD), and filter (FIL) stage of extractions. Bars are standard error, dashed line are amount spiked. 296

Figure 9.86 Fluopyram internal standard recovery before freeze-drying (BFD), after freeze-drying (AFD), and filter (FIL) stage of extractions. Bars are standard error, dashed line are amount spiked. 296

Figure 9.87 Boscalid internal standard recovery before freeze-drying (BFD), after freeze-drying (AFD), and filter (FIL) stage of extractions. Bars are standard error, dashed line are amount spiked. 297

Figure 9.88 Metolachlor internal standard recovery before freeze-drying (BFD), after freeze-drying (AFD), and filter (FIL) stage of extractions. Bars are standard error, dashed line are amount spiked. 297

Figure 9.89 Malathion internal standard recovery before freeze-drying (BFD), after freeze-drying (AFD), and filter (FIL) stage of extractions. Bars are standard error, dashed line are amount spiked. 297

Figure 9.90 Fenoxycarb internal standard recovery before freeze-drying (BFD), after freeze-drying (AFD), and filter (FIL) stage of extractions. Bars are standard error, dashed line are amount spiked. 297

Figure 9.91 Tebufenozide internal standard recovery before freeze-drying (BFD), after freeze-drying (AFD), and filter (FIL) stage of extractions. Bars are standard error, dashed line are amount spiked. 298

Figure 9.92 Friponil internal standard recovery before freeze-drying (BFD), after freeze-drying (AFD), and filter (FIL) stage of extractions. Bars are standard error, dashed line are amount spiked. 298

Figure 9.93 Tetrachlorvinphos internal standard recovery before freeze-drying (BFD), after freeze-drying (AFD), and filter (FIL) stage of extractions. Bars are standard error, dashed line are amount spiked. 298

Figure 9.94 Propiconazole internal standard recovery before freeze-drying (BFD), after freeze-drying (AFD), and filter (FIL) stage of extractions. Bars are standard error, dashed line are amount spiked. 298

Figure 9.95 Kresoxim-Methyl internal standard recovery before freeze-drying (BFD), after freeze-drying (AFD), and filter (FIL) stage of extractions. Bars are standard error, dashed line are amount spiked. 299

Figure 9.96 Diazinon internal standard recovery before freeze-drying (BFD), after freeze-drying (AFD), and filter (FIL) stage of extractions. Bars are standard error, dashed line are amount spiked. 299

Figure 9.97 Benzovindiflupyr internal standard recovery before freeze-drying (BFD), after freeze-drying (AFD), and filter (FIL) stage of extractions. Bars are standard error, dashed line are amount spiked. 299

Figure 9.98 Prallethrin internal standard recovery before freeze-drying (BFD), after freeze-drying (AFD), and filter (FIL) stage of extractions. Bars are standard error, dashed line are amount spiked. 299

Figure 9.99 Pyraclostrobin internal standard recovery before freeze-drying (BFD), after freeze-drying (AFD), and filter (FIL) stage of extractions. Bars are standard error, dashed line are amount spiked. 300

Figure 9.100 MGK 264 internal standard recovery before freeze-drying (BFD), after freeze-drying (AFD), and filter (FIL) stage of extractions. Bars are standard error, dashed line are amount spiked. 300

Figure 9.101 Allethrin internal standard recovery before freeze-drying (BFD), after freeze-drying (AFD), and filter (FIL) stage of extractions. Bars are standard error, dashed line are amount spiked. 300

Figure 9.102 Tetramethrin internal standard recovery before freeze-drying (BFD), after freeze-drying (AFD), and filter (FIL) stage of extractions. Bars are standard error, dashed line are amount spiked. 300

Figure 9.103 Spiromesifen internal standard recovery before freeze-drying (BFD), after freeze-drying (AFD), and filter (FIL) stage of extractions. Bars are standard error, dashed line are amount spiked. 301

Figure 9.104 Hexythiazox internal standard recovery before freeze-drying (BFD), after freeze-drying (AFD), and filter (FIL) stage of extractions. Bars are standard error, dashed line are amount spiked. 301

Figure 9.105 Spirodiclofen internal standard recovery before freeze-drying (BFD), after freeze-drying (AFD), and filter (FIL) stage of extractions. Bars are standard error, dashed line are amount spiked. 301

1. INTRODUCTION

1.1 Pesticide Usage and Management

Although inorganic chemicals have been used for pest control for several thousands of years, current-use pesticides are primarily synthetic organic chemicals (Patinha et al. 2018). Such pesticides have become an integral part of Prairie agricultural production systems within Canada ever since the green revolution of the 1950s because of their proven contribution to increased crop yields and labour cost reduction (Sánchez-Bayo and Wyckhuys 2018; Waschuk et al. 2021). The expansion of agriculture in the Prairie region has resulted in a large landscape conversion from natural grasslands to intensive annual cropping systems (Sánchez-Bayo and Wyckhuys 2018; Grab et al. 2019; Tscharntke et al. 2005; Samson and Knopf 1994). Due to the expansion of agricultural land and increased pesticide use, pesticides are now detected in Prairie surface waters, either in the water-column or sorbed to sediments, and, to a lesser extent, groundwaters (Carter 2000; Gamhewage et al. 2019; Munira at el. 2018). Unlike many other xenobiotics (such as personal care products and pharmaceuticals, or industrial coatings and surfactants), pesticides are directly applied over large areas of land, making them prone to distribute from applied areas into the broader environment by processes such as snowmelt, rainfall, runoff, and leaching (Munira at el. 2018; Waite et al 2005). When pesticides are released into the environment their physicochemical properties play a role in both their biological effects to target and non-target organisms and their persistence and distribution in soil and water (Gamhewage et al. 2021; van Stempvoort et al. 2014;

Limay-Rios et al. 2015). The fate of pesticides in soil can also be influenced by fertilizer and manure applications to agricultural land (Jing et al. 2017; de Wilde et al. 2009a). For example, although glyphosate is readily and strongly sorbed by soil consituents, high concentrations of phosphate fertilizers in soil can reduce glyphosate sorption (Munira and Farenhorst 2017). Another example is applications of manure or biosolids to soils that can encourage microbial communities present to convert the herbicide 2,4-D (2,4-dichlorophenoxyacetic acid) into CO_2 and other inorganic chemicals (Farenhorst et al. 2006).

Current-use pesticides account for the majority of pesticides detected in the water-column and bottom sediments of Prairie rivers; legacy pesticides continue to be detected at low concentrations as well (Gamhewage et al. 2019). Pesticide contamination in water is a result of non-point and point source pollution. Non-point source pollution refers to contamination in which pesticides are released from large areas into the broader environment by processes such as spray drift (Zhang et al. 2018), volatilization of pesticides from agricultural fields and subsequent atmospheric deposition (Waite et al. 2005), or pesticide surface runoff and leaching in agricultural fields (Larsbo et al. 2016; Rosenbom et al. 2015). Point-source pollution refers to contamination that originates from a single source that could be traced, such as pesticides being present in the release of treated wastewater in rivers by wastewater treatment plants (Ryu et al. 2022). Another example of pesticide point-source pollution is the area in which pesticides are handled to fill and clean the application sprayer (Carter 2000; Elibariki and Maguta 2017).

Following pesticide application, it is important to rinse the sprayer tank to remove pesticide residues in the tank to prevent cross-contamination and accidental crop damage when spraying subsequent crops that might be sensitive to these pesticide residues (Osbourne et al. 2015). Tank rinsing is also an integral process of crop production for maintaining pest management product

regulations and ultimately the safety of consumers because pesticides may only be applied to the crops that they are registered for (Osbourne et al. 2015); the products of the tank rinsing procedure is known colloquially as “rinsate”. Although not broadly discussed in the agricultural community or the general public, there is a lack of regulation regarding rinsate disposal (Torstensson 2000; Carter 2000). This is a concern, as the areas where the tank filling, rinsing, and cleaning occur have been shown to be significant pathways for contamination of surface and groundwater (Spliid and Köppen 1998; Helweg et al. 2002; Müller et al. 2002; Reichenberger et al. 2007).

Unlike the spraying of cropped fields, in which pesticide residues are applied at rates involving low concentrations distributed over large areas, handling areas result in pesticides ending up in relatively high concentrations with large water volumes in small areas, resulting in greater risks of pesticide mass flow into surface water (e.g., by snowmelt and rainfall runoff) and groundwater (e.g., by bulk or preferential flow) (Suleman and Keely 2019; Rosenbom 2015). Many previous efforts have focused on mitigating pesticide non-point source pollution such as through the invention and use of low-drift nozzle applicators or implementing riparian buffer zones near waterways (Aguiar et al. 2015); however, the lack of regulation and management strategies for rinsate disposal makes it of utmost importance to study additional mitigation strategies to intercept a major pesticide point-source pollution site.

1.2 Rinsate Management Using Bioreactors: Biobeds

Biobeds were invented by a Swedish farmer, Mr. Göran Olsson, to lower the concentration of pesticides in rinsate before the final disposal to fields, thereby also reducing the mass of pesticides entering surface waters and groundwaters (Carter 2000; Castillo et al 2008; Fogg et al. 2003). Biobeds are above- or in-ground containers that are filled with lignin-rich, slightly acidic, and high organic matter biomixtures. Biomixtures are created by mixing soil, humified organic matter (e.g., compost, peat), and dry plant matter (e.g., wood chips, straw) in a 1:1:2 volumetric ratio (Carter 2000), and in creating such biomixtures it is most common to utilize local resources such as local top soil and crop residues (de Wilde et al. 2009a,b; Rezende et al .2021; Fatema et al. 2022). Because biomixtures are rich in organic matter, they are ideal media to sorb and mineralize the high pesticide concentrations in the rinsate applied to the biobed, resulting in effluent with significantly reduced pesticide concentrations (Karanasios et al. 2010; de Wilde et al. 2009a). Biobeds are implemented on farms and in municipalities across Europe and Latin America but are not widely used in Canada or the United States (Torstensson 2000; de Wilde et al. 2009c,d). More than 80% of annual cropland within Canada is situated within the Prairies, therefore an important region for considering the adoption of on-farm biobeds. Most recently, several biobeds were installed in each of three Prairie provinces (Alberta, Saskatchewan, and Manitoba) in Canada; published studies have included performance evaluations (i.e., the efficacy of the biobed to turn pesticide rinsate into relatively clean water) in the provinces of Saskatchewan and Alberta at two locations each (Bergsveinsons et al. 2018; Fatema et al. 2022) and, more recently, a biobed study was initiated in the Province of Manitoba (Johnson 2024). Performance evaluations of biobeds operating under Prairie conditions provide for essential data to assess best

management practices that can potentially contribute to Canada's green economy and sustainability goals.

The performances of biobeds needs to be evaluated in the context of agricultural practices relevant to the Prairies within Canada. For example, relative to Latin America, agricultural practices in the Prairies are much more reliant on herbicides (which tend to be hydrophilic [water-loving]) rather than fungicides and insecticides (which tend to be more hydrophobic [water-repelling]) (Lewis et al. 2016; Fatema et al. 2022). The Prairies within Canada also have among the shortest growing season in the world (Morrison 2021), leaving limited time for both crop development as well as pesticide degradation within the environment. Therefore, unlike some countries in Latin America where biobeds have been readily and practically adopted with limited augmentation, Canadian settings require further research to help optimize biobed systems, including under harsh environmental conditions (e.g., extreme temperatures, short growing seasons, freeze-thaw cycles, etc.) typical in the Prairies.

1.3 Pesticide Fate Processes in Biomatrix Materials

Biobeds are designed for continuous exposure to moderate-to-high levels of pesticide residues. For example, pesticide rinsate can be applied to biobed systems at a rate equivalent to 10 to 20 L m^{-2} day^{-1} (Braul et al. 2018). This pesticide rinsate can contain total pesticide concentrations ranging from 5 to 80 mg L^{-1} (Fatema et al. 2022). As such, as per the two references, biobeds may receive pesticide mass loading ranging from 50 to 1,600 mg m^{-2}. Pesticide fate processes relevant to biomatrix materials include: (1) sorption to, and desorption from, biomatrix constituents, (2) transport of pesticides in water flowing through biomatrix, and (3) transformation

through degradation and mineralization of pesticides within biomatrix (Karanasios et al. 2010; Fogg and Boxall 2004). Sorption/desorption, transport, and transformation processes all interact with one another that determine the ability of biomatrix to efficiently dissipate pesticides, which ultimately affect the final concentrations of pesticides in biobed effluent, hence the remediation capabilities of the biobed (Rezende et al. 2021; Fogg and Boxall 2004; Fogg et al. 2003). Volatilization is not expected to be a significant pathway of pesticide dissipation in biobed systems due to the small surface area of the biobed system (Córdova-Méndez et al. 2021); photolysis is also not a major route since biobed systems usually involve roofs that reduce the irradiation of the biomixture surface by direct sunlight.

There is evidence from the existing literature that pesticide dissipation in biomatrices are influenced by the pesticides physicochemical properties as well as biomatrix composition, water management, and environmental conditions. Much of the current literature has involved laboratory studies (e.g., Coppola et al. 2007, Karanasio et al. 2010, Lescano et al. 2018) rather than field studies. As well, given that there are very limited Canadian studies (Knight et al. 2016; Cessna et al. 2017), the pesticides examined in these labaratory studies are not necessarily reflective of the wide rage of pesticide active ingredients used on the Prairies within Canada. There is also a lack of knowledge on the desorption of pesticides from biomatrices, a process that would increase the likelihood of pesticide transport through the biobed and subsequent release in effluent.

Biobeds are known to contain elevated pesticide concentrations with biomatrices being at at or near-field capacity water content. As such, it is possible that there is high desorption and leaching potential within the biomatrix, especially during days when the rinsate added is relatively clean (pesticide concentrations are low) since the cleaner rinsate would allow for the release of sorbed pesticides back into the biobed water phase, hence into effluent and environment (Fogg et

al. 2004). Like in soils and biosolids (Parker and Doxtader 1983; Schroll et al. 2006; Shymko et al. 2013; Pereira et al. 2017; Adesanya et al. 2021), the moisture content and temperature of the biomatrix has been shown to impact the pesticide fate in laboratory studies (Cessna et al 2017; Córdova-Méndez et al. 2021). Overall, there is a need for in-situ field studies on pesticide fate in biobed systems to augment the information currently available based on laboratory studies.

There are a limited number of biobeds in operation in the Prairies within Canada including two single-cell biobeds in Alberta, two dual-cell biobeds in Saskatchewan (Fatema et al. 2022) and one-dual cell biobed in Manitoba (this study; see below). It is expected that the first biobed cell in a dual-cell biobed contains pesticides at greater concentration than the second biobed cell. Currently, there is no information available for dual-cell biobeds on how the fate of pesticides in the biomatrix might differ between cells, for example because the biomatrix in the cells differ in chemical concentrations, microbial activities might also differ, and hence pesticide degradation rates.

1.4 Canadian Contexts of Biobeds Operation and Application

Since the annual cropping systems on the Prairies are predominantly herbicide based (Government of Canada 2022), many of the pesticides applied tend to be rather hydrophilic. Although many different herbicides are applied, the PMRA (2024) sales report indicates that of these herbicides, the top 10 herbicide active ingredients account for ~90% of total herbicide sales. Insecticides and fungicides utilized also account for a diverse array of active ingredients but again the top 10 active ingredients account for most of the sales (~83 and ~75% respectively) (PMRA 2024). For the four biobeds operating in Saskatchewan and Alberta, Fatema et al. (2022)

demonstrated that they were highly effective in retaining and/or degrading pesticide active ingredients, thereby reducing pesticide concentrations in effluents. However, this same study identified five herbicides (bentazon, clopyralid, diclofop, fluoxypyr, and imazethapyr) that remain in the effluent of biobed systems at concentrations greater than 50% of initial input concentrations (Fatema et al. 2022). The agricultural regions of Saskatchewan and in particular Alberta are largely classified as semi-arid and fall within the mixed- and short-grass prairie ecoregions, corresponding to a combination of Køppen climate class Dfb (humid continental) and Bsk (cold semi-arid); the agricultural region in Manitoba is primarily classified as sub-humid continental within the tall-grass prairie and boreal plains ecoregions, corresponding to Køppen Dfb only (Smith et al. 1998; Cardillo 2014). Given that environmental conditions can influence pesticide fate within biobeds (Córdova-Méndez 2021; Fatema et al. 2022), and that there are climatic differences between Saskatchewan-Alberta versus Manitoba ecoregions, there is a need for further investigations on the efficiencies of biobed systems under Manitoba conditions. Similarly, it is also true that most previous studies have been conducted in Europe and Latin America under climate conditions different from the Prairies within Canada (Spliid et al. 2006; Fogg et al 2004; Rezende et al 2021); biobeds must be optimized for Prairie environments, including the wetter regions of Manitoba. Sustainable management practices that minimize the transport of pesticides to the broader environment are recommended in prairie agriculture within Canada, e.g., for reducing the risk of non-target organisms being exposed to pesticides and their metabolites as well as lessening the potential for pesticide resistance development within pest populations (McCallum et al. 2021).

1.5 The Biobed System in Carman, Manitoba

The University of Manitoba's Ian N. Morrison Research Farm in Carman, Manitoba (MB), is the first biobed to be both established in Manitoba and was designed for research purposes (Figure 1.1). The biobed is designed to: 1) mitigate point-source pesticide pollution from the Ian N. Morrison Research Farm; 2) increase awareness of biobeds through education and outreach, and; 3) model and study the operation and management of biobeds. The Morrison Research Farm will be the focus of this research.



Figure 1.1 The Ian. N. Morrsion Research Farm two-cell biobed located in Carman, MB, showing a) the collection trough and rinsate storage tanks, and b) the roofed, dual-cell biobed filled with biomixture.

The biobed at the Carman farm is an above-ground, dual-cell biobed that is designed to process the 10,000 L of rinsate produced on-farm annually; the biobed actively treats rinsate on the farm from pest control products utilized in a variety of on-farm research projects. Both biobed

cells have the same dimensions, each having a 9.3 m^2 surface area and a depth of 0.7 m consisting of 15 to 20 cm of 10-mm diameter pea gravel at the base and 50-55 cm of biomixture above (Figure 1.2). The biomixture within the Morrison Reasearch Farm biobed cells (Figure 1.3) was developed from locally sourced materials and composed of (by volume) 25% on-farm topsoil (0-15 cm, Denham series, Orthic Black Chernozem), 50% on-farm wheat stubble, and 25% peat (Sunshine Sphagnum Peat). The biomixture was aged for 8 weeks based on guideline recommendations (Braul et al. 2018), with an excess amount of biomixture produced so that the cells could be topped up annually with fresh biomixture.

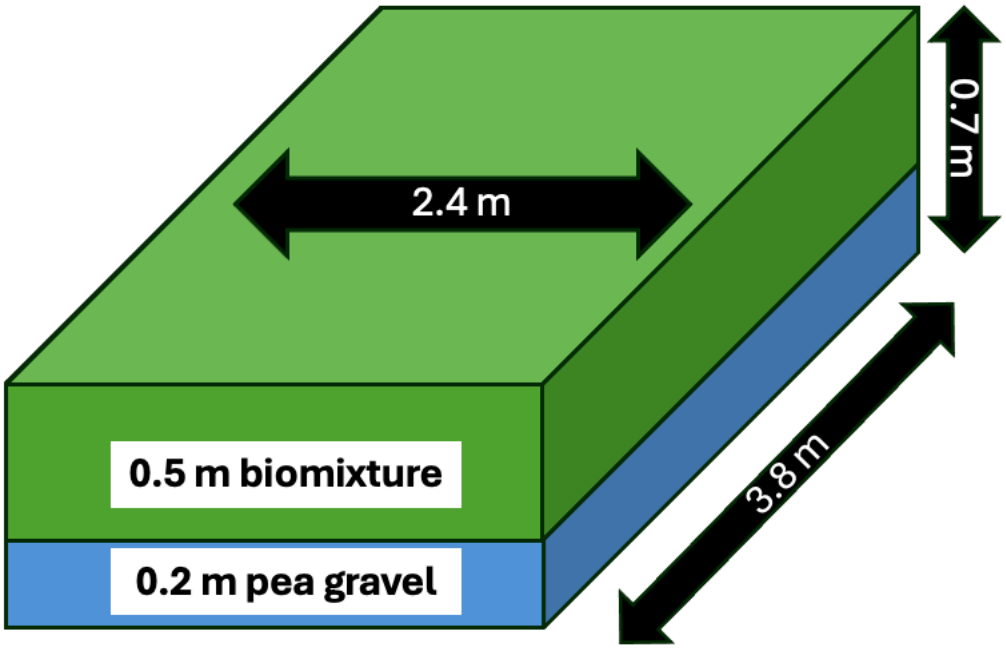

Figure 1.2 Overview of biobed cell set up with black arrows representing the dimensions of the cell and white labels indicating layer composition within the cell.



Figure 1.3 The biomixture utilized in the biobed at the Morrsion Research Farm, developed from a 1:1:2 volume ratio of soil, peat, and wheat stubble.

The Morrison Research Farm biobed was built with the intention of being able to quantitatively determine the remediation capacity of biobeds. The Morrison Research Farm biobed has five pumps that regulate the flow of the biobed installed at: 1) rinsate collection sump pump; 2) rinsate tank agitator; 3) rinsate applicator to biobed cell one; 4) biobed cell one effluent applicator to biobed cell two, and; 5) final effluent release pump (Figure 1.4). Pumps 1, 4, and 5 are controlled by float switches that, once activated, collect rinsate, apply effluents, or release effluents, respectively. Pumps 2 and 3 are powered by solar panels and are activated with a timed irrigator that recirculates or applies rinsate at set time intervals and time of day, respectively. In addition to the pumps, five flow meters were installed to model water flow and monitor: 1) incoming fresh water; 2) rinsate input; 3) biobed cell one input; 4) biobed cell two input, and; 5) final effluent release (Figure 1.5). All of the above both control the water volume applied to biobeds daily and monitor water flux within the biobed; the water was applied at a range of 10 - 20 L m^{-2} day^{-1} on cell one for optimal performance (Braul et al. 2018); in total, the Carman biobed

is able to process an estimated 16,000 L annually over 100 days of operation, more than its estimated 10,000 L production (Johnson 2024).

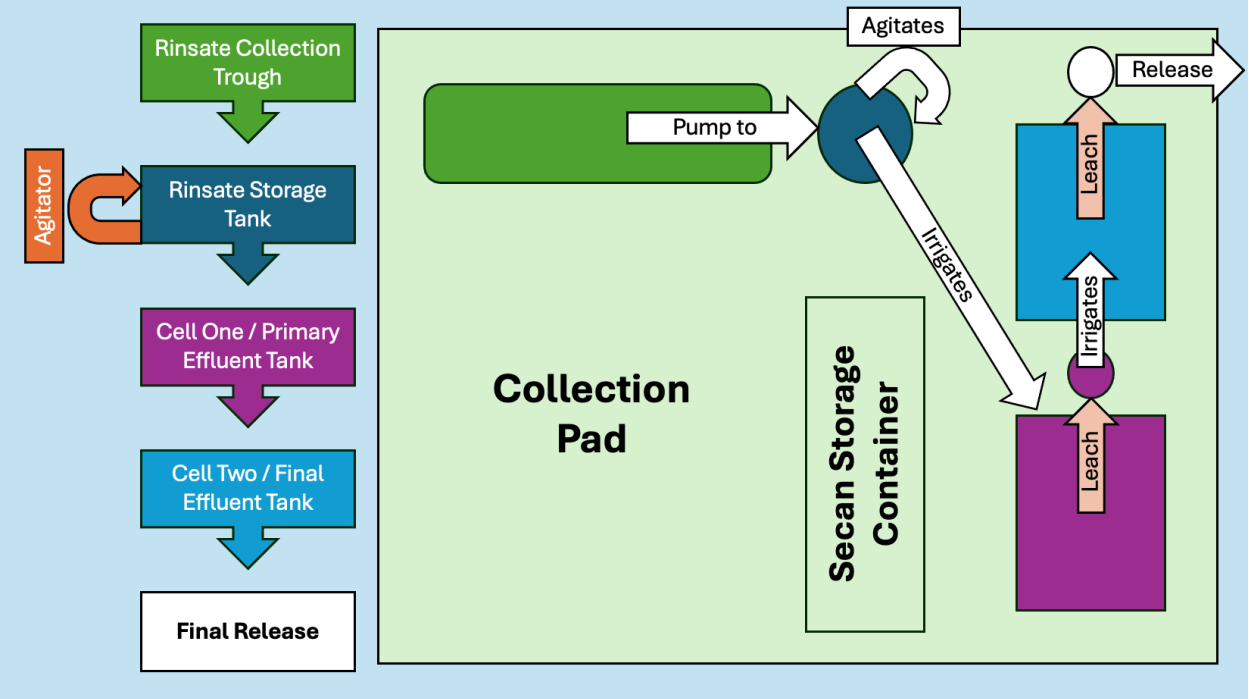

Figure 1.4 Technical diagram of the biobed layout. The left hand side represent the flow sequence and corresponds to colour on the right hand side. White arrows of the right hand side represent pump-operated flows while orange represent gravity mediated flows.

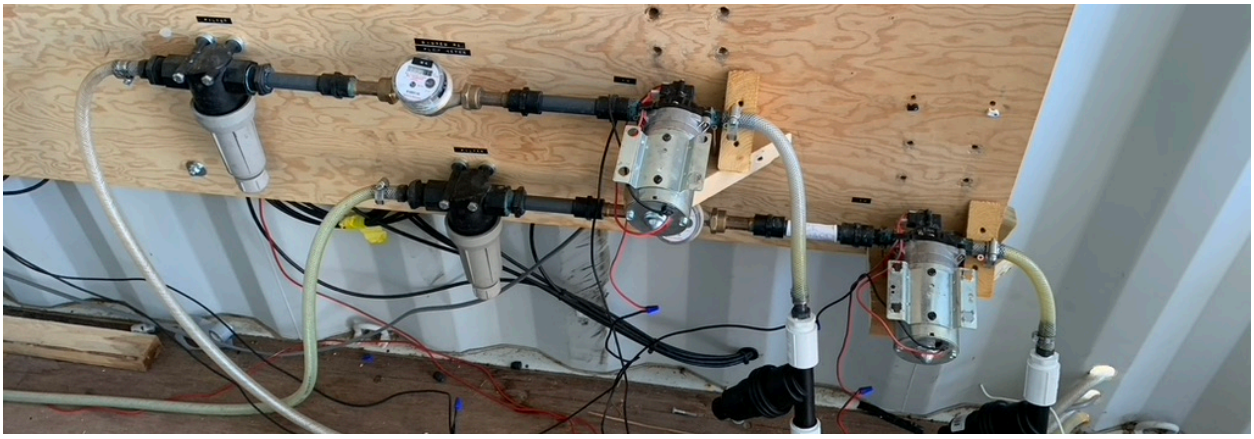

Figure 1.5 Pumps and flow meters installed at the Ian N. Morrison Research Farm biobed for biobed cell one (bottom) and biobed cell two (top).

To monitor the biobed cell conditions at the Morrison Research Farm biobed, Sentek Drill and Drop Sensors and Hydraprobes were installed. Sentek probes are cylindrical probes that were

installed in the center-left, center-middle, and center-right of each biobed cell to measure volumetric water content, volumetric ion content, and temperature at 10, 20, 30, 40, and 50 cm depth. Hydraprobes are cylindrical probes that were installed in the center-left of the biobed to measure water fraction by volume, temperature, and dielectric permittivity at 10, 25, and 40 cm depths (Johnson 2024).

The Morrison Research Farm biobed design (Figure 1.4) makes it the optimal biobed to study the fate of pesticides within biobeds due to its robust scientific design and research farm location that utilizes a broad range of pesticides. Unlike previous field studies in the prairies (Fatema et al. 2022), this study focuses on the fate processes within the biobed cell biomixtures and comparison of single or dual-cell treatment of rinsate.

1.6 Validation, UHPLC-MS/MS, and Pesticide Quantification

To determine the pesticide residue levels within the biomatrix, rinsate, and effluents from the biobed, a validated method of extraction and analysis is required to ensure that all values reported are real, accurate, and quantitative. However, there have been no Canadian studies that have applied a thoroughly validated method to assess pesticide concentrations in both the water and solid fractions of a biobed system. Validation is the process of proving the realness of a number; it is an answer to the philosophical question of *am I seeing a real number?* Quantification of any compound in the enivornment requires validation to determine the consistency, accuracy, and limits of the analytical equipment used to determine residue levels. There are many validation guidelines for different applications and analytical applications; this thesis will utilize Magnusson and Örnemark (2014) *EURACHEM* guidelines to help validate pesticide concentrations since it is

considered standard in European and North American contexts (see Table 1.1 for validation parameter descriptions and determinations). This thesis will solely focus on the application of Ultra-High Performance Liquid Chromatography – Tandem Mass Spectrometry (UHPLC-MS/MS) due to its ability to analyze herbicides.

Table 1.1 Overview of Magnusson and Örnemark's (2014) *EURACHEM* validation parameters, purpose of the parameter, and determination method used in this thesis.

Parameter	Purpose	Determination
Selectivity	Does the method target the compound(s) of interest?	Ion fragments
Working Range	What range of concentrations do responses correspond linearly?	Calibration curve range
Linearity	What is the response variation of the calibration curve?	R^2
LOD/MLD	What are the limits of the machine (LOD) or method (MLD) to determine the **presence** of a compound(s)?	Standard error * 3
LOQ/MLQ	What are the limits of the machine (LOQ) or method (MLQ) to determine the **concentration** of a compound(s)?	Standard error * 10
Accuracy	How well do the concentrations quantified represent what is present in the sample?	Percent recovery
Precision	How consistent are the quantified values from the sample over time?	Coefficient of variation
Matrix Effects	How much do the method co-extractives affect compound(s) response?	ANOVA/ ANCOVA
Internal Standard Loss	How much of the compound(s) is lost between extraction steps developed?	ANOVA/ ANCOVA

A wide variety of analytical equipment has been developed for the purpose of trace level pesticide analysis, however, the most prominent detectors are mass spectrometers (Kebarle 2000). Mass spectrometers fragment molecules to produce unique ion fragments that are passed though an orthogonal quadrupole (diagonally, two with radiofrequencies and two with direct currents) in a vacuum to filter out any non-select ions (Fenn et al. 1989; Ho et al. 2003). There are two major forms of ionization; hard ionization, which fragments molecules directly with electrons, and soft ionization, which fragments molecules through a matrix such as solvents or solids (Siuzdak 2004).

Soft ionization will be discussed further since this is the ionization technique of UHPLC-MS/MS since it utilizes volatile acids/bases and various solvents to help ionize molecules before entering the mass spectrometer via Coulombic explosion (Kebarle 2000). Although single quadrupole mass spectrometers are powerful instruments, they are frequently only able to quantify between high parts-per-billion (ppb) to parts-per-million (ppm) levels of molecules; trace levels analyses require triple quadrupoles, which adds a secondary collision cell and quadrupole, to further reduce background noise and increase fragment ions response (Rosenberg 2003; Siuzdak, 2004). Through the addition of a secondary quadrupole, measurements are able to range from parts-per-quadrillion (ppq) to ppm (through dilution) levels of pesticides. In addition to ion fragmentation of mass spectrometers, they are also able to simultaneously utilize internal standards that allow for isotope dilution, thereby decreasing measurement variability by having isotopically-labelled sister compounds at known concentrations to correct for losses and noise present in a sample vs standard, undisturbed calibration curves (Rosenberg 2003; Siuzdak, 2004).

Although mass spectrometers are incredibly powerful, issues regarding detector oversaturation cause issues since multiple trace compounds interfer with the detector sensitivity; if directly injected into a mass spectrometer, significant background noise will impact the detector's ability to quantify the compound (Rosenberg 2003; Siuzdak, 2004). Through the application of UHPLC, compounds are able to interact with columns before the mass spectrometer, thereby reducing noise by delaying the release of multiple compounds and increasing sample response by spreading out other compounds from the detector (Vogeser and Parhofer 2007; Pitt 2009). Further addition of dynamic chromatographies via differing miscible mobile phases (e.g. water with acetonitrile or methanol), compounds are able to elute from the column into mass spectrometer at known times, thereby significantly reducing noise and allowing for the

quantification of multiple compounds through dynamic multiple reaction monitoring (dMRM) (Vogeser and Parhofer 2007; Pitt 2009). Through the exploitation of the varying physicochemical properties of pesticides, this thesis will utilize UHPLC-MS/MS to determine pesticide concentrations in the Carman biobed system. Although previous research has identified that concentrations of high ppb to ppm in biobeds, a tandem mass spectrometry was utilized to mitigate matrix effects (the inherent noise of co-extractants that remains post-extraction of samples) of rinsates, effluents, and biomixtures through isotope and sample dilution.

In summary, past research on biobeds has focused on Europe and Latin America where the types of pesticides used might not necessarily directly reflect the pesticides dominating Canadian agriculture. For example, Latin America is proportionally using more insecticides and fungicides that tend to be relatively hydrophobic, whereas Canadian is proportionally using more herbicides that tend to be relatively hydrophilic (Sharma et al. 2019); however, the higher proportion of herbicides are with fewer active ingredients when compared to insecticides and fungicides (PMRA 2024). As well, although the herbicides atrazine and glyphosate are widely used in North American cropping systems, atrazine has been deregistered for use in most European Union countries due to groundwater concentrations exceeding 0.1 ug L^{-1}, whereas the use of glyphosate in agriculture is severely restricted (EFSA 2022). The Ian N. Morrison Research Farm's biobed has been developed to monitor, measure, and quantify biobed efficacy for pesticides typically applied in the Prairies of Canada. This research will monitor the pesticide concentrations in the biobed influent (rinsate), the biobed effluents from cell one and two, and whether the pesticides dissipate or remain within the biobed cells (biomixture). Understanding how pesticides behave within biomixtures is required to optimize the function of biobeds within the Canadian Prairie setting.

1.7 Research Objectives and Thesis Outline

The objectives of this M.Sc. research are to:

Chapter 2 Objectives: (1) Apply the *EURACHEM* Validation guidelines (Magnussson and Örnemark 2014) with UHPLC-MS/MS to validate a quantitative method for the analyses of glyphosate, glufosinate, and AMPA in biobed rinsate, effluent, and biomixtures to (2) determine the efficacy of an above-ground, dual-cell biobed system to determine the efficacy of a biobed system to remediate pesticide rinstate into cleaner effluent.

Chapter 3 Objective: (1) Apply the *EURACHEM* Validation guidelines (Magnussson and Örnemark 2014) with UHPLC-MS/MS to validate a quantitative method for the analyses of 84 pesticide compounds in biobed rinsate, effluent, and biomixtures to (2) determine the efficacy of an above-ground, dual-cell biobed system to determine the efficacy of a biobed system to remediate pesticide rinstate into cleaner effluent.

This thesis is organized into four major written chapters, with the first chapter as a general introduction into the topic of pesticides and biobeds. The following two chapters (2 and 3) written in a manuscript format for publication; chapters 5 and 6, 7, 8, 9, and 10 are the appendices for each research chapter, respectively (see *Foreward* for further details). Chapters two and three validate then apply a method developed on an UHPLC-MS/MS to monitor the fate of pesticide rinsate through to the final effluent within a biobed for the operation season of 2023 and the fate of those pesticides within the biomixture for 2022 and 2023. Chapter 2 focuses on the highly hydrophilic ($\log P < -2$) compounds of glyphosate, glufosinate, and AMPA while chapter 3 focuses on a broad spectrum of 84 compounds that are more hydrophobic ($\log P > -2$). Finally, chapter 4 is a synthesis chapter that discusses the final conclusions and findings of the two research chapters and reccomendations for future research work.

1.8 References

Adesanya, T., Zvomuya, F., and Farenhorst, A. 2021. Sulfamethoxazole sorption by cattail and switchgrass roots. J. Environ. Sci. Health - B Pestic. Food Contam. Agric. Wastes **55(1)**: 1021-1031.

Aguiar, T.R.Jr., Bortolozo, F.R., Hansel, F.A., Rasera, K., and Ferreira, M.T. 2015. Riparian buffer zones as pesticide filters of no-till crops. Environ. Sci. Pollut. Res. **22**: 10618-10626.

Bergsveinson, J., Perry, B. J., Sheedy, C., Braul, L., Reedyk, S., Gossen, B. D., and Yost, C. K. 2018. Identifying the core bacterial and fungal communities within four agricultural biobeds used for the treatment of pesticide rinsates. J. Appl. Microbiol. **125(5)**: 1333-1342.

Braul, L., Reedyk, S., and Sheedy, C. 2018. A robust biobed design for managing pesticide rinsate under Canadian conditions – construction, operation and maintenance manual. Agriculture and Agri- Food Canada, Regina, SK. Available from: https://publications.gc.ca/collections/collection_2018/aac-aafc/A42-123-2018-eng.pdf [Accessed 18 March 2025]

Cardillo, J. 2014. Stubble management effects on microclimate and performance of canola across different climactic regions in western Canada. Masters of Science Thesis. University of Manitoba, Winnipeg, Manitoba, Canada. Available from https://mspace.lib.umanitoba.ca/server/api/core/bitstreams/6dd8e01d-eed6-4508-8dc9-98d28dac4f64/content?authentication-token=eyJhbGciOiJIUzI1NiJ9.eyJlaWQiOiIwNjZmMGEzNS1lNWYxLTRiY2EtOTlkZS0wODEyYzZkZWJkZDAiLCJzZyI6WyIxNzVmYjI4MC1mMGM0LTQ1YjQtYWJhZi0yM2YwMTBkNzAxMTciXSwiYXV0aGVudGljYXRpb25NZXRob2QiOiJsZGFwIiwiZXhwIjoxNzQyNzg5MjU4fQ.N5EwNfYJSgBqTXJ14XfIdyD5-z75qhbmOPiMRdio6kM [Accessed 23 March 2025].

Carter, A. 2000. How pesticides get into water – and proposed reduction measures. Pestic. Outlook, **11(4)**: 149-156.

Castillo, M.D., Torstensson, L., and Stenström, J. 2008. Biobeds for environmental protection from pesticide use – a review. J. Agri. Food Chem. **56**: 6206-6219.

Cessna, A., Knight, J.K., Ngombe, D., and Wolf, T.M. 2017. Effect of temperature on the dissipation of seven herbicides in a biobed matrix. Can. J. Soil Sci. **97(4)**: 717-731.

Coppola, L., Castillo, M. D. P., Monaci, E., and Vischetti, C. 2007. Adaptation of the biobed composition for chlorpyrifos degradation to southern Europe conditions. J. Agri. Food Chem. **55(2)**: 396–401.

Córdova-Méndez, E.A., Góngora-Echeverría, V.R., González-Sánchez, A., Quintal-Franco, C., Giácoman-Vallejos, G., and Ponce-Caballero, C. 2021. Pesticide treatment in biobed systems at microcosm level under critical moisture and temperature range using an orthic solonchaks soil from southeastern Mexico amneded with corn husks as support. Sci. Total Environ. **772**: 145038.

Elibariki, R., and Maguta, M.M. 2017. Status of pesticides pollution in Tanzania – a review. Chemosphere, **178**: 154-164.

Farenhorst, A., Reimer, M., Londry, K., and Saiyed, I. 2006. 2,4-dichlorophenoxy acetic acid mineralization in amended soil. J. Environ. Sci. Health - B Pestic. Food Contam. Agric. Wastes **41**: 509–522.

Fatema, M., Farenhorst, A., and Sheedy, C. 2022. Using the pesticide toxicity index to show the potential ecosystem benefits of on-farm biobeds. J. Environ. Quality. **51(5)**: 1044-1053.

Fenn, J. B., Mann, M., Meng, C. K., Wong, S. F., and Whitehouse, C. M. 1989. Electrospray ionization for mass spectrometry of large biomolecules. Science, **246**: 64–71.

Fogg, A., Boxall, A.B.A., Walker, A., and Jukes, A.A. 2003. Pesticide degradation in a 'biobed' composting substrate. Pest Manag. Sci. **59**: 527–537.

Fogg, A., and Boxall, A.B.A. 2004. Effect of different soil textures on leaching potential and degradation of pesticides in biobeds. J. Agric. Food Chem. **52**: 5643-5652.

Fogg, P., Boxall, A., Walker, A., and Jukes, A. 2004. Leaching of pesticides from biobeds: effect of biobed depth and water loading. J. Agri. Food Chem. **52**: 6217-6227.

Gamhewage, M., Farenhorst, A., and Sheedy, C. 2019. Phenoxy herbicides' interactions with river bottom sediments. J. Soils Sediments **19**: 3620-3630.

Gamhewage, M., Sheedy, C., Munira, S., and Farenhorst, A. 2021. Pesticide mixtures in the water-column versus bottom-sediments of prairie rivers. Bull. Environ. Contam. Toxicol. **106**: 936–941.

Government of Canada. 2022. Pesticides indicator. Available from https://agriculture.canada.ca/en/agricultural-production/water/pesticides-indicator [Accessed 13 Feb 2023].

Grab, H., Branstetter, M.G., Amon, N., Urban-Mead, K.R., Park, M.G., Gibbs, J., Blitzer, E.J., Poveda, K., Loeb, G., and Danforth, B.N. 2019. Agriculturally dominated landscapes reduce bee phylogenetic diversity and pollination services. Science, **363(6424)**: 282- 284.

Helweg, A., Bay, H., Hansen, H.P.B., Rabølle, M., Sonnenborg, A., and Stenvang, L. 2002. Pollution at and below-sites used for mixing and loading of pesticides. Intern. J. Environ. Anal. Chem. **82(8-9)**: 583-590.

Ho, C. S., Lam, C. W. K., Chan, M. H. M., Cheung, R. C. K., Law, L. K., Lit, L. C. W., Ng, K.F., Suen, M.W.M., and Tai, H.L. 2003. Electrospray ionisation mass spectrometry: principles and clinical applications. Clin Biochem Rev. **24**: 3–12.

Jing, X., Yao, G., Liu, D., Liang, Y., Luo, M., Zhou, Z., and Wang, P. 2017. Effects of wastewater irrigation and sewage sludge application on soil residues of chiral fungicide benalaxyl. Environ. Pollut., **224**: 1-6.

Johnson, S. 2024. Management of agricultural pesticide rinsate using a biobed under Manitoba conditions. MSc. Thesis, University of Manitoba, Winnipeg, Canada. Available from https://mspace.lib.umanitoba.ca/server/api/core/bitstreams/05b7f34e-0fb0-4cb9-8c12-1057271e8d95/content [Accessed 18 March 2025].

Karanasios, E., Tsiropoulos, N.G., Karpouzas, D.G., and Ehaliotis, C. 2010. Degradation and adsorption of pesticides in compost-based biomisxtures as potential substrates for biobeds in southern Europe. J. Agric. Food Chem. **58**: 9147-9156.

Kebarle, P. 2000. A brief overview of the present status of the mechanisms involved in electrospray mass spectrometry. J. Mass Spectrom. **35**: 804–817.

Knight, J.D., Cessna, A.J., Ngombe, D., and Wolfe, T.M. 2016. Mineralisation and degradation of 2,4-dichlorophenoxyacetic acid dimethylamine salt in a biobed matrix and in topsoil. Pest Manag. Sci. **72**: 1965–1976.

Larsbo, M., Sandin, M., Jarvis, N., Etana, A., and Kreuger, J. 2016. Surface runoff of pesticides from a clay loam field in Sweden. J. Environ. Qual. **45**: 1367-1374.

Lescano, M.R., Pizzul, L., Castillo, M.d.P., and Zalazar, C.S. 2018. Glyphosate and aminomethylphosphonic acid degradation in biomixtures based on alfalfa straw, wheat stubble, and river waste. J. Environ. Manag. **228**: 451-457.

Lewis, K.A., J. Tzilivakis, D.J. Warner, and A. Green. 2016. An international database for pesticide risk assessments and management. Human Ecol. Risk Assess. **22**:1050–1064.

Limay-Rios, V., Forero, L.G., Xue, Y., Smith, J., Baute, T., and Schaafsma, A. 2015. Neonicotinoid insecticide residues in soil dust and associated parent soil in fields with a history of seed treatment use on crops in southwestern Ontario. Environ. Toxicol. Chem. **35(2)**: 303-310.

Magnusson, B., and Örnemark, U. 2014. EURACHEM guide: the fitness for purpose of analytical methods – a laboratory guide to method validation and related topics, (2nd ed.). ISBN 978-91-87461-59-0. Available from www.eurachem.org [Accessed 15 Nov 2024].

McCallum, B.D., Geddes, C.M., Chatterton, S., Peng, G., Carisse, O., Turkington, T.K., Olfert, O., Leeson, J., Sharpe, S., Stephens, E., Hervet, V., Aboukhaddour, R. and Vankosky, M. 2021. We stand on guard for thee: a brief history of pest surveillance on the Canadian prairies. Crop Prot. **149**: 105748.

Morrison, C. 2021. Cover cropping on the prairies. The Canadian Agri-Food Policy Institute. Available from https://capi-icpa.ca/explore/resources/cover-cropping-on-the-prairies/ (Accessed 20 Oct. 2022).

Müller, K., Bach, M., Hartmann, H., Spiteller, M., and Fredem, H-G. 2002. Point- and nonpoint-source pesticide contamination in the Zwester-Ohm catchment, Germany. J. Environ. Qual. **31**: 309-318

Munira, S., and Farenhorst, A. 2017. Sorption and desorption of glyphosate, MCPA and tetracycline and their mixtures in soil as influenced by phosphate. J. Environ. Sci. Health B Pestic. Food Contam. Agric. Wastes **52(12)**: 887 – 895.

Munira, S., Farenhorst, A., Saptoka, K., Nilsson, D., and Sheedy., C. 2018. Auxin herbicides and pesticide mixtures in groundwater of a Canadian prairie province. J. Environ. Qual., **47**: 1462-1467.

Osbourne, P.P., Xu, Z., Swanson, K.D., Walker, T., and Farmer, D.K. 2015. Dicamba and 2,4-D residues following applicator cleanout: a potential point source to the environment and worker exposure. J. Air Waste Manag. Assoc., **65(9)**: 1153-1158.

Parker, L.W. and Doxtader, K.G.. 1983. Kinetics of microbial degradation of 2,4-D in soil: effects of temperature and moisture. J. Environ. Qual. **12(4)**: 553-558.

Patinha, C., Durães, N., Claudia Dias, A., Pato, P., Fonseca, R., Janerio, A., Barriga, F., Paula Reis, A., Duarte, A., de Silva, E.F., Sousa, A.J., and Cachada, A. 2018. Long-term application of the organic and inorganic pesticides in vineyards: environmental record of past use. Appl. Geochem. **88(B)**: 226-238.

Pereira, F.G., Amarakoon, I.D., Zvomuya, F., and Jeke, N.N. 2017. Kinetics and thermodynamics of phosphorus sorption on goethites: effects of biochar application. Can. J. Soil Sci. **0**: 1–8.

Pest Management Regulatory Agency (PMRA). 2024. Pest control products sales report for 2022. Available from https://publications.gc.ca/collections/collection_2025/sc-hc/H111-3-2022-eng.pdf [Accessed 9 June 2025]

Pitt J.J. 2009. Principles and applications of liquid chromatography-mass spectrometry in clinical biochemistry. Clin Biochem Rev. **30(1)**: 19–34.

Reichenberger, S., Bach, M., Skitschak, A. and Frede, H-G. 2007. Mitigation strategies to reduce pesticide inputs into ground- and surface water and their effectiveness: a review. Sci. Total Environ. **384**: 1-35

Rezende, S., Cesio, M.V., Acrhondo, L., Russi, C., Martínez, P., Rivero, A., Hladki, R., Heinzen, H., and Besil, N. 2021. Pilot study of biobeds application for the remediation of citrus agro-industrial wastewaters. Int. J. Environ. Anal. Chem., **103(20)**: 9698-9714.

Rosenberg E. 2003. The potential of organic (electrospray- and atmospheric pressure chemical ionisation) mass spectrometric techniques coupled to liquid-phase separation for speciation analysis. J. Chromatogr. A **1000**:841–89.

Rosenbom, A.E., Olsen, P., Plauborg, F., Grant, R., Juhler, R.K., Brüschm W., and Kjær, J. 2015. Pesticide leaching through sandy and loamy fields – long-term lessons learnt from the Danish pesticide leaching assessment programme. Environ. Pollut. **201**: 75-90.

Ryu, H-D., Han, H., Park, J-H, and Kim, Y.S. 2022. New insights into the occurance and removal of 36 pesticides in pesticide wastewater treatment plants in Korea. Chemosphere, **309**: 136717.

Samson, F., and Knopf, F. 1994. Prairie conservation in north america. BioScience **44(6)**: 418-421.

Sánchez- Bayo, F., and Wyckhuys, K.A.G. 2018. Worldwide decline of the entomofauna: a review of its drivers. Biol. Conserv. **232**: 8-27.

Schroll, R., Becher, H.H., Dörfler, U., Gayler, S., Grundmann, S., Hartmann, H.P., and Ruoss, J. 2006. Quantifying the effect of soil moisture on the aerobic microbial mineralization of selected pesticides in different soils. Environ. Sci. Technol. **40**: 3306-3312.

Sharma, A., Kumar, V., Shahzad, B., Tanveer, M., Singh Sidhu, G.P., Handa, N., Kohli, S.K., Yadav, P., Bali, A.S., Parihaur, R.D., Dar, O.I., Singh, K., Jasrotia, S., Bakshi, P., Ramakrishnan, M., Kumar, S., Bhardwak, R., and Thurkal, A.K. 2019. Worldwide pesticide usage and its impacts on ecosystem. SN Appl. Sci. **1**:1446.

Shymko, J., Farenhorst, A., and Francis, Z. 2011. Polynomial response of 2,4-D mineralization to temperature in soils at varying soil moisture contents, slope positions, and depths. J. Environ. Sci. Health. **46(4)**: 301-312.

Siuzdak G. 2004. An Introduction to Mass Spectrometry Ionization: An Excerpt from The Expanding Role of Mass Spectrometry in Biotechnology, 2nd ed.; MCC Press: San Diego, 2005. J. Lab. Autom. **9(2):** 50-63.

Smith, R.E., Veldhuis, H., Mills, G.F., Eilers, R.G., Fraser, W.R., and Lelyk, G.W. 2001. Terrestrial ecozones, ecoregions, and ecodistricts of Manitoba – an ecological stratification of Manitoba's natural landscapes. Research Branch Technical Bulletion 1998-9E. Available from https://www.thinktrees.org/wp-content/uploads/2019/07/Manitobas-Eco-Regions.pdf [Accessed 14 Nov. 2022].

Spliid, P., and Køppen, B. 1998. Occurrence of pesticides in Danish shallow ground water. Chemosphere **37(7)**: 1307-1316.

Spliid, N.H., Helweg, A., and Heinrichson, K. 2006. Leaching and degradation of 21 pesticides in a full-scale model biobed. Chemosphere, **65**: 2223-2232.

van Stempvoort, D.R., Roy, J.W., Brown, S.J., and Bickerton, G. 2014. Residues of the herbicide glyphosate in riparian groundwater in urban catchments. Chemosphere **95**: 455-463.

Suleman, M., and Keely, B.J. 2019. Laboratory simulation studies of leaching of the priority and their transformation products in soils. J. Anim. Plant Sci. **29(4)**: 1112-1126.

Torstensson, L. 2000. Experiences of biobeds in practical use in Sweden. Pestic. Outlook, **11(5)**: 206-211.

Tscharntke, T., Klein, A.M., Kruess, A., Steffan-Dewenter, I., and Thies, C. 2005. Landscape perspectives on agricultural intensification and biodiversity – ecosystem service management. Ecol. Lett., **8(8)**: 857-874.

Vogeser, M., and Parhofer, K.G. 2007. Liquid chromatography tandem-mass spectrometry (LC-MS/MS)-technique and applications in endocrinology. Exp. Clin. Endocrinol. Diabetes **115(9)**: 59-70.

Waschuk, N., Hanson, M., and Prosser, R. 2021. Yield to the data: some perspective on crop productivity and pesticides. Pest. Manag. Sci. **78(5)**: 1765-1771.

de Wilde,T., Spanoghe, P., Ryckeboer, J., Jaekan, P, and Springael, D. 2009a. Sorption Characteristics of pesticides on matrix substances used in biopurification systems. Chemosphere **75**: 100-108.

de Wilde, T., Mertens, J., Šimůnek, J., Sniegowski, K., Ryckeboer, J., Jaeken, P., Springael, D., and Spanoghe, P. 2009b. Characterizing pesticide sorption and degradation in microscale biopurification systems using column displacement experiments. Environ. Pollu. **157**: 463-473.

de Wilde, T., Spanoghe, P., Mertens, J., Sniegowski, K., Ryckeboer, J., Jaeken, P., and Springael, D. 2009c. Characterizing pesticide sorption and degradation in macro scale biopurification systems using column displacement experiments. Environ. Pollu. **157**: 1373-1381.

de Wilde, T., Spanoghe, P., Ryckeboer, J., Jaeken, P. and and Springael, D. 2009d. Sorption characteristics of pesticides on matrix substrates used in biopurification systems. Chemosphere **75**: 100–108.

Zhang, X., Luo, Y., and Goh, K.S. 2018. Modeling spray drift and runoff-related inputs of pesticides to receiving water. Environ. Pollut. **234**: 48-58.

2. ANALYTICAL METHOD FOR TESTING BIOBED SYSTEM EFFICACY: QUANTIFYING GLUFOSINATE, GLYPHOSATE AND AMPA IN RINSATE, EFFLUENT, AND BIOMATRIX SAMPLES

2.1 Abstract

Glyphosate (N-(phosphonomethyl)glycine) and glufosinate (2-amino-4-(hydroxymethylphosphinyl)butanoic acid) are among the most commonly used herbicides in the world. Biobed systems to manage pesticide rinsate have been proposed to reduce the risk of water contamination by current-use pesticides. This study validated a rapid analytical method to simultaneously analyze for glyphosate and glufosinate in biobed samples, while also analyzing for AMPA (2-Amino-3-(3-hydroxy-5-methyl-isoxazol-4-yl) propanoic acid) which is glyphosate's primary and environmentally persistent metabolite. The method was applied to rinsate, effluent, and biomixture samples from an on-farm, dual-cell biobed under a humid continental climate (Köppen climate classification Dfb) to examine the contribution of each cell in recycling glufosinate and glyphosate rinsate into cleaner water. Glyphosate had the largest mean concentration in the rinsate (193 mg L^{-1}) and was often quantified (78%) in primary effluent but only quantified once (11%) in the final effluent (0.0028 mg L^{-1}). On average, the mean glufosinate concentration was reduced by 86% in primary effluent from cell one and then by a total of 99% in the final effluent from cell two, again showing the important contribution of a second biobed cell for improving the dissipation of both aminophosphate herbicides in biobed systems. Transformation of glyphosate to AMPA was rapid, and AMPA was detected 77% of final effluent samples at a mean concentration of 0.046 mg L^{-1}; this was statistically significantly less from the

mean AMPA concentrations in rinsate (2.0 mg L^{-1}) = primary effluent (1.0 mg L^{-1}). The mean AMPA concentration in the biomixture (187 mg kg^{-1}) was much larger than the mean concentrations of glyphosate (5.9 mg kg^{-1}) or glufosinate (7.0 mg kg^{-1}). This study demonstrates the important contribution of the second cell in enhancing the dissipation of glufosinate and glyphosate in biobed systems. As well, our findings underscore the need to include primary metabolites in biobed efficacy trials, and that additional innovations might be required for dealing with persistent metabolites in biobed systems.

2.2 Introduction

Glufosinate ((*DL*-)2-amino-4-(hydroxymethylphosphinyl)butanoic acid) and glyphosate (N-(phosphonomethyl)glycine) were registered for use in North America around the mid-70s and mid-90s, respectively. Due to the expansion of herbicide-tolerant cropping systems, glyphosate is now the top herbicide sold in North America as well as globally (Benbrook 2016; Klingelhöfer et al. 2021). Current-use of glufosinate is expected to rise globally for the increasing need to control glyphosate-resistance weeds in soil-landscapes (Takano and Dayan 2020).

Canola (*Brassica napus* L.) is grown throughout the Northern Great Plains of the Americas (Johnston et al. 2002). Since the mid-2000s, almost all the canola grown in this region consisted of glyphosate-tolerant varieties followed by glufosinate- and imidazolinone-tolerant varieties (Wilson 2012; Chasto et al. 2024). Several thousand water and sediment samples taken between 2001-2010 in 38 USA states showed that glyphosate was frequently detected in streams and rivers and almost always (97.7%) in combination with its primary metabolite AMPA (2-amino-3-(3-hydroxy-5-methyl-isoxazol-4-yl)propanoic acid) (Battaglin et al. 2014). Thus, despite the

relatively short soil half-life of glyphosate in soil (Table 2.1), its non-labile fraction has been shown to persist for several years (Padilla and Salim 2020). In contrast, AMPA is more environmentally persistent (Table 2.1) and a study across Canada in 2007 also frequently detected both glyphosate and AMPA in surface waters (Glozier et al. 2012). The environmental persistence of glufosinate is short, with soil-half lives less than five days due to rapid mineralization (conversion to CO_2) (Zhang et al 1990); however, it is occasionally detected in Praire waters (Glozier et al. 2012; Brown and Farenhorst 2023).

Table 2.1 2D chemical structures and physico-chemical properties of herbicide glyphosate and its primary metabolite AMPA, as well as the herbicide glufosinate.

Compounds	Glyphosate	AMPA	Glufosinate
Molecule	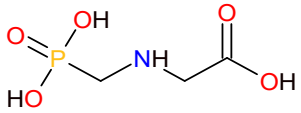	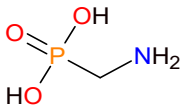	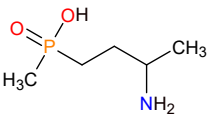
Water solubility (mg L^{-1})	100,000 [a]	1,470,000 [a]	500,000 [b]
Log P[e]	-6.28 [a]	-1.63 [a]	-4.01 [b]
pKa[f]	0.78, 2.6, 5.6, 10.6 [c]	1.8, 5.4, 10.2 [c]	2.0, 2.9, 9.8 [d]
K_{oc}[g] (mL g^{-1})	1400 [a]	2000 [a]	600 [b]
Half-life soil (days)	17.3 [a]	114 [a]	7.4 [b]
Half-life sediment (days)	20.8 [a]	132 [a]	24.5 [b]
Half-life water (days)	9.9 [a]	5.5 [a]	7.2 [b]

[a]Lewis et al. (2016); [b]Lewis et al. (2016), for *glufosinate-ammonium*; [c] Trinh and Schäfer (2024), and; [d]Takano and Dayan (2020). [e]Log P = Octanol- water partitioning coefficient; [f]pKa = acid dissociation constant; [g]K_{oc} = organic carbon-water partitioning coefficient.

Glufosinate and glyphosate are broad-spectrum, non-selective herbicides, hence, the triple-rinsing of the tank post-spray to remove remaining residues is particularly important for preventing cross-contamination and accidental damage when spraying subsequent, non-resistant crops (Osbourne et al. 2015). As well, tank rinsing is an integral process of ensuring consumer safety since pesticides may only be applied to the crops that they are registered for (Osbourne et al. 2015); this remaining rinse material produced is colloquially known as *rinsate*. The use of biobeds for the recycling of rinsate water can be seen as a best management practice in the same way as the

recycling of pesticide containers are industry recommendations (Braul et al. 2018). Specifically, using biobeds can strongly reduce point-source pollution by lessening total pesticide loadings in water bodies.

Few biobed studies have evaluated glyphosate dissipation and no studies have been reported for glufosinate. For a study in a temperate oceanic climate (Köppen climate classification Cfb), Spliid et al. (2006) constructed a single cell biobed and twice applied a batch of 21 pesticides in two, 1.25 m^2 areas on the biobed surface; this study reported no detectable ($<1.0X10^{-5}$ mg/L) glyphosate and AMPA concentrations in (vertical) leachate, limiting further analyses. In contrast, Fatema et al. (2022) detected glyphosate in the effluent of a single cell biobed that had a surface area of 8 m^2 and operated under a humid continental climate (Köppen climate classification Dfb). Córdova-Méndez et al. (2021) constructed miniature biobeds (~ 100 cm^3) and exposed them to different temperatures and moisture conditions to study the dissipation of several pesticides, including glyphosate which dissipated the fastest (half-life ~ 2.3 days). In another controlled incubation study, Lescano et al. (2018) also concluded that glyphosate dissipated quickly in biomatrix material (7.5 – 22 days), but that AMPA was formed and persisted until the end of the two-month experiment.

Glufosinate (Log P = -4.01), glyphosate (-6.28), and AMPA (-1.63) have low octanol-water partitioning coefficients (Lewis et al. 2016; Takano and Dayan 2020) and are hence challenging to extract from matrices with organic solvents. In fact, glyphosate remains among the most difficult agrochemicals to quantify due to its low volatility, requiring molecule derivatization in analyses by gas chromatography (Valle et al. 2019). Glyphosate and AMPA's typical quantification method involves molecule derivatization using 9-fluorenylmethylchloroformate (FMOC-Cl) followed by quantification with either tandem mass spectrometry or fluorescence spectrometry (Glass 1983;

Miles et al. 1985; Ibañez et al. 2005; Todorovic et al. 2013; Marin et al. 2020; Alonso et al. 2022); however, this poses challenges for rinsate samples that often resemble cloudy or milky looking solutions because of the presence of formulation adjuvants. Although many other analytical methods have been developed for glyphosate, AMPA, and glufosinate, few methods analyze for all three compounds such as in a recently developed direct-inject method (i.e., only syringe filtration) that required no derivatization (Brown and Farenhorst 2024). This rapid method has been applied to municipal tap water and surface water samples and, with appropriate dilutions, might be adaptable to biobed samples that can contain glyphosate concentrations that are more than 20,000-fold greater (as demonstrated by Fatema et al. (2022)) than the levels observed in water samples collected in Brown and Farenhorst (2024). Previous studies quantifying glyphosate and AMPA in soils have reported signficant matrix effects (Botero-Coy et al. 2013; de Gerónimo et al. 2018); in some studies, dilution has been shown to successfully reduce matrix interferences for a wide range of pesticides (Ferrer et al. 2011), including glyphosate and AMPA (de Gerónimo et al. 2018).

The two objectives of this study were to 1) develop and validate an analytical technique to simultaneously analyze without derivatization for glyphosate, AMPA and glufosinate in biobed samples, and 2) assess the efficacy of an above-ground dual cell biobed for removing glufosinate and glyphosate from rinsate under humid continental climate (Dfb).

2.3 Material and Methods

2.3.1 Chemicals

Aminomethanephosphonic acid (AMPA; lot#: 7-JTN-125-1), glufosinate (lot#: 59-GHZ-182-1), glyphosate (lot#: 1-AFB-72-1), AMPA-^{13}C,^{15}N (lot#: 4-GMG-129-1), glufosinate-d_3 • HCl (lot#: 8-NZZ-176-4), and glyphosate-$^{13}C_2$,^{15}N (lot#: 14-JUZ-144-2) were purchased from Toronto Research Chemicals (Toronto, ON, Canada). Potassium hydroxide (lot#: 225063), 37% hydrochloric acid (lot#: 222041), Optima™ grade water (lot#: 235186), Optima™ grade methanol (lot#: 223213), isopropanol (lot# 214580), glacial acetic acid (lot#: 213861), and formic acid (lot#: 232523) were purchased from Fisher Scientific (Ottawa, ON, Canada). InfinityLab™ deactivator (lot#: 0006598114) was purchased from Agilent Technologies (Santa Clara, CA, USA).

2.3.2 Description of the Dual-Cell Biobed System.

An above-ground, dual-cell biobed was constructed to process a predicted 10,000 L of pesticide rinsate produced by annual spraying operations at the Ian N. Morrison Research Farm in Carman, MB, Canada (Johnson 2024). The biobed system consists of a collection trough and rinsate holding tank (Figure 2.1a) and two biobed cells with their effluent tanks (Figure 2.1b); primary effluent refers to effluent from cell one while final effluent refers to effluent from cell two. Each biobed cell is filled with 4.65 m^3 of biomixture (9.3 m^2 surface area, 0.5 m deep, bulk density of 1.07 g cm^{-3}, measured in 2022) that was prepared following the recommendations of Braul et al. (2018); the biomixture was placed ontop of 0.15-0.20 cm of 10 mm pea gravel. The biomixture

is a mixture in a 2:1:1 volumetric ratio of peat (Sunshine® Sphagnum Peat Moss, Homestead Co-op in Carman, MB, Canada), a sandy-loam soil (Ap-horizon, Denham series, Orthic Black Chernozem [Mills and Haluschuk 1993]) and chopped wheat straw (3 to 7 cm in size). Soil and straw were obtained on- farm, which is a common approach to develop biomixtures (de Wilde et al. 2009; Rezende et al .2021; Fatema et al. 2022). Biomixture characteristics (measured in 2020) were an organic carbon content of 2.82%; pH of 5.96; cation exchange capacity of 179.5 meq kg^{-1}; electrical conductivity of 115.2 µS cm^{-1}; macro nutrient concentrations of 21.8 (N), 26.0 (P), 382.5 (K) and 27.5 (S) mg kg^{-1}, and; micro nutrient concentrations of 0.7 (B), 3.6 (Zn), 164.9 (Fe), 12.6 (Mn), and 0.9 (Cu) mg kg^{-1}.

Installed over each biobed cell are irrigation pipes with drip emitters (Figure 2.1c, d), allowing for the timed application of rinsate and effluent across the surface of cell one and two, respectively. Such applications are facilitated by a series of pumps and tanks, the latter also being equipped with valves to serve as sampling stations. Rinsate, effluent from cell one (primary effluent), and effluent from cell two (final effluent) are collected at these three sampling stations in the biobed. Prior to any pesticide rinsate applications, over a time span of about one-month, sufficient water was run through the biobed system (about 2,000 liters) to generate effluent from cell two. The water added induced favourable moisture conditions in the biomixtures for supporting microbial populations prior to the commencement of biobed operations. The source of the water was a municipal water line that is used on the farm for preparing all tank mixtures and for rinsing spraying tanks. Free chlorine concentrations ranges from 0.10 mg/L to 0.13 mg/L, which is consistent with the guideline range for free chlorine in Canadian potable water distribution systems (Health Canada 2009). The biobed was built in 2020 with some delays caused by the COVID-19 pandemic (i.e., laboratory closures, disruption of the supply chain); it became

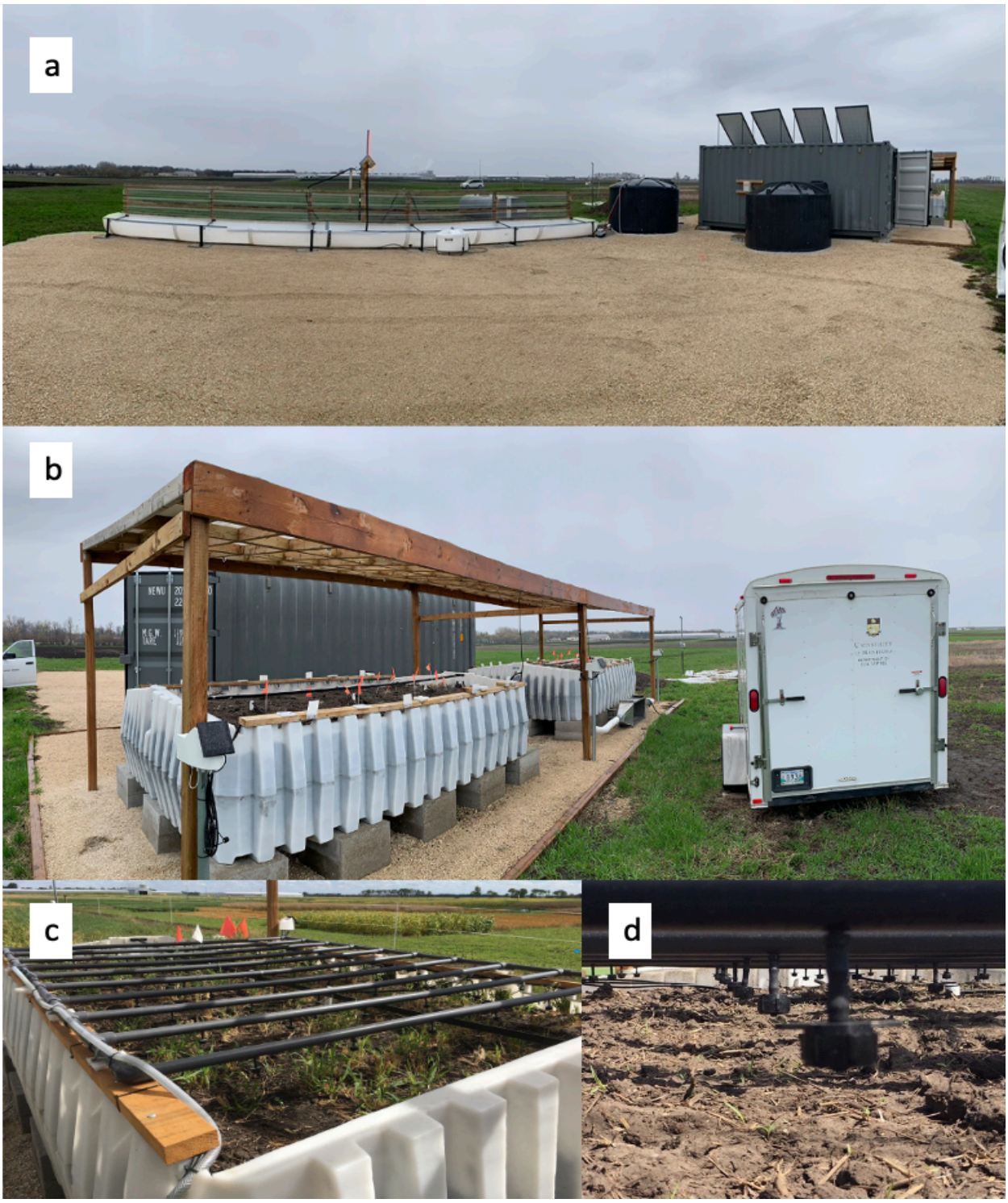

Figure 2.1 Visual overview photos of the biobed system in Carman, MB,with a) rinsate collection area (white trough – bending is an optical illusion due to panoramic photo) with a black, 1,000 L rinsate storage vessel, b) biobed cells that processes rinsate (foreground cell) and primary effluent (background cell), c) close-up of cell two with the drip-emitter manifold that irrigates the cell, and d) close-up of drip emitters that applies of rinsate (cell one) or effluent (cell two) onto biomatrix surfaces.

operational with the first pesticide rinsate being applied by drip irrigation on August 25, 2020 (Johnson 2024). The biobed system was winterized on September 28, 2020, and reopened between early June to early October 2021 (Johnson 2024) which is the time-period during which pesticides are typically applied on the farm. The current study commenced in 2022 with method development and biomatrix sampling, followed by all other biobed sampling and analyses in 2023.

2.3.3 Analytical Method Validation.

The EURACHEM validation guidelines (Magnusson and Örnemark 2014) were followed to determine method accuracy, precision (intra- and inter-day), method detection and quantification limits, and matrix effects (details in Chapter 5.1 for calculations and process). Due to consistent glyphosate, AMPA and glufosinate detections within samples obtained from the biobed system, the rinsate and effluent validation experiments utilized artificially created solutions as described below. As well, the biomixture validation experiments utilized biomixture that was obtained from the centre of an on-site storage pile that is used to top-up the biobed cells annually. The biomixture in the storage pile is identical in composition as the biomixture in the biobed cells but had never received pesticide rinsate. No glufosinate or glyphosate was detected in this biomixture, but AMPA was detected at low levels ($<1.0 \times 10^{-6}$ mg g^{-1}); this is most likely because it had been present in the sandy-loam soil (0-15 cm) that was a component used in preparing the biomixture (see above). Therefore, for AMPA in biomixture only, blank-corrected validation was conducted with a separate calculation recommended by EURACHEM (Chapter 5.1, equation 5-4). The biomatrix was air-dried and sieved (2 mm) prior to use in the validation experiments. The artificial rinsate solution was prepared using the on-farm water supply and mixing two herbicide products, Dual II Magnum® (915 g L^{-1} metolachlor) and AAtrex® Liquid 480 (480 g L^{-1} atrazine)

with the insecticide product Decis® 50 EC (50 g L^{-1} deltamethrin) to yield a concentration of 500 mg L^{-1} metolachlor plus 500 mg L^{-1} atrazine plus 50 mg L^{-1} deltamethrin. These pest control products are commonly used on the farm and in corn cropping systems throughout the Northern Great Plains of the Americas. The artificial effluent solution was prepared by mixing the biomixture (300 g) from the storage pile with on-farm water (3 L) and shaking vigorously (5 min) before allowing solids to settle for 48 h at room temperature. Subsequently, the artificial effluent solution was filtered through a 2 µm Whatman® 45 mm glass filter paper to remove significant suspended particles. The artificial effluent solution showed no detectable concentrations of glyphosate, AMPA and glyphosate.

2.3.4 Collection and Extraction of Rinsate, Effluent and Biomatrix Samples.

Rinsate and effluent samples were collected biweekly from June 20th until October 10th, 2023, using 50-mL Falcon® (lot#: 10922042) centrifuge tubes. Samples were processed within two days of collection and kept in coolers during transportation and in a laboratory fridge when not being handled. Field blanks included and opened during each collection showed no detections. A method adapted from Brown and Farenhorst (2024) was used to quantify glufosinate, glyphosate and AMPA concentrations by Ultra-High Performance Liquid Chromatography-Tandem Mass Spectrometry (UHPLC-MS-MS) as described below. This direct-inject method was developed for environmental samples such as surface waters with analytes being in the ng L^{-1} range. As such, in the current study, rinsate and effluent samples were diluted 10, 100, 1,000, and 10,000 (rinsate only) fold prior to quantifications by UHPLC -MS-MS. Diluted rinsate and effluent samples were vortexed for 30 seconds and a 980 µL aliquot was spiked with 20 µL of an internal standard

solution containing glufosinate-d_3, AMPA-^{13}C,^{15}N, and glyphosate-$^{13}C_2$,^{15}N for a final concentration of 20 ng mL^{-1} per internal standard. Samples were then syringe filtered (3 mL polypropylene (PP) plastic syringes, lot#:21L04C0, with 0.22 µm white polytetrafluoroethylene (PTFE) filters, lot#: 310098157, from Thermo Fisher Scientific) into 2-mL screw vials (lot#: 436022305V3) and capped with 9 mm bonded blue PTFE screw cap with red silicone septas (lot#: 299471) from Agilent Technologies. For each analyte, when two dilutions were within the calibration curve and both showed good peaks on the chromatograms, the more concentrated dilution was chosen (i.e., 10-fold over 100-fold dilution).

Biomixture samples were collected before (pre) and after (post) the growing season (i.e., "*time variable*") in both years 2022 and 2023 (i.e., "*year variable*"). Samples were collected at 0-5, 5-15, and 15-30 cm from the surface (i.e., "*depth variable*") from three marked locations of both biobed cells one and two (i.e., "*cell variable*"). All samples were collected with a tulip planter and inserted into amber, polypropylene bags (VWR® brand Re-closable UV-Protectant Amber Bags (lot#: 89005-324), VWR International, Mississauga, Canada), then transported in coolers to the laboratory and immediately frozen (-20° C) to prevent further glufosinate, glyphosate or AMPA degradation. Prior to extractions, samples were freeze-dried for 24 hours in a FreeZone Benchtop Freeze-Dryer at 1.000 mbar with a -20° C sample temperature and -80° C collection vessel temperature.

The biomixture extraction method was adapted from Ibañez et al. (2005). Briefly, subsamples (4.0 g) of the freeze-dried biomatrix were weighed into 50 mL Falcon® tubes to which 10 mL of 0.1 M KOH in deionized (DI) water was added. Biomixture slurries were rotated for 120 min at 40 revolutions per minutes (rpm) then centrifuged at 10,000 rpm at 20° C for 10 min (IEC CL31R Multispeed Centrifuge, Thermo Fisher Scientific, Ottawa, Canada). Biomixture slurry

aliquots (3 mL) were added to 15 mL Falcon® centrifuge tubes (lot#: 25423012) with 0.1 M HCl and 1% acetic acid in DI water (3 mL). These aliquots (6 mL) were then vortexed for 30 sec then centrifuged at 3,750 rpm at 4° C for 15 minutes (Sorvall Legend RT Centrifuge). 1,960 µL of samples were spiked with 40 µL of internal standard solutions and passed through a 60 mg, 3 cc HLB SPE Cartridge (lot#: 016732020A) from Waters Corporation® (Milford, USA), that were pre-equilibrated with 3 mL methanol then 3 mL DI water; eluents were collected in 15 mL Falcon® centrifuge tubes. Finally, 1 mL of eluents were syringe filtered through 0.22 µm PTFE filters and PP syringes directly into PP vials for quantification. Samples were diluted 10, 100 and 1,000-fold with the internal standard concentration set at 20 ng mL^{-1}.

2.3.5 Separations and Quantifications by UHPLC-MS-MS

For separations, an Agilent 1260 UHPLC Infinity Pump plus multi-sampler with a InfinityLab Agilent Poroshell 120 CS-C_{18} column (2.1 mm x 150 mm x 2.7 µm dp) attached to a InfinityLab Agilent Poroshell 120 CS-C_{18} guard column (2.1 mm x 5 mm x 2.7 µm dp). Column temperature was maintained at 42º C while flow rate was set at 0.35 mL min^{-1}. Mobile phases were DI water with 0.1% FA and 0.1% InfinityLab Deactivator (A) and Methanol with 0.1% FA and 0.1% InfinityLab Deactivator (B). Pump conditions were as follows: 0.1% B from 0.00 to 1.50 min; ramp up to 20% B until 2.00 min; ramp up to 40% B until 3.00 min; hold at 40% B until 3.50 min; ramp down to 0.1% B until 4.00 min; finally, re-equilibration at 0.1% B until 15.00 min. At the end of each batch, a column flush of 15 min 100% B then 30 min 0.1% B was conducted for column maintenance; retention times (Rt) are listed Table 5.1.

Quantitation was conducted with a 6470 Triple Quadrupole coupled to the UHPLC system using dynamic multiple reaction monitoring (dMRM) in both positive and negative mode; specific fragments and associated parameters are found in Table 5.1. As with Brown and Farenhorst (2024), mass spectrometer conditions are desolvation and drying gas flow rate was 11 L min^{-1} with a temperature of 220 º C, a sheath gas flow rate of 11 L min^{-1} and temperature of 300 º C; desolvation, drying, and sheath gases were ≥99.5% nitrogen.. Capillary voltages were +3000 and -3500 V while nebulizer voltage were +1500 and -800 V for positive and negative mode, respectively, while nebulizer pressure was 30 psi. Mass spectrometer one and two were both set to 100º C while ultrapure nitrogen (99.9999%) was used as the collision gas at 16.8 L min^{-1}.

2.3.6 Statistical Analyses

Calculations for accuracy, precision, and detection and quantification limits were conducted in Excel® version 16.78. Statistical analyses were conducted in R version 4.3.2 *Eye Holes* (R Core Team 2023, Vienna, Austria). A total of twelve samples showed detections below method limit of quantification (i.e., <MLQ). For the purpose of the Analyses of Variance (ANOVAs), the R package *censlm* (Regression by Maximum Likelihood Estimation for Left-Censored Data) (Martilla 2023) was used to randomly assign an analyte concentration to these samples with the value ranging from greater than zero and less than the respective MLQ. This was done for ten samples for glyphosate (two in primary effluent, eight in final effluent) and two samples for AMPA (final effluent only) on log_{10}-transformed values to estimate non-quantifiable values; R seed was set at *10*.

For each analyte (glyphosate, AMPA or glufosinate), Welch's ANOVA for Heterogenous Variance was applied using the base R code to test for significant differences in concentrations (log_{10}-transformed for normality) between rinsate, primary effluent, and final effluent samples; subsequent pairwise comparisons were performed using the Games-Howell Post-Hoc Test for Heterogenous Variance. Only log_{10}-transformed glufosinate in the final effluent violated the normality assumption; since ANOVA's are robust to mild normality violations ($p > 0.01$), analysis proceeded. In addition, each analyte (glyphosate, AMPA or glufosinate) had a four-way repeated measures ANOVA (RM ANOVA) applied to the biomatrix data with *cell* and *year* as the between-subject factors as well as *depth* and *time* as the within-subject factors using the package *rstatix* (Pipe-Friendly Framework for Basic Statistical Tests) (Kassambara 2023b). Biomixture values were log_{10}-transformed and run through the Shapiro-Wilk Test for Normality, Levene's Test for Heterogeneity, and Mauchly's Test for Sphericity to test RM ANOVA assumptions; log_{10}-transformations were required for homogeneity of variance and normality of data. Only two violations of normality were detected (Table 5.10) in log_{10}-transformed glufosinate ($W = 0.75$) and AMPA ($W = 0.76$), however, boxplots visually demonstrated normality as well as the robustness of ANOVA to normality violations, the analysis proceeded. RM ANOVA results always showed significant interactions, so the interactions with the greatest number of factors were followed-up with Benjamini-Hochberg Post-Hoc Test for pairwise comparisons.

For validation studies that used the artificially created rinsate, artificially created effluent, and the stock-piled biomixture, matrix effects were tested for each analyte separately using a one-way ANOVA using base R code and tested for both normality (Shapiro-Wilk Test) and homogeneity of variance (Bartlett's Test); log_{10}-transformed AMPA for undiluted biomixture and glufosinate for 100-fold diluted biomixture were non-normal, but was proceeded due to the

aforementioned ANOVA robustness. Matrix effect pairwise comparisons were compared by Dunnet's Post Hoc Test to test differences between the control (deionized solutions) and treatments (matrix extracts). The internal standard losses were also evaluated through a one-way ANOVA, comparing concentrations extracted to spiking stage (before freeze-drying, after freeze-drying, and post-SPE spikes) using base R code; if significant, pairwise comparisons were done using the Tukey's Post-Hoc Test to compare differences between all freeze-drying stages. No violations of assumptions were detected with internal standard losses.

In the above analyses, the R environment was organized and labelled using *DescTools* (Tools for Descriptive Statistics) (Signorell et al. 2017) and *dplyr* (Grammar of Data Manipulation) (Wickham et al. 2023). In addition, plots were created using *ggplot2* (Wickham 2016) and were adjusted with *ggbreak* (Xu et al. 2021), *ggpubr* (Kassambara 2023a), and *plotrix* (Lemon 2006).

2.4 Results and Discussion

2.4.1 Analytical Method Validation

Overall, considering EURACHEM validation criteria (Magnusson and Örnemark 2014), the method developed was appropriate for monitoring the efficacy of the dual-cell biobed (discussed below). The calibration curves of all three compounds had linearity $R^2 > 0.98$ and a working range of 1×10^{-4} to 0.4 mg L^{-1}, providing excellent responses for quantitation (Table 2.2). Chromatograms are shown in Figures 5.1, 5.2, and 5.3 while mass spectrometric and chromatographic parameters are shown in Table 5.1. Mean accuracy measurements for glyphosate,

AMPA and glufosinate ranged from 118% to 133% for rinsate and from 116% to 132% for effluent, with glufosinate being the only compound with recoveries slightly above the 70% to 130% recovery range recommended by EURACHEM (Table 2.2). Intra- and interday precision for rinsate and effluent measurements were all below 10% (Table 2.2), indicating excellent consistency of the method. For biomixtures, mean accuracy measurements showed a recovery between 94 to 120% recoveries for all three compounds, with intra- and inter-day performances showing coefficients of variation < 6%; These results indicate excellent method performance for biomixture extractions, particularly for glufosinate (Table 2.2).

AMPA was not measurable at 0.1 mg kg^{-1} in biomixture since it was below the method quantification limits (Table 2.2). MLDs/MLQs numerically decreased from biomixture > rinsate > effluent (Table 2.2). Both rinsate and biomixture MLDs/MLQs were greater than the LODs/LOQs, as expected. For effluent, MLDs/MLQs were smaller that the LODs/LOQs for AMPA and glufosinate. MLDs/MLQs (artificially created effluent) and LOD/LOQs (DI water with 0.1% FA) had the same recovery (75%) for AMPA, the mean recovery for glufosinate was numerically greater for MLDs/MLQs (110%) than LOD/LOQs (100%) (Table 2.3). Interestingly, for both AMPA and glufosinate, the standard error of the mean is greater for LOD/LOQs than MLDs/MLQs, indicating effluent reduced AMPA and glufosinate response variance, thereby quantification (Table 2.3). Glyphosate recoveries were higher than AMPA and glufosinate for both effluent (240%) and DI water (240%), standard errors and quantification limits did not follow the same trend with LOQs lower than MLQs.

Glyphosate ($F_{5,25}$ = 0.432, P = 0.822) did not show significant matrix effects for rinsate and effluent (Figure 2.2; Table 5.2, 5.3). Matrix effects were significant for both glufosinate ($F_{5,25}$ = 60.2, P < 0.001) and AMPA ($F_{5,25}$ = 6.07, P < 0.001) (Figure 2.2; Table 5.2). When contrasted

with the control, the pairwise comparison showed significant decreased responses for glufosinate in the 10-fold diluted rinsate. Effluent contrasts were only significant for AMPA in the undiluted and 10-fold diluted effluent, with no effect on glufosinate. Without a 10-fold dilution, matrix effects prevented of glyphosate, AMPA and glufosinate quantitation in rinsate; quantifications were not acceptable since peaks were supressed and right-tailed.

For biomixture, matrix effects were significant for glyphosate ($F_{4,20}$ = 7.902, p < 0.001), glufosinate ($F_{4,20}$ = 60.2, p < 0.001), and AMPA ($F_{4,20}$ = 366, p < 0.001) (Figure 2.2; Table 5.4, 5.5). Other studies have reported on matrix effects when quantifying glyphosate and AMPA, particularly for soils with large organic carbon contents (Botero-Coy et al. 2013; de Gerónimo et al. 2018). Dilution has been shown to successfully reduce matrix interferences for a wide range of pesticides (Ferrer et al. 2011), including glyphosate and AMPA (de Gerónimo et al. 2018). In our study, relative to the control (deionized water with 0.1% FA), Dunnett's Test revealed that AMPA had significantly decreased responses in undiluted, 10-fold and 100-fold dilutions but not in the 1,000-fold dilution (Figure 2.2; Table 5.3). For both glyphosate and glufosinate, all dilutions had similar responses to the control except the undiluted extracts, which showed a significantly decreased response. Similar to rinsate, the quantification of AMPA in biomixture required an initial 10-fold dilution to ensure good chromatograms and peaks.

Internal standard losses (Figure 2.3; Table 5.6, 5.7) throughout the biomixture extractions were not significant for glyphosate ($F_{2,12}$ = 0.502, p = 0.618) but were significant for AMPA ($F_{2,12}$ = 8.236, p = 0.005) and glufosinate ($F_{2,12}$ = 34.58, p < 0.001). Regardless of the significance, all spiking stages remained above the 70% accuracy threshold, indicating minimal-to-no method significance. For both AMPA and glufosinate, Tukey's HSD tests showed significant differences between the post-SPE spike versus the spiking before freeze-drying = the spiking after freeze-

drying (Figure 2.3; Table 5.6, 5.7) Interestingly, glufosinate quantification performed better with later spiking stages, indicating that spiking post-SPE had more accurate recoveries for glufosinate.

2.4.2 Biobed Efficacy: Rinsate versus Effluent

Rinsate samples that were diluted 10 -fold often visually showed the best peaks and were the dilution used to quantify glufosinate in 55% of the nine rinsate samples. Rinsate samples that were diluted 1,000-fold for 55% of samples and 10-fold for 89% of samples showed the best peaks for glyphosate and AMPA, respectively. Primary effluent samples that were diluted 10-fold (78% of samples) were most often the best peaks for glufosinate, while samples that were undiluted and 10-fold dilution showed the best peaks for glyphosate (89% of samples) and AMPA (55% of samples), respectively. Finally, undiluted samples for glufosinate, glyphosate, and AMPA (100% of samples) showed the best peaks for secondary effluent. Glufosinate was quantified at all sampling times, while AMPA and glyphosate were only consistently quantified in rinsate.

Glufosinate concentrations in rinsate ranged from 0.31 to 31 mg L^{-1} (Figure 2.4) and significantly decreased from rinsate (mean = 6.4 mg L^{-1}) > primary effluent (mean = 0.89 mg L^{-1}) > final effluent (mean = 0.086 mg L^{-1}) ($F_{2,15.7}$ = 13.2, p = 0.00043; Table 5.8). Glufosinate concentrations in primary effluent ranged from 0.036 to 3.9 mg L^{-1} and in final effluent from 0.0014 to 0.28 mg L^{-1}. Relative to rinsate, the mean glufosinate concentration was first reduced by 86% in primary effluent and then 99% in secondary effluent (Figure 2.4). These results indicate that the second cell played an important role in enhancing glufosinate dissipation, however, all effluent samples contained quantifiable concentrations of glufosinate (>7.6×10^{-4} mg L^{-1}).

Table 2.2 Linearity (R^2), working range (WR), limits of detection (LOD) and limits of quantification (LOQ), method limits of detection (MLD) and method limits of quantification (MLQ), accuracy [as percent recovery (% Rec)], and intra- and interday (Intra/Inter) precision [as percent coefficient of variation (% CV)] for AMPA, glufosinate, and glyphosate for biobed effluent, rinsate, and biomixture. *NQ* = not quantifiable.

Validation Parameter		AMPA	Glufosinate	Glyphosate
Instrument (mg L^{-1})				
R^2		0.9863	0.9992	0.9993
WR		$1.0 \times 10^{-4} – 4.0 \times 10^{-1}$		
LOD		2.2×10^{-5}	3.2×10^{-6}	2.2×10^{-6}
LOQ		7.5×10^{-5}	1.1×10^{-5}	7.3×10^{-6}
Effluent (mg L^{-1})				
MLD		1.3×10^{-5}	2.2×10^{-6}	3.3×10^{-6}
MLQ		4.2×10^{-5}	7.5×10^{-6}	1.1×10^{-5}
Accuracy (% Rec)	**0.02**	125	130	116
	0.2	122	132	118
Intra/Inter (% CV)	**0.02**	4.2 / 8.6	5.8 / 8.8	5.6 / 11
	0.2	6.8 / 8.1	6.5 / 6.9	7.7 / 8.3
Rinsate (mg L^{-1})				
MLD		1.4×10^{-4}	2.3×10^{-5}	1.5×10^{-4}
MLQ		4.6×10^{-4}	7.6×10^{-5}	5.1×10^{-4}
Accuracy (% Rec)	**0.2**	120	133	118
	2	123	132	118
	20	120	132	118
Intra/Inter (% CV)	**0.2**	6.5 / 3	6.4 / 5.7	7.0 / 7.0
	2	7.2 / 6.4	9.0 / 6.0	9.2 / 8.7
	20	7.6 / 4.8	7.2 / 6.1	7.1 / 8.2
Biomixture (mg kg^{-1})				
MLD		7.3×10^{-2}	5.5×10^{-3}	8.3×10^{-3}
MLQ		1.2×10^{-1}	9.1×10^{-3}	1.4×10^{-2}
Accuracy (% Rec)	**0.1**	*NQ*	99	110
	1	100	94	100
	10	120	100	120
	100	100	95	110
Intra/Inter (% CV)	**0.1**	*NQ*	2.7 / 3.3	3.1 / 5.5
	1	5.5 / 6	1.8 / 2.5	1.4 / 1.5
	10	3 / 3.2	3.0 / 3.9	2.7 / 2.4
	100	5.6 / 5.7	1.2 / 1.9	3.7 / 5.5

Table 2.3 Comparison of instrument and effluent mean of replicates, standard error of the mean, and limits of quantifications (ng mL^{-1}) for AMPA, glufosinate, and glyphosate across ten replicates samples used to determine quantification limits.

Compound	Matrix	Mean of Replicates	Standard Error of the Mean	Limits of Quantification
AMPA	Instrument	1.0	0.0075	0.075
	Effluent	1.1	0.0042	0.042
Glufosinate	Instrument	0.75	0.0011	0.011
	Effluent	0.75	0.00075	0.0075
Glyphosate	Instrument	2.4	0.00073	0.0073
	Effluent	2.4	0.0011	0.011

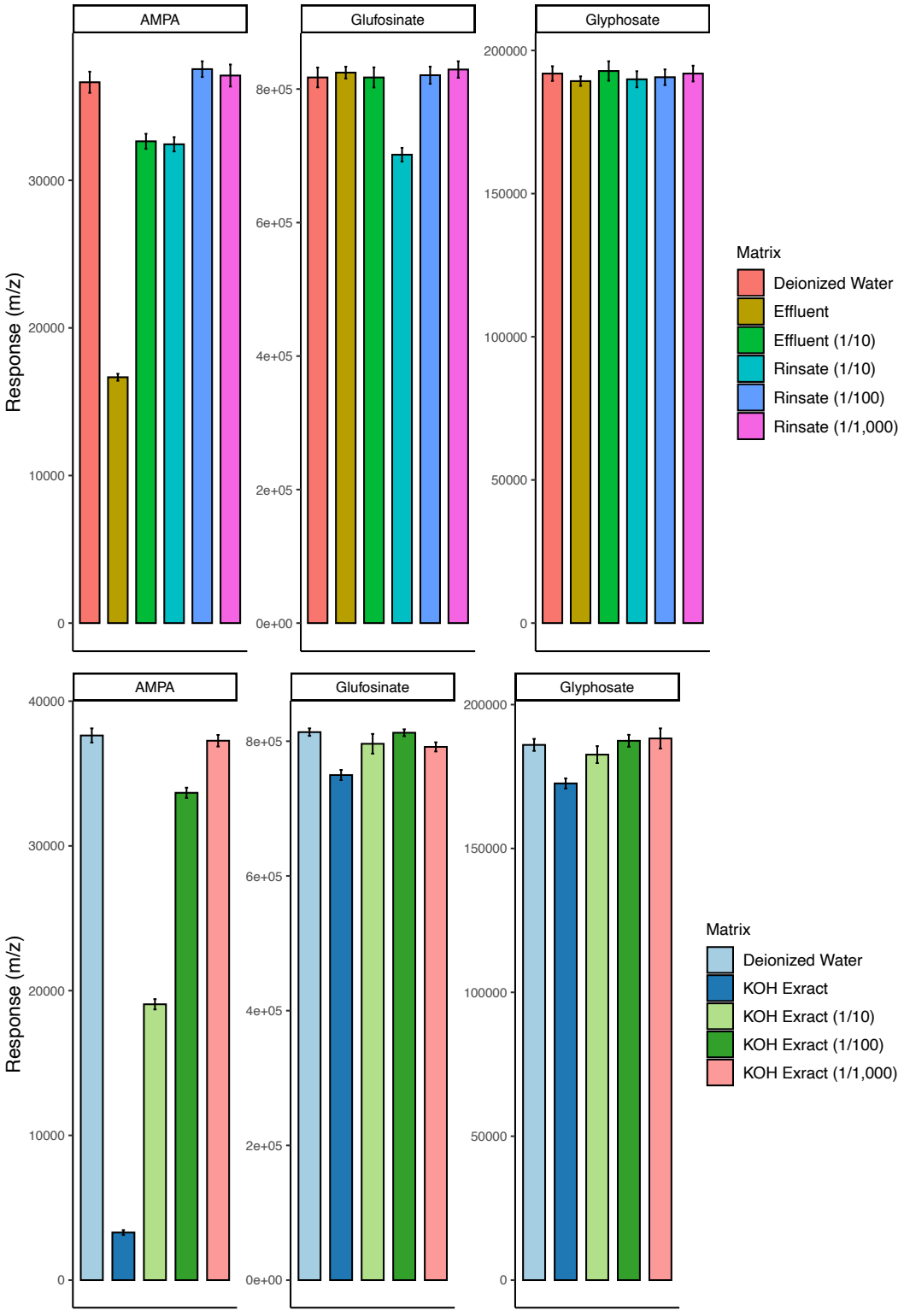

Figure 2.2 Matrix effects on compound responses (*m/z* units) in rinsate and effluent (top) and biomixture fractions (bottom) for AMPA, glufosinate, and glyphosate at 100 ng mL^{-1} in-vial. Error bars represent standard error; note y-axis for each facet are different scales. Paranthesis indicate dilution level.

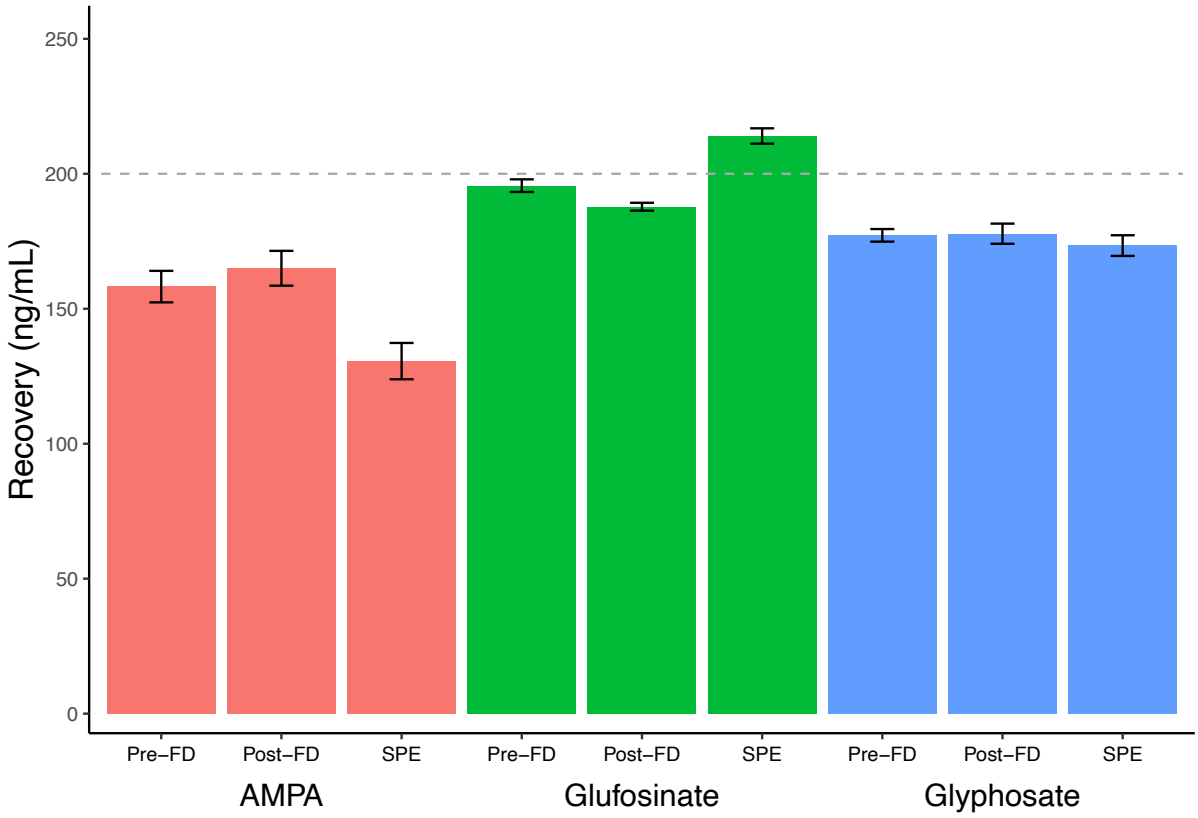

Figure 2.3 Recoveries from internal standard spikes before freeze-drying (Pre-FD), after freeze-drying (Post-FD), and final solid-phase extraction clean-up (SPE) steps for AMPA (red), glufosinate (green), and glyphosate (blue). Dotted line represents the in-vial spiked concentration of 200 ng mL^{-1}.

Glufosinate has low toxicity to aquatic organisms and all detected concentrations including in rinsate were below acute exposure scenarios for formulated glufosinate-ammonium with ErC_{50} = 80 mg L^{-1} for *Raphidocelis subcapitata* (Korshikov) Nygaard, Komárek, Kristiansen, Skulberg, EC_{50} > 100 mg L^{1} *Daphnia magna* Straus 1820, and LC50 = 100 mg L^{-1} for *Oncorhynchus mykiss* (Walbaum,1792) (EFSA 2005). However, chronic toxicity values were exceeded in rinsate (ErC_{50} = 8.9 mg L^{-1} *R. subcapitata*, EC50 = 2.7 mg L^{-1} *D. magna*, and LC50 = 1.9 mg L^{-1} *O. mykiss*) but were lower than the final effluent, indicating importance of dual cell biobeds in reducing glufosinate toxicity (EFSA 2005). The glufosinate concentration in the final effluent were always greater than the generic drinking water quality guidelines ($1x10^{-4}$ mg L^{1}) set for individual

pesticides by the European Union. When compared to the Health Canada's aquatic life reference values (ALRV), final effluent glufosinate concentrations only exceed values for non-vascular (0.072 mg L^{-1}) and vascular plants (1.5 mg L^{-1}), indicating possible risk for aquatic plants (PMRA 2024).

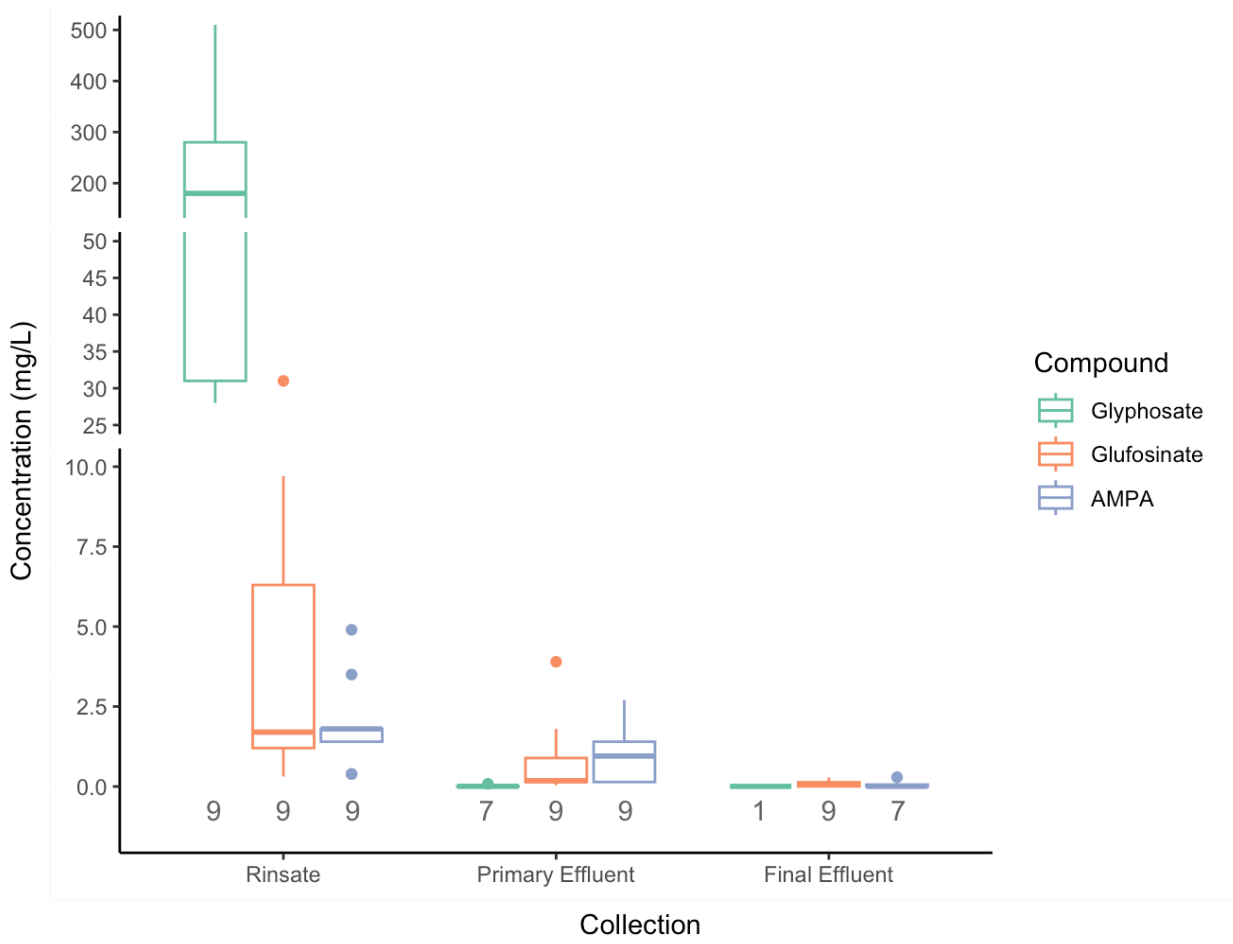

Figure 2.4 Water concentrations of glyphosate, glufosinate, and AMPA within the collection areas of rinsate, primary effluent, and final effluent for the 2023 growing season. Values below boxplots represent number of samples >MLQ.

Glyphosate had much greater concentration in rinsate than glufosinate but was only detected once in the final effluent at a concentration of 0.0028 mg L^{-1} (Figure 2.4). Glyphosate concentrations in rinsate ranged from 140 to 510 mg L^{-1} and significantly decreased from rinsate

(mean = 193 mg L^{-1}) > primary effluent (mean = 0.012 mg L^{-1} [1]) > final effluent (mean = 3.1 x 10^{-4} mg L^{-1} [2]) ($F_{2,11.8}$ = 88.4, p = <0.0001; Table 5.8). One-fifth of the primary effluent samples did not contain quantifiable levels of glyphosate (>1.1×10^{-5} mg L^{-1}) with quantifiable values in other samples ranging from 0.0028 to 0.084 mg L^{-1} (Figure 2.4). Both primary and final effluent concentrations for glyphosate are below the Canadian Water Quality Guidelines for the Protection of Aquatic Life, including for long-term exposure (0.8 mg L^{1}) (CCME 2012). Effluent concentrations are also lower than the range of acute toxicities (LC50 96-h) reported for glyphosate in studies that focused on species of fish (~ 0.3 to 645 mg L^{1}), amphibians (~ 6.5 to 115 mg L^{1}), and invertebrates (~ 35 to 462 mg L^{1}) (Tresnakova et al. 2021).

AMPA was also detected in the rinsate and hence was applied onto the biobed surface by drip irrigation (Figure 2.1, 2.4); this suggests that glyphosate is transformed to AMPA while in the application tanks during spraying or when it was present in the rinsate storage tank at the biobed. Summaries of studies pertaining glyphosate (CCME 2012) indicate that AMPA is the main transformation product of glyphosate in water under both anaerobic and aerobic conditions, with other transformation product accounting for < 1% of total glyphosate; this process occurs through biodegradation rather than hydrolysis. All rinsate samples contained quantifiable levels of AMPA with concentrations ranging from 0.39 to 4.9 mg L^{-1} (Figure 2.4). AMPA was detected in 100% and 78% of the primary and final effluent samples, respectively. ANOVA analyses of AMPA ($F_{2,14.1}$ = 18.0, p = 0.00013; Table 5.8) showed significantly larger AMPA concentrations in rinsate (mean 2.0 mg L^{-1}) = primary effluent samples (mean 1.0 mg L^{-1}) > final effluent samples mean 0.046 mg L^{-1} [3]). Concentrations in primary effluent ranged from 0.11 to 2.7 mg L^{-1} and, omitting

[1] Calculated with seven quantified and two MLE estimated values due to no response (<MLQ).
[2] Calculated with one quantified and eight MLE estimated values due to no response (<MLQ).
[3] Calculated with seven quantified and two MLE estimated values due to no response (<MLQ).

two values <MLQ (< 4.2×10^{-5}), in the final effluent from 0.0020 to 0.29 mg L^{-1}, demonstrating that AMPA was transformed or mineralized in biobed cell one and two.

2.4.3 Analyte Persistence in Biobed Cell One and Two

For glyphosate concentrations in biomatrix, the interactions *cell*depth*time* ($F_{2,16}$ = 6.537, p = 0.008) and *cell*year*depth* ($F_{2,16}$ = 5.564, p = 0.015) were significant (Figure 2.5; Table 5.9, 5.10, 5.11, and 5.12). *Cell*depth*time* pairwise comparisons found minimal differences among depths and between sampling time within cells, particularly in cell two. However, across depths and sampling times, the biomatrix of cell two often showed significantly less glyphosate concentrations relative to biomatrix of cell one (Table 5.13). A clear exception was the 0-5 cm layer in cell one that also had relatively small glyphosate concentrations due to the yearly top-up (Figure 2.5). Similarly, *cell*year*depth* pairwise comparisons also showed few significant differences among depths and between sampling years within cells. As well, across all depths and in both sampling years, the biomatrix of cell two almost always showed significantly less glyphosate concentrations relative to the biomatrix of cell one (Table 5.14).

At the start (pre-operation) of the 2023 growing season, cell one showed mean glyphosate concentrations of 16 mg kg^{-1} in the 5-15 cm layer and 5.4 mg kg^{-1} in the 15-30 cm layer (the 0-5 cm layer showed mean glyphosate concentration of 0.63 mg kg^{-1} due to the top-up). The relatively greater glyphosate concentrations at deeper depths in cell one would have been glyphosate residues that remained in the biobed from applications in 2022. Glyphosate concentrations in cell two were always ≤ 2.5 mg kg^{-1}, regardless of sampling year or depth, suggesting that majority of glyphosate was retained in the biomatrix of cell one. The post-growing season sampling event in 2022 showed

substantial glyphosate concentrations in the 0-5 cm (34 mg kg^{-1}), 5-15 cm (8.8 mg kg^{-1}) and 15-30 cm (25 mg kg^{-1}) layers of cell one. Glyphosate concentrations in the 0-5 cm layer were largest because the last documented application of glyphosate in 2022 was on September 30th and the biomixture sampling was done on October 1st. The post-growing season sampling event in 2023 showed that the mean glyphosate concentrations in cell one were 1.1 mg kg^{-1}, 1.4 mg kg^{-1}, and 0.71 mg kg^{-1} in 0-5, 5-15 and 15-30 cm, respectively; hence, in addition to being retained, glyphosate was also degraded in cell one. The last application of glyphosate in 2023 was on October 3rd while the biomixture sampling was done on October 10th, 2023. As such, glyphosate degradation in the biomixture might be relatively fast. A rapid glyphosate degradation within biomatrices has been reported in controlled-laboratory studies (Spliid et al. 2006; Góngora-Echeverría et al. 2017; Góngora-Echeverría et al. 2018; Lescano et al. 2018; ; Góngora-Echeverría et al. 2019; Lescano et al. 2020; Córdova-Méndez et al. 2021). Previous studies on soils showed that glyphosate degradation was optimal when relatively large moisture conditions prevail (e.g., -15 kPa water tension) (Schroll et al. 2006; Kah et al. 2007; Nguyen et al. 2018), and such conditions occur in the biobed with the biomatrix being near water holding capacity with little moisture variations over time (Johnson 2024).

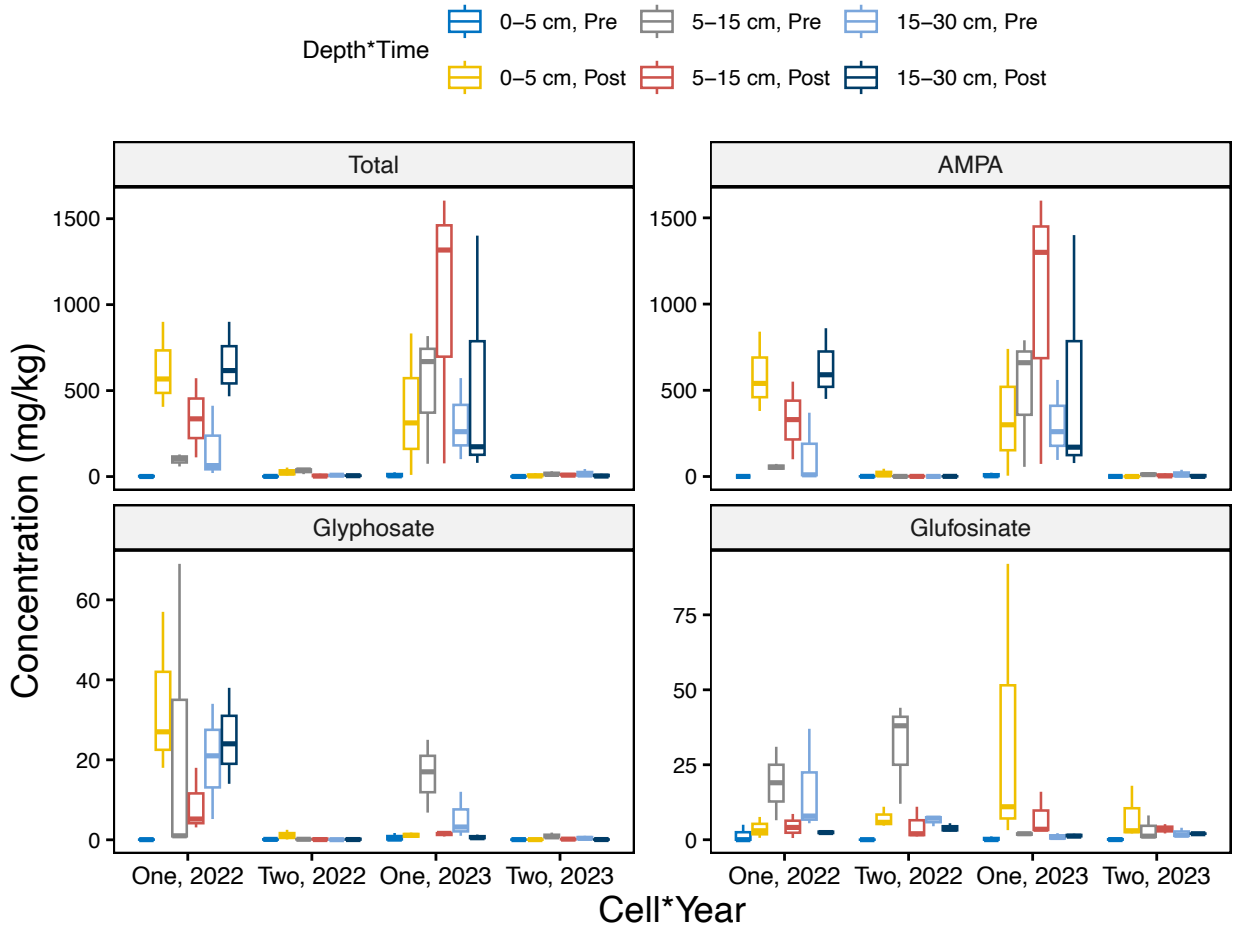

Figure 2.5 Total, AMPA, glyphosate, and glufosinate biomixture concentrations quantified across cells and years (one, 2022; two, 2022; one 2023, and; two 2023) at sampling times (Pre and Post) and depths (0-5, 5-15, and 15-30 cm). "Pre" represents pre-season operation of biobed while "Post" represents post-season operation of biobed.

AMPA concentrations were numerically much larger than that of glyphosate in biomixture (Figure 2.5). Biomatrix samples taken at the end of the growing season (0.09 - 1,600 mg kg^{-1}) typically showed numerically greater AMPA concentrations than samples taken at the beginning of the growing season (0.25 - 790 mg kg^{-1}), confirming that glyphosate was readily transformed to AMPA in the biomatrix during the growing season. The AMPA RM ANOVA showed significant interactions for which the highest order was *cell*year*depth* ($F_{2,16} = 4.164$, $p = 0.035$; Table 5.9, 5.10, 5.11, and 5.12). AMPA concentrations were significantly greater in the biomixture of cell

one (0.33 - 1,600 mg kg^{-1}) than cell two (0.09 - 45 mg kg^{-1}), again suggesting that AMPA was readily formed due to the degradation of glyphosate in the biomatrix. AMPA was largely retained in the biomatrix of cell one because, in both 2022 and 2023, AMPA concentrations were significantly greater in cell one than cell two, except for the top 0-5 cm in cell one (Figure 2.5; Table 5.15). In cell two, AMPA concentrations in the deeper layers were significantly greater in 2023 than 2022, suggesting that AMPA was also accumulating in the second biobed cell. Depth did not influence AMPA concentrations in cells, except that cell two in 2023 showed AMPA concentrations at 0-5 cm (0.09 - 1.4 mg kg^{-1}) that were significantly smaller than at 5-15 cm (2.8 - 21 mg kg^{-1}) and 15-30 cm (0.33 - 39 mg kg^{-1}).

Glufosinate's RM ANOVA showed three significant two-way interactions, i.e., *year: depth* ($F_{2,16}$ = 4.162, *p-value* = 0.035), *year: time* ($F_{1,8}$ = 24.14.052, *p-value* = 0.005), and *depth: time* ($F_{2,16}$ = 24.012, *p-value* = 0.00015) (Table 5.9, 5.10, 5.11, and 5.12). The *depth:tim*e pairwise comparisons showed that, for the samples taken pre-application, mean glufosinate concentrations were significantly smaller at 0-5 cm (0.012 - 92 mg kg^{-1}) than the 5-15 cm (0.57 - 44 mg kg^{-1}) and 15-30 cm (0.095 - 37 mg kg^{-1}) (Table 5.16). This was expected as clean biomixture had been added to each cell to rejuvenate the biobed at the start of the growing season. The *year:time* pairwise comparisons indicated that the mean glufosinate concentrations were significantly smaller in pre-application in 2023 (0.012 – 8.1 mg kg^{-1}) relative to biomatrix samples that were taken post-application in 2023 (1.1 - 92 mg kg^{-1}) and both 2022 pre- (0.012 - 92 mg kg^{-1}) and post-application (0.57 - 11 mg kg^{-1}) (Table 5.17). Finally, the *year:depth* pairwise comparisons showed that the 5-15 (0.57 - 44 mg kg^{-1}) and 15-30 cm (2.1 - 37 mg kg^{-1}) in 2022 were significantly lower than 2023 15-30 cm (0.095 – 4.0 mg kg^{-1}) (Table 5.18).

In 2021, a large amount of glufosinate had entered the biobed system as a tank that had been prepared was not sprayed in the field and thus needed to be cleaned and recycled. Glufosinate was still present at relatively large concentrations when the biomatrix was sampled pre-application in 2022 (Figure 2.5). Overall, mean glufosinate concentrations at 5-15 cm depth in cell one decreased from 19 mg kg^{-1} at pre-application to 4.4 mg kg^{-1} at post-application. Mean glufosinate concentrations in cell two decreased from 31 mg kg^{-1} to 4.7 mg kg^{-1} at the depth of 5-15 cm. Glufosinate concentrations also numerically decreased at 15-30 cm depth, from 17 to 2.5 and from 6.5 to 4.0 mg kg^{-1} in cell one and two, respectively. Overall, these results show that glufosinate is being degraded in the biobed during the growing season. Glufosinate was only applied once to the biobed in 2022 (June 20th), and was more frequently applied in 2023. In 2023, relative to the pre-application samples, glufosinate concentrations were numerically increased in the post-application samples, with increases in cell one from 0.39 to 35 mg kg^{-1} at 0-5 cm, from 1.9 to 7.5 mg kg^{-1} at 5-15 cm and from 1.0 to 1.4 mg kg^{-1} at 15-30 cm. In cell two, glufosinate concentrations increased from 0.12 to 7.7 mg kg^{-1} at 0-5 cm depth and from 3.3 to 3.6 mg kg^{-1} at 5-15 cm; however, at 15-30 cm, mean glufosinate concentrations decreased from 2.2 in the pre-application samples to 2.0 mg kg^{-1} in the post-application samples. Overall, a portion of the glufosinate entering the biobed system appears to persist in the biomatrix.

Overall, the biobed system drastically reduced glyphosate concentrations with significant reductions in glyphosate concentration between rinsate and primary effluent, with only one detection of glyphosate in the final effluent. Both glyphosate and AMPA concentrations were greater in the biomixture of cell one than two, suggesting that substantial sorption of these compounds occurred in the biomatrix of cell one. It is well known that glyphosate and AMPA are strongly sorbed by soils and sediments (de Jonge et al. 2001; Autio et al. 2004; Dion et al. 2001;

Gimsing and Borggaard 2001; Fatema and Farenhorst 2021). The sorption of glyphosate is enhanced in acidic soils and soils rich in iron and aluminum oxides (Dion et al. 2001; Gimsing and Borggaard 2001; Piccolo and Celano 1994). The biomixture in this study contains the Denham soil series which has a relatively large iron- and aluminum-oxide content, and is acidic. The humus-rich peat would also have provided sorption sites for glyphosate. For example glyphosate is adsorbed by metal-humin complexes by hydrogen bonding, or is partitioned into humified organic matter to form humin-glyphosate complexes (McConnell and Hossner 1985; Piccolo and Celano 1994; Piccolo et al. 1996; Morillo et al. 2000; Morillo et al. 2002; Ololade et al. 2014).

Laboratory studies have shown rapid glyphosate degradation within biomatrices, with the primary metabolite being AMPA (Spliid et al. 2006; Góngora-Echeverría et al. 2017; Góngora-Echeverría et al. 2018; Lescano et al. 2018; Góngora-Echeverría et al. 2019; Lescano et al. 2020; Córdova-Méndez et al. 2021). In this field study, glyphosate degradation occurred within the rinsate collection vessel before biobed application (Figure 2.4). Primary effluent concentrations of AMPA were not significantly different from the rinsate values and were higher than that of glyphosate; it is not known if AMPA competes with glyphosate for sorption but both have a phosphate moiety (Table 2.1). In previous studies, phosphate ions outcompeted glyphosate for sorption sites in soil due to its smaller ion diameter (Dion et al. 2001; Gimsing and Borggaard 2001; de Jonge et al. 2001; Vereecken 2005; Munira et al. 2016; Munira and Farenhorst 2017). In addition, lower soil pH is known to increase the sorption of glyphosate, indicating a lower pH biomixture could retain more glyphosate (de Jonge et al. 2001; McConnel and Hossner 1985); the effects of soil pH on AMPA are still unknown. The majority of studies focus on AMPA production from degradation; no studies were found regarding the sorption mechanisms and persistence of AMPA within environmental matrices.

Glyphosate and AMPA data indicate that it is rapidly dissipated within cell one, with little glyphosate detected within the biomixture even though large reductions between rinsate and primary effluent were noted; large increases in AMPA concentrations within biomixtures support this hypothesis. This indicates that glyphosate is adequately removed between rinsate and primary effluent with a single cell biobed, falling below aforementioned toxicity values; this contrasts to AMPA, which required a secondary cell to significantly reduce concentrations between the rinsate and final effluent. As a major metabolite of glyphosate, AMPA concentrations increase drastically within the biomixture, predominantely residing within cell one; however, tandem leaching or formation of AMPA is not understood. Since AMPA has a greater GUS and DT_{50} value than glyphosate (Table 2.1), a greater leaching probability is associated with the more persistent metabolite than its parent.

Glufosinate concentrations were reduced at each step of processing. Although the extent of glufosinate sorption by biomixture is unknown, studies have shown that there is little to no sorption of glufosinate in soils (Autio et al. 2004; Laitnen et al. 2006; Laitnen et al. 2008). Thus, decreases in glufosinate concentrations are associated with mineralization instead of sorption, with glufosinate DT_{50} <5 days within soils (Behrendt et al. 1990; Gallina and Stephenson 1992; Autio et al. 2004; Laitnen et al. 2008; Table 2.1). Biomixture extractions demonstrated that glufosinate was evenly distributed in the biomatrix across cells (Figure 2.5), regardless of concentration reductions from rinsate to final effluent (Table 5.17). This is likely because glufosinate is weakly sorbed in the biomatrix and remains within the soil water fraction; since biomixtures are near or at field capacity, glufosinate appears to distribute with water transport througout the biomixture. Daily irrigation would generate the transport of such glufosinate molecules with water in the biobed system, perhaps somewhat reducing the likelihood of these molecules to be mineralized by

the microbial consortium. Unlike glyphosate and AMPA, glufosinate is a racemic mixture of both the dextrorotary (*D*) and levorotary (*L*) isomers, with most glufosinate formulated products being racemic mixtures; it is believed that the *L*-isomer is the bioactive form since it is a direct analogue of *L*-glutamic acid (Takano and Dayan 2020). Only one study investigated differences between the two isomers, noting that the *D*-isomer dissipates faster than the *L*-isomer; this indicates that the mixture may degrade the inactive *D*-isomer while the more labile *L*-isomer is able to leach from the biomixture and into the environment (Jia et al. 2019).

2.6 Conclusion

This study successfully validated and quantified the herbicide glyphosate and its primary metabolite AMPA, as well as the herbicide glufosinate in an operational above-ground, two-cell biobed located in Carman, Manitoba. Glyphosate concentrations were significantly reduced from rinsate to final effluent, with only one detection of glyphosate within the final effluent. Glyphosate was also rapidly dissipated within biomixtures, especially cell one, with glyphosate concentrations being much less compared to its metabolite AMPA. AMPA concentrations were concentrated in biobed cell one while cell two had relatively small concentrations of AMPA; concentrations of AMPA decreased in the order of rinsate = primary effluent > final effluent. This study finds that a single cell is adequate for glyphosate treatment. Glufosinate concentrations were consistent across both biobed cells, and the use of the second cell lowered glufosinate concentrations to below the acute toxicity thresholds resported for indicator species, indicating the necessity of two or more cells for glufosinate treatment. The large 2021 glufosinate influx continued to degrade into 2022 with pre-operation concentrations higher than post, demonstrating the importance of multi-year

sampling; 2023 glufosinate concentrations increased from pre- to post-operation. Final effluent concentrations resulted in concentrations below most acute toxicity thresholds for glufosinate and CCME guidelines for glyphosate, indicating the effectiveness of biobeds reducing point-source pollution of glufosinate and glyphosate in the environment.

2.7 References

Alonso, B., Griffero, L., Pereira, H.B., Pareja, L., and Parada, A.P. 2022. Determination of glyphosate and AMPA in freshwater and soil from agroecosystems by 9-fluorenylmethoxycarbonyl chloride derivatization and liquid chromatography - fluorescence detection and tandem mass spectrometry. MethodsX **9**: 101730.

Autio, S., Siimes, K., Laitinen, P., Rämö, S., Oinonen, S., and Eronen, L. 2004. Adsorption of sugar beet herbicides to finnish soils. Chemosphere **55**: 215-226.

Battaglin, W.A., M.T. Meyer, K.M. Kuivila, and J.E. Dietze. 2014. Glyphosate and its degradation product AMPA occur frequently and widely in U.S. soils, surface water, groundwater, and precipitation. J. Am. Water Resour. Assoc. **50(2)**: 275-290.

Behrendt, H., Matthies, M., Gilfemeister, H., and Görlitz, G. 1990. Leaching and transformation of glufosinate-ammonium and its main metabolite in a layered soil column. Environ. Toxicol. Chem. **9**: 541-549.

Benbrook, C.M. 2016. Trends in glyphosate herbicide use in the united states and globally. Environ. Sci. Eur. **28**: 3.

Botero-Coy, A.M., Ibáñez, M., Sancho, J.V. and Hernandez, F., 2013. Improvements in the analytical methodology for the residue determination of the herbicide glyphosate in soils by liquid chromatography coupled to mass spectrometry. J. Chromatogr. A **1292**: 132-141.

Braul, L., Reedyk, S., and Sheedy, C. 2018. A robust biobed design for managing pesticide rinsate under Canadian conditions – Construction, operation and maintenance manual. Agriculture and Agri- Food Canada, Regina, SK. Available from: https://publications.gc.ca/collections/collection_2018/aac-aafc/A42-123-2018-eng.pdf [Accessed 18 March 2025]

Brown, A.K., and Farenhorst, A. 2024. Quantitation of glyphosate, glufosinate, and AMPA in drinking water and surface waters using direct injection and charged-surface ultra-high performance liquid chromatography-tandem mass spectrometry. Chemosphere **349**: 140924.

Canadian Council of Ministers of the Environment (CCME). 2012. Canadian water quality guidelines for the protection of aquatic life: Glyphosate. In: Canadian environmental quality guidelines. Canadian Council of Ministers of the Environment, Winnipeg, MB. Available from: https://ccme.ca/en/res/glyphosate-en-canadian-water-quality-guidelines-for-the-protection-of-aquatic-life.pdf [Accessed 14 March 2025].

Chasto, T. Benaragama, D.I., Leeson, J., and Willenborg, C.J. 2024. The impact of herbicide-resistant canola systems on the weed community dynamics in the Canadian Prairies. Can. J. Plant Sci. **104**: 514–528.

Córdova-Méndez, E.A., Góngora-Echeverría, V.R., González-Sánchez, A., Quintal-Franco, C., Giácoman-Vallejos, G., and Ponce-Caballero, C. 2021. Pesticide treatment in biobed systems at microcosms level under critical moisture and temperature range using an orthic

solonchaks soil from southeastern Mexico amended with corn husk as support. Sci. Total Environ. **772**: 145038.

Dion, H.M., Harsh, J.B., and Hill Jr., H.H. 2001. Competitive sorption between glyphosate and inorganic phosphate on clay minerals and low organic matter. J. Radioanal. Nucl. Chem. **249(2)**: 385-390.

European Food Safety Authority (EFSA). 2005. Conclusion regarding the peer review of the pesticide risk assessment of the active substance glufosinate. Available from https://www.efsa.europa.eu/en/efsajournal/pub/rn-27 [accessed 14 Mar. 2025].

Fatema, M., and Farenhorst, A. 2021. Sorption of pesticides by microplastics, charcoal, ash, and river sediments. J. Soils Sediments **22**: 1876-1884.

Fatema, M., Farenhorst, A., and Sheedy, C. 2022. Using the pesticide toxicity index to show the potential ecosystem benefits of on-farm biobeds. J. Environ. Quality. **51(5)**: 1044-1053.

Ferrer, C., Lozano, A., Agüera, A., Girón, A.J. and Fernández-Alba, A.R. 2011. Overcoming matrix effects using the dilution approach in multiresidue methods for fruits and vegetables. J. Chromatogr. A **1218(42)**: 7634-7639.

Gallina, M.A., and Stephenson, G.R. 1992. Dissipation of [^{14}C]glufosinate-ammonium in two ontario soils. J. Agric. Food Chem. **40**: 165-168.

de Gerónimo, E., Lorenzón, C., Iwasita, B. and Costa, J.L. 2018. Evaluation of two extraction methods to determine glyphosate and aminomethylphosphonic acid in soil. Soil Sci. **183(1)**: 34-40.

Gimsing, A.L., and Borggaard, O.K. 2001. Effect of KCl and $CaCl_2$ as background electrolytes on the competitive adsorption of glyphosate and phosphate on goethite. Clays Clay Miner. **49(3)**: 270-275.

Glass, R.L. 1983. Liquid chromatographic determination of glyphosate in fortified soil and water samples. J. Agric. Food Chem. **31**: 280-282.

Glozier, N.E., Struger, J., Cessna, A.J., Gledhill, M., Rondeau, M., Ernst, W.R., Sekela, M.A., Cagampan, S.J., Sverko, E., Murphy, C.,Murray, J.L., and Donald, D.B. 2012. Occurrence of glyphosate and acidic herbicides in select urban rivers and streams in Canada, 2007. Environ. Sci. Pollut. Res. **19**:821-834.

Góngora-Echeverría, V.R., Martin-Laurent, F., Quintal,-Franco, C., Giácoman-Vallejos, G., and Ponce-Caballero, C. 2017. Agricultural effluent treatment in biobed systems using novel substrates from southeastern Mexico: the relationship with physicochemical parameters of biomixtures. Environ. Sci. Pollut. Res. **24**: 9741-9753.

Góngora-Echeverría, V.R. Quintal-Franco, C., Arena-Ortiz, M.L., Giácoman-Vallejos, G., and Ponce-Caballero, C. 2018. Identification of microbial species present in a pesticide

dissipation process in biobed systems using typical substrates from southeastern Mexico as a biomixture at a laboratory scale Sci. Total Environ. **628-629**: 528-538.

Góngora-Echeverría, V.R., Martin-Laurent, F., Quintal-Franco, C., Lorenzo-Flores, A., Giácoman-Vallejos, G., and Ponce-Caballero, C. 2019. Dissipation and adsorption of 2,4-D, atrazine, diazinon, and glyphosate in an agricultural soil from Yucatan State, Mexico. Water Air Soil Pollut. **230**: 131.

Health Canada. 2009. Guidelines for canadian drinking water quality – guideline technical document: chlorine. Available from https://www.canada.ca/content/dam/canada/health-canada/migration/healthy-canadians/publications/healthy-living-vie-saine/water-chlorine-chlore-eau/alt/water-chlorine-chlore-eau-eng.pdf [accessed 18 Mar. 2025].

Ibañez, M., Pozo, Ó.J., Sancho, J.V., López, F.J., and Hernández, F. 2005. Residue determination of glyphosate, glufosinate and aminomethylphosphonic acid in water and soil samples by liquid chromatography coupled to electrospray tandem mass spectrometry. J. Chromatogr. A **1081**: 145-155.

Jia, G., Xu, J., Long, X., Ge, S., Chen, L., Hu, D., and Zhang, Y. 2019. Enantioselective degradation and chiral stability of glufosinate in soil and water samples and formation of 3-methylphosphinicopropionic acid and N-acetyl-glufosinate metabolites. J. Agric. Food. Chem. **67**: 11312-11321.

Johnson, S. 2024. Management of agricultural pesticide rinsate using a biobed under Manitoba conditions. MSc. Thesis, University of Manitoba, Winnipeg, Canada. Available from https://mspace.lib.umanitoba.ca/server/api/core/bitstreams/05b7f34e-0fb0-4cb9-8c12-1057271e8d95/content [Accessed 18 March 2025].

Johnston, A.M., Tanaka, D.L., Miller, P.R., Brandt, S.A., Nielsen, D.C., Lafond, G.P., and Riveland, N.R. 2002. Oilseed crops for semiarid cropping systems in the northern great plains. Agron. J., **94**: 231-240.

de Jonge, H., de Jonge, L.W., Jacobsen, O.H., Yamaguchi, T., and Moldrup, P. 2001. Glyphosate sorption in soils of different pH and phosphorous content. Soil Sci. **166(4)**: 230-238.

Kah, M., Beulke, S., and Brown, C.D. 2007. Factors influencing degradation of pesticides in soil . J. Agric. Food Chem. **55**: 4487-4492.

Kassambara, A. 2023a. ggpubr: 'ggplot2' based publication ready plots. R package version 0.6.0, https://CRAN.R-project.org/package=ggpubr.

Kassambara, A. 2023b. rstatix: pipe-friendly framework for basic statistical tests. R package version 0.7.2, https://CRAN.R-project.org/package=rstatix.

Klingelhöfer, D., Braun, M., Brüggmann, D., and Groneberg, D.A. 2021. Glyphosate: how do ongoing controversies, market characteristics, and funding influence the global research landscape? Sci. Total Environ. **765**: 144271

Laitnen, P., Siimes, K., Eronen, L., Rämö, S., Welling, L., Oinonen, S., Mattsoffm L., and Ruohonen-Lehto, M. 2006. Fate of the herbicides glyphosate, glufosinate-ammonium, phenmedipham, ethofumesate and metamitron in two Finnish arable soils. Pest Manag. Sci. **62**: 473-491.

Laitnen, P., Siimes, K., Rämö, S., Jauhianen, L., Eronen, L., Oinonen, S., and Hartikainen, H. 2008. Effects of soil phosphorous status on environmental risk assessment of glyphosate and glufosinate-ammonium. J. Environ. Qual. **37(3)**: 830-838.

Lemon, J. 2006. plotrix: a package in the red light district of R. R-News, **6(4)**: 8-12.

Lescano, M.R., Pizzul, L., Castillo, M.d.P., and Zalazar, C.S., 2018. Glyphosate and aminomethylphosphonic acid degradation in biomixtures based on alfalfa straw, wheat stubble, and river waste. J. Environ. Manag. **228**: 451-457.

Lescano, M.R., Masin, C.E., Rodríguez, A.R., Godoy, J.L., and Zalasar, C.S. 2020. Earthworms to improve glyphosate degradation in biobeds. Environ. Sci. Pollut. Res. **27**: 27023-27031.

Lewis, K.A., Tzilivakis, J., Warner, D. and Green, A. 2016. An international database for pesticide risk assessments and management. Hum. Ecol. Risk Assess. **22(4)**: 1050-1064.

Magnusson, B., and Örnemark, U. (eds.) 2014. EURACHEM guide: the fitness for purpose of analytical methods – a laboratory guide to method validation and related topics, 2nd ed. Available from www.eurachem.org. [Accessed 18 March 2025].

Marin, J., Campillo, N., Hernández-Cordoba, M., Garrido, I., Fenoll, J., and Viñas, P. 2020. Liquid–liquid microextraction of glyphosate, glufosinate and aminomethylphosphonic acid for the analysis of agricultural samples by liquid chromatography. Anal. Method. **12**: 2039-2045.

Marttila, M. 2024. censlm: censored linear models. R package version 0.0.0.9001, commit 8b43af1e5ed8601c7705043d3d82f3450bbe651d, https://github.com/mikmart/censlm.

McConnell, J.S., and Hossner, L.R. 1985. pH-dependent adsorption isotherms of glyphosate. J. Agric. Food Chem. **33**: 1075-1078.

Miles, C.J., Wallace, L. R., and Moye, H.A. 1985. Determination of glyphosate herbicide and (aminomethyl)phosphonic acid in natural waters by liquid chromatography using pre-column fluorogenic labelling with 9-fluorenylmethyl chloroformate. J. Assoc. Off. Anal. Chem. **69(3)**: 458-461.

Mills, G.F., and Haluschuk, P. 1993. Canada-Manitoba soil survey: soils of the carman research station N½ 23-6-5W. Special Report Series No. 93-1. Available from https://www.gov.mb.ca/agriculture/soil/soil-survey/pubs/fss02s00931.pdf [Accessed 22 February 2025]

Morillo, E., Undabeytia, T., Maqueda, C., and Ramos, A. 2000. Glyphosate adsorption on soils of different characteristics. influence of copper addition. Chemosphere **40**: 103-107.

Morillo, E, Undabeytia, T., Maqueda, C., and Ramos, A. 2002. The effect of dissolved glyphosate upon the sorption of copper by three selected soils. Chemosphere **47**: 747-752.

Munira, S., Farenhorst, A., Flaten, D., and Grant, C. 2016. Phosphate fertilizer impacts on glyphosate sorption by soil. Chemosphere **153**: 471-477.

Munira, S., and Farenhorst, A. 2017. Sorption and desorption of glyphosate, MCPA, and tetracycline and their mixtures as influenced by phosphate. J. Environ. Sci. Health - B Pestic. Food Contam. Agric. Wastes **52(12)**: 887-895.

Nguyen, N.G., Dörfler, U., Welzl, G., Munch, J.C., Schroll, R., and Suhadolc, M. 2018. Large variation in glyphosate mineralization in 21 different agricultural soils explained by soil properties. Sci. Total Environ. **627**: 544-552.

Ololade, I.A., Oladoja, N.A., Oloye, F.F., Alomaja, F., Akerele, D.D., Iwaye, J., and Aikpokpodion, P. 2014. Sorption of glyphosate on soil components: the roles of metal oxides and organic materials. Soil Sediment Contam. **23**: 571-585.

Osbourne, P.P., Xu, Z., Swanson, K.D., Walker, T., and Farmer, D.K. 2015. Dicamba and 2,4-D residues following applicator cleanout: a potential point source to the environment and worker exposure. J. Air Waste Manag. Assoc. **65(9)**: 1153-1158.

Padilla, J.T., and Selim, H.M. 2020. Chapter one - environmental behavior of glyphosate in soils. Adv. Agron. **159**: 1-34.

Pest Management Regulatory Agency (PMRA). 2024. Aquatic life reference values (ARLVs). Available from: https://www.canada.ca/en/health-canada/services/consumer-product-safety/pesticides-pest-management/public/protecting-your-health-environment/programs-initiatives/water-monitoring-pesticides/aquatic-life-reference-values.html [Accessed 8 June 2025].

Piccolo, A., and Celano, G. 1994. Hydrogen-bonding interactions between the herbicide glyphosate and water-soluble humic substances. Environ. Toxicol. Chem. **13(11)**: 1737-1741.

Piccolo, A., Celano, G., and Conte, P. 1996. Adsorption of glyphosate by humic substances. J. Agric. Food Chem. **44**: 2442-2446.

R Core Team. (2023). R: a language and environment for statistical computing. R Foundation for Statistical Computing, Vienna, Austria. https://www.R-project.org/.

Rezende, S., Cesio, M.V., Acrhondo, L., Russi, C., Martínez, P., Rivero, A., Hladki, R., Heinzen, H., and Besil, N. 2021. Pilot study of biobeds application for the remediation of citrus agro-industrial wastewaters. Int. J. Environ. Anal. Chem., **103(20)**: 9698-9714.

Schroll, R., Becher, H.H., Förfler, U., Gayler, S., Grundmann, S., Hartmann, H.P., and Ruoss, J. 2006. Quantifying the effect of soil moisture on the aerobic microbial mineralization of selected pesticides in different soils. Environment. Sci. Technol. **40**: 3305-3312.

Signorell, A. 2024. DescTools: tools for descriptive statistics. R package version 0.99.54, https://CRAN.R-project.org/package=DescTools.

Spliid, N.H., Helweg, A., and Heinrichson, K. 2006. Leaching and degradation of 21 pesticides in a full-scale model biobed. Chemosphere. **65**: 2223-2232.

Takano, H.K., and Dayan, F.E. 2020. Glufosinate-ammonium: a review of the current state of knowledge. Pest Manag. Sci. **76**: 3911-3925.

Todorovic, G.R., Mentler, A., Popp, M., Hann, S., Köllensperger, G., Rampazzo, N., and Blum, W.E.H. 2013. Determination of glyphosate and AMPA in three representative agricultural soils with a HPLC-MS/MS method. Soil Sediment Contam. **22**: 332-350.

Tresnakova, N., Alzbeta, S., and Josef, V. 2021. Effects of glyphosate and its metabolite AMPA on aquatic organisms. Appl. Sci. **11(19)**: 9004.

Valle, A.L., Mello, F.C.C., Alves-Balvedi, R.P., Rodrigues, L.P. and Goulart, L.R., 2019. Glyphosate detection: methods, needs and challenges. Environ. Chem. Lett. **17**: 291-317.

Vereecken, H. 2005. Mobility and leaching of glyphosate: A Review. Pest Manag. Sci. **61**: 1139-1151.

Wickham, H. 2016. ggplot2: Elegant graphics for data analysis. Springer-Verlag, New York.

Wickham, H., François, R., Henry, L., Müller, K., and Vaughan, D. 2023. dplyr: A grammar of data manipulation. R package version 1.1.4, https://CRAN.R-project.org/package=dplyr

de Wilde, T., Mertens, J., Šimůnek, J., Sniegowski, K., Ryckeboer, J., Jaeken, P., Springael, D., and Spanoghe, P. 2009. Characterizing pesticide sorption and degradation in microscale biopurification systems using column displacement experiments. Environ. Pollu., **157**: 463-473.

Wilson, J.L. 2012. Agricultural pesticide use trends in manitoba and 2,4-D fate in soil. Ph.D. Thesis, The University of Manitoba, Available from: https://mspace.lib.umanitoba.ca/server/api/core/bitstreams/b778cd5d-03dc-48c3-_83ba-b9fbfb0eef4d/content [Accessed March 18 2025].

Xu, S., Chen, M., Feng, T., Zhan, L., Zhou, L., Yu, G. 2021. Use ggbreak to effectively utilize plotting space to deal with large datasets and outliers. Front. Genet. **12**:774846.

3. ANALYTICAL METHOD FOR TESTING BIOBED SYSTEM EFFICACY: A METHOD FOR QUANTIFYING 84 PESTICIDE ANALYTES IN RINSATE, EFFLUENT, AND BIOMATRIX SAMPLES

3.1 Abstract

Agricultural pesticides are frequently used in the Prairie region within Canada. The current study validated an analytical method that analyzed for up to 83 commonly-used pesticide active ingredients (52 insecticides, 22 fungicides, and eight herbicides), as well as the adjuvant MGK-264 in both the water fractions (rinsate and effluents) and the biomixtures within biobed systems. A total of two insecticides, three fungicides and eight herbicides were detected in the samples collected from an on-farm, dual-cell biobed located in Carman, Manitoba, which has a Köppen climate classification Dfb (humid continental climate). Rinsate and effluent samples in 2023 showed that metolachlor was the most dominant pesticide in rinsate and primary effluent with a mean concentration 68 mg L^{-1} and 18 mg L^{-1}, respectively. Metolachlor was detected in all nine final effluent samples at concentrations ranging from 0.037 mg L^{-1} to 7.0 mg L^{-1} with a mean of 2.4 mg L^{-1}. Biomixture samples in 2022 and 2023 found that mean pesticide concentrations were greater within biobed cell one (46 mg kg^{-1}) than cell two (7.8 mg kg^{-1}), while mean concentrations were greater in 2023 (43 mg kg^{-1}) than 2022 (11 mg kg^{-1}). Boscalid continued to dissipate from 2022 to 2023, while all other pesticidies were retained at higher concentrations in 2023 than 2022. Bentazon had the highest pesticide concentration in the final effluent with a mean concentration of 5.0 mg L^{-1}. Both bentazon (GUS = 1.95) and clopyralid (GUS = 3.02) were frequently detected in both rinsate and effluent samples and thus the biobed system did appear to be less effective for

these compounds. Imazethapyr appeared to accumulate across both cell one and two with the concentrations being greater in 2023 than 2022. 2,4-D, boscalid, tebuconazole, and pyraclostrobin were not detected in final effluent while chlorantraniliprole, dicamba, and imazamox were detected in ~50% of the final effluent samples. Regardless, the overall data also show that the dual-cell biobed significantly reduced pesticide concentrations in the order of rinsate > primary effluent > final effluent samples.

3.2 Introduction

The cleaning of sprayer equipment produces rinsate that contains pesticide active ingredients at relatively large concentrations whereas the safe disposal of rinsate is important for protecting water resources (Spliid and Køppen 1998; Müller et al. 2002; Helweg et al. 2002; Spanoghe et al 2004; Reichenberger et al. 2007). To prevent pesticide point-source pollution arising from rinsate, biobed systems are used to reduce pesticide concentrations before rinsate is released into the broader environment (Carter 2000; Braul et al. 2018). Among the many strategies that can be used to protect water resources from pesticide contamination (Guyot 1994; Ahmad and Sharma 2023), biobed have gained acceptance in Europe and Latin America for freshwater stewardship (Carter 2000; Góngora-Echeverría et al. 2018; Córdova-Méndez et al. 2021).

Biobeds are either above or below ground bioreactors that are filled with biomixtures developed from a 2:1:1 volumetric ratio of crop residues, peat, and local topsoil, or other mixtures of organic rich substrates (Carter 2000; Bergsveinson et al. 2018). Biomixtures are optimized for promoting the retention of relevant pesticide active ingredients, and for inducing environmental conditions that stimulate microbial consortia capable of transforming pesticide residues into

metabolites, CO_2, and other inorganic chemicals (Carter 2000; Bergsveinson et al. 2018; Góngora-Echeverría et al. 2018; Córdova-Méndez et al. 2021). Biobed systems have been shown to reduce by more than 90% of the pesticide active ingredients concentrations in rinsate (de Wilde et al. 2009 a,b,c; Karanasios et al. 2010; Rezende et al. 2021; Fatema et al. 2022).

In Canada, large-scale grain and oilseed production systems cover more than 278,000 km^2 of relatively flat land in the Prairies (McCallum et al. 2021; AAFC 2025). Pest control products are applied on most farms (>95%) to manage pest populations and prevent weed seedbank increases (Wilson 2012; Chasto et al. 2024). Many of the same pesticide active ingredients are registered for use in both agricultural and non-agricultural applications, and both agricultural and urban sites contribute to the pollution of water resources by pesticides (Sheedy et al. 2019; Izma et al. 2024). The current study focuses on 84 pesticide active ingredients typically applied in grain and oilseed production systems, such as those also frequently detected in surface waters of relatively flat land in the prairies (Glozier et al. 2012; Gamhewage et al. 2021) and sometimes in groundwater (Munira et al. 2018).

There are currently no studies reporting on a fully validated method to assess pesticide concentrations in liquid (rinsate and effluents) and biomatrix samples from biobed systems. This research validated an analytical metod to quantify up to 84 pesticide active ingredients in rinsate, effluent and biomatrix samples; these are insecticides (52), fungicides (22), herbicides (8) as well as N-Octyl bicycloheptene dicarboximide, which is also known as MGK-264, developed but the McLaughlin Gormley King Company; this is an adjuvant in pest control products (e.g., pyrethroid insecticides). The method validation reported here followed Magnusson and Örnemark (2014) *EURACHEM* guidelines which are highly regarded as the standard particularly in North American and European contexts. One of the 84 compounds was the herbicide atrazine which is severely

restricted in Europe because of its “unacceptable effect on groundwater” (Sass and Colangelo 2006). Based on their Groundwater Ubiquity Scores (GUS) (Gustafson 1989), about 12 of the 84 analytes have a high potential for movement toward groundwater (GUS >2.8). Fatema et al. (2022) found that operational biobeds in the Prairies can perform relatively poor for active ingredients that have GUS > 2.8.

Biobed applications in North America have only recently been explored, particulalry in the Prairies within Canada (Bergsveinson et al. 2018; Braul et al. 2018; Fatema et al. 2022). There are frequent detections of pesticides in Prairie surface waters (Glozier et al. 2012; Gamhewage et al. 2021) and sometimes groundwater (Munira et al. 2018). Fatema et al. (2022) found that dual-cell biobeds were better at the complete removal of pesticide analytes than single-cell biobeds for biobed systems operating in the Prairies. However, Fatema et al. (2022) only measured rinsate and final effluent, and not the primary effluent in the dual biobed systems; in addition, each of four biobeds had a different structural design and biomatrix composition and received different pest control products, hence no clear conclusions could be made. In the current study, we applied the validated method to a dual-cell biobed system to examine the contribution of either cells towards reducing the concentrations of pesticide active ingredients typically in rinsate generated in grain and oilseed production systems. The dual-cell biobed system used was designed to annually process up to 10,000 L of rinsate. The study objective was to develop and validate an analytical method relevant of the pesticide active ingredients typically detected in rinsate generated in large-scale grain and oilseed production systems, and monitor their fate in a high-volume dual-cell biobed system. The adoption of biobed systems in the prairies might help to reduce such pollution.

3.3 Materials and Methods

3.3.1 Analytes and Analyses

Optima®-grade acetonitrile (lot #: 219296), Optima®-grade methanol (lot#: 223213), Optima®-grade ultra-pure deionized water (lot#: 224871), formic acid (lot#: 220621), and isopropanol (lot#: 214580) were purchased from Fisher Scientific (Ottawa, ON, Canada). The 99 pesticide *Canadian Cannabis Pesticide Kit* was purchased from Agilent Technologies Ltd for monitoring (Table 6.1; lot#: 0006686504 and 0006686507); all pesticides were >95% purity. Table 6.1 shows additional details on each of the compounds included in the *Canadian Cannabis Pesticide Kit* that was used for optimization, validation, and calibration curves. The pesticide mixtures were received in five glass ampules and each transferred into clean amber glass vials with the concentration maintained for each of the 99 compounds at 100 μg mL^{-1} in 1 ml of acetonitrile; and stored at -20° C. 76 of the 99 analytes were required to do develop the calibration curves, validate the method, and to optimize the Ultra High Performance Liquid Chromatography (UHPLC) – Tandem Mass Spectrometer (MS/MS) for ion fragments and retention times (see Chapter 6 for more detail regarding selected pesticides); the remaining 23 pesticides were not compatible with UHPLC-MS/MS. This analytical technique was deemed most appropriate because many of the pesticide active increadients screened for are relatively hydrophilic compounds with low volatility.For optimization, pesticides from the *Canadian Cannabis Pesticide Mixture* were optimized with in consulation with an Agilent Technologies Ltd. Associate for quantitative use (specific pesticides listed in Table 6.1).

Analytical-grade herbicides purchased from Toronto Research Chemicals (Toronto, Ontario, Canada) were used to prepare individual master solutions in 25 ml of methanol at

concentrations of 200 ug mL^{-1}. Individual herbicide solutions were stored in certified clean amber glass bottles (Thermo®) at -20° C. This included analytical-grade 2,4-D (lot#: 1-TIF-38-1; 98% purity), atrazine (lot#: 4-XJZ-154-1; 98% purity) bentazon (lot#: 22-SCC-125-1; 98% purity), clopyralid (lot# 21-AUR-67-1; 96% purity), dicamba (lot#: 2-JLW-142-1; 96% purity), imazethapyr (lot#: 2-MLM-80-1; 98% purity), imazamox (lot# 6-SX6-14-1; 98% purity), and metolachlor (lot# 5-SCC-20-1; 98% purity) as well as isotopically-labelled standards 2,4-D-$^{13}C_6$ (lot#: 6-NVG-96-1; 98% purity), bentazon-d_7 (lot#: 26-MVI-73-1; 97% purity), tebuconazole-d_9 (lot#: 14-FLI-37-1; 97% purity), thiamethoxam-d_4 (lot#: 7-TKN-94-1; 97% purity), and metolachlor-d_6 (lot#: 10-MP-42-3; 97% purity).

The analyses for sepration and quanitification was adapted from the application note of Stone et al. (2020); equilibration time was extended by 1 minute for a total of 13 minute run time. An Agilent 1260 UHPLC quaternary pump and multi-sampler with a InfinityLab™ Agilent Poroshell 120 Phenyl-Hexyl column (3.0 mm x 100 mm x 2.7 μm dp) attached to a matching Poroshell 120 Phenyl-Hexyl guard column (3.0 mm x 5 mm x 2.7 μm dp) were used for separation. Injections were sandwich injections with one sample aliquot (10 μL) between two 10 μL of deionized water with 0.1% FA above and below; sandwich's were pre-mixed by 5 times before injection into the column. The column temperature was maintained at 55° C, a flow rate of 0.5 mL min^{-1}; deionized water with 0.1% FA and acetonitrile with 0.1% FA were the mobile phases A and B, respectively. The solvent gradient was as follows: 0-1 min 30% B hold; 1.01-2.00 min 75% B ramp; 2.01-8.00 min 96% B ramp; 8.01-9.00 min 100% B ramp; 9.01-9.50 min 100% B hold; finally, 9.51-13.00 min 30% B for re-equilibration. At the end of all runs, a 45-minute flush method for column storage was conducted at 42° C column temperature was performed to maintain column

health using a gradient of deionized water (C) and acetonitrile (D) using the following gradient: 0-15 min 5% D, 15.01-20 min ramp to 100% D, then 100% D hold until 45 min.

An Agilent 6470 triple quadrupole mass spectrometer was used to identify and quantify all compounds eluted from the UHPLC. Individually purchased pesticides and internal standards were optimized separately in both negative and positive mode with 10 µL injections; the highest yielding ion being the quantifier and the second highest being the qualifier ion. Polarity switching between electrospray ionization (ESI) positive (Capillary Voltage [CV] 5,000 V) and negative (CV 3,500 V) modes was employed. Drying gas temperature and flow rate were 200° C and 13 L min^{-1}, respectively; nebulizer pressure was 55 psi; sheath gas temperature and flow rate of 200° C and 10 L min^{-1}, respectively; nozzle voltage was 500 to 1,000 V, and; desolvation gas flow rate was 13 L min^{-1}. Sheath, drying, and nebulizer gas nitrogen were produced from an Agilent Nitrogen Gas Generator while the collision cell was supplied with Ultra High Purity Nitrogen (5.0; 99.9999%). Chromatographic and mass spectrometric conditions found in Chapter 6.2.1 and Table 6.2.

3.3.2 Validation Experiments

Biweekly, working solutions were prepared at 1 µg mL^{-1} for both labelled and unlabelled standards and an additional 0.05 ug mL^{-1} for unlabelled standards only. Calibration curves were prepared from the working solutions in deionized water for direct-inject rinsate and effluent analyses, in acetonitrile for the Quick, Easy, Cheap, Effective, Rugged, and Safe (QuEChERS) biomixture extractions, and in 50:50 methanol:deionized water for for the Quick Polar Pesticides – Plant Origin (QuPPe) biomixture extractions. Concentrations were 1 x 10^{-4}, 1 x 10^{-3}, 2.5 x 10^{-3},

5 x 10^{-3}, 1 x 10^{-2}, 2.5 x 10^{-2}, 5 x 10^{-2}, and 1 x 10^{-1} µg mL^{-1} with 5 x 10^{-2} µg mL^{-1} internal standard for quantitation.

All validation followed Magnusson and Örnemark (2014); parameters validated were instrument selectivity, working range, both limits of detection and quantification (LOD/LOQs). For rinsate and effluents method limits of detection and quantification at 5 x 10^{-3} µg mL^{-1} (MLD/MLQs), both accuracy and precision (intra- and interday) at 2 x 10^{-2} (effluent only), 2 x 10^{-1}, 2, 20 and 200 (rinsate only) µg mL^{-1}, and matrix effects at 5 x 10^{-3}, 10 x 10^{-2}, and 20 x 10^{-2} µg mL^{-1}. Detailed descriptions of measurements and calculations are described in Chapter 6.1. For biomixture, concentrations tested for validation were method limits of detection and quantification at 2.5 x 10^{-2} µg kg^{-1} (MLD/MLQs), both accuracy and precision (intra- and interday) at 1 x 10^{-1} and 1 µg kg^{-1}, and matrix effects at 5 x 10^{-3}, 10 x 10^{-2}, and 20 x 10^{-2} µg mL^{-1}.

For validation, artificial rinsate was prepared to mimic the pest control suspensions typically in the field samples. The pesticide mixture that was prepared contained 50 mg L^{-1} deltamethrin (Decis® 5 EC), 500 mg L^{-1} glyphosate (Roundup Transorb® HC), and 500 mg L^{-1} glufosinate (Liberty® 150) were mixed with tap water on the farm, so that the total pesticide concentration was 1.05 g L^{-1}. This concentration was ten-times greater than the mean pesticide concentration (105 mg L^{-1}) in rinsate collected from the biobed in 2020-2021 by Johnson (2024). Glyphosate, glufosinate, and deltamethrin are widely used in grain and oilseed production in the Prairies, as well as on the research farm in Carman, but not targeted as analytes in the multi-residue method developed and validated in this study. The artificial rinsate was prepared to take into consideration the possibility of strong matrix effects. Articifial solutions were stored for no more than 30 days at 4° C in amber glass bottles. All validation parameters for rinsate required an initial

1/10 dilution due to significant matrix effects that either significantly impacted recoveries, altered internal standard relative response, or caused no signal to appear for compounds.

Artificial effluent solutions were made with the expectations that humic substances will be abundantly present in the effluent (Figure 3.1) of the biomatrix cells, thereby complicating the quantifications of pesticide active ingredients by UHPLC-MS-MS in this research. In order to obtain a representative sample of the potentially large concentraitons of humic substances present in effluent samples obtained in the field, biomixture (300 g) (collected as stated in 2.4.2) and tapwater (3 L) was was shaking vigourosly 3 L high-density prolypropylene bottle for 5 min. and allowed to sit for 48 h. at room temperature to settle solids. No pesticides were detected in the laboratory made effluent before use in the validation experiments, so the matrix effects observed were due to the humic substances expected to be dissolved in the effluent (Figure 3.1). A 10:1 ratio was selected to simulate the addition of water:biomixture ratio expected for the biobed system on an annula basis (1,200 kg biomixture to 10,000 L water).



Figure 3.1 Photo of rinsate (left glass cylinder), primary effluent (middle) and final effluent (right) during sample collection in 2023. Rinsate solution is cloudy from adjuvants in formulation while effluents are yellow-brown from humic substances leached from biomixtures.

3.3.3 Research Site and Biobed System

Research was conducted at the above-ground, dual-cell biobed (Figure 2.1) located at the Ian N. Morrison Research Farm in Carman Manitoba. This biobed system was established during the COVID-19 pandemic and began its operation in fall 2020 (Johnson 2024). The biobed system has installed a series of five pumps that 1) collect rinsate, 2) agitate rinsate within a tank, 3) applies rinsate to cell one, 4) applies primary effluent from cell one to cell two, and 5) triggers a release of final effluent from a tank into the broader environment. Each cell of the biobed were filled with 7.44 m^3 of biomixture (9.3 m^2 surface area x 0.7 m deep [0.50-0.55 m biomixture, 0.15-0.20 pea gravel]). The biomixture was prepared as a mixture of wheat straw, topsoil (0-15 cm, Denham series, Orthic Black Chernozem), and peat (Sunshine Sphagnum Peat) in a 2:1:1 volumetric ratio (Braul et al. 2018) (Table 3.1). Macro and micronutrient profiles from 2020 are as follows: 21.8 (N), 26.0 (P), 382.5 (K) and 27.5 (S) mg kg^{-1}, 0.7 (B), 3.6 (Zn), 164.9 (Fe), 12.6 (Mn), and 0.9 (Cu) mg kg^{-1} (Johnson 2024).

Table 3.1 Selected properties determined for the biomatrix in the dual-cell biobed system.

B.D.[1] (g cm^{-3})	Poro[2] (%)	P.D.[2] (g cm^{-3})[3]	EC[4] (µS/cm)	pH[5]	OC[6] (%)	CEC[7] (meq)	Soil Text.[8]	FC[9] (%)
1.07	53	2.27	115.2	5.96	2.82	17.95	S.L.[a]	31

[1]Bulk Density, 100cc sample dried at 105°C for 24 hours; [2]Porosity, slurry volume/(50 mL biomix + 70 ml dH_2O); [3]Particle Density, B.D./(1-Porosity); [4]Electrical Conductivity, 2:1 biomix:dH_2O; [5]pH, 2:1 biomix:dH_2O; [6]Organic Carbon, loss-on-ignition divided by 1.72; [7]Cation Exchange Capacity, Barium Chloride Displacement; [8]Soil Texture, Hydrometer Method; [9]Field Capacity, percolation technique; [a]Sandy Loam.

3.3.4 Samples Collected.

Biomixture sampling was conducted twice a year in both 2022 and 2023 (*year* factor) with the sampling rounds being pre- and post-biobed operation (*time* factor). Pre-biobed operation

refers to the time period between applying the first rinsate but after a 5 cm biomixture top-up which is a standard procedure every year. Post-biobed sampling was done within a week after biobed operations ceased for the season. Biobed samples were collected from three randomized spots per cell that were flagged and geolocated on a GPS so that post samples could be collected from approximately the same area in the biobed cell; both biobed cell one and two were sampled for comparison (hereafter *cell* factor) at three locations each. At each sampling spot, samples were collected at 0-5, 5-15, and 15-30 cm deep (*depth* factor). All samples were collected with a clean tulip planter and transfered to 6"x 8" VWR® brand Re-closable UV-Protectant Amber Bags (lot#: 89005-324). Samples were transported over ice to the laboratory and frozen at -20º C until analysis.

Rinsate, primary effluent, and final effluent samples were collected biweekly June 20 to October 10, 2023, for a total of 27 samples. For each sampling event, samples were taken from each of three sampling ports and collected in 15 mL clear glass vials (lot#: 14-959-25B) with a rubber lined black caps. Glass vials were capped then inserted into a singular 500 mL certified clean glass amber bottle (ThermoScientific©) to prevent photodegradation. During each sampling round, a field blank (deionized water in a sampling vial) was opened for about 30 seconds then closed and processed in the same way as collected samples. Samples were stored over ice for transport to the laboratory, and then stored at 4º C and extracted within 2 days of arrival.

3.3.5 Analyte Extractions and Quantifications.

Rinsate samples were diluted 1/10 before extraction to reduce matrix effects. For the extractions, rinsate and effluent samples were vortexed for 30 seconds, then 950 µL samples aliquots were spiked with 50 µL internal standard (IS; 0.05 µg mL^{-1} each) solutions. Spiked

samples were syringe filtered through a 0.22 μm polytetrafluoroethylene (PTFE) syringe filter (lot#: 310098157) into a two mL amber glass vials (lot#: 23288413) with BONDED blew screw PTFE-red silicone screw caps (lot#: 306034). Extracts were diluted in deionized water with rinsate dilutions of 1/10, 1/100, 1/1,000, and 1/10,000 and effluent dilutions of no dilution, 1/10, 1/100, and 1/1,000 times were quantified.

Biomatrix samples were freeze-dried for 24 hours using a sample temperature of -20 º C and a collector temperature of -80º C under a vacuum of 1.000 mbar. Freeze-dried samples were subjected to both QuEChERS and QuPPe extractions as follows. The QuEChERS extraction followed a procedure adapted from Rezende et al. (2021). Freeze-dried biomixture samples (2 g) were added to a 50 mL Falcon® tube (lot#: 10922042) with 8 mL of deionized water. Tubes were rotated for 30 min on an end-to-end rotameter at 30 revolutions per minute (rpm); post-rotation, slurries had 10 mL of acetonitirile added, then shaken by hand for 1 min, sonicated for 15 min at 30º C, 80 hz, at 100% power with a FisherBrand™ 112xx Series Advanced Ultrasonicator. After sonication, 3 g of NaCl (>99.5% purity, lot#: A0448895) and 4 g of $MgSO_4$ (>99.5% purity, lot#: Q14J043) were added and tubes were shaken again by hand for 3 min. Tubes were then centrifuged at 6,000 rpm at 20 º C for 10 min. in a Thermo® IEC CL31R Multispeed Centrifuge. Subsequently, a 6 mL aliquot of the upper solvent layer was added to a 15 mL Falcon® tube (lot#: 25423012) with 0.90 g of $MgSO_4$. Falcon tubes were vortexed for 30 sec then centrifuged at 3,750 rpm at 4º C in a Thermo® Sorvall Legened RT Refrigerated Benchtop Centrifuge. Finally, a 950 μL sample aliquot was spiked with 50 μL IS solution and syringe filtered through a 0.22 μm PTFE syringe filter into a 2 mL glass amber vial, capped, and stored at 4º C until quantification by UHPLC-MS/MS; samples were analyzed within 7 days of extraction.

For the QuPPE extraction procedures adapted from Anastassiades et al. (2023). Freeze-dried biomixtures (4 g) were weighed into 50 ml Falcon® tube with 10 mL of deionized water. Tubes were rotated for 30 min at 30 rpm as described above prior to adding 10 mL methanol with 1% formic acid to the slurries. Tubes were shaken by hand for 1 min and then sonicated for 15 min as described above. Samples were then centrifuged at 10,000 rpm for 10 min at 20 º C in a Thermo® CL31R Multispeed Centrifuge. A 950 µL aliquot was spiked with 50 µL IS, syringe filtered through a 0.22 µm PTFE syringe filter into a 2 mL glass amber vial, capped, and stored at 4º C until quantification by UHPLC-MS/MS; as with QuEChERS, samples were analyzed within 7 days of extraction.

For quantification, the biomatrix extracts were diluted 1/10, 1/100 and 1/1,000 times in acetonitrile for the QuEChERS extracts and 50:50 methanol:deionized water for the QuPPe extracts.

3.3.6 Statistical Analysis

MLD and MLQs, accuracy, and precision were determined in Microsoft® Excel for Mac v.16.78 (see Chapter 6.1 for details). Matrix effects and freeze-drying statistical analyses were conducted in R v.4.3.2. "Eye Holes" (R Core Team 2023; Vienna, Austria).

Matrix effects were analyzed through ANCOVA[4] analysis with the response vs. extraction matrix across three concentrations (see Chapter 6.1 for detail); rinsate and effluent, QuPPe, and QuEChERS and their dilutions were all compared against solvent-matched controls. Data for

[4] ANCOVA is *analysis of covariance* which includes a covariate that is continuous with categorical factors; it is an extension of an ANOVA (*analysis of variance*), which typically are applied for only categorical factors. Both stem from a linar regression model.

ANCOVA's were transformed (as indicated in Chapter's 7, 8, and 9) and residuals were tested for the assumptions of normality with Shapiro-Wilk Test, homoscedascity with Breusch-Pagan Test, and equal slopes with an interactive vs. additive model ANOVA test (all using the base R code; α = 0.05); when ANCOVA's were significant, a Dunnett's post-hoc test was used to compare the differences between pure, control matrix to extractant effects on molecule response with the *emmeans* package (Lenth 2024). If responses were only quantifiable at one concentration, then an ANOVA was conducted with Shapiro-Wilk Test (α = 0.05) and Bartlett's Test of homogeneity (α = 0.05) to test assumptions. Dunnett's post-hoc test was used to compare pure, analytical solutions to matrix solutions when significant using the base R code.

Biomixture freeze-drying losses were analyzed in a one-way ANOVA model with spike stage as the factor; both the assumptions of normality (Shapiro-Wilk Test) and homogeneity of variance (Bartletts Test) were tested. When significant, ANOVA mean's were compared using the Tukey's post-hoc test[5] with the *emmeans* to compare differences in concentrations quantified by spiking stage of internal standards.

When data were <MLQ values, concentrations were randomly imputed from 0 to MLQ through Maximum Likelihood Estimation on log-transformed values with *censlm* package and then further analyzed (Martilla 2023). Welch's ANOVA was used to analyze differences in concentrations between rinsate, primary, and final effluent with the base R code; when significant, a Games-Howell Post-Hoc Test was used to compare means with the *rstatix* package (Kassamabra 2023a). A repeated measures ANOVA (RM ANOVA) was also analyzed through *rstatix* for biomixtures, with depth and time as a within-subject factors and cell and year as between-subject

[5] Dunnet's post-hoc test was utilized when comparing pure, analytical solutions to matrix solutions, thereby quantifying the effect of the matrix itself on the molecular response. Tukey's test was utilized for internal standard losses since comparisons are looking for at which stage(s) result in the greatest losses of standard.

factors. When RM ANOVA's were significant, Benjamini-Hochberg Post Hoc comparisons were used to compare factor means within the significant highest order interaction with the base R code. Responses were transformed as necessary while assumptions were tested with Levene's Test of Equal Variance, Shapiro-Wilk test for normality, and Mauchly's Test for Sphericity. If Mauchly's test for sphericity was significant then a Greenhouse-Geisser correction was applied. When significant, a Benjamini-Hochberg post hoc test was conducted on the highest order interaction.

ggbreak (Xu et al. 2021), *ggplot2* (Wickham 2016), *ggpubr* (Kassamabra 2023b), and *plotrix* (Lemon 2006) were used to make plots for this manuscript.

3.4 Results and Discussion

3.4.1 Validations

Pesticide linearity, working range, associated internal standard, and machine limits of detection and quantification were assessed and are discussed in Chapter 6, with the compound and internal standard chromatograms displayed in Figure 6.1 to 6.90. Calibration curves for each pesticide had R^2 values greater than 0.9900 within the working range, with only eight pesticides having values less than 0.9800; working ranges of pesticides were 1×10^{-4} to 1×10^{-2} µg mL^{-1}, with the exception of four compounds that were not detected until the 1×10^{-3} to 2.5×10^{-3} µg mL^{-1} range as well as twelve compounds that couldn't be quantified when concentrations $>2.5 \times 10^{-2}$ µg mL^{-1} (concentrations increases after 2.5×10^{-2} µg mL^{-1} did not have a proportional increase in molecular response) (Table 6.3). Internal standards were predominantely associated with

bentazon-d_7 (39 pesticides) and tebuconazole-d_9 (33), and also with 2,4-D-$^{13}C_6$ (4), thiamethoxam-d_4 (5), and metolachlor-d_6 (4). Instrument limits of detection and quantification were low for all compounds (Table 6.3).

3.4.1.1 Rinsate and Effluent. Almost all compounds and concentrations fell between the 70 - 130% recovery for rinsate accuracy except for six compounds at 2 x 10^{-1} µg mL^{-1} and three compounds at both 2 µg mL^{-1} and 20 µg mL^{-1}; both buprofezin and fenoxycarb were not detected at 2 x 10^{-1} µg mL^{-1} (Table 7.1). MLQs were between 1 x 10^{-2} – 1 x 10^{-3} µg mL^{-1} for 29 compounds and <1 x 10^{-2} µg mL^{-1} for 51 compounds; only fensulfothion, cyantraniliprole, dimetamorph II, and fludioxinil had quantification limits >1 x 10^{-1} ng mL^{-1}, with dimetamorph II and fludioxinil exceeding 1 µg mL^{-1} (Table 7.1). As discussed below, these pesticides were not detected within the biobed system.

Method limits of detection (MLD) and quantification (MLQ) for compounds in effluents ranged between 5 x 10^{-5} - 1 x 10^{-2} µg mL^{-1} for all compounds, with only dinotefuran and methomyl MLD and Qs requiring an additional dilution due to matrix effects causing recoveries >130% (Table 7.1). Only oxamyl quantification limits reached 1.1 x 10^{-2} µg mL^{-1}; the remaining MLQ's did not exceed 1.0 x 10^{-2} µg mL^{-1}. For accuracy, only buprofezin was not detected at 2 x 10^{-2} µg mL^{-1} in effluent. Dinotefuran and methomyl elicited an increased response at 2 x 10^{-2} µg mL^{-1}; oxamyl response was > 130% at 2 x 10^{-1} µg mL^{-1}.

Rinsate precision was much more pronounced than effluent for both intra- and inter-day precision, with compounds exceeding 20% CV for 15 compounds at 2 x 10^{-1} µg mL^{-1}, 5 at 2 µg mL^{-1}, 6 at 20 µg mL^{-1}, and 10 at 200 µg mL^{-1} (Table 7.2). Effluent intraday variation were below 20% variation except for four compounds at 2 x 10^{-2} µg mL^{-1} and fludioxinil at 2 x 10^{-1} and 200

μg mL^{-1}, exceeding 20% CV. Interday variation had found two compounds exceeding 20% CV variation at 2 x 10^{-2} μg mL^{-1} while bifenthrin exceeded 20% CV at 2 and 20 μg mL^{-1} (Table 7.2).

Significant matrix effects analysis were found for 75 compounds (Table 7.3, 7.4, and 7.5 and Figure 7.1-7.3); metolachlor and tetrachlorvinphos required a seperation analysis of 1/10 dilution rinsate due to non-normality of residuals (Table 7.3). Out of the 75 significant tests, Dunnett's Post Hoc test were insignificant for fenoxycarb, kresoxim-methyl, MGK-264 and tetramethrin, demonstrating no significant differences detected between each matrix water and the deionized water solution. The remaining treatment-control post-hoc comparisons revealed that significant differences between deionized water and matrix water, with 38 in effluent, 22 in 1/10 diluted effluent, 17 in 1/100 diluted effluent, 1 in 1/1,000 diluted effluent, 48 in /10 diluted rinsate, 38 in 1/100 diluted rinsate, 13 in 1/1,000 diluted rinsate, and 7 in 1/10,000 diluted rinsate (Figures 7.4 to 7.87). Data indicates that greater dilution effectively reduces matrix effects on compounds; isotope dilution with internal standard was able to counter matrix effects of both rinsate and effluents for most compounds within the method.

3.4.1.2 Biomatrix. QuEChERS was able to extract 67 of the 85 compounds within the method; most non-quantifiable compounds had either unacceptable recoveries or no response. Detection and quantification limits of QuEChERS were mostly below 1 x 10^{-2} μg kg^{-1} except for 7 compounds; no compound exceed 5 x 10^{-2} μg kg^{-1} (Table 8.1). Almost all compounds were within the 70 - 130% accuracy range demonstrating good performance, with the exception of azoxystrobin (140% at 1 μg kg^{-1}) and thiophanate-methyl (68% at 1 μg kg^{-1}); few compounds went beyond 80 - 120% range (Table 8.1). Intra-day precision were predominantly < 20%, with only pyrethrin II and chlorpyrifos for both 1 x 10^{-1} and 1 μg kg^{-1} > 20%; inter-day precision only had thiophanate-methyl exceed 20% variation for both 1 x 10^{-1} and 1 μg mL^{-1} (Table 8.1). Matrix

effects were found across all QuEChERS dilutions, predominantly as a decreased response (Table 8.2 - 8.4; Figures 8.1 – 8.69). Diluted QuEChERS extractants had less matrix effects than the raw extractant, with only 3 compounds having an increased response in both the 1/100 and 1/1,000 diluted QuEChERS. Overall, internal standards were able to counteract compound ionization effects in quantification of biomixture extracted by QuEChERS. Internal standard losses were all > 70% accuracy threshold, so losses were considered negligible, though significant differences were detected in 50 compounds (Table 8.5 and 8.6; Figure 8.70 – 8.136).

QuPPe was able to extract 51 compounds, however QuPPe was able to extract clopyralid; most compound quantification limits were below 1 x 10^{-2} µg kg^{-1}, with the exceptions of five compounds; no quantification limit exceeded 3 x 10^{-2} µg kg^{-1} (Table 9.1). Almost all compounds extracted were within the 70-130% accuracy range; only oxamyl exceeded the maximum 130% threshold for accuracy at 1 x 10^{-1} µg kg^{-1} (Table 9.1). Intra or Inter-day precision never exceeded 20% CV (Table 9.1). QuPPe matrix effects ANCOVA's were significant for 32 of the 51 compounds that were extractable (Figure 9.1). Within the 32, Dunnet's post-hoc tests for five compounds found no differences between the control and treatment matrices (Tables 9.2 – 9.4; Figures 9.2 – 9.52). The raw QuPPe extractant experienced the greatest matrix effect while the 1/100 dilutions had no more than 4 compounds experiencing matrix effect; 1/1,000 diluted QuPPe experienced no matrix effects for any compounds. Internal standards were able to counteract the majority of matrix effects during extraction. Internal standard losses were significant for 48 of the 51 compounds (Table 9.5 and 9.6; Figures 9.53 – 9.104), however, these differences were considered negligible since extractions remained within the 70-130% accuracy range.

3.4.2 Biobed Performance

3.4.2.1 Rinsate and Effluent. Twelve pesticide active ingredients were detected in the rinsate for which the GUS ranged from 0.05 to 3.90, the soil half-lives ranged from 4.4 to 597 $days^{-1}$, and Koc values ranged from 5 to 9,304 ml g^{-1}. Mean total pesticide concentrations decreased from 84 mg L^{-1} in rinsate (range 18 - 210 mg L^{-1}) to 26 mg L^{-1} in primary effluent (range 12 - 39 mg L^{-1}) to 9.4 mg L^{-1} in final effluent (range 4.6 - 12 mg L^{-1}). As such, the first biobed cell reduced the pesticide concentration in the biobed flow by about 69%. Relative to the primary effluent, the second biobed cell resulted in another 64% reduction in total pesticide concentration for a total 88% concentration reduction from rinsate to final effluent (Figure 3.2). Rinsate concentration on June 20th was the highest concentration quantified with a gradual decline over time; primary and final effluent gradually increased in concentrations from June 20th to August 17th then plateaud until operations ceased on October 10th, 2023 (Figure 3.3).

For the eight pesticides detected in the final effluent, the GUS ranged from 1.94 to 3.90, and thus these were all compounds that have either a moderate (1.8-2.8) or high (>2.8) potential for movement toward ground water. Fatema et al. (2022) found that bentazon, clopyralid, diclofop, and fluoxypyr were pesticides of concern within biobed systems and concluded that pesticides with larger GUS scores (>2.8) have greater risk in biobed system leaching. In this study, bentazon (GUS 1.95) was indeed (also among) the most dominant analyte in the final effluent with a mean of 5.0 mg L^{-1} (range 2.2 - 9.5 mg L^{-1}).

The type of pest control products applied on the farm during the growing season influenced the types of analytes detected in the rinsate as mixtures, and hence in effluent. For example, metolachlor was more consistently used on the farm than imazethapyr. Metolachlor (GUS = 2.36) had the highest concentration detected in both the rinsate (mean of 68 mg L^{-1} ranging from 14-200

mg L^{-1}) and primary effluent (18 mg L^{-1} range of 1-30 mg L^{-1}) (Figure 3.2). Atrazine, bentazon, clopyralid, imazethapyr, and metolachlor were detected in all twenty-seven samples (9 rinsate, 9 primary effluent, and 9 final effluent) collected in 2023. Off these, only atrazine ($F_{2,\ 10.7}$ = 16.8, *p-value* = 0.0003) and metolachlor ($F_{2,\ 12.8}$ = 19.0, *p-value* = 0.0005) showed significant decreasing mean concentrations in the order of rinsate > primary effluent > final effluent (Figure 3.2). For imazethapyr ($F_{2,14.0}$ = 10.1, *p-value* = 0.0019), rinsate was not significantly different from either primary or final effluent, while primary effluent > final effluent; note the large variations in imazethapyr concentrations across means (Figure 3.2 and 3.3). Mean imazethapyr concentrations was numerically greater in rinsate (mean = 0.22 mg L^{-1}; range = 0.0092 – 0.66 mg L^{-1}) than primary effluent (mean = 0.13 mg L^{-1}; range = 0.085 – 0.17 mg L^{-1}), and in rinsate than final effluent (mean = 0.082 mg L^{-1}; range = 0.056 – 0.11 mg L^{-1}). Clopyralid (GUS = 3.02) ($F_{2,15.0}$ = 0.371, *p-value* > 0.05) and bentazon (GUS = 1.95) ($F_{2,14.4}$ = 1.47, *p-value* > 0.05) concentrations were not significantly different across rinsate, primary, or final effluent samples; interestingly, these compounds variation around the mean decreased from rinsate > primary > final effluent (Figure 3.2).

Although not consistently detected in each sample, chlorantraniliprole ($F_{2,11.7}$ = 43.3, *p-value* < 0.0001), dicamba ($F_{2,15.4}$ = 13.51, *p-value* = 0.0004), and imazamox ($F_{2,14.5}$ = 30.7, *p-value* < 0.0001) were additional compounds that showed significantly decreasing mean concentrations in the order of rinsate > primary effluent > final effluent (Figure 3.2). Thus, including atrazine and metolachlor, a dual-cell biobed was sufficient for 41% (5) of the twelve pesticides entering the biobed. Chlorantraniliprole (GUS = 3.51) was detected/quantifiable in 100% of the rinsate and primary effluent samples, but only 78% of the final effluent samples. Dicamba (GUS = 1.94) was detected/quantifiable in 89% of rinsate samples, 100% of primary effluent samples, and 44% of

final effluent samples. Imazamox (GUS = 3.59) was detected in 100% of rinstate samples, 78% in the primary effluent, and 33% in the final effluent samplest. Adding an additional, third cell might decrease the concentrations of these pesticides further.

The four other pesticide active ingredients that were efficiently processed in the biobed system were: 2,4-D, boscalid, pyraclostrobin, and tebuconazole. No statistical analyses were applied as these analytes because they were not (consistenly) detected in primariy effluent and/or final effluent. Neither 2,4-D (GUS = 3.82) nor tebuconazole (GUS = 1.86) were detected in the primary effluent, and of the ten pesticides detected in the primary effluent and entering the second biobed cell, boscalid (GUS = 2.68) and pyraclostrobin (GUS = 0.05) were not detected in the final effluent. The herbicide 2,4-D has the shortest soil half-life (Table 3.2), thus was likely rapidly degraded in the biomatrix of cell one; indeed the fact that 2,4-D was never detected in biomatrix supports this (see below *Biomixture Concentrations 2022 and 2023*). Tebuconazole has a relatively large K_{oc} and small GUS (Table 3.2) and was retained in the biomatrix of cell one with lesser concentrations in cell two (see below *Biomixture Concentrations 2022 and 2023*). This suggests both retention and degradation of tebuconazole in the biobed system. Boscalid has a large K^{oc} and its very short-half life in the water column of aquatic systems is because of boscalid's rapid sorption to sediments including dissolved sediments (Table 3.2). As expected, based on its relatively large soil half-life (Table 3.2), it is also relatively persistent in biomatrix (see below *Biomixture Concentrations 2022 and 2023*). Of any compounds detected in this study, pyraclostrobin was the compound with the largest K_{oc} value and smallest GUS (Table 3.2) hence it was not expected to be detected in the final effluent.

Table 3.2 Water solubility (Water sol.), LogK_{ow} (Log_{10} octanol-water partitioning coefficient), pKa (Log_{10} acid-dissociation constant), half-lives in days (DT_{50}) in lab soil (L), field soil (F), and water-phase only (W), K_{oc} (soil organic carbon-water partitioning coefficient), and GUS (Groundwater Ubiquity Score) of compounds as described in Lewis et al. (2016).

Com.[1]	Mat-rix[2]	Water sol.[3]	Log-K_{ow}	pKa	DT_{50} (L)[4]	DT_{50} (F)[4]	DT_{50} (W)[4]	K_{oc}[5]	GUS
2,4-D	W only	24,300	-0.82	3.4	4.4	29	7.7	39.3	3.82
ATRA	W/B	35	2.7	1.7	66	29	*ND*[6]	100	2.57
BENT	W/B	7,112	-0.46	3.5	20	7.5	80	55.3	1.95
BOSC	W/B	4.6	2.96	*NA*	484	254	5	*772*	2.68
CHLO	W/B	0.88	2.86	11	597	204	23.5	362	3.51
CLOP	W/B	7,850	-2.63	2.0	23	8.2	148	5	3.02
CLTH	B only	327	0.905	11	545	121	40.3	123	3.74
DICA	W/B	250,000	-1.8	1.9	9.6	3.9	40	*5.7*[6]	1.94
IMAX	W only	626,000	-2.9	2.3, 3.3, 11	200	17	132	*11.6*	3.59
IMZR	W/B	1,400	1.49	2.1, 3.9	513	51	*ND*	52	3.90
METO	W/B	530	3.4	*NA*	15	21	88	120	2.36
PYRA	W/B	1.9	3.9	*NA*	2.2	33.3	2	9304	0.05
TEBU	W/B	36	3.7	5.0	365	47	43	*769*	1.86

[1]Acronyms: ATRA = atrazine, BENT = betnazon, BOSC = boscalid, CHLO = chlorantraniliprole, CLOP = clopyralid, CLTH = clothianidin, DICA = dicamba, IMAX, imazamox, IMZR = imazethapyr, METO = metolachlor, PYRA = pyraclostrobin, and TEBU = tebuconazole. [2]W = water, B = biomixture; [3]mg L^{-1}; [4]$days^{-1}$; [5]g mL^{-1}; [6]ND = Not documented, [7]italisized values indicate K_{oc} for the Freundlich Isotherm.

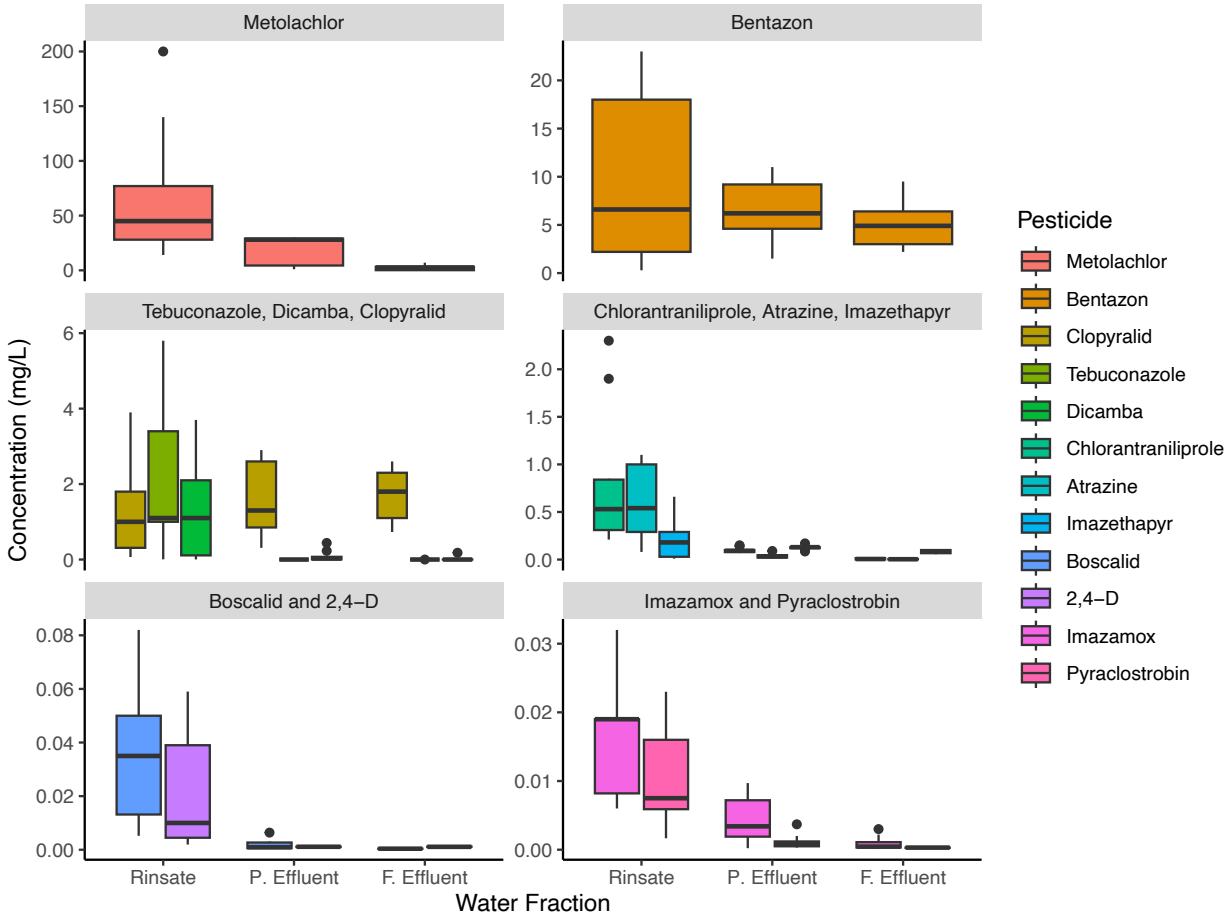

Figure 3.2 Ordered in decreasing rinsate concentration, concentrations of metolachlor, bentazon, clopyralid, tebuconazole, dicamba, chlorantraniliprole, atrazine, imazethapyr, boscalid, 2,4-D, imazamox, and pyraclostrobin quantified in the 2023 operation season for the rinsate, primary effluent, and final effluent. Figure includes imputed <MLQ values for visual clarity.

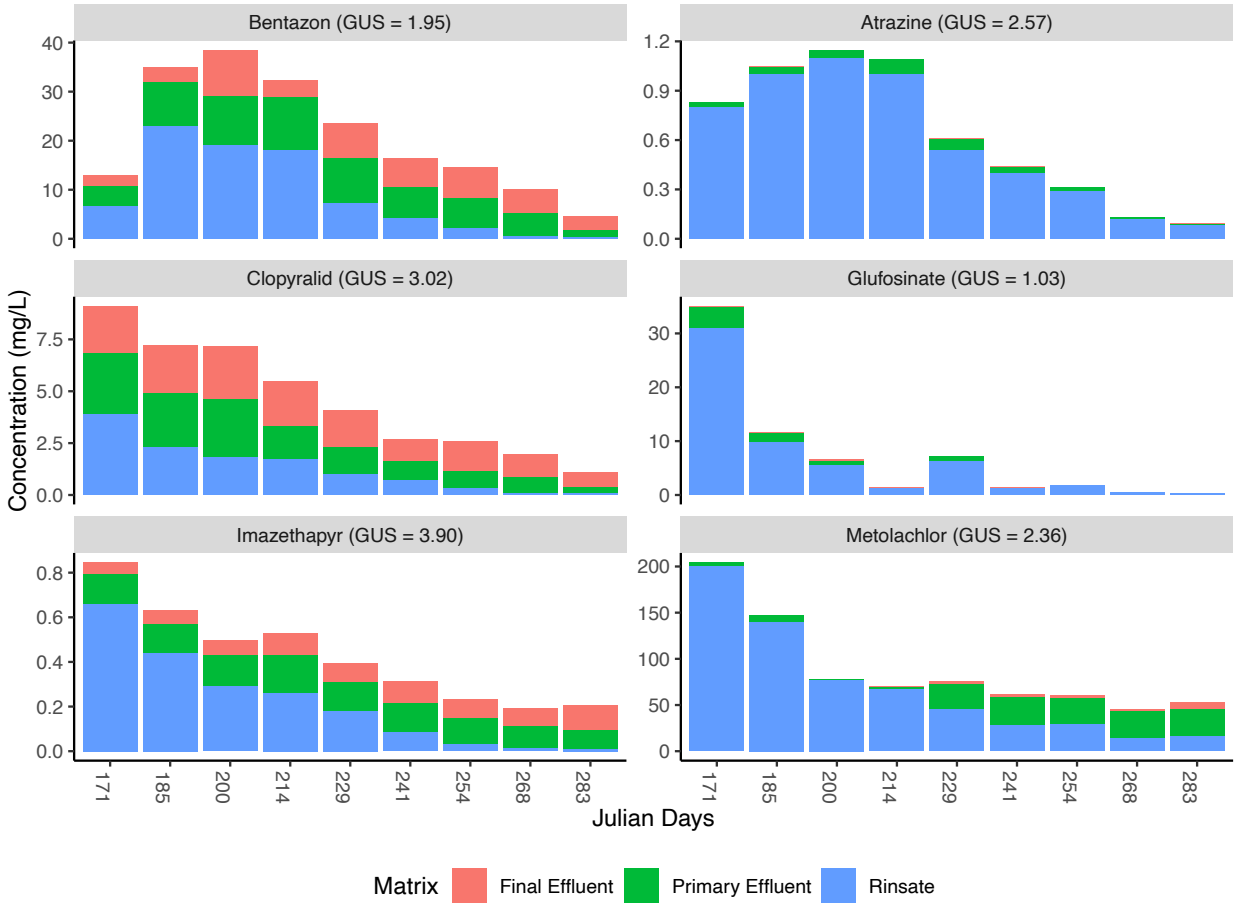

Figure 3.3 Concentrations of bentazon, atrazine, clopyralid, glufosinate (from Chapter 2), imazethapyr, and metolachlor within rinsate, primary effluent, and final effluent across julian days. GUS values are included for posterity.

3.3.2.2 Biomatrix. Overall, concentrations within biobed cell one (46 mg kg^{-1}) > biobed cell two (7.8 mg kg^{-1}), demonstrating that the concentration of pesticides within the water phase effect concentrations within the biomixtures. In addition 2023 (43 mg kg^{-1}) > 2022 (11 mg kg^{-1}) concentrations, indicating a greater pesticide application during the 2023 growing season rather than the 2022 growing season. 2022 was the wettest year recorded in Manitoba (Government of Manitoba 2022) with large delays in planting and farming operations while 2023 conditions, although drier-than-normal, had no delays or major issues; this impacted the type and rates of pesticides that were sprayed due to pest growth and development changing in variable moisture

conditions (Government of Manitoba 2023). Post-operation concentrations (620 mg kg^{-1}) > pre-operation concentrations (30 mg kg^{-1}), demonstrating that pesticides accumulate when rinsate or effluent is applied onto the biobed. Finally, 0-5 cm (250 mg kg^{-1}) > 5-15 cm (190 mg kg^{-1}) = 15-30 cm (200 mg kg^{-1}), indicating that the top 5 cm of the biobed retains the most pesticides due to the intial contact from the irrigation systems.

Clothianidin was detected in the biomatrix in both biobed cell one and two as well as the biomixture compost pile but was never detected in the rinsate or documented that it was sprayed in either 2022 or 2023 (Figure 3.4, 3.5); no other pesticide was detected or quantfied in the biomixture compost pile. Previous studies have shown that clothianidin is a persistent insecticide (Table 3.2) that can remain at low concentrations in soil for ~3 years (Jones et al. 2014; Li et al. 2018). Clothianidin-treated canola was seeded on the farm in the fall 2020 and hence clothianidin residues could have been in the soil used to prepare the biomixture in the fall of 2020.

2,4-D and imazamox were not detected in the biomixture even though both were applied in 2022 and 2023, indicating rapid degradation. This was expected for 2,4-D which had the smallest soil half-life of the twelve pesticides that entered the biobed system (Table 3.1) and was never detected in primary or final effluent. Cessna et al. (2017) demonstrated the rapid and complete dissipation of 2,4-D in biomatrix incubated at 13 °C and 20 °C. However, imazamox has been documented to have greater environmental persistence (Table 3.2) and was quantified in 78% of the primary and 33% of the final effluent samples, so no detections within the biomixture was not expected. Imazamox degradation and sorption is pH-dependent and has greater persistence at pH < 5 and is rapidly degraded at pH > 6.3 (Buerge et al. 2019) and pH = 7 (Aichele and Penner 2005). Substantial sorption of imazamox was observed at soil pH = 5, but was readily desorbed as well (Buerge et al. 2019, Aichele and Penner 2005). Hence, in the biobed system context, it is

possible that imazamox was readily degraded while some imazamox residues leached from biomixtures into effluents whenever rinsate or primary effluent were applied on surfaces. It is also possible that aged sorption of imazamox onto biomixture colloids made imazamox unextractable from the biomatrix.

Other than 2,4-D, clothianidin, and imazamox, ten pesticides were quantifiable within the biomixture (Figure 3.4 and 3.5), in order of increasing concentrations: imazethapyr, atrazine, dicamba, chlorantraniliprole, clopyralid, boscalid, tebuconazole, pyraclostrobin, bentazon, and metolachlor. These ten pesticides had significant interactions across the four factors included in the RM ANOVA: cell (cell *one* and *two*), year (*2022* and *2023*), depth (*0-5*, *5-15*, and *15-30* cm), and time (*pre*- and *post*-operation). However, unlike water fractions, no clear physicochemical characteristic indicated possible biomixture persistence or dissipation. In general, pesticide concentrations in the biomatrix were greater in 2023 than 2022, with data suggesting that pesticide residues remaining post-operation in 2022 are carried over and persist into the 2023 operating season. Pesticide concentrations were typically greater in biobed cell one than biobed cell two. However, 2022 concentrations post-operation were much lower than the post-operation 2023 concentrations. For imazethapyr, metolachlor, chlorantraniliprole, atrazine, and boscalid, since the interactions are ≥3 interaction factors (i.e., *cell x year x depth* or *year x depth x time* comparisons) there were between 28 to 276 comparisons, so comparisons will be discussed in general with means represent general trends.

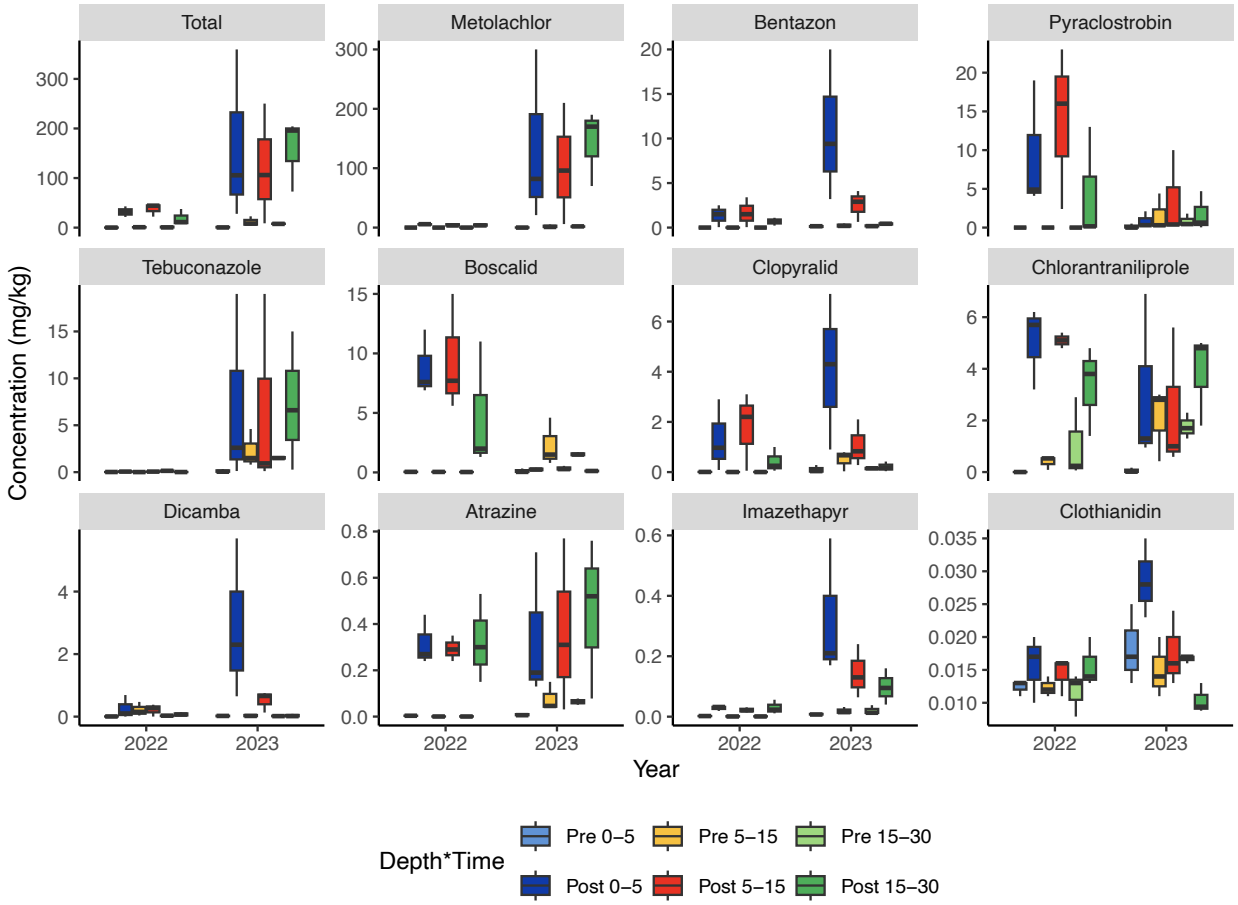

Figure 3.4 Pesticide concentrations quantified within cell one in 2022 and 2023 (including imputed values for visual clarity). Depth* Time factors are highlighted with boxplot colours. “Pre” prefix indicates pre-season operation, “Post” indicate post-season operation; the suffix “0-5”, “5-15”, and “15-30” indicate respective biobed sampling depths in cm.

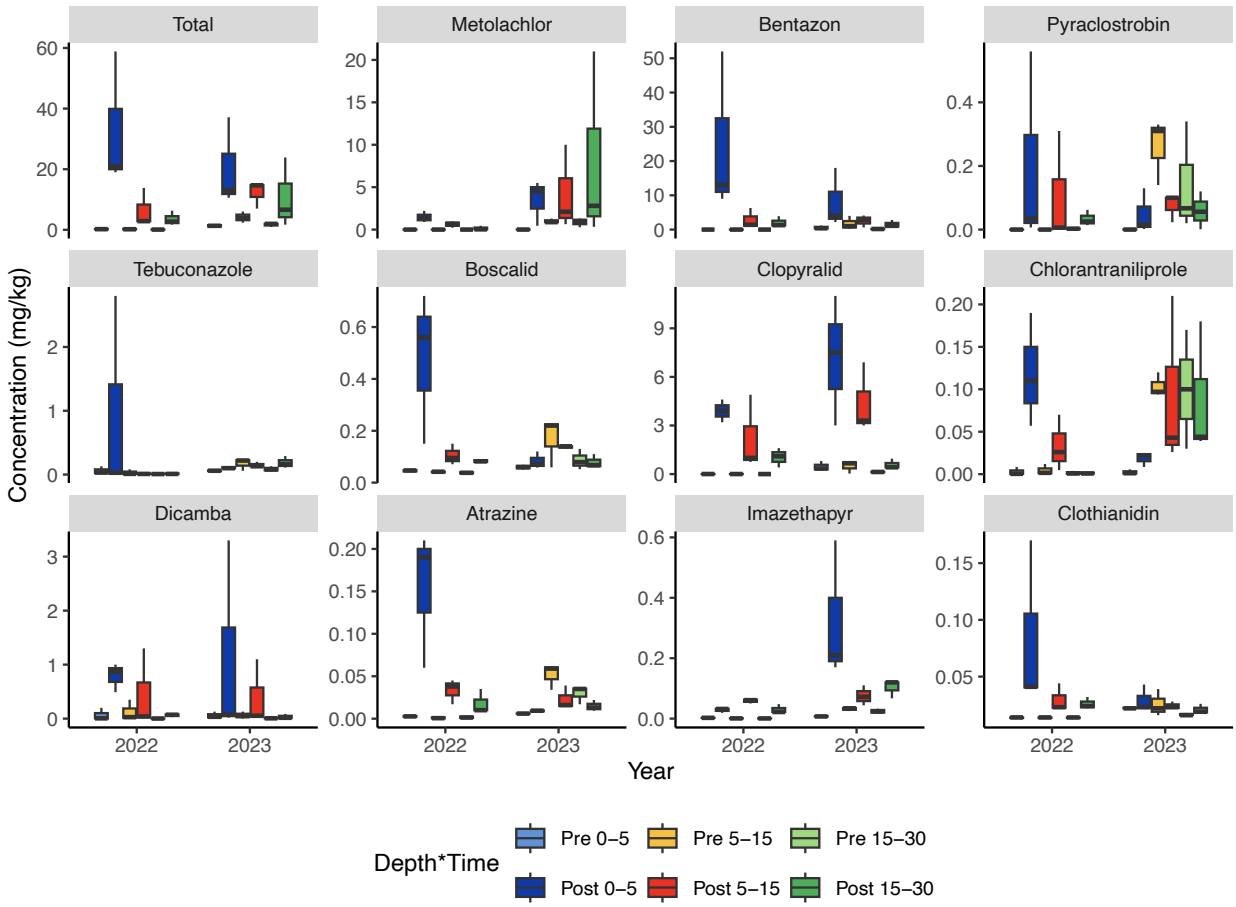

Figure 3.5 Pesticide concentrations quantified within cell two in 2022 and 2023 (including imputed values for visual clarity). Depth* Time factors are highlighted with boxplot colours. "Pre" prefix indicates pre-season operation, "Post" indicate post-season operation; the suffix "0-5", "5-15", and "15-30" indicate respective biobed sampling depths in cm.

Both bentazon and clopyralid showed significant two-way interactions for *depth:time* ($F_{2,16}$ = 59.8, *p-value* < 0.0001 and $F_{2,16}$ = 68.1, *p-value* < 0.0001, respectively) and *year:time* ($F_{1,8}$ = 8.253 *p-value* = 0.0003 and $F_{1,8}$ = 8.126, *p-value* < 0.0001, respectively); no *cell* interaction was found, indicating that bentazon and clopyralid concentrations in cell one (1.5 and 0.86 mg kg^{-1}, respectively) = cell two (3.7 and 1.7 mg kg^{-1}, respectively) (Table 10.2 – 10.5). In general, post season showed significantly greater concentrations than pre-operation samples (Table 3.3; Table 10.6 and 10.8). Depth was not a significant factor pre-operation, but post-operation concentrations

were significantly greater at 0-5 cm depth than the other two depths (Table 3.3). Both bentazon and clopyralid *year:time* interactions (Table 10.7 and 10.9) showed that post-operation concentrations were not significantly different between 2022 and 2023 but post-operation were greater than either pre-operation concentrations (Table 3.3). Thus, concentrations were always greater post season, and compound residues were at the same concentrations in 2022 and 2023. Only bentazon has been studied within biobeds (de Wilde et al. 2009a,b,c) and was found to be homogenous across the matrix regardless of depth. However, in this study, bentazon had homogenous concentrations across depths only pre-operation and not post-operation. Clopyralid has not been previously studied within biomatrix, however this study indicates that its fate is similar to that of bentazon. Bentazon and clopyralid have relatively large water solubilities and similar soil half-lives (Table 3.2).

Tebuconazole showed relatively large variations in concentrations across and within cells, with the following four significant two-way interactions: *cell:year* ($F_{1,8}$ = 6.34, *p-value* = 0.036), *cell:depth* ($F_{2,16}$ = 11.7, *p-value* = 0.0075), *year:depth* ($F_{2,16}$ = 17.7, *p-value* < 0.0001), and *depth:time* ($F_{2,16}$ = 4.62, *p-value* = 0.026) (Table 3.3; Table 10.2 - 10.5). In general, tebuconazole concentrations in cell one (2.1 mg kg^{-1}) > cell two (0.15 mg kg^{-1}), but pairwise comparisons of *depth:time* yielded no significant difference (Table 10.10), while *cell:depth* yielded minimal differences (Table 10.11), therefore will not be discussed further (Table 3.3). *Year:depth* tebuconazole concentration comparisons found that 2023 > 2022 with no differences across depth in either years (Table 3.3; Table 10.12). *Cell:year* tebuconazole interactions found that there were no differences between cells in 2022, however, cell one in 2023 was greater than cell two; 2023 concentrations were greater than in 2022 (Table 3.3; Table 10.13). Romero et al. (2019) found that tebuconazole had minimal degradation within biomixtures, with ~ 90% of applied tebuconazole

remaining within the biomixture after 15 days. Masís-Mora et al. (2020) found no changes in tebuconazole concentration within biomixtures for 50 days. Bernadelli et al. (2021) reported that it required 168 days for complete dissipation of tebuconazole, however, a pre-application advanced oxidative process with UV/H_2O_2 reduced complete dissipation to 84 days. This study supported the current literature that indicates the persistence of tebuconazole within the biomixture.

Pyraclostrobin also had three significant two-way interactions including *year:depth* ($F_{2,16}$ = 5.83, *p-value* = 0.013), *year:time* ($F_{1,8}$ = 9.31, *p-value* = 0.016), and *depth:time* ($F_{2,16}$ = 17.3, *p-value* = 0.0001) (Table 10.2 - 10.5); since *year:depth* had only one difference, it will not be discussed further (Table 3.3; Table 10.14). In general, post operation (2.9 mg kg^{-1}) > pre operation (0.26 mg kg^{-1}), cell one (3.0 mg kg^{-1}) > cell two (0.077 mg kg^{-1}), and 2023 (2.3 mg kg^{-1}) > 2022 (0.79 mg kg^{-1}) concentrations for pyraclostrobin within the biobed. *Depth:time* showed that 0-5 cm pre-operation < all other depths or operation periods, indicating that the yearly biobed top up for biobed rejuvenation influences the biobed; the high heterogeneity found in the data also contributed to a lack of differences (Figure 3.3 and 3.4; Table 10.15). *Year:time* comparisons (Table 10.16) found that the pre-operation 2022 < all other year and time combinations; high variance of the data rendered many pairwise comparisons insignificant. As of writing this thesis, no study (known to the author) currently quantifies or monitors pyraclostrobin fate within biobeds, demonstrating a first describing pyraclostrobin fate within biobed systems.

Dicamba had a significant three-way interaction of *cell:year:depth* ($F_{2,16}$ = 4.48, *p-value* = 0.028), however, no significant differences were detected in follow-up pairwise comparisons; therefore, two-way interactions of *cell:depth* ($F_{2,16}$ = 3.72, *p-value* = 0.047), *year:depth* ($F_{2,16}$ = 4.91, *p-value* = 0.022), and *depth:time* ($F_{2,16}$ = 6.6, *p-value* = 0.008) were tested (Table 3.3; Table 10.2 - 10.5). Minimal differences were detected for *cell:depth* (Table 3.3; Table 10.17) or

year:depth (Table 10.18), therefore both will not be discussed further due to limited inference. Finally, *depth:time* interaction showed that there were significant increases of concentration top 5 cm of the biomixture from pre- to post-operation (Table 3.3; Table 10.19), but no differences were detected between pre- and post- operation for 5-15 and 15-30 cm depths. *Depth:time* interactions indicate an accumulation of dicamba in the top 5 cm of the biomatrix over the operation season while there are minimal differences between the deeper layers due to limited concentrations reaching lower depths. Fatema et al. (2022) found that ~88% of dicamba is removed from the water phase while ~80% was removed in Cooper et al. (2016); however, there are currently no studies monitoring dicamba fate within biomixtures. This study indicates that dicamba is retained within the top 5 cm of biomixture with minimal differences >5 cm depths.

Imazethapyr showed two three-way interactions to be significant, *cell:year:time* (*F-value* = 10.9, *p-value* = 0.011) and *year:depth:time* (*F-value* = 11.2, *p-value* = 0.0009) (Table 10.2 – 10.5); although significant, *cell* appears to have little to no influence on significant pairwise effects. Pairwise comparisons of imazethapyr *cell:year:time* interaction suggested that imazethapyr concentrations increased after each operation season (Table 3.4; Table 10.20) within the biobed system but no difference was detected between the non-operational period between 2022 and 2023. For *year:depth:time*, 0-5 cm was only significant after the yearly 5 cm top-up of biobed cells due to concentrations being <MLQ, experiencing the greatest concentration fluctuation between pre- and post-operation (Table 3.4); all other depths were equivalent to each other with differences predominantely from year of operation (Table 10.21). Imazethapyr was detectable within biomixture and this persistence is consistent with what has been observed for the behaviour of imazethapyr in soils. Imazethapyr sorption is enhanced at lower pH (~5.5) and has relatively long half-lives in soil including detectable levels remaining in soil within the next year (Bresnahan et

Table 3.3 Overview of compounds with two-way interactions. Mean concentrations are indicated in case of significant two-way interactions and all numbers are in mg kg^{-1}. *Cell:time* had no significance, so was not included. *Italics* indicate significantly different interactions but yields no additional information about compound fate. PO = Post, PR = Pre, '22 = 2022, '23 = 2023, C1 = Cell 1, C2 = Cell 2.

Compound	*year:time*	*depth:time*	*year:depth*	*cell:depth*	*cell:year*
Bentazon	PO (4.9) > PR (0.25) PO: '22 (5.5) = '23 (4.3) 2023 PR (0.51) > 2022 PR (<MLQ)	PO (15) > PRE (0.77) PR: 0-5 cm (0.18) = 5-15 cm (0.50) = 15-30 cm (0.09) PO: 0-5 cm (11) > 5-15 cm (2.4) = 15-30 cm (1.2)	-	-	-
Clopyralid	PO (2.3) > PR (0.15) PO: '22 (2.9) = '23 (1.8) PR: '23 PR (0.3) > '22 PR (<MLQ)	PO (7.0) > PRE (0.46) PR: 0-5 cm (0.14) = 5-15 cm (0.25) = 15-30 cm (0.067) PO: 0-5 cm (4.1) > 5-15 cm (2.4) = 15-30 cm (0.57)	-	-	-
Tebuconazole	-	-[1]	'23 (2.2) > '22 (0.11) '22: 0-5 cm (0.27) = 5-15 cm (0.029) = 15-30 cm (0.042)	*C2 15-30* cm *(0.074)* < *C1 5-15* cm *(2.2)* = *C1 15-30* cm *(2.3)* *C1 15-30* cm *(2.3)* > *C2 5-15* cm *(0.093)* = *C2 15-30* cm *(0.074)*	'22 (0.11) > '23 (2.2) C1 '22 (0.05) = C2 '22 (0.18) C1 '23 (4.2) > C2 '23 (0.13)

			’23: 0-5 cm (1.9) = 5-15 cm (2.3); 5-15 cm = 15-30 cm (2.3); but 0-5 cm < 15-30 cm		
Pyraclostrobin	PR ’22 (<MLQ) < ’23 (0.79) PR ’22 < PO ’22 (4.6) PO’22 = ‘23	PR 0-5 cm (<MLQ) < PO cm (2.9) PR cm 0-5 < PR cm 5-15 cm (0.47) = PR 15-30 cm (0.25) PO = PR 5-15 cm = PR 15-30 cm	*’22 15-30* cm *(1.1) < ’23 5-15* cm *(1.4)*	-	-
Dicamba	-	PR 0-5 cm (0.037) > PO 0-5 cm (1.3) = PO 5-15 cm (0.39) PR 15-30 cm (0.013) < PO 0-5 cm = PR cm 5-15 (0.11) = PO cm 5-15 PO cm 0-5 > PO cm 15-30 (0.051)	*’23 0-5* cm *(1) = ’23 5-15* cm *(0.25) > ’22 5-15* cm *(0.025) = ’22 15-30 cm (0.04)*	*C2 15-30* cm *(0.04) > C2 5-15* cm *(0.25) = C2 0-5* cm *(0.51) = C1 5-15* cm *(0.25)*	-

[1]RM ANOVA was significant but no significant post-hoc comparison emerged.

Table 3.4 An overview of general trends for compounds in the case of three-way significant interactions; mean concentrations are not statistical tests but general trends seen within the data for simpler interpretation. All values within parantheses are mg kg^{-1}. PO = Post, PR = Pre, '22 = 2022, '23 = 2023, C1 = Cell 1, C2 = Cell 2.

Compound	Year	Cell	Time	Depth	Interaction	Interaction of interest
Imazethapyr	'23 > '22	C1 = C2	PO > PR	0-5 cm = 5-15 cm = 15-30 cm	*cell:year:time*	PR '22 (<MLQ) < PO '22 (0.061) = PR '23 (0.037) < PO '23 (0.37)
					year:depth:time	PR 0-5 cm (<MLQ) < PO 0-5 cm (0.17)
Metolachlor	'23 > '22	C1 > C2	-	-	*cell:year:depth*	'23 C1 > '22 C1 > '23 C2 > '22 C2 '22 C1 = '23 C2
Chlorantraniliprole	'23 = '22	C1 > C2	-	0-5 cm > 5-15 cm or 15-30 cm	*cell:year:depth*	C1 '22 = C1 '23 C2 '22 = C2 '23
Atrazine	'23 > '22	-	PO > PR	0-5 cm = 5-15 cm = 15-30 cm	*year:depth:time*	PO '22 = PO '23 PR '23 = PO '23 PR '22 < PO '23

Table 3.5 An overview of general trends for boscalid, which had a significant four-way interaction; mean concentrations are not statistical tests but general trends seen within the data for simpler interpretation. PO = Post, PR = Pre, ’22 = 2022, ’23 = 2023, C1 = Cell 1, C2 = Cell 2.

Compound	Interaction	Cell	Year	Intra-Year	Time	Depth
Boscalid	*cell:year:depth:time*	C1 > C2	‘22 = ‘23	‘22	PO (3.9) > PR (0.041)	0-5 cm (2.3) = 5-15 cm (2.4) > 15-30 cm (1.2)
				‘23	PO (0.71) > PR (0.17)	0-5 cm (0.13) < 5-15 cm (0.74) > 15-30 cm (0.45) 0-5 cm < 15-30 cm

al. 2000; Aichele and Penner 2005).

Metolachlor had a significant three-way interaction with *cell:year:depth* (*F-value* = 5.65, *p-value* = 0.014) (Table 10.2 – 10.5). Concentrations were generally larger in 2023 than 2022, and in cell one than cell two (Table 3.4). Thus, not surprisingly, across *cell* years* combinations, significantly higher concentrations were found in cell one in 2023 relatively to 2022 or cell two (Table 10.22). In addition, cell comparisons across found that cell one concentrations in 2022 were generally lower than in 2023, while cell two had a little-to-no difference in concentrations between years. No differences across *depths* were observed within each *cell*year* combination (Table 3.4). Chlorantraniliprole had a significant three-way interaction with *cell:year:depth* (*F-value* = 17.2, *p-value* = 0.0001) (Table 10.2 – 10.5). Like metolachlor, concentrations were generally larger in in cell one than cell two (Table 3.4; Table 10.23). Concentrations in 2023 were similar to those in 2022 and the concentrations of cell one in 2022 were statistically similar to the concentrations of cell two in 2023. Chlorantraniliprole appeared to be influenced by depth with visual inspection of graphs indicating that there were large concentration increases in the top 5 cm that were comparable to the deeper levels.

Atrazine had a significant three-way interaction with *year:depth:time* ($F_{2,16}$ = 8.87, *p-value* = 0.003); interestingly, although numerically greater in cell one (0.18 mg kg^{-1}) > two (0.029 mg kg^{-1}), it was not statistically significant in the RM ANOVA (Table 3.4; Table 10.2 - 10.5). All pre depths in 2022 (0.0014 mg kg^{-1}) < all 2022 post depths (0.19 mg kg^{-1}), however when comparing *depth* and *time* across both *years*, all 2022 pre-operation depths were significantly different in concentrations from post 2022 and 2023 samples, but 2023 post depths were not different from 2022 post and 2023 pre depths (Table 3.4; Table 10.24). Atrazine has been frequently studied within biobed systems and is shown to rapidly disspate within biomixtures, achieving >90%

degradation within 60 days of application (Diez et al. 2015; Elgueta et al. 2016; Córdova-Méndez et al. 2021). Guillen Garcés (2007) indicated that low nitrogen conditions increase atrazine dissipation due to the microbial communties utilizing the triazine ring as a nitrogen source; since no fertilizer is applied to the biobed, low nitrogen conditions within the biobed could explain the atrazine fate within the biobed, specifically with the low carry-over between years.

Boscalid was the only pesticide with a significant four-way interaction between *cell:year:depth:time* ($F_{2,16}$ = 7.32, *p-value* = 0.006) with 276 pairwise comparisons (Table 3.5; Table 10.2-10.5). No statistical differences were detected for cell two between 2022 (0.13 mg kg^{-1}) and 2023 (0.10 mg kg^{-1}); boscalid appears to be predominantely retained in cell one, therefore cell two will not be discussed further. Boscalid concentrations generally were retained within cell one (Table 3.5; Table 10.25), with significant differences in 2022 pre operation < 2022 post operation; the top 15 cm had greater concentrations than the 15-30 cm depth. However, in 2023, cell one concentrations in pre operation > post operation; the top 5 cm had lower concentrations than the bottom layers, indicating that boscalid applied in 2022 persisted into 2023 and continued to degrade. Based off of the concentrations, boscalid was still prevalent within the biomixture after the 2022 applications, but the amount of boscalid applied to the biobed in 2023 was lower, resulting in continued decrease of boscalid concentrations from pre to post operation in 2023. Mukherjee et al. (2016a) found that ^{14}C-labelled boscalid half-lives in biomixtures composed of digestate and biochar varied between 25 to 195 $days^{-1}$; this was indicated to be related to total adsorption of boscalid onto biomixtures (Mukherjee et al. 2016b). Boscalid half-lives in biobeds appear to be shorter or equal to in-field values found in Table 3.2; as boscalid concentrations did not move within the biobed, the strong sorption of boscalid within the biomixtures prevented leaching from the biomixture into effluents.

3.5 Conclusions

An analytical method for analyzing 84 pesticides was successfully developed, validated, and applied to an operational biobed in Carman, Manitoba. Validation data indicate good method performance and the method was able to counter matrix effects through isotope dilution. Field data indicated that pesticide concentrations are signficiantly reduced from rinsate to final effluent. Pesticide concentrations were significantly reduced with one biobed cell, with no detections of 2,4-D, boscalid, pyraclostrobin, tebuconazole in the final effluent. However, chlorantraniliprole, dicamba, metolachlor, imazamox, and imazethapyr remediation was improved with a second cell. Bentazon and clopyralid experienced no reduction in the dual-cell biobed. Biomixtures retained most pesticides within cell one, except for bentazon, clopyralid, and imazethapyr, which were found equally distributed across cells. 2,4-D and imazamox rapidly dissipated within biomixtures, while pyraclostrobin, tebuconazole, and imazethapyr accumulated within cells. Overall, biobeds are effective tools at reducing point-source pollution from agricultural spraying activities; one biobed cell is adequate, two cells are able to further reduce pesticide concentrations, especially for imazethapyr and metolachlor.

3.6 References

Agriculture and Agri-Food Canada (AAFC). 2025. Canada: outlook for principal field crops, 2025. Available from https://agriculture.canada.ca/sites/default/files/documents/2025-03/canada_outlook_for_principal_field_crops_202503.pdf

Ahmad, U., and Sharma, L. 2023. A review of Best Management Practices for potato crop using Precision Agricultural Technologies. Smart Agric. Technol. **4**: 100220.

Aichele, T.M. and Penner, D. 2005. Adsorption, desorption, and degradation of imidazolinones in soil. Weed Technol. **19(1)**: 154-159.

Anastassiades, M., Schäfer, A-K., Kolberg, D.I., Eichhorn, E., Dias, A., Benkenstein, A., Zechmann, S., Mack, D., Wildgrube, C., Barth, A., Sigalov, I., Goerlich, S., Dörk, D., and Cerchia, G. 2023. Quick method for the analysis of highly polar pesticides in food involving extraction with acidified methanol and LC- or IC-MS/MS Measurement I. Food of Plant Origin (QuPPe-PO-Method) Version 12.2. Available from https://www.eurl-pesticides.eu/userfiles/file/EurlSRM/EurlSrm_meth_QuPPe_PO_V12_2.pdf [Accessed 23 July 2025].

Bergsveinson, J., Perry, B.J., Sheedy, C., Braul, L., Reedyk, S., Gossen, B.D., and Yost, C.K. 2018. Identifying the core bacterial and fungal communities within four agricultural biobeds used for the treatment of pesticide rinsates. J. Appl. Microbiol. **125(5)**: 1333-1342.

Bernardelli, P.V., Nagel-Hassemera, M.E., and Geblerb, L. 2021. Introduction of advanced oxidative pre-treatment in the Biobed reactor system in the final disposal process of pesticide effluents. Chem. Eng. Trans., **86**: 685-690.

Braul, L., Reedyk, S., and Sheedy, C. 2018. A robust biobed design for managing pesticide rinsate under Canadian conditions – Construction, operation and maintenance manual. Agriculture and Agri- Food Canada, Regina, Saskatchewan, Canada.

Bresnahan, G., Koskinen, W., Dexter, A., and Lueschen, W. 2000. Influence of soil pH-sorption interactions on imazethapyr carry-over. J. Agric. Food Chem. **48**: 1929-1934.

Buerge, I.J., Bächli, A., Kasteel, R., Portmann, R., López-Cabeza, R., Schwab, L.F., and Poiger, T. 2019. Behavior of the chiral herbicide imazamox in soils: pH-dependent, enantioselective degradation, formation and degradation of several chiral metabolites. Environ. Sci. Technol. **53**: 5725−5732

Carter, A. 2000. How pesticides get into water – and proposed reduction measures. Pestic. Outlook, **11(4)**: 149-156.

Cessna, A., Knight, J.K., Ngombe, D., and Wolf, T.M. 2017. Effect of temperature on the dissipation of seven herbicides in a biobed matrix. Can. J. Soil Sci. **97(4)**: 717-731.

Chasto, T. Benaragama, D.I., Leeson, J., and Willenborg, C.J. 2024. The impact of herbicide-resistant canola systems on the weed community dynamics in the Canadian Prairies. Can. J. Plant Sci. 104: 514–528.

Cooper, R.J., Fitt, P., Hiscock, K.M, Lovett, A.A., Gumm, L., Dugdale, S.J., Rambohul, J., Williamson, A., Noble, L., Beamish, J., and Hovesen, P. 2016. Assessing the effectiveness of a three-stage on-farm biobed in treating pesticide contaminated wastewater. J. Environ. Manag. **181**: 874-882

Córdova-Méndez, E.A., Góngora-Echeverría, V.R., González-Sánchez, A., Quintal-Franco, C., Giácoman-Vallejos, G., and Ponce-Caballero, C. 2021. Pesticide treatment in biobed systems at microcosms level under critical moisture and temperature range using an orthic solonchaks soil from southeastern Mexico amended with corn husk as support. Sci. Total Environ. **772**: 145038.

Diez, M.C., Schalchli1, H., Elgueta, S., Salgado, E., Millahueque, N., Rubilar, O., Tortella, G.R., and Briceño, G. 2015. Rhizosphere effect on pesticide degradation in biobeds under different hydraulic loads. J. Soil Sci. & Plant Nutr. **15(2)**: 410-421.

Elgueta, S.,, Santosa, C., Limab, N., and Diez, M.C. 2016. Atrazine dissipation in a biobed system inoculated with immobilized white-rot fungi. Arch. Agron. Soil Sci. **62(10)**: 1451–1461.

Farenhorst, A., and Bowman, B. 1998. Competitive sorption of atrazine and metolachlor in soil. J. Environ. Sci. Health B **33(6)**: 671-682.

Fatema, M., Farenhorst, A., and Sheedy, C. 2022. Using the Pesticide Toxicity Index to Show the Potential Ecosystem Benefits of On-farm Biobeds. J. Environ. Quality. **51(5)**: 1044-1053.

Gamhewage, M., Sheedy, C., Munira, S., and Farenhorst, A. 2021. Pesticide mixtures in the water-column versus bottom-sediments of prairie rivers. Bull. Environ. Contam. Toxicol. **106**: 936–941.

Glozier, N.E., Struger, J., Cessna, A.J., Gledhill, M., Rondeau, M., Ernst, W.R., Sekela, M.A., Cagampan, S.J., Sverko, E., Murphy, C.,Murray, J.L., and Donald, D.B. 2012. Occurrence of glyphosate and acidic herbicides in select urban rivers and streams in Canada, 2007. Environ. Sci. Pollut. Res. **19**:821-834.

Góngora-Echeverría, V.R. Quintal-Franco, C., Arena-Ortiz, M.L., Giácoman-Vallejos, G., and Ponce-Caballero, C. 2018. Identification of microbial species present in a pesticide dissipation process in biobed systems using typical substrates from southeastern Mexico as a biomixture at a laboratory scale. Sci. Total Environ. **628-629**: 528-538.

Government of Manitoba. 2022. Issue 26 (Week 44) – November 1, 2022 Seasonal Summary Crop Report. Available from https://www.gov.mb.ca/agriculture/crops/seasonal-reports/crop-report-archive/pubs/seasonal-summary-11-01-2022.pdf [Accessed 11 June 2025].

Government of Mantioba. 2023. Issue 24 (Week 43) – October 25, 2023 Seasonal Summary Crop Report. Available from https://www.gov.mb.ca/agriculture/crops/seasonal-reports/crop-report/pubs/crop-seasonal-summary-10-25-2023.pdf [Accessed 11 June 2025].

Guillen Garcés, R.A. Hansen, A.M., and van Afferden, M. 2007. Mineralization of atrazine in agricultural soil: inhibition by nitrogen. Environ. Toxicol. Chem. **26(5)**: 844–850.

Gustafson, D.I. 1989. Groundwater ubiquity score: a simple method for assessing pesticide leachability. Environ. Toxicol. Chem. **8**: 339-357.

Guyot, C. 1994. Strategies to Minimize the Pollution of Water by Pesticides. Börner, H. (Eds.) Pesticides in Ground and Surface Water. Chemistry of Plant Protection, Volume 9. Springer, Berlin, Heidelberg.

Helweg, A., Bay, H., Hansen, H.P.B., Rabølle, M., Sonnenborg, A., and Stenvang, L. 2002. Pollution at and below sites used for mixing and loading of pesticides. Intern. J. Environ. Anal. Chem. **82(8-9)**: 583-590.

Izma, G., Raby, M., Prosser, R. and Rooney, R., 2024. Urban-use pesticides in stormwater ponds and their accumulation in biofilms. Sci. Total Environ. **918**: 170534.

Johnson, S. 2024. Management of agricultural pesticide rinsate using a biobed under Manitoba conditions. MSc. Thesis, University of Manitoba, Winnipeg, Canada. Available from https://mspace.lib.umanitoba.ca/server/api/core/bitstreams/05b7f34e-0fb0-4cb9-8c12-1057271e8d95/content [Accessed 18 March 2025].

Jones, A., Harrington, P., and Turnbull, G. 2014. Neonicotinoid concentrations in arable soils after seed treatment applications in preceding years. Pest Manag. Sci. **70**: 1780–1784.

Karanasios, E., Tsiropoulos, N.G., Karpouzas, D.G., and Ehaliotis, C. 2010. Degradation and Adsorption of Pesticides in Compost-Based Biomixtures as Potential Substrates for Biobeds in Southern Europe. J. Agric. Food Chem., **58**: 9147–9156.

Kassambara, A. 2023a. rstatix: pipe-friendly framework for basic statistical tests. R package version 0.7.2, https://CRAN.R-project.org/package=rstatix.

Kassambara, A. 2023b. ggpubr: 'ggplot2' based publication ready plots. R package version 0.6.0, https://CRAN.R-project.org/package=ggpubr.

Lemon, J. 2006. plotrix: a package in the red light district of R. R-News, **6(4)**: 8-12.

Lenth, R. 2024. emmeans: Estimated Marginal Means, aka Least-Squares Means. R package version 1.10.0, https://CRAN.R-project.org/package=emmeans.

Lewis, K.A., Tzilivakis, J., Warner, D. and Green, A. 2016. An international database for pesticide risk assessments and management. Human and Ecological Risk Assessment: An International Journal, 22(4), 1050-1064.

Li, Y., Su, P., Li, Y., We, K., Bi, G., and Cox, M. 2018. Adsorption-desorption and degradation of insecticides clothianidin and thiamethoxam in agricultural soils. Chemosphere **207**: 708-714

Magnusson, B., and Örnemark, U. (eds.) 2014. Eurachem Guide: The Fitness for Purpose of Analytical Methods – A Laboratory Guide to Method Validation and Related Topics, 2nd ed. Available from www.eurachem.org.

Marttila, M. 2024. censlm: censored linear models. R package version 0.0.0.9001, commit 8b43af1e5ed8601c7705043d3d82f3450bbe651d, https://github.com/mikmart/censlm.

Masís-Mora, M., Beita-Sandí, W., Rodríguez-Yáñez, J., and Rodríguez-Rodríguez, C.E. 2020. Validation of a methodology by LC-MS/MS for the determination of triazine, triazole and organophosphate pesticide residues in biopurification systems. J. Chromatogr. B, **1156**: 122296.

McCallum, B.D., Geddes, C.M., Chatterton, S., Peng, G., Carisse, O., Turkington, T.K., Olfert, O., Leeson, J., Sharpe, S., Stephens, E., Hervet, V., Aboukhaddour, R. and Vankosky, M. 2021. We stand on guard for thee: a brief history of pest surveillance on the Canadian prairies. Crop Prot. **149**: 105748.

Mukherjee, S., Tappe, W., Weihermüller, L., Hofmann, D., Köppchen, S., Laabs, V., Schroeder, T., Vereecken, H., and Burauel, P. 2016a. Dissipation of bentazone, pyrimethanil and boscalid in biochar and digestate based soil mixtures for biopurification systems. Sci. Total Environ. **544**: 192-202.

Mukherjee, S., Weihermüller, L., Tappe, W., Hofmann, D., Köppchen, S., Laabs, V., Schroeder, T., Vereecken, H., and Burauel, P. 2016b. Sorption–desorption behaviour of bentazone, boscalid and pyrimethanil in biochar and digestate based soil mixtures for biopurification systems. Sci. Total Environ. **559**: 63-73.

Müller, K., Bach, M., Hartmann, H., Spiteller, M., and Fredem H-G. 2002. Point- and nonpoint-source pesticide contamination in the Zwester Ohm catchment, Germany. J. Environ. Qual. **31**:309–318.

Munira, S., Farenhorst, A., Saptoka, K., Nilsson, D., and Sheedy., C. 2018. Auxin herbicides and pesticide mixtures in groundwater of a Canadian prairie province. J. Environ. Qual., **47**: 1462-1467.

Popov, V.H., Cornish, P.S., and Sun, H. 2006. Vegetated biofilters: The relative importance of infiltration and adsorption in reducing loads of water-soluble herbicides in agricultural runoff. Agric. Ecosyst. Environ. **114**: 351-359.

R Core Team. 2023. R: A Language and Environment for Statistical Computing. R Foundation for Statistical Computing, Vienna, Austria. https://www.R-project.org/.

Reichenberger, S., Bach, M., Skitschak, A., and Frede, H-G. 2007. Mitigation strategies to reduce pesticide inputs into ground- and surface water and their effectiveness: a review. Sci. Total Environ. **384**: 1-35.

Rezende, S., Cesio, M.V., Acrhondo, L., Russi, C., Martínez, P., Rivero, A., Hladki, R., Heinzen, H., and Besil, N. 2021. Pilot study of biobeds application for the remediation of citrus agro-industrial wastewaters. Int. J. Environ. Anal. Chem., **103(20)**: 9698-9714.

Romero, E., Delgado-Moreno, L., and Nogales, R. 2019. Pesticide Dissipation and Enzyme Activities in Ungrassed and Grassed Biomixtures, Composed of Winery Wastes, Used in Biobed Bioremediation Systems. Water Air Soil Pollut **230**: 33.

Sass, J.B., and Colangelo, A. 2006. European Union bans atrazine, while the United States negotiates continued use. Int. J. Occup. Environ. Health **12(3)**: 260-267.

Sheedy, C., Kromrey, N., Nilsson, D., and Armitage, T., 2019. From peaks to prairies: a time-of-travel synoptic survey of pesticides in watersheds of southern Alberta, Canada. Inland Waters **9(4)**: 438-452.

Spanoghe, P., Maes, A., and Steurbaut, W. 2004. Limitation of point source pesticide pollution: results of bioremediation system.Comm. Appl. Biol. Sci. **69(4)**: 719-732.

Spliid, N.H., and Køppen, B. 1998. Occurrence of pesticides in Danish shallow ground water. Chemosphere **37(7)**: 1307-1316.

Stone, P.J., Hitchcock, J., Roy, J-F., and Deckers, C. 2020. Determination of pesticides and mycotoxins in cannabis flower as defined by legalized U.S. state recreational cannabis regulations: a combined LC/MS/MS analysis method. Agilent Technologies Application Note 5994-1734EN.

Wickham, H. 2016. ggplot2: Elegant Graphics for Data Analysis. Springer-Verlag New York.

de Wilde, T., Mertens, J., Šimůnek, J., Sniegowski, K., Ryckeboer, J., Jaeken, P., Springael, D., and Spanoghe, P. 2009a. Characterizing pesticide sorption and degradation in microscale biopurification systems using column displacement experiments. Environ. Pollu., **157**: 463-473.

de Wilde, T., Spanoghe, P., Mertens, J., Sniegowski, K., Ryckeboer, J., Jaeken, P., and Springael, D. 2009b. Characterizing pesticide sorption and degradation in macro scale biopurification systems using column displacement experiments. Environ. Pollu., **157**: 1373-1381.

de Wilde, T., Spanoghe, P., Ryckeboer, J., Jaeken, P. and and Springael, D. 2009c. Sorption characteristics of pesticides on matrix substrates used in biopurification systems. Chemosphere **75**: 100–108.

Wilson, J.L. 2012. Agricultural Pesticide Use Trends in Manitoba and 2,4-D Fate in Soil. Ph.D. Thesis, The University of Manitoba, Available from: https://mspace.lib.umanitoba.ca/server/api/core/bitstreams/b778cd5d-03dc-48c3-_83ba-b9fbfb0eef4d/content [Accessed 9 April 2025].

Xu, S., Chen, M., Feng, T., Zhan, L., Zhou, L., Yu, G. 2021. Use ggbreak to effectively utilize plotting space to deal with large datasets and outliers. Front. Genet. **12**: 774846.

4. OVERALL CONCLUSIONS

4.1 Summary of Research

This research validated analytical methods to assess the performance of a dual-cell biobed system designed to process pesticide rinsate into cleaner water prior to disposal into the broader environment. For the multi-residue method that was developed (Chapter 3), five internal standards were used for isotope dilution (2,4-D-$^{13}C_6$, bentazon-d_7, tebuconazole-d_9, thiamethoxam-d_4, and metolachlor-d_6), thereby reducing analytical costs while providing good internal standard relative responses for all compounds quantified. The use of internal standards countered rinsate matrix effects for all compounds except fensulfothion, cyantraniliprole, dimethomorph II, and fludioxinil accuracies with unreliable recoveries (<70% or >130%) based on EURACHEM guidelines. Due to strong matrix effects, rinsate samples needed to be diluted ten times as part of the the broad-spectrum method delevoped in this study (Chapter 3). Effluent samples did not require an initial dilution for compounds to be quantified but both oxamyl and dinotefuran showed unreliable recoveries, i.e., >130% for the initial and 1/10 diluted sample, respectively. Similar to Chapter 2, the direct-injection and minimal processing of samples resulted in an extraction that could be completed within two hours with minimal risks for errors, while also being cost-efficient.

The analytical methods were successfully applied to rinsate, effluent and biomixture samples taken from the operational biobed situated on the University of Manitoba's Ian N. Morrison Research Farm in Carman, Manitoba. In total, 27 rinsate and effluent samples, and 72 biomixture samples were processed. With the ability for direct injection in the analytical methods,

sample processing time was rapid (< one day), including sample filtering, dilution and LC-MS/MS worklist set-up and quantifications. For the biomixture extractions, the broad-spectrum method required phase-separation with QuEChERS (for compounds with larger K_{ow}'s) or protic, acidic solvents with QuPPe (for acidic and mobile (GUS > 2.8) pesticides such as clopyralid) (Chapter 3). Unlike the negative K_{ow}'s and zwitterionic nature of glyphosate, glufosinate, and AMPA (Chapter 2), the use of an organic solvent is required to counter sorption forces of the predominantly positive K_{ow} compounds for quantification in Chapter 3. Although not all compounds that could be analyzed for were extracted by broad-spectrum method, the majority of compounds (80% of total) were extractable with a modified QuEChERS and QuPPe extraction. Each of these extractions had a similar time-commitment as the extraction that was separately developed for quantifying glyphosate, glufosinate, and AMPA in biomixtures (~6 hours for 18 samples).

The pesticide active ingredients detected had water solubilities ranging from 0.88 to 1,470,000 mg L^{-1} and GUS ranging from 0.05 to 3.9 (Table 4.1) with the following distributions: 37.5% compounds with a GUS > 2.8 (high potential for movement to groundwater); 37.5% compounds with a GUS ranging from 1.8 to 2.8 (moderate potential for movement to groundwater) and 25 % compounds with a GUS ranging from 0 to 1.8 (low potential for movement to groundwater). GUS was not a strong indicator in predicting compounds detected in effluent because the 11 different compounds detected in the final effluent ranged in GUS values from 0.29 to 3.9 (versus 0.05 to 3.9 for the 14 pesticide active ingredients and AMPA in rinsate). The 14 different compounds detected in the biomatrix of the biobed cells also had GUS values ranging from 0.05 to 3.9. Clothianidin was only detected within the biomixture and never in rinsate or

effluent; with no indication of previous application via rinsate prior to 2023, however, it was applied as a seed treatment to soil in 2022.

Rinsate was applied to the biobed using drip irrigation and for most pesticide active ingredients, the biobed system was able to effectively reduce the pesticide concentrations from rinsate to effluents. Generally, total pesticide concentrations were greater in the biomatrix of cell one than cell two, suggesting pesticide sorption. For most pesticides, significant concentration reductions were found between rinsate and primary effluent samples, particularly for pesticide active ingredients with large soil or sediment K_{oc} values. Overall, the research conducted shows the effectiveness of the dual-cell biobed in reducing large pesticide concentrations in rinsate from sprayer cleaning to much smaller levels, with some compounds not detected in primary and/or final effluents and showing 100% dissipation.

Summarizing the biobed efficacy for 14 pesticide active ingredients and AMPA detected in the biobed system (Table 4.2): two (13%) compounds primarily dissipated, ten (66%) compounds were predominantly retained within the first biobed cell, and three (21%) compounds were equally distributed across cell one and two (Table 4.2). Specifically, 2,4-D, boscalid, pyraclostrobin, and tebuconazole were not detected in either primary or final effluent. 2,4-D has a short soil half-life (4.4 days: Table 4.1) and was not detected in the biomatrix of either biobed cells, hence rapidly degraded. Boscalid, pyraclostrobin, and tebuconazole were detected in the biomatrix and each of these compounds have large Koc values (Table 4.1) hence were persistent and strongly retained in the biomatrix rather than having the tendency to be transported within the biobed system.

Table 4.1 Pesticide active ingredient and one metabolite detected in one sample in rinsate, effluent, or biomixture analysed for in this study, and their physicochemical properties.

Compound	Water solubility (mg L^{-1})	Log P	pKa	Half-life soil (days)	K_{oc} (mL g^{-1})	GUS
2,4-D	24,300	-0.82	3.4	4.4	39.3	3.82
AMPA	1,470,000 [a]	-1.63	1.8, 5.4, 10.2 [c]	114	2,000	1.56
Atrazine	35	2.7	1.7	75	100	2.57
Bentazon	7,112	-0.46	3.51	20	55.3	1.95
Boscalid	4.6	2.96	*NA*	484	*772*	2.68
Chlorantraniliprole	0.88	2.86	10.88	597	362	3.51
Clopyralid	7,850	-2.63	2.01	23.2	5	3.02
Clothianidin	327	0.905	11.1	545	123	3.74
Dicamba	250,000	-1.8	1.87	9.6	*5.3*	1.94
Glufosinate	500,000	-4.01	2.0, 2.9, 9.8	7.4	600	1.03
Glyphosate	100,000	-6.28	0.78, 2.6, 5.6, 10.6	17.3	1,400	0.29
Imazamox	626,000	-2.9	2.3, 3.3, 10.8	200	*11.6*	3.59
Imazethapyr	1,400	1.49	2.1, 3.9	90	52	3.90
Metolachlor	530	3.4	*NA*	90	120	2.36
Pyraclostrobin	1.9	3.9	*NA*	41.9	9304	0.05
Tebuconazole	36	3.7	5	63	*769*	1.86

Nine (60%) compounds required two cells to effectively reduce in their concentrations in the biobed system. Atrazine, chlorantraniliprole, dicamba, glyphosate, and imazamox experienced large decreases in concentrations between rinsate and primary effluent, but a second cell did further reduce concentrations between primary and final effluent further.

AMPA was produced within the rinsate tank and detected at similar concentrations within the rinsate and primary effluent, however, a significant decrease was found between primary and final effluent. Glufosinate, which is known to be weakly retained in soil (K_D ~ 1-5 L kg^{-1}), found decreases with only one cell, but cell two further reduced glufosinate concentrations suggesting rapid dissipation. Both imazethapyr and metolachlor were relatively persistent with some indication of transport as these herbicide active ingredients were detected in effluent samples.

Table 4.2 General overview of the cells required for the dissipation of pesticide active ingredients and metabolite AMPA from rinsate applied to the operational biobed in Carman, Manitoba. Compounds of concern are also highlighted.

Biobed Efficacy		
Cell one	Cell one and two	Compounds of Concern
2,4-D	AMPA	Bentazon
Boscalid	Atrazine	Clopyralid
Pyraclostrobin	Chlorantraniliprole	
Tebuconazole	Dicamba	
	Glufosinate	
	Glyphosate	
	Imazamox	
	Imazethapyr	
	Metolachlor	

Furthermore, imazethapyr was found to accumulate within both cells across years. Imazethapyr concentrations showed large variations in the rinstate samples, but imazethapyr concentrations were numerically greater in rinsate (mean = 0.22 mgL^{-1}) than primary effluent (mean = 0.13 mg L^{-1}) or final effluent (mean = 0.083 mg L^{-1}). Metolachlor was found to have

greater concentrations in cell one than cell two as well as greater concentrations in 2023 than in 2022; decreases were detected with each successive cell from rinsate to final effluent. Metolachlor had the second-highest concentrations within the rinsate (after glyphosate). A visual look at both imazethapyr and metolachlor concentrations across rinsate, primary, and final effluent appeared to leach from cell one mid-season; this may be due to their longer half-lives within soils (Jensen et al. 1995), interactions with adjuvants of pesticide formulations (Hernández-Soriano et al. 2007), or competitive sorption with other compounds (Farenhorst and Bowman 1998; de Wilde et al. 2009).

There were two herbicide active ingredients, bentazon (K_{oc}= 55.3 L kg^{-1}; half-life = 20 days) and clopyralid (K_{oc}= 5 L kg^{-1}; half-life = 23 days) for which the final effluent showed similar mean concentrations to the rinsate but with less variation surrounding the mean. As well, based on the quantifications of bentazon and clopyralid concentrations in the biomatrix samples, each of these herbicides had no differences in the post-operation concentrations for 2022 (mean = 5.5 and 1.8 mg kg^{-1}, respectively) versus 2023 (mean = 4.3 and 2.9 mg kg^{-1}, respectively), suggesting that concentrations do not exceed an upper threshold; future sorption experiments could be conducted to determine the such thresholds. Many studies have reported that both bentazon and clopyralid have low K_{oc} or K_d values, hence these herbicides are not strongly sorbed by matrices such as soils, sediments, and biomixtures regardless of the physicochemical properties of these matrices (Gaston et al. 1996; Wagner et al. 1996; Shang and Arshad 1998; de Wilde et al. 2009; Bukun et al. 2010; Rosenbom et al. 2015). Although previous studies have shown that bentazon and clopyralid are not persistent (Wagner et al. 1996; Ahmad et al. 2003), including bentazon within biomatrices (Coppola et al. 2010), the daily irrigation of the biobed cells could have resulted in the weakly-

sorbed bentazon and clopyralid to readily move with the leachate in the biobed system, thereby eluting in effluents before degradation.

4.2 Practical Implications of the Research

The pest control products used on the University of Manitoba's Ian N. Morrison Research Farm are typical of crop production systems in the Americas and may other regions in the world. These products contain active ingredients that can be analyzed for by the analytical methods that was developed in this M.Sc. study and so this will allow the biobed to be monitored in future years; as well, other researchers working on the fate of pesticides in soil, biobeds and water can adapt these methods.

One analytical method focused on three compounds that have negative octanol-water partitioning coefficients, i.e., herbicides glyphosate (-6.28) and glufosinate (-4.01), and glyphosate's primary metabolite AMPA (-1.63). Given that these compounds have a greater affinity for water than for organic solvents, these compounds are challenging to extract from matrices such as water and soil. As well, existing methods for these compounds typically require molecule derivatization and quantification using fluorescence spectrometry (Glass 1983; Miles et al. 1985; Ibañez et al. 2005; Todorovic et al. 2013; Marin et al. 2020; Alonso et al. 2022) which is problematic for rinsate samples that often resemble cloudy or milky looking solutions because of the presence of formulation adjuvants that can interfere with light fluorescence. The method that was developed in this study (Chapter 2) relied on recent advances in mass spectrometry and column chemistry (Brown and Farenhorst 2024) that allows for the separation of glyphosate, glufosinate, and AMPA without derivatization. This eliminated the time needed for derivatization

reactions to occur, and possible operator errors related to the derivatization process for all extractions.

Glyphosate and AMPA are very strongly sorbed in soils and similar matrices such biomixtures, increasing extraction challenges for hydrophilic compounds (Sprankle et al. 1975a, b; de Jonge et al. 2001; Autio et al. 2004). Previous studies have utilized phosphate ions to extract AMPA and glyphosate, however glufosinate does not compete with phosphate sorption sites, therefore could not be extracted with phosphate-rich solvents (Autio et al. 2004). As such, the extraction method that was developed in this study (Chapter 2) utilized strong base solutions (pH ~ 13) to repel the negatively charged molecules from the negatively charged biomixture surfaces. The biomixture extraction method developed in this study streamlined sample processing so that glyphosate, glufosinate, and AMPA could be rapidly quantified, i.e., ~6 hours for 18 samples, with good recoveries (100-120%). In addition, rinsate and effluent samples were quickly processed and diluted, i.e. < 2 hours total, with good recoveries across all three compounds, providing the ability to process multiple samples within or across biobeds.

The broad-spectrum analytical method can simultaneously analyze for up to 82 pesticide active ingredients and one adjuvant in rinsate, effluent and biomixture samples (Chapter 3). All compounds were extractable from rinsate and effluent, (Table 4.3); for biomixture, QuPPe was able to extract 60% (51) of compounds while QuEChERS was able to extract 80% (67). Although less compounds were extracted, QuPPe was able to extract clopyralid (a compound of concern within biobed systems (Braul et al. 2018)) and is a much faster method in comparison to QuEChERS (~4 hours for QuPPe vs ~8 hours for QuEChERS for 18 samples). The quicker biomixture processing times allow for a greater number of samples to be analyzed within quicker

time-frames and less resources, i.e., labour, thereby allowing larger sample sizes for future experiments.

Previous studies have indicated optimal glyphosate degradation conditions when soils were at -15 kPa water tension, which is just above the theoretical water holding capacity of -33 kPa (Schroll et al. 2006; Kah et al. 2007; Nguyen et al. 2018); although these studies focused on glyphosate, most laboratory conditions used for any pesticide degradation assessment are near or at field-capacity (~ -33 kPa). The low variation of volumetric water content of the biobed are ideal conditions for pesticides to degrade (Johnson 2024). In this field study, biobed cells were irrigated at rates of 10 – 20 L m^{-2} day^{-1}, thereby consistently maintaining near water holding capacity with only small variations in volumetric water content throughout its seasonal operation. Anaerobic or anoxic conditions within the biomixture were largely minimized because of the use of a pea gravel layer below the biomixture that allowed excess water to leach from the biobed cell. Because moisture conditions were optimal for biodegradation, compounds such as glyphosate, 2,4-D, and imazamox were able to dissipate rapidly within the biomatrix without leaching into the effluents.
at rates of 10 – 20 L m^{-2} day^{-1}, thereby consistently maintaining near water holding capacity with only small variations in volumetric water content throughout its seasonal operation. Anaerobic or anoxic conditions within the biomixture were largely minimized because of the use of a pea gravel layer below the biomixture that allowed excess water to leach from the biobed cell. Because moisture conditions were optimal for biodegradation, compounds such as glyphosate, 2,4-D, and imazamox were able to dissipate rapidly within the biomatrix

Table 4.3 Summary of extractable compounds with QuEChERS and QuPPe. Dashed lines indicate the inability to extract while yes indicates extractable. The 46 compounds that were extractable in both QuEChERS and QuPPe are omitted.

Compound	QuEChERS	QuPPe	Compound	QuEChERS	QuPPe
Acephate	Yes	-	Buprofenzin	Yes	-
Clopyralid	-	Yes	Teflubenzuron	Yes	-
Methomyl	-	-	Pyrethin II	Yes	-
Pirimicarb	-	-	Piperonyl Butoxide	-	-
Imazalil	Yes	-	Clofentazine	Yes	-
Thiophanate-Methyl	Yes	-	Trifloxystrobin	-	-
Imazamox	Yes	-	Etoxazole	Yes	-
Dodemorph	Yes	-	Pyrethrin I	Yes	-
Fensulfothion	-	-	Chlorpyrifos	Yes	-
Cyantraniliprole	-	-	Pyridaben	Yes	-
Spiroxamine	-	-	Resmethrin	-	-
Fludioxinil	-	-	Coumaphos	Yes	-
Cyprodinil	Yes	-	Permethrin	-	-
Spinosyn A	-	-	Etofenprox	-	-
Spinosyn D	-	-	Bifenthrin	-	-
Phosmet	-	-	Acequinocyl	-	-
Spinetoram J	Yes	-	Fenpyroximate	-	-

The two chromatographic methods developed in this M.Sc. research are able to quantify a total of 87 different compounds (1 metabolite, 1 adjuvants, and eighty-four active ingredients) with minimal processing effort that allows for rapid analysis of pesticide active ingredients typically sold in Canada. These methods were validated then successfully applied to a dual-cell biobed system under a humid continental climate (Köppen climate classification Dfb) to monitor pesticide remediation of agricultural rinsate; results show the reduction of pesticides from rinsate to the final effluent release. The methods developed for this study can be utilized in other biobed contexts and climates and augments the methods that were previously developed for biobeds in Europe and Latin America.

In chapter 2, all compounds were successfully extracted regardless of the matrix (rinsate, effluent, or biomixutre); these compounds are glyphosate, AMPA, and glufosinate. Glyphosate and glufosinate are the top two herbicides used in Canada, with ~50,000,000 and ~5,000,000 kg of active ingredient sold in 2022 (PMRA 2024). The study demonstrated that biobeds are effective tools for recycling the rinsate of applications associated with these sales. Glyphosate reductions went from an average of 193 mg L^{-1} in rinsate to an average of 0.012 mg L^{-1} in primary effluent, demonstrating the potential of single-cell biobeds to be effective. Glufosinate concentrations were reduced from an average of 6.4 mg L^{-1} in rinsate to an average of 0.89 mg L^{-1} in primary effluent, and the second biobed cell further reduced glufosinate concentrations to an average of 0.086 mg L^{-1} in the final effluent. Regardless, if construction costs need to be considered, even a single cell biobed can significantly reduce effluent concentrations released into the environment, thereby reducing contamination of surface waters.

This study has reaffirmed the results of Johnson (2024) regarding on-farm rinsate management, which is that pesticide concentrations decreased in the order of rinsate > primary

effluent > final effluent; biomixture concentrations also indicated that the concentrations of pesticides decreased in the order of biobed cell one > biobed cell two. Although a relatively new technology within Canada, research is promising regarding the practical applications of biobeds on farms to protect waterways and thereby also safeguarding Indigenous lands and furthering decolonization. The Pest Management Regulatory Agency, under the jurisdiction of the Pest Control Products Act (2002), has increased effort for both water and field monitoring for pesticides in the environment; biobeds are a proposal to help prevent concentrations from being present.

4.3 Limitations of the Research and Recommendations for Future Studies.

The 16 compounds that were non-extractable using either QuEChERS or QuPPe shared the common characters to have one of the following characteristics: 1) high volatility that resulted in major losses during the freeze-drying (methomyl, trifloxystrobin), or 2) compounds that are more hydrophobic (large K_{ow}'s) or insoluble in water, methanol, or acetonitrile that require water-immiscible solvents for extraction (permethrin, acequinocyl). Further research is required to optimize the extractions for these compounds.

The Denham series soil was used for the inoculation of the biomixture (consisting of ~22% of the soil series on the land associated with the research farm in Carman); local soils range in pH from 4.8 to 7.4 and in soil organic carbon content from 0.87 to 4.9% (Mills and Haluschuk 1993). Such characteristics can incluence the sorption of glyphosate, AMPA, and some phenoxyacetic herbicides (Schwandt et al. 1992; Vasudevan and Cooper 2004; Werner et al. 2013; Dion et al. 2001; Gimsing and Borggaard 2001; Piccolo and Celano 1994). The biomixture utilized for this study had a pH of 5.96 and an organic carbon content of 2.82%; the addition of peat moss lowered

biomixture pH, while both peat and wheat straw also increased organic carbon content; this would have enhanced the sorption capacity of acidic compounds (Kah and Brown 2006, 2007). However, further research could be conducted in how the composition of biomixtures could improve the degradation or retention of some of the compounds that were frequently detected in the final effluent in this study.

Previous studies demonstrated the need to utilize concentrations of base >0.1 M KOH to overcome the sorption of glyphosate to loamy-clay, clay, and heavy clay soils (Miles and Moye 1988; Todorovic et al. 2013; Zhang et al. 2019). Since the glyphosate biomixture extractions were based off of the sandy-loam soil of the Carman biobed, the method developed by this study may not be utilizable for all soil textures. To apply the biobed research across Manitoba, clay-rich prairie soils of the Red River floodplains may require more basic solutions or basic cations (Ca, Mg, Na, etc.) to extract glyphosate and AMPA. However, the stronger base solutions would require more sample clean-up due to humic and fluvic acids coextraction; the KOH solution required to extract glyphosate, glufosinate, and AMPA resulted in visibly dark brown-black extraction solutions. Cleanup procedures through precipitating humic acids with HCl-acetic acid solution then adsorbing fulvic acids to HLB cartridges was conducted to reduce matrix effects in extractants, but were time-exhaustive. Future research is needed on how best to optimize this workflow while reducing matrix effects, such as utilizing dispersive-SPE instead of cartridges, glyphosate-glufosinate-AMPA extractable SPE cartidges to further clean up solutions, or weaker acids and bases that compete with sorption sites of both glufosinate and glyphosate-AMPA.

Across all three biomixture extraction methods, internal standards were added in-vial (for QuEChERS and QuPPe) or pre-SPE (for KOH) to minimize cost due to internal standard wastage, i.e., volume of extractant and mass of biomixture samples needed to spike at the beginning of

extraction would result in greater internal standard losses since extracted mass is greater than the final in-vial mass (4 g extracted vs. 0.2 g/mL final extract). Although a smaller amount of biomixture could be weighed out and extracted, biomixture heterogeneity would result in unrepresentative concentrations. Therefore, future studies should focus on: 1) developing matrix-matched calibration curves that also utilize internal standards to quantify extraction losses without high internal standard uses; 2) sub-sampling multiple, 0.2 g duplicates of a sample to account for biomixture heterogeneity, and; 3) develop back-calculating methods that account for water content within the sample. Regardless of the solution, future projects should focus on maintaining the 4 g minimum to ensure ample sample representation without excessive internal standard losses.

AMPA was the only metabolite monitored in this study, with rinsate concentrations closely following the trends of glyphosate concentrations, indicating glyphosate degradation within the rinsate collection tank before biobed application. However, this degradation in the tank is minimal when compared to the degradation of glyphosate to AMPA occurring in the biobed, particularly in biobed cell one. Primary effluent concentrations of AMPA were not significantly different from the rinsate values and were higher than that of glyphosate; it is not known if AMPA competes with glyphosate for sorption but it is likely because both have the phosphate moiety. In addition, AMPA concentrations was significantly higher in cell one than in cell two but there were no differences in AMPA concentrations between rinsate and primary effluent, this indicates that glyphosate entering cell one is degraded to AMPA which is retained within the biomixture of cell one. Other common metabolites such as 3-methyl-phosphinico-propionic acid (glufosinate), 2,4-dichlorophenol, 4-chlorophenol, and 2,4-dichloroanisole (2,4-D), *N*-methyl bentazon (bentazon), 6-deisopropyl atrazine and desethylatrazine (atrazine), and metolachlor-oxalinic acid and metolachlor-ethane sulfonic acid (metolachlor) were not monitored in this study. Future studies

should, in tandem with pesticide fate within biobed systems, study the environmental fate of metabolites for assessment biobed efficacy and mineralization capacity.

Unlike most pesticides, both glufosinate, imidazolinones, and metolachlor, are racemic mixtures of dextrorotary (*D*)-levorotary (*L*), rectus (*R*)-sinister (*S*), and *RS* isomers, respectively. In addition, metolachlor has two additional *M/P* atropisomers from the sterically inhibited aromatic ring-nitrogen bond site, resulting in four possible isomers total. Due to the cost of separation, most pesticide formulations consist of both isomers with on effective, bioactive (*L*-glufosinate, *S*-metolachlor, and *R*-imidazolinones) versus an ineffective, nonactive form (*D*-glufosinate, *R*-metolachlor, and *S*-imidazolinones) (Takano and Dayan 2020). One study investigated differences between the two glufosinate isomers, noting that the *D*-isomer half-lives quicker than *L*-isomer, indicating that the mixture may degrade the inactive *D*-isomer while the bioactive *L*-isomer is able to leach from the biomixture and into the environment (Jia et al. 2019). Future studies should monitor enantiomers to assess whether 1) bioactive forms are being degraded, and 2) how different isomers impact modelling of pesticide fate. This could be of great impact on biobed performance since both pesticides are detected within the primary effluent and final effluent; which isomer is present within the effluent's would influence the toxicity of the effluent. Although glufosinate, imazethapyr, imazamox, and metoachlor were quantified in the primary effluent, if they were not the bioactive *L*-glufosinate, *R*-imathapyr, *R*- imazamox, and *S*-metolachlor, then one biobed cell may be acceptable. However, if the bioactive forms are present in the final effluent, this would indicate a need for future research.

Pesticide fate parameters, such as sorption-desorption, degradation, and volatilization are not well understood within the biobed, especially for metolachlor, bentazon, imazethapyr, glufosinate, and clopyralid. The lack of studies in compounds of concerns, especially bentazon

and clopyralid, make it difficult to infer whether the pesticides are degrading within biomatrices or rinsate, if they are volatilizing from biomixture surfaces, or rapidly desorbed from biomixture colloids. Since biobeds are variable systems, the influence of competitive adsorption-desorption, heat flux, and variable-concentration degradation rates should be studied to be able to adequately model biobed performance as well as indicate possible future studies that should be conducted *in-situ*.

4.4 References

Ahmad, R., James, T.K., Rahman, A., and Holland, P.T. 2003. Dissipation of the herbicide clopyralid in an allophanic soil: laboratory and field studies. J. Environ. Sci. Health B **38(6)**: 683-695.

Alonso, B., Griffero, L., Pereira, H.B., Pareja, L., and Parada, A.P. 2022. Determination of glyphosate and AMPA in freshwater and soil from agroecosystems by 9-fluorenylmethoxycarbonyl chloride derivatization and liquid chromatography - fluorescence detection and tandem mass spectrometry. MethodsX **9**: 101730.

Autio, S., Siimes, K., Laitinen, P., Rämö, S., Oinonen, S., and Eronen, L. 2004. Adsorption of sugar beet herbicides to finnish soils. Chemosphere **55**: 215-226.

Brown, A.K., and Farenhorst, A. 2024. Quantitation of glyphosate, glufosinate, and AMPA in drinking water and surface waters using direct injection and charged-surface ultra-high performance liquid chromatography-tandem mass spectrometry. Chemosphere **349**: 140924.

Bukun, B., Shaner, D.L., Nissen, S.J., Phillip, W., and Brunk, G. 2010. Comparison of the interactions of aminopyralid vs. clopyralid with soil. Weed Sci. **58(4)**: 473-477.

Coppola, L., Castillo, M.d.P., and Vischetti, C. 2010. Degradation of isoproturon and bentazone in peat- and compost-based biomixtures. Pest Manag. Sci. **67**: 107-113.

Dion, H.M., Harsh, J.B., and Hill Jr., H.H. 2001. Competitive sorption between glyphosate and inorganic phosphate on clay minerals and low organic matter. J. Radioanal. Nucl. Chem. **249(2)**: 385-390.

Farenhorst, A., and Bowman, B.T. 1998. Competitive sorption of atrazine and metolachlor in soil. J. Environ. Sci. Health B **33(6)**: 671-682.

Gaston, L.A., Locke, M.A., Wagner, S.C., Zablotowicz, R.M., and Reddy, K.N. 1996. Sorption of bentazon and degradation products in two Mississippi soils. Weed Sci. **44(3)**: 678-682.

Gimsing, A.L., and Borggaard, O.K. 2001. Effect of KCl and $CaCl_2$ as background electrolytes on the competitive adsorption of glyphosate and phosphate on goethite. Clays Clay Miner. **49(3)**: 270-275.

Glass, R.L. 1983. Liquid chromatographic determination of glyphosate in fortified soil and water samples. J. Agric. Food Chem. **31**: 280-282.

Hérnandez-Soriano, M.C., Mingorance, M.D., and Peña, A. 2007. Interaction of pesticides with a surfactant-modified soil interface: effect of soil properties. Colloids Surf. A: Physicochem. Eng. Asp. **306**: 49-55.

Ibañez, M., Pozo, Ó.J., Sancho, J.V., López, F.J., and Hernández, F. 2005. Residue determination of glyphosate, glufosinate and aminomethylphosphonic acid in water and soil

samples by liquid chromatography coupled to electrospray tandem mass spectrometry. J. Chromatogr. A **1081**: 145-155.

Jensen, K.I.N., Ivany, J.A., and King, R.R. 1995. Persistence of Imazethapyr in two Atlantic Canada soils. Can. J. Soil Sci. **75**: 525-527.

Jia, G., Xu, J., Long, X., Ge, S., Chen, L., Hu, D., and Zhang, Y. 2019. Enantioselective degradation and chiral stability of glufosinate in soil and water samples an formation of 3-methylphosphinicopropionic acid and N-acetyl-glufosinate metabolites. J. Agric. Food. Chem. **67**: 11312-11321.

Johnson, S. 2024. Management of agricultural pesticide rinsate using a biobed under Manitoba conditions. MSc. Thesis, University of Manitoba, Winnipeg, Canada. Available from https://mspace.lib.umanitoba.ca/server/api/core/bitstreams/05b7f34e-0fb0-4cb9-8c12-1057271e8d95/content [Accessed 18 March 2025].

de Jonge, H., de Jonge, L.W., Jacobsen, O.H., Yamaguchi, T., and Moldrup, P. 2001. Glyphosate sorption in soils of different pH and phosphorous content. Soil Sci. **166(4)**: 230-238.

Kah, M., and Brown, C.D. 2006. Adsorption of ionisable pesticides in soils. Rev. Environ. Contam. Toxicol. **188**: 149-217.

Kah, M., and Brown, C.D. 2007. Prediction of the adsorption of ionizable pesticides in soils. J. Agric. Food Chem. **55**: 2312-2322.

Kah, M., Beulke, S., and Brown, C.D. 2007. Factors influencing degradation of pesticides in soil . J. Agric. Food Chem. **55**: 4487-4492.

Lewis, K.A., Tzilivakis, J., Warner, D. and Green, A. 2016. An international database for pesticide risk assessments and management. Hum. Ecol. Risk Assess. **22(4)**: 1050-1064.

Marin, J., Campillo, N., Hernández-Cordoba, M., Garrido, I., Fenoll, J., and Viñas, P. 2020. Liquid–liquid microextraction of glyphosate, glufosinate and aminomethylphosphonic acid for the analysis of agricultural samples by liquid chromatography. Anal. Method. **12**: 2039-2045.

Miles, C.J., Wallace, L. R., and Moye, H.A. 1985. Determination of glyphosate herbicide and (aminomethyl)phosphonic acid in natural waters by liquid chromatography using pre-column fluorogenic labelling with 9-fluorenylmethyl chloroformate. J. Assoc. Off. Anal. Chem. **69(3)**: 458-461.

Miles, C.J., and Moye, H.A. 1988. Extraction of glyphosate herbicide from soil and clay minerals and determination of residues in soil. J. Agric. Food Chem. **36**: 486-491.

Mills, G.F., and Haluschuk, P. 1993. Canada-Manitoba soil survey: soils of the carman research station N½ 23-6-5W. Special Report Series No. 93-1. Available from https://www.gov.mb.ca/agriculture/soil/soil-survey/pubs/fss02s00931.pdf [Accessed 22 February 2025].

Nguyen, N.G., Dörfler, U., Welzl, G., Munch, J.C., Schroll, R., and Suhadolc, M. 2018. Large variation in glyphosate mineralization in 21 different agricultural soils explained by soil properties. Sci. Total Environ. **627**: 544-552.

Pest Control Products Act. **SC 2002**. c. 28. Available from: https://laws-lois.justice.gc.ca/PDF/P-9.01.pdf [Accessed 12 June 2025].

Pest Management Regulatory Agency (PMRA). 2024. Pest control products sales report for 2022. Available from https://publications.gc.ca/collections/collection_2025/sc-hc/H111-3-2022-eng.pdf [Accessed 9 June 2025].

Piccolo, A., and Celano, G. 1994. Hydrogen-bonding interactions between the herbicide glyphosate and water-soluble humic substances. Environ. Toxicol. Chem. **13(11)**: 1737-1741.

Rosenbom, A.E., Olsen, P., Plauborg, F., Grant, R.M., Juhler, R.K., Brüsch, W., and Kjær, J. 2015. Pesticide leaching through sandy and loamy-fields – long-term lessons learnt from the Danish Pesticide Leaching Assessment Programme. Environ. Pollut. **201**: 75-90.

Schroll, R., Becher, H.H., Förfler, U., Gayler, S., Grundmann, S., Hartmann, H.P., and Ruoss, J. 2006. Quantifying the effect of soil moisture on the aerobic microbial mineralization of selected pesticides in different soils. Environment. Sci. Technol. **40**: 3305-3312.

Schwandt, H., Kögel-Knaber, I., Stanjek, H., and Totsche, K. 1992. Sorption of an acidic herbicide on synthetic iron oxides and soils: sorption isotherms. Sci. Total Environ. **123/124**: 121-131.

Shang, C., and Arshad, M.A. 1998. Sorption of clopyralid, dicamba, and MCPA by two soils with conventional and no-till management. Can J. Soil Sci. **78**: 181-186.

Sprankle, P., Meggitt, W.F., and Penner, D. 1975a. Rapid inactivation of glyphosate in the soil. Weed Sci. **23(3)**: 224-228.

Sprankle, P., Meggitt, W.F., and Penner, D. 1975b. Adsorption, mobility, and microbial degradation of glyphosate in the soil. Weed Sci. **23(3)**: 229-234.

Takano, H.K., and Dayan, F.E. 2020. Glufosinate-ammonium: a review of the current state of knowledge. Pest Manag. Sci. **76**: 3911-3925.

Todorovic, G.R., Mentler, A., Popp, M., Hann, S., Köllensperger, G., Rampazzo, N., and Blum, W.E.H. 2013. Determination of glyphosate and AMPA in three representative agricultural soils with a HPLC-MS/MS method. Soil Sediment Contam. **22**: 332-350.

Vasudevan, D., and Cooper, E.M. 2004. 2,4-D sorption in iron oxide-rich soils: role of soil phosphate and exchangeable Al. Environ. Sci. Technol. **38**: 163-170.

Wagner, S.C., Zablotowicz, R.M., Gaston, L.A., Locke, M.A., and Kinsiella, J. 1996. Bentazon degradation in soil: influence of tillage and history of bentazon application. J. Agric. Food Chem. **44**: 1593-1598.

Werner, D., Garratt, J.A., and Pigott, G. 2013. Sorption of 2,4-D and other phenoxy herbicides to soil, organic matter, and minerals. J. Soils. Sediments **13**: 129-139.

de Wilde, T.D., Spanoghe, P., Ryckeboer, J., Jaeken, P., and Springael, D. 2009. Sorption characteristics of pesticides on matrix substrates used in biopurification systems. Chemosphere **75**: 100-108.

Zhang, P., Rose, M., and van Zwieten, L. 2019. Direct determination of glyphosate and its metabolite AMPA in soil using mixed-mode solid-phase purification and LC-MS/MS determination on a hypercarb column. J. AOAC Int. **10(3)**: 952-965.

5. APPENDIX I: CHAPTER TWO VALIDATION AND SUPPLEMENTARY MATERIALS

5.1 Eurachem Method Validation Calculations

A seven-point calibration curve (0.1, 1, 5, 10, 50, 100, 400 ng mL^{-1}) was used for quantitation with an internal standard concentration of 20 ng mL^{-1} for relative response correction. Linearity was determined with an unweighted calibration curve (x) from seven independent calibration curve R^2 values; all calibration curves were made from DI water with 0.1% FA.

For water fractions, ten replicates of 1 ng mL^{-1} samples in deionized water (LOD/LOQ), artificial rinsate, and artificial effluent (MLDs/MLQs) were run. Values were then inputted into the following formula:

$$S_0' = \frac{S_0}{\sqrt{n}} \tag{5-1}$$

$$Detection\ Limit = S_0'\ x\ 3 \tag{5-2}$$

$$Quantification\ Limit = S_0'\ x\ 10 \tag{5-3}$$

Where; n = number of replicates, S_0 = the standard deviation of the sample runs, and S'_0 = the standard error of the sample run, Detection Limit = Instrument or Method Limit of Detection, Quantification Limit = Instrument Method Limit of Quantification.

For biomixture, due to detectable concentrations of glyphosate and AMPA within, an adjusted formula using twelve replicates of 1 ng mL^{-1} spiked and six replicates of unspiked samples were run. Values were then inputted into the following formula:

$$S'_0 = S_0 * \sqrt{\frac{1}{n_s} + \frac{1}{n_b}} \quad (5\text{-}4)$$

Where all of the parameters are the same as above except for the inclusion of n_s and n_b, the spiked samples and blank samples, respectively.

Accuracy and precision were measured at three effluent (20, 200, and 2,000 ng mL^{-1}) and rinsate (200, 2,000, 20,000 ng mL^{-1}) concentrations and four (100, 1,000, 10,000, and 100,000 ng g^{-1}) concentrations for biomixture. Accuracy measurements were conducted in five replicates per concentration for rinsate and effluents and six replicates per concentration for biomixture. Intraday (0, 12, 24 hours) and interday (0, 24, 48 hours) were measured with two replicates per concentration at each time period. 3 blank replicates were run with biomixture to correct for AMPA and glyphosate detections.

Accuracy results inputted into the following formula:

$$R(\%) = \left(\frac{\bar{x}}{x_{spk}}\right) * 100 \quad (5\text{-}5)$$

in which $R(\%)$ is percent recovery, $\bar{x}$ = mean analyte recovery, and x_{spk} = spiked analyte concentration.

Precision results were inputted into the following formula:

$$CV\ (\%) = \left(\frac{SD}{\bar{x}}\right) * 100 \quad (5\text{-}6)$$

where $CV\ (\%)$ = percent coefficient of variation (relative standard deviation), SD = standard deviation, and $\bar{x}$ = mean analyte recovery.

Matrix effects were determined by spiking all matrices and their dilutions at 100 ng mL^{-1} and compared to a deioinized water matrix; each matrix had five replicates. Rinsate matrices used were 1/10, 1/100, and 1/1,000 dilutions while effluent matrices were undiluted and 1/10 dilution.

Biomixture tested were undiluted plus 1/10, 1/100, 1/1,000, and 1/10,000 diluted matrices. Water and biomixture were conducted in separate chromatographic runs and statistical analyses.

Since biomixture was freeze-dried to asses dry-weight corrected concentrations, losses of glyphosate, glufosinate, and AMPA were assessed; each spike stage had five replicates. Samples were all initially spiked at 1,000 ng g^{-1} for all for unlabelled glyphosate, glufosinate, and AMPA; internal standards were then spiked at three stages of free-drying; pre-freeze-drying, post-freeze-drying, and pre-SPE.

5.2 Supplementary Materials for Chapter Two

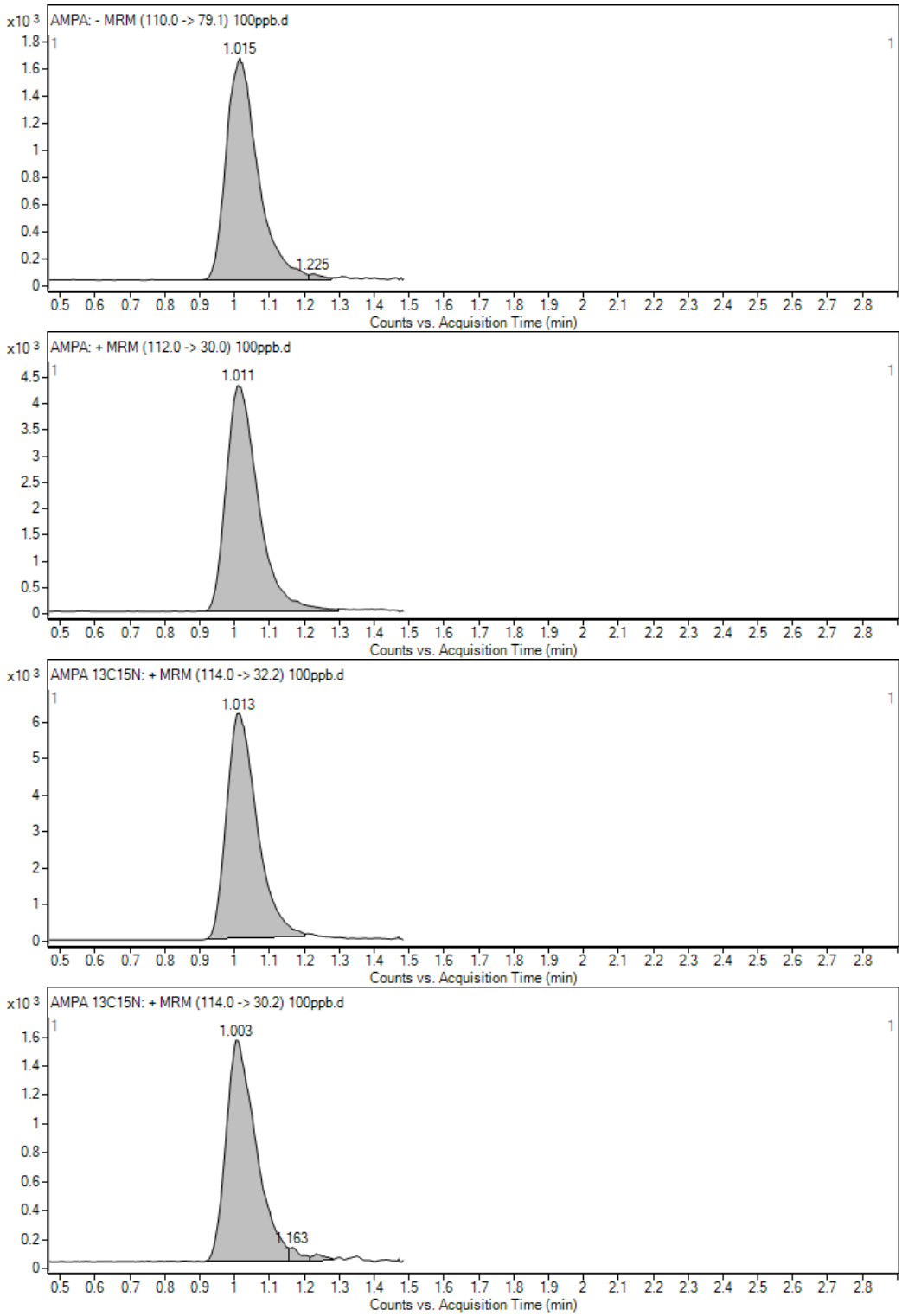

Figure 5.1 Chromatograms for AMPA (top two) and AMPA^{13}C,^{15}N (bottom two) and quantifiers (top, third) and qualifiers (second, bottom).

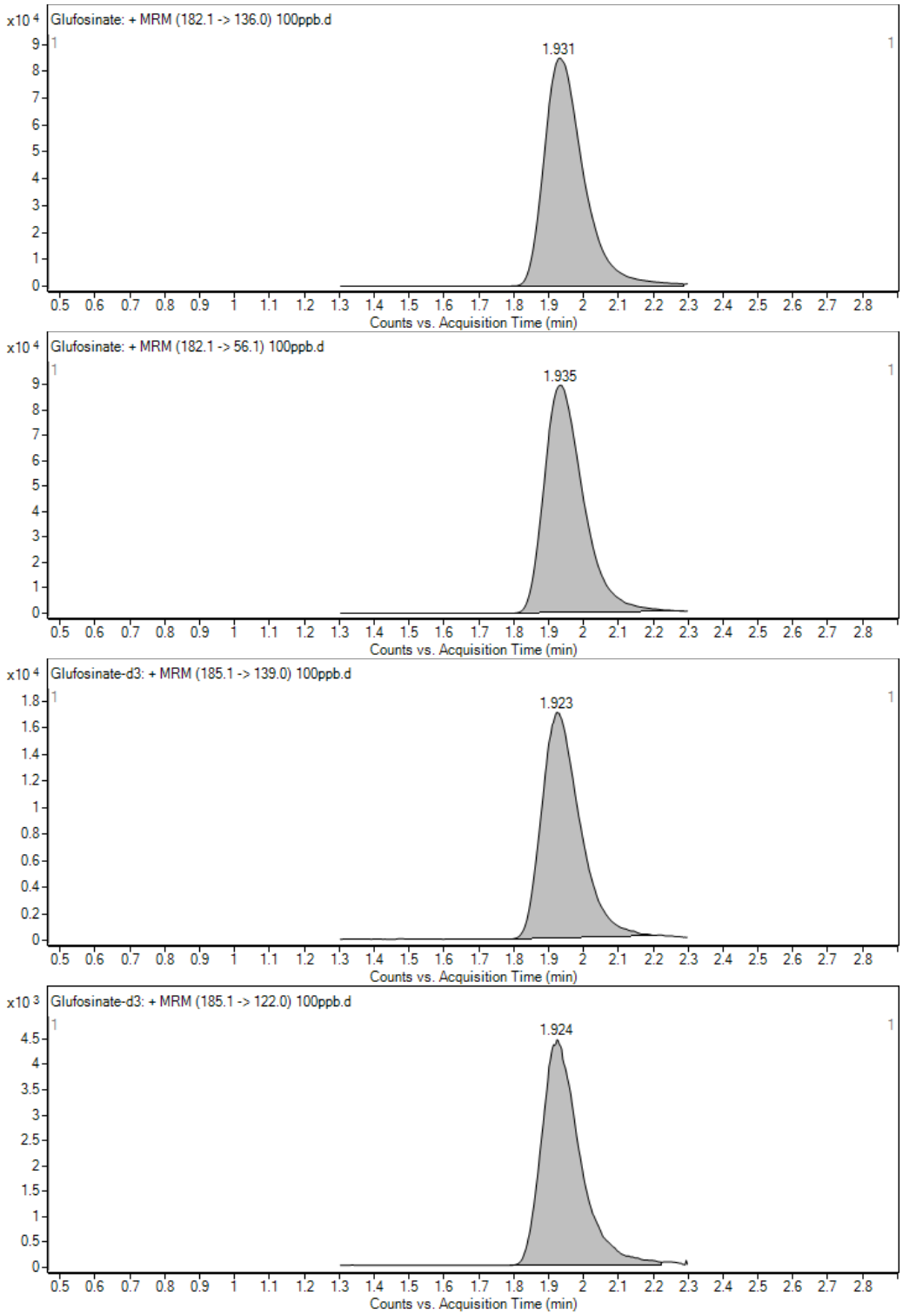

Figure 5.2 Chromatograms for glufosinate (top two) and glufosinate-d_3 (bottom two) and quantifiers (top, third) and qualifiers (second, bottom).

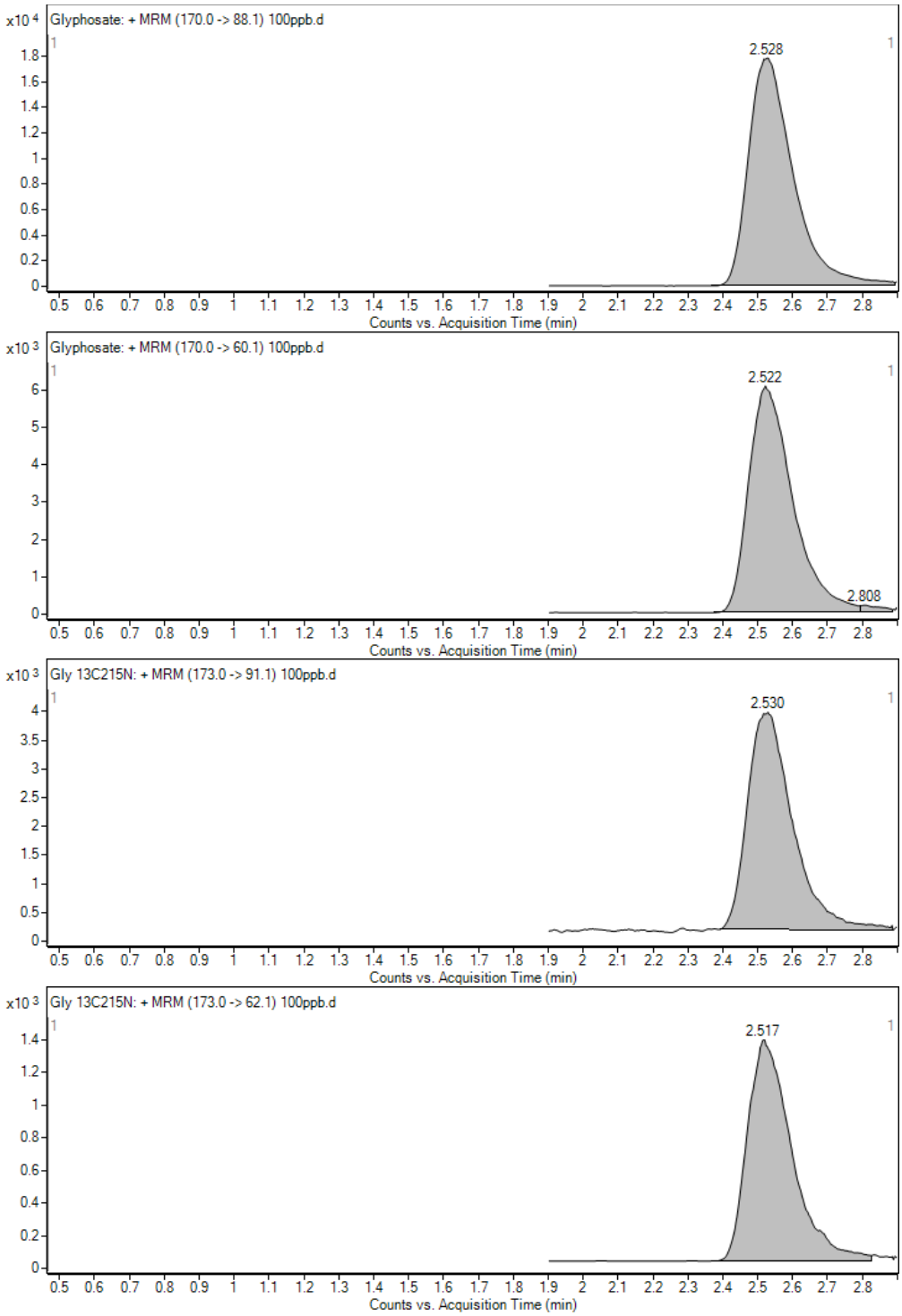

Figure 5.3 Chromatograms for glyphosate (top two) and glyphosate-$^{13}C_2$,^{15}N (bottom two) and quantifiers (top, third) and qualifiers (second, bottom).

Table 5.1 The method retention time (Rt), electrospray ionization (ESI), precsuor ion, product ions [both the quantitative (Q) and qualitative (q) product ions], fragmentation voltage (FV), and collision energy (CE).

Compound		AMPA	Glufosinate	Glyphosate
Rt (min)		0.97	1.82	2.34
ESI		Negative and Positive	Positive	Positive
Precusor Ion (m/z)		112 (Negative)	182.1	170
Q	Product Ion (m/z)	79.1 (Negative)	136	88.1
	FV (V)	108	87	65
	CE (eV)	36	12	8
q	Product Ion (m/z)	30 (Positive)	56.1	60.1
	FV (V)	56	87	65
	CE (eV)	0	28	16

Table 5.2 Assumptions of ANOVA tested for the water matrix effects. Homogeneity of variance was tested with Bartlett's Test while normality was assessed with Shapiro-Wilk's Test. DI = Deionized Water, EF = Effluent Mimic, RN = Rinsate Mimic. Parenthesis indicate dilution level.

Compound	Homogeneity of Variance	Normality					
		DI	EF	EF (1/10)	RN (1/10)	RN (1/100)	RN (1/1,000)
AMPA	0.3022	0.2307	0.8575	0.4878	0.3424	0.7055	0.8858
Glufosinate	0.8653	0.9673	0.3727	0.5852	0.4279	0.975	0.9335
Glyphosate	0.8207	0.09259	0.3306	0.639	0.9496	0.8659	0.6199

Table 5.3 ANOVA tests and values for compound response within water matrix effects with a follow-up Dunnett's Post-Hoc Test if significant. - = reduced response; 0 = no response change, and; NA = Not Applicable.

ANOVA (df = 5,25)		Dunnett's Test Pairwise									
		DI v EF		DI v EF10DIL		DI v RN10DIL		DI v RN100DIL		DI v RN1000DIL	
Compound	p-value	p-value	response	p-value	response	p-value	response	p-value	response	p-value	response
AMPA	<0.0001	<0.0001	-	<0.0001	-	<0.0001	-	0.6966	0	0.9684	0
GLUF	<0.0001	0.9927	0	1	0	<0.0001	-	0.9998	0	0.9416	0
GLYP	0.82203	NA	NA	NA	NA	NA	NA	NA	NA	NA	NA

Table 5.4 Assumptions of ANOVA tested for the biomixture matrix effects. Homogeneity of variance was tested with Bartlett's Test while normality was assessed with Shapiro-Wilk's Test. DI = Deionized Water, KOH = Potassium Hydroxide Extractant. Parenthesis indicate dilution level.

Compound	Homogeneity of Variance	Normality				
		DI	KOH	KOH (1/10)	KOH (1/100)	KOH (1/1,000)
AMPA	0.3247	0.02127	0.945	0.9949	0.4465	0.9847
Glufosinate	0.1078	0.2809	0.5496	0.1293	0.0242	0.7659
Glyphosate	0.5465	0.3384	0.2566	0.1308	0.3376	0.8389

Table 5.5 ANOVA tests and values for compound response within biomatrix matrix effects with a follow-up Dunnett's Post-Hoc Test if significant. - = reduced response; 0 = no response change, and; NA = Not Applicable.

ANOVA(df = 4,20)		Dunnett's Test Pairise							
		DI v GLYRAW		DI v GLY10DIL		DI v GLY100DIL		DI v GLY1000DIL	
Compound	p-value	p-value	response	p-value	response	p-value	response	p-value	response
AMPA	<0.0001	<0.0001	-	<0.0001	-	<0.0001	-	0.8934	0
Glufosinate	<0.0001	<0.0001	-	0.4372	0	1	0	0.2444	0
Glyphosate	0.000544	0.0037	-	0.7567	0	0.9843	0	0.9265	0

Table 5.6 Assumptions of ANOVA tested for the internal standard losses of biomixture extractions. Homogeneity of variance was tested with Bartlett's Test while normality was assessed with Shapiro-Wilk's Test. FD = freeze-drying, SPE = solid-phase extraction.

Compound	Homogeneity	Normality		
		Pre-FD	Post-FD	SPE
AMPA	0.9629	0.7369	0.3798	0.7532
Glufosinate	0.4738	0.9189	0.9144	0.4162
Glyphosate	0.6117	0.5591	0.,9489	0.8674

Table 5.7 ANOVA tests for internal standard losses of compounds followed up by Tukey's post-hoc test if significant. From preceding to succeeding step, - = reduced response; 0 = no change; + = increased response; and; NA = Not Applicable.

ANOVA (df = 2,12)		Tukey's Test Pairise					
		BFD v AFD		AFD v SPE		BFD v SPE	
Compound	p-value	p-value	response	p-value	response	p-value	response
AMPA	0.00561	0.735	0	0.0062	-	0.024	-
Glufosinate	<0.0001	0.078	0	<0.0001	+	0.00027	+
Glyphosate	0.618	NA	NA	NA	NA	NA	NA

Table 5.8 Welch's ANOVA table for glufosinate, glyphosate, and AMPA for water concentrations across all three matrices as well as the Games-Howell Post-Hoc comparisons. Data transformation and Shapiro-wilk Test for Normality also shown for Welch's ANOVA assumptions.

Compound	Transformation	Shapiro-Wilk			Welch's ANOVA			Games-Howell Post-Hoc		
		RIN	PEF	FEF	*df*	*F-value*	*p-value*	RIN v PEF	PEF v FEF	RIN v FEF
AMPA	Log10	0.0983	0.116	0.24	2.00, 14.1	17.9	0.000183	0.182	0.000431	0.001
Glufosinate	Log10	0.812	0.729	0.0345	2.00, 15.7	13.2	0.0004296	0.037	0.03	0.000326
Glyphosate	Log10	0.0858	0.0604	0.12	2.00, 11.8	88.4	<0.0001	<0.0001	0.00029	<0.0001

Table 5.9 ANOVA tables for glufosinate (GLU), glyphosate (GLY), and AMPA for biomixture analyses. Acronyms for parameters are: SS_n = Sum of Squares (numerator), SS_d = Sum of Squares (denominator), *F* = F-Statistic, and *p* = p-value. Acronyms for factors are: (I) = Model Intercept, C = Cell, Y = Year, T = Time, and D = Depth. Orange highlighted cells are significant factors; bolded values are significant p-values. Fact = Factor, df = degrees of freedom.

Fact		(I)	C	Y	D	T	C:Y	C:D	Y:D	C:T	Y:T	D:T	C:Y :D	C:Y :T	C:D :T	Y:D :T	C:Y :D:T
df		1,8	1,8	1,8	2,16	1,8	1,8	2,16	2,16	1,8	1,8	2,16	2,16	1,8	2,16	2,16	2,16
GLU	SS_n	4115.571	0.039	6.622	54.156	27.976	0.003	2.509	12.281	0.152	11.424	100.407	1.996	3.5	1.687	4.419	2.046
	SS_d	9.668	9.668	9.668	23.605	6.302	9.668	23.605	23.605	6.302	6.302	33.453	23.605	6.302	33.453	33.453	33.453
	F	3405.504	0.032	5.48	18.354	35.514	0.003	0.85	4.162	0.193	14.502	24.012	0.677	4.443	0.403	1.057	0.489
	p	**8.26E-12**	8.62E-01	**4.70E-02**	**7.21E-05**	**3.38E-04**	9.61E-01	4.46E-01	**3.50E-02**	6.72E-01	**5.00E-03**	**1.52E-05**	5.22E-01	6.80E-02	6.75E-01	3.71E-01	6.22E-01

GLY	SSn	2905.249	165.69	5.871	20.95	2.352	8.178	12.224	9.945	3.662	32.573	41.439	11.722	1.713	10.635	0.997	2.223
	SSd	15.537	15.537	15.537	16.853	5.665	15.537	16.853	16.853	5.665	5.665	13.035	16.853	5.665	13.035	13.035	13.035
	F	1495.959	85.316	3.023	9.945	3.321	4.211	5.803	4.721	5.172	45.996	25.433	5.564	2.419	6.527	0.612	1.364
	p	**2.19E-10**	**1.53E-05**	1.20E-01	**2.00E-03**	1.06E-01	7.40E-02	**1.30E-02**	**2.40E-02**	5.30E-02	**1.40E-04**	**1.07E-05**	**1.50E-02**	1.58E-01	**8.00E-03**	5.55E-01	2.84E-01
AMPA	SS_n	6240.644	303.165	7.865	47.736	37.083	0.023	12.304	23.272	28.2	24.696	27.263	10.404	0.33	8.849	2.933	0.546
	SS_d	38.305	38.305	38.305	19.989	5.475	38.305	19.989	19.989	5.475	5.475	24.369	19.989	5.475	24.369	24.369	24.369
	F	1303.364	63.316	1.643	19.105	54.189	0.005	4.924	9.314	41.208	36.087	8.95	4.164	0.483	2.905	0.963	0.179
	p	**3.80E-10**	**4.54E-05**	2.36E-01	**5.76E-05**	**7.91E-05**	9.47E-01	**2.20E-02**	**2.00E-03**	**2.05E-04**	**3.21E-04**	**2.00E-03**	**3.50E-02**	5.07E-01	8.40E-02	4.03E-01	8.38E-01

Table 5.10 Results from the Shapiro-Wilk's Test for normality for glufosinate, glyphosate, and AMPA for biomixture analyses. Acronyms for parameters are: C_Y = Cell_Year, T = Time, D = Depth, *W* = W-statistic, and *p* = p-value. Orange highlighted cells are significant factors that, when viewed with boxplots, were visually normally distributed.

Factors			Glufosinate		Glyphosate		AMPA	
D	T	C_Y	*W*	*p*	*W*	*p*	*W*	*p*
0,5	Pre	BB1_2022	0.821	0.166	0.894	0.366	0.999	0.942
0,5	Post	BB1_2022	0.979	0.723	0.972	0.676	0.996	0.874
5,15	Pre	BB1_2022	0.956	0.595	0.8	0.113	1	0.976
5,15	Post	BB1_2022	0.936	0.51	0.946	0.554	0.949	0.566
15,30	Pre	BB1_2022	0.886	0.343	0.927	0.477	0.84	0.215
15,30	Post	BB1_2022	0.979	0.725	0.998	0.912	0.991	0.82
0,5	Pre	BB1_2023	0.944	0.545	0.994	0.856	0.988	0.793
0,5	Post	BB1_2023	0.977	0.71	0.981	0.734	0.879	0.321
5,15	Pre	BB1_2023	0.9	0.385	0.948	0.559	0.801	0.116
5,15	Post	BB1_2023	0.818	0.159	0.813	0.146	0.8	0.115
15,30	Pre	BB1_2023	0.97	0.665	0.999	0.93	0.994	0.857
15,30	Post	BB1_2023	0.857	0.258	0.957	0.603	0.934	0.504
0,5	Pre	BB2_2022	0.97	0.669	0.901	0.389	1	0.976
0,5	Post	BB2_2022	0.922	0.458	0.959	0.611	0.99	0.81
5,15	Pre	BB2_2022	0.833	0.197	0.952	0.578	0.886	0.343
5,15	Post	BB2_2022	0.928	0.483	0.888	0.347	0.762	**0.026**
15,30	Pre	BB2_2022	0.857	0.258	0.992	0.829	0.95	0.57
15,30	Post	BB2_2022	0.963	0.631	0.816	0.154	0.957	0.603
0,5	Pre	BB2_2023	0.999	0.939	0.853	0.249	0.998	0.91
0,5	Post	BB2_2023	0.871	0.297	0.994	0.847	0.848	0.236
5,15	Pre	BB2_2023	0.9	0.385	0.87	0.297	0.947	0.555
5,15	Post	BB2_2023	0.995	0.86	0.88	0.324	0.816	0.152
15,30	Pre	BB2_2023	0.917	0.443	0.987	0.778	0.995	0.862

15,30	Post	BB2_2023	0.75	**0**	0.97	0.665	0.886	0.341

Table 5.11 Results from the Mauchly's Test for sphericity for glufosinate, glyphosate, and AMPA for biomixture analyses. Acronyms for parameters are: W = W-statistic, and p = p-value. Factor Acronyms are the same as Table 5.9.

		D	C:D	Y:D	C:Y:D	D:T	C:D:T	Y:D:T	C:Y:D:T
Glufosinate	*W*	0.492	0.492	0.492	0.492	0.459	0.459	0.459	0.459
	p	0.083	0.083	0.083	0.083	0.065	0.065	0.065	0.065
Glyphosate	*W*	0.705	0.705	0.705	0.705	0.813	0.813	0.813	0.813
	p	0.295	0.295	0.295	0.295	0.484	0.484	0.484	0.484
AMPA	*W*	0.988	0.988	0.988	0.988	0.869	0.869	0.869	0.869
	p	0.958	0.958	0.958	0.958	0.613	0.613	0.613	0.613

Table 5.12 Results from Levene's Test for homogeneity of variance for glufosinate, glyphosate, and AMPA for biomixture analyses. Acronyms for parameters are: W = W-statistic, and p = p-value. Factor Acronyms are the same as Table 5.9.

				Glufosinate		Glyphosate		AMPA	
D	T	df1	df2	*W*	*p*	*W*	*p*	*W*	*p*
0,5	Pre	3	8	0.454	0.722	2.29	0.155	2.94	0.0988
0,5	Post	3	8	0.523	0.678	1.04	0.426	0.567	0.652
5,15	Pre	3	8	0.518	0.682	0.719	0.568	0.427	0.739
5,15	Post	3	8	0.329	0.805	0.454	0.722	0.0986	0.959
15,30	Pre	3	8	0.794	0.531	0.722	0.606	0.677	0.59
15,30	Post	3	8	0.762	0.546	0.454	0.722	0.954	0.459

Table 5.13 Pairwise comparisons for glyphosate tested using the Benjamini-Hochberg correction for the significant Cell*Depth*Time interaction. White "=" values were insignificant, magenta ">" values indicate column value was greater than the row value, and yellow "<" values indicate column value was lesser than the row value. C1 = Cell 1, C2 = Cell 2, Pre = Pre-operation, Pos = Post-operation, 0-5 = 0-5 cm, 5-15 = 5-15 cm, and 15-30 = 15-30 cm.

Row Labels	Conc	C1 0-5 Pre	C1 0-5 Pos	C1 5-15 Pre	C1 5-15 Pos	C1 15-30 Pre	C1 15-30 Pos	C2 0-5 Pre	C2 0-5 Pos	C2 5-15 Pre	C2 5-15 Pos	C2 15-30 Pre
		0.34 (0.67)	18 (22)	20 (26)	5.1 (6.5)	13 (13)	13 (16)	0.069 (0.033)	0.6 (0.98)	0.6 (0.65)	0.18 (0.19)	0.26 (0.39)
C1 0-5 Pos	18 (22)	>										
C1 5-15 Pre	20 (26)	>	=									
C1 5-15 Pos	5.1 (6.5)	>	=	=								
C1 15-30 Pre	13 (13)	>	=	=	<							
C1 15-30 Pos	13 (16)	=	=	=	=	=						
C2 0-5 Pre	0.069 (0.033)	=	<	<	<	<	<					
C2 0-5 Pos	0.6 (0.98)	=	<	<	<	<	<	=				
C2 5-15 Pre	0.6 (0.65)	=	=	<	=	<	=	=	=			
C2 5-15 Pos	0.18 (0.19)	=	<	<	<	<	<	=	=	=		
C2 15-30 Pre	0.26 (0.39)	=	=	<	<	<	=	=	=	<	=	
C2 15-30 Pos	0.13 (0.15)	=	<	<	<	<	<	=	=	=	=	=

Table 5.14 Pairwise comparisons for glyphosate tested using the Benjamini-Hochberg correction for the significant Cell*Year*Depth interaction. White "=" values were insignificant, magenta ">" values indicate column value was greater than the row value, and yellow "<" values indicate column value was lesser than the row value. C1 = Cell 1, C2 = Cell 2, '22 = 2022, '23 = 2023, 0-5 = 0-5 cm, 5-15 = 5-15 cm, and 15-30 = 15-30 cm.

Row Labels	Conc	C1 '22 0-5	C1 '22 5-15	C1 '22 15-30	C2 '22 0-5	C2 '22 5-15	C2 '22 15-30	C1 '23 0-5	C1 '23 5-15	C1 '23 15-30	C2 '23 0-5	C2 '23 5-15
		17 (23)	16 (27)	23 (12)	0.62 (0.97)	0.18 (0.18)	0.11 (0.16)	0.88 (0.77)	8.8 (10)	3.1 (4.5)	0.049 (0.014)	0.6 (0.65)
C1 '22 5-15	16 (27)	=										
C1 '22 15-30	23 (12)	=	=									
C2 '22 0-5	0.62 (0.97)	=	<	<								
C2 '22 5-15	0.18 (0.18)	=	<	<	=							
C2 '22 15-30	0.11 (0.16)	=	<	<	=	=						
C1 '23 0-5	0.88 (0.77)	=	=	>	=	=	=					
C1 '23 5-15	8.8 (10)	=	=	=	=	>	>	=				
C1 '23 15-30	3.1 (4.5)	=	=	>	=	>	>	=	<			
C2 '23 0-5	0.049 (0.014)	=	<	<	=	=	=	<	<	<		
C2 '23 5-15	0.6 (0.65)	=	=	<	=	=	=	=	<	<	>	
C2 '23 15-30	0.27 (0.37)	=	=	<	=	=	=	=	<	<	=	=

Table 5.15 Pairwise comparisons for AMPA tested using the Benjamini-Hochberg correction for the significant Cell*Year*Depth interaction. White "=" values were insignificant, magenta ">" values indicate column value was greater than the row value, and yellow "<" values indicate column value was lesser than the row value. C1 = Cell 1, C2 = Cell 2, '22 = 2022, '23 = 2023, 0-5 = 0-5 cm, 5-15 = 5-15 cm, and 15-30 = 15-30 cm.

Row Labels	Conc	C1 '22 0-5	C1 '22 5-15	C1 '22 15-30	C2 '22 0-5	C2 '22 5-15	C2 '22 15-30	C1 '23 0-5	C1 '23 5-15	C1 '23 15-30	C2 '23 0-5	C2 '23 5-15
		290 (350)	190 (210)	380 (330)	9.4 (18)	1.5 (1.8)	0.62 (0.31)	180 (300)	750 (630)	430 (510)	0.44 (0.48)	11 (7.5)
C1 '22 5-15	190 (210)	=										
C1 '22 15-30	380 (330)	=	=									
C2 '22 0-5	9.4 (18)	=	<	<								
C2 '22 5-15	1.5 (1.8)	=	<	<	=							
C2 '22 15-30	0.62 (0.31)	=	<	<	=	=						
C1 '23 0-5	180 (300)	=	=	=	=	=	=					
C1 '23 5-15	750 (630)	=	=	=	>	>	>	=				
C1 '23 15-30	430 (510)	=	=	=	>	>	>	=	=			
C2 '23 0-5	0.44 (0.48)	=	<	<	=	<	=	=	<	<		
C2 '23 5-15	11 (7.5)	=	<	=	=	>	>	=	<	<	>	
C2 '23 15-30	10 (15)	=	<	=	=	=	=	=	<	<	>	=

Table 5.16 Pairwise comparisons for glufosinate tested using the Benjamini-Hochberg Correction for the significant Depth*Time interaction. White "=" values were insignificant, magenta ">" values indicate column value was greater than the row value, and yellow "<" values indicate column value was lesser than the row value. Pre = Pre-operation, Pos = Post-operation, 0-5 = 0-5 cm, 5-15 = 5-15 cm, and 15-30 = 15-30 cm.

Row Labels	Conc	0-5 Pre	0-5 Pos	5-15 Pre	5-15 Pos	15-30 Pre
		0.55 (1.4)	14 (25)	14 (16)	5.1 (4.6)	6.6 (10)
0-5 Pos	14 (25)	<				
5-15 Pre	14 (16)	<	=			
5-15 Pos	5.1 (4.6)	<	=	=		
15-30 Pre	6.6 (10)	<	=	=	=	
15-30 Pos	2.5 (1.2)	<	=	<	=	=

Table 5.17 Pairwise comparisons for glufosinate tested using the Benjamini-Hochberg correction for the significant Year*Time interaction. White "=" values were insignificant, magenta ">" values indicate column value was greater than the row value, and yellow "<" values indicate column value was lesser than the row value. '22 = 2022, '23 = 2023, Pre = Pre-operation, Pos = Post-operation.

Row Labels	Conc	'22_Pre	'22_Post	'23_Pre
		13 (15)	4.4 (3.3)	1.5 (2)
'22 Pos	4.4 (3.3)	=		
'23 Pre	1.5 (2)	<	<	
'23 Pos	9.6 (21)	=	=	>

Table 5.18 Pairwise comparisons for glufosinate tested using the Benjamini-Hochberg correction for the significant Year*Depth interaction. White "=" values were insignificant, magenta ">" values indicate column value was greater than the row value, and yellow "<" values indicate column value was lesser than the row value. '22 = 2022, '23 = 2023, 0-5 = 0-5 cm, 5-15 = 5-15 cm, and 15-30 = 15-30 cm.

Row Labels	Conc	'22 0-5	'22 5-15	'22 15-30	'23 0-5	'23 5-15
		3.2 (3.7)	15 (15)	7.4 (9.5)	11 (26)	4.1 (4.3)
'22 5-15	15 (15)	=				
'22 15-30	7.4 (9.5)	=	=			
'23 0-5	11 (26)	=	=	=		
'23 5-15	4.1 (4.3)	=	=	=	=	
'23 15-30	1.7 (0.98)	=	<	<	=	=

6. APPENDIX II: CHAPTER THREE VALIDATION OVERVIEW LC-MS/MS PARAMETERS

6.1 Eurachem Method Validation Calculations

Selectivity was determined through a dynamic Multiple Reaction Monitoring by selection of a parent ions (of greatest abundance) and selection of a quantitative (greatest abundance) and qualitative (second most abundant) product ions. Linearity as determined through seven independent runs of an eight-point calibration curve spiked with 50 ng mL^{-1} IS; concentration was determined through isotope dilution. Working range were determined through qualitative assessment of calibration curves that maximized R^2 values with the most calibration points in an unweighted calibration curve.

LOD/LOQ and MLD/MLQ were determined in solution at 5 ng mL^{-1} in-vial concentration. LOD/LOQ was determined in acetonitrile while MLD/MLQ were determined in sample extracts. Each were with ten replicates and used:

$$S'_0 = \frac{S_0}{\sqrt{n}} \tag{6-1}$$

$$Detection\ Limit = S'_0\ x\ 3 \tag{6-2}$$

$$Quantification\ Limit = S'_0\ x\ 10 \tag{6-3}$$

Where S'_0 is the standard error of the mean, S_0 is the standard deviation of all runs, and n is the total number of samples.

Most pesticides in bimoixture extractions utilized the same formula as above for MLD/MLQ determination; biomixture samples that did have quantifiable pesticide concentrations

were determined with twelve spiked samples and six blank corrections samples. For compounds with endmemic concentrations, MLD/MLQs were determined by:

$$S'_0 = S_0 * \sqrt{\frac{1}{n_s} + \frac{1}{n_b}} \quad (6\text{-}4)$$

Where n_s is total number of spiked samples while n_b is the total number of blank samples.

Effluent and rinsate accuracy and precisions were conducted at all dilutions. Effluent samples were spiked at 20, 200, 2,000, and 20,000 μg L^{-1}; rinsate was spiked at 200, 2,000, 20,000, and 200,000 ng mL^{-1}. Biomixture was conducted at 100 and 1,000 ng g^{-1}.

Accuracies results were conducted with six replicates per matrix; for biomixtures, three blanks were run in tandem for correction. Results were calculated with the following equation:

$$R(\%) = \left(\frac{\bar{x}}{x_{spk}}\right) * 100 \quad (6\text{-}5)$$

Where $R(\%)$ is percent recovery, $\bar{x}$ = mean analyte recovery, and x_{spk} = spiked analyte concentration.

Both intra- and interday precision were determined at 0, 12, 24 hours and 0, 24, and 48 hours, respectively, with two replicates at each time point; one blank per time period was also run for biomixture. A total of six replicates (and three blanks) for both intra- and interday precision with and calculated with the following equation:

$$CV\ (\%) = \left(\frac{SD}{\bar{x}}\right) * 100 \quad (6\text{-}6)$$

Where CV (%) = percent coefficient of variation (relative standard deviation), SD = standard deviation, and $\bar{x}$ = mean analyte recovery.

Matrix effects were determined for all levels of dilutions, across s linear range for all compounds of 5, 10, and 20 ng mL^{-1} in four replicates; runs were conducted in a randomized

complete block design with one replicate of each concentration and matrix run in four separate runs to compare raw response changes across matrices. Biomixtures freeze-drying losses were compared for pesticide losses by spiking internal standard before freeze-drying, after freeze-drying, and at syringe filtering to test changes in pesticide concetrations quantified. Initial pesticide concentrations were set at 1,000 ppb while internal standards were added for a final in-vial concentration of 50 ppb.

6.2 Supplementary Materials for Chapter Three: Instrument Chromatograms, Mass Spectrometric and Chromatographic Conditions, and Chemical Characteristics

6.2.1 Chromatograms for Pesticides

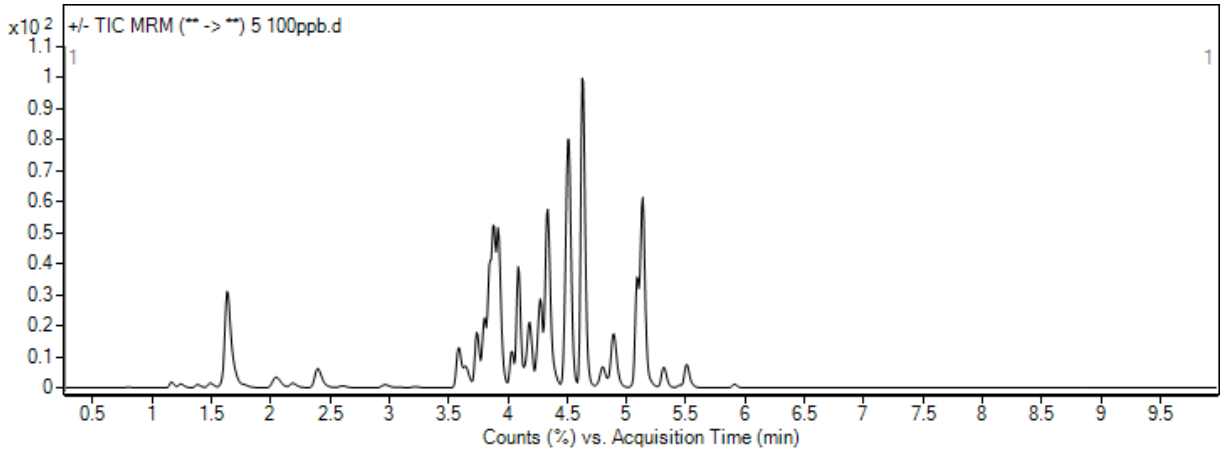

Figure 6.1 Total ion chromatogram for the method.

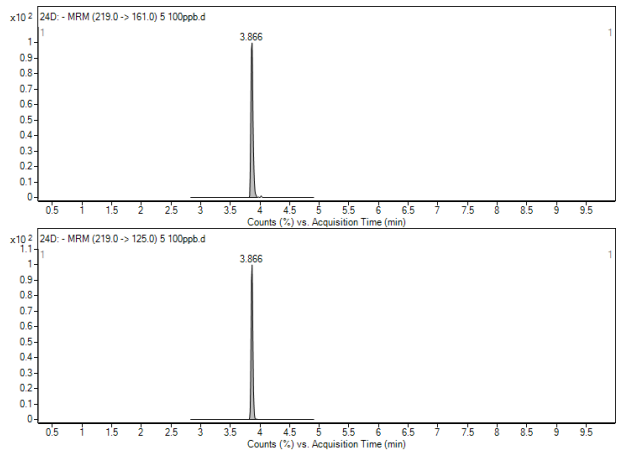

Figure 6.2 2,4-D chromatograms for the quantifier (top) and qualifier (bottom).

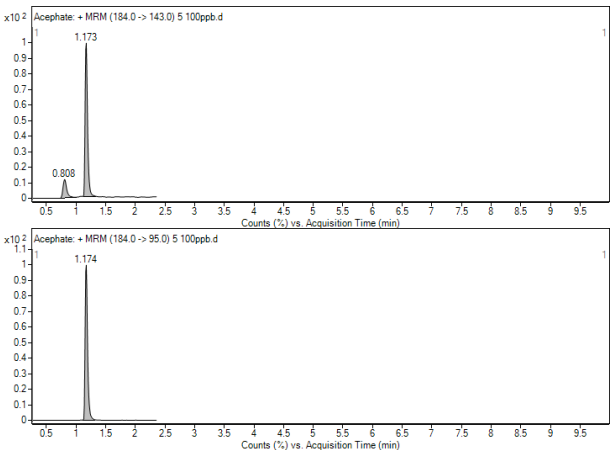

Figure 6.4 Acephate chromatograms for the quantifier (top) and qualifier (bottom).

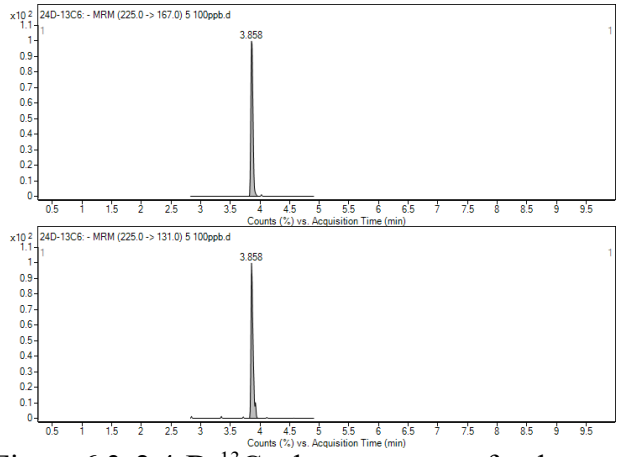

Figure 6.3 2,4-D-$^{13}C_6$ chromatograms for the quantifier (top) and qualifier (bottom).

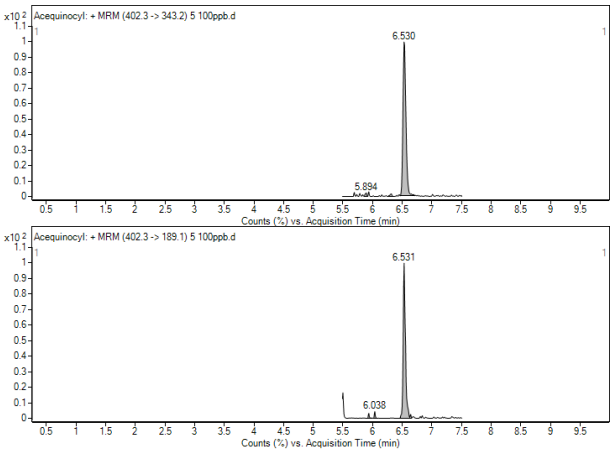

Figure 6.5 Acequinocyl chromatograms for the quantifier (top) and both qualifier (bottom).

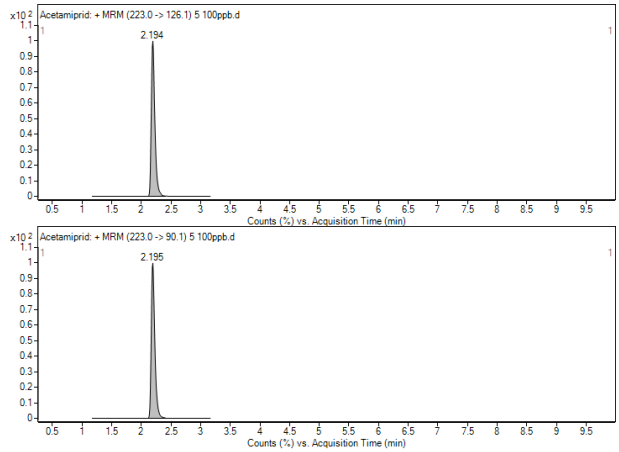

Figure 6.6 Acetamiprid chromatograms for the quantifier (top) and qualifier (bottom).

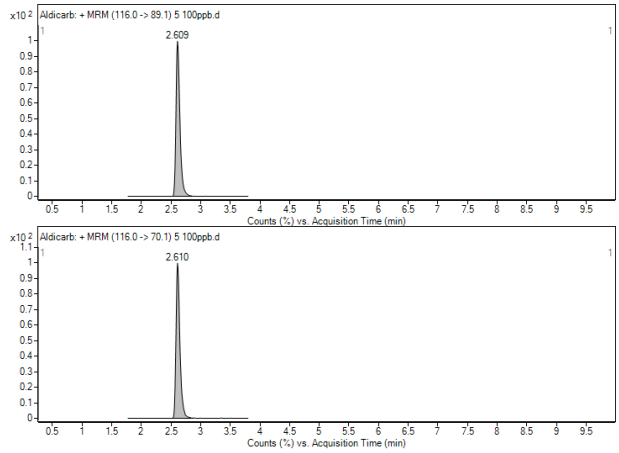

Figure 6.7 Acetamiprid chromatograms for the quantifier (top) and qualifier (bottom).

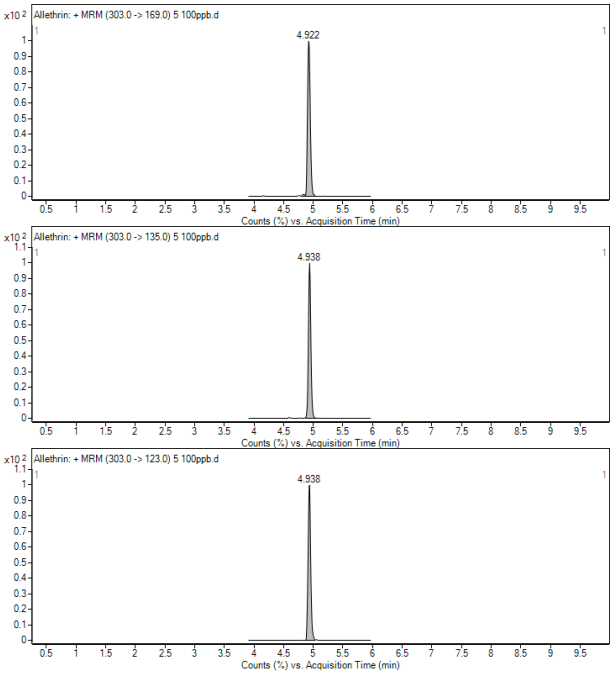

Figure 6.8 Allethrin chromatograms for the quantifier (top) and qualifiers (middle and bottom).

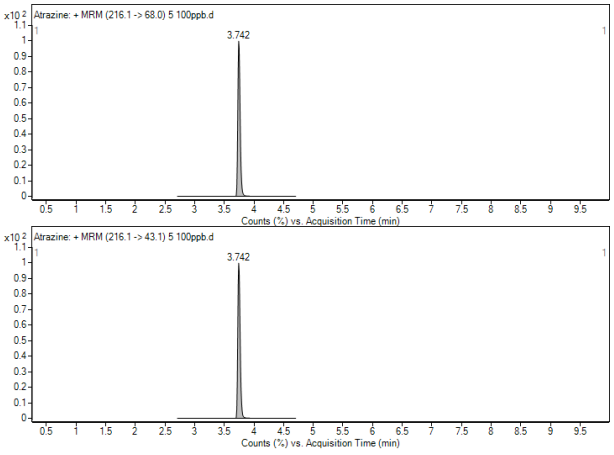

Figure 6.9 Atrazine chromatograms for the quantifier (top) and qualifier (bottom).

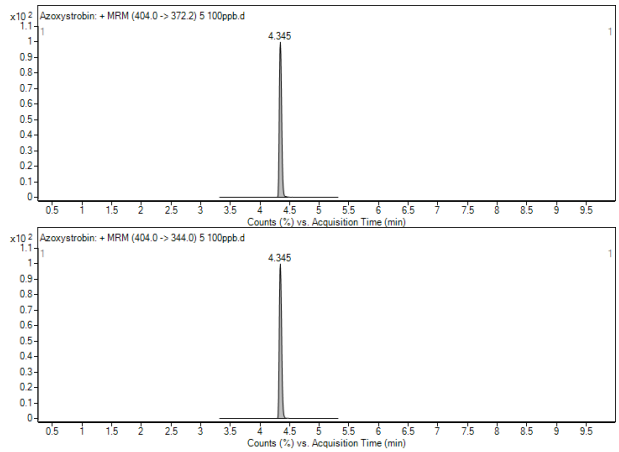

Figure 6.10 Azoxystrobin chromatograms for the quantifier (top) and qualifier (bottom).

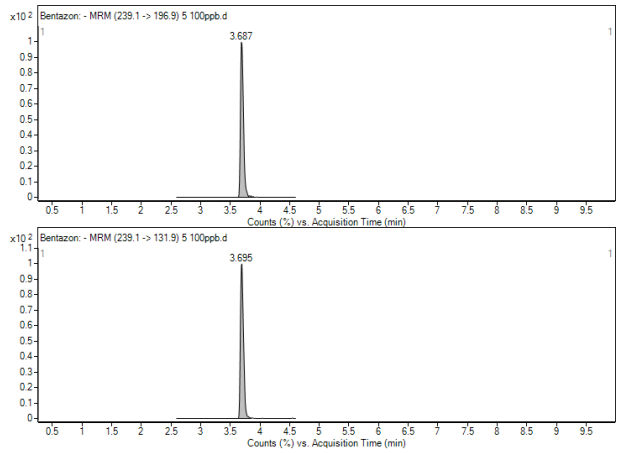

Figure 6.11 Bentazon chromatograms for the quantifier (top) and qualifier (bottom).

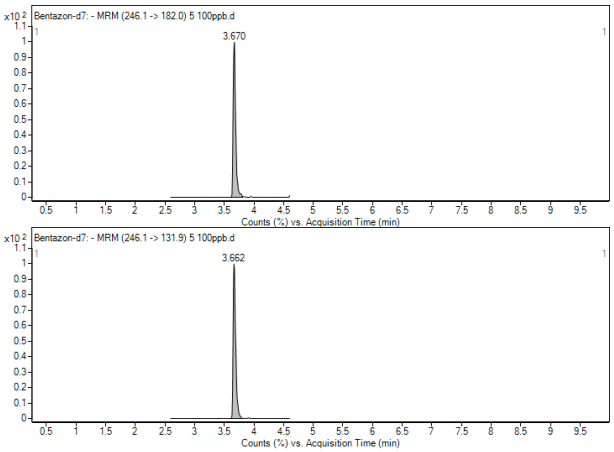

Figure 6.12 Bentazon-d_7 chromatograms for the quantifier (top) and qualifier (bottom).

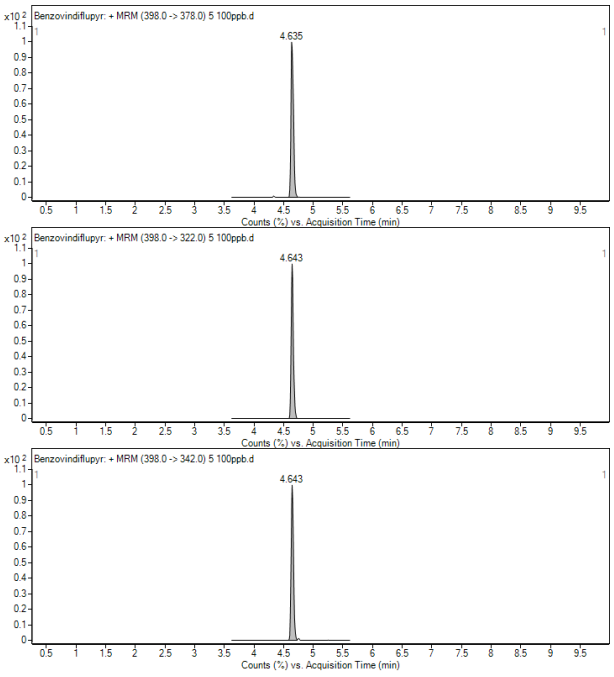

Figure 6.13 Benzovindiflupyr chromatograms for the quantifier (top) and qualifiers (bottom).

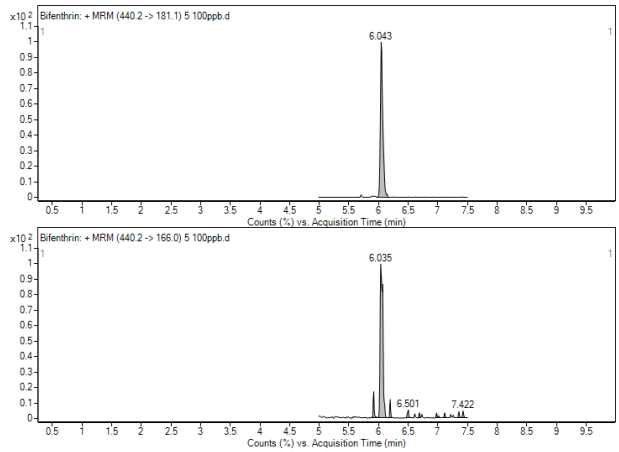

Figure 6.14 Bifenthrin chromatograms for the quantifier (top) and qualifier (bottom).

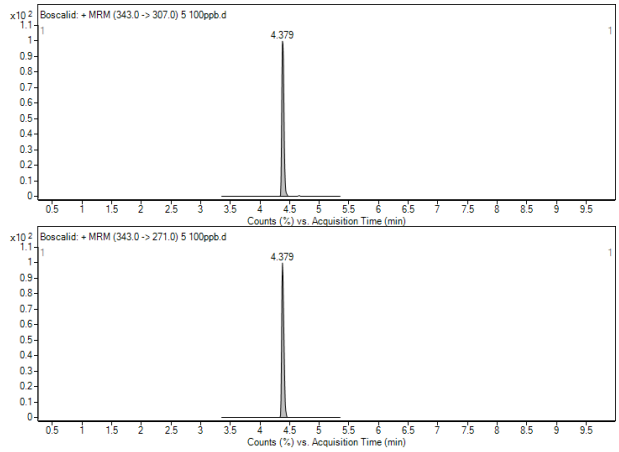

Figure 6.15 Boscalid chromatograms for the quantifier (top) and qualifier (bottom).

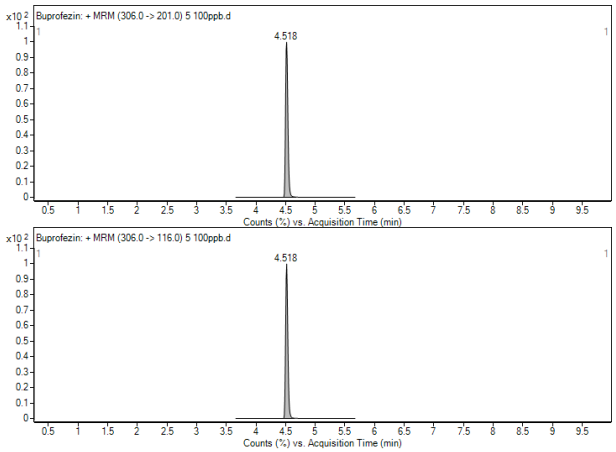

Figure 6.16 Buprofezin chromatograms for the quantifier (top) and qualifier (bottom).

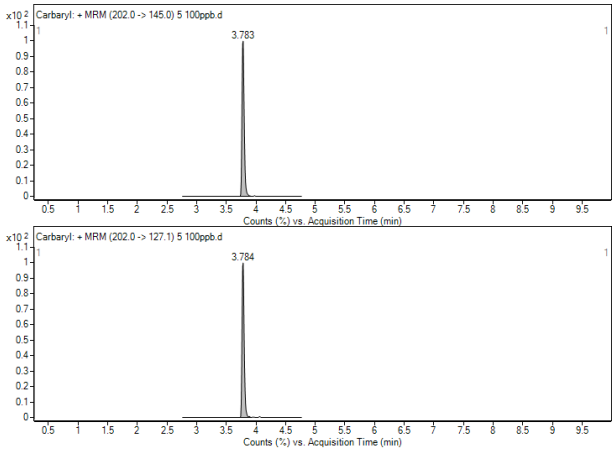

Figure 6.17 Carbaryl chromatograms for the quantifier (top) and qualifier (bottom).

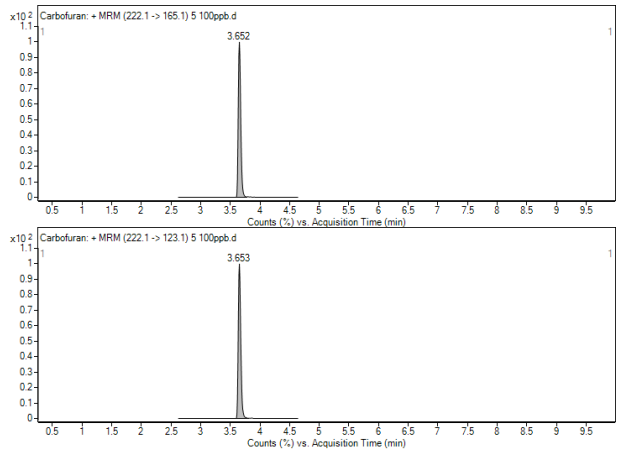

Figure 6.18 Carbofuran chromatograms for the quantifier (top) and qualifier (bottom).

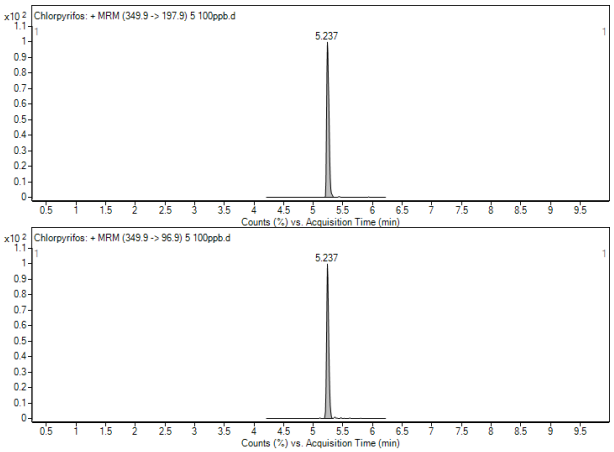

Figure 6.20 Chlorpyrifos chromatograms for the quantifier (top) and qualifier (bottom).

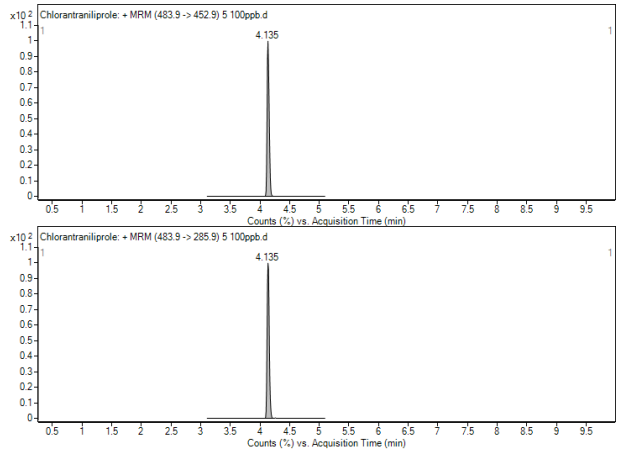

Figure 6.19 Chlorantraniliprole chromatograms for the quantifier (top) and qualifier (bottom).

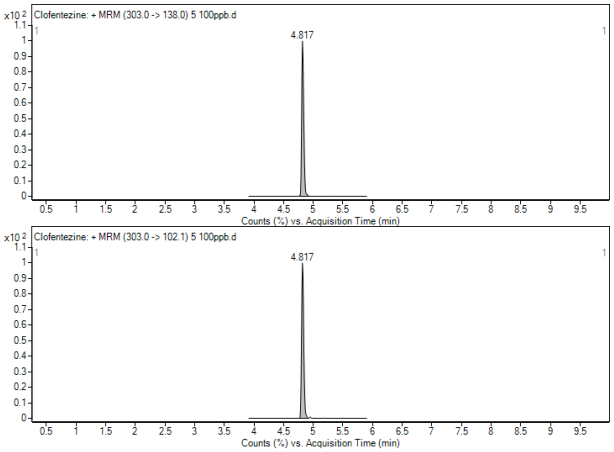

Figure 6.21 Clofentezine chromatograms for the quantifier (top) and qualifier (bottom).

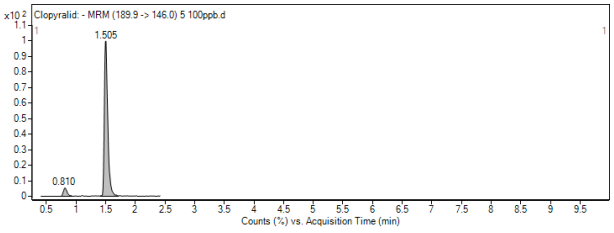

Figure 6.22 Clopyralid chromatogram for the quantifier.

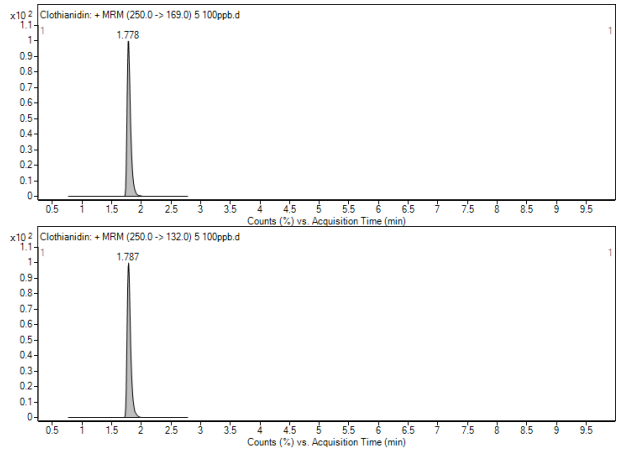

Figure 6.23 Clothianidin chromatograms for the quantifier (top) and qualifier (bottom).

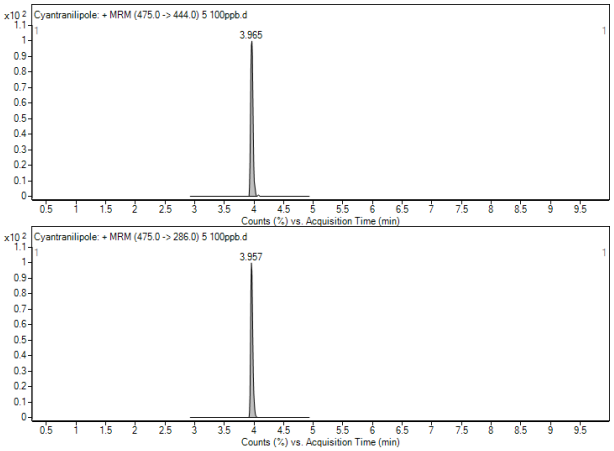

Figure 6.25 Cyantraniliprole chromatograms for the quantifier (top) and qualifier (bottom).

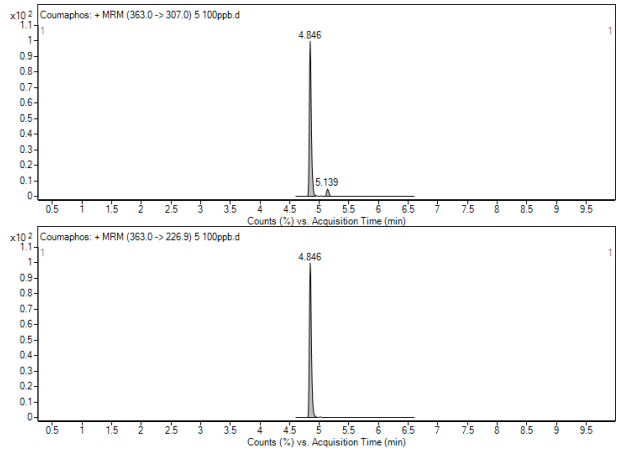

Figure 6.24 Coumaphos chromatograms for the quantifier (top) and qualifier (bottom).

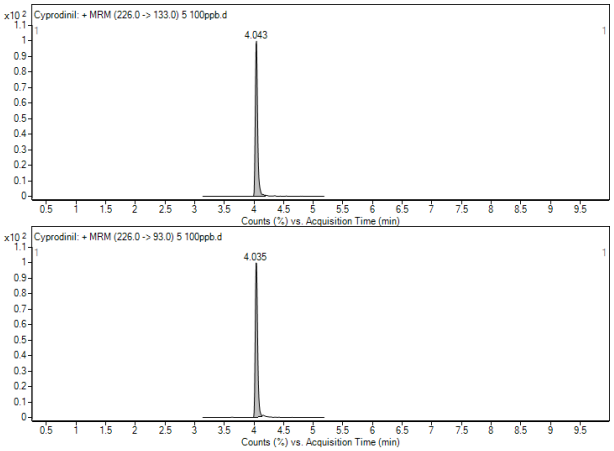

Figure 6.26 Cyprodinil chromatograms for the quantifier (top) and qualifier (bottom).

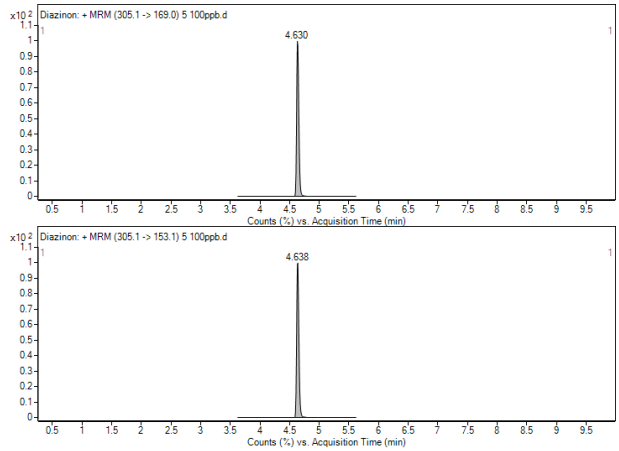

Figure 6.27 Diazinon chromatograms for the quantifier (top) and qualifier (bottom).

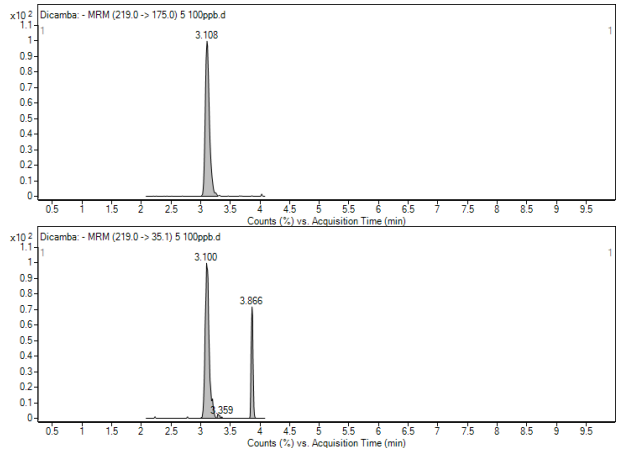

Figure 6.28 Dicamba chromatograms for the quantifier (top) and qualifier (bottom).

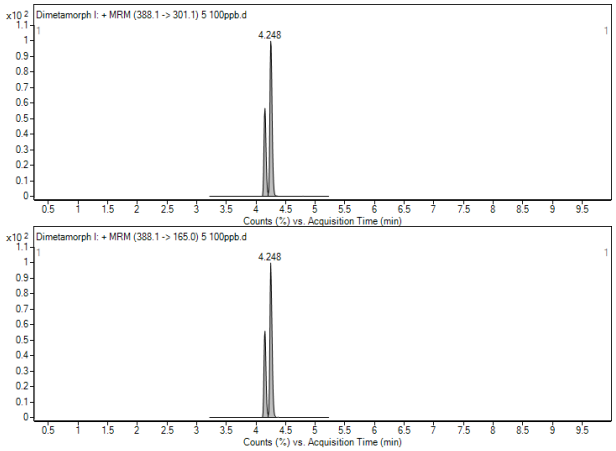

Figure 6.29 Dimethomorph I (right peak) chromatograms for the quantifier (top) and qualifier (bottom).

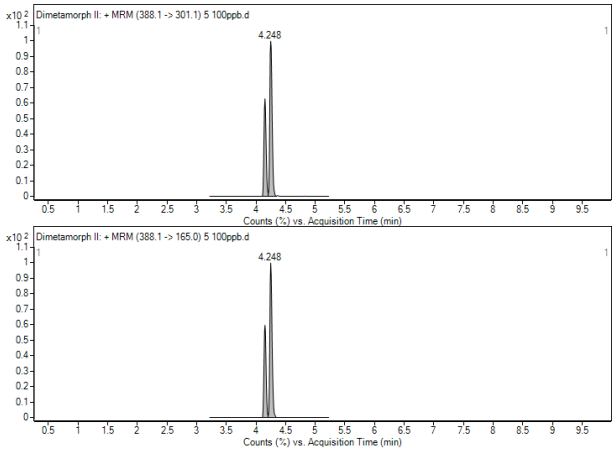

Figure 6.30 Dimethomorph II (left peak) chromatograms for the quantifier (top) and qualifier (bottom).

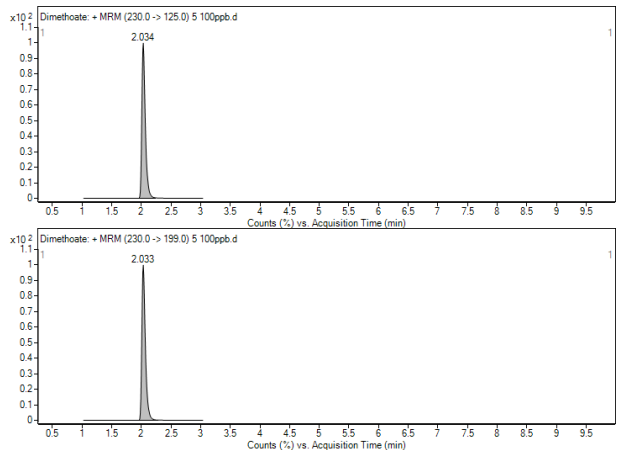

Figure 6.31 Dimethoate chromatograms for the quantifier (top) and qualifier (bottom).

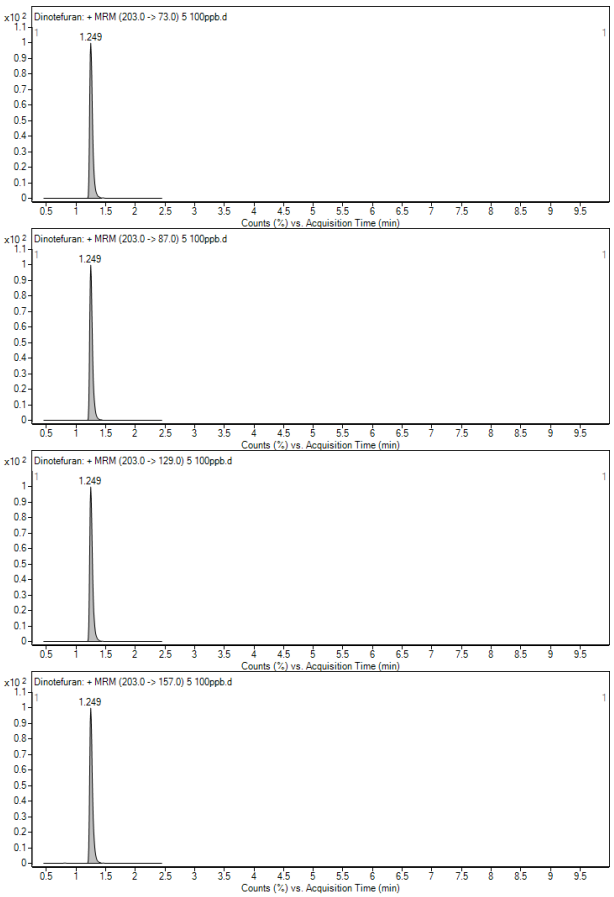

Figure 6.32 Dinotefuran chromatograms for the quantifier (top) and qualifiers (mid-up, mid-bottom, and bottom).

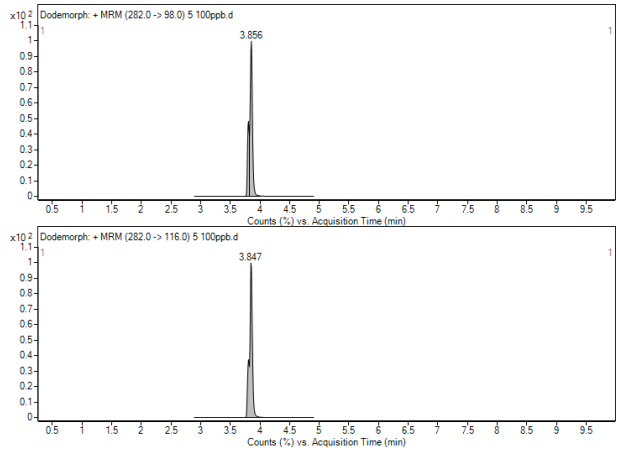

Figure 6.33 Dodemorph chromatograms for the quantifier (top) and qualifier (bottom).

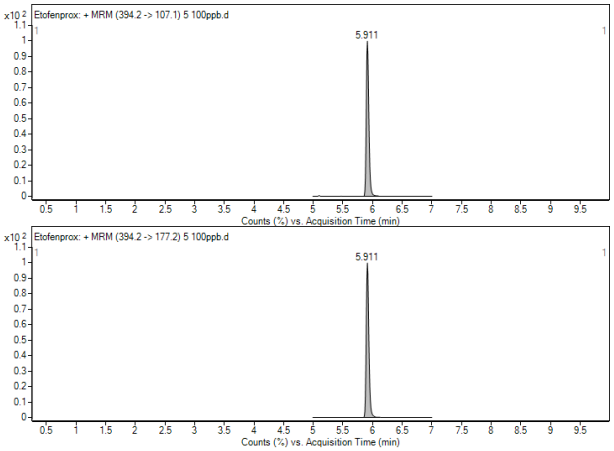

Figure 6.35 Etofenprox chromatograms for the quantifier (top) and qualifier (bottom).

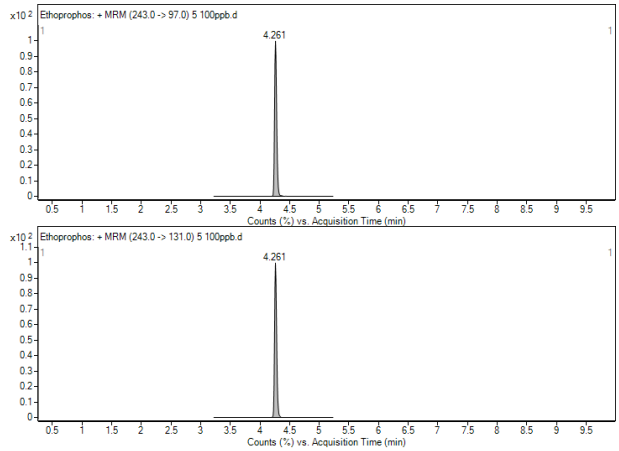

Figure 6.34 Ethoprophos chromatograms for the quantifier (top) and qualifier (bottom).

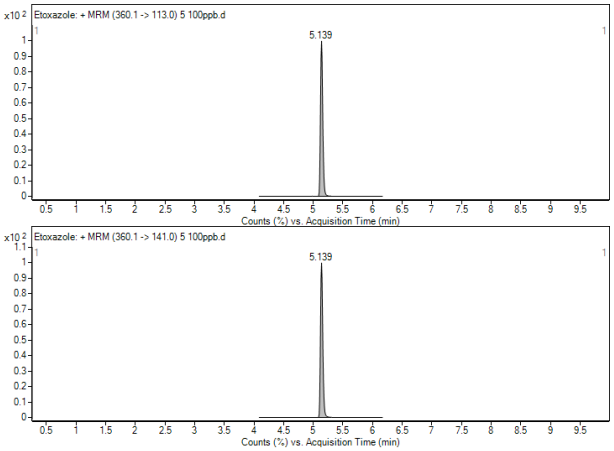

Figure 6.36 Etoxazole chromatograms for the quantifier (top) and qualifier (bottom).

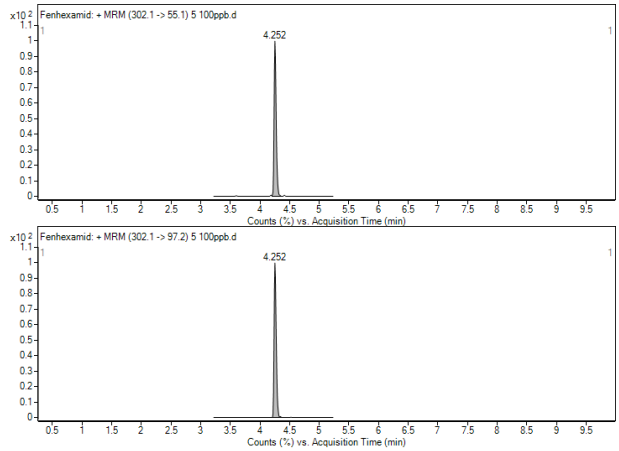

Figure 6.37 Fenhexamid chromatograms for the quantifier (top) and qualifier (bottom).

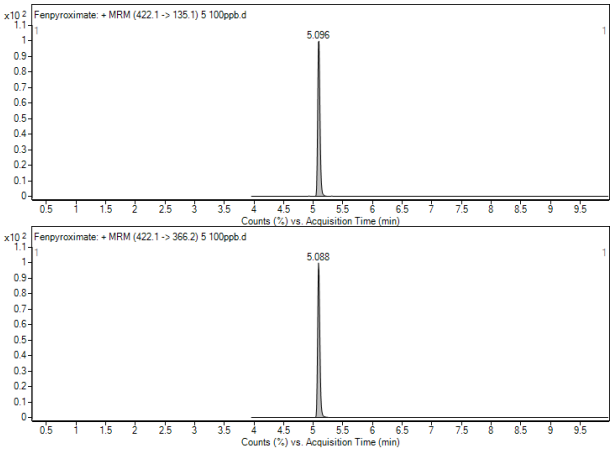

Figure 6.39 Fenpyroximate chromatograms for the quantifier (top) and qualifier (bottom).

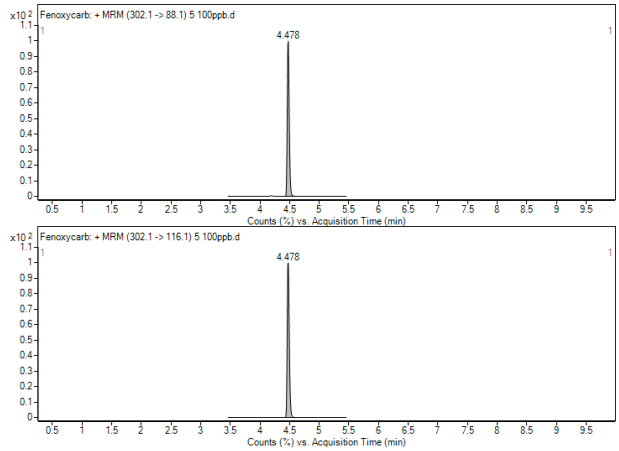

Figure 6.38 Fenoxycarb chromatograms for the quantifier (top) and qualifier (bottom).

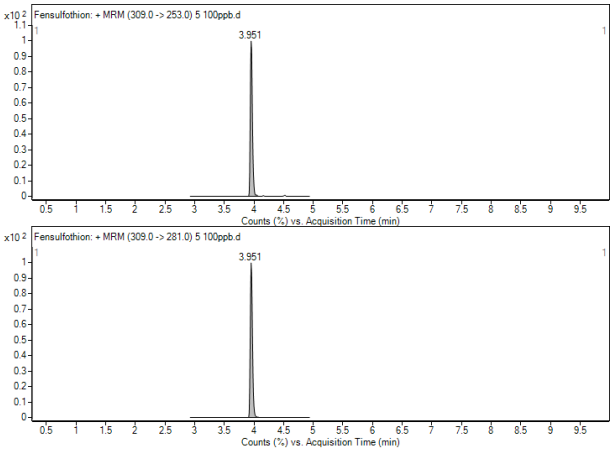

Figure 6.40 Fensulfothion chromatogram for the quantifier (top) and qualifiers (bottom).

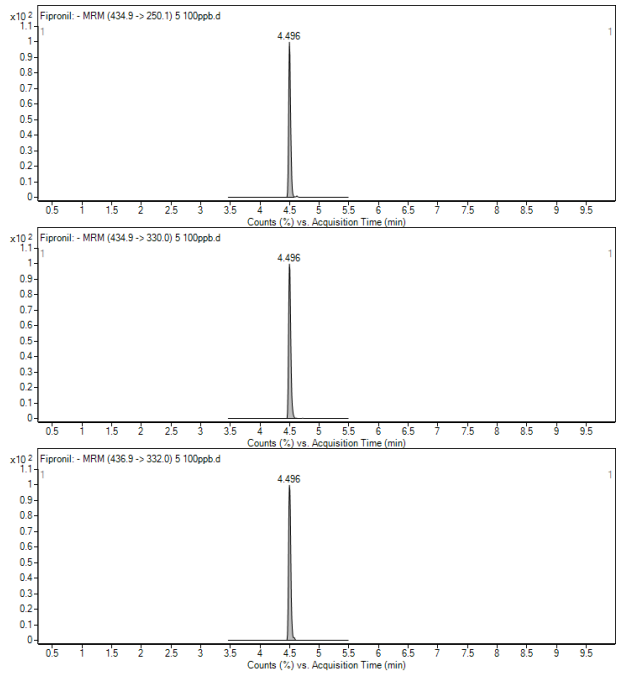

Figure 6.41 Fipronil chromatograms for the quantifier (top) and qualifiers (middle and bottom).

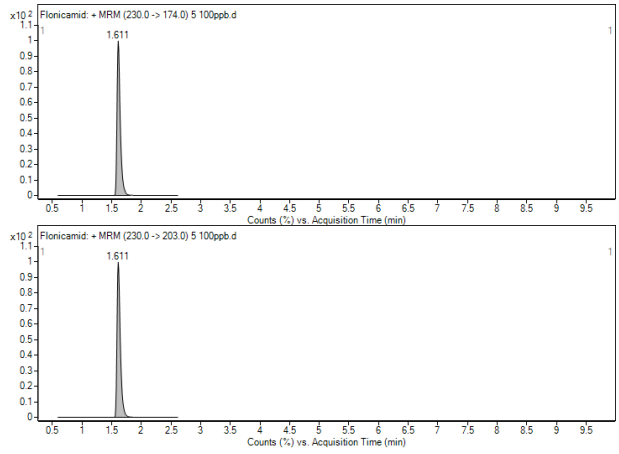

Figure 6.42 Flonicamid chromatogram for the quantifier (top) and qualifiers (bottom).

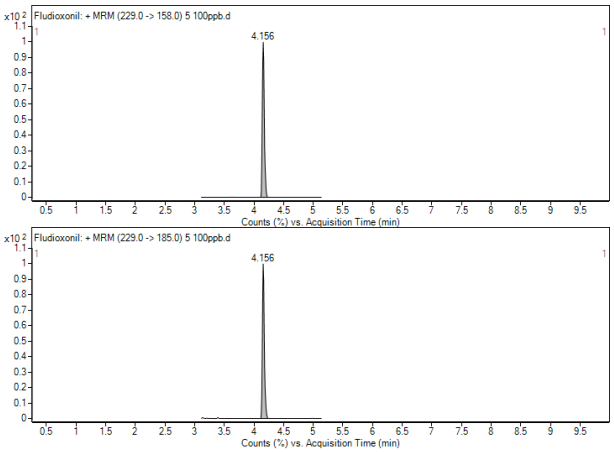

Figure 6.43 Fludioxinil chromatograms for the quantifier (top) and qualifier (bottom).

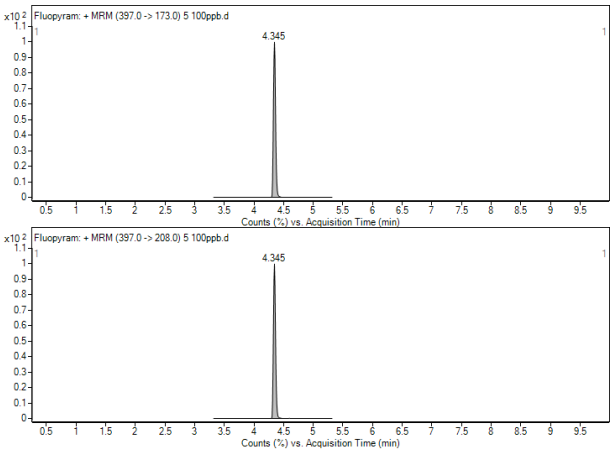

Figure 6.44 Fluopyram chromatogram for the quantifier (top) and qualifiers (bottom).

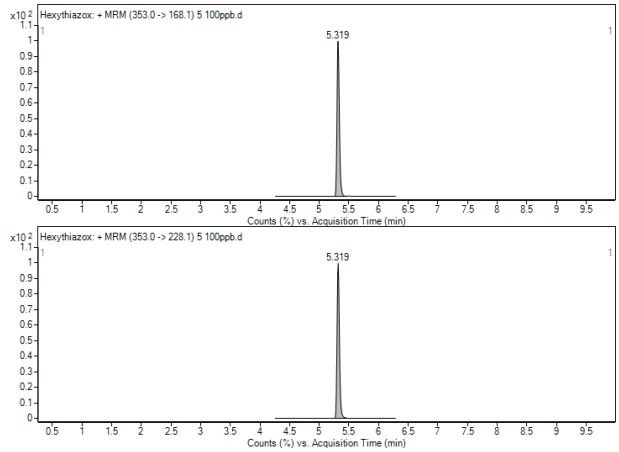

Figure 6.45 Hexythiazox chromatograms for the quantifier (top) and qualifier (bottom).

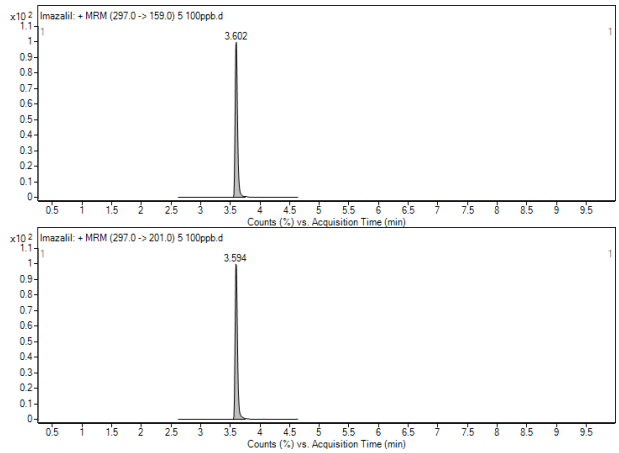

Figure 6.46 Imazalil chromatograms for the quantifier (top) and qualifier (bottom).

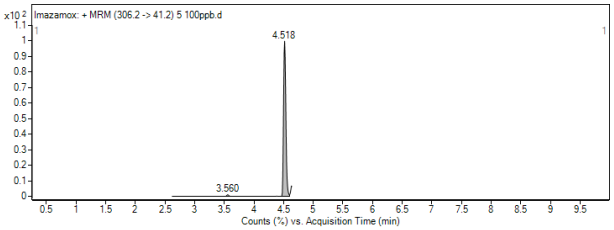

Figure 6.47 Imazamox chromatogram for the quantifier.

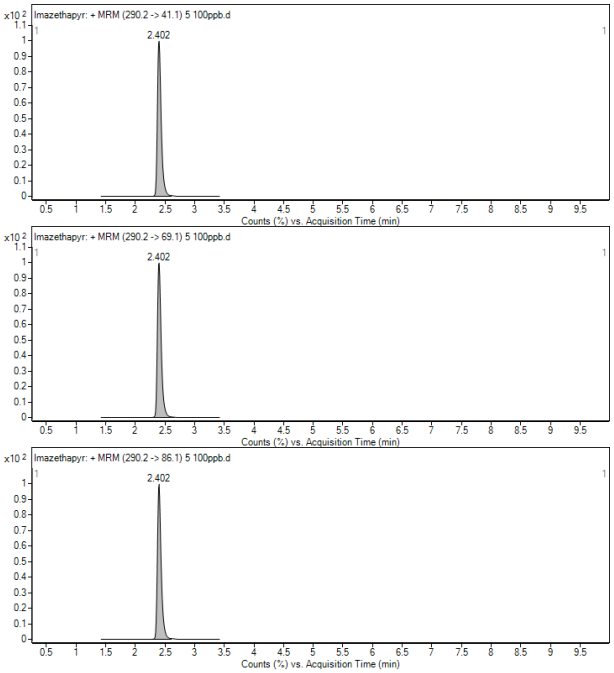

Figure 6.48 Imazethapyr chromatograms for the quantifier (top) and qualifiers (middle and bottom).

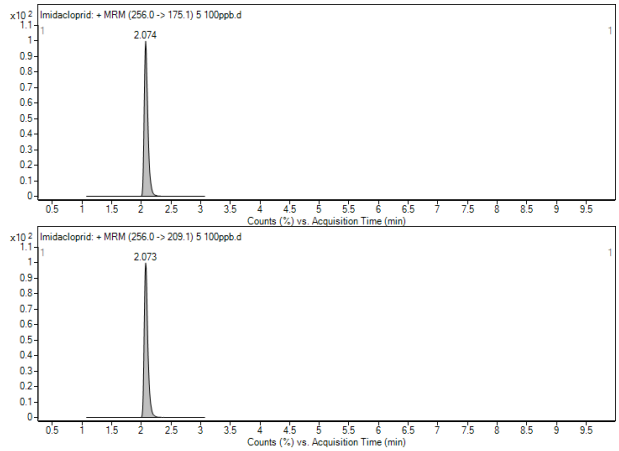

Figure 6.49 Imidacloprid chromatograms for the quantifier (top) and qualifier (bottom).

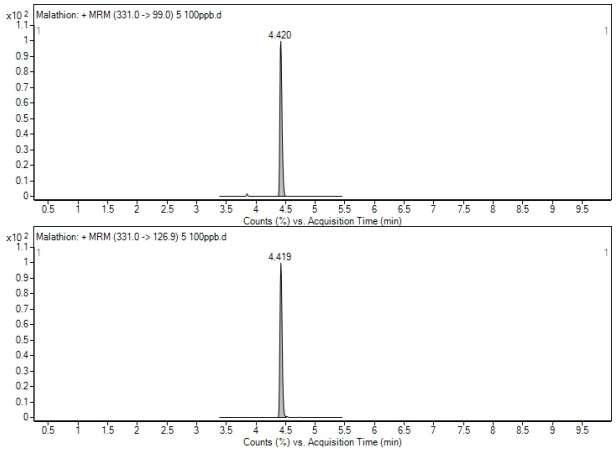

Figure 6.51 Malathion chromatograms for the quantifier (top) and qualifier (bottom).

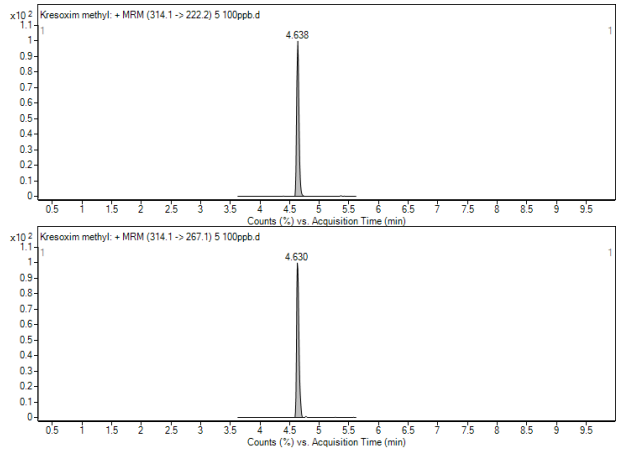

Figure 6.50 Kresoxim-methyl chromatograms for the quantifier (top) and qualifier (bottom).

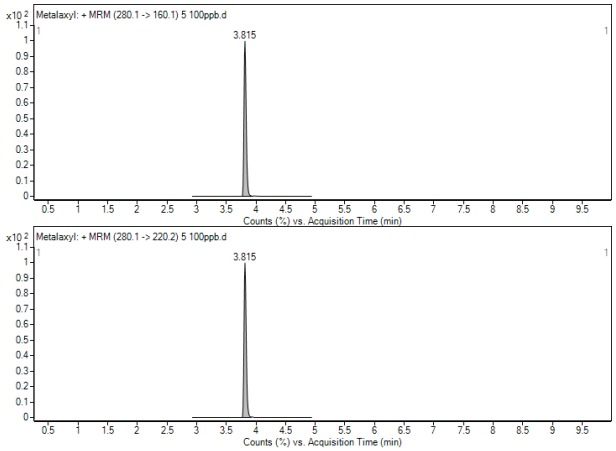

Figure 6.52 Metalaxyl chromatograms for the quantifier (top) and qualifier (bottom).

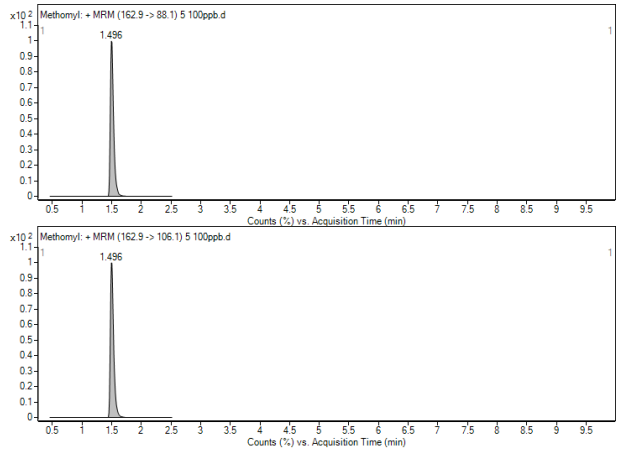

Figure 6.53 Methomyl chromatograms for the quantifier (top) and qualifier (bottom).

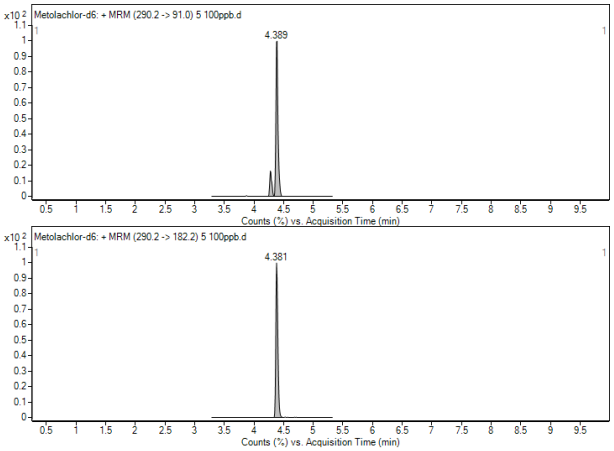

Figure 6.55 Metolachlor-d_6 chromatograms for the quantifier (top) and qualifier (bottom).

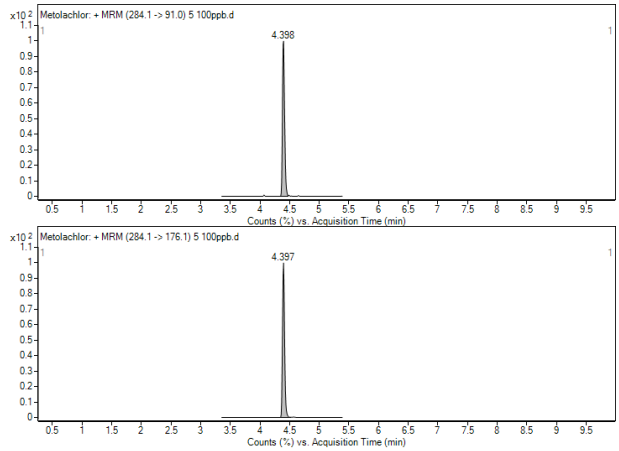

Figure 6.54 Metolachlor chromatograms for the quantifier (top) and qualifier (bottom).

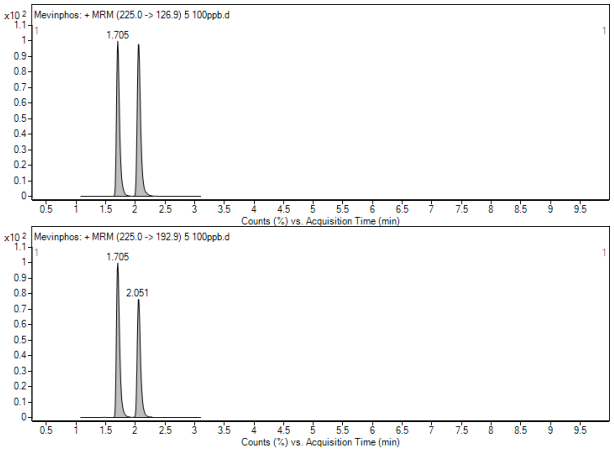

Figure 6.56 Mevinphos chromatograms for the quantifier (top) and qualifier (bottom).

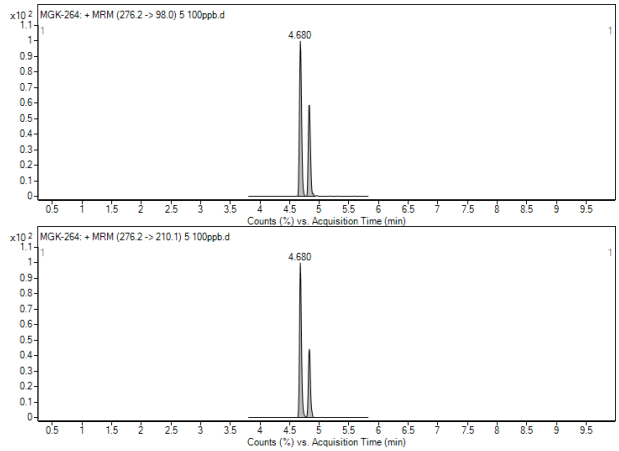

Figure 6.57 MGK-264 chromatograms for the quantifier (top) and qualifier (bottom).

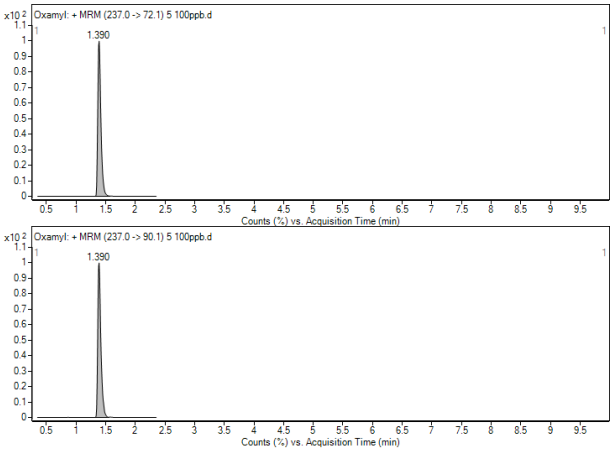

Figure 6.59 Oxamyl chromatograms for the quantifier (top) and qualifier (bottom).

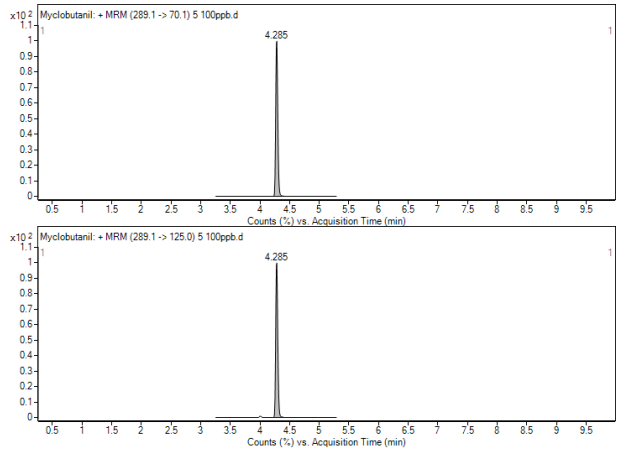

Figure 6.58 Myclobutanil chromatograms for the quantifier (top) and qualifier (bottom).

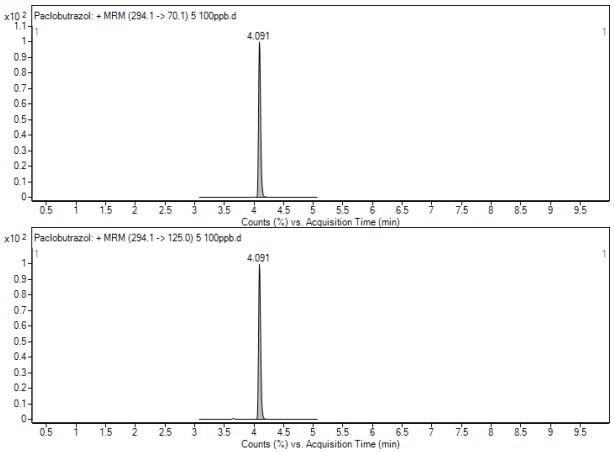

Figure 6.60 Paclobutrazol chromatograms for the quantifier (top) and qualifier (bottom).

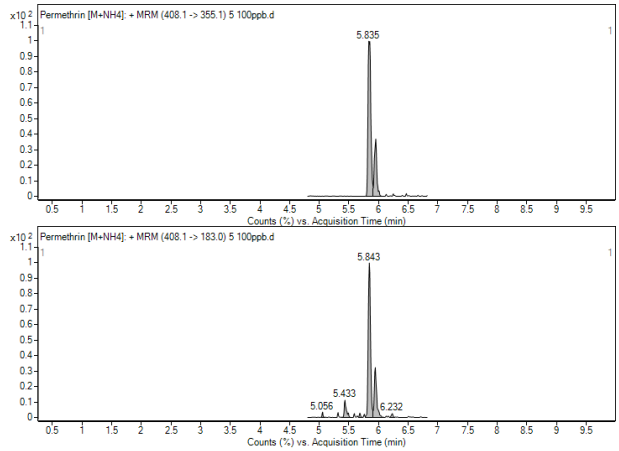

Figure 6.61 Permethrin [$NH4^{+}$] chromatograms for the quantifier (top) and qualifier (bottom).

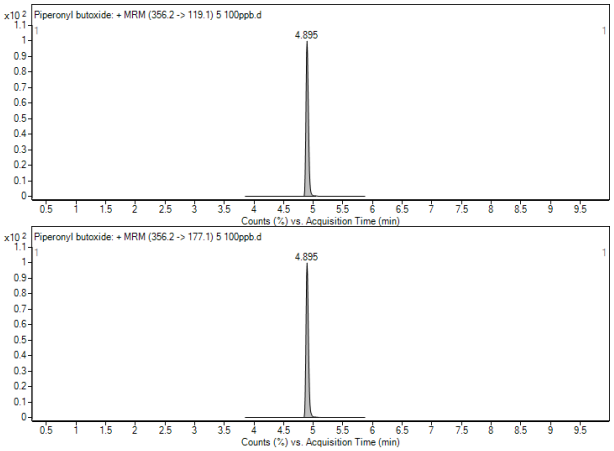

Figure 6.63 Piperonyl Butoxide chromatograms for the quantifier (top) and qualifier (bottom).

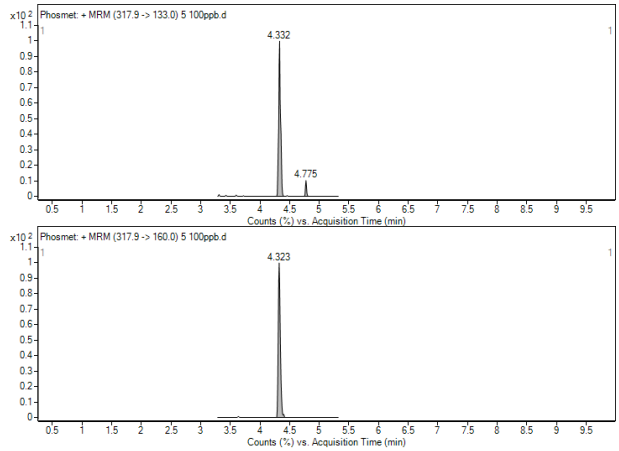

Figure 6.62 Phosmet chromatograms for the quantifier (top) and qualifier (bottom).

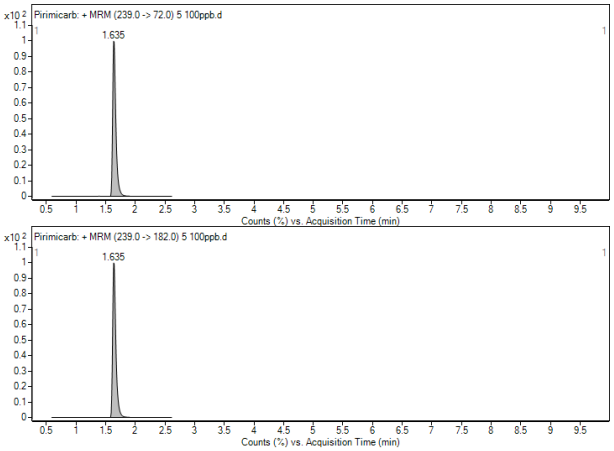

Figure 6.64 Pirimicarb chromatograms for the quantifier (top) and qualifier (bottom).

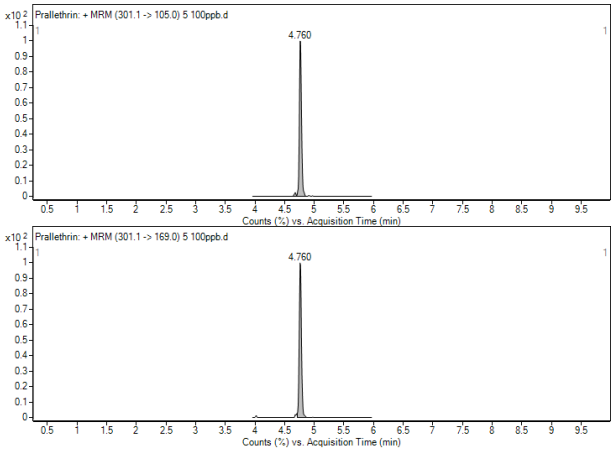

Figure 6.65 Prallethrin chromatograms for the quantifier (top) and qualifier (bottom).

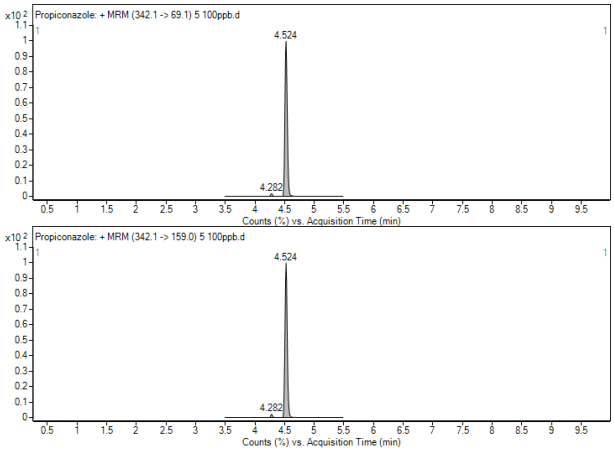

Figure 6.66 Propiconazole chromatograms for the quantifier (top) and qualifier (bottom).

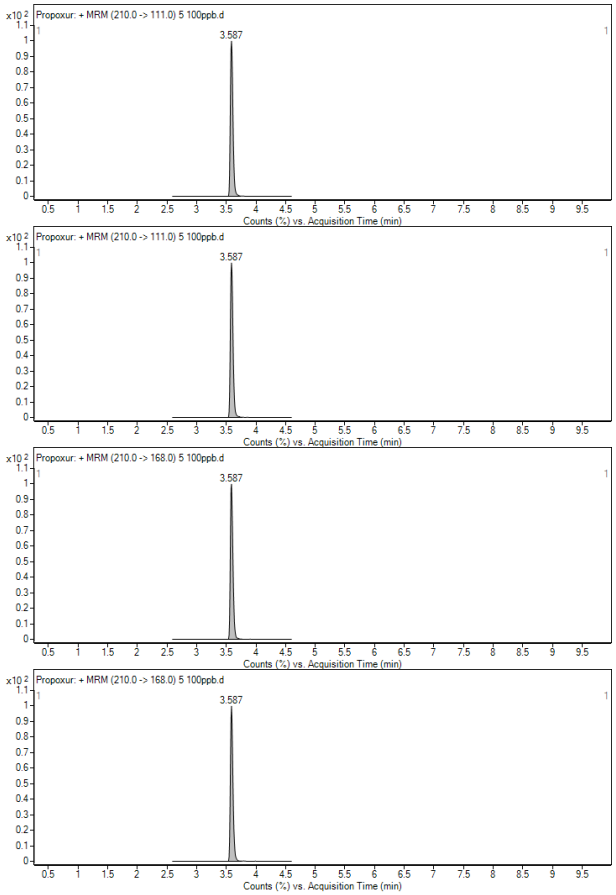

Figure 6.67 Propoxur chromatograms for the quantifier (top) and qualifiers (mid-top, mid-bottom, and bottom).

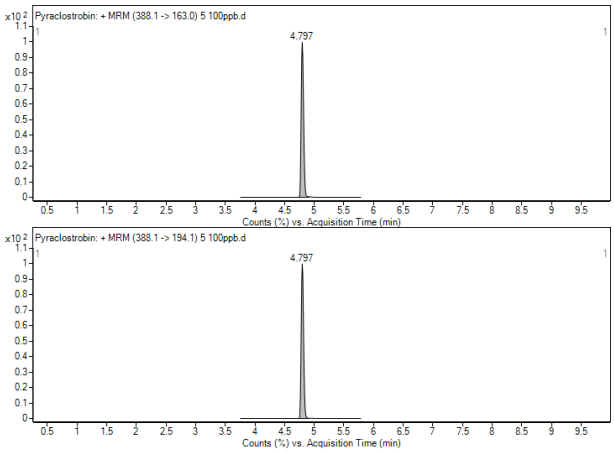

Figure 6.68 Pyraclostrobin chromatograms for the quantifier (top) and qualifier (bottom).

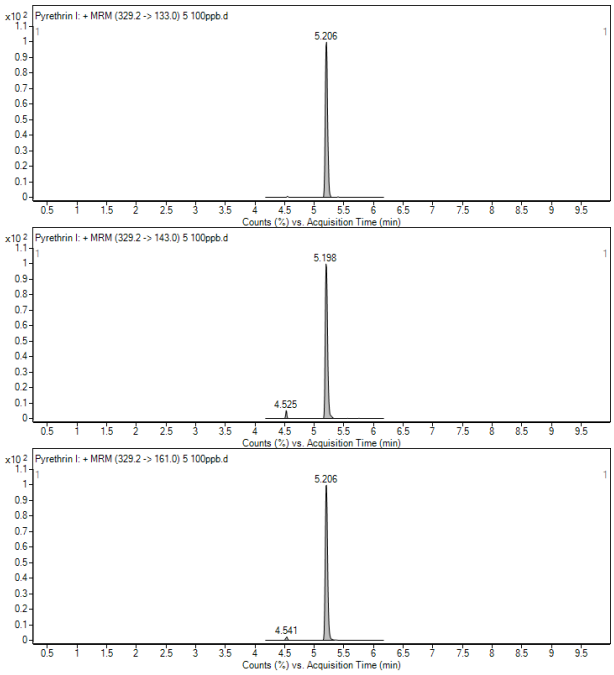

Figure 6.69 Pyrethrin I chromatograms for the quantifier (top) and qualifiers (middle and bottom).

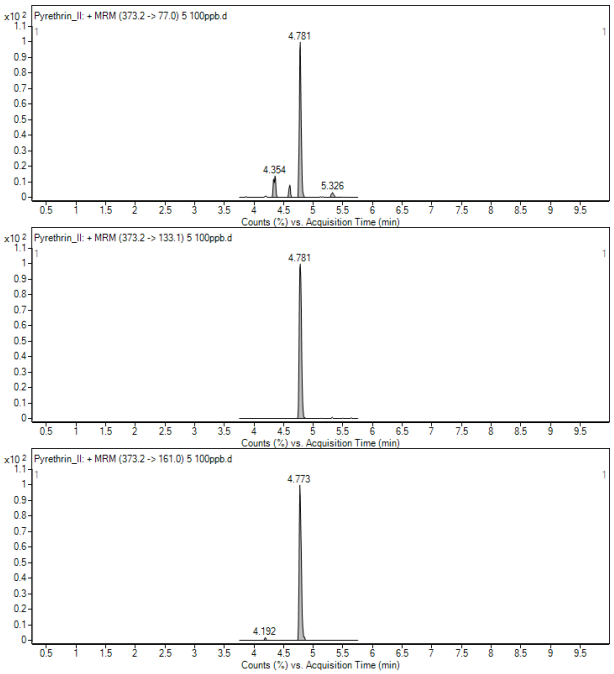

Figure 6.70 Pyrethrin II chromatograms for the quantifier (top) and qualifiers (middle and bottom).

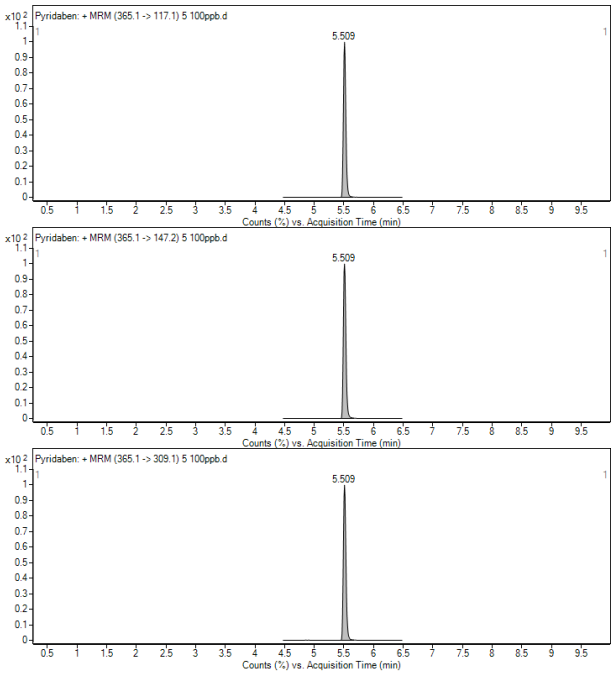

Figure 6.71 Pyridaben chromatograms for the quantifier (top) and qualifiers (middle and bottom).

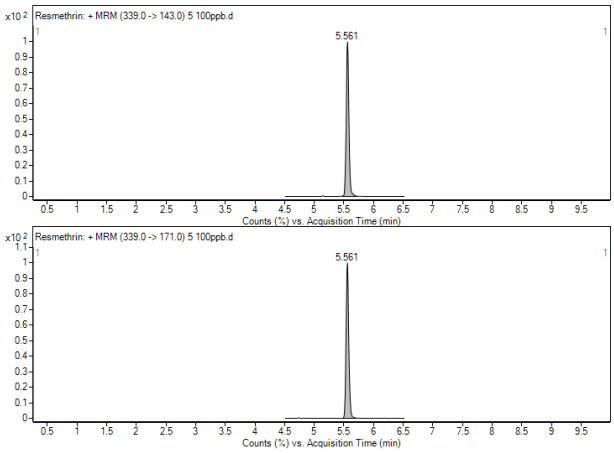

Figure 6.72 Resmethrin chromatograms for the quantifier (top) and qualifier (bottom).

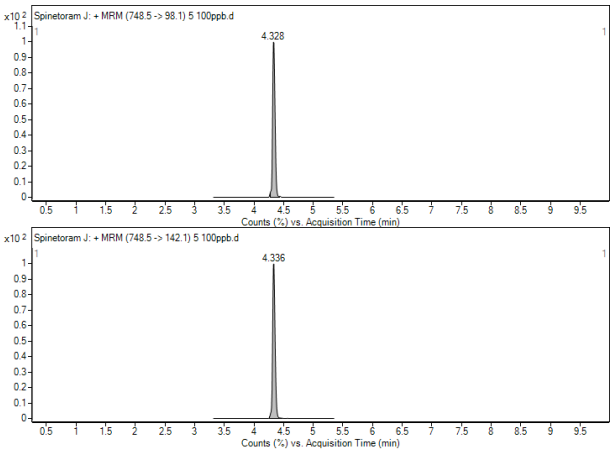

Figure 6.73 Spinetoram J chromatograms for the quantifier (top) and qualifier (bottom).

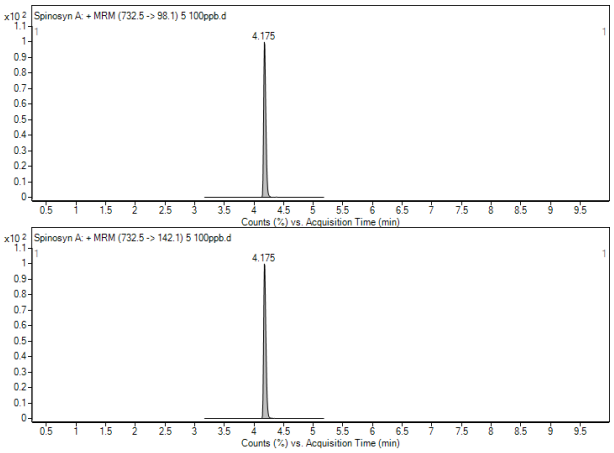

Figure 6.74 Spinosyn A chromatograms for the quantifier (top) and qualifier (bottom).

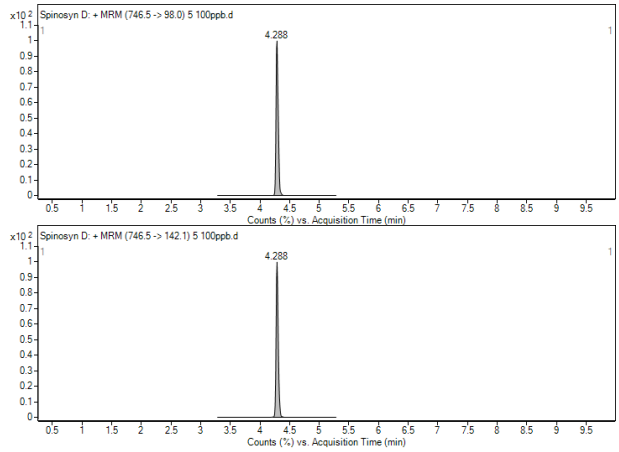

Figure 6.75 Spinosyn D chromatograms for the quantifier (top) and qualifier (bottom).

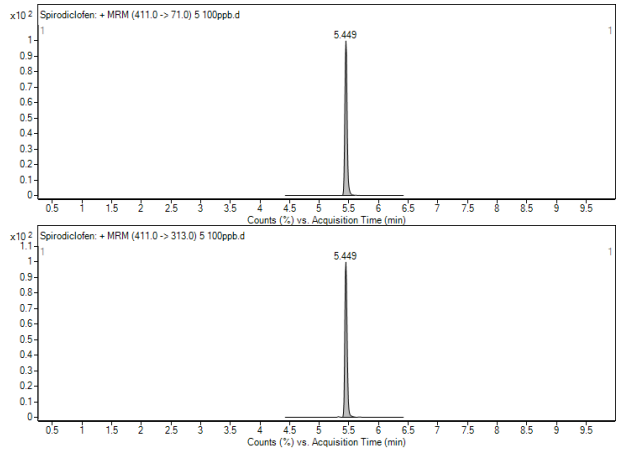

Figure 6.76 Spirodiclofen chromatograms for the quantifier (top) and qualifier (bottom).

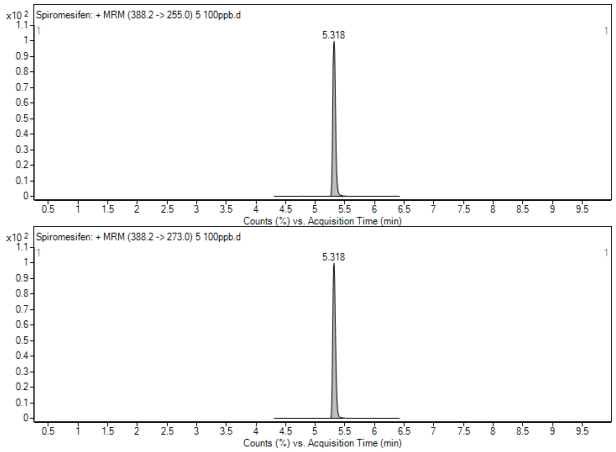

Figure 6.77 Spiromesifen chromatograms for the quantifier (top) and qualifier (bottom).

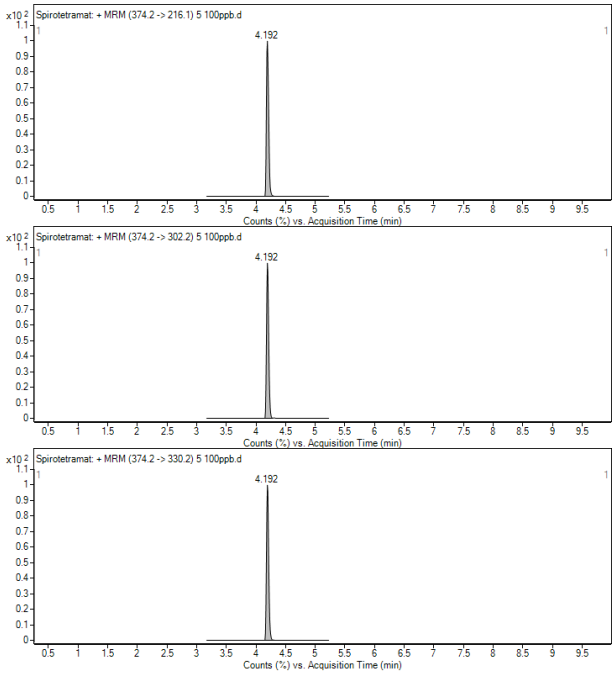

Figure 6.78 Spirotetramat chromatograms for the quantifier (top) and qualifiers (middle and bottom).

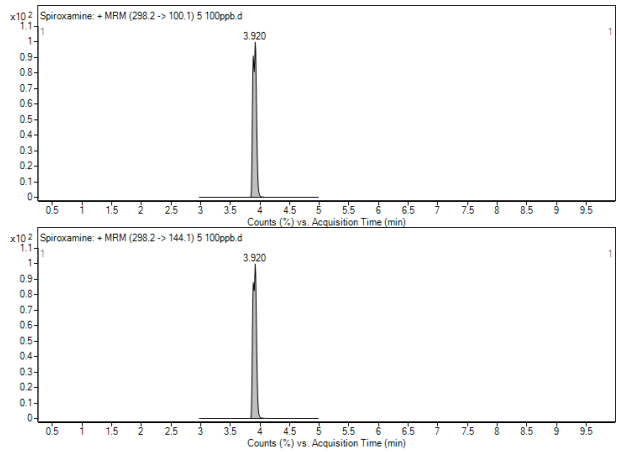

Figure 6.79 Spiroxamine chromatograms for the quantifier (top) and qualifier (bottom).

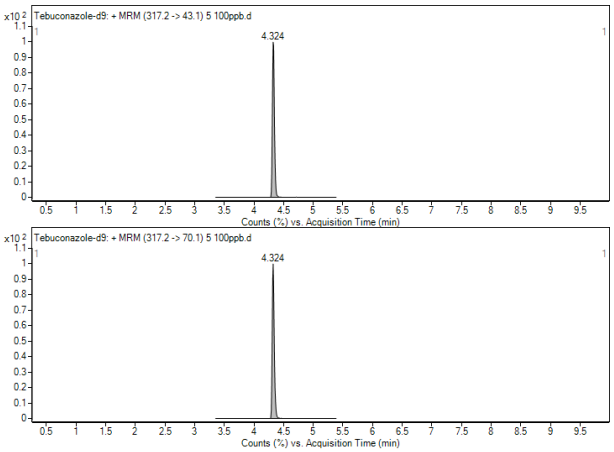

Figure 6.81 Tebuconazole-d_9 chromatograms for the quantifier (top) and qualifier (bottom).

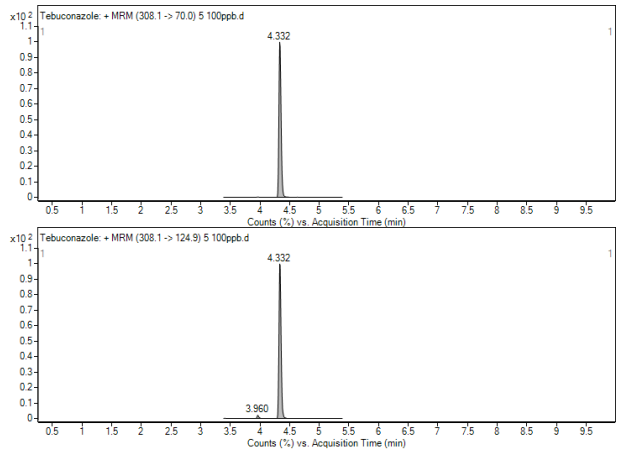

Figure 6.80 Tebuconazole chromatograms for the quantifier (top) and qualifier (bottom).

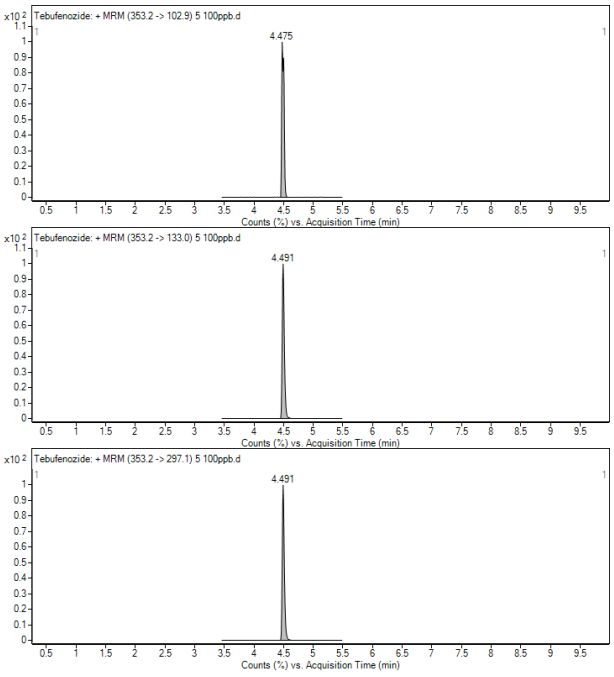

Figure 6.82 Tebufenozide chromatograms for the quantifier (top) and qualifier (bottom).

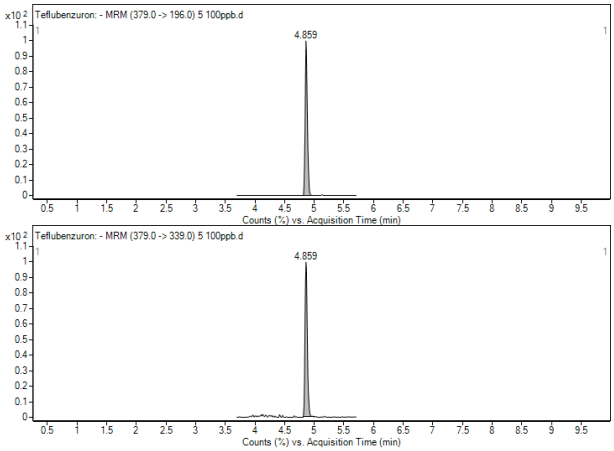

Figure 6.83 Teflubenzuron chromatograms for the quantifier (top) and qualifier (bottom).

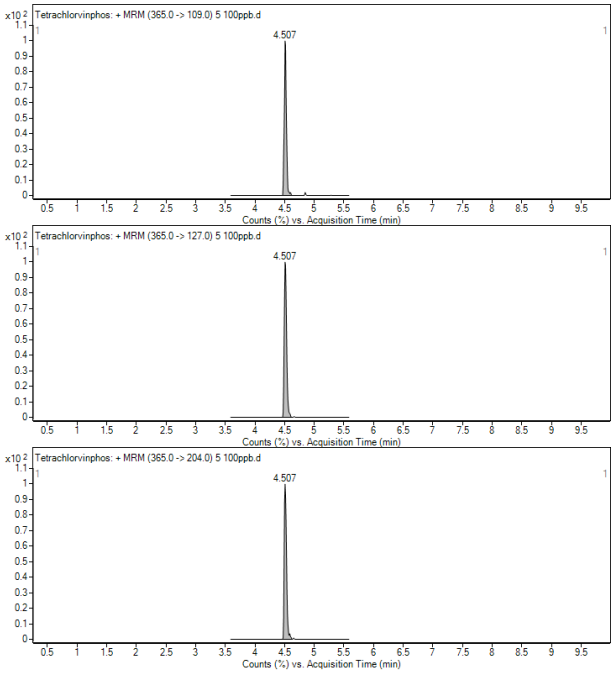

Figure 6.84 Tetrachlorvinphos chromatograms for the quantifier (top) and qualifiers (middle and bottom).

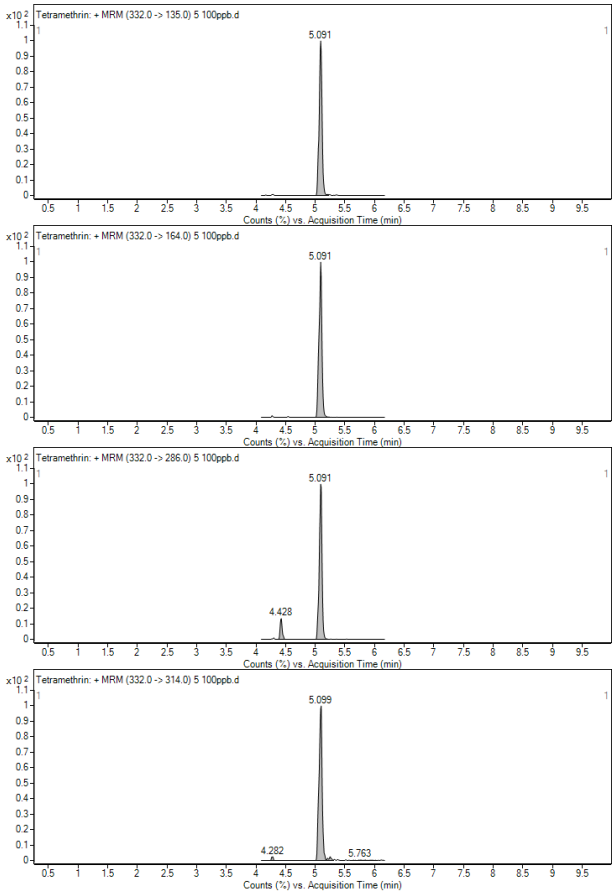

Figure 6.85 Tetramethrin chromatograms for the quantifier (top) and qualifiers (mid-top, mid-bottom, and bottom).

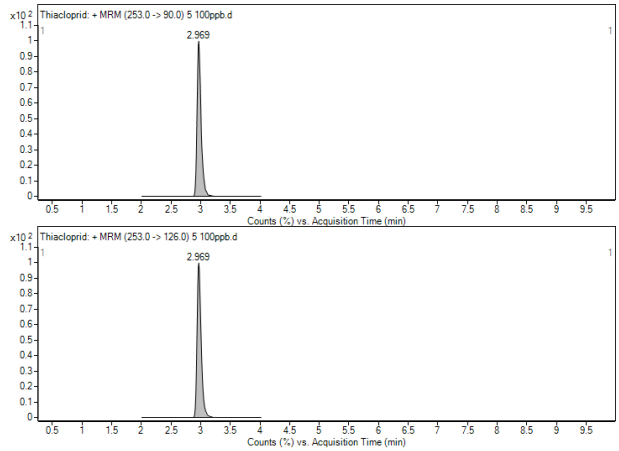

Figure 6.86 Thiacloprid chromatograms for the quantifier (top) and qualifier (bottom).

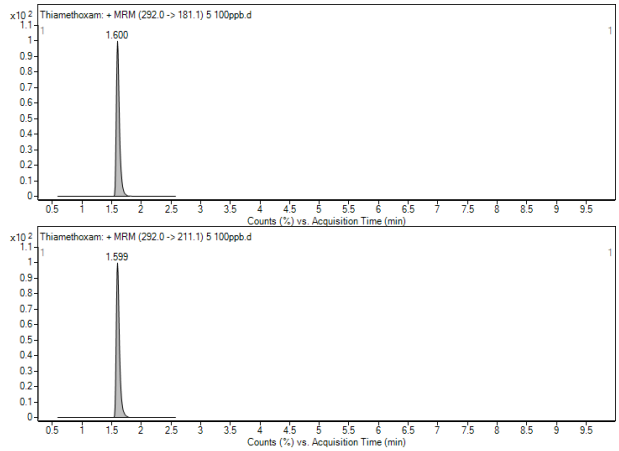

Figure 6.87 Thiamethoxam chromatograms for the quantifier (top) and qualifier (bottom).

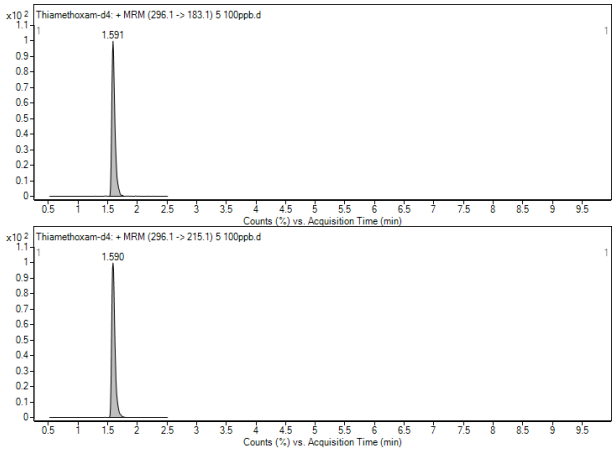

Figure 6.88 Thiamethoxam-d_4 chromatograms for the quantifier (top) and qualifier (bottom).

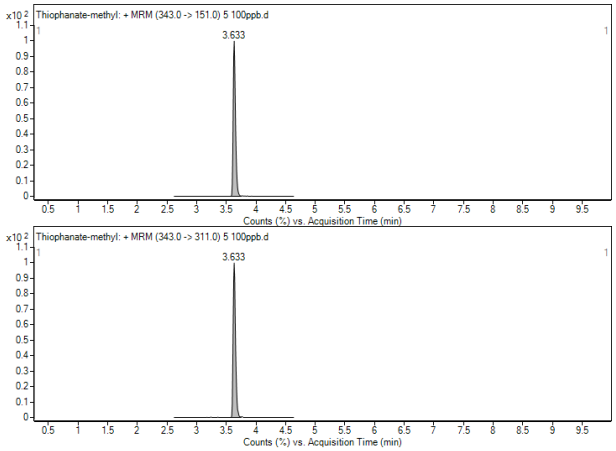

Figure 6.89 Thiophanate-Methyl chromatograms for the quantifier (top) and qualifier (bottom).

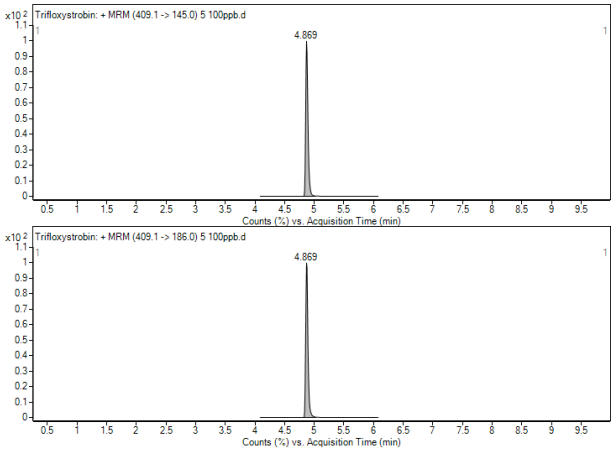

Figure 6.90 Trifloxystrobin chromatograms for the quantifier (top) and qualifier (bottom).

6.2.2 Compounds, Solubility, Fragments, Energies, and Other Parameters for Pesticides Selectivity

Table 6.1 List of pesticides analyzed in the analytical method with LogP and pKa values as well as acetone, dichloromethane, ethyl acetate, methanol, toluene, and water solubilites. **Bolded** pesticides are independent of the Agilent 96 pesticides Canadian Cannabis Mixture. *Italicized* pesticides have deuterated or ^{13}C labelled internal standards. Pesticides written with ~~strikethroughs~~ were removed from the final chromatography since they are analyzed by GC-MS/MS. All values were retrieved from Lewis et al. (2016).

Pesticide	LogP	pKa	Acetone (g/l)	Dichloro-methane (g/l)	Ethyl Acetate (g/l)	Methanol (g/l)	Toluene (g/l)	Water (g/l)
2,4-D	***-0.82***	***3.4***	***212***	***8***	***NA***	***810***	***6.4***	***24.3***
~~Abamectin~~	~~4.4~~	~~NA~~	~~72~~	~~470~~	~~160~~	~~13~~	~~23~~	~~0.00121~~
Acephate	-0.85	8.35	151	515	34.7	575	6.8	700
Acequinocyl	6.2	NA	250	NA	250	6	NA	0.0000067
Acetamiprid	0.8	0.7	200	200	NA	NA	NA	4.25
Aldicarb	1.15	NA	373	578	NA	NA	NA	4.93
Allethrin	4.96	NA	miscible	NA	NA	NA	NA	0.0000001
Atrazine	**2.7**	**1.7**	**NA**	**28**	**24**	**NA**	**4**	**0.035**
~~Azadirachtin~~	~~0.99~~	~~NA~~	~~77.9~~	~~NA~~	~~75.1~~	~~92.9~~	~~65~~	~~2.9~~
Azoxystrobin	2.5	NA	86	400	NA	20	55	0.006
Bentazon	***-0.46***	***3.51***	***300***	***250***	***300***	***300***	***24.5***	***7.7***
Benzovindiflupyr	4.3	NA	350	450	190	76	48	0.98
~~Bifenazate~~	~~3.4~~	~~12.94~~	~~210~~	~~NA~~	~~102~~	~~44.7~~	~~24.7~~	~~2.06~~
Bifenthrin	6.6	NA	735.7	NA	579.8	48	NA	1.4E-09
Boscalid	2.96	NA	180	NA	NA	45	22.5	0.0046
Buprofezin	4.5	NA	253.4	586.9	240.8	86.6	17.9	0.000458
Carbaryl	2.36	10.4	255	NA	175	87.5	NA	0.12
Carbofuran	1.8	NA	105.2	NA	61.5	71.7	NA	0.322
Chlorantraniliprole	2.86	10.88	3.4	2.5	1.1	1.7	NA	0.00088
~~Chlorphenapyr~~	~~5.21~~	~~NA~~	~~1140~~	~~1410~~	~~NA~~	~~7.09~~	~~75.4~~	~~0.00012~~
Chlorpyrifos	4.7	NA	1000	NA	1000	500	NA	0.00039

Clofentezine	4.09	NA	9.3	NA	5.67	NA	NA	0.0000342
Clopyralid	**-2.63**	**2.01**	**250**	**102**	**NA**	**NA**	**4.6**	**7.8**
Clothianidin	0.905	11.1	15.2	1.32	2.03	6.26	NA	0.327
Coumaphos	3.86	NA	238.2	63.9	NA	NA	NA	0.0015
Cyantraniliprole	2.02	8.8	6.54	5.05	1.96	4.73	NA	0.01233
~~Cyfluthrin~~	~~6~~	~~NA~~	~~NA~~	~~200~~	~~NA~~	~~NA~~	~~200~~	~~2.2~~
~~Cypermethrin~~	~~5.55~~	~~NA~~	~~450~~	~~NA~~	~~2500~~	~~450~~	~~NA~~	~~0.000009~~
Cyprodinil	4	4.44	500	500	NA	NA	440	0.013
~~Daminozide~~	~~-1.53~~	~~4.68~~	~~1.6~~	~~NA~~	~~0.27~~	~~48~~	~~NA~~	~~128~~
~~Deltamethrin~~	~~4.6~~	~~NA~~	~~250~~	~~250~~	~~250~~	~~NA~~	~~250~~	~~0.0000013~~
Dicamba	**-1.8**	**1.87**	**500**	**500**	**NA**	**500**	**NA**	**250**
Diazinon	3.69	2.6	9000	NA	250	9000	9000	0.06
~~Dichlorvos~~	~~1.9~~	~~NA~~	~~miscible~~	~~NA~~	~~NA~~	~~NA~~	~~miscible~~	~~18~~
Dimethoate	0.75	NA	NA	NA	NA	1590	1030	25.9
~~Dimethomorph~~	~~2.68~~	~~-1.3~~	~~100.4~~	~~461~~	~~48.3~~	~~39~~	~~49.5~~	~~0.05~~
Dinotefuran	-0.549	12.6	NA	NA	NA	NA	150	39.8
Dodemorph	4.6	8.08	57	NA	185	NA	NA	0.1
~~Endosulfan sulfate~~	~~3.66~~	~~NA~~	~~NA~~	~~NA~~	~~NA~~	~~NA~~	~~NA~~	~~0.48~~
~~Endosulfan-alpha~~	~~4.74~~	~~NA~~	~~NA~~	~~200~~	~~200~~	~~NA~~	~~200~~	~~0.33~~
~~Endosulfan-beta~~	~~3.83~~	~~NA~~	~~NA~~	~~200~~	~~200~~	~~NA~~	~~200~~	~~0.32~~
Ethoprophos	2.99	NA	500	NA	500	500	500	1.3
Etofenprox	6.9	NA	877	924	837	49	862	0.00002
Etoxazole	5.52	NA	309	NA	249	104	NA	0.07
~~Etridiazole~~	~~3.37~~	~~2.77~~	~~NA~~	~~NA~~	~~NA~~	~~miscible~~	~~miscible~~	~~0.088~~
Fenoxycarb	4.07	NA	500	NA	500	NA	500	7.9
Fenpyroximate	5.7	NA	150	201	1307	15.3	268	0.0000231
Fensulfothion	2.23	NA	NA	250	NA	NA	250	0.0042
~~Fenthion~~	~~4.84~~	~~NA~~	~~250~~	~~NA~~	~~250~~	~~NA~~	~~250~~	~~0.0042~~
~~Fenvalerate~~	~~5.01~~	~~NA~~	~~NA~~	~~NA~~	~~NA~~	~~84~~	~~NA~~	~~0.000001~~
Fipronil	3.75	NA	545.9	22.3	264.9	137.5	3	3.35
Flonicamid	-0.24	11.6	163.5	4.5	34.2	104.3	0.55	5.2
Fludioxonil	4.12	0, 14.12	190	NA	NA	420	2.7	1.8
Fluopyram	3.3	NA	250	250	250	250	62.2	0.016

Hexythiazox	2.67	NA	159	619	148	17.6	233	0.00012
Imazalil	2.56	6.49	500	500	500	500	500	0.184
Imazamox	**5.36**	**2.3, 3.3, 10.8**	**29.3**	**10.2**	**143**	**66.8**	**2.1**	**643**
Imazethapyr	**1.49**	**2.1, 3.9**	**48.2**	**184.8**	**NA**	**105**	**5**	**5**
Imidacloprid	0.57	NA	50	67	6.7	NA	0.69	0.61
~~Iprodione~~	~~3~~	~~NA~~	~~342~~	~~NA~~	~~225~~	~~NA~~	~~147~~	~~0.68~~
~~Kinoprene~~	~~6.68~~	~~NA~~	~~NA~~	~~NA~~	~~NA~~	~~NA~~	~~NA~~	~~0.000211~~
Kresoxim-methyl	3.4	NA	217	NA	123	14.9	NA	0.002
Malathion	2.75	NA	250	NA	NA	250	250	0.148
Metalaxyl	1.75	0	miscible	NA	NA	miscible	miscible	26
~~Methiocarb~~	~~3.18~~	~~NA~~	~~144~~	~~NA~~	~~87~~	~~NA~~	~~NA~~	~~0.027~~
Methomyl	0.09	NA	250	NA	NA	1000	NA	55
~~Methoprene~~	~~5~~	~~NA~~	~~500~~	~~NA~~	~~NA~~	~~450~~	~~NA~~	~~0.00685~~
Metolachlor	***3.4***	***NA***	***miscible***	***NA***	***NA***	***NA***	***NA***	***0.53***
Mevinphos	0.127	NA	miscible	NA	NA	NA	NA	600
MGK-264	3.7	NA	miscible	NA	miscible	miscible	miscible	0.000015
Myclobutanil	2.89	2.3	250	NA	NA	250	270	0.132
~~Naled~~	~~2.18~~	~~NA~~	~~NA~~	~~NA~~	~~NA~~	~~NA~~	~~NA~~	~~2~~
~~Novaluron~~	~~4.3~~	~~NA~~	~~198~~	~~NA~~	~~113~~	~~14.5~~	~~NA~~	~~0.000003~~
Oxamyl	-0.44	-2.11	250	NA	NA	250	NA	148.1
Paclobutrazol	3.11	NA	72.4	NA	NA	150	NA	0.0229
~~Parathion-methyl~~	~~3~~	~~NA~~	~~NA~~	~~200~~	~~NA~~	~~NA~~	~~200~~	~~0.055~~
Permethrin	6.1	NA	NA	NA	NA	258	NA	0.0002
~~Phenothrin~~	~~6.01~~	~~NA~~	~~5~~	~~NA~~	~~NA~~	~~NA~~	~~NA~~	~~0.0000097~~
Phosmet	2.8	NA	143	NA	57	29.2	NA	15.2
Piperonyl butoxide	4.75	NA	300	NA	300	NA	300	0.0289
Pirimicarb	1.7	4.4	370	NA	280	350	NA	3.1
Prallethrin	4.49	NA	NA	NA	NA	500	NA	0.00803
Propiconazole	3.72	1.09	miscible	NA	NA	miscible	NA	0.15
Propoxur	0.14	NA	NA	NA	NA	NA	94	1.8
Pyraclostrobin	3.99	NA	500	NA	NA	100.8	NA	0.0019
~~Pyrethrins (Cinerin I, II, Jasmolin I, II, Pyrethrin I, II)~~	~~4.26 – 6.04~~	~~NA~~	~~250~~	~~NA~~	~~NA~~	~~250~~	~~NA~~	~~0.00096 – 0.0107~~

Pyridaben	6.37	NA	333	NA	NA	494	NA	0.000022
~~Quintozene~~	~~4.46~~	~~NA~~	~~NA~~	~~NA~~	~~NA~~	~~20~~	~~1140~~	~~0.00044~~
Resmethrin	5.43	NA	NA	NA	NA	NA	NA	0.00001
Spinetoram	4.2	7.7	250	NA	NA	250	NA	0.029
Spinosyn (A, D)	3.91-4.38	8	10.1 – 168	448-525	19-194	2.52 – 190	152 – 457	0.000331 – 0.235
Spirodiclofen	5.83	NA	250	250	250	NA	NA	0.00005
Spiromesifen	4.55	NA	250	NA	NA	250	NA	0.000013
Spirotetramat	2.51	10.7	100	67	600	NA	60	0.0299
Spiroxamine	2.89	6.9	200	NA	NA	200	200	0.405
Tebuconazole	*3.7*	*5*	*200*	*200*	*NA*	*NA*	*57*	*0.032*
Tebufenozide	4.25	NA	74.8	NA	23.8	130	3.2	0.00083
Teflubenzuron	4.3	9.2	8.85	1.51	6.28	1.06	0.74	0.00001
Tetrachlorvinphos	3.53	NA	NA	NA	NA	NA	NA	0.0116
Tetramethrin	4.6	NA	200	NA	NA	200	200	0.00183
Thiacloprid	1.26	NA	64	9.4	NA	NA	NA	0.184
Thiamethoxam	*-0.13*	*NA*	*48*	*7*	*NA*	*NA*	*0.68*	*4.1*
Thiophanate-methyl	1.4	7.28	NA	NA	8.4	0.0078	0.11	0.0185
Trifloxystrobin	4.5	NA	500	500	NA	76	500	0.00061

Table 6.2 Pesticide analytical method's retention time (Rt), retention window (ΔRt), electrospray ionization mode (ESI: + = positive; - = negative), parent ions, product ions [both quantitative (Q) or qualitative (l) product ions], fragmentation voltage (frag), and collision energies (CE).

Pesticide	Rt (min)	DRt (min)	ESI Mode	Precusor Ion (m/z)	Frag (V)	Product Ions (m/z)	CE (eV)	Q/l
Acephate	1.267	2	+	184.0	60	143.0	5	Q
						95.0	20	l
Oxamyl	1.355	2	+	237.0	60	90.1	0	Q
						72.1	15	l
Clopyralid	1.410	2	-	189.9	61	146.0	4	Q
						157.0	4	Q
Dinotefuran	1.458	2	+	203.0	90	129.0	8	l
						87.0	16	l
						73.0	20	l
Methomyl	1.470	2	+	162.9	60	106.1	5	Q
						88.1	0	l
Thiamethoxam-d4	1.520	2	+	296.1	97	215.1	8	Q
						183.1	24	l
Thiamethoxam	1.590	2	+	292.0	80	211.1	8	Q
						181.1	20	l
Flonicamid	1.597	2	+	230.0	120	203.0	15	Q
						174.0	20	l
Pirimicarb	1.610	2	+	239.0	100	182.0	16	Q
						72.0	24	l
Clothianidin	1.778	2	+	250.0	95	169.0	12	Q
						132.0	16	l
Dimethoate	2.025	2	+	230.0	70	199.0	5	Q
						125.0	21	l

Imidacloprid	2.070	2	+	256.0	90	209.1	16	Q
						175.1	20	1
Mevinphos	2.100	2	+	225.0	60	192.9	5	Q
						126.9	17	1
Acetamiprid	2.172	2	+	223.0	100	126.1	25	Q
						90.1	35	1
Imazethapyr	2.417	2	+	290.2	142	86.1	32	Q
						69.1	32	1
						41.1	60	1
Aldicarb	2.772	2	+	116.0	50	89.1	4	Q
						70.1	4	1
Thiacloprid	3.010	2	+	253.0	100	126.0	16	Q
Dicamba	3.080	2	-	219.0	56	175.0	0	Q
						35.1	24	1
Propoxur	3.600	2	+	210.0	60	168.0	5	Q
						111.0	10	1
Bentazon	3.600	2	-	239.1	141	196.9	20	Q
						131.9	28	1
Bentazon-d7	3.600	2	-	246.1	135	182.0	20	Q
						131.9	32	1
Imazalil	3.620	2	+	297.0	120	201.0	15	Q
						159.0	20	1
Thiophanate-Methyl	3.620	2	+	343.0	105	311.0	8	Q
						151.0	20	1
Imazamox	3.627	3	+	306.2	147	69.1	32	Q
Carbofuran	3.641	2	+	222.1	90	165.1	5	Q
						123.1	20	1
Atrazine	3.700	2	+	216.1	127	68.0	44	Q
						43.1	48	1

Carbaryl	3.765	2	+	202.0	70	145.0	0	Q
						127.1	25	1
2,4-D	3.820	2	-	219.0	72	161.0	12	Q
						125.0	28	1
2,4-D-13C6	3.820	2	-	225.0	77	167.0	12	Q
						131.0	32	1
Dodemorph	3.899	2	+	282.0	145	116.0	24	Q
						98.0	32	1
Fensulfothion	3.930	2	+	309.0	125	281.0	12	Q
						253.0	16	1
Cyantraniliprole	3.937	2	+	475.0	115	444.0	20	Q
						286.0	12	1
Metalaxyl	3.940	2	+	280.1	100	220.2	10	Q
						160.1	20	1
Spiroxamine	3.980	2	+	298.2	120	144.1	16	Q
						100.1	32	1
Paclubutrazol	4.070	2	+	294.1	110	125.0	40	Q
						70.1	20	1
Chlorantraniliprole	4.107	2	+	483.9	100	452.9	15	Q
						285.9	10	1
Fludioxinil	4.128	2	+	229.0	144	185.0	13	Q
						158.0	25	1
Cyprodinil	4.150	2	+	226.0	160	133.0	28	Q
						93.0	40	1
Spinosyn A	4.177	2	+	732.5	160	142.1	28	Q
						98.1	60	1
Spirotetramat	4.194	2	+	374.2	110	330.2	12	Q
						302.2	12	1
						216.1	36	1

Dimetamorph I	4.228	2	+	388.1	145	301.1	20	Q
						165.0	32	1
Dimetamorph II	4.228	2	+	388.1	145	301.1	20	Q
						165.0	32	1
Fenhexamid	4.230	2	+	302.1	145	97.2	25	Q
						55.1	45	1
Ethoprophos	4.240	2	+	243.0	90	131.0	15	Q
						97.0	30	1
Myclobutanil	4.255	2	+	289.1	110	125.0	35	Q
						70.1	15	1
Metolachlor	4.270	2	+	284.1	117	176.1	28	Q
						91.0	68	1
Metolachlor-d6	4.270	2	+	290.2	112	182.2	28	Q
						91.0	64	1
Spinosyn D	4.291	2	+	746.5	160	142.1	35	Q
						98.0	55	1
Phosmet	4.302	2	+	317.9	80	160.0	10	Q
						133.0	40	1
Azoxystrobin	4.324	2	+	404.0	100	372.2	10	Q
						344.0	25	1
Fluopyram	4.324	2	+	397.0	150	208.0	24	Q
						173.0	36	1
Spinetoram J	4.338	2	+	748.5	165	142.1	26	Q
						98.1	50	1
Boscalid	4.357	2	+	343.0	140	307.0	12	Q
						271.0	28	1
Tebuconazole	4.389	2	+	308.1	120	124.9	47	Q
						70.0	40	1
Tebuconazole-d9	4.389	2	+	317.2	142	70.1	24	Q

						43.1	108	1
Malathion	4.400	2	+	331.0	80	126.9	5	Q
						99.0	10	1
Fenoxycarb	4.450	2	+	302.1	100	116.1	5	Q
						88.1	15	1
						297.1	4	Q
Tebufenozide	4.469	2	+	353.2	100	133.0	20	1
						102.9	20	1
						332.0	18	Q
Fipronil	4.475	2	+	436.9	100	330.0	18	1
						250.1	30	1
Propiconazole	4.490	2	+	342.1	130	159.0	32	Q
						69.1	16	1
						204.0	48	Q
Tetrachlorvinphos	4.590	2	+	265.0	125	127.0	12	1
						109.0	48	1
						378.0	12	Q
Benzovindiflupyr	4.620	2	+	398.0	150	342.0	20	1
						322.0	24	1
Kresoxim-Methyl	4.623	2	+	314.1	80	267.1	0	Q
						222.2	10	1
Diazinon	4.623	2	+	305.1	100	169.0	20	Q
						153.1	20	1
Buprofezin	4.660	2	+	306.0	105	201.0	8	Q
						116.0	16	1
Teflubenzuron	4.696	2	+	379.0	125	339.0	8	Q
						196.0	24	1
Pyrethin II	4.750	2	+	373.2	102	161.0	2	Q
						133.1	24	1

						77.0	98	1
Pyraclostrobin	4.780	2	+	388.1	82	194.1	8	Q
						163.0	24	1
MGK-264	4.816	2	+	276.2	100	210.1	12	Q
						98.0	28	1
Piperonyl Butoxide	4.860	2	+	356.2	90	177.1	5	Q
						119.1	35	1
Clofentezine	4.900	2	+	303.0	90	138.0	10	Q
						102.1	40	1
						169.0	4	Q
Allethrin	4.910	2	+	303.0	85	135.0	10	1
						123.0	16	1
Prallethrin	4.960	2	+	301.1	90	169.0	5	Q
						105.0	20	1
Trifloxystorbin	5.085	2	+	409.1	100	186.0	12	Q
						145.0	52	1
						314.0	8	Q
Tetramethrin	5.100	2	+	332.0	100	286.0	8	1
						164.0	28	1
						135.0	16	1
Etoxazole	5.100	2	+	360.1	140	141.0	28	Q
						113.0	50	1
						161.0	5	Q
Pyrethrin I	5.170	2	+	329.2	90	143.0	20	1
						133.0	20	1
Chlorpyrifos	5.210	2	+	349.9	100	197.9	20	Q
						96.9	41	1
Hexythiazox	5.281	2	+	353.0	90	228.1	10	Q
						168.1	25	1

Spiromesifen	5.300	2	+	388.2	80	273.0	6	Q
						255.0	26	1
Spirodiclofen	5.420	2	+	411.0	140	313.0	8	Q
						71.0	16	1
Pyridaben	5.480	2	+	365.1	90	309.1	4	Q
						147.2	20	1
						117.1	20	1
Resmethrin	5.515	2	+	339.0	135	171.0	12	Q
						143.0	28	1
Coumaphos	5.600	2	+	363.0	125	307.0	15	Q
						226.9	33	1
Permethrin [M+NH4]	5.812	2	+	408.1	72	355.1	4	Q
						183.0	20	1
Etofenprox	6.000	2	+	394.2	90	177.2	10	Q
						107.1	45	1
Bifenthrin	6.016	2	+	440.2	90	181.1	5	Q
						166.0	20	1
Acequinocyl	6.499	2	+	402.3	90	343.2	10	Q
						189.1	41	1
Fenpyroximate	6.979	2	+	422.1	130	366.2	15	Q
						135.1	30	1

Table 6.3 Method linearity (R^2) and working range (WR) in each of the solvents used for each extraction, associated internal standards (IS), and machine limits of detection and quantification (LOD/LOQ).

Compound	Deionized Water		Acetonitrile[1]		50:50 Methanol:Water[1]		Internal Standard[2]	LOD/LOQ (ng mL^{-1})
	R^2	WR (ng mL^{-1})	R^2	WR (ng mL^{-1})	R^2	WR (ng mL^{-1})		
Acephate	0.9934	2.5-100	0.9618	2.5-100	0.9833	2.5-100	B-d7	0.23/0.76
Oxamyl	0.9982	0.1-100	0.9105	0.1-100	0.9657	0.1-100	Th-d4	0.13/0.44
Clopyralid	0.9916	1-100	0.9862	2.5-100	0.9555	2.5-100	2-C6	0.35/1.2
Dinotefuran	0.9914	1-100	0.9727	1-100	0.9802	0.1-100	B-d7	0.12/0.41
Methomyl	0.9917	0.1-100	0.9718	0.1-100	0.9927	0.1-100	B-d7	0.10/0.34
Thiamethoxam	0.9989	0.1-100	0.9956	1-100	0.9992	0.1-100	Th-d4	0.098/0.33
Flonicamid	0.9938	0.1-100	0.9758	0.1-100	0.9788	0.1-100	B-d7	0.09/0.30
Pirimicarb	0.9873	0.1-100	0.9767	0.1-100	0.9896	0.1-100	B-d7	0.073/0.24
Clothianidin	0.9944	1-100	0.9807	1-100	0.9611	0.1-100	B-d7	0.090/0.30
Dimethoate	0.9912	0.1-100	0.9569	0.1-100	0.9795	0.1-100	B-d7	0.13/0.42
Imidacloprid	0.9947	0.1-100	0.9812	1-100	0.9664	0.1-100	B-d7	0.13/0.43
Mevinphos	0.9886	0.1-100	0.9559	1-100	0.9897	0.1-100	B-d7	0.18/0.59
Acetamiprid	0.9901	0.1-100	0.9661	1-100	0.987	0.1-100	B-d7	0.12/0.40
Imazethapyr	0.994	0.1-100	0.982	0.1-100	0.9806	0.1-100	2-C6	0.26/0.86
Aldicarb	0.9895	0.1-100	0.974	1-100	0.9896	0.1-100	B-d7	0.15/0.49
Thiacloprid	0.9907	0.1-100	0.9714	1-100	0.9871	0.1-100	B-d7	0.13/0.43
Dicamba	0.9943	1-100	0.9908	2.5-100	0.9852	1-100	2-C6	0.43/1.4

Propxur	0.9987	0.1-100	0.9886	1-100	0.9802	0.1-100	Tc-d9	0.20/0.66
Bentazon	0.9977	0.1-100	0.9974	0.1-100	0.9915	0.1-50	B-d7	0.34/1.1
Imazalil	0.9912	0.1-100	0.9824	1-100	0.9906	0.1-100	B-d7	0.13/0.42
Thiophanate-Methyl	0.9881	0.1-100	0.9499	1-100	0.9866	1-100	B-d7	0.26/0.88
Imazamox	0.9976	0.1-100	0.9845	0.1-100	0.9854	0.1-100	Tc-d9	0.26/0.85
Carbofuran	0.9949	0.1-100	0.962	0.1-100	0.9853	0.1-100	B-d7	0.11/0.35
Atrazine	0.9886	0.1-100	0.979	0.1-100	0.9898	0.1-100	B-d7	0.075/0.25
Carbaryl	0.9931	0.1-100	0.9654	1-100	0.9856	1-100	B-d7	0.27/0.89
2,4-D	0.992	0.1-100	0.9853	5-100	0.9832	1-100	2-C6	1.2/4.0
Dodemorph	0.9585	0.1-100	0.9762	0.1-100	0.978	0.1-100	B-d7	0.48/1.6
Fensulfothion	0.9938	0.1-100	0.9805	0.1-100	0.9877	0.1-100	B-d7	0.27/0.89
Cyantraniliprole	0.9927	0.1-100	0.9678	1-100	0.966	1-100	B-d7	0.28/0.94
Metalaxyl	0.9938	0.1-100	0.9712	0.1-100	0.9827	0.1-100	B-d7	0.14/0.45
Spiroxamine	0.9923	0.1-100	0.9777	0.1-100	0.9855	0.1-100	B-d7	0.56/1.9
Paclubutrazol	0.992	0.1-100	0.9759	0.1-100	0.9849	0.1-100	B-d7	0.11/0.36
Chlorantraniliprole	0.9961	0.1-100	0.9794	1-100	0.9892	1-100	M-d6	0.77/2.6
Fludioxinil	0.99	0.1-100	0.9126	2.5-100	0.9263	2.5-100	B-d7	1.1/3.8
Cyprodinil	0.99	0.1-100	0.9828	0.1-100	0.9883	0.1-100	B-d7	0.11/0.38
Spinosyn A	0.996	0.1-100	0.9962	0.1-100	0.9899	0.1-100	Tc-d9	0.33/1.1
Spirotetramat	0.9979	0.1-100	0.9948	0.1-100	0.9929	1-100	Tc-d9	0.30/0.99

Dimetamorph I	0.993	0.1-100	0.9513	1-100	0.9629	0.1-100	B-d7	0.31/1.0
Dimetamorph II	0.997	0.1-100	0.9841	1-100	0.9875	1-100	M-d6	0.76/2.5
Fenhexamid	0.9953	0.1-100	0.9904	1-100	0.9921	0.1-100	M-d6	0.62/2.1
Ethoprophos	0.9955	0.1-100	0.9822	0.1-100	0.9353	0.1-100	Th-d4	0.40/1.3
Myclobutanil	0.9994	0.1-100	0.9954	0.1-100	0.994	0.1-100	Tc-d9	0.15/0.49
	0.9978	0.1-100	0.9925	1-100	0.9959	0.1-100	M-d6	0.31/1.0
Spinosyn D	0.9831	0.1-100	0.9934	1-100	0.9857	0.1-100	Tc-d9	1.1/3.8
Phosmet	0.9745	0.1-100	0.9411	1-100	-	-	Tc-d9	0.27/0.91
Azoxystrobin	0.9936	0.1-25	0.9895	0.1-100	0.9155	0.1-100	Th-d4	0.26/0.88
Fluopyram	0.9921	0.1-50	0.9937	0.1-100	0.944	0.1-100	Th-d4	0.38/1.3
Spinetoram J	0.991	0.1-100	0.9947	0.1-100	0.9857	0.1-100	Tc-d9	0.41/1.4
Boscalid	0.9945	0.1-100	0.9632	1-100	0.9593	1-100	B-d7	0.61/2.0
Tebuconazole	0.9991	0.1-100	0.9975	0.1-100	0.955	0.1-100	Tc-d9	0.13/0.42
Malathion	0.9931	0.1-50	0.981	1-100	0.9877	1-100	Tc-d9	0.48/1.6
Fenoxycarb	0.9966	0.1-100	0.9918	1-100	0.9892	1-100	Tc-d9	0.61/2.0
Tebufenozide	0.9983	0.1-25	0.9987	0.1-100	0.9851	0.1-50	Tc-d9	0.21/0.68
Fipronil	0.9933	0.1-100	0.9537	1-100	0.8912	1-100	Tc-d9	0.71/2.4

Propiconazole	0.9977	0.1-50	0.9952	0.1-100	0.9922	0.1-100	Tc-d9	0.32/1.1
Tetrachlorvinphos	0.9943	0.1-25	0.9774	1-100	0.9827	0.1-25	Tc-d9	0.69/2.3
Benzovindiflupyr	0.9902	0.1-50	0.9808	0.1-100	0.9803	0.1-50	Tc-d9	1.1/3.8
Kresoxim-Methyl	0.9897	0.1-50	0.9495	1-100	0.9794	1-100	Tc-d9	1.1/3.7
Diazinon	0.9915	0.1-100	0.9789	0.1-100	0.9866	0.1-100	B-d7	0.084/0.28
Buprofenzin	0.9971	0.1-100	0.983	1-100	0.9817	0.1-100	Tc-d9	0.16/0.53
Teflubenzuron	0.9916	0.1-100	0.957	1-100	0.8537	2.5-100	Tc-d9	0.86/2.9
Pyrethin II	0.988	0.1-100	0.9834	2.5-100	0.9758	5-100	Tc-d9	1.8/6.0
Pyraclostrobin	0.9974	0.1-25	0.9828	0.1-50	0.9715	0.1-100	Tc-d9	0.25/0.83
MGK-264	0.9946	0.1-100	0.9588	2.5-100	0.9843	1-100	Tc-d9	0.75/2.5
Piperonyl Butoxide	0.998	0.1-25	0.9643	0.1-100	0.9421	0.1-50	Tc-d9	0.24/0.79
Clofentazine	0.9975	0.1-100	0.9852	1-100	0.991	1-100	Tc-d9	0.77/2.6
Allethrin	0.9947	0.1-100	0.9953	1-100	0.987	1-100	Tc-d9	0.32/1.1
Prallethrin	0.9946	0.1-100	0.9814	1-100	0.9866	1-100	Tc-d9	0.71/2.4
Trifloxystrobin	0.9872	0.1-25	0.9782	0.1-25	0.9702	0.1-25	Tc-d9	0.20/0.66
Tetramethrin	0.9872	0.1-100	0.9545	1-100	0.9669	1-100	B-d7	0.28/0.93

Etoxazole	0.9825	0.1-100	0.9815	0.1-100	0.9841	0.1-100	B-d7	0.12/0.39
Pyrethrin I	0.9912	0.1-100	0.989	1-100	0.9833	1-100	Tc-d9	0.40/1.3
Chlorpyrifos	0.9934	0.1-100	0.9667	2.5-100	0.9801	2.5-100	Tc-d9	0.70/2.3
Hexythiazox	0.9884	0.1-100	0.9748	1-100	0.9648	1-100	B-d7	0.15/0.48
Spiromesifen	0.9902	0.1-100	0.9862	0.1-100	0.9691	0.1-100	B-d7	0.21/0.69
Spirodiclofen	0.9905	0.1-100	0.9827	1-100	0.979	0.1-100	Tc-d9	0.33/1.1
Pyridaben	0.9941	0.1-100	0.9954	0.1-100	0.9919	0.1-100	Tc-d9	0.16/0.53
Resmethrin	0.9647	0.1-100	0.9506	1-100	0.9379	2.5-100	B-d7	0.32/1.1
Coumaphos	0.996	0.1-100	0.99	1-100	0.9923	1-100	Tc-d9	0.64/2.1
Permethrin [M+NH4]	0.9647	0.1-100	0.9653	5-100	0.9132	2.5-100	B-d7	1.2/4.1
Etofenprox	0.9646	0.1-100	0.8713	1-100	0.9137	1-100	B-d7	0.25/0.83
Bifenthrin	0.978	0.1-100	0.9428	2.5-100	0.9321	1-100	B-d7	1.0/3.5
Acequinocyl	0.9616	0.1-50	-	-	-	-	B-d7	0.34/1.1
Fenpyroximate	0.9773	0.1-100	0.9618	1-100	0.9661	0.1-100	B-d7	0.09/0.30

[1] - = no responses were recorded due to instability in solvent.

[2] B-d7 = Bentazon-d_7; Th-d4 = Thiamethoxam-d_4; 2-C6 = 2,4-D-$^{13}C_6$; Te-d9 = Tebuconazole-d_9; M-d6 = Metolachlor-d_6

7. APPENDIX II: CHAPTER THREE VALIDATION OF WATER FRACTIONS

7.1 Chapter 3 Water Fraction Method Limits of Detection/Quantification, Accuracy, and Precision Validation for Biobeds

Table 7.1 Method limits of detection and quantification (MLD/MLQ) and accuracy at four spike levels for effluent and rinsate water fractions. *Italicized* values represent recoveries below <70%, **bolded** values represent values >130%, and – represents no response detected.

Pesticide	Rinsate	Rinsate Accuracy (%)				Effluent	Effluent Accuracy (%)			
	MLD/MLQ (ng mL^{-1})	200 ng mL^{-1}	2,000 ng mL^{-1}	20,000 ng mL^{-1}	200,000 ng mL^{-1}	MLD/MLQ (ng mL^{-1})	20 ng mL^{-1}	200 ng mL^{-1}	2,000 ng mL^{-1}	20,000 ng mL^{-1}
Acephate	2.9 / 9.6	79	81	84	81	0.44 / 1.5	130	130	75	82
Oxamyl	0.53 / 1.8	78	85	89	90	0.41 / 1.4	87	**140**	97	96
Clopyralid	3.1 / 10	110	100	110	100	0.23 / 0.78	110	100	100	110
Dinotefuran	2.7 / 9.0	120	86	91	78	3.3 / 11	**240**	130	86	79
Methomyl	1.6 / 5.4	89	83	85	82	1.8 / 6.0	180	98	84	81
Thiamethoxam	0.82 / 2.7	93	96	97	100	0.16 / 0.54	96	100	100	99
Flonicamid	1.6 / 5.2	87	89	88	87	0.10 / 0.34	*66*	80	84	81
Pirimicarb	1.0 / 3.3	81	83	83	82	0.094 / 0.31	83	83	82	79
Clothianidin	1.9 / 6.2	100	91	91	86	0.14 / 0.48	74	81	84	80
Dimethoate	1.7 / 5.7	89	85	86	83	0.29 / 0.96	130	93	84	80
Imidacloprid	2.2 / 7.3	89	87	88	85	0.14 / 0.46	*67*	79	83	82
Mevinphos	1.7 / 5.8	79	83	83	82	0.088 / 0.29	92	86	83	80
Acetamiprid	1.6 / 5.4	89	85	86	83	0.17 / 0.57	91	83	82	79
Imazethapyr	1.4 / 4.7	100	99	100	100	0.18 / 0.62	120	110	110	110
Aldicarb	1.6 / 5.2	82	84	84	83	0.23 / 0.76	92	83	81	77

Thiacloprid	1.3/4.3	89	86	85	83	0.15/0.51	81	80	78	75
Dicamba	3.1/10	100	100	110	100	0.21/0.69	110	110	110	110
Propxur	2.8/9.5	100	92	95	97	0.13/0.44	110	110	100	100
Bentazon	4.2/14	96	97	98	95	0.36/1.2	100	100	100	94
Imazalil	1.9/6.2	76	85	83	84	0.14/0.46	84	86	83	81
Thiophanate-Methyl	2.2/7.3	88	89	91	85	0.23/0.76	120	90	78	70
Imazamox	1.5/5	98	100	110	100	0.3/1	97	100	99	100
Carbofuran	2.2/7.3	81	85	86	84	0.2/0.67	100	90	85	81
Atrazine	1.5/4.9	82	86	85	85	0.13/0.44	84	84	84	81
Carbaryl	4.4/15	86	87	85	86	0.34/1.1	92	87	85	82
2,4-D	5.6/19	100	99	110	94	1/3.4	120	100	100	110
Dodemorph	4.2/14	81	87	87	80	0.51/1.7	87	84	99	86
Fensulfothion	30/99	*45*	72	71	82	0.26/0.86	83	82	82	80
Cyantraniliprole	53/180	*42*	*68*	*68*	79	0.49/1.6	81	83	83	82
Metalaxyl	2.2/7.2	84	84	86	84	0.23/0.76	97	86	86	82
Spiroxamine	1.3/4.2	100	83	92	83	0.71/2.4	100	110	110	110
Paclubutrazol	1.2/4.1	79	85	87	85	0.07/0.23	85	85	84	80
Chlorantraniliprole	5.2/17	110	110	120	87	0.54/1.8	110	100	98	94
Fludioxinil	910/3,000	*15*	*41*	*43*	79	0.5/1.7	*61*	76	76	81
Cyprodinil	1.7/5.7	81	83	84	83	0.21/0.7	84	83	82	78
Spinosyn A	1.7/5.7	99	98	100	100	0.26/0.87	90	84	81	75
Spirotetramat	3.2/11	81	87	92	96	0.31/1	110	100	100	98
Dimetamorph I	3.6/12	96	80	84	83	0.29/0.98	96	83	78	78
Dimetamorph II	590/2,000	**160**	**160**	**170**	90	0.59/2	110	100	97	88
Fenhexamid	3.2/11	*59*	82	83	93	0.48/1.6	97	95	96	98
Ethoprophos	1.2/4.1	94	98	96	110	0.17/0.57	*68*	97	94	95

Myclobutanil	2/6.6	86	93	96	98	0.11/0.38	97	100	99	99
Metolachlor	2.7/9	84	92	98	79	0.51/1.7	93	79	78	*68*
Spinosyn D	25/83	100	120	110	130	0.93/3.1	78	110	100	95
Phosmet	1.3/4.5	93	100	100	93	0.17/0.57	73	95	94	94
Azoxystrobin	1.4/4.6	92	99	100	110	0.17/0.58	*67*	92	91	95
Fluopyram	1.5/4.8	86	99	99	99	0.22/0.74	97	97	98	96
Spinetoram J	2.3/7.7	100	100	110	88	0.35/1.2	100	90	86	79
Boscalid	6.6/22	110	87	89	80	0.39/1.3	87	91	82	84
Tebuconazole	1.1/3.5	99	95	98	97	0.19/0.62	98	98	97	98
Malathion	5.8/19	*66*	77	83	86	0.33/1.1	110	110	110	100
Fenoxycarb	50/170	-	79	78	88	0.41/1.4	100	100	99	100
Tebufenozide	2.1/7.1	80	91	93	96	0.19/0.62	100	99	98	97
Fipronil	5.6/19	78	110	100	110	0.54/1.8	95	97	100	96
Propiconazole	2.5/8.2	81	88	91	92	0.23/0.77	110	100	100	100
Tetrachlorvinphos	3.5/12	*69*	78	86	99	0.34/1.1	100	100	99	96
Benzovindiflupyr	9.9/33	100	100	96	98	0.53/1.8	120	110	110	100
Kresoxim-Methyl	12/41	**140**	120	120	110	0.88/2.9	120	100	100	110
Diazinon	1.5/5.1	78	84	84	85	0.076/0.25	84	84	84	81
Buprofenzin	1.5/5	-	89	92	99	0.26/0.86	-	100	100	110
Teflubenzuron	11/37	94	100	110	110	0.57/1.9	110	110	110	110
Pyrethin II	21/69	110	97	100	100	1.4/4.7	90	83	100	100
Pyraclostrobin	2.2/7.3	120	100	110	99	0.27/0.89	100	100	100	100
MGK-264	10/34	110	93	91	100	0.65/2.2	110	100	110	110
Piperonyl Butoxide	3.1/10	87	94	96	97	0.26/0.85	98	99	98	99
Clofentazine	9.0/30	110	100	100	100	0.59/2.0	97	100	99	110
Allethrin	4.6/15	110	86	89	89	0.41/1.4	91	92	90	91

Prallethrin	9.2/31	94	84	86	91	0.56/1.9	100	110	100	110
Trifloxystrobin	3.9/13	94	100	100	100	0.38/1.3	110	100	98	98
Tetramethrin	3.1/10	83	89	89	83	0.32/1.1	*62*	73	74	*65*
Etoxazole	1.2/3.9	75	88	89	86	0.11/0.35	85	84	83	81
Pyrethrin I	4.7/16	130	100	110	100	0.35/1.2	97	92	94	94
Chlorpyrifos	22/74	100	97	88	86	1.8/6	87	98	97	97
Hexythiazox	2.3/7.6	83	93	93	91	0.33/1.1	86	86	84	81
Spiromesifen	1.5/5	83	97	98	91	0.26/0.85	96	91	88	87
Spirodiclofen	2.9/9.8	120	110	110	100	0.35/1.2	100	99	95	99
Pyridaben	2.4/8	120	110	120	100	0.25/0.82	110	100	96	98
Resmethrin	3.2/11	79	110	120	98	0.42/1.4	92	90	81	87
Coumaphos	5.8/19	120	100	100	100	1/3.3	94	96	91	91
Permethrin [M+NH4]	9.1/30	73	120	120	110	0.87/2.9	100	96	95	98
Etofenprox	1.5/5.2	72	110	110	100	0.24/0.79	100	98	86	93
Bifenthrin	7.1/24	91	120	120	110	0.89/3	110	110	100	100
Acequinocyl	4.7/16	80	120	130	120	0.47/1.6	110	110	110	110
Fenpyroximate	2/6.6	76	92	97	82	0.16/0.54	78	73	71	70

Table 7.2 Intra- and interday percent coefficient of variation (CV) at four spike levels for both effluent and rinsate water fractions. *Italicized* values represent CV's that exceed 20% while **bolded** values represent CV's that exceed 30%.

Pesticide	Rinsate Precision (Intraday/Interday)				Effluent Precision (Intraday/Interday)			
	200 ng mL^{-1}	**2,000 ng mL^{-1}**	**20,000 ng mL^{-1}**	**200,000 ng mL^{-1}**	**20 ng mL^{-1}**	**200 ng mL^{-1}**	**2,000 ng mL^{-1}**	**20,000 ng mL^{-1}**
Acephate	5.3/2.1	*8.1/30*	10/5.1	12/5.2	**9.5/38**	6.2/7.6	12/8.2	9.7/5.6
Oxamyl	11/11	8.7/5.1	11/4.5	18/14	*12/26*	9/6.9	9.7/2	8.5/4.4
Clopyralid	7.3/6.3	6.4/11	5.2/12	8.1/7.7	5.9/7	9.3/13	8.6/13	8.4/5.2
Dinotefuran	*24/25*	17/9.9	12/0.91	13/11	13/8.4	11/11	16/4.9	17/6.9
Methomyl	15/7.8	13/7.6	13/3.6	15/5	9.5/20	11/5.4	15/6.3	15/5.7
Thiamethoxam	4.6/2.6	3.3/1.4	4.9/2.1	8.4/5.8	5.2/2.4	6.5/1.9	6.4/3.2	7.1/5.3
Flonicamid	13/6.7	12/5.5	10/1.8	14/5.5	17/2.7	11/2.1	14/5.3	14/6.3
Pirimicarb	14/4.1	13/4.8	13/1.9	17/4.4	16/4.3	12/2.7	15/5.2	16/5.4
Clothianidin	17/13	13/7.7	11/1	12/5.8	17/6.9	12/4	14/4.8	15/8.4
Dimethoate	14/8.3	14/6.5	13/2.2	15/5.2	11/8.5	10/3.7	15/5.7	15/6
Imidacloprid	15/8.6	13/6.4	11/1.4	15/4.6	16/3.6	13/2.8	15/6.1	14/5.3
Mevinphos	12/3.5	12/5.3	13/3.7	16/5.5	14/4.7	11/1.9	15/5.5	15/5
Acetamiprid	15/8.2	13/6.9	12/3	14/4.8	14/6.8	12/4.2	15/6.3	15/7.6
Imazethapyr	10/6.8	11/9.8	7/9.6	13/6.8	11/9.8	12/11	6.6/9.4	8.8/6
Aldicarb	14/6.1	14/6.3	13/4.8	17/5.8	15/5.5	12/4.7	16/5.5	16/5.8
Thiacloprid	15/7.9	13/6.1	13/3.2	16/5.6	15/5.5	13/3.8	16/8	16/5.5
Dicamba	7.2/4.4	8.3/5.4	4.1/7	12/8.6	8.2/11	14/13	5.3/9.3	7.8/9.3
Propxur	9.7/4.9	4.9/3.4	8.6/5.1	7.6/5.8	6.9/1.8	8.8/2.7	8.8/2.1	8.9/4.4
Bentazon	12/2.5	12/6.6	7.5/3.5	8.1/4.2	7.4/6.2	5.9/5.9	12/5.2	9.6/5.1
Imazalil	9.6/2.9	11/5.2	10/3.2	17/7.5	14/5.2	11/4	15/8.2	15/5.5
Thiophanate-Methyl	9.9/6.7	11/9.3	8.6/3	7.7/9	17/13	7.3/3.9	16/14	15/8.2

Imazamox	6.5/3.6	8.8/5.6	6.9/4.1	13/10	12/5.9	8/3.7	8.8/2.8	12/6.4
Carbofuran	10/4.5	11/5.4	10/2.1	17/6.2	12/5.4	9.9/3.7	14/7.7	12/6.3
Atrazine	14/5.2	14/5	13/2.6	15/3.4	14/4.4	11/4.2	15/7.6	14/4.9
Carbaryl	13/6	13/8	11/3.2	17/9.1	14/5.5	13/5.9	16/6.8	14/5.8
2,4-D	15/11	10/8.5	11/11	16/9.4	10/12	14/11	11/13	13/14
Dodemorph	8.3/5.8	14/7.8	8.9/5.5	16/16	17/9.7	14/7.6	14/5.6	17/8.5
Fensulfothion	**22/31**	12/7.3	19/17	**43/40**	20/19	10/7.7	14/9.2	15/9
Cyantraniliprole	**26/33**	8.5/9.7	15/18	**43/40**	17/20	9.5/9.9	12/13	14/11
Metalaxyl	13/5.7	12/6.7	12/4.2	14/5	14/7.1	9.9/2	15/7	16/7.7
Spiroxamine	14/5.5	16/11	14/6.5	*21/12*	*24/20*	14/6.4	16/8.1	18/10
Paclubutrazol	9/5.8	10/7.6	9.6/4.7	17/11	12/7	8.5/4	14/8.8	12/8.5
Chlorantraniliprole	16/16	13/7.9	16/20	13/13	7.6/9.4	12/9.1	12/7.9	11/13
Fludioxinil	**67/82**	**31/30**	**40/34**	**58/57**	*25/11*	*25/16*	16/14	*23/15*
Cyprodinil	15/9.2	10/7.5	15/10	15/10	12/9.7	12/9.2	10/5.2	14/7.3
Spinosyn A	12/3.6	6.7/3.2	7.5/7.3	9.9/11	13/11	13/6.6	9/6.3	9.7/7
Spirotetramat	8/8.4	8.1/5.6	14/9.3	18/13	5.7/4.8	11/3.4	10/4.2	12/4.1
Dimetamorph I	*21/13*	13/8	9.7/3.4	13/15	14/7.1	13/5	16/8.6	15/6.4
Dimetamorph II	**45/45**	**32/31**	*26/27*	**25/30**	9.1/9.4	11/7.3	14/10	17/14
Fenhexamid	**31/35**	12/11	9.6/8.8	19/15	12/9	14/9.1	10/3.7	7.8/6.8
Ethoprophos	15/3.2	10/6.8	12/5.8	8.7/12	12/3.1	11/3.4	13/7.6	13/8.1
Myclobutanil	8.2/12	6.7/3.9	10/4.5	*25/21*	8/2.9	9.1/1.8	8.3/2.2	10/4.6
Spinosyn D	15/6.1	20/20	15/16	14/19	17/11	15/11	8.9/7.1	10/8.6
Phosmet	*25/22*	11/9.7	*21/18*	11/5.9	14/18	8/9.5	11/10	11/14
Azoxystrobin	4.9/4.9	4.5/4.6	10/10	15/17	8.5/8.7	8.3/8.4	8.9/8.5	6.2/5.7
Fluopyram	5.3/7.4	5.4/5.3	1.3/1.5	7.2/9.3	9.6/8.1	5.9/5.4	8.1/7.3	4.7/6
Metolachlor	14/4.4	14/7.3	11/6.8	18/6.5	9.4/4.4	15/2.5	13/6.1	17/7
Spinetoram J	16/15	17/14	14/13	11/16	18/8.3	16/8.3	5.6/1	8.3/7.4

Boscalid	*21/22*	16/16	11/11	13/10	19/15	12/4	*21/12*	18/14
Tebuconazole	5.7/3.1	6.5/2.7	7.7/3.4	13/8.6	8.4/1.8	9.2/2.8	9.4/2.3	9.4/4.8
Malathion	16/18	9.7/9.9	12/8.2	19/15	11/8.2	9.3/8.3	9.9/3.7	7.4/3.9
Fenoxycarb	-	8/9.4	17/15	*23/20*	11/4.1	11/3.1	8.4/3.7	17/13
Tebufenozide	16/20	8.8/6.4	11/5	*25/19*	7.1/5.7	7.6/4.2	9.7/3	9.7/6.7
Fipronil	16/18	3.1/3.3	9.2/11	11/12	9.3/8.3	7.7/3.6	4.6/7.6	8.2/5.6
Propiconazole	6.1/4.7	5.7/3.4	8.9/6.9	14/10	8.9/3	11/6	8.3/2.8	9.7/5.8
Tetrachlorvinphos	*19/26*	15/12	20/9.5	**33/25**	16/7.8	*22/5.9*	15/4.6	15/7.7
Benzovindiflupyr	10/5	8.8/4.2	16/6.7	12/9.5	6.6/5.6	14/11	14/8.7	9.5/4.9
Kresoxim-Methyl	17/12	8.1/8.5	*21/11*	10/8.8	15/10	11/4.3	14/5.7	11/9.3
Diazinon	6.6/2.9	8.5/4.4	8.2/2.2	15/8.6	11/4	7.8/4.2	12/8.1	11/6.5
Buprofenzin	-	6.2/4.3	13/8.7	20/14	-	12/2.5	10/2.1	12/5.5
Teflubenzuron	12/17	12/14	12/8.1	7.7/16	11/8	11/12	6/11	17/20
Pyrethin II	13/19	9.5/8.2	20/16	*23/23*	13/13	23/19	17/17	14/9.7
Pyraclostrobin	7.9/8	8.6/8.5	4.3/3.8	16/14	5/2.1	7.2/5.7	5.2/2.7	8/6.1
MGK-264	*21/8.3*	12/9.8	12/11	15/16	17/8.2	13/3.7	*22/14*	17/9.2
Piperonyl Butoxide	8.8/5.2	7.3/5	11/5.6	14/11	9.7/3.6	11/3.3	10/2.6	11/5.8
Clofentazine	13/9.8	12/12	16/14	*22/20*	10/5.4	18/10	*23/20*	16/13
Allethrin	16/9.5	8.4/7.7	11/6.7	9.2/4.6	12/5.4	12/6.5	12/3.5	15/12
Prallethrin	11/5.9	11/13	12/8.2	9.9/11	8.3/7.7	16/9.3	6.4/8.8	13/12
Trifloxystrobin	9.7/8.6	4.9/4	8.3/9.5	12/11	8.2/4.9	8.8/5.4	9/7.1	9.8/7.8
Tetramethrin	7.9/8.1	7.2/8.1	11/12	8.1/5.8	9/7.1	6.7/6.4	14/13	12/9.8
Etoxazole	8.1/3.6	9.2/5.8	8.8/2.5	16/8.7	13/5.7	9.6/4.2	12/5.7	12/7.5
Pyrethrin I	*22/13*	6.6/4.3	14/6.3	14/15	15/9.6	15/6.7	13/7.5	11/10
Chlorpyrifos	*23/16*	*24/16*	12/14	18/16	13/18	13/14	14/12	17/14
Hexythiazox	6.3/4.2	8.3/6.2	6.4/5.9	15/9.2	11/5.5	8.7/5.8	13/9.8	13/6.6
Spiromesifen	7.5/5.4	12/9.9	9/4.3	16/11	14/6.1	9.8/5	10/2.8	12/6.6

Spirodiclofen	17/13	9.1/8	9.3/5.1	8.6/1.6	13/8.9	11/3.2	9.3/5.9	10/7.2
Pyridaben	17/12	7/2.9	8.8/6.4	12/13	11/3.4	12/4	9.4/7.5	10/5.7
Resmethrin	20/17	11/5.3	11/10	18/12	17/8	13/7.5	14/6.7	11/9.1
Coumaphos	14/6.8	7.7/4.2	15/10	7.6/11	11/6.4	16/11	8.2/7.4	14/8.3
Permethrin [M+NH4]	*20/22*	18/20	12/20	20/20	13/6	17/20	9.8/18	13/8.9
Etofenprox	20/20	9.6/6.1	8.3/3.7	*24/21*	14/7.9	11/3.4	10/2.1	14/9.8
Bifenthrin	**32/29**	*19/21*	*27/21*	*19/23*	20/20	20/19	*19/21*	*17/23*
Acequinocyl	*24/24*	5.4/5.8	6/6.5	19/17	12/6.9	12/8.7	7.4/6.5	9.8/11
Fenpyroximate	11/5.7	14/11	9.1/6.4	16/13	16/5.9	13/7	14/7.4	13/6.8

7.2 Chapter 3 Water Fraction Method Matrix Effect Validation for Biobeds

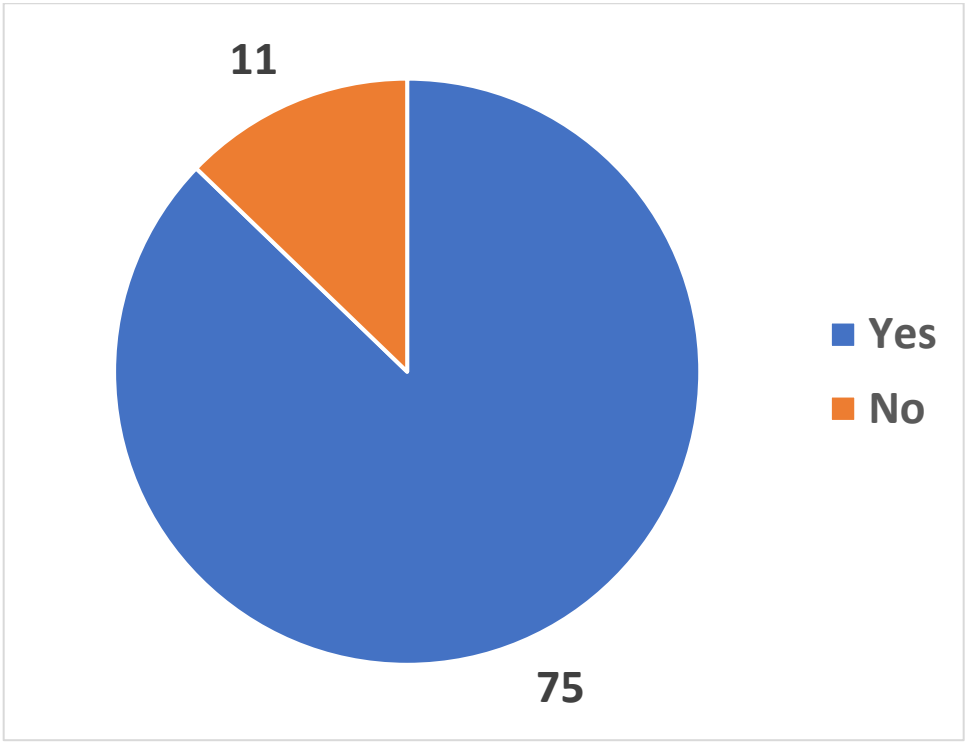

Figure 7.1 ANCOVA's conducted that were found to have a significant matrix effect (yes) vs. no effect (no).

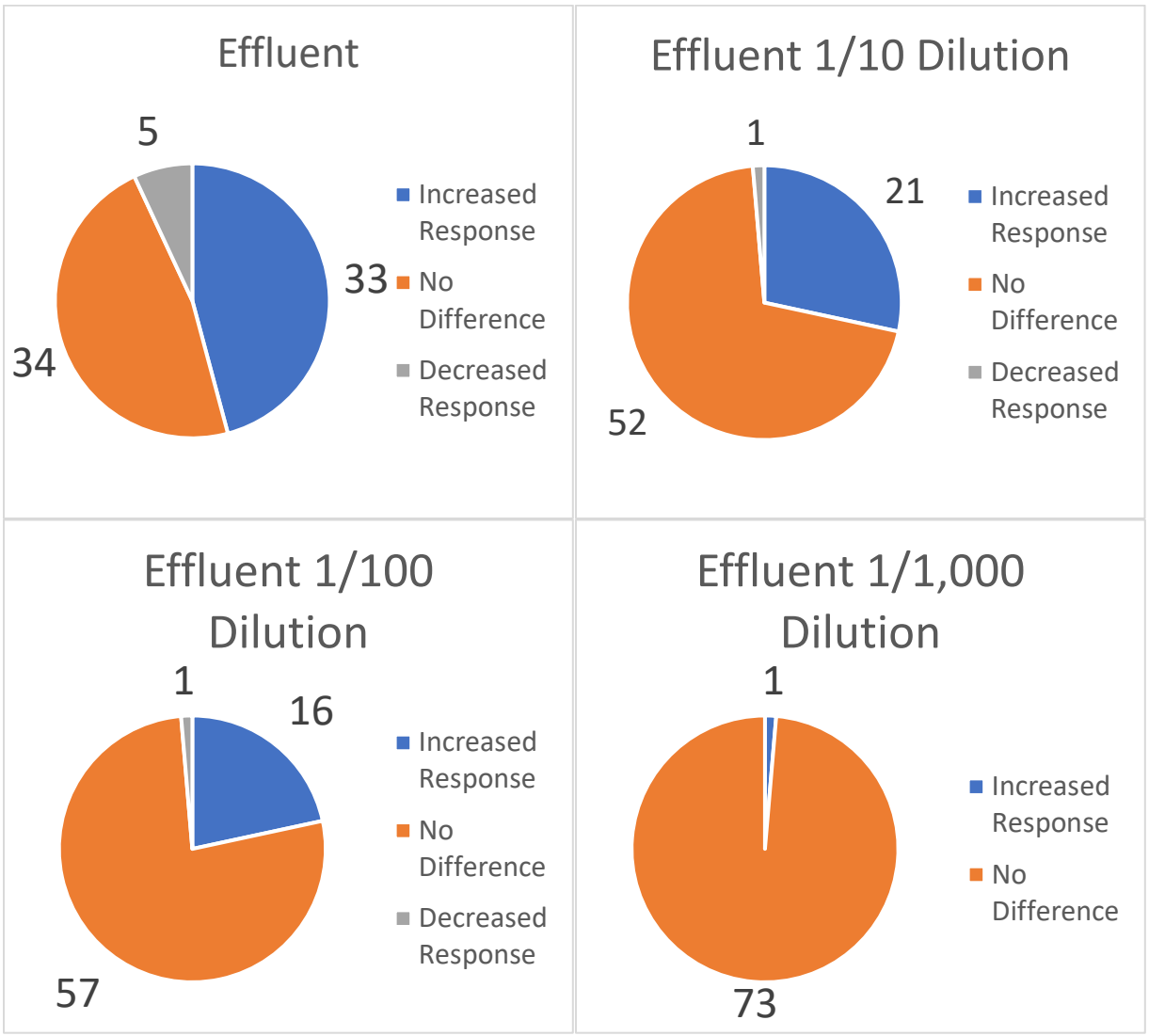

Figure 7.2 Summary of molecule responses from matrix effect found to be significant in an ANOVA and analyzed through Dunnett's test (control vs. matrices) for effluent.

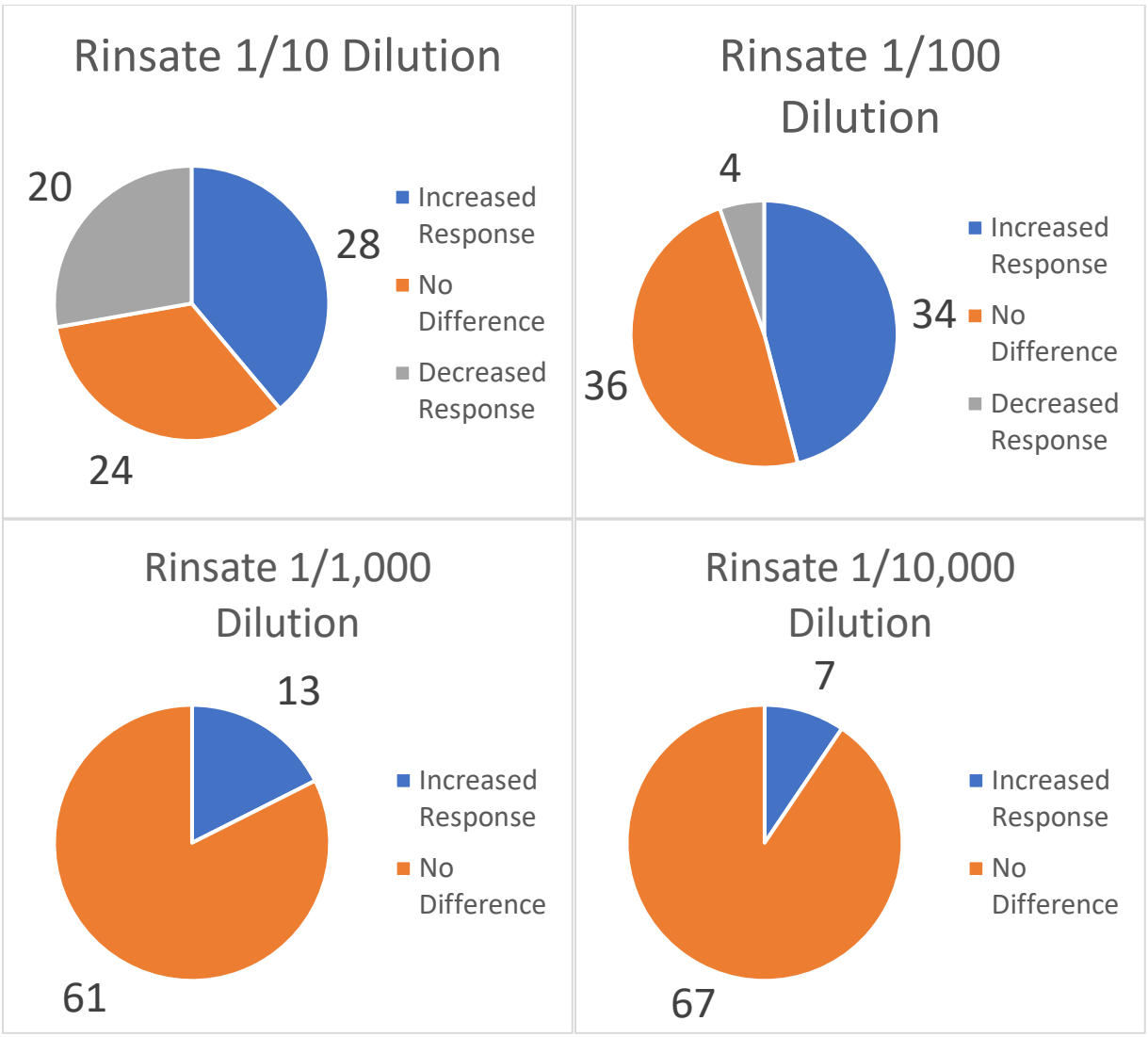

Figure 7.3 Summary of molecule responses from matrix effect found to be significant in an ANOVA and analyzed through Dunnett's test (control vs. matrices) for rinsate.

Table 7.3 Table of ANOVA "Matrix" significance for the water factions and associated *p-values* (*P*) and responses (R) from Dunnett's Post Hoc Test. + = increased molecule response, - = decreased molecule response, and 0 = no molecule response change. Green highlights indicate two seperate ANOVA's to meet assumptions; blue highlights represent a significant matrix effect *but* no differences in Dunnett's test; yellow highlights represent a removal of rn10dil due to a lack of machine response, and; orange highlights represents the removal of rn10dil *and* undiluted effluent due to no machine responses.

Matrix vs Control Solutions	ANOVA "Matrix" Significance	Effluent								Rinsate							
		Undiluted		1/10 Dil		1/100 Dil		1/1,000 Dil		1/10 Dil		1/100 Dil		1/1,000 Dil		1/10,000 Dil	
	P	*P*	R	*P*	R	*P*	R	*P*	R	*P*	R	*P*	R	*P*	R	*P*	R
Acephate	**<0.001**	**0.0118**	+	**<0.0001**	+	0.9095	0	0.9907	0	0.4099	0	0.9855	0	0.9999	0	0.9989	0
Dinotefuran	**<0.001**	**<0.0001**	+	**<0.0001**	+	**<0.0001**	+	0.66	0	**<0.0001**	+	**0.00004**	+	0.1096	0	0.1556	0
Oxamyl	**<0.001**	**<0.0001**	+	**<0.0001**	+	0.2897	0	0.9512	0	0.8939	0	0.6217	0	0.6698	0	0.9685	0
Clopyralid	**<0.05**	1	0	0.7825	0	0.1381	0	0.828	0	0.3405	0	0.136	0	**0.0285**	+	0.6909	0
Methomyl	**<0.001**	**<0.0001**	+	**<0.0001**	+	0.4734	0	1	0	0.0516	0	0.9893	0	0.9998	0	0.9443	0
Thiamethoxam	**<0.001**	**<0.0001**	+	**0.0009**	+	0.0557	0	0.3544	0	**<0.0001**	+	**0.0009**	+	0.2649	0	0.1266	0
Flonicamid	**<0.001**	0.9992	0	**0.0283**	+	**0.0054**	+	0.3859	0	**<0.0001**	+	**0.0003**	+	**0.0432**	+	**0.0045**	+
Clothianidin	**<0.001**	0.4092	0	**0.0024**	+	**0.0118**	+	0.3678	**0**	**<0.0001**	+	**<0.0001**	+	**0.0341**	+	**0.0082**	+
Dimethoate	**<0.001**	**<0.0001**	+	**<0.0001**	+	**0.032**	+	0.7082	0	**<0.0001**	+	**0.0472**	+	0.4209	0	0.6044	0
Pirimicarb	**<0.001**	**0.0003**	+	**0.0074**	+	0.1001	0	0.8279	0	**0.0002**	+	**0.139**	+	0.2057	**0**	0.2142	0
Mevinphos	**<0.001**	**<0.0001**	+	0.0697	0	0.2723	0	0.9635	0	0.1221	0	0.4277	0	0.1442	0	0.3657	0
Imidacloprid	**<0.001**	0.9004	0	0.6226	0	0.1384	0	0.9245	0	**<0.0001**	+	**0.0007**	+	0.241	0	0.1192	0

Acetamiprid	**<0.001**	**<0.0001**	+	**0.0382**	+	0.2018	0	0.9247	0	**<0.001**	+	**0.0247**	+	0.0922	0	0.1623	0
Imazethapyr	**<0.001**	**0.0004**	+	**0.0088**	+	0.0904	0	0.8987	0	**0.0007**	+	**0.006**	+	**0.039**	+	0.1964	0
Aldicarb	**<0.001**	**<0.0001**	+	**0.0028**	+	**0.0067**	+	0.557	0	**0.0003**	+	**0.0408**	+	**0.0403**	+	**0.0209**	+
Thiacloprid	**<0.001**	**0.0002**	+	**0.123**	+	0.2046	0	0.4195	0	**<0.001**	+	**0.0073**	+	0.1556	0	0.1413	0
Dicamba	>0.05	NA	NA	NA	NA	NA	NA	NA	NA	NA	NA	NA	NA	NA	NA	NA	NA
Propoxur	**<0.001**	**<0.0001**	+	**0.0302**	+	0.0723	0	0.9333	0	*<0.001*	-	0.9787	0	0.1157	0	0.3585	0
Imazalil	**<0.001**	**<0.0001**	+	**0.0026**	+	**0.0042**	+	0.5187	0	0.9863	0	**0.0048**	+	**0.0011**	+	0.055	0
Thiophanate-Methyl	**<0.001**	**<0.0001**	+	*0.0134*	-	*0.044*	-	0.6961	0	0.133	0	0.1259	0	**0.0217**	+	0.5528	0
Carbofuran	**<0.001**	**<0.0001**	+	0.0632	0	0.8239	0	0.8506	0	0.9997	0	0.2992	0	0.6293	0	0.613	0
Bentazon	**<0.01**	0.1809	0	0.5406	0	**0.0048**	+	0.1809	0	**0.0012**	+	0.2609	0	0.2566	0	0.0865	0
Atrazine	**<0.001**	**0.0007**	+	**0.0224**	+	0.0634	0	0.7932	0	**0.0006**	+	**0.0116**	+	0.2229	0	0.1693	0
Carbaryl	**<0.001**	**0.0291**	+	0.0898	0	**0.017**	+	0.9733	0	**0.0008**	+	**0.0122**	+	0.7856	0	**0.0472**	+
Metalaxyl	**<0.01**	**0.0014**	+	0.3509	0	0.5147	0	1	0	0.523	0	0.1856	0	0.968	0	0.9292	0
Dodemorph	**<0.001**	**0.007**	+	**0.007**	+	**0.0042**	+	0.5281	0	**<0.001**	+	**0.0005**	+	**0.0026**	+	0.0842	0
2,4-D	>0.05	NA	NA	NA	NA	NA	NA	NA	NA	NA	NA	NA	NA	NA	NA	NA	NA
Spiroxamine	**<0.001**	**0.0014**	+	**0.0149**	+	**0.002**	+	0.1057	0	0.9896	0	**<0.001**	+	**0.0004**	+	0.4227	0
Fensulfothion	**<0.001**	0.9015	0	0.1068	0	0.611	0	0.521	0	*<0.001*	-	*0.0067*	-	0.3134	0	0.3206	0
Cyantraniliprole	**<0.001**	0.9668	0	0.9997	0	0.8965	0	0.9945	0	*<0.001*	-	0.0532	0	1	0	0.996	0

Cyprodinil	**<0.001**	**<0.0001**	+	**0.0025**	+	**0.0155**	+	0.3324	0	**<0.001**	+	**0.0001**	+	**0.0155**	+	**0.0255**	+
Paclobutrazol	**<0.01**	**<0.0001**	+	**0.009**	+	**0.0113**	+	0.3358	0	0.8076	0	**0.0079**	+	**0.0016**	+	0.0591	0
Chlorantraniliprole	**<0.001**	0.1037	0	0.8648	0	0.9929	0	0.9847	0	**<0.001**	+	**<0.001**	+	0.12	0	0.9315	0
Dimetamorph II	**<0.001**	0.1035	0	0.343	0	0.8657	0	1	0	**<0.001**	+	**<0.001**	+	0.8644	0	0.9892	0
Fludioxinil	**<0.001**	0.8583	0	0.9545	0	0.9703	0	0.9686	0	*<0.001*	-	0.0943	0	0.998	0	0.7639	0
Spinosyn A	**<0.001**	0.0925	0	0.3441	0	0.8739	0	0.8731	0	0.6648	0	**<0.001**	+	0.932	0	0.8596	0
Spirotetramat	**<0.001**	0.1575	0	0.3243	0	0.4531	0	0.9918	0	*<0.001*	-	*<0.001*	-	0.1668	0	0.6533	0
Dimetamorph I	**<0.01**	0.2768	0	0.9386	0	0.9452	0	0.6941	0	**0.0042**	+	1	0	0.9995	0	0.9999	0
Fenhexamid	**<0.001**	0.2673	0	0.5152	0	0.9997	0	0.2337	0	**<0.001**	+	0.9397	0	0.5439	0	0.9961	0
Ethoprophos	**<0.001**	**0.0006**	+	0.3108	0	0.3338	0	0.928	0	**<0.001**	+	0.9268	0	0.8571	0	0.7676	0
Myclobutanil	**<0.001**	**0.04**	+	0.0629	0	0.0962	0	0.5515	0	*<0.001*	-	0.8319	0	0.1151	0	0.0842	0
Spinosyn D	**<0.001**	0.0884	0	0.4823	0	0.9978	0	0.8365	0	**0.0045**	+	**<0.001**	+	0.9849	0	0.7347	0
Phosmet	>0.05	NA	NA	NA	NA	NA	NA	NA	NA	NA	NA	NA	NA	NA	NA	NA	NA
Tebuconazole	**<0.001**	**<0.0001**	+	**0.001**	+	**0.0168**	+	0.4299	0	*<0.001*	-	**0.0002**	+	**0.0043**	+	**0.0268**	+
Spinetoram J	**<0.001**	0.188	0	0.5673	0	0.9701	0	0.9553	0	**0.0003**	+	**<0.001**	+	0.8934	0	0.9899	0
Azoxystorbin	**<0.001**	**0.0204**	+	0.9978	0	0.9815	0	0.4375	0	**<0.001**	+	**<0.001**	+	0.706	0	0.9881	0
Fluopyram	**<0.001**	**0.0009**	+	0.2092	0	0.1802	0	0.946	0	**<0.001**	+	**0.0003**	+	0.1929	0	0.1382	0
Boscalid	**<0.001**	0.9689	0	0.9999	0	0.9786	0	0.5812	0	**<0.001**	+	0.6427	0	0.931	0	0.931	0

Metolachlor	**<0.001**	**0.0326**	+	0.7228	0	0.2568	0	0.9882	0	NA	NA	**<0.0001**	+	0.9355	0	0.9885	0
	<0.001 (rinsate only)	NA	NA	NA	NA	NA	NA	NA	NA	**<0.0001**	+	NA	NA	NA	NA	NA	NA
Malathion	**<0.001**	0.108	0	0.6351	0	**0.0068**	+	0.94	0	**<0.0001**	+	0.4022	0	0.9219	0	0.7502	0
Fenoxycarb	**<0.001**	0.3476	0	0.056	0	0.1067	0	0.5934	0	NA	NA	0.3141	0	0.6904	0	0.0912	0
Tebufenozide	**<0.001**			0.1454	0	0.3954	0	0.4563	0	*<0.001*	-	0.9998	0	0.1387	0	0.1677	0
Fipronil	**<0.001**	0.1373	0	0.2204	0	**0.0048**	+	**0.0318**	+	*<0.001*	-	**0.0013**	+	0.3704	0	0.231	0
Tetrachlorvinphos	**<0.01**	**0.0317**	+	0.1345	0	0.9634	0	0.9891	0	NA	NA	NA	NA	**0.0385**	+	0.9996	0
	<0.001 (rinsate only)	NA	NA	NA	NA	NA	NA	NA	NA	*<0.001*	-	*0.0002*	-	NA	NA	NA	NA
Propiconazole	**<0.001**	**0.0033**	+	0.166	0	0.5602	0	0.8875	0	*<0.001*	-	0.6396	0	0.304	0	**0.0256**	+
Imazamox	**<0.001**	0.6937	0	0.9687	0	0.3749	0	0.9997	0	*<0.001*	-	**0.0282**	+	0.21	0	0.6585	0
Buprofezin	**<0.001**	NA	NA	0.5894	0	0.441	0	0.9737	0	NA	NA	*0.0001*	-	0.7629	0	0.4393	0
Kresoxim-Methyl	**<0.01**	0.3666	0	0.9993	0	0.8252	0	0.8968	0	0.0701	0	0.9201	0	0.9986	0	0.9862	0
Diazinon	**<0.01**	**0.0073**	+	0.0839	0	0.4657	0	0.8528	0	0.9462	0	0.095	0	0.1435	0	0.3518	0
Benzovindiflupyr	**<0.001**	0.9979	0	0.58	0	0.832	0	0.6623	0	*<0.001*	-	0.8986	0	0.7347	0	0.8876	0
Prallethrin	**<0.001**	0.8945	0	0.9908	0	0.4012	0	0.9762	0	*0.0051*	-	0.7	0	0.9978	0	0.4973	0
Pyrethrin II	**<0.01**	0.993	0	0.9962	0	0.7359	0	0.9759	0	0.681	0	0.0609	0	0.8002	0	0.1384	0
Pyraclostrobin	**<0.001**	0.1306	0	0.5908	0	0.8852	0	0.9953	0	*<0.001*	-	**<0.0001**	+	0.6311	0	1	0
Clofentazine	**<0.001**	0.1062	0	0.9907	0	0.8315	0	0.9653	0	*0.0005*	-	0.949	0	0.9651	0	0.8668	0

MGK.264	**<0.05**	0.9952	0	0.9333	0	0.9485	0	0.6659	0	0.1189	0	1	0	0.9757	0	0.9772	0
Coumaphos	**<0.01**	**0.0216**	+	0.1267	0	0.1151	0	0.3927	0	0.9451	0	0.096	0	0.9666	0	0.111	0
Teflubenzuron	**<0.001**	0.9017	0	0.9987	0	0.7809	0	0.954	0	*<0.001*	-	0.9173	0	0.1457	0	0.9315	0
Trifloxystrobin	**<0.001**	0.9032	0	0.6803	0	0.871	0	0.7411	0	*<0.001*	-	0.0712	0	0.2385	0	0.6045	0
Piperonyl Butoxide	**<0.001**	0.5506	0	0.1319	0	**0.0218**	+	0.5281	0	*<0.001*	-	0.1308	0	0.3625	0	0.7304	0
Allethrin	>0.05	NA	NA	NA	NA	NA	NA	NA	NA	NA	NA	NA	NA	NA	NA	NA	NA
Fenpyroximate	>0.05	NA	NA	NA	NA	NA	NA	NA	NA	NA	NA	NA	NA	NA	NA	NA	NA
Tetramethin	**<0.01**	0.3422	0	0.8975	0	0.9056	0	0.4503	0	0.0987	0	0.9959	0	0.3677	0	0.7273	0
Etoxazole	>0.05	NA	NA	NA	NA	NA	NA	NA	NA	NA	NA	NA	NA	NA	NA	NA	NA
Pyrethrin I	**<0.001**	*<0.0001*	-	0.9924	0	0.9999	0	0.8526	0	0.0506	0	**0.0008**	+	0.6863	0	0.7863	0
Chlorpyrifos	**<0.05**	0.6825	0	1	0	0.8676	0	0.5829	0	0.0664	0	0.8041	0	0.9781	0	0.9999	0
Spiromesifen	**<0.01**	*<0.0001*	-	0.3054	0	0.7127	0	0.2354	0	0.759	0	**0.0247**	+	0.9998	0	0.889	0
Hexythiazox	>0.05	NA	NA	NA	NA	NA	NA	NA	NA	NA	NA	NA	NA	NA	NA	NA	NA
Spirodiclofen	**<0.01**	0.1209	0	0.9989	0	0.9572	0	0.9913	0	0.9175	0	0.188	0	0.9637	0	0.8154	0
Pyridaben	**<0.05**	*<0.0001*	-	0.5208	0	0.593	0	0.6681	0	0.102	0	**<0.0001**	+	0.8722	0	0.531	0
Resmethrin	**<0.01**	*<0.0001*	-	0.5845	0	0.4691	0	0.7306	0	0.8747	0	**0.0325**	+	0.9604	0	0.9348	0
Permethrin-NH4+	>0.05	NA	NA	NA	NA	NA	NA	NA	NA	NA	NA	NA	NA	NA	NA	NA	NA
Etofenprox	**<0.01**	*0.0004*	-	0.7289	0	0.9947	0	0.8188	0	*0.001*	-	0.5299	0	0.9371	0	0.5302	0

Bifenthrin	>0.05	NA	NA	NA	NA	NA	NA	NA	NA	NA	NA	NA	NA	NA	NA	NA	NA
Acequinocyl	>0.05	NA	NA	NA	NA	NA	NA	NA	NA	NA	NA	NA	NA	NA	NA	NA	NA

Table 7.4 Transformation method, Shapiro-Wilk's Test for normality and Breusch-Pagan's Test for homoscedascity on model residuals and slope homogeneity assumption ANOVA test p-values and notes regarding issues in analysis for water matrix effects ANCOVA's for each compound. *Italicized* values had no response below 20 ppb, so were run as an ANOVA and are found in Table 7.5. NA = not applicable; green highlighted rows were separated into two analyses due to strength of matrix effects causing non-homogenous slopes with transformations.

Compounds	Transfor-mation	Norma-lity	Homosce-dascity	Slope Homogeneity	Notes
Acephate	Cube Root	0.9364	0.5726	0.1124	
Dinotefuran	Log10	0.2689	0.7503	0.1224	
Oxamyl	Log10	0.4894	0.8934	0.1007	
Clopyralid	Square Root	0.5529	0.7347	0.4723	
Methomyl	Log10	0.5013	0.1908	0.7779	
Thiamethoxam	Log10	0.9249	0.2854	0.2096	
Flonicamid	Square Root	0.5537	0.8245	0.5717	
Clothianidin	Cube Root	0.6204	0.6181	0.1546	
Dimethoate	Log10	0.2506	0.2049	0.6626	
Pirimicarb	Square Root	0.5903	0.4296	0.6705	
Mevinphos	Square Root	0.2923	0.8003	0.4681	
Imidacloprid	Square Root	0.4024	0.3827	0.6337	
Acetamiprid	Square Root	0.5785	0.9736	0.1644	
Imazethapyr	Square Root	0.4996	0.2107	0.9192	
Aldicarb	Square Root	0.7411	0.8682	0.3265	
Thiacloprid	Square Root	0.7566	0.5086	0.5768	
Dicamba	Square Root	0.4114	0.47	0.8779	Block A Removal (Heteroscedascity)
Propoxur	Log10	0.6393	0.0768	0.43	

Imazalil	Square Root	0.4743	0.7956	0.589	
Thiophanate-Methyl	*None*	*NA*	*NA*	*NA*	*Response at 20 ppb*
Carbofuran	Log10	0.5443	0.6608	0.7545	
Bentazon	Cube Root	0.6409	0.137	0.8214	
Atrazine	Square Root	0.7597	0.9081	0.4495	
Carbaryl	Square Root	0.6949	0.06414	0.2495	
Metalaxyl	Square Root	0.5221	0.918	0.3596	
Dodemorph	Log10	0.128	0.6319	0.701	
2,4-D	Square Root	0.9487	0.4479	0.8441	
Spiroxamine	Square Root	0.4602	0.2124	0.2975	Block D Removal (Heteroscedascity)
Fensulfothion	*Log10*	*NA*	*NA*	*NA*	*Response at 20 ppb*
Cyantraniliprole	Square Root	0.2369	0.953	0.07143	Block A Removal (Heteroscedascity)
Cyprodinil	Square Root	0.3255	0.485	0.916	
Paclobutrazol	Square Root	0.09704	0.5745	0.4115	
Chlorantraniliprole	Log10	0.1126	0.2357	0.639	5 ppb Removal (No Response)
Dimetamorph II	*Log10*	*NA*	*NA*	*NA*	*Response at 20 ppb*
Fludioxinil	*Square Root*	*NA*	*NA*	*NA*	*Response at 20 ppb*
Spinosyn A	*Square Root*	*NA*	*NA*	*NA*	*Response at 20 ppb*
Spirotetramat	Log10	0.7021	0.1664	0.06533	Block A Removal (Heteroscedascity)
Dimetamorph I	Cube Root	0.1128	0.2766	0.2053	Block A, C Removal (Heteroscedascity)
Fenhexamid	Cube Root	0.5308	0.6986	0.326	
Ethoprophos	Cube Root	0.4671	0.5643	0.5782	
Myclobutanil	Log10	0.4311	0.056425	0.7287	
Spinosyn D	*Square Root*	*NA*	*NA*	*NA*	*Response at 20 ppb*
Phosmet	*None*	*NA*	*NA*	*NA*	*Response at 20 ppb*
Tebuconazole	Log10	0.9633	0.1305	0.37	
Spinetoram J	*None*	*NA*	*NA*	*NA*	*Response at 20 ppb*
Azoxystorbin	Cube Root	0.613	0.1332	0.1732	Block B Removal (Heteroscedascity)

Fluopyram	Log10	0.138	0.1158	0.8671	
Boscalid	Square Root	0.1635	0.9128	0.1303	
Metolachlor	Cube Root	0.9487	0.2646	0.2677	Excluding RN10DIL
	Log10	0.1634	0.2748	0.4032	DI Water vs RN10DIL
Malathion	Cube Root	0.4782	0.6961	0.1789	5 ppb Removal (No Response)
Fenoxycarb	Square Root	0.6225	0.4792	0.5318	RN10DIL Removed (No Response)
Tebufenozide	Log10	0.05128	0.10859	0.2758	
Fipronil	Log10	0.2867	0.5218	0.899	5 ppb Removal (No Response)
Tetrachlorvinphos	Cube Root	0.8824	0.6716	0.8457	Excluding RN10DIL and RN100DIL
	Log10	0.2726	0.1849	0.0604	DI Water vs RN10DIL and RN100DIL
Propiconazole	Log10	0.7369	0.1076	0.8934	
Imazamox	Square Root	0.6111	0.06484	0.078	
Buprofezin	Log10	0.053541	0.8184	0.1515	RN10DIL and EF Removed (No Response)
Kresoxim-Methyl	Square Root	0.396	0.1072	0.9722	
Diazinon	Square Root	0.9565	0.5275	0.6389	
Benzovindiflupyr	Cube Root	0.7564	0.3762	0.1549	Block B Removal (Heteroscedascity)
Prallethrin	Square Root	0.7305	0.0802	0.6605	
Pyrethrin II	Square Root	0.241	0.9555	0.8142	
Pyraclostrobin	Log10	0.0842	0.305	0.4605	
Clofentazine	Square Root	0.2671	0.5974	0.0666	
MGK.264	Cube Root	0.8702	0.8499	0.0957	Block A Removal (Cal Curve Error)
Coumaphos	Square Root	0.5912	0.1374	0.9881	5 ppb Removal (No Response)
Teflubenzuron	Square Root	0.9838	0.4005	0.4943	Block A Removal (Heteroscedascity)
Trifloxystrobin	Square Root	0.9021	0.4635	0.255	
Piperonyl Butoxide	Cube Root	0.3805	0.2638	0.07245	Block A Removal (Heteroscedascity)
Allethrin	Square Root	0.4306	0.9822	0.2822	
Fenpyroximate	*Square Root*	*NA*	*NA*	*NA*	*Response at 20 ppb*

Tetramethin	Cube Root	0.5684	0.7301	0.6377	Block C, D Removal (Heteroscedascity)
Etoxazole	Log10	0.2262	0.982	0.1584	Block C, D Removal (Heteroscedascity)
Pyrethrin I	*Square Root*	*NA*	*NA*	*NA*	*Response at 20 ppb*
Chlorpyrifos	Square Root	0.5684	0.9624	0.701	
Spiromesifen	*Square Root*	*NA*	*NA*	*NA*	*Response at 20 ppb*
Hexythiazox	Square Root	0.2881	0.684	0.9665	
Spirodiclofen	Log10	*0.0856*	*0.6398*	*0.1235*	Block B Removal (Heteroscedascity)
Pyridaben	*Square Root*	*NA*	*NA*	*NA*	*Response at 20 ppb*
Resmethrin	*Square Root*	*NA*	*NA*	*NA*	*Response at 20 ppb*
Permethrin-NH4+	*Square Root*	*NA*	*NA*	*NA*	*Response at 20 ppb*
Etofenprox	*Square Root*	*NA*	*NA*	*NA*	*Response at 20 ppb*
Bifenthrin	*Square Root*	*NA*	*NA*	*NA*	*Response at 20 ppb*
Acequinocyl	*Square Root*	*NA*	*NA*	*NA*	*Response at 20 ppb*

Table 7.5 Transformation method, Shapiro-Wilk Test for normality for each matrix, Bartlett's Test for homogeneity of variance, and notes regarding issues in analysis for water matrix effects ANOVA's for compounds only detected at 20 ppb.

ANOVA	Transformation	Normality								Homogeneity of Variance	Notes
		Deionized Water	Effluents				Rinsate				
		Control	0 Dil	10 Dil	100 Dil	1,000 Dil	10 Dil	100 Dil	1,000 Dil	10,000 Dil	
Thiophanate-Methyl	None	0.9085	0.7238	0.2271	0.3078	0.01599	0.9739	0.3091	0.3493	0.1871	0.9822
Fensulfothion	Log10	0.4758	0.6708	0.9508	0.5705	0.4989	0.2523	0.9978	0.9496	0.8728	0.1247
Dimetamorph II	Log10	0.8832	0.2154	0.992	0.4025	0.5395	0.5094	0.7929	0.7368	0.2071	0.8407
Fludioxinil	Square Root	0.9032	0.7181	0.4432	0.2645	0.3584	0.2755	0.6983	0.5806	0.9286	0.6965
Spinosyn A	Square Root	0.7838	0.6727	0.6629	0.8912	0.2605	0.2966	0.0791	0.0852	0.9393	0.7758

Spinosyn D	Square Root	0.6692	0.2818	0.1154	0.8031	0.2793	0.3904	0.6513	0.06547	0.8946	0.221	Block A Removal (Quantification Issue)
Phosmet	None	0.8738	0.186	0.8107	0.3831	0.5651	0.6274	0.5901	0.05277	0.1363	0.2373	Block A 20 ppb DI Water removed (Qant issues)
Spinetoram J	None	0.1113	0.3714	0.6773	0.465	0.3326	-0.844	0.9918	0.4986	0.4618	0.105	Block A 20 ppb RN 10DIL removed (Qant issues)
Fenpyroximate	Square Root	0.1316	0.6602	0.181	0.1889	0.1067	0.1439	0.6292	0.9951	0.0201	0.1313	Block A Removal (Heterogenous Variance)
Pyrethrin I	Square Root	0.4806	0.4884	0.3247	0.2755	0.2382	0.9067	0.6696	0.7022	0.8765	0.0901	
Spiromesifen	Square Root	0.7193	0.6256	0.6307	0.1373	0.4273	0.9955	0.5052	0.5075	0.6896	0.9053	
Pyridaben	Square Root	0.2085	0.8642	0.1206	0.9938	0.2594	0.9993	0.4686	0.7899	0.9833	0.7533	
Resmethrin	Square Root	0.1435	0.4977	0.7726	0.6879	0.1284	0.1666	0.4402	0.7317	0.6619	0.7208	
Permethrin-NH4+	Square Root	0.9169	0.2812	0.9443	0.06636	0.4053	0.7565	0.9971	0.8053	0.2919	0.8289	
Etofenprox	Square Root	0.4324	0.2122	0.7668	0.3575	0.9555	0.3306	0.595	0.611	0.8423	0.1218	Block A Removal (Heterogenous Variance)
Bifenthrin	Square Root	0.6976	0.3991	0.0922	0.4071	0.1946	0.1044	0.7885	0.9529	0.9515	0.7335	Block A Removal (Heterogenous Variance)
Acequinocyl	Square Root	0.6388	0.3297	0.5673	0.07716	0.0977	0.6357	0.1975	0.9101	0.4105	0.5748	Block C Removal (Heterogenous Variance)

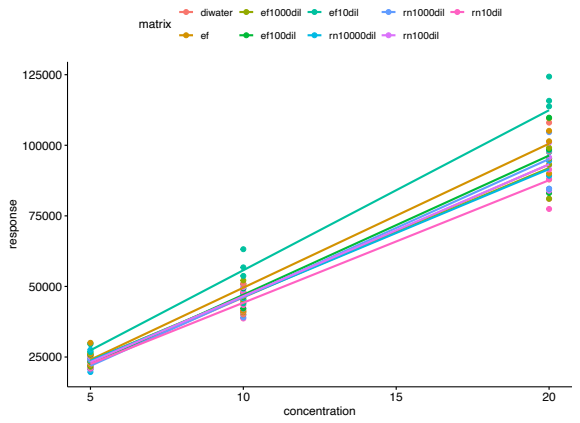

Figure 7.4 Acephate response across concentration in a pure water matrix vs effluents and rinsates.

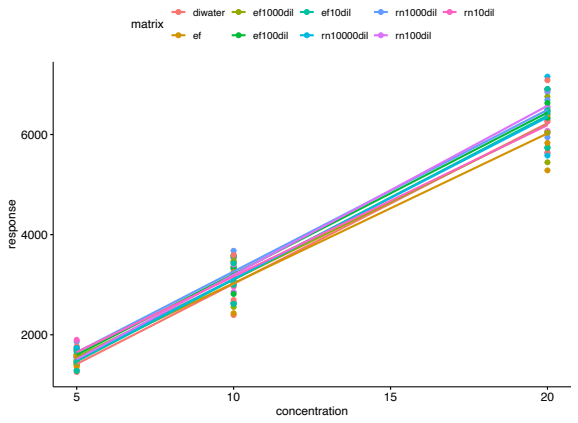

Figure 7.7 Clopyralid response across concentration in a pure water matrix vs effluents and rinsates.

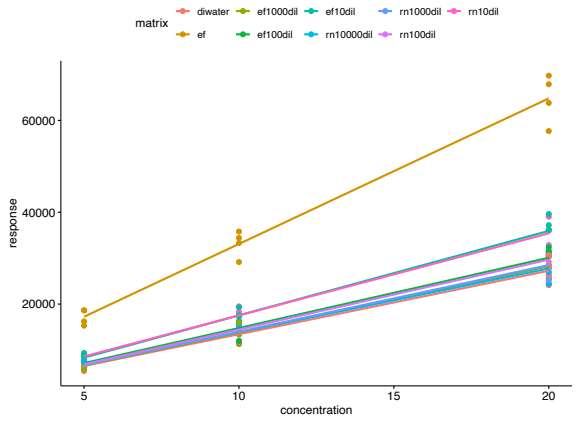

Figure 7.5 Dinotefuran response across concentration in a pure water matrix vs effluents and rinsates.

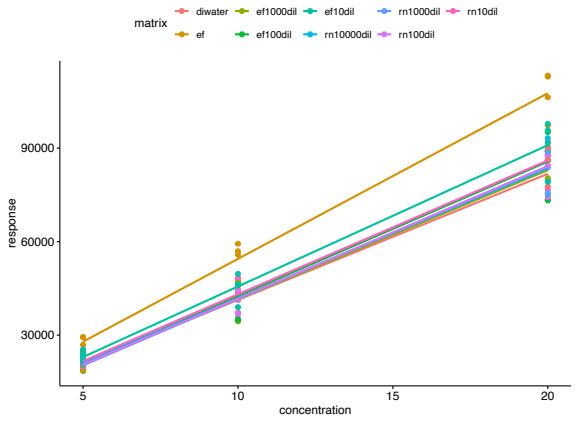

Figure 7.8 Methomyl response across concentration in a pure water matrix vs effluents and rinsates.

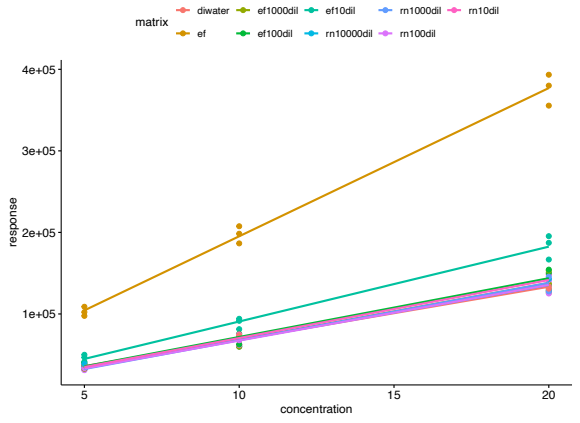

Figure 7.6 Oxamyl response across concentration in a pure water matrix vs effluents and rinsates.

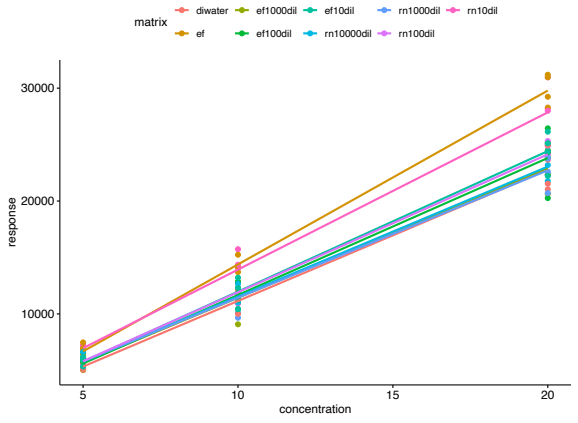

Figure 7.9 Thiamethoxam response across concentration in a pure water matrix vs effluents and rinsates.

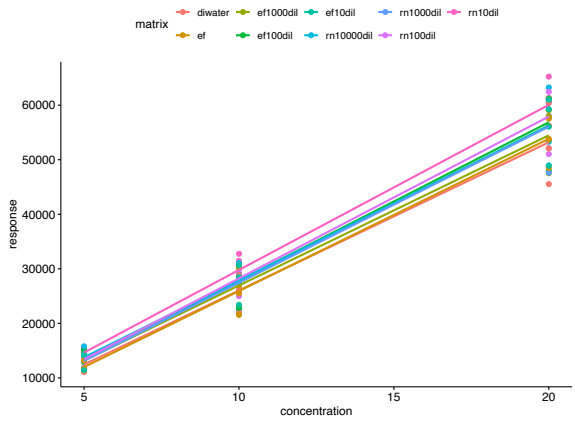

Figure 7.10 Flonicamid response across concentration in a pure water matrix vs effluents and rinsates.

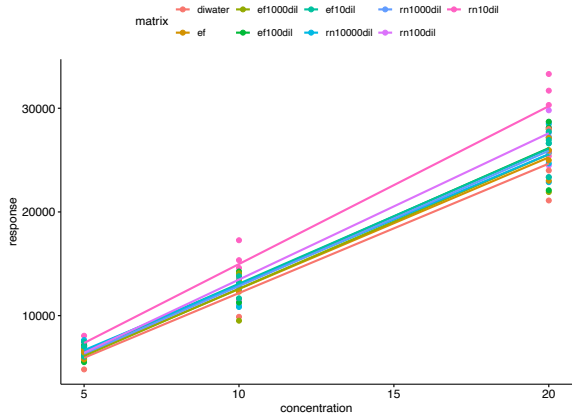

Figure 7.11 Clothianidin response across concentration in a pure water matrix vs effluents and rinsates.

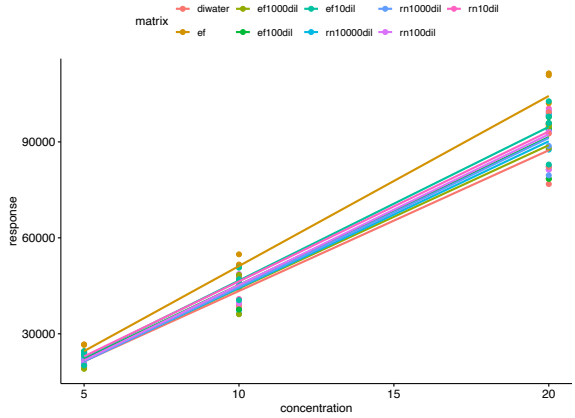

Figure 7.12 Dimethoate response across concentration in a pure water matrix vs effluents and rinsates.

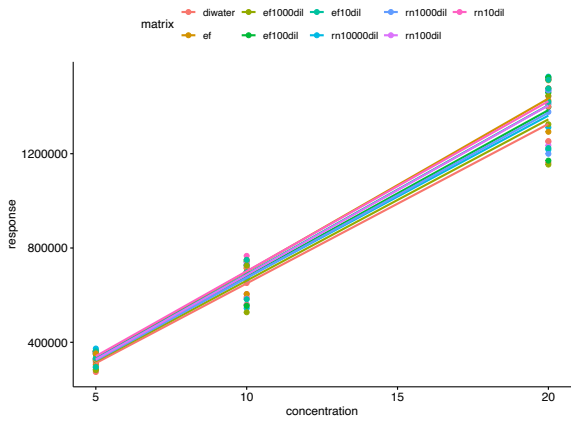

Figure 7.13 Pirimicarb response across concentration in a pure water matrix vs effluents and rinsates.

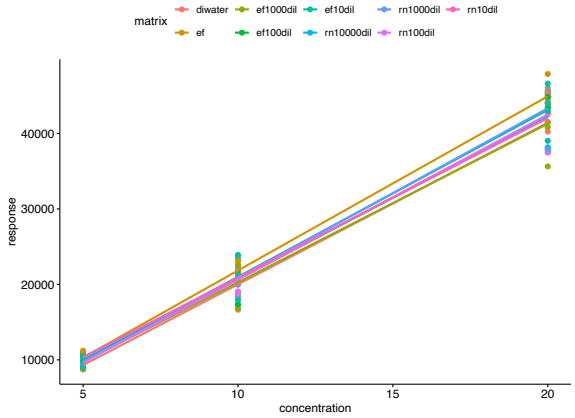

Figure 7.14 Mevinphos response across concentration in a pure water matrix vs effluents and rinsates.

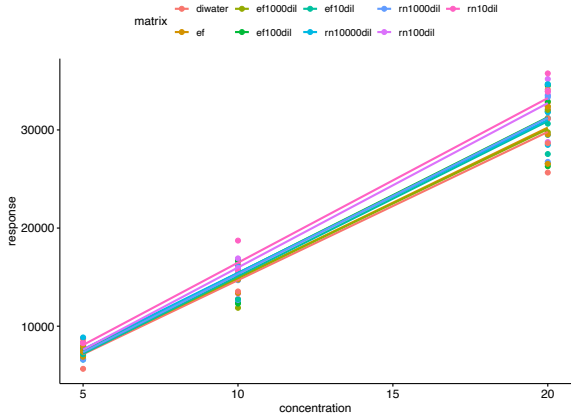

Figure 7.15 Imidacloprid response across concentration in a pure water matrix vs effluents and rinsates.

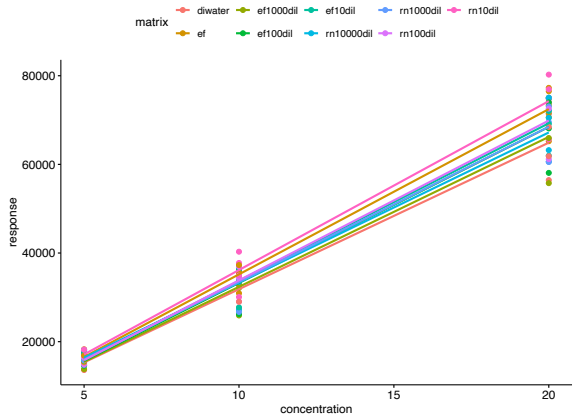

Figure 7.16 Acetamiprid response across concentration in a pure water matrix vs effluents and rinsates.

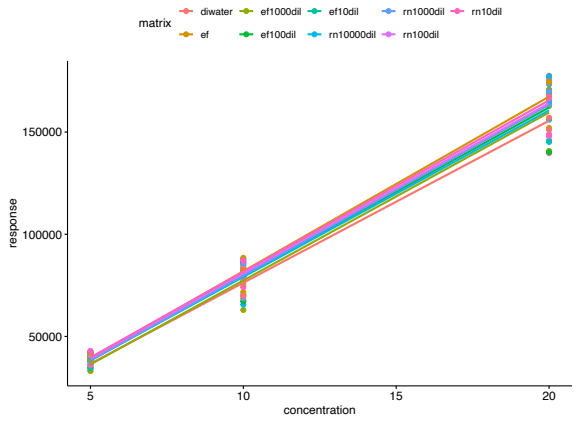

Figure 7.17 Imazethapyr response across concentration in a pure water matrix vs effluents and rinsates.

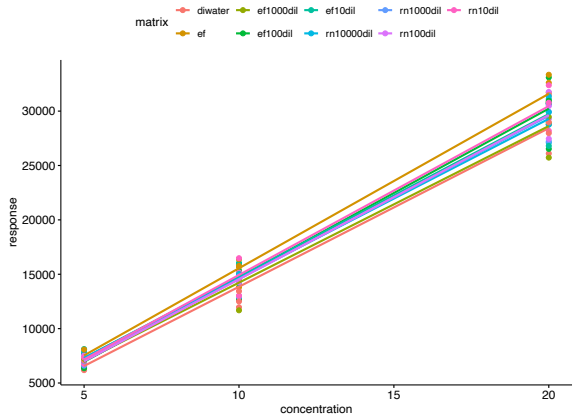

Figure 7.18 Aldicarb response across concentration in a pure water matrix vs effluents and rinsates.

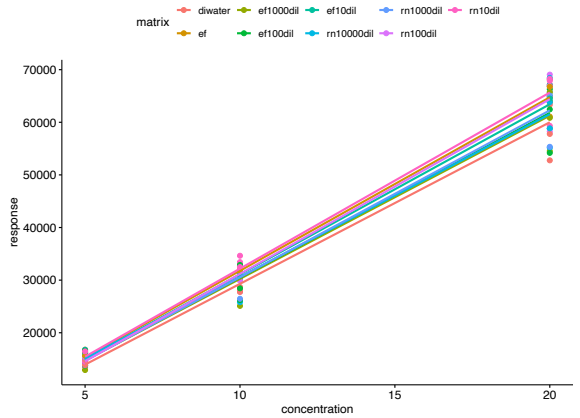

Figure 7.19 Thiacloprid response across concentration in a pure water matrix vs effluents and rinsates.

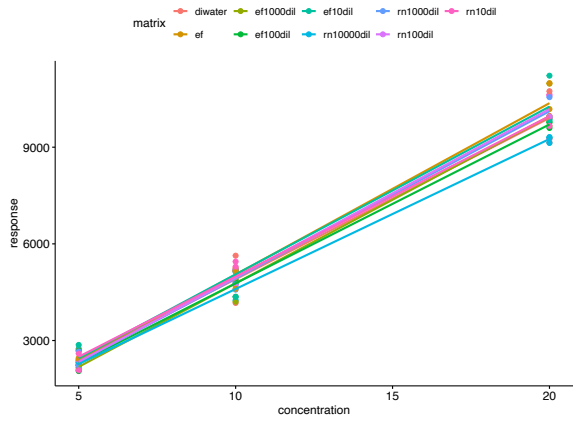

Figure 7.20 Dicamba response across concentration in a pure water matrix vs effluents and rinsates.

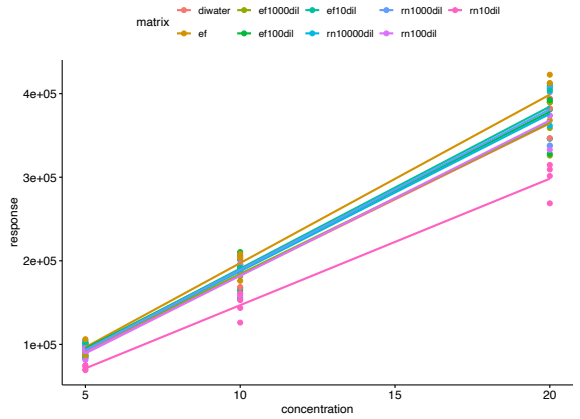

Figure 7.21 Propoxur response across concentration in a pure water matrix vs effluents and rinsates.

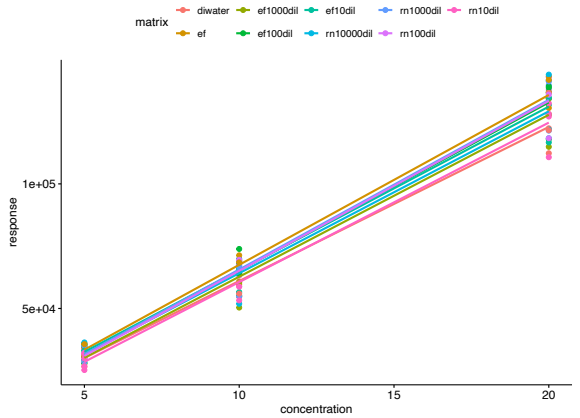

Figure 7.22 Imazalil response across concentration in a pure water matrix vs effluents and rinsates.

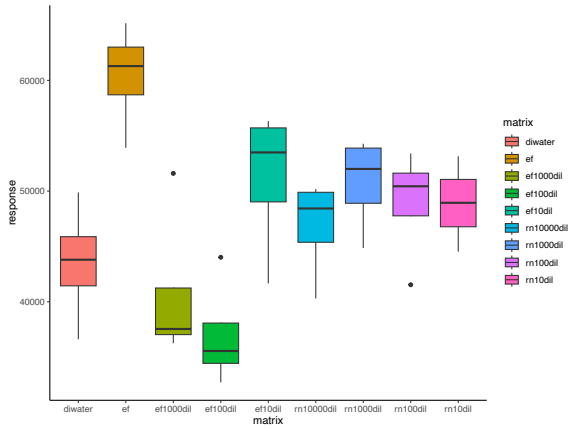

Figure 7.23 Thiophanate-Methyl response at 20 ppb in a pure water matrix vs effluents and rinsates.

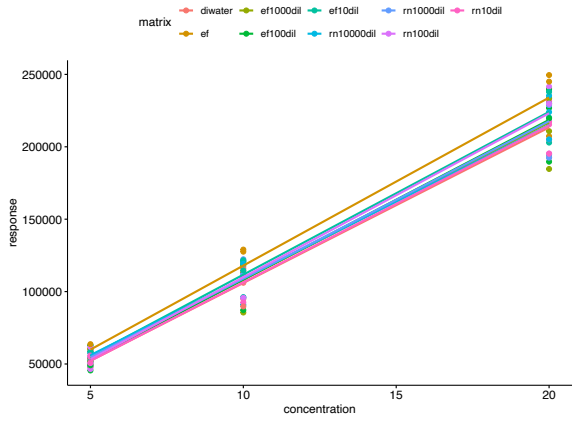

Figure 7.24 Carbofuran response across concentration in a pure water matrix vs effluents and rinsates.

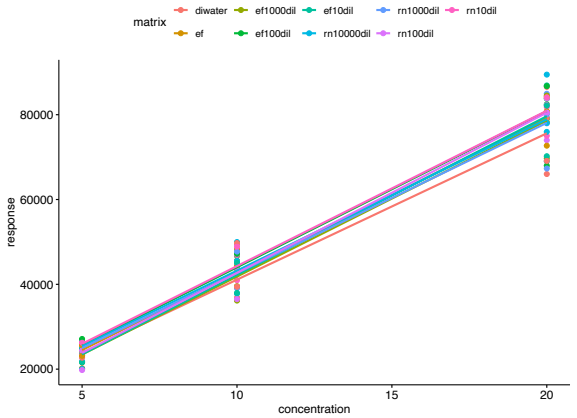

Figure 7.25 Bentazon response across concentration in a pure water matrix vs effluents and rinsates.

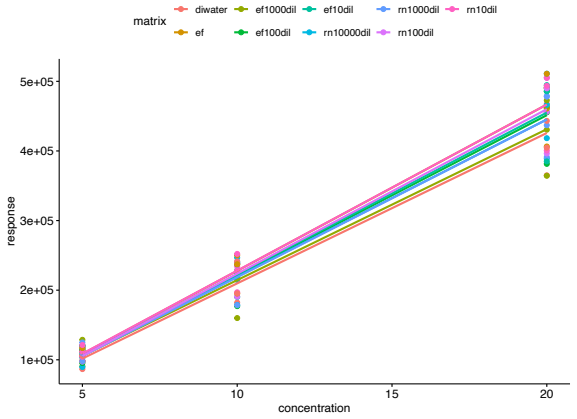

Figure 7.26 Atrazine response across concentration in a pure water matrix vs effluents and rinsates.

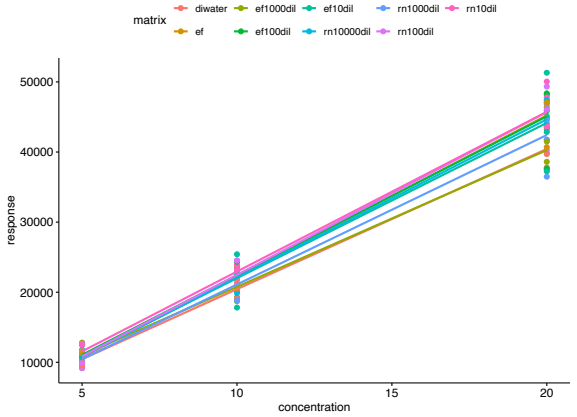

Figure 7.27 Carbaryl response across concentration in a pure water matrix vs effluents and rinsates.

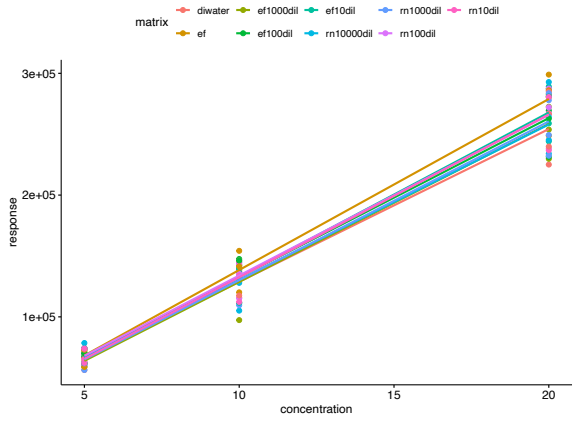

Figure 7.28 Metalaxyl response across concentration in a pure water matrix vs effluents and rinsates.

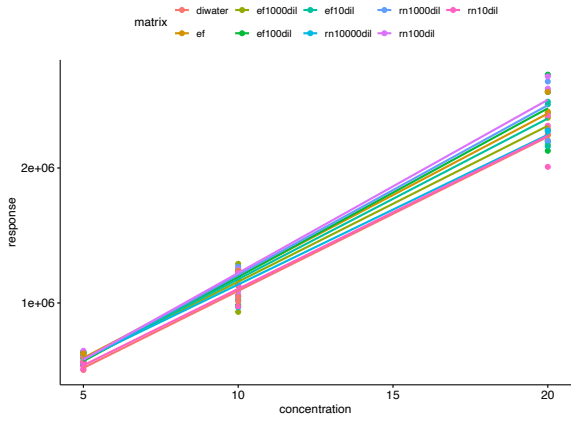

Figure 7.31 Spiroxamine response across concentration in a pure water matrix vs effluents and rinsates.

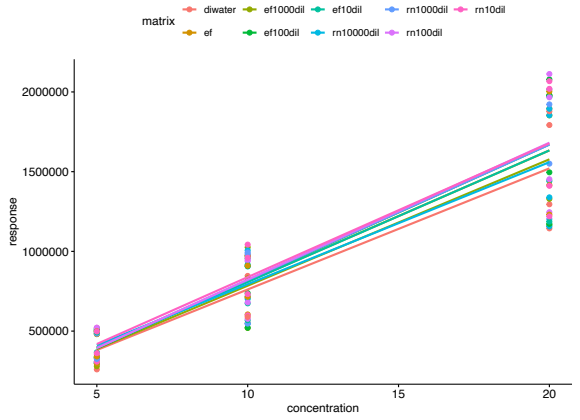

Figure 7.29 Dodemorph response across concentration in a pure water matrix vs effluents and rinsates.

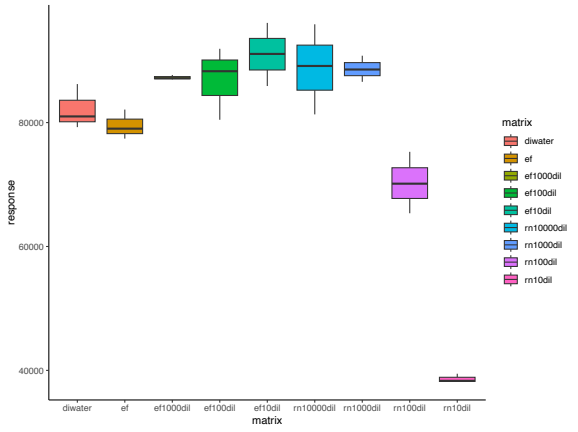

Figure 7.32 Fensulfothion response at 20 ppb in a pure water matrix vs effluents and rinsates.

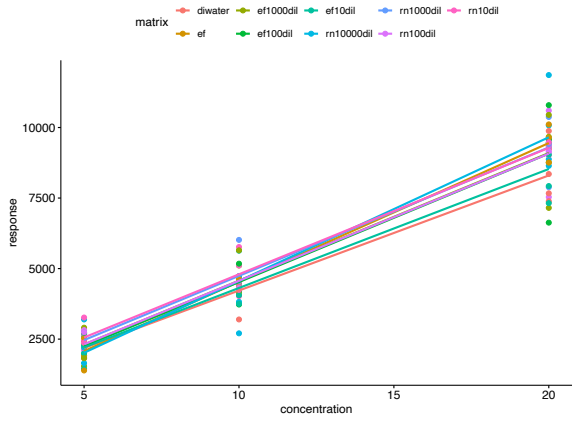

Figure 7.30 2,4-D response across concentration in a pure water matrix vs effluents and rinsates.

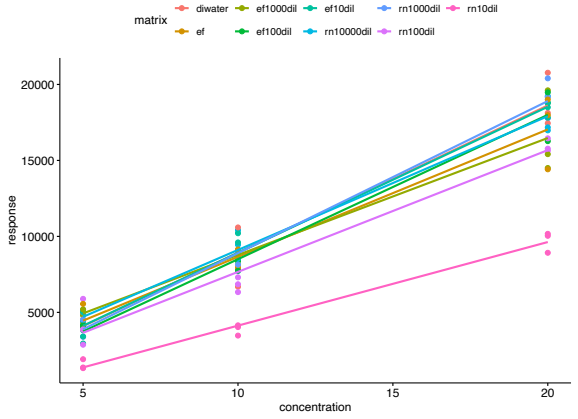

Figure 7.33 Cyantraniliprole response across concentration in a pure water matrix vs effluents and rinsates.

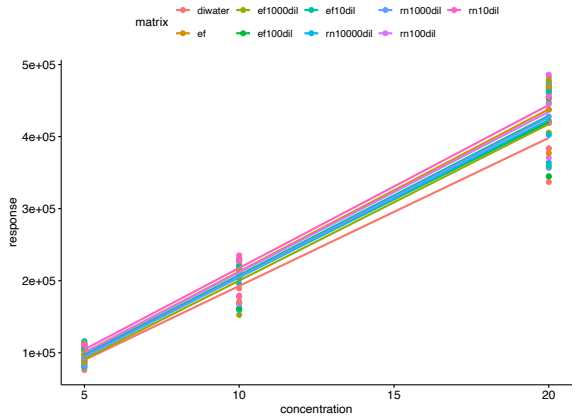

Figure 7.34 Cyprodinil response across concentration in a pure water matrix vs effluents and rinsates.

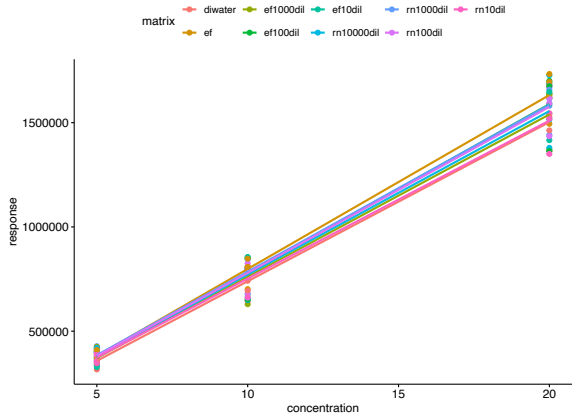

Figure 7.35 Paclobutrazol response across concentration in a pure water matrix vs effluents and rinsates.

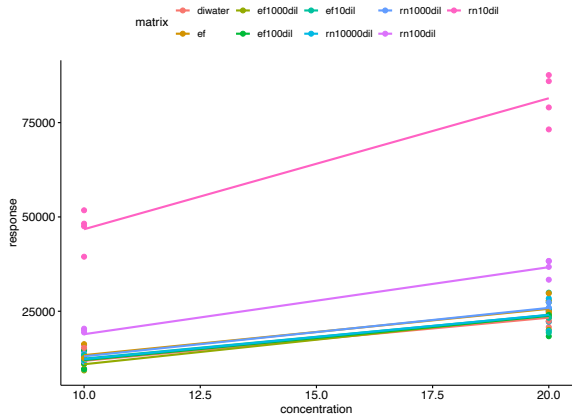

Figure 7.36 Chlorantraniliprole response across concentration in a pure water matrix vs effluents and rinsates.

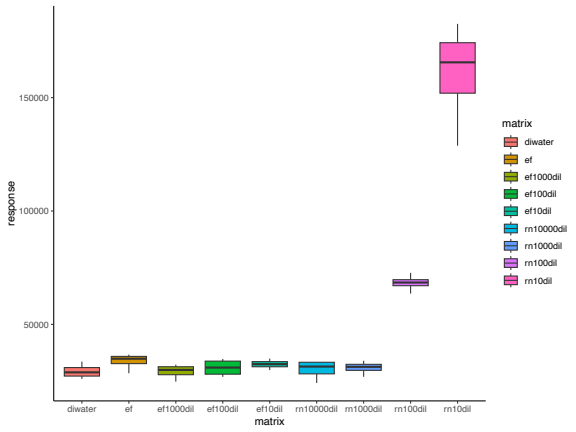

Figure 7.37 Dimethomorph II response at 20 ppb in a pure water matrix vs effluents and rinsates.

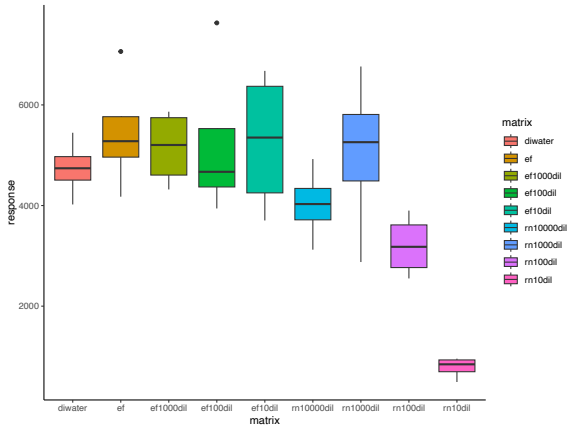

Figure 7.38 Fludioxinil response at 20 ppb in a pure water matrix vs effluents and rinsates.

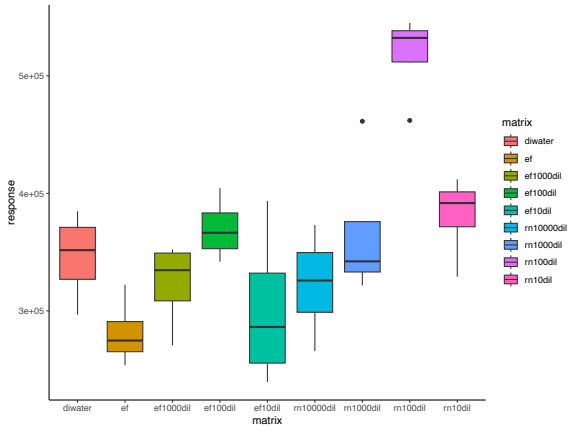

Figure 7.39 Spinosyn A response at 20 ppb in a pure water matrix vs effluents and rinsates.

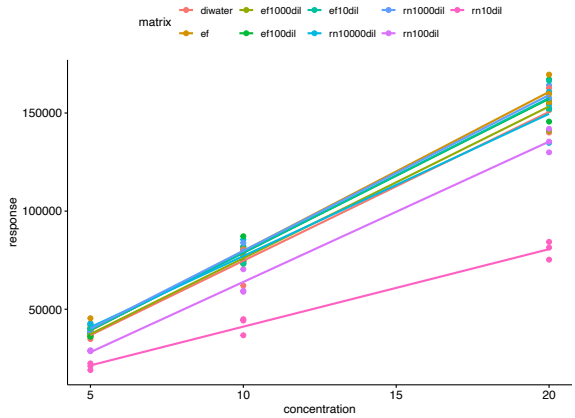

Figure 7.40 Spirotetramat response across concentration in a pure water matrix vs effluents and rinsates.

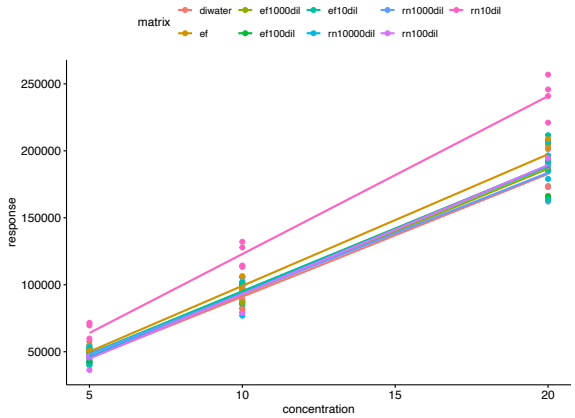

Figure 7.43 Ethoprophos response across concentration in a pure water matrix vs effluents and rinsates.

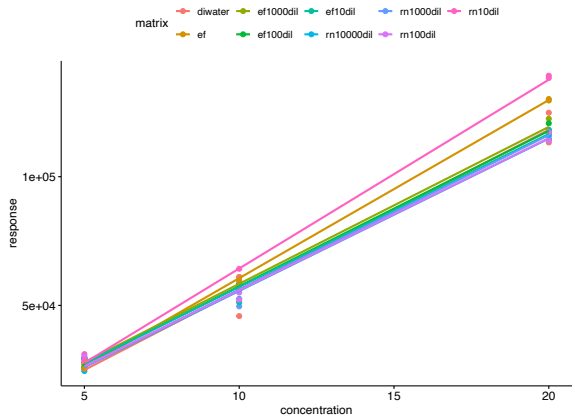

Figure 7.41 Dimethomorph I response across concentration in a pure water matrix vs effluents and rinsates.

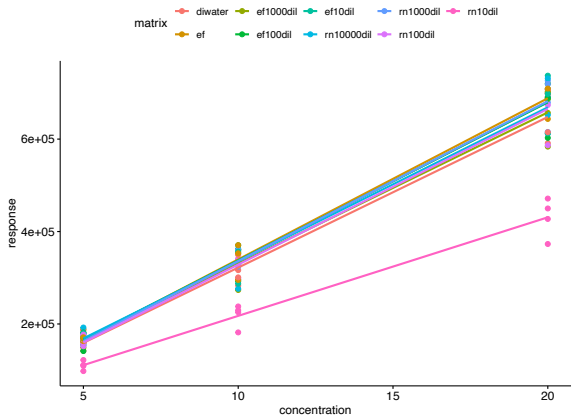

Figure 7.44 Myclobutanil response across concentration in a pure water matrix vs effluents and rinsates.

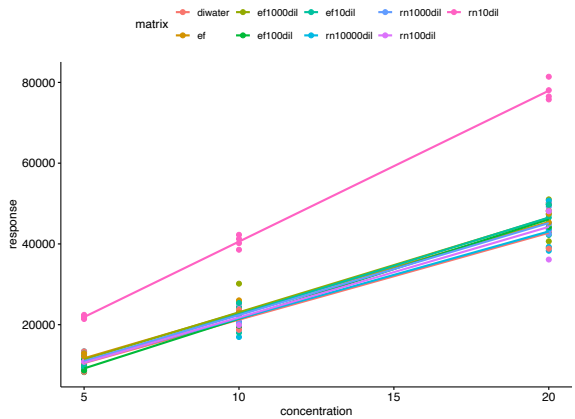

Figure 7.42 Fenhexamid response across concentration in a pure water matrix vs effluents and rinsates.

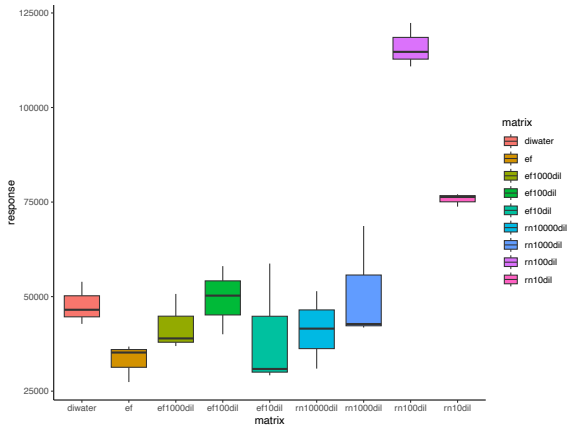

Figure 7.45 Spinosyn D response at 20 ppb in a pure water matrix vs effluents and rinsates.

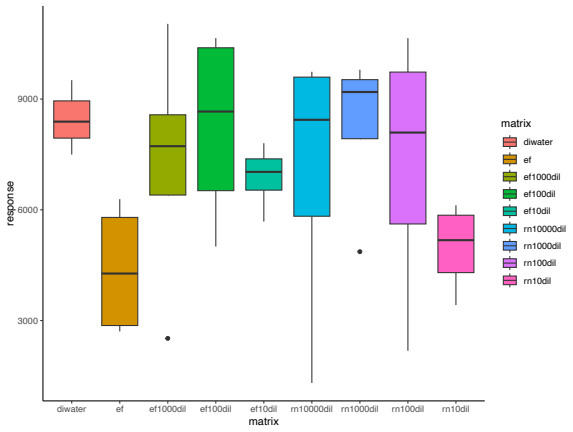

Figure 7.46 Phosmet response at 20 ppb in a pure water matrix vs effluents and rinsates.

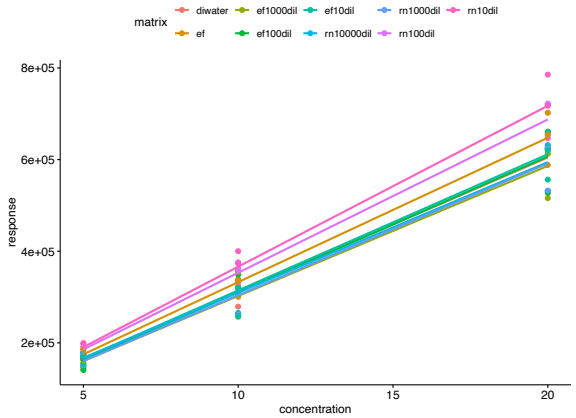

Figure 7.49 Azoxystrobin response across concentration in a pure water matrix vs effluents and rinsates.

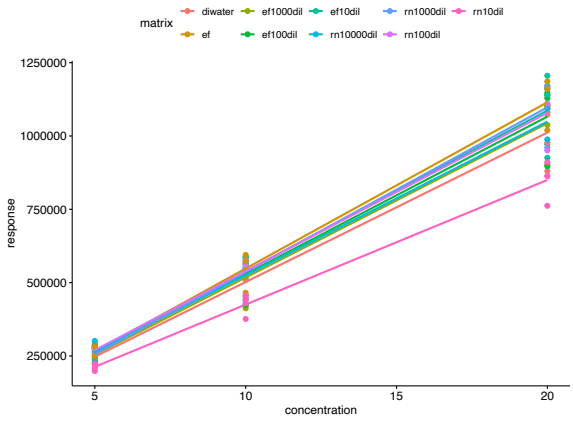

Figure 7.47 Tebuconazole response across concentration in a pure water matrix vs effluents and rinsates.

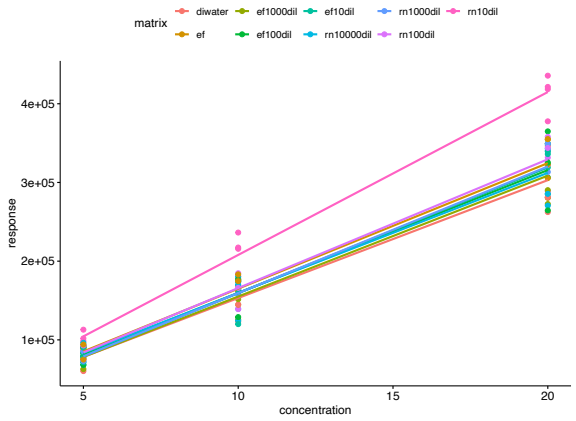

Figure 7.50 Fluopyram response across concentration in a pure water matrix vs effluents and rinsates.

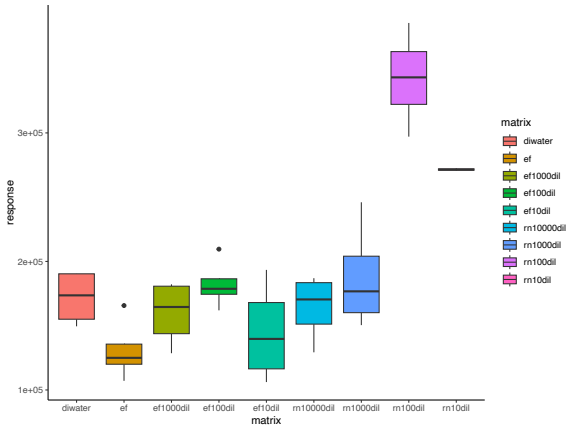

Figure 7.48 Spinetoram J response at 20 ppb in a pure water matrix vs effluents and rinsates.

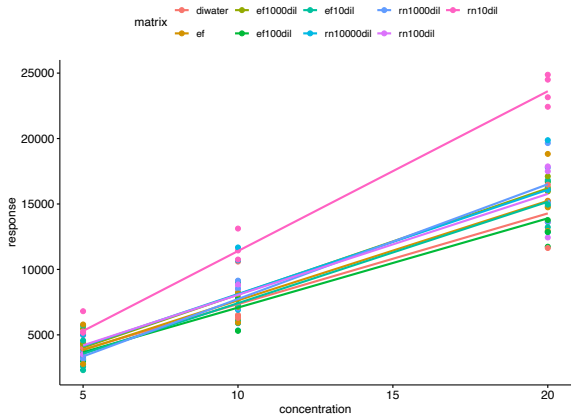

Figure 7.51 Boscalid response across concentration in a pure water matrix vs effluents and rinsates.

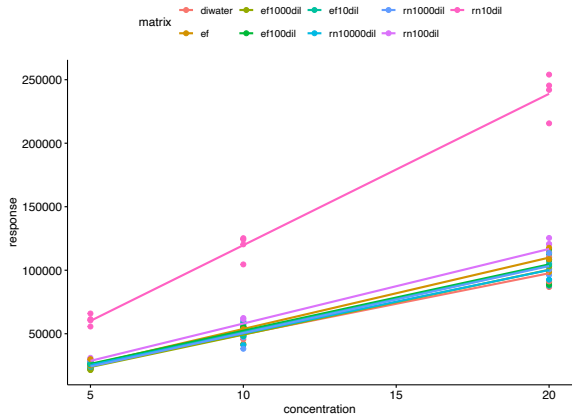

Figure 7.52 Metolachlor response across concentration in a pure water matrix vs effluents and rinsates.

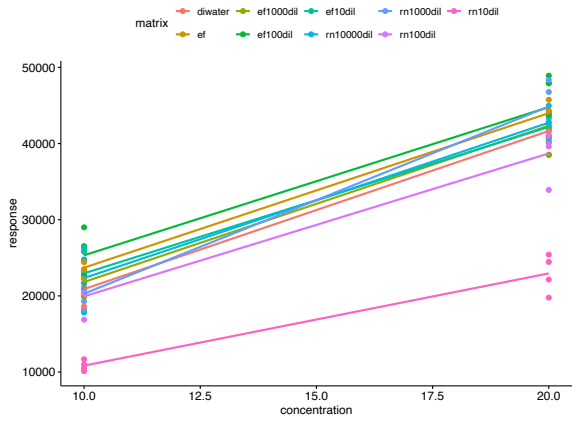

Figure 7.53 Malathion response across concentration in a pure water matrix vs effluents and rinsates.

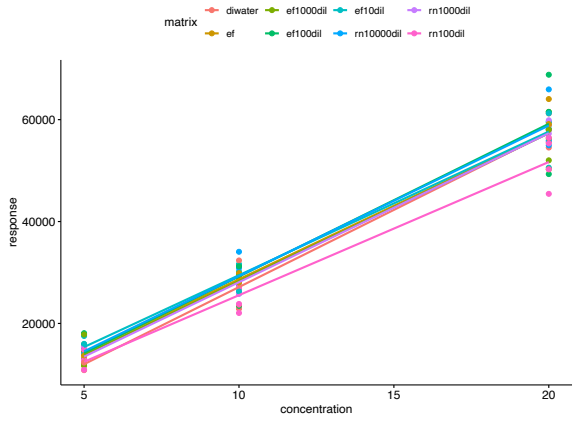

Figure 7.54 Fenoxycarb response across concentration in a pure water matrix vs effluents and rinsates.

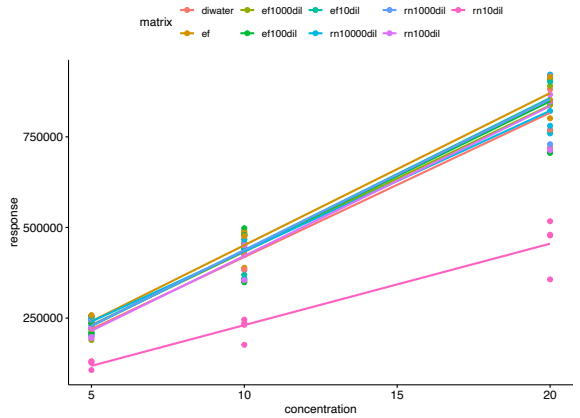

Figure 7.55 Tebufenozide response across concentration in a pure water matrix vs effluents and rinsates.

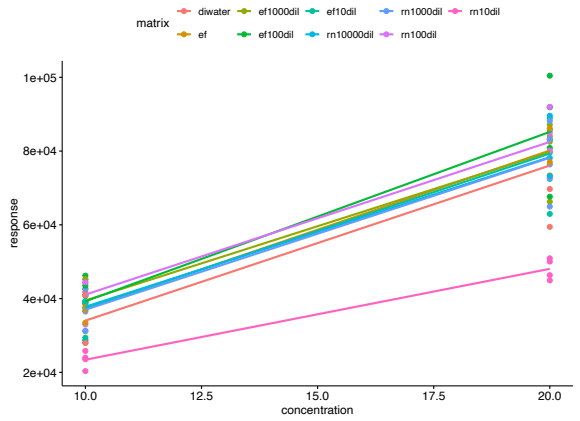

Figure 7.56 Fipronil response across concentration in a pure water matrix vs effluents and rinsates.

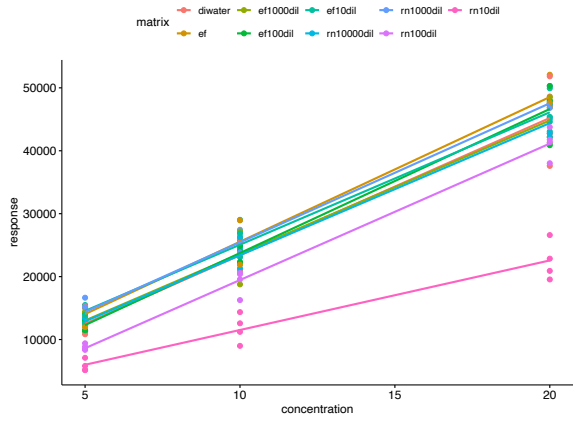

Figure 7.57 Tetrachlorvinphos response across concentration in a pure water matrix vs effluents and rinsates.

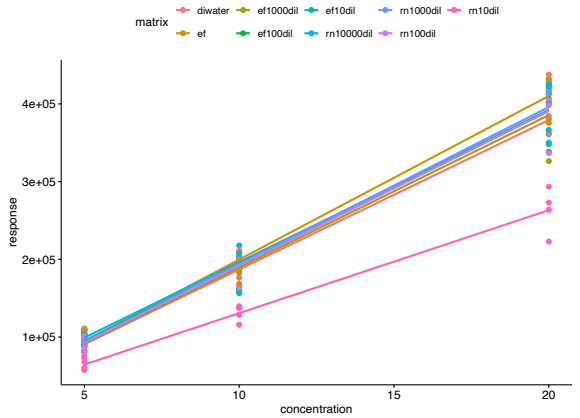

Figure 7.58 Propiconazole response across concentration in a pure water matrix vs effluents and rinsates.

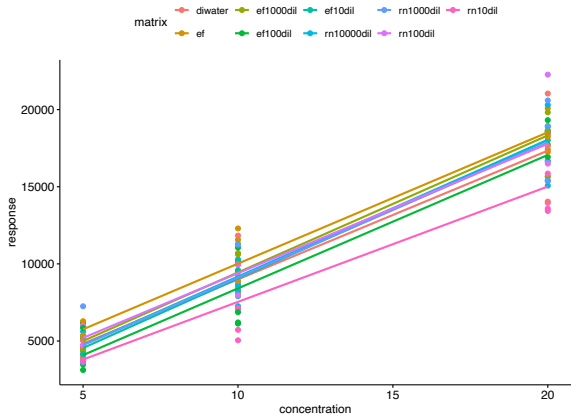

Figure 7.61 Kresoxim-Methyl response across concentration in a pure water matrix vs effluents and rinsates.

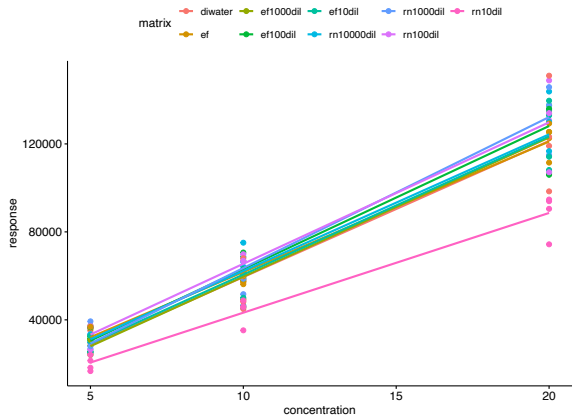

Figure 7.59 Imazamox response across concentration in a pure water matrix vs effluents and rinsates.

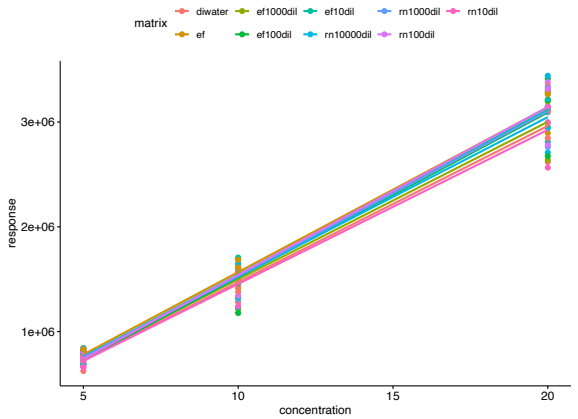

Figure 7.62 Diazinon response across concentration in a pure water matrix vs effluents and rinsates.

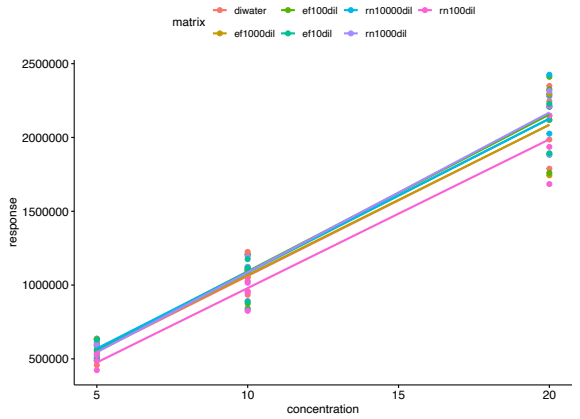

Figure 7.60 Buprofezin response across concentration in a pure water matrix vs effluents and rinsates.

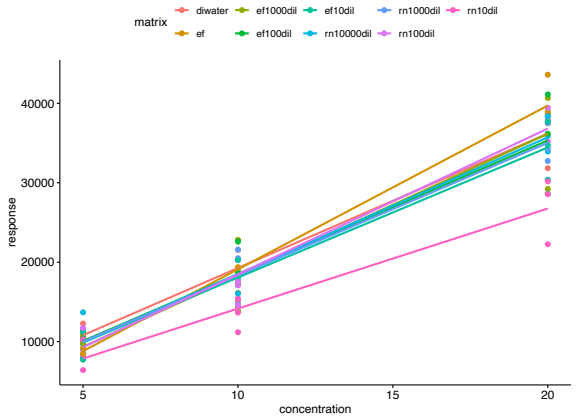

Figure 7.63 Benzodiflupyr response across concentration in a pure water matrix vs effluents and rinsates.

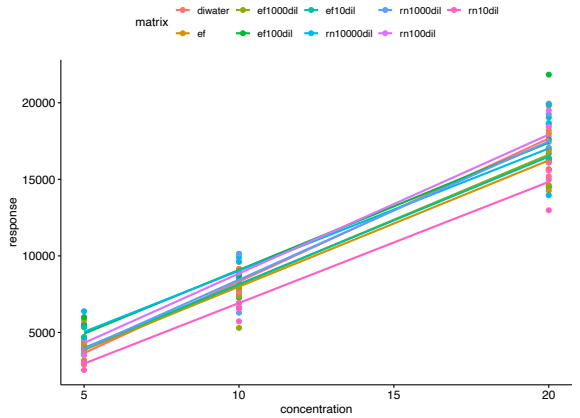

Figure 7.64 Prallethrin response across concentration in a pure water matrix vs effluents and rinsates.

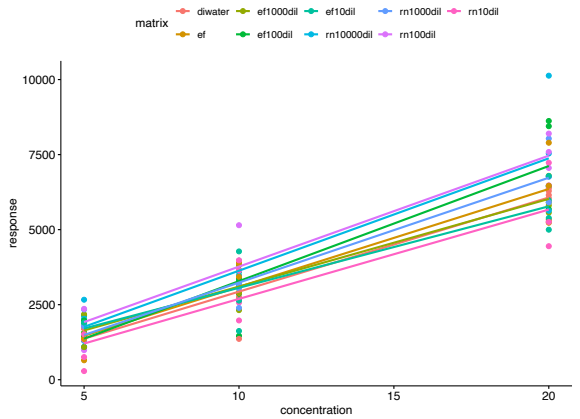

Figure 7.65 Pyrethrin II response across concentration in a pure water matrix vs effluents and rinsates.

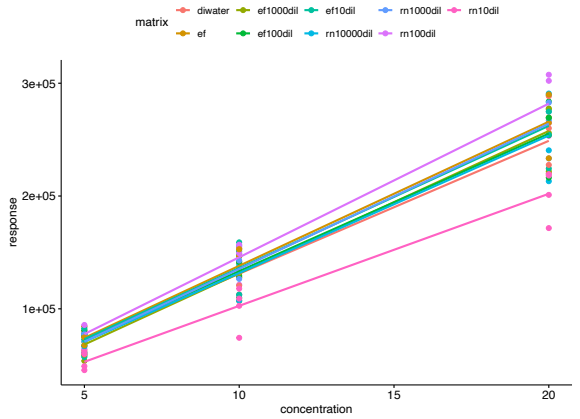

Figure 7.66 Pyraclostrobin response across concentration in a pure water matrix vs effluents and rinsates.

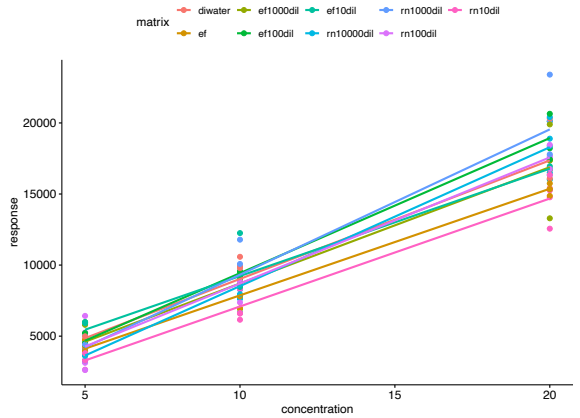

Figure 7.67 Clofentazine response across concentration in a pure water matrix vs effluents and rinsates.

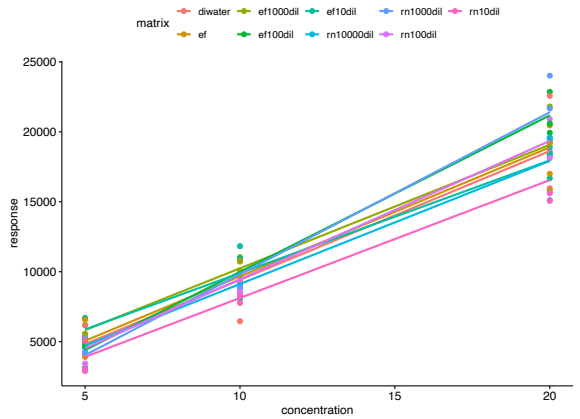

Figure 7.68 MGK 264 response across concentration in a pure water matrix vs effluents and rinsates.

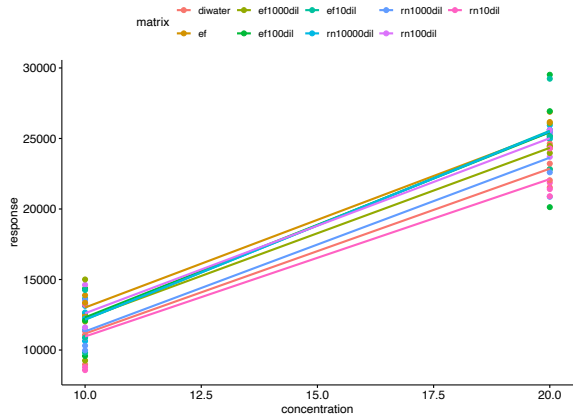

Figure 7.69 Coumaphos response across concentration in a pure water matrix vs effluents and rinsates.

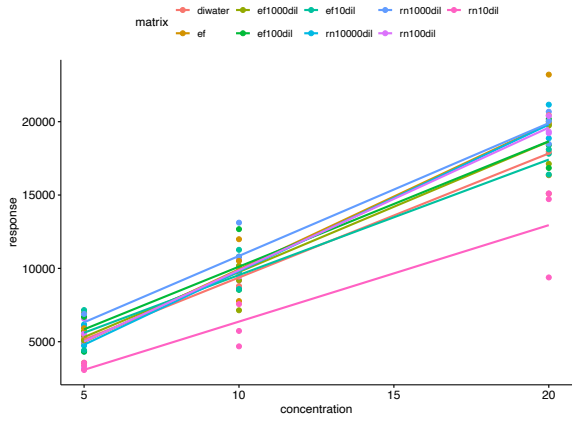

Figure 7.70 Teflubenzuron response across concentration in a pure water matrix vs effluents and rinsates.

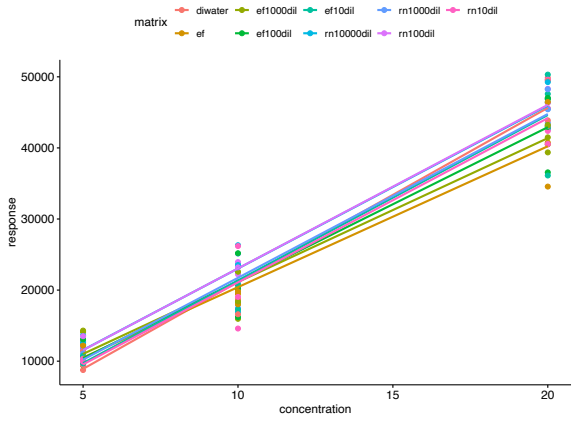

Figure 7.73 Allethrin response across concentration in a pure water matrix vs effluents and rinsates.

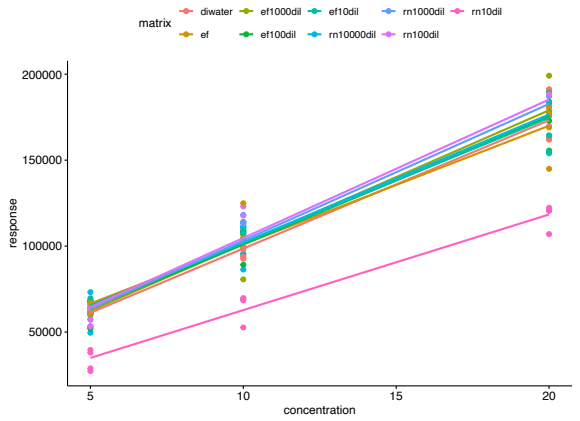

Figure 7.71 Trifloxystrobin response across concentration in a pure water matrix vs effluents and rinsates.

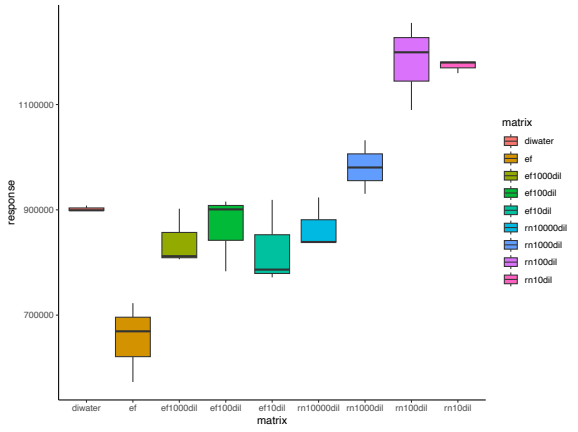

Figure 7.74 Fenpyroximate response at 20 ppb in a pure water matrix vs effluents and rinsates.

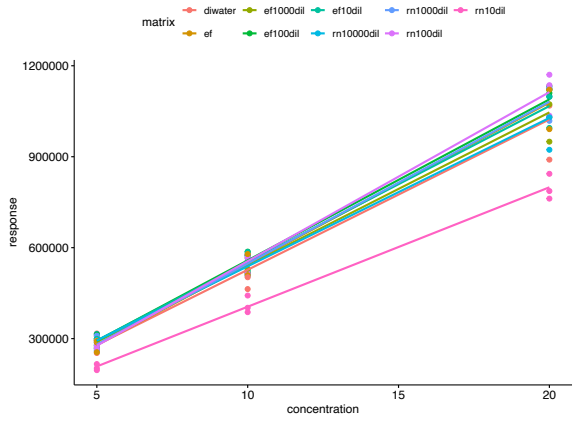

Figure 7.72 Piperonyl Butoxide response across concentration in a pure water matrix vs effluents and rinsates.

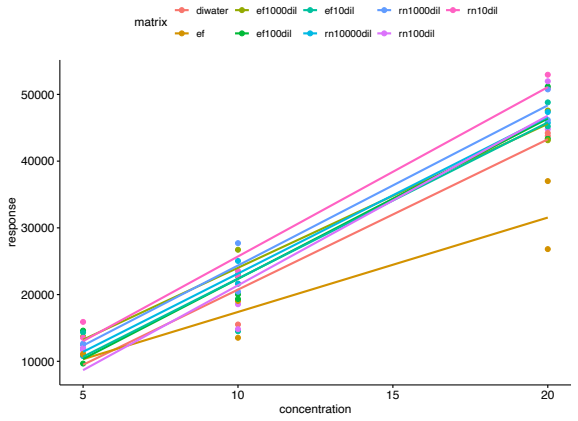

Figure 7.75 Tetramethrin response across concentration in a pure water matrix vs effluents and rinsates.

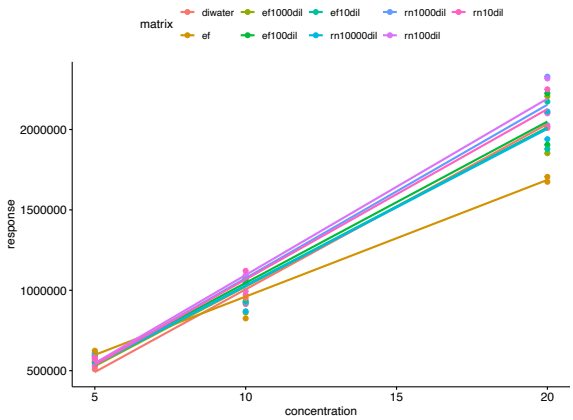

Figure 7.76 Etoxazole response across concentration in a pure water matrix vs effluents and rinsates.

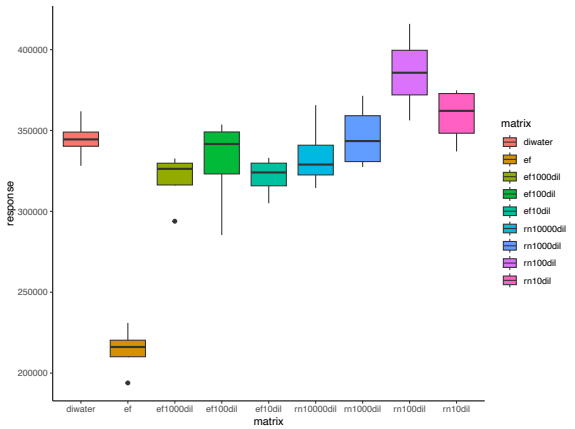

Figure 7.79 Spiromesifen response at 20 ppb in a pure water matrix vs effluents and rinsates.

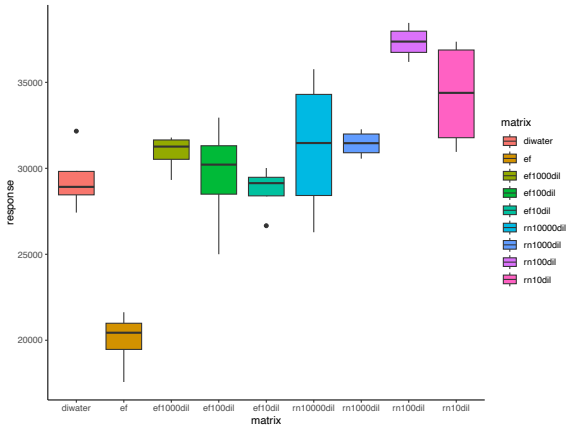

Figure 7.77 Pyrethrin I response at 20 ppb in a pure water matrix vs effluents and rinsates.

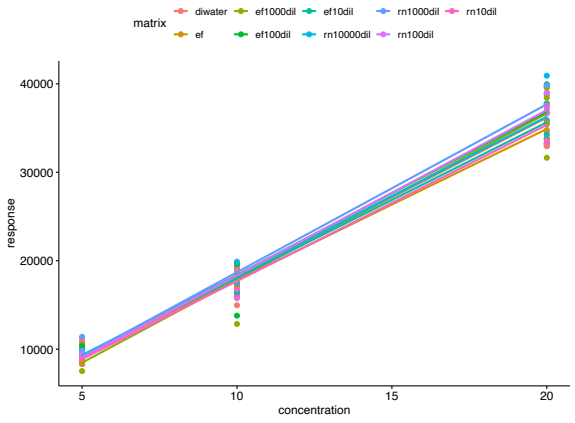

Figure 7.80 Hexythiazox response across concentration in a pure water matrix vs effluents and rinsates.

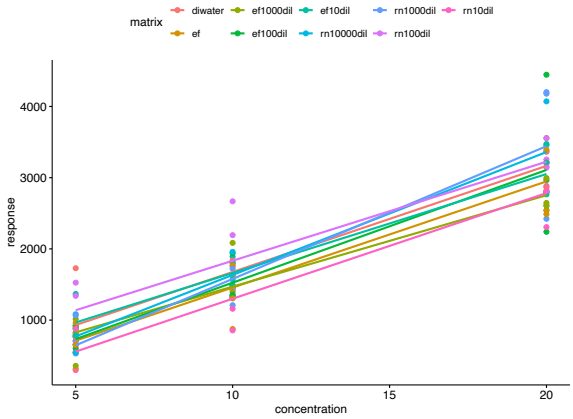

Figure 7.78 Chlorpyrifos response across concentration in a pure water matrix vs effluents and rinsates.

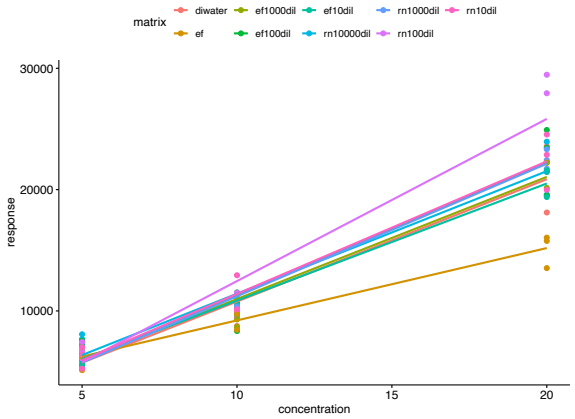

Figure 7.81 Spirodiclofen response across concentration in a pure water matrix vs effluents and rinsates.

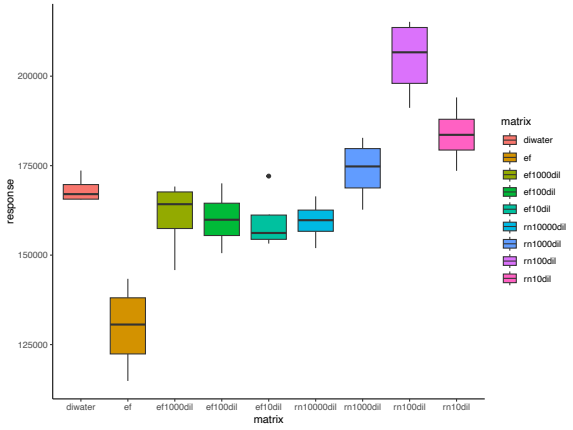

Figure 7.82 Pyridaben response at 20 ppb in a pure water matrix vs effluents and rinsates.

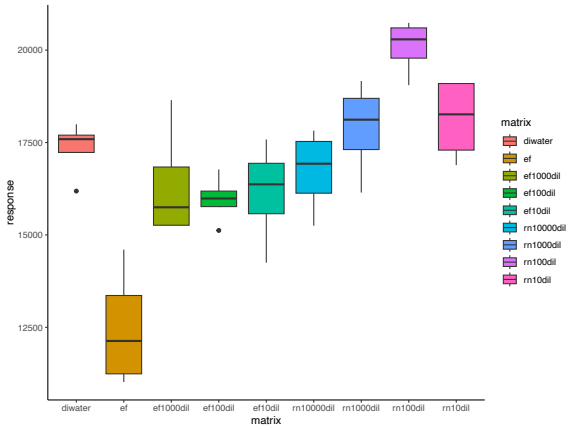

Figure 7.83 Resmethrin response at 20 ppb in a pure water matrix vs effluents and rinsates.

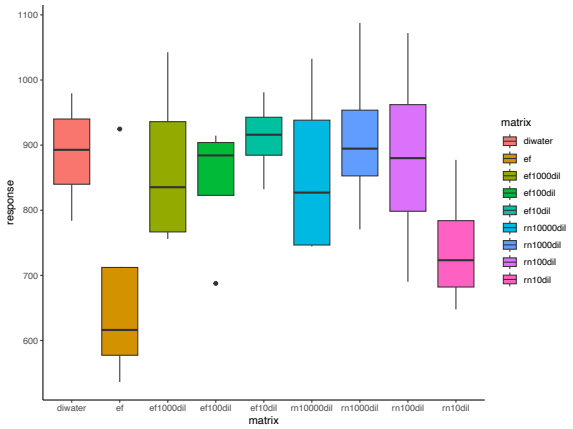

Figure 7.84 Permethrin response at 20 ppb in a pure water matrix vs effluents and rinsates.

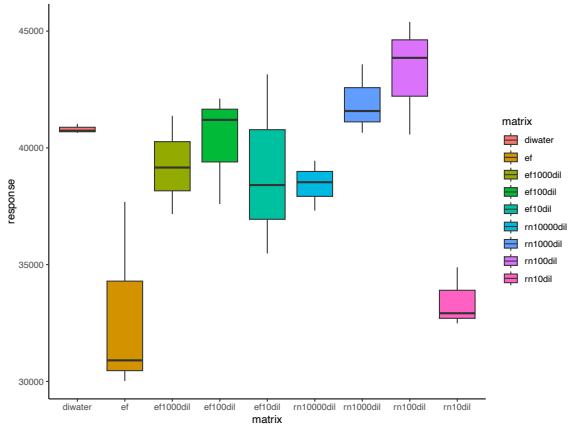

Figure 7.85 Etofenprox response at 20 ppb in a pure water matrix vs effluents and rinsates.

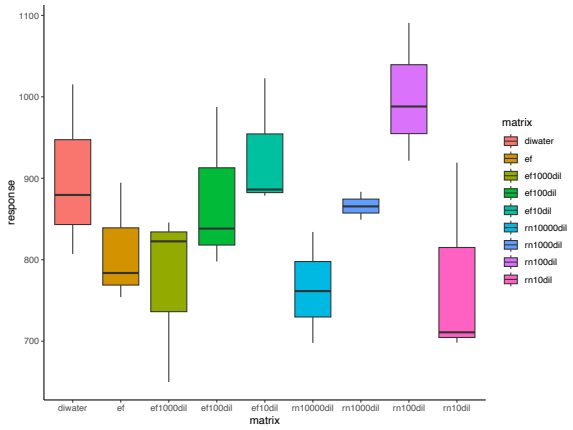

Figure 7.86 Bifenthrin response at 20 ppb in a pure water matrix vs effluents and rinsates.

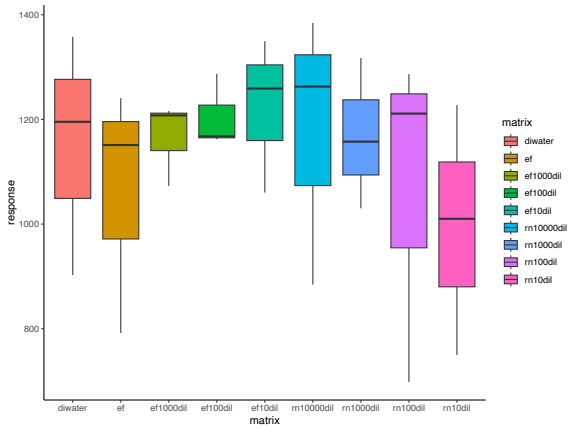

Figure 7.87 Acequinocyl response at 20 ppb in a pure water matrix vs effluents and rinsates.

8. APPENDIX II: CHAPTER THREE VALIDATION OF QUECHERS EXTRACTION

8.1 Chapter 3 QuEChERS Method Limits of Detection/Quantification, Accuracy, Precision, and Matrix Effect Validation for Biobeds

Non-extractable pesticides: Acequinocyl, Bifenthrin, Etofenprox, Permethrin, Resmethrin, Fenpyroximate, Piperonyl Butoxide, Trifloxystrobin, Fludioxinil, Cyantraniliprole, Fensulfothion, Pirimicarb, Spiroxamine, Spinosyn A, Spinosyn D, and Clopyralid.

Table 8.1 Method detection and quantification limits (MLD/MLQ), intra- and interday precision, and accuracy for QuEChERS extraction method. **Bolded** values represent recoveries greater than 130%, *italicized* values represent recoveries below 70%, and – represent non-extractable pesticides with the method.

Pesticides	QuEChERS				
	MLD/MLQ	Precision (Intra, Inter)		Accuracy	
		100 ppb	1,000 ppb	100 ppb	1,000ppb
	ng/g	% CV	% CV	% Rec	% Rec
Acephate	1.5 / 5.1	2.8 / 3	1.8 / 5.9	82	86
Oxamyl	1.1 / 3.6	5.7 / 6.9	8.7 / 8.9	110	87
Clopyralid	-	-	-	-	-
Dinotefuran	1.6 / 5.3	8.2 / 6.4	6.6 / 5	84	93
Methomyl	-	-	-	-	-
Thiamethoxam	3.1 / 10	3.8 / 7.6	4.4 / 7.9	96	110
Flonicamid	0.49 / 1.6	6.4 / 4	6.2 / 5.2	93	120
Pirimicarb	-	-	-	-	-
Clothianidin	1.1 / 3.6	6.3 / 5.8	5.8 / 6.9	86	96
Dimethoate	0.65 / 2.2	5 / 5.2	5.6 / 7.4	91	100
Imidacloprid	3.1 / 10	8.6 / 8.1	8.7 / 9.3	83	94
Mevinphos	0.74 / 2.5	5.1 / 6.9	5.1 / 8.3	88	100
Acetamiprid	0.48 / 1.6	5.3 / 4.2	5.6 / 5.1	98	110
Imazethapyr	1.1 / 3.7	15 / 13	14 / 13	100	130
Aldicarb	1.1 / 3.8	5.7 / 4.4	6 / 6.5	84	88
Thiacloprid	0.76 / 2.5	6.9 / 4.5	5.6 / 7.2	89	97
Dicamba	2.2 / 7.2	11 / 13	12 / 14	95	120
Propxur	1.3 / 4.3	3 / 5.1	2.7 / 4.4	98	120
Bentazon	1.4 / 4.7	4.7 / 5	4.4 / 7.8	100	120
Imazalil	0.66 / 2.2	3.1 / 2.5	2.7 / 3.8	85	100

Thiophanate-Methyl	1.5 / 4.9	*13 / 26*	*13 / 23*	84	*68*
Imazamox	2.5 / 8.3	7.8 / 5.4	7.2 / 7.3	98	110
Carbofuran	0.78 / 2.6	3.3 / 2.8	3.1 / 6.9	95	110
Atrazine	1.3 / 4.3	5.0 / 4.3	4.6 / 7.3	99	120
Carbaryl	0.88 / 2.9	7.7 / 4.6	10 / 4.6	83	110
2,4-D	2.0 / 6.5	15 / 15	16 / 9.2	120	140
Dodemorph	0.49 / 1.6	2.8 / 4.0	3.0 / 7.2	75	90
Fensulfothion	-	-	-	-	-
Cyantraniliprole	-	-	-	-	-
Metalaxyl	0.77 / 2.6	8.1 / 2.8	8 / 5.8	93	110
Spiroxamine	-	-	-	-	-
Paclubutrazol	0.37 / 1.2	5.2 / 4.0	5.7 / 5.1	82	110
Chlorantraniliprole	3.1 / 10	12 / 15	12 / 16	84	120
Fludioxinil	-	-	-	-	-
Cyprodinil	0.59 / 2.0	5.8 / 3.0	5.3 / 6.4	82	97
Spinosyn A	-	-	-	-	-
Spirotetramat	1.5 / 4.9	11 / 5.6	9.6 / 5.6	100	110
Dimetamorph I	1.2 / 4.0	6.6 / 2.2	6.6 / 7.9	85	110
Dimetamorph II	2.0 / 6.7	8.8 / 5.9	9.4 / 5.0	92	130
Fenhexamid	4.3 / 14	10 / 12	10 / 13	110	130
Ethoprophos	0.96 / 3.2	4.8 / 5.7	3.8 / 6.5	89	120
Myclobutanil	0.79 / 2.6	4.1 / 5.1	4.3 / 5.2	89	110
Spinosyn D	-	-	-	-	-
Phosmet	-	-	-	-	-
Azoxystrobin	1.1 / 3.8	3.4 / 5.4	3.6 / 6.5	130	**140**
Fluopyram	1.9 / 6.5	5.7 / 7.8	4.8 / 7.9	93	120
Metolachlor	1.2 / 4.1	7.6 / 5.8	7.7 / 8.3	110	130
Spinetoram J	1.3 / 4.5	5.4 / 6.1	5.1 / 6.2	93	120
Boscalid	8.6 / 29	9 / 12	8.9 / 14	120	110
Tebuconazole	1.7 / 5.6	7.8 / 3.9	7.7 / 4.9	100	110
Malathion	2.2 / 7.4	13 / 13	13 / 14	73	100
Fenoxycarb	2.5 / 8.5	1.3 / 9.8	3.9 / 12	94	130
Tebufenozide	1.1 / 3.7	6.4 / 4.7	5.9 / 6.3	94	120
Fipronil	2.0 / 6.7	7.6 / 7.4	7.3 / 7	96	130
Propiconazole	2.6 / 8.6	8.2 / 5.9	7.1 / 5.0	100	110
Tetrachlorvinphos	2.2 / 7.4	9.4 / 13	9.8 / 12	82	110
Benzovindiflupyr	1.3 / 4.5	9.5 / 5.0	9.1 / 9.0	86	130

Kresoxim-Methyl	2.8 / 9.3	6.8 / 15	8.5 / 6.1	77	120
Diazinon	0.75 / 2.5	5.1 / 3.4	5.9 / 7.1	92	110
Buprofenzin	0.89 / 3.0	2.6 / 3.6	2.6 / 4.9	90	110
Teflubenzuron	6.9 / 23	13 / 4.4	13 / 13	130	130
Pyrethin II	7.4 / 25	*23 / 12*	*21 / 16*	130	130
Pyraclostrobin	1.6 / 5.3	10 / 8.4	7.7 / 3.8	130	130
MGK-264	2.9 / 9.6	15 / 10	16 / 11	130	130
Piperonyl Butoxide	-	-	-	-	-
Clofentazine	1.5 / 5	14 / 9.4	12 / 9.8	130	130
Allethrin	1.7 / 5.7	9.7 / 14	7.5 / 12	130	130
Prallethrin	4.1 / 14	20 / 17	20 / 17	83	89
Trifloxystrobin	-	-	-	-	-
Tetramethrin	1.3 / 4.3	8.5 / 8.5	5.9 / 10	130	130
Etoxazole	0.66 / 2.2	5.1 / 4.3	5.7 / 7.7	130	130
Pyrethrin I	1.5 / 5.1	12 / 12	12 / 11	130	130
Chlorpyrifos	4.8 / 16	*21 / 17*	*24 / 19*	130	130
Hexythiazox	1.7 / 5.8	8.6 / 6.2	8.9 / 6	130	130
Spriomesifen	1.1 / 3.8	6.6 / 5.5	6.5 / 9.8	130	130
Spriodiclofen	1.5 / 5.2	11 / 5.1	9.5 / 6.1	130	130
Pyridaben	0.88 / 2.9	6.3 / 4.7	7.1 / 3.4	130	130
Resmethrin	-	-	-	-	-
Coumaphos	4.4 / 15	7.1 / 11	5.4 / 9.4	130	130
Permethrin [M+NH4]	-	-	-	-	-
Etofenprox	-	-	-	-	-
Bifenthrin	-	-	-	-	-
Acequinocyl	-	-	-	-	-
Fenpyroximate	-	-	-	-	-

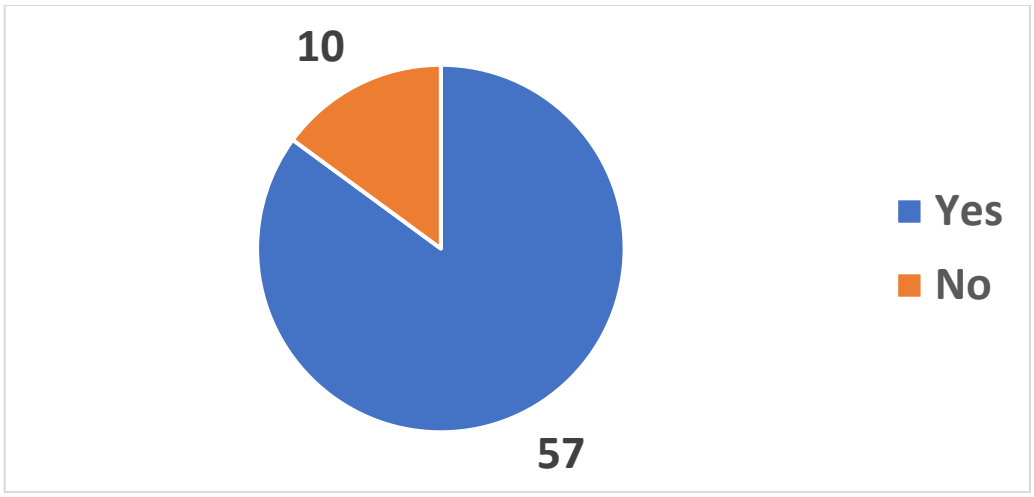

Figure 8.1 ANOVA's conducted that were found to have a significant matrix effect vs. no effect.

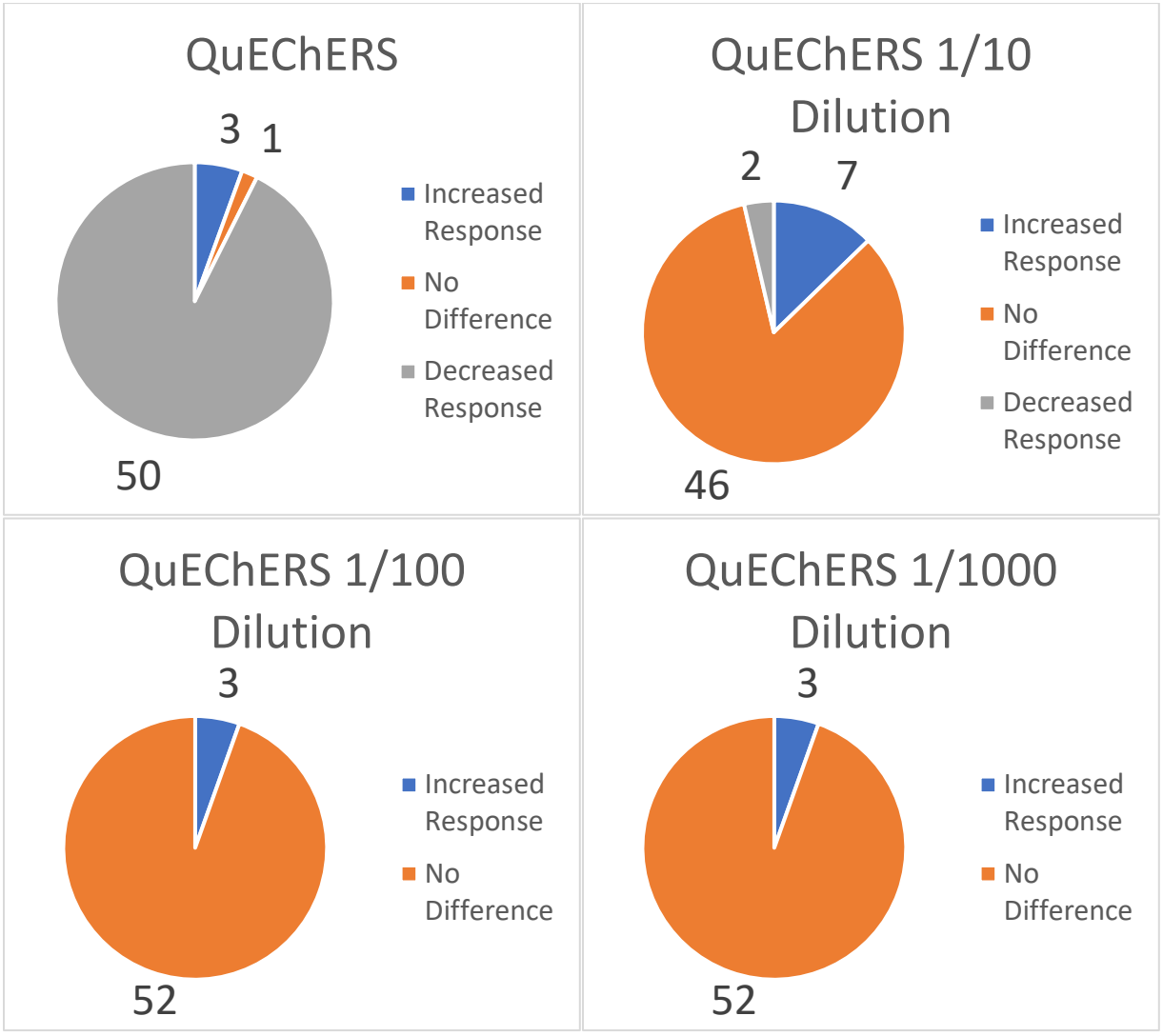

Figure 8.2 Summary of molecule responses from matrix effect found to be significant in an ANOVA and analyzed through Dunnett's test (control vs. matrices) for QuEChERS.

Table 8.2 Table of ANOVA "Matrix" significance as well as the *p-values* (*P*) and responses (R) from Dunnett's Post Hoc Test for QuEChERS. + = increased molecule response, - = decreased molecule response, and 0 = molecule response did not change. Green highlights mean that the matrices had to be separated to meet ANOVA assumptions; blue highlights represent a significant matrix effect *but* no significant differences found in Dunnett's test.

QuEChERS Matrix vs Control Solutions	ANOVA "Matrix" Significance	Undiluted		1/10 Dilution		1/100 Dilution		1/1,000 Dilution	
		P	R	*P*	R	*P*	R	*P*	R
Acephate	**<0.001**	*0.0001*	-	0.9311	0	*0.0455*	-	0.9897	0
Dinotefuran	**<0.001**	*0.0042*	-	0.2913	0	0.7593	0	0.3784	0
Oxamyl	**<0.001**	**<0.0001**	+	**0.0013**	+	0.6359	0	0.4973	0
Thiamethoxam	**<0.001**	*<0.0001*	-	0.9857	0	0.7147	0	0.7837	0
Flonicamid	**<0.001**	*<0.0001*	-	0.9814	0	0.9631	0	0.2807	0
Clothianidin	**<0.001**	*<0.0001*	-	0.9152	0	0.5194	0	0.5956	0
Dimethoate	**<0.01**	*0.0012*	-	0.9072	0	0.6346	0	0.9046	0
Mevinphos	>0.05	NA	NA	NA	NA	NA	NA	NA	NA
Imidacloprid	**<0.001**	*0.0003*	-	0.6319	0	0.6776	0	0.9686	0
Acetamiprid	**<0.001**	*0.0007*	-	0.2475	0	0.9979	0	0.3684	0
Imazethapyr	**<0.001**	**<0.0001**	+	**<0.0001**	+	0.1919	0	0.9287	0
Aldicarb	>0.05	NA	NA	NA	NA	NA	NA	NA	NA
Thiacloprid	**<0.001**	*0.0001*	-	0.7907	0	0.6407	0	0.9991	0
Dicamba	>0.05	NA	NA	NA	NA	NA	NA	NA	NA
Propoxur	**<0.001**	*<0.0001*	-	0.9893	0	0.6807	0	0.9841	0
Imazalil	**<0.001**	*<0.0001*	-	0.9841	0	0.6807	0	0.9841	0
Thiophanate-Methyl	**<0.001**	**<0.0001**	+	**<0.0001**	+	**<0.0001**	+	**<0.0001**	+
Carbofuran	>0.05	NA	NA	NA	NA	NA	NA	NA	NA
Bentazon	**<0.001**	*<0.0001*	-	0.174	0	0.7404	0	0.9566	0
Atrazine	**<0.001**	*0.0002*	-	0.1813	0	0.9793	0	0.9	0
Carbaryl	>0.05	NA	NA	NA	NA	NA	NA	NA	NA
Metalaxyl	>0.05	NA	NA	NA	NA	NA	NA	NA	NA
Dodemorph	**<0.001**	<0.0001	-	0.9412	0	0.9903	0	0.8788	0

2,4-D	**<0.05**	0.1081	0	0.9833	0	0.0515	0	0.9314	0
Spiroxamine	**<0.001**	<0.0001	-	0.4626	0	0.861	0	0.254	0
Cyprodinil	**<0.001**	<0.0001	-	0.4763	0	0.8393	0	0.9896	0
Paclobutrazol	**<0.001**	<0.0001	-	0.9994	0	0.9994	0	0.5408	0
Chlorantraniliprole	**<0.001**	<0.0001	-	0.6237	0	1	0	0.9824	0
Dimetamorph II	**<0.001**	<0.0001	-	0.9653	0	0.8573	0	0.9512	0
Spirotetramat	>0.05	NA	NA	NA	NA	NA	NA	NA	NA
Dimetamorph I	**<0.001**	<0.0001	-	0.0616	0	0.9232	0	0.9919	0
Fenhexamid	**<0.01**	0.0117	-	0.9966	0	0.9885	0	0.9931	0
Ethoprophos	>0.05	NA	NA	NA	NA	NA	NA	NA	NA
Myclobutanil	**<0.001**	<0.0001	-	0.5308	0	0.7066	0	0.8965	0
Tebuconazole	**<0.001**	<0.0001	-	0.6878	0	0.732	0	0.4637	0
Spinetoram J	**<0.001**	<0.0001	-	0.2715	0	0.9292	0	0.7527	0
Azoxystrobin	**<0.001**	<0.0001	-	<0.0001	+	0.9232	0	0.8721	0
Fluopyram	**<0.001**	<0.0001	-	0.9423	0	0.9981	0	0.9355	0
Boscalid	>0.05	NA	NA	NA	NA	NA	NA	NA	NA
Metolachlor	**<0.001**	<0.0001	-	0.934	0	0.4671	0	0.7412	0
Malathion	**<0.001**	<0.0001	-	0.9334	0	0.3072	0	0.9327	0
Fenoxycarb	**<0.001**	<0.0001	-	0.3244	0	0.9228	0	0.376	0
Tebufenozide	**<0.001 (undiluted only)**	<0.0001	-	NA	NA	NA	NA	NA	NA
	>0.05	NA	NA	NA	NA	NA	NA	NA	NA
Fipronil	**<0.001**	<0.0001	-	0.0299	+	0.6183	0	0.9253	0
Tetrachlorvinphos	**<0.001**	<0.0001	-	1	0	0.0361	+	0.7332	0
Propiconazole	**<0.001**	<0.0001	-	0.7342	0	0.6	0	0.7342	0
Imazamox	**<0.01**	0.0019	-	0.6748	0	0.1343	0	0.9118	0
Buprofezin	**<0.001**	<0.0001	-	0.6117	0	0.8586	0	0.9477	0
Kresoxim Methyl	**<0.001**	0.0002	-	0.3797	0	0.3633	0	0.9997	0
Diazinon	**<0.001**	<0.0001	-	0.9138	0	0.9756	0	0.4805	0
Benzovindiflupyr	**<0.001**	<0.0001	-	0.9242	0	0.3773	0	0.9997	0

Prallethrin	**<0.05**	0.0194	-	0.9528	0	0.9443	0	0.9966	0
Pyrethrin II	**<0.001**	0.0228	-	0.0629	0	0.357	0	0.0155	+
Pyraclostrobin	**<0.001**	0.0228	-	0.0001	+	0.0212	+	0.044	+
Clofentazine	**<0.05**	0.0222	-	0.9251	0	0.9464	0	0.9879	0
MGK 264	**<0.001**	<0.0001	-	0.9876	0	0.7752	0	0.9817	0
Coumaphos	**<0.001**	<0.0001	-	0.9974	0	0.7432	0	0.9974	0
Allethrin	**<0.001**	<0.0001	-	0.8483	0	0.9889	0	0.9998	0
Tetramethrin	**<0.001**	<0.0001	-	0.2792	0	0.7925	0	0.8653	0
Etoxazole	**<0.001**	<0.0001	-	0.9974	0	0.9968	0	0.9429	0
Pyrethrin I	**<0.001**	<0.0001	-	0.4039	0	0.2665	0	0.328	0
Chlorpyrifos	**<0.001**	<0.0001	-	0.1442	0	0.8378	0	0.8661	0
Spiromesifen	**<0.001**	NA	NA	<0.0001	-	0.9793	0	0.913	0
Hexythiazox	**<0.001**	<0.0001	-	0.0254	-	0.546	0	0.31	0
Spirodiclofen	**<0.001**	<0.0001	-	0.0327	+	0.3119	0	0.9104	0
Pyridaben	**<0.001**	<0.0001	-	0.1059	0	0.8539	0	0.838	0

Table 8.3 Transformation method, Shapiro-Wilk'a Test for normality, and Bresuch-Pagan Test for homoscedascity, and addition vs. interaction model ANOVA on model residuals; notes for all compounds extractable with the QuEChERS extraction method. Blue highlights represents a need to separate matrices for analysis due to non-normality of residuals. *Italicized* values only had detects at 20 ppb, so were proceeded with an ANOVA model in Table 8.4. NA = Not Applicable.

Compound	Transformation	Normality	Homoscedascity	Slope Homogeneity	Notes
Acephate	Square Root	0.8035	0.1892	0.3961	
Oxamyl	Square Root	0.8146	0.436	0.1336	
Dinotefuran	Log10	0.2258	0.8797	0.2583	5 ppb removed (Heteroscedascity)
Thiamethoxam	Cube Root	0.5353	0.7626	0.103	
Flonicamid	Log10	0.9538	0.9394	0.2181	5 ppb removed (No Response)
Clothianidin	Square Root	0.8389	0.1186	0.1036	Block A Removed (Heteroscedascity)
Dimethoate	Square Root	0.8307	0.8614	0.9309	
Mevinphos	Cube Root	0.124	0.8293	0.7561	
Imidacloprid	Square Root	0.0967	0.7513	0.1388	
Acetamiprid	Square Root	0.5696	0.4076	0.8118	
Imazethapyr	Square Root	0.8413	0.1574	0.6478	
Aldicarb	Square Root	0.1178	0.3034	0.9508	Block A Removed (Heteroscedascity)
Thiacloprid	Square Root	0.1427	0.1415	0.8818	
Dicamba	Square Root	0.4419	0.4378	0.2623	
Propxur	Cube Root	0.106	0.7039	0.5332	

Imazalil	Square Root	0.2044	0.6672	0.6412	
Thiophanate-Methyl	Cube Root	0.9301	0.5828	0.5745	
Carbofuran	Square Root	0.6362	0.6615	0.0549	
Bentazon	Square Root	0.4548	0.0771	0.6565	
Atrazine	Square Root	0.9491	0.6268	0.7904	
Carbaryl	Square Root	0.8313	0.4264	0.3842	5 ppb removed (No Response)
Metalaxyl	Square Root	0.1918	0.7962	0.9318	
Dodemorph	Cube Root	0.088	0.09966	0.209	
2,4-D	Cube Root	0.544	0.8721	0.8796	
Spiroxamine	Square Root	0.7637	0.1931	0.1399	
Cyprodinil	Square Root	0.4991	0.4238	0.1306	
Paclobutrazol	Square Root	0.6748	0.4116	0.0562	
Chlorantraniliprole	Square Root	0.6627	0.6004	0.4697	Block D Removed (Heteroscedascity)
Dimetamorph II	Square Root	0.6223	0.9829	0.4681	
Spirotetramat	Square Root	0.9677	0.379	0.0719	Block C Removed (Heteroscedascity)
Dimetamorph I	Log10	0.6696	0.456	0.0978	
Fenhexamid	Log10	0.4005	0.2509	0.0665	
Ethoprophos	*Cube Root*	*NA*	*NA*	*NA*	*Required ANOVA*

Myclobutanil	Log10	0.2591	0.4149	0.5243	5 ppb removed (Heteroscedascity)
Tebuconazole	Square Root	0.7808	0.3187	0.0508	
Spinetoram J	Cube Root	0.2978	0.7521	0.2215	
Azoxystrobin	Square Root	0.5361	0.9088	0.2755	
Fluopyram	Cube Root	0.6451	0.3666	0.1175	
Boscalid	*Square Root*	*NA*	*NA*	*NA*	*Required ANOVA*
Metolachlor	Square Root	0.7882	0.9924	0.4938	
Malathion	Cube Root	0.3648	0.7531	0.1165	
Fenoxycarb	Log10	0.2857	0.3312	0.4706	5 ppb removed (No Response)
Tebufenozide	Cube Root	0.72	0.1922	0.5096	QuEChERS 0DIL vs DIWATER only
	Cube Root	0.6953	93,305	0.4833	Excluding QuEChERS 0DIL
Fipronil	Log10	0.4994	0.7805	0.1099	5 ppb removed (No Response)
Tetrachlorvinphos	Log10	0.9391	0.3406	0.5646	Block A, C Removed (Heteroscedascity)
Propiconazole	Square Root	0.5219	0.3831	0.1788	
Imazamox	Square Root	0.9011	0.5638	0.7944	
Buprofezin	Cube Root	0.3662	0.4192	0.2305	
Kresoxim-Methyl	Square Root	0.569	0.6259	0.1524	
Diazinon	Square Root	0.1659	0.5798	0.0609	

Benzodiflupyr	*Square Root*	*NA*	*NA*	*NA*	*Required ANOVA*
Prallethrin	Square Root	0.125	0.2703	0.4094	
Pyrethrin II	*Cube Root*	*NA*	*NA*	*NA*	*Required ANOVA*
Pyraclostrobin	Cube Root	0.4265	0.3693	0.6551	5 ppb removed (Non-Normal)
Clofentazine	*Square Root*	*NA*	*NA*	*NA*	*Required ANOVA*
MGK-264	Square Root	0.9765	0.1235	0.1696	
Coumaphos	Square Root	0.4763	0.4481	0.7157	
Teflubenzuron	Log10	0.3698	0.7673	0.4025	5 ppb removed (No Response)
Allethrin	Square Root	0.9581	0.2062	0.1701	
Tetramethrin	Square Root	0.5388	0.2767	0.144	
Etoxazole	Square Root	0.7812	0.5907	0.0683	Block C Removed (Heteroscedascity)
Pyrethrin I	Log10	0.6387	0.81	0.455	
Chlorpyrifos	*Square Root*	*NA*	*NA*	*NA*	*Required ANOVA*
Spiromesifen	Square Root	0.2869	0.8029	0.8528	QuEChERS 0DIL Removed (No Response)
Hexythiazox	*Square Root*	*NA*	*NA*	*NA*	*Required ANOVA*
Spirodiclofen	Square Root	0.6569	0.3921	0.4188	
Pyridaben	Log10	0.31	0.688	0.3595	

Table 8.4 Transformation method, Shapiro-Wilk Test for normality, and Bartlett's Test for homogeneity of variance for compounds extractable with the QuEChERS extraction method detected at 20 ppb only.

		Normality					
		Acetonitrile	QuEChERS Extract				
Compound	Transformation	Control	0 Dil	10 Dil	100 Dil	1,000 Dil	Homogeneity of Variance
Ethoprophos	Cube Root	0.4476	0.8209	0.5743	0.9153	0.7808	0.4933
Boscalid	Square Root	0.0606	0.0721	0.0586	0.089	0.058	0.9128
Benzodiflupyr	Square Root	0.6205	0.491	0.929	0.5708	0.1656	0.1873
Pyrethrin II	Cube Root	0.5978	0.5254	0.8756	0.0854	0.023	0.7629
Clofentazine	Square Root	0.3297	0.8217	0.3836	0.7642	0.8748	0.7196
Chlorpyrifos	Square Root	0.5767	0.174	0.2813	0.0798	0.3495	0.8338
Hexythiazox	Square Root	0.1642	0.6015	0.3106	0.1573	0.7923	0.4625

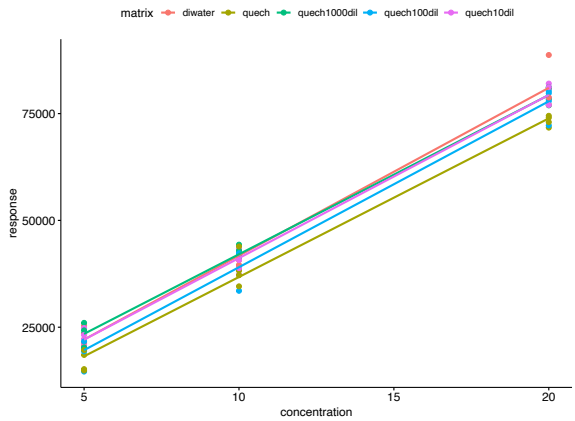

Figure 8.3 Acephate response across concentrations in a pure acetonitrile matrix vs QuEChERS extracts.

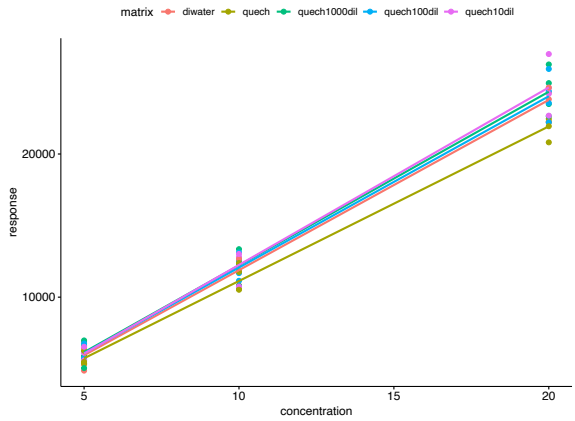

Figure 8.4 Dinotefuran r response across concentrations in a pure acetonitrile matrix vs QuEChERS extracts.

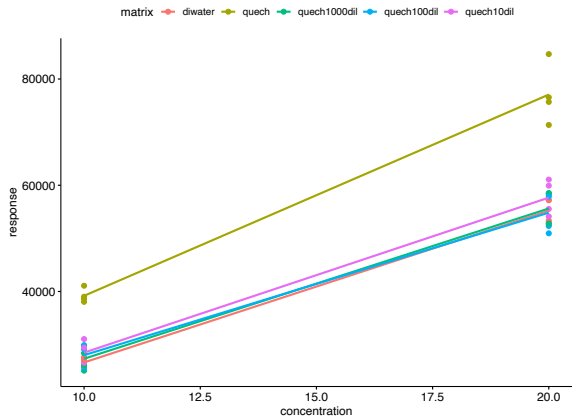

Figure 8.5 Oxamyl response across concentrations in a pure acetonitrile matrix vs QuEChERS extracts.

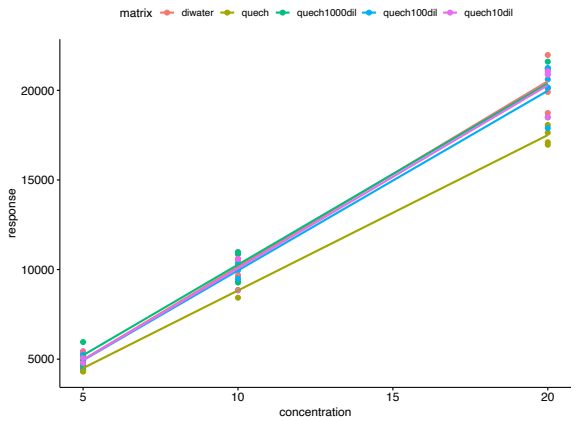

Figure 8.6 Thiamethoxam response across concentrations in a pure acetonitrile matrix vs QuEChERS extracts.

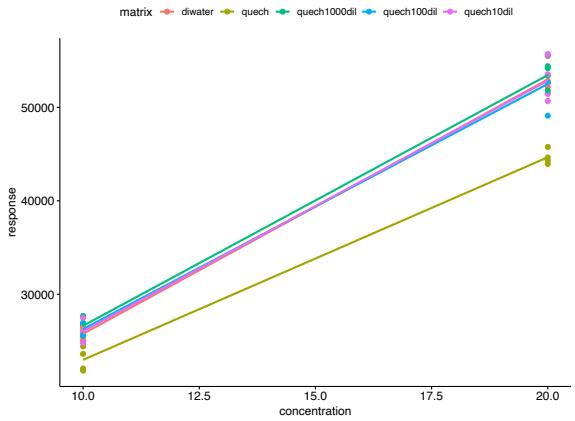

Figure 8.7 Flonicamid response across concentrations in a pure acetonitrile matrix vs QuEChERS extracts.

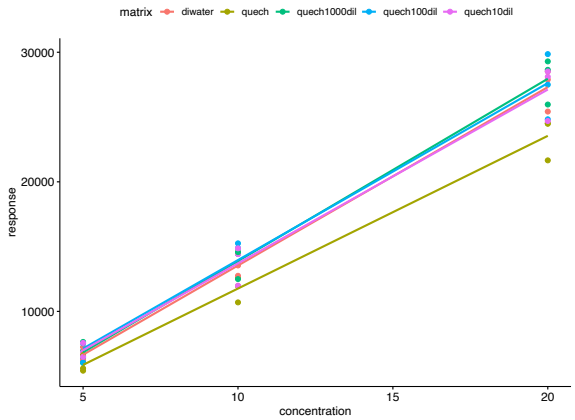

Figure 8.8 Clothianidin response across concentrations in a pure acetonitrile matrix vs QuEChERS extracts.

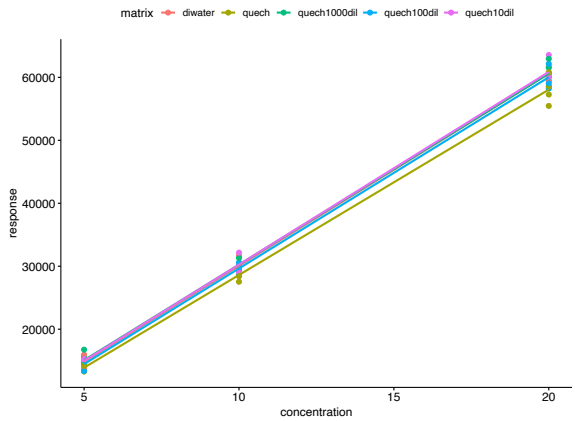

Figure 8.9 Dimethoate response across concentrations in a pure acetonitrile matrix vs QuEChERS extracts.

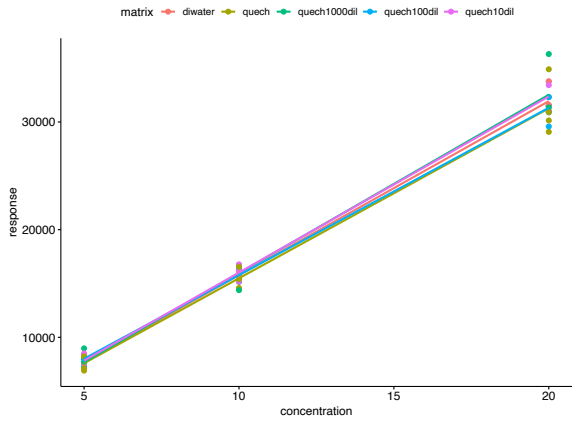

Figure 8.10 Mevinphos response across concentrations in a pure acetonitrile matrix vs QuEChERS extracts.

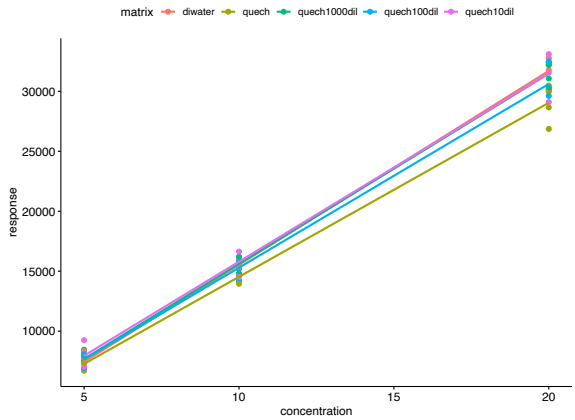

Figure 8.11 Imidacloprid response across concentrations in a pure acetonitrile matrix vs QuEChERS extracts.

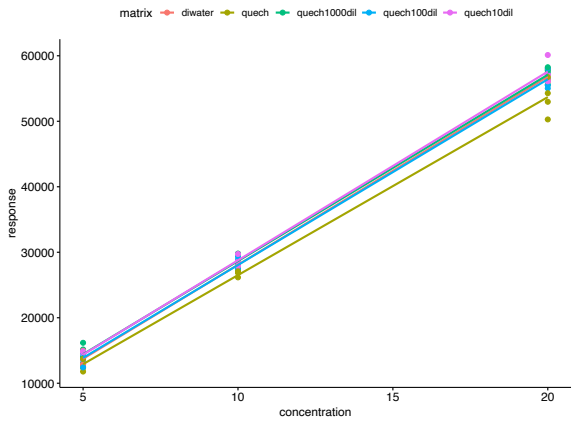

Figure 8.12 Acetamiprid response across concentrations in a pure acetonitrile matrix vs QuEChERS extracts.

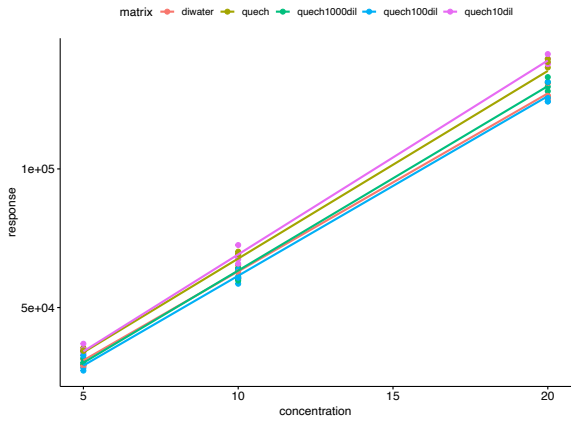

Figure 8.13 Imazethapyr response across concentrations in a pure acetonitrile matrix vs QuEChERS extracts.

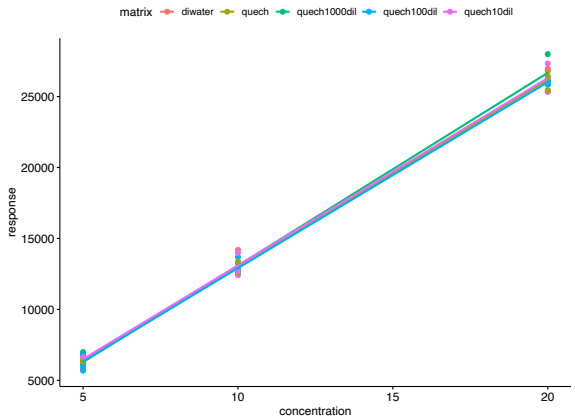

Figure 8.14 Aldicarb response across concentrations in a pure acetonitrile matrix vs QuEChERS extracts.

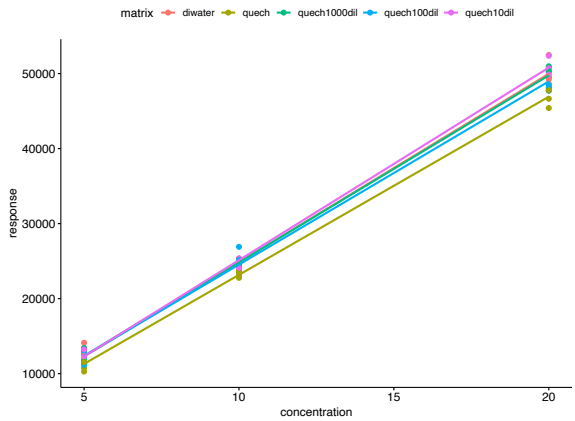

Figure 8.15 Thiacloprid response across concentrations in a pure acetonitrile matrix vs QuEChERS extracts.

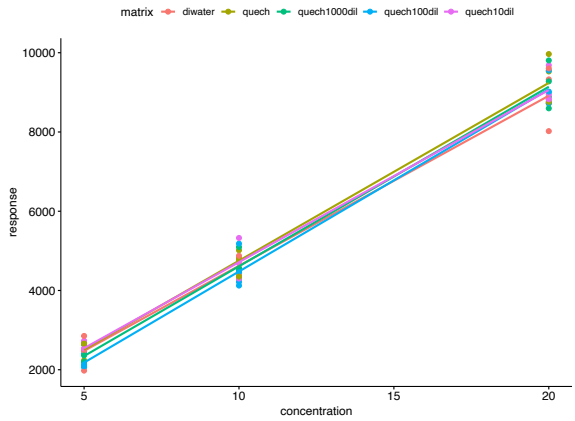

Figure 8.16 Dicamba response across concentrations in a pure acetonitrile matrix vs QuEChERS extracts.

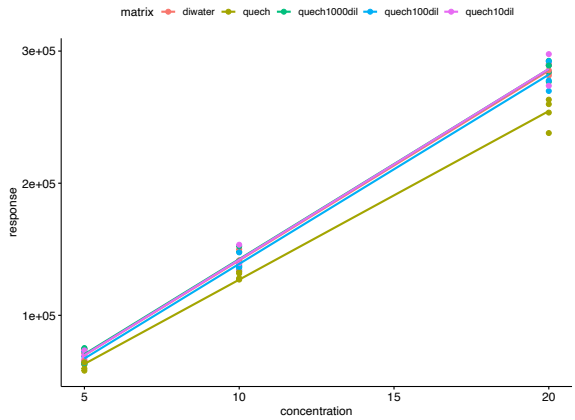

Figure 8.17 Propoxur response across concentrations in a pure acetonitrile matrix vs QuEChERS extracts.

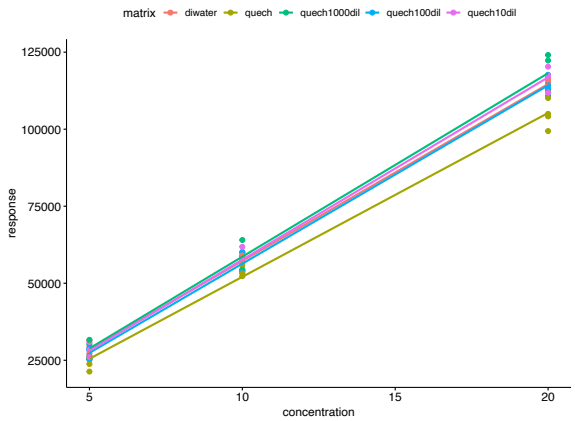

Figure 8.18 Imazalil response across concentrations in a pure acetonitrile matrix vs QuEChERS extracts.

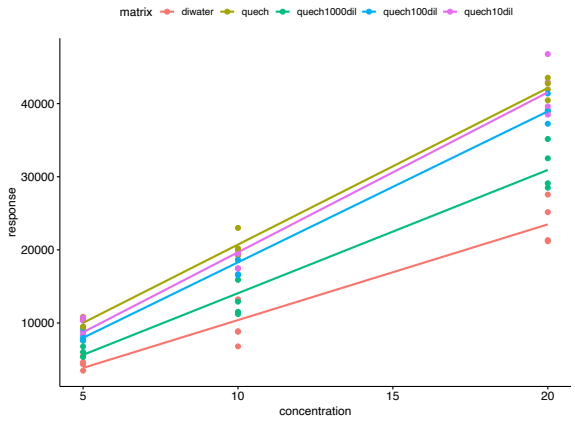

Figure 8.19 Thiophanate-Methyl response across concentrations in a pure acetonitrile matrix vs QuEChERS extracts.

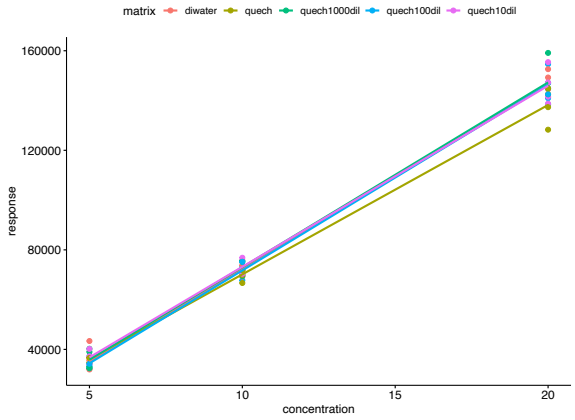

Figure 8.20 Carbofuran response across concentrations in a pure acetonitrile matrix vs QuEChERS extracts.

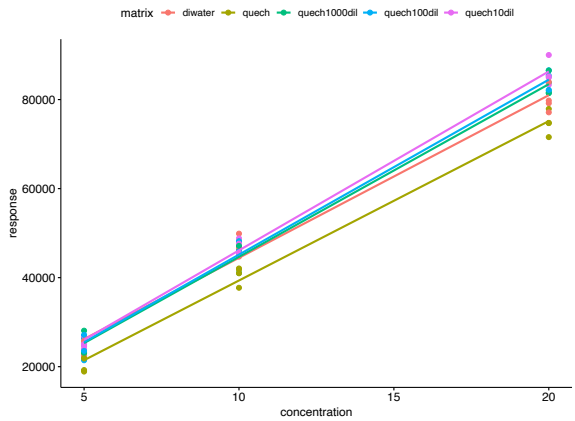

Figure 8.21 Bentazon response across concentrations in a pure acetonitrile matrix vs QuEChERS extracts.

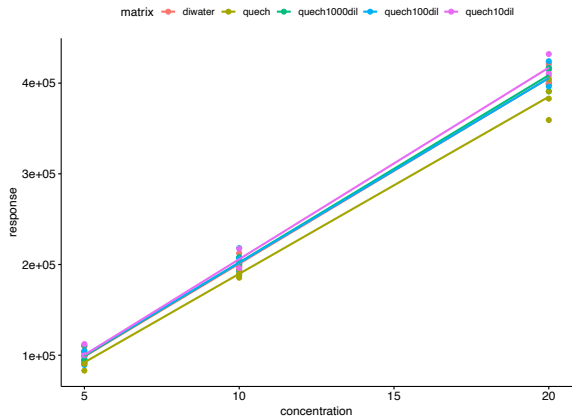

Figure 8.22 Atrazine response across concentrations in a pure acetonitrile matrix vs QuEChERS extracts.

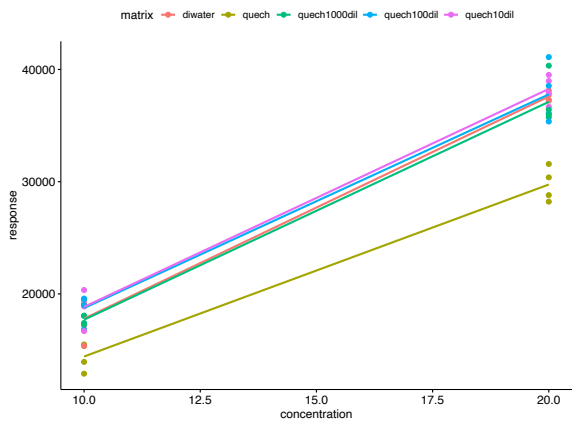

Figure 8.23 Carbaryl response across concentrations in a pure acetonitrile matrix vs QuEChERS extracts.

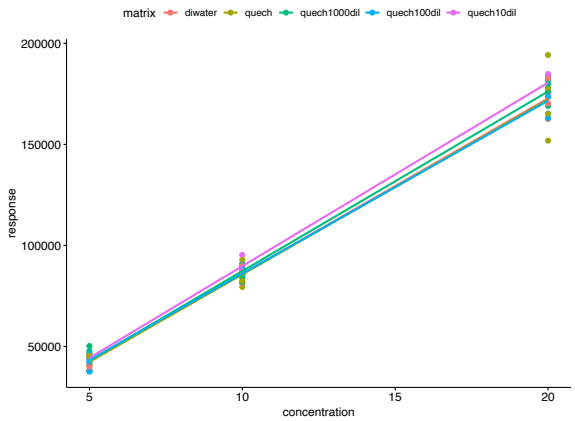

Figure 8.24 Metalaxyl response across concentrations in a pure acetonitrile matrix vs QuEChERS extracts.

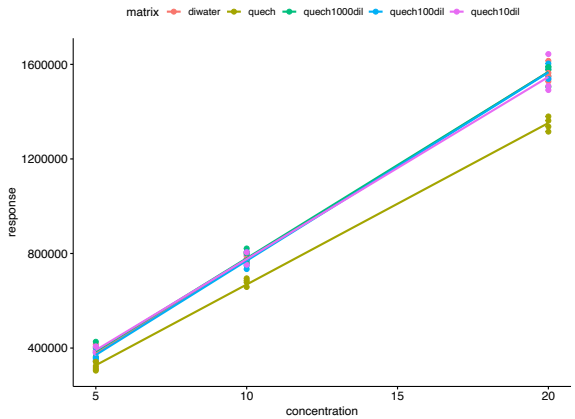

Figure 8.25 Dodemorph response across concentrations in a pure acetonitrile matrix vs QuEChERS extracts.

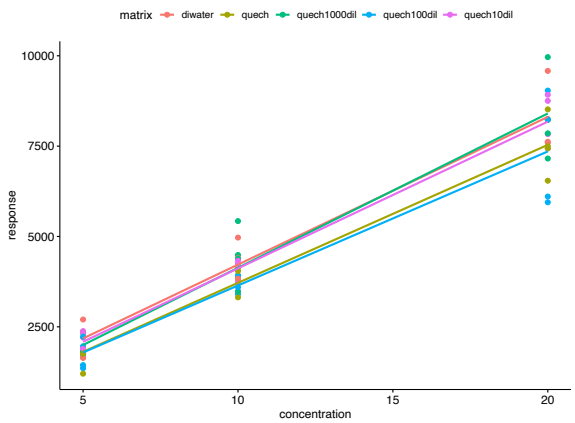

Figure 8.26 2,4-D response across concentrations in a pure acetonitrile matrix vs QuEChERS extracts.

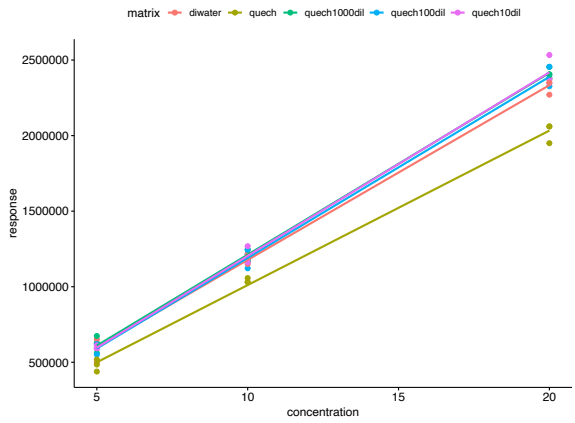

Figure 8.27 Spiroxamine response across concentrations in a pure acetonitrile matrix vs QuEChERS extracts.

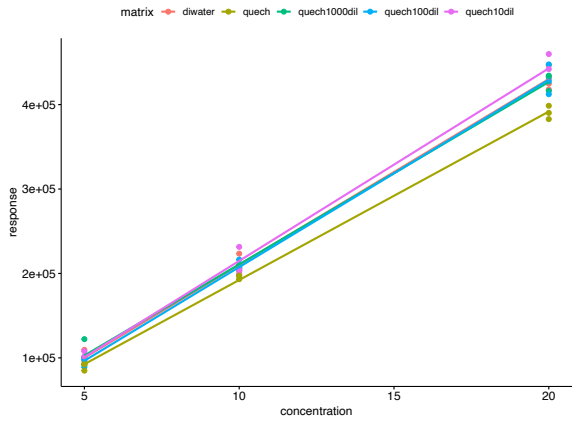

Figure 8.28 Cyprodinil response across concentrations in a pure acetonitrile matrix vs QuEChERS extracts.

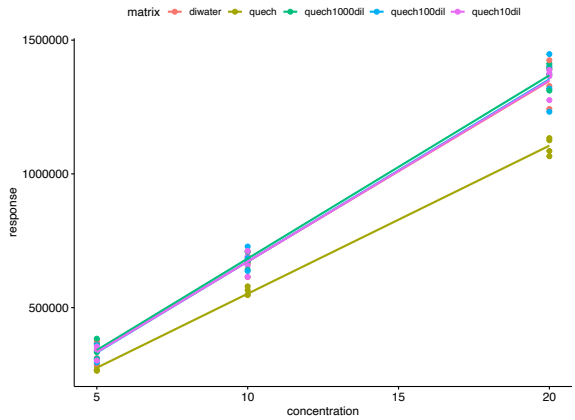

Figure 8.29 Paclobutrazol response across concentrations in a pure acetonitrile matrix vs QuEChERS extracts.

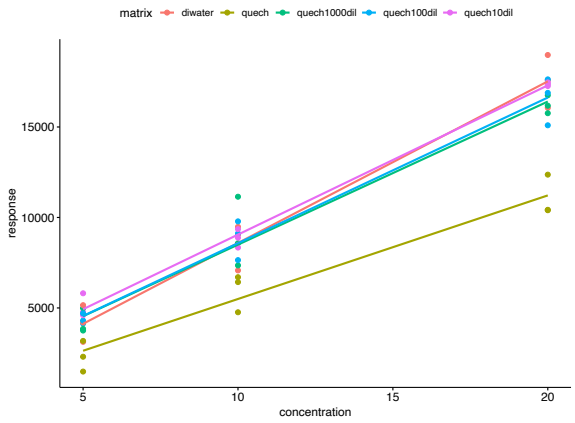

Figure 8.30 Chlorantraniliprole response across concentrations in a pure acetonitrile matrix vs QuEChERS extracts.

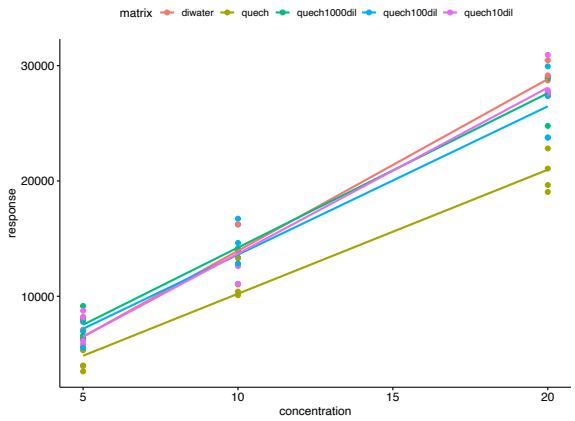

Figure 8.31 Dimethomorph II response across concentrations in a pure acetonitrile matrix vs QuEChERS extracts.

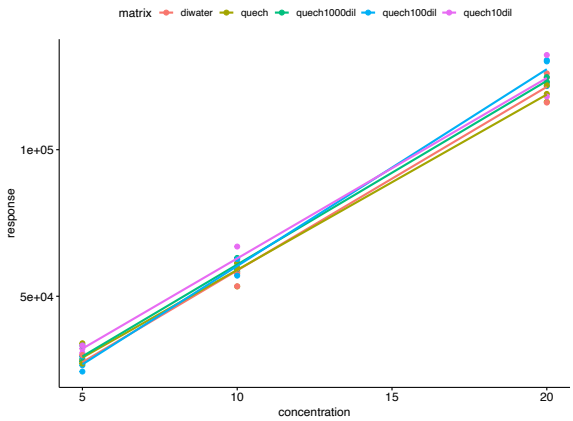

Figure 8.32 Spirotetramat response across concentrations in a pure acetonitrile matrix vs QuEChERS extracts.

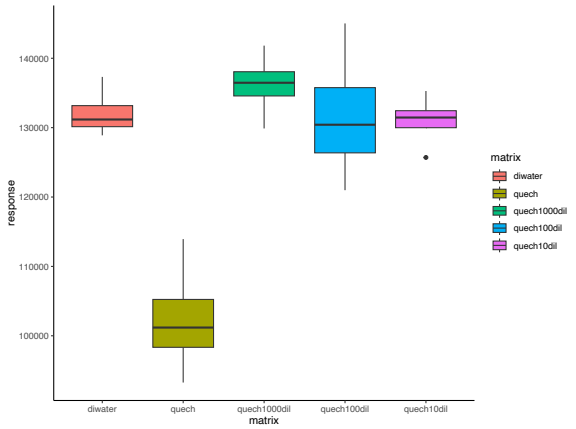

Figure 8.35 Ethoprophos response at 20 ppb in a pure acetonitrile matrix vs QuEChERS extracts.

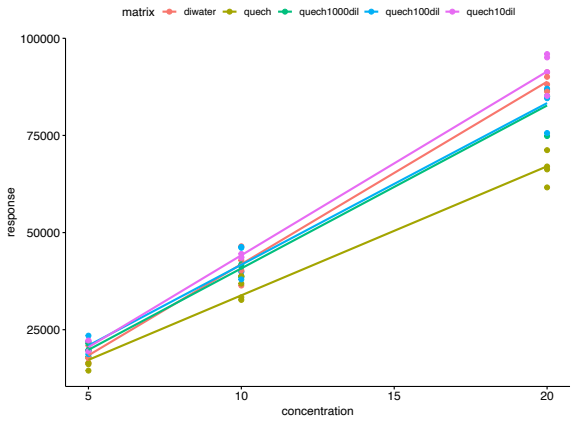

Figure 8.33 Dimethomorph I response across concentrations in a pure acetonitrile matrix vs QuEChERS extracts.

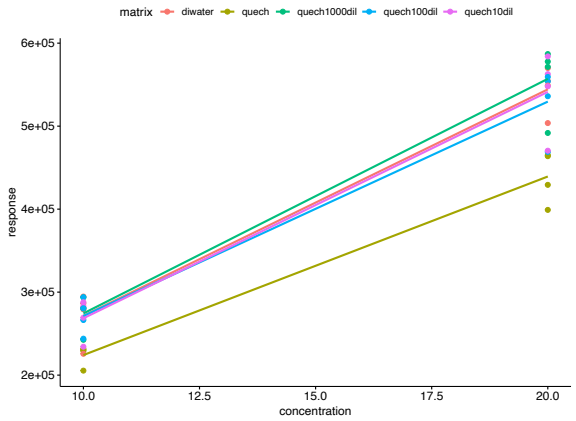

Figure 8.36 Myclobutanil response across concentrations in a pure acetonitrile matrix vs QuEChERS extracts.

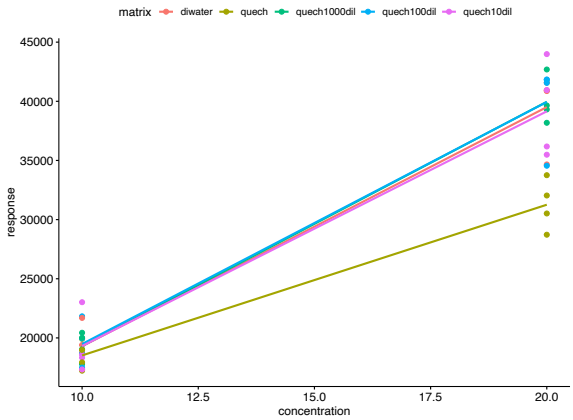

Figure 8.34 Fenhexamid response across concentrations in a pure acetonitrile matrix vs QuEChERS extracts.

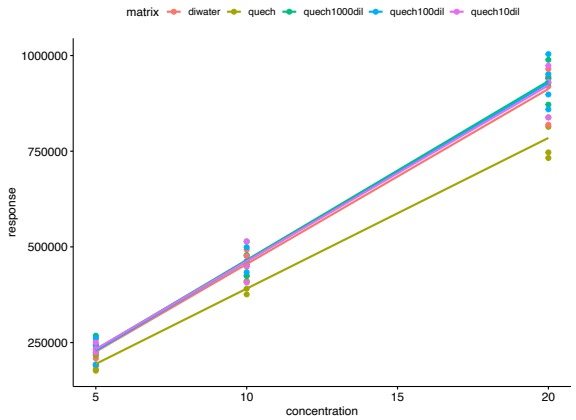

Figure 8.37 Tebuconazole response across concentrations in a pure acetonitrile matrix vs QuEChERS extracts.

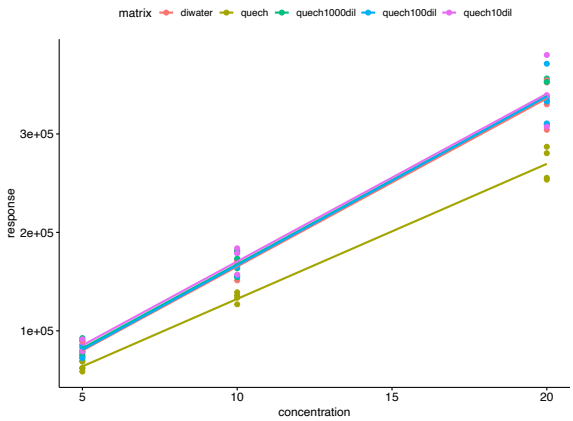

Figure 8.38 Spinetoram J response across concentrations in a pure acetonitrile matrix vs QuEChERS extracts.

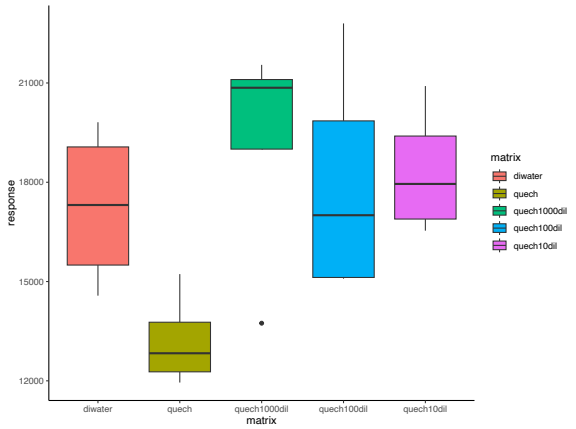

Figure 8.41 Boscalid response at 20 ppb in a pure acetonitrile matrix vs QuEChERS extracts.

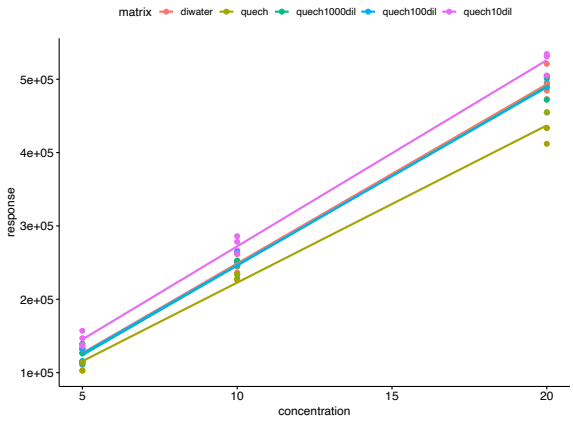

Figure 8.39 Azoxystrobin response across concentrations in a pure acetonitrile matrix vs QuEChERS extracts.

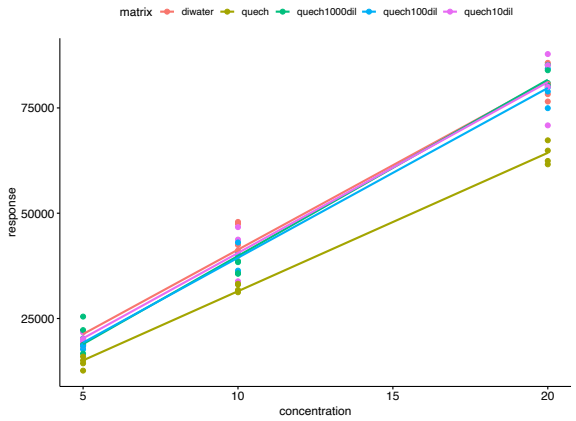

Figure 8.42 Metolachlor response across concentrations in a pure acetonitrile matrix vs QuEChERS extracts.

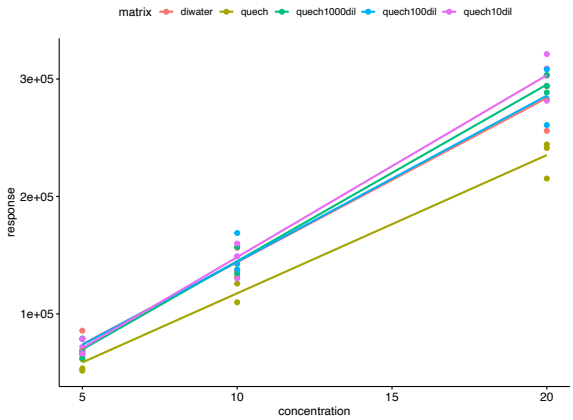

Figure 8.40 Fluopyram response across concentrations in a pure acetonitrile matrix vs QuEChERS extracts.

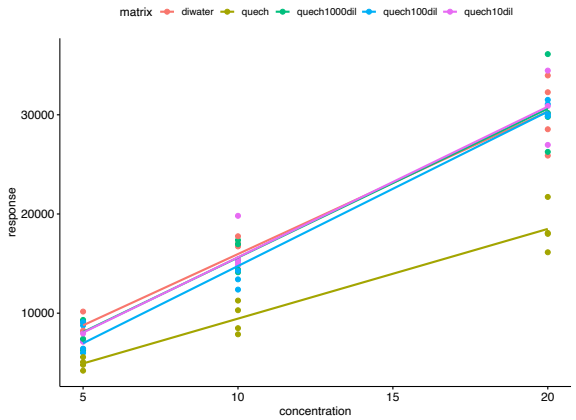

Figure 8.43 Malathion response across concentrations in a pure acetonitrile matrix vs QuEChERS extracts.

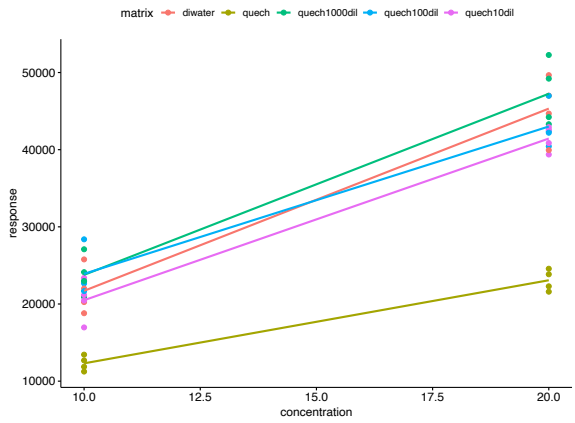

Figure 8.44 Fenoxycarb response across concentrations in a pure acetonitrile matrix vs QuEChERS extracts.

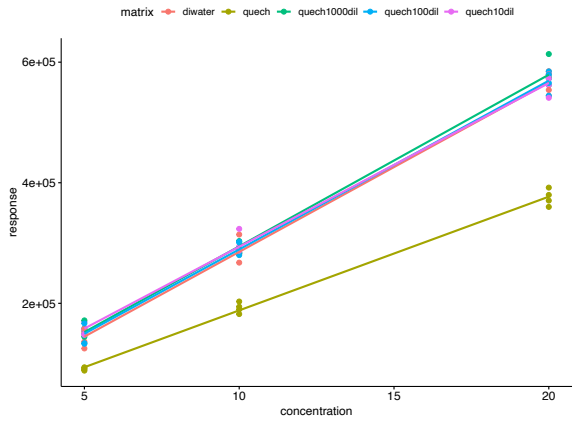

Figure 8.45 Tebufenozide response across concentrations in a pure acetonitrile matrix vs QuEChERS extracts.

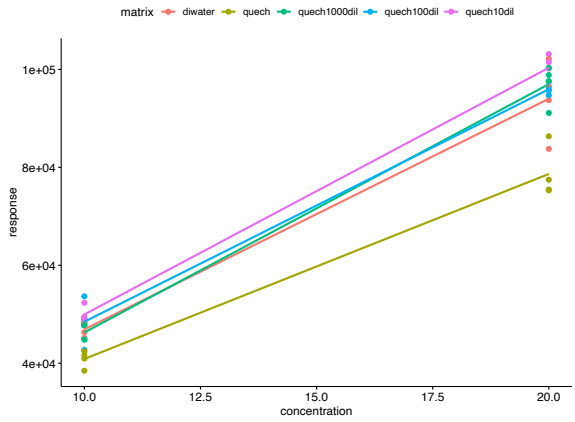

Figure 8.46 Fipronil response across concentrations in a pure acetonitrile matrix vs QuEChERS extracts.

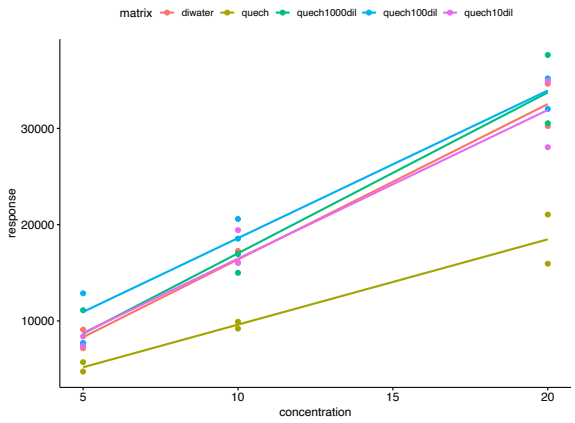

Figure 8.47 Tetrachlorvinphos response across concentrations in a pure acetonitrile matrix vs QuEChERS extracts.

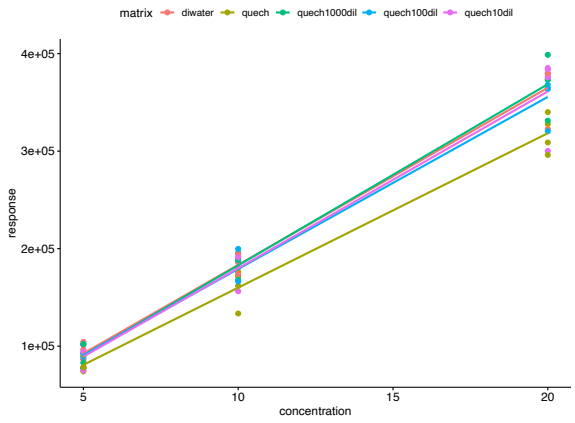

Figure 8.48 Propiconazole response across concentrations in a pure acetonitrile matrix vs QuEChERS extracts.

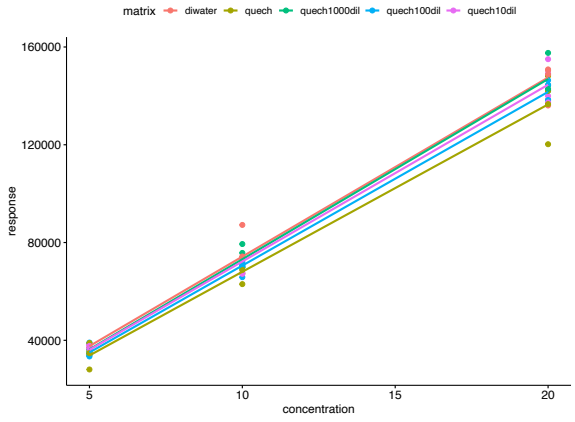

Figure 8.49 Imazamox response across concentrations in a pure acetonitrile matrix vs QuEChERS extracts.

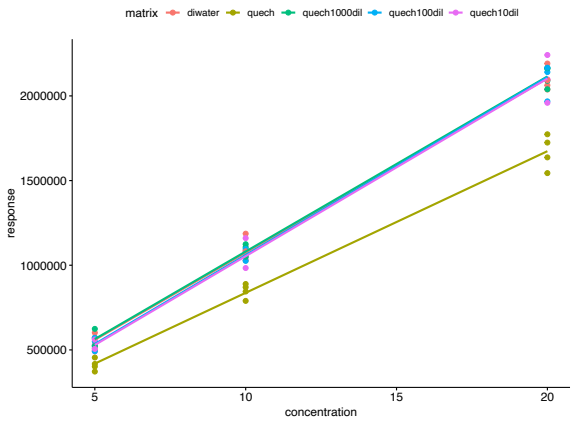

Figure 8.50 Buprofezin response across concentrations in a pure acetonitrile matrix vs QuEChERS extracts.

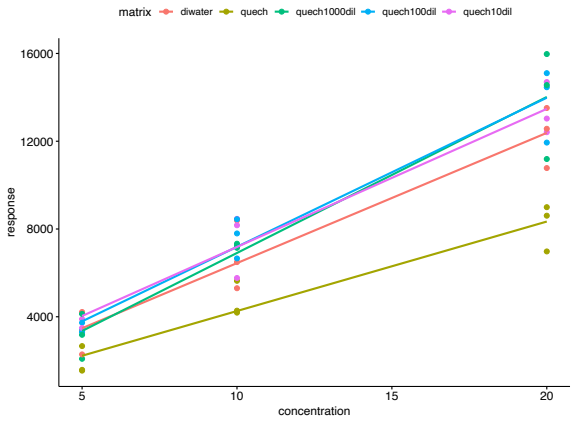

Figure 8.51 Kresoxim-Methyl response across concentrations in a pure acetonitrile matrix vs QuEChERS extracts.

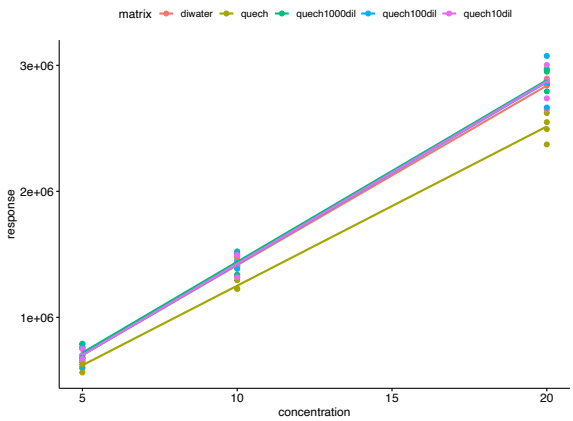

Figure 8.52 Diazinon response across concentrations in a pure acetonitrile matrix vs QuEChERS extracts.

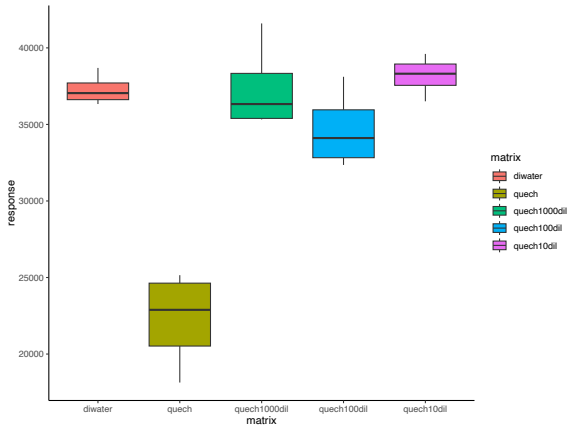

Figure 8.53 Benzovindiflupyr response at 20 ppb in a pure acetonitrile matrix vs QuEChERS extracts.

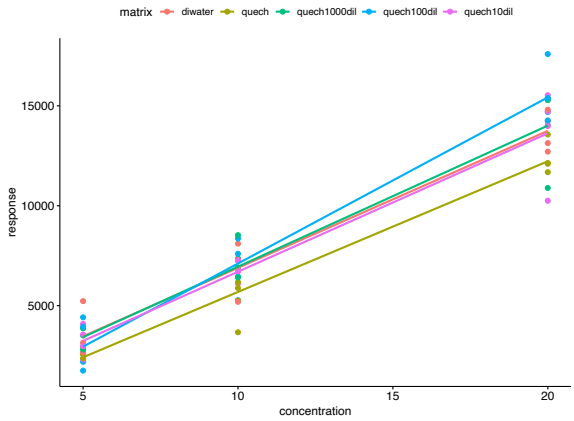

Figure 8.54 Prallethrin response across concentrations in a pure acetonitrile matrix vs QuEChERS extracts.

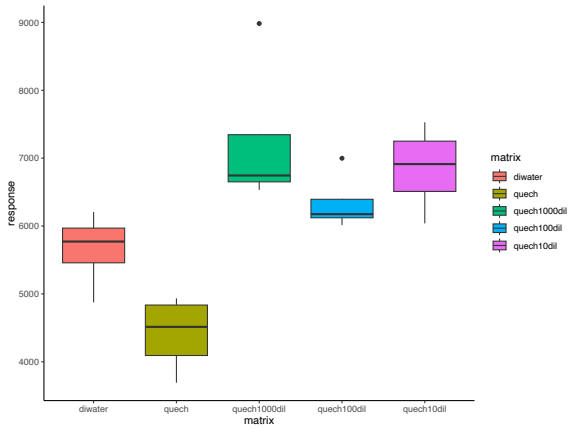

Figure 8.55 Pyrethrin II response at 20 ppb in a pure acetonitrile matrix vs QuEChERS extracts.

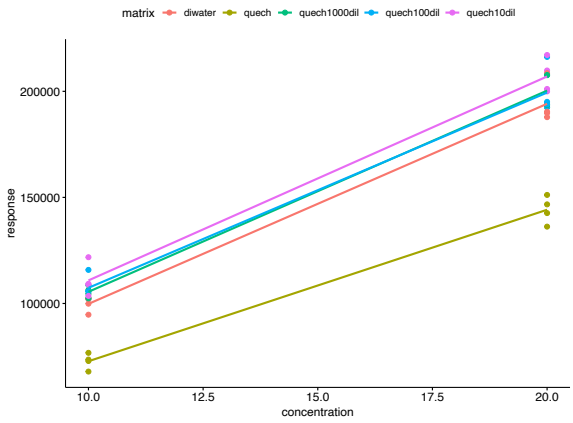

Figure 8.56 Pyraclostrobin response across concentrations in a pure acetonitrile matrix vs QuEChERS extracts.

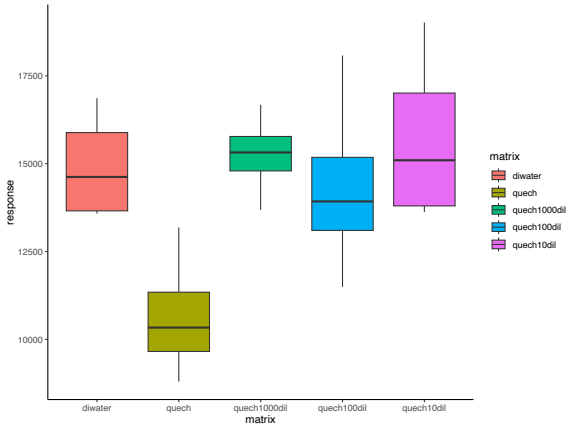

Figure 8.57 Clofentazine response at 20 ppb in a pure acetonitrile matrix vs QuEChERS extracts.

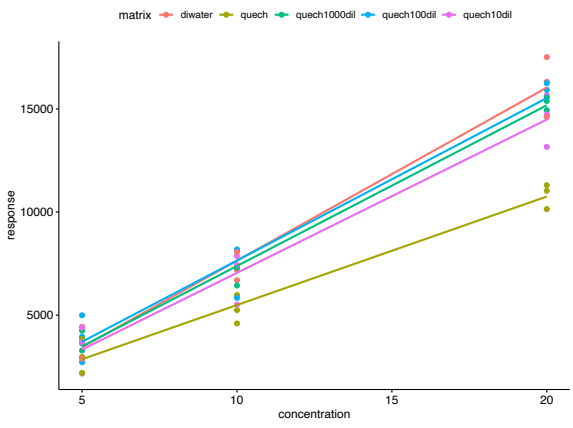

Figure 8.58 MGK 264 response across concentrations in a pure acetonitrile matrix vs QuEChERS extracts.

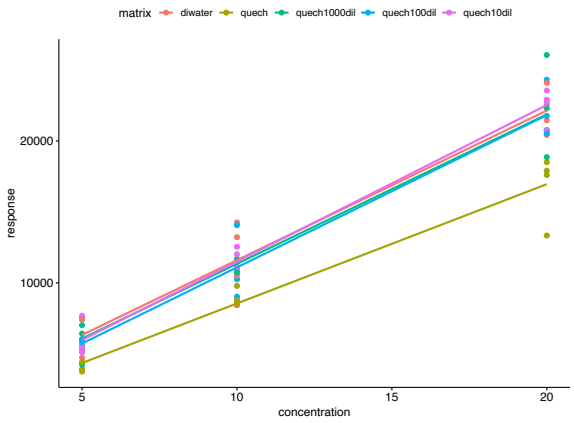

Figure 8.59 Coumaphos response across concentrations in a pure acetonitrile matrix vs QuEChERS extracts.

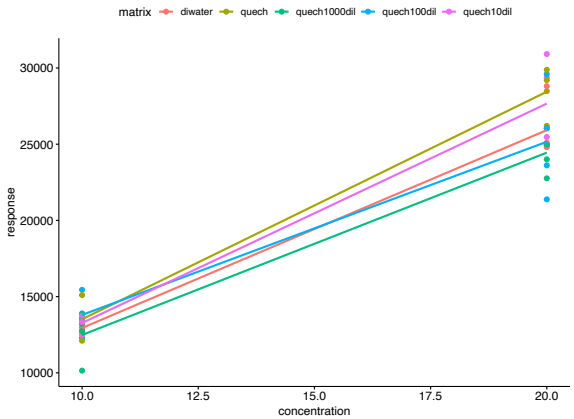

Figure 8.60 Teflubenzuron response across concentrations in a pure acetonitrile matrix vs QuEChERS extracts.

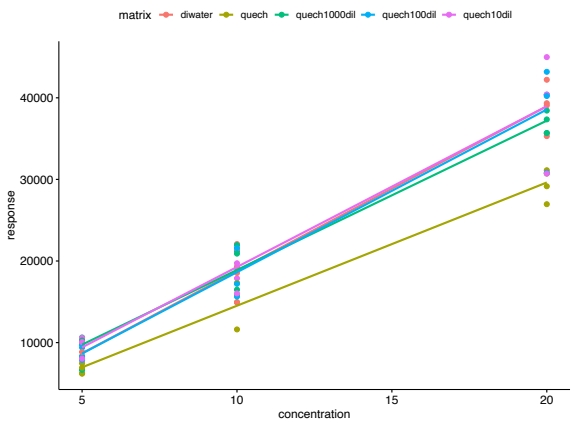

Figure 8.61 Allethrin response across concentrations in a pure acetonitrile matrix vs QuEChERS extracts..

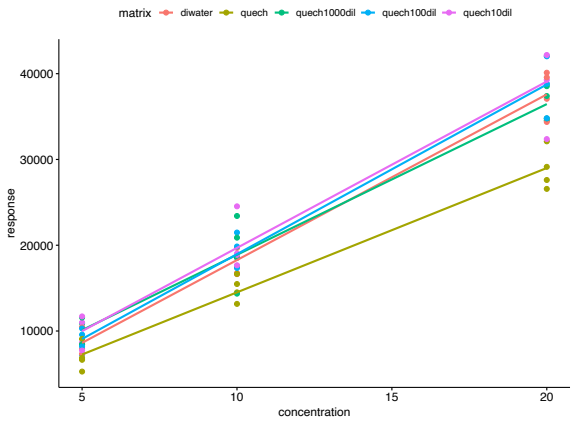

Figure 8.62 Tetramethrin response across concentrations in a pure acetonitrile matrix vs QuEChERS extracts.

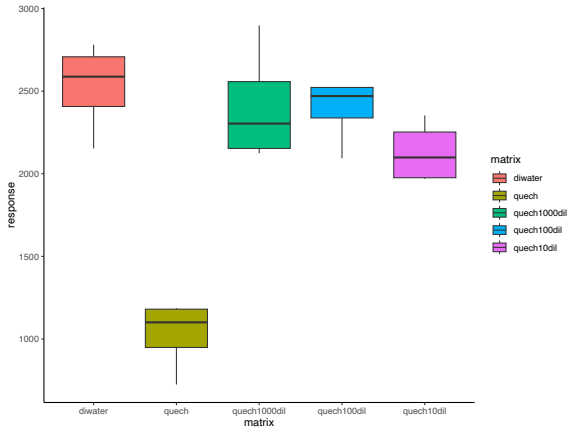

Figure 8.65 Chlorpyrifos response at 20 ppb in a pure acetonitrile matrix vs QuEChERS extracts.

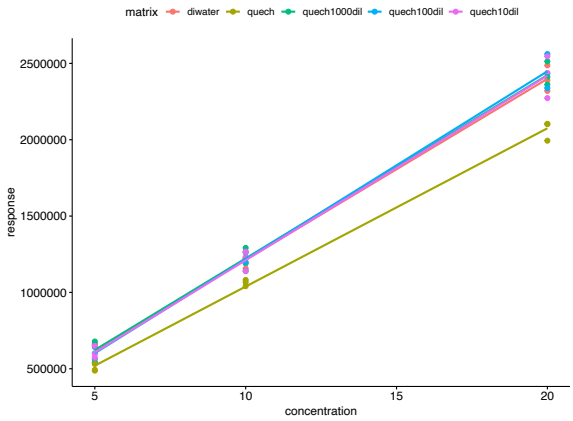

Figure 8.63 Etoxazole response across concentrations in a pure acetonitrile matrix vs QuEChERS extracts.

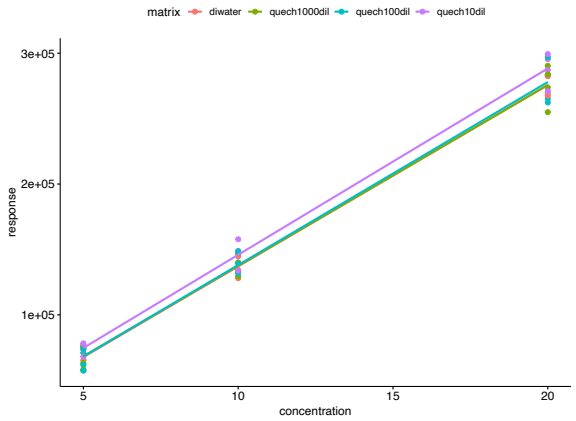

Figure 8.66 Spiromesifen response across concentrations in a pure acetonitrile matrix vs QuEChERS extracts.

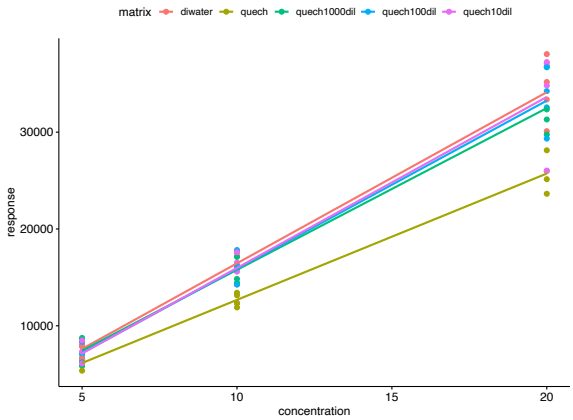

Figure 8.64 Pyrethrin I response across concentrations in a pure acetonitrile matrix vs QuEChERS extracts.

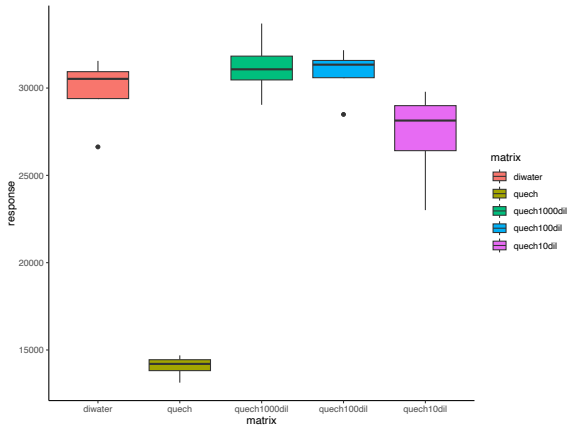

Figure 8.67 Hexythiazox response at 20 ppb in a pure acetonitrile matrix vs QuEChERS extracts.

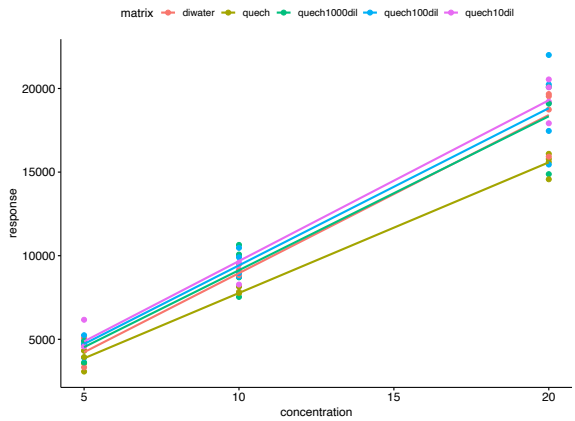

Figure 8.68 Spirodiclofen response across concentrations in a pure acetonitrile matrix vs QuEChERS extracts.

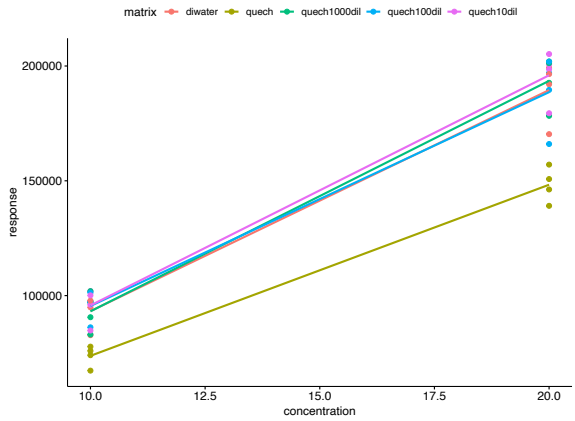

Figure 8.69 Pyridaben response across concentrations in a pure acetonitrile matrix vs QuEChERS extracts.

8.2 Chapter 3 QuEChERS Internal Standard Loss for Biobeds

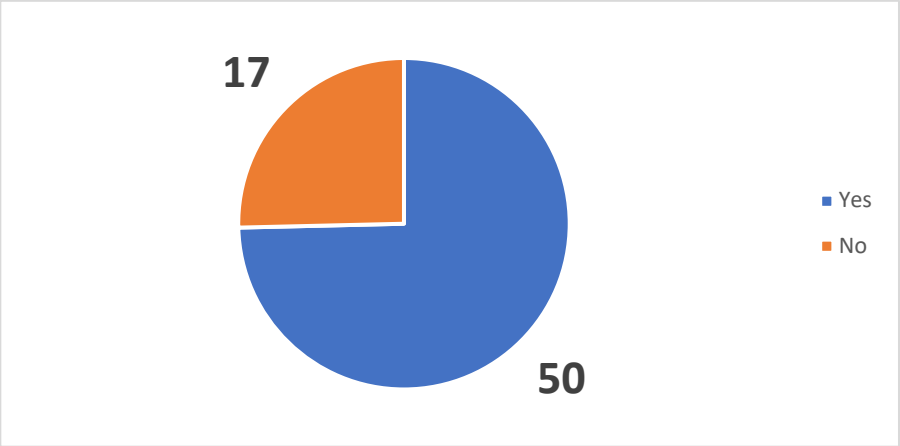

Figure 8.70 Quick Summary of freeze-drying losses detected by an ANOVA for QuEChERS.

Table 8.5 Table of internal standard loss ANOVA p-values as well as the p-values from the Tukey's Post Hoc Test for QuEChERS. *Italicized* values represent square-root transformation.

Compound	ANOVA	BFD v AFD	AFD v FIL	BFD v FIL
Acephate	0.02499	0.7318	0.0246	0.0938
Dinotefuran	0.000932	0.3619	-0.0008	0.0097
Oxamyl	<0.0001	<0.0001	0.1968	<0.0001
Thiamethoxam	0.05115	NA	NA	NA
Flonicamid	<0.0001	0.0001	<0.0001	0.671
Clothianidin	0.0001716	0.0024	0.0002	0.2584
Dimethoate	<0.0001	0.3145	<0.0001	0.0002
Mevinphos	<0.0001	0.3145	<0.0001	0.0002
Imidacloprid	0.00104	0.149	0.0008	0.027
Acetamiprid	0.0002088	0.0767	0.0002	0.0088
Imazethapyr	0.004866	0.76	0.0056	0.0202
Aldicarb	0.0002672	0.9981	0.0007	0.0006
Thiacloprid	0.0001571	0.0804	0.0001	0.0061
Dicamba	0.007317	0.6673	0.0075	0.0357
Propoxur	<0.0001	0.0003	<0.0001	0.0056
Imazalil	0.0003358	0.0923	0.0002	0.0126
Thiophanate-Methyl	0.08034	NA	NA	NA
Carbofuran	<0.0001	0.7403	0.0001	0.0002
Bentazon	0.006595	0.6154	0.0065	0.0361
Atrazine	0.0004329	0.007	0.0004	0.2349
Carbaryl	*0.08732*	*NA*	*NA*	*NA*
Metalaxyl	0.0004706	0.8211	0.002	0.0007

Dodemorph	<0.0001	0.0016	<0.0001	0.1015
2,4-D	0.06563	NA	NA	NA
Cyprodinil	0.01281	0.339	0.0011	0.148
Paclobutrazol	0.002711	0.3301	0.0023	0.0319
Chlorantraniliprole	0.3482	NA	NA	NA
Dimetamorph II	0.6279	NA	NA	NA
Spirotetramat	0.001873	0.0427	0.0014	0.1734
Dimetamorph I	0.0826	NA	NA	NA
Fenhexamid	0.04546	0.8643	0.0489	0.1186
Ethoprophos	0.007292	0.0894	0.305	0.0057
Myclobutanil	<0.0001	0.0037	<0.0001	0.0058
Phosmet	0.3773	NA	NA	NA
Tebuconazole	0.0002683	0.0118	0.0002	0.0302
Spinetoram J	0.0004687	0.0254	0.0652	0.0003
Azoxystrobin	0.1216	NA	NA	NA
Fluopyram	0.01882	0.9755	0.0274	0.0399
Boscalid	0.0686	NA	NA	NA
Metolachlor	0.03677	0.4219	0.0297	0.2594
Malathion	0.02471	0.151	0.5063	0.0208
Fenoxycarb	0.2864	NA	NA	NA
Tebufenozide	0.005221	0.1603	0.0039	0.1269
Fipronil	0.01819	0.9632	0.0255	0.0407
Tetrachlorvinphos	0.125	NA	NA	NA
Propiconazole	0.0001936	0.0997	0.0001	0.0063
Imazamox	0.007581	0.091	0.006	0.3104
Buprofezin	<0.0001	0.0009	<0.0001	0.1103
Kresoxim-Methyl	0.8692	NA	NA	NA
Diazinon	<0.0001	0.3598	0.0001	0.0008
Benzodiflupyr	0.07329	NA	NA	NA
Prallethrin	0.1645	NA	NA	NA
Pyrethrin II	0.04563	0.2425	0.5242	0.0382
Pyraclostrobin	0.003385	0.0109	0.0049	0.8908
Clofentazine	0.04481	0.1151	0.0488	0.8722
MGK-264	0.01163	0.0134	0.0392	0.8236
Coumaphos	<0.0001	0.0001	0.0113	0.0216
Teflubenzuron	0.006212	0.0448	0.0056	0.4951
Allethrin	0.0003254	0.0206	0.0002	0.0528
Tetramethrin	0.04573	0.5398	0.0385	0.2347
Etoxazole	<0.0001	0.047	0.0001	0.0045
Pyrethrin I	0.0007747	0.0009	0.0047	0.614

Chlorpyrifos	0.1595	NA	NA	NA
Spiromesifen	0.001155	0.0133	0.001	0.339
Hexythiazox	0.1349	NA	NA	NA
Spirodiclofen	0.02709	0.3723	0.0216	0.2306
Pyridaben	0.00105	0.0261	0.0008	0.1561

Table 8.6 Table of Shaprio-Wilk Test and Bartlett's Test results for ANOVA assumptions of QuEChERS internal standard loss. *Italicized* values represent square-root transformation. **Bold** values were significantly different from normal, but boxplots demonstrated normal distribution.

Compound	Normality			Homogeneity of Variance
	BFD	AFD	FIL	
Acephate	0.7546	0.9375	0.7794	0.2778
Dinotefuran	0.122	0.5322	0.7557	0.245
Oxamyl	0.9698	0.665	0.821	0.3702
Thiamethoxam	0.4337	0.2979	0.06588	0.7105
Flonicamid	0.3392	0.8991	0.7185	0.6853
Clothianidin	0.2017	0.2524	0.5553	0.1207
Dimethoate	0.6661	0.4712	0.5495	0.5391
Mevinphos	0.09972	0.9761	0.3417	0.6492
Imidacloprid	0.651	0.6105	0.5232	0.5095
Acetamiprid	0.3247	0.8152	0.3363	0.09591
Imazethapyr	0.1871	0.3218	0.8566	0.5058
Aldicarb	0.3209	0.8033	0.2657	0.346
Thiacloprid	0.3682	0.5689	0.4783	0.5214
Dicamba	0.1372	0.09386	0.9922	0.3966
Propoxur	0.3147	0.5082	0.3832	0.8724
Imazalil	0.3543	0.06313	0.3629	0.682
Thiophanate-Methyl	0.3026	0.5364	0.9897	0.4061
Carbofuran	0.6126	0.4607	0.4265	0.06356
Bentazon	0.3355	0.6093	0.07381	0.9585
Atrazine	0.3713	0.76	0.1152	0.8896
Carbaryl	0.9962	0.6816	0.2529	0.7419
Metalaxyl	0.09108	0.5782	0.5416	0.05858
Dodemorph	0.7188	0.2697	0.9408	0.1184
2,4-D	0.9805	0.4499	0.2915	0.07303
Cyprodinil	0.2095	0.9959	0.06498	0.2625
Paclobutrazol	0.8736	0.831	0.1456	0.2625
Chlorantraniliprole	0.528	0.957	0.6072	0.5774
Dimetamorph II	0.9168	0.8329	0.8377	0.9923

Spirotetramat	0.3557	0.3716	0.8998	0.06772
Dimetamorph I	0.8903	0.8376	0.3204	0.154
Fenhexamid	0.7765	0.461	0.9628	0.2503
Ethoprophos	0.7077	0.8089	0.08152	0.983
Myclobutanil	0.3674	0.9623	0.9075	0.1181
Phosmet	0.5175	0.1808	0.8112	0.2395
Tebuconazole	0.2851	0.5182	0.8159	0.1577
Spinetoram J	**0.01375**	0.9182	0.3885	0.08064
Azoxystrobin	0.05828	0.1657	0.8879	0.3633
Fluopyram	0.4364	0.3941	0.65	0.05921
Boscalid	0.6161	0.7447	0.9514	0.633
Metolachlor	0.1928	0.9978	0.9857	0.8164
Malathion	0.07847	0.3752	0.5452	0.6158
Fenoxycarb	0.654	0.4238	0.2863	0.3269
Tebufenozide	0.8907	0.7837	0.4793	0.648
Fipronil	0.5204	0.9805	0.2928	0.1323
Tetrachlorvinphos	0.7775	0.927	0.1234	0.7299
Propiconazole	0.8914	0.27	0.182	0.07255
Imazamox	0.8266	0.5696	0.6519	0.1728
Buprofezin	0.2888	0.554	0.1863	0.9
Kresoxim-Methyl	0.3345	0.3398	0.4316	0.8492
Diazinon	0.8019	0.5995	0.1812	0.0724
Benzodiflupyr	0.3042	0.9959	0.4179	0.5588
Prallethrin	0.1201	0.6604	0.1667	0.3134
Pyrethrin II	0.8698	0.9596	0.7839	0.8208
Pyraclostrobin	0.6401	0.8797	0.3883	0.2846
Clofentazine	0.3042	0.3883	0.7739	0.8268
MGK-264	0.5605	**0.03885**	0.3883	0.3819
Coumaphos	0.965	0.7374	0.3681	0.9781
Teflubenzuron	0.5315	0.6371	0.7807	0.9721
Allethrin	0.9991	0.5603	0.5611	0.9824
Tetramethrin	0.9412	0.9549	0.3953	0.09614
Etoxazole	**0.04501**	0.8854	0.3536	0.8922
Pyrethrin I	0.1615	0.4592	0.3403	0.444
Chlorpyrifos	0.922	0.8604	0.7968	0.7488
Spiromesifen	0.1007	0.1039	0.6998	0.9666
Hexythiazox	0.597	0.9062	0.8102	0.7273
Spirodiclofen	0.2347	0.4596	0.1956	0.1826
Pyridaben	0.5936	0.7937	0.07856	0.7026

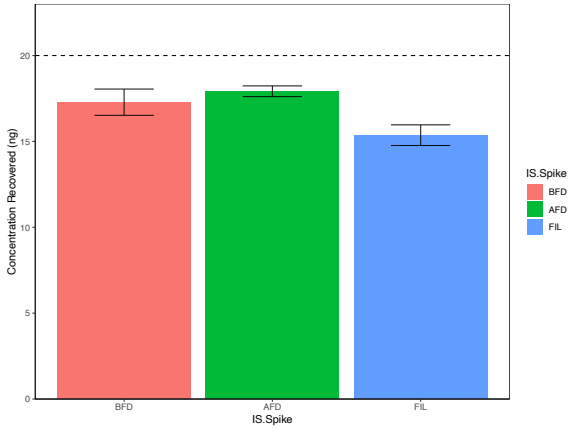

Figure 8.71 Acephate internal standard recovery before freeze-drying (BFD), after freeze-drying (AFD), and filter (FIL) stage of extractions. Bars are standard error, dashed line are amount spiked.

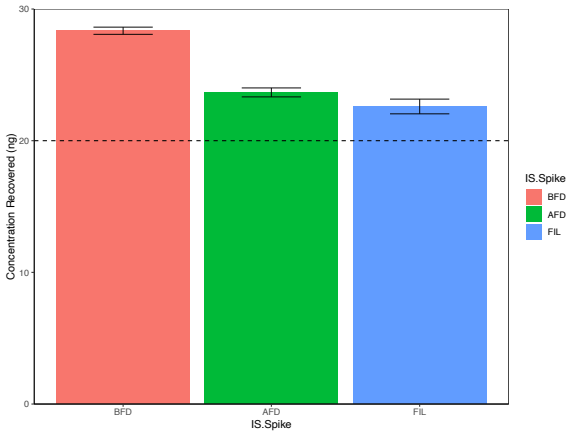

Figure 8.73 Oxamyl internal standard recovery before freeze-drying (BFD), after freeze-drying (AFD), and filter (FIL) stage of extractions. Bars are standard error, dashed line are amount spiked.

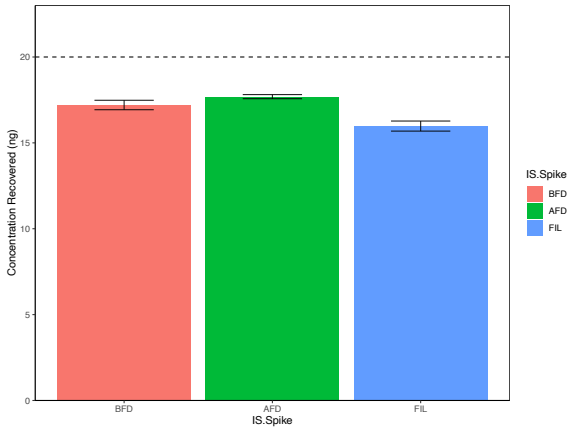

Figure 8.72 Dinotefuran internal standard recovery before freeze-drying (BFD), after freeze-drying (AFD), and filter (FIL) stage of extractions. Bars are standard error, dashed line are amount spiked.

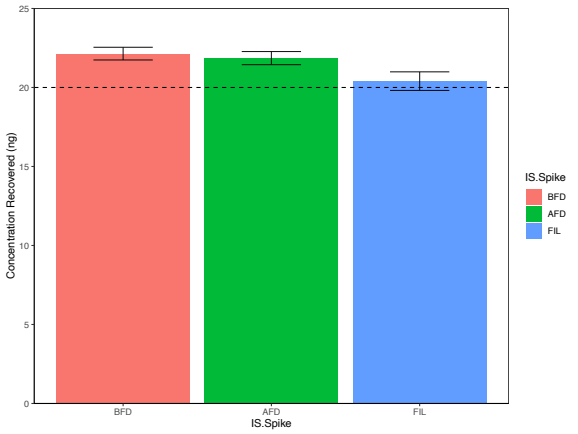

Figure 8.74 Thiamethoxam internal standard recovery before freeze-drying (BFD), after freeze-drying (AFD), and filter (FIL) stage of extractions. Bars are standard error, dashed line are amount spiked.

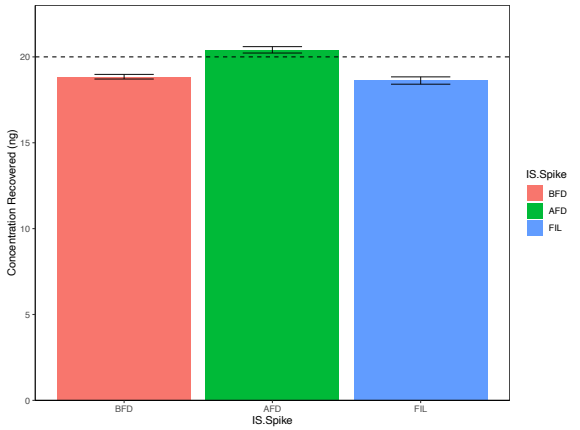

Figure 8.75 Flonicamid internal standard recovery before freeze-drying (BFD), after freeze-drying (AFD), and filter (FIL) stage of extractions. Bars are standard error, dashed line are amount spiked.

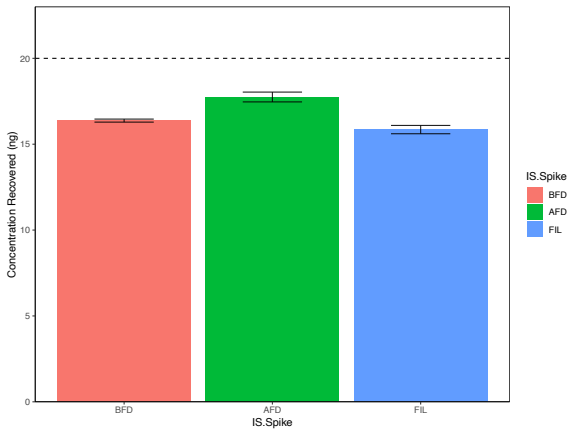

Figure 8.76 Clothianidin internal standard recovery before freeze-drying (BFD), after freeze-drying (AFD), and filter (FIL) stage of extractions. Bars are standard error, dashed line are amount spiked.

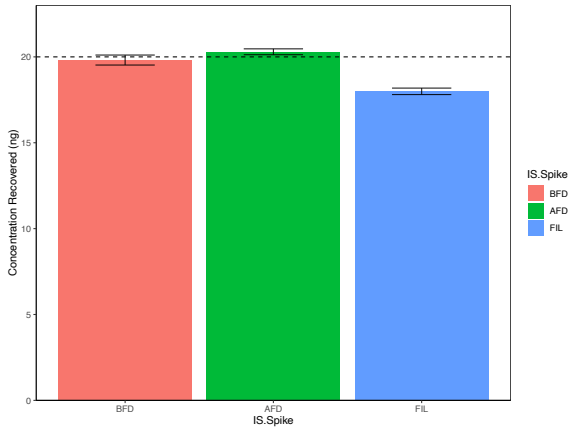

Figure 8.77 Dimethoate internal standard recovery before freeze-drying (BFD), after freeze-drying (AFD), and filter (FIL) stage of extractions. Bars are standard error, dashed line are amount spiked.

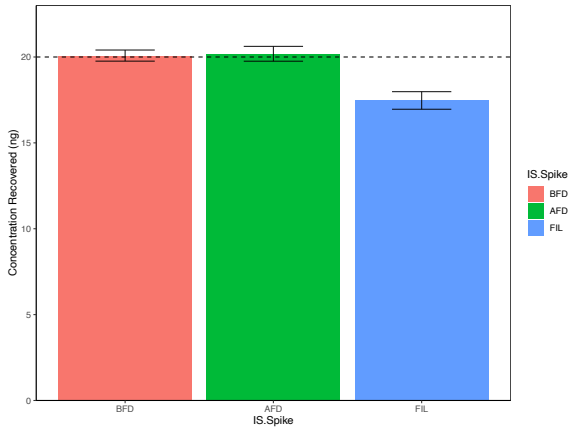

Figure 8.78 Mevinphos internal standard recovery before freeze-drying (BFD), after freeze-drying (AFD), and filter (FIL) stage of extractions. Bars are standard error, dashed line are amount spiked.

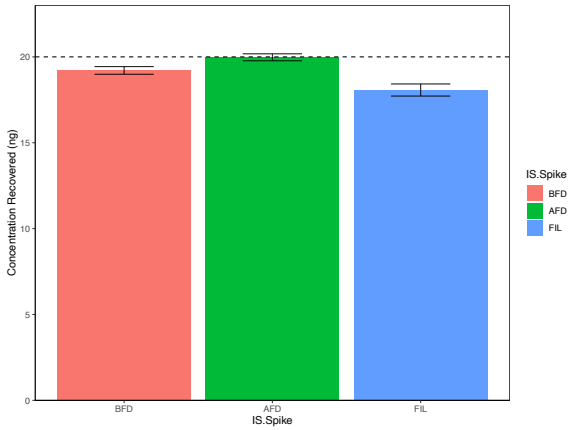

Figure 8.79 Imidacloprid internal standard recovery before freeze-drying (BFD), after freeze-drying (AFD), and filter (FIL) stage of extractions. Bars are standard error, dashed line are amount spiked.

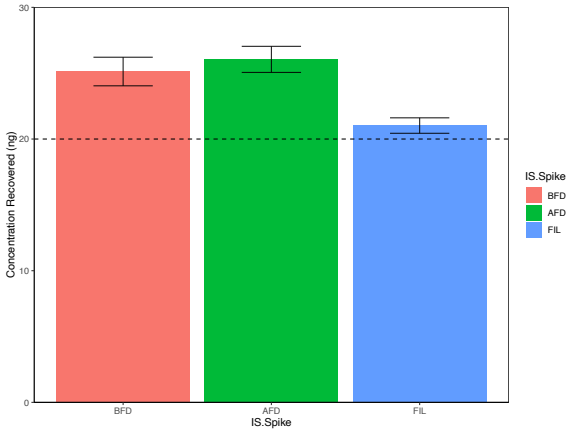

Figure 8.81 Imazethapyr internal standard recovery before freeze-drying (BFD), after freeze-drying (AFD), and filter (FIL) stage of extractions. Bars are standard error, dashed line are amount spiked.

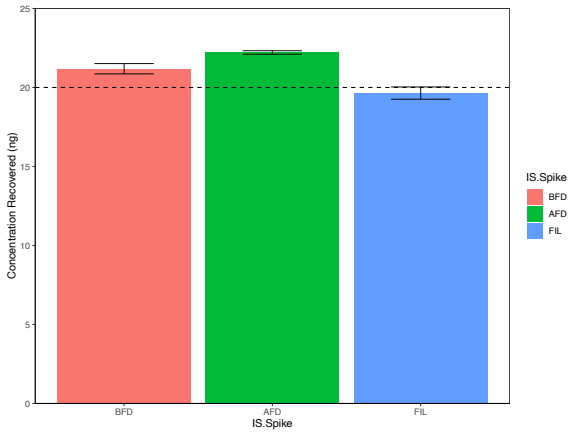

Figure 8.80 Acetamiprid internal standard recovery before freeze-drying (BFD), after freeze-drying (AFD), and filter (FIL) stage of extractions. Bars are standard error, dashed line are amount spiked.

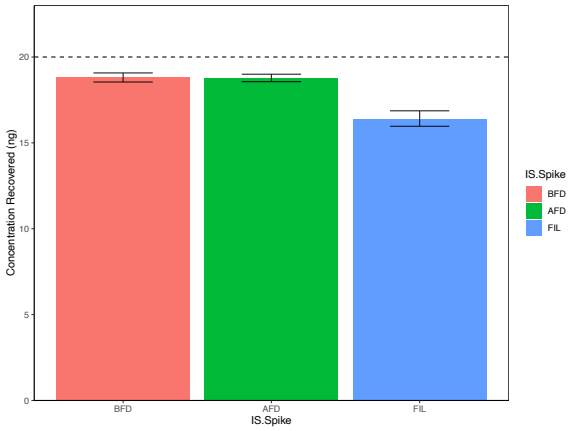

Figure 8.82 Aldicarb internal standard recovery before freeze-drying (BFD), after freeze-drying (AFD), and filter (FIL) stage of extractions. Bars are standard error, dashed line are amount spiked.

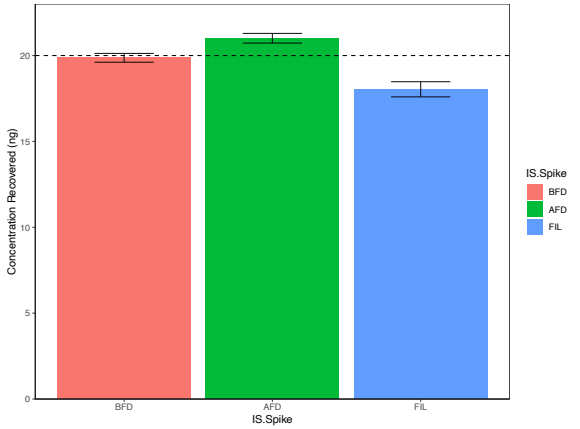

Figure 8.83 Thiacloprid internal standard recovery before freeze-drying (BFD), after freeze-drying (AFD), and filter (FIL) stage of extractions. Bars are standard error, dashed line are amount spiked.

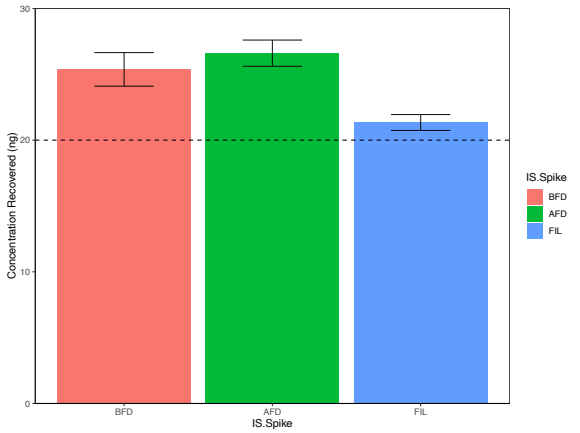

Figure 8.84 Dicamba internal standard recovery before freeze-drying (BFD), after freeze-drying (AFD), and filter (FIL) stage of extractions. Bars are standard error, dashed line are amount spiked.

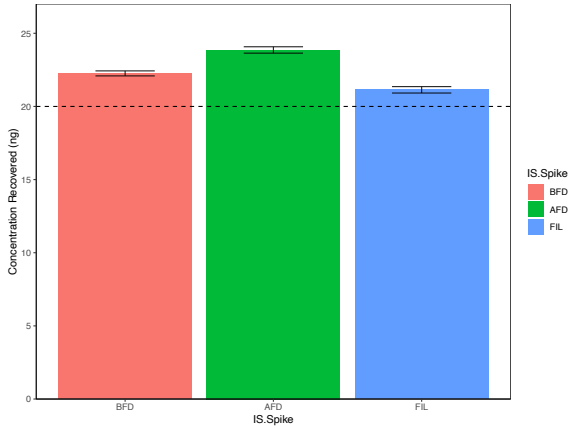

Figure 8.85 Propoxur internal standard recovery before freeze-drying (BFD), after freeze-drying (AFD), and filter (FIL) stage of extractions. Bars are standard error, dashed line are amount spiked.

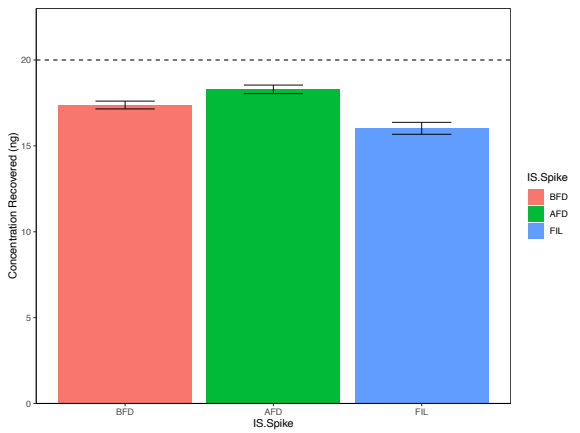

Figure 8.86 Imazalil internal standard recovery before freeze-drying (BFD), after freeze-drying (AFD), and filter (FIL) stage of extractions. Bars are standard error, dashed line are amount spiked.

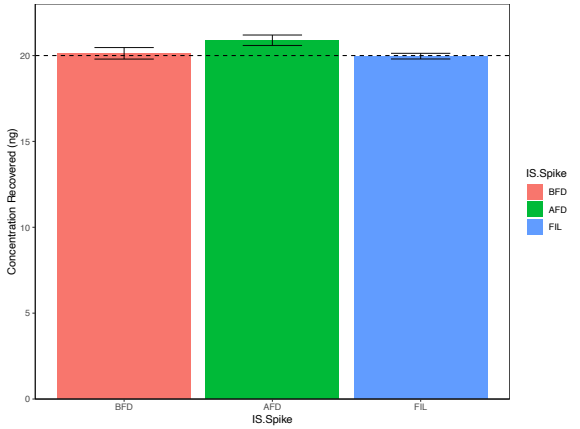

Figure 8.87 Thiophanate-Methyl internal standard recovery before freeze-drying (BFD), after freeze-drying (AFD), and filter (FIL) stage of extractions. Bars are standard error, dashed line are amount spiked.

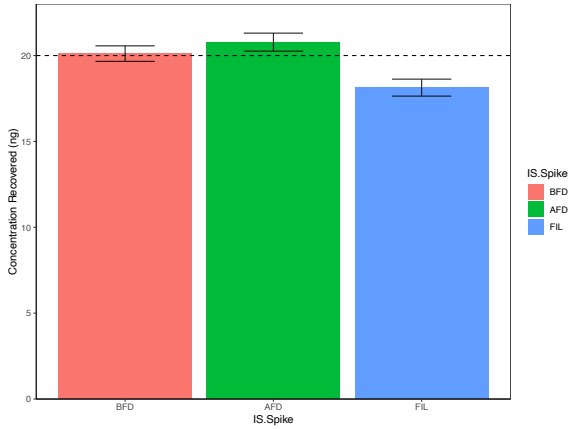

Figure 8.89 Bentazon internal standard recovery before freeze-drying (BFD), after freeze-drying (AFD), and filter (FIL) stage of extractions. Bars are standard error, dashed line are amount spiked.

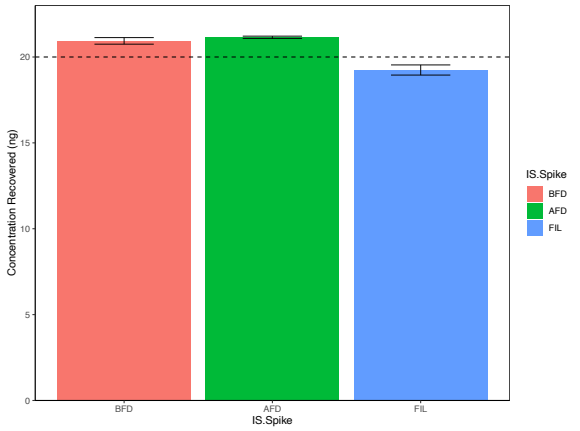

Figure 8.88 Carbofuran internal standard recovery before freeze-drying (BFD), after freeze-drying (AFD), and filter (FIL) stage of extractions. Bars are standard error, dashed line are amount spiked.

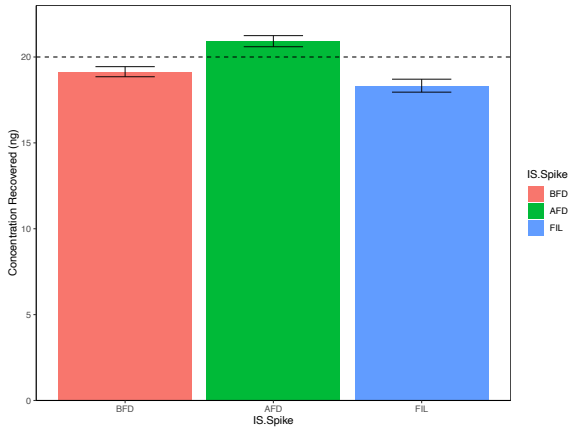

Figure 8.90 Atrazine internal standard recovery before freeze-drying (BFD), after freeze-drying (AFD), and filter (FIL) stage of extractions. Bars are standard error, dashed line are amount spiked.

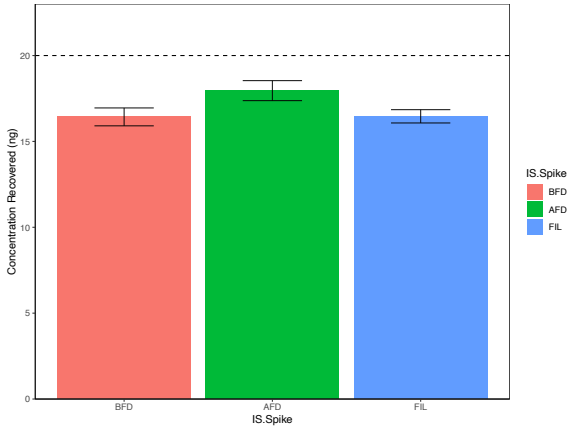

Figure 8.91 Carbaryl internal standard recovery before freeze-drying (BFD), after freeze-drying (AFD), and filter (FIL) stage of extractions. Bars are standard error, dashed line are amount spiked.

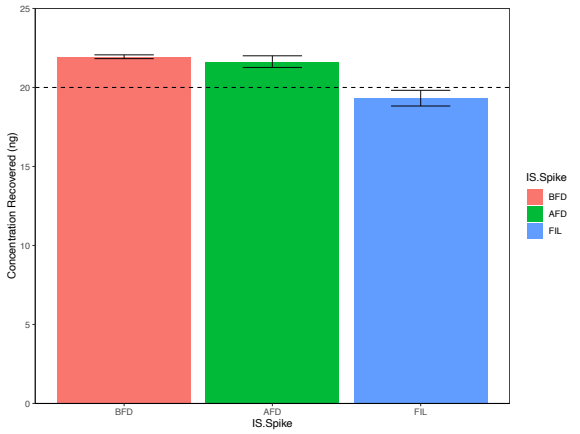

Figure 8.92 Metalaxyl internal standard recovery before freeze-drying (BFD), after freeze-drying (AFD), and filter (FIL) stage of extractions. Bars are standard error, dashed line are amount spiked.

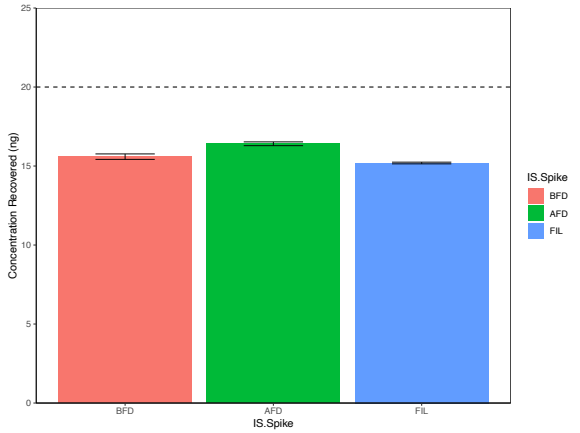

Figure 8.93 Dodemorph internal standard recovery before freeze-drying (BFD), after freeze-drying (AFD), and filter (FIL) stage of extractions. Bars are standard error, dashed line are amount spiked.

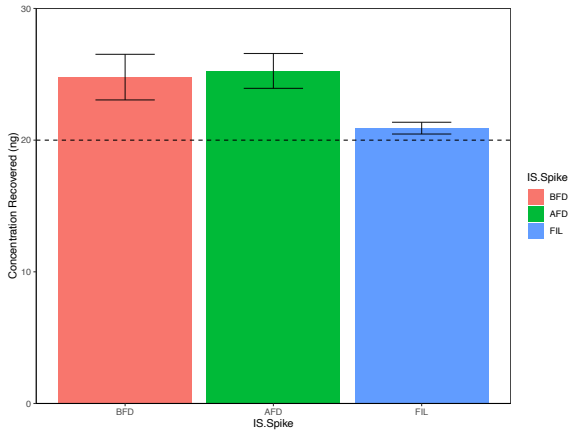

Figure 8.94 2,4-D internal internal standard recovery before freeze-drying (BFD), after freeze-drying (AFD), and filter (FIL) stage of extractions. Bars are standard error, dashed line are amount spiked.

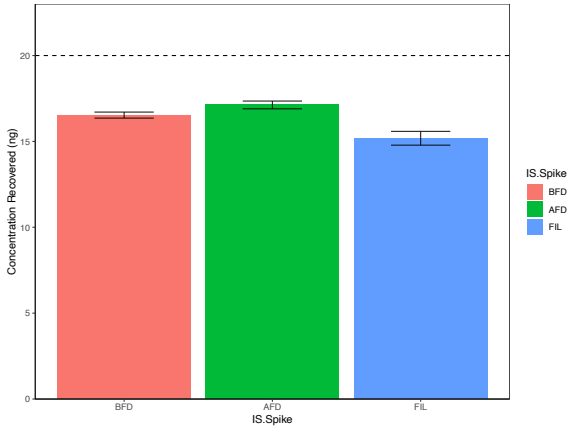

Figure 8.95 Cyprodinil internal standard recovery before freeze-drying (BFD), after freeze-drying (AFD), and filter (FIL) stage of extractions. Bars are standard error, dashed line are amount spiked.

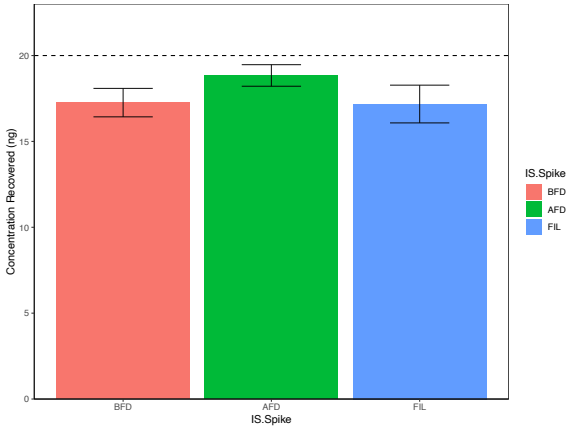

Figure 8.97 Chlorantraniliprole internal standard recovery before freeze-drying (BFD), after freeze-drying (AFD), and filter (FIL) stage of extractions. Bars are standard error, dashed line are amount spiked.

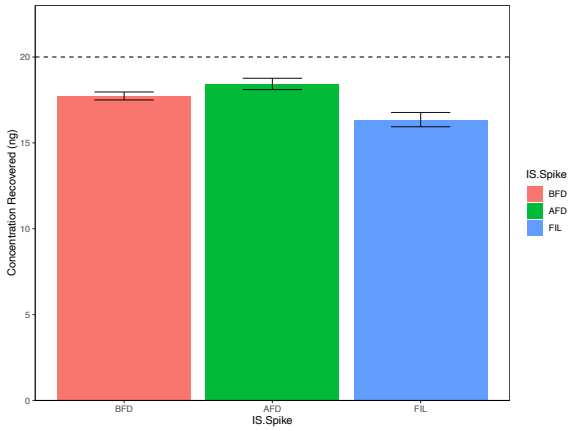

Figure 8.96 Paclobutrazol internal standard recovery before freeze-drying (BFD), after freeze-drying (AFD), and filter (FIL) stage of extractions. Bars are standard error, dashed line are amount spiked.

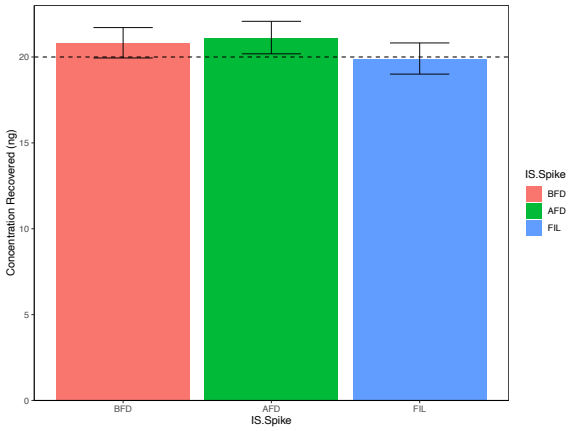

Figure 8.98 Dimethomorph II internal standard recovery before freeze-drying (BFD), after freeze-drying (AFD), and filter (FIL) stage of extractions. Bars are standard error, dashed line are amount spiked.

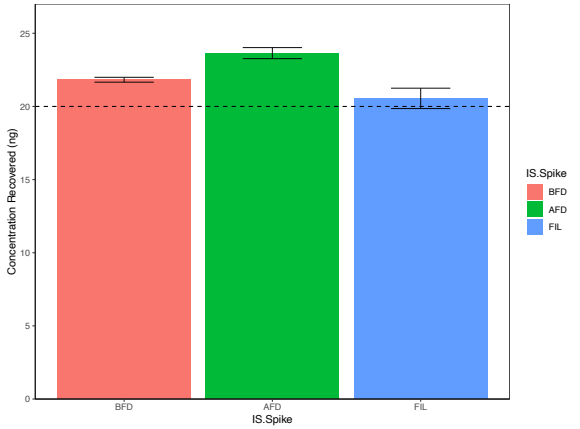

Figure 8.99 Spirotetramat internal standard recovery before freeze-drying (BFD), after freeze-drying (AFD), and filter (FIL) stage of extractions. Bars are standard error, dashed line are amount spiked.

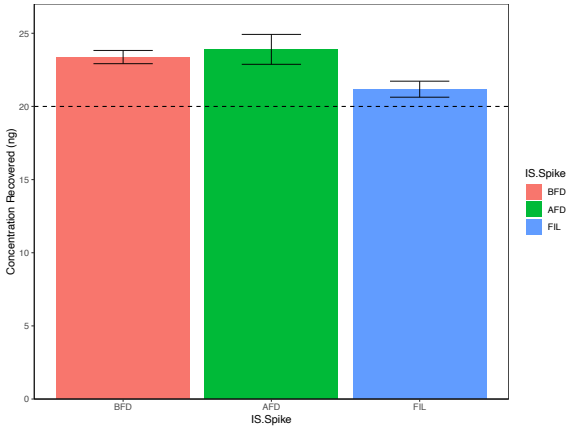

Figure 8.101 Fenhexamid internal standard recovery before freeze-drying (BFD), after freeze-drying (AFD), and filter (FIL) stage of extractions. Bars are standard error, dashed line are amount spiked.

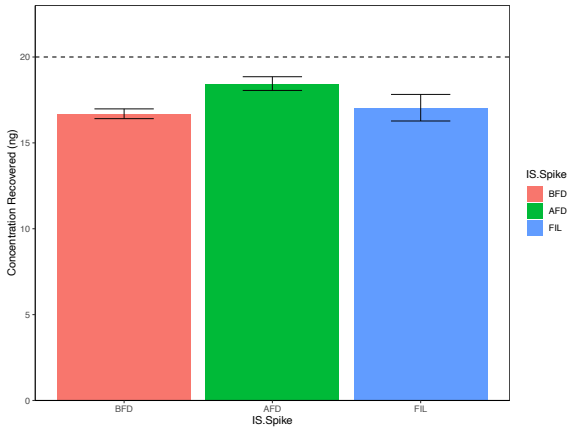

Figure 8.100 Dimethomorph I internal standard recovery before freeze-drying (BFD), after freeze-drying (AFD), and filter (FIL) stage of extractions. Bars are standard error, dashed line are amount spiked.

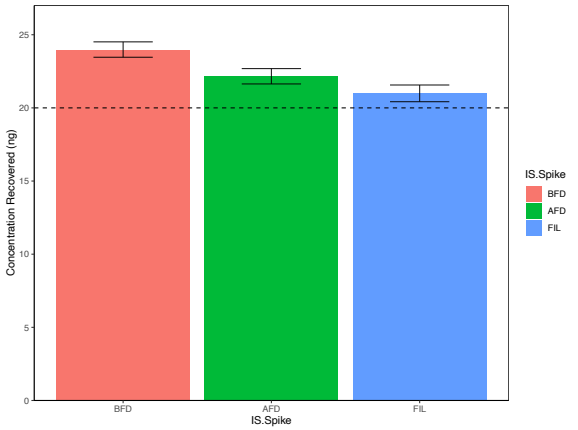

Figure 8.102 Ethoprophos internal standard recovery before freeze-drying (BFD), after freeze-drying (AFD), and filter (FIL) stage of extractions. Bars are standard error, dashed line are amount spiked.

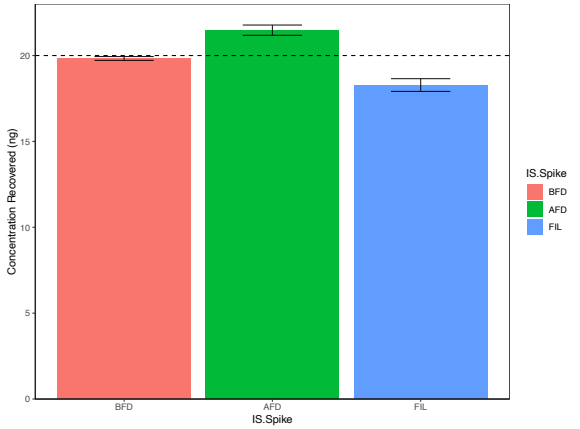

Figure 8.103 Myclobutanil internal standard recovery before freeze-drying (BFD), after freeze-drying (AFD), and filter (FIL) stage of extractions. Bars are standard error, dashed line are amount spiked.

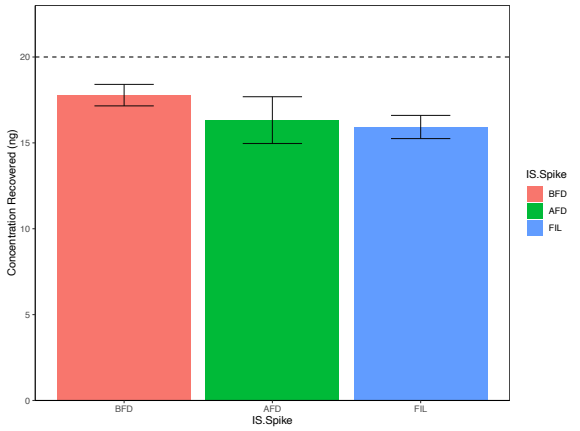

Figure 8.104 Phosmet internal standard recovery before freeze-drying (BFD), after freeze-drying (AFD), and filter (FIL) stage of extractions. Bars are standard error, dashed line are amount spiked.

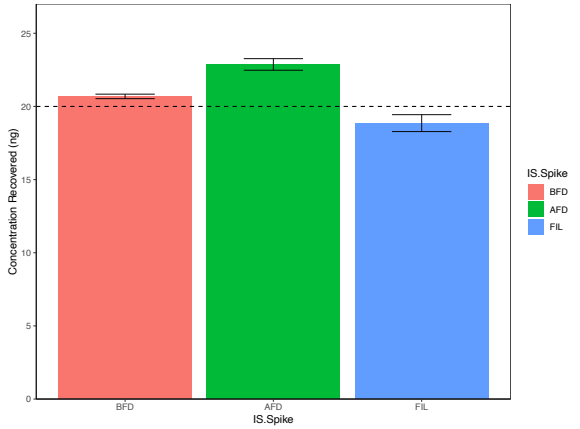

Figure 8.105 Tebuconazole internal standard recovery before freeze-drying (BFD), after freeze-drying (AFD), and filter (FIL) stage of extractions. Bars are standard error, dashed line are amount spiked.

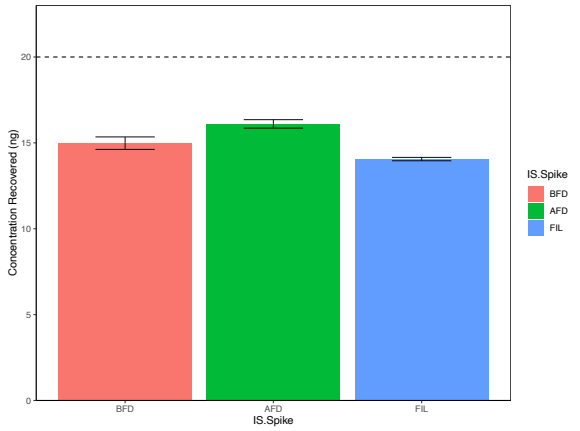

Figure 8.106 Spinetoram J internal standard recovery before freeze-drying (BFD), after freeze-drying (AFD), and filter (FIL) stage of extractions. Bars are standard error, dashed line are amount spiked.

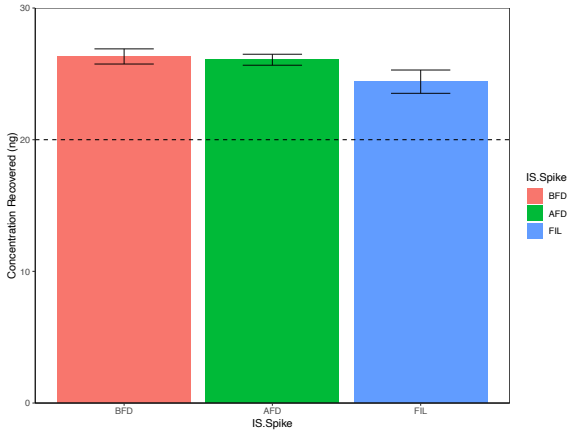

Figure 8.107 Azoxystrobin internal standard recovery before freeze-drying (BFD), after freeze-drying (AFD), and filter (FIL) stage of extractions. Bars are standard error, dashed line are amount spiked.

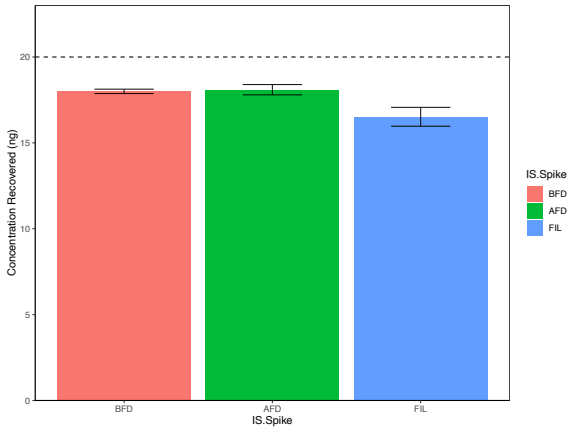

Figure 8.108 Fluopyram internal standard recovery before freeze-drying (BFD), after freeze-drying (AFD), and filter (FIL) stage of extractions. Bars are standard error, dashed line are amount spiked.

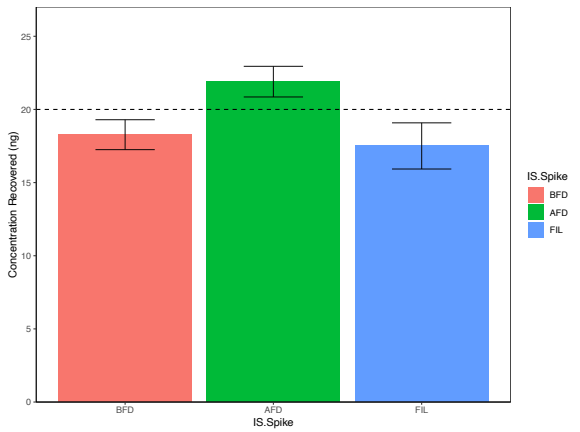

Figure 8.109 Boscalid internal standard recovery before freeze-drying (BFD), after freeze-drying (AFD), and filter (FIL) stage of extractions. Bars are standard error, dashed line are amount spiked.

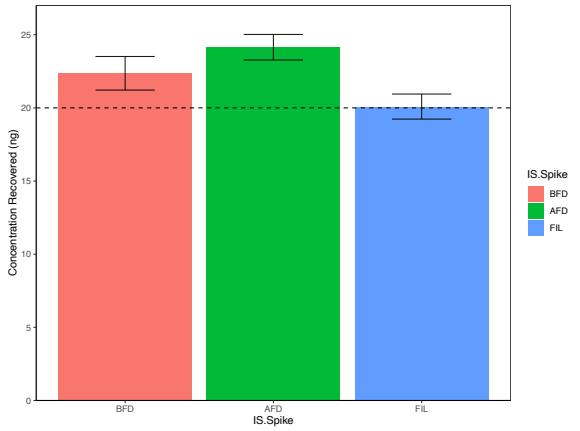

Figure 8.110 Metolachlor internal standard recovery before freeze-drying (BFD), after freeze-drying (AFD), and filter (FIL) stage of extractions. Bars are standard error, dashed line are amount spiked.

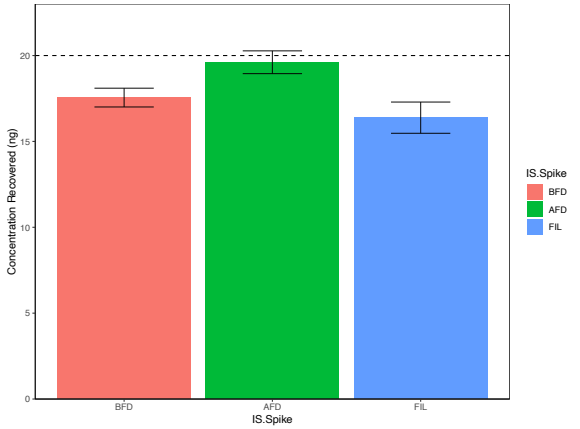

Figure 8.111 Malathion internal standard recovery before freeze-drying (BFD), after freeze-drying (AFD), and filter (FIL) stage of extractions. Bars are standard error, dashed line are amount spiked.

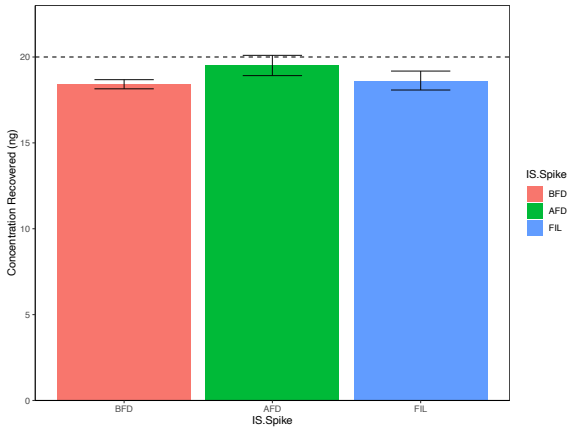

Figure 8.112 Fenoxycarb internal standard recovery before freeze-drying (BFD), after freeze-drying (AFD), and filter (FIL) stage of extractions. Bars are standard error, dashed line are amount spiked.

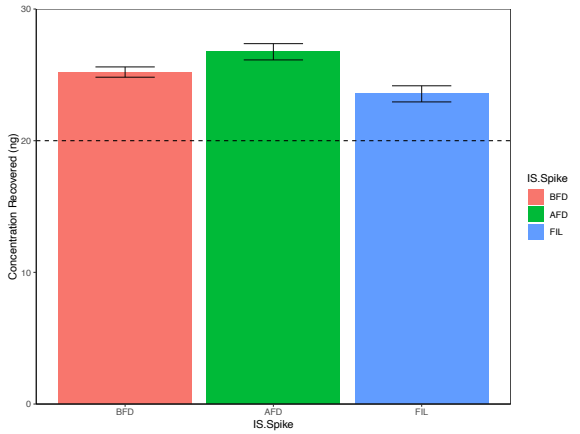

Figure 8.113 Tebufenozide internal standard recovery before freeze-drying (BFD), after freeze-drying (AFD), and filter (FIL) stage of extractions. Bars are standard error, dashed line are amount spiked.

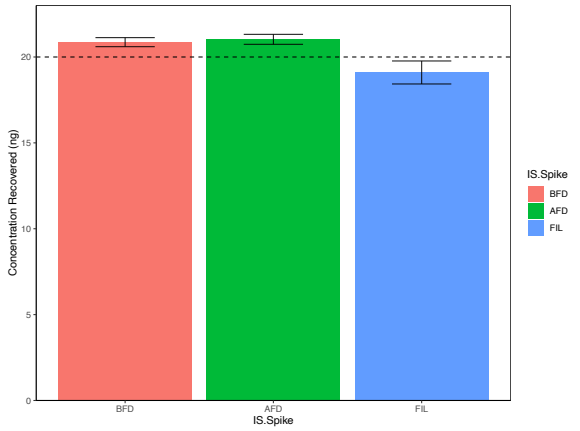

Figure 8.114 Fipronil internal standard recovery before freeze-drying (BFD), after freeze-drying (AFD), and filter (FIL) stage of extractions. Bars are standard error, dashed line are amount spiked.

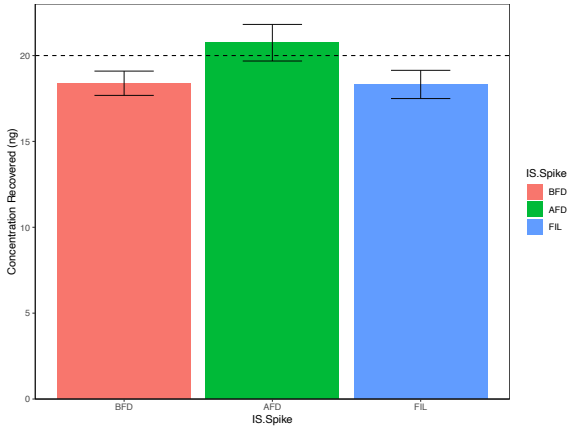

Figure 8.115 Tetrachlorvinphos internal standard recovery before freeze-drying (BFD), after freeze-drying (AFD), and filter (FIL) stage of extractions. Bars are standard error, dashed line are amount spiked.

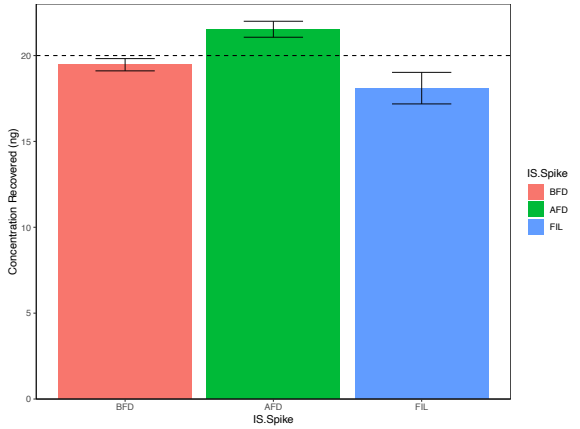

Figure 8.117 Imazamox internal standard recovery before freeze-drying (BFD), after freeze-drying (AFD), and filter (FIL) stage of extractions. Bars are standard error, dashed line are amount spiked.

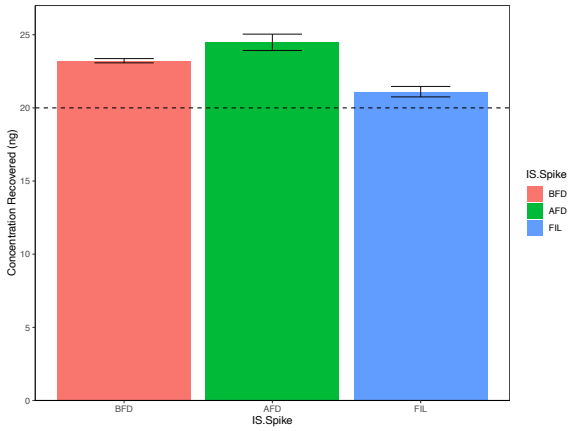

Figure 8.116 Propiconazole internal standard recovery before freeze-drying (BFD), after freeze-drying (AFD), and filter (FIL) stage of extractions. Bars are standard error, dashed line are amount spiked.

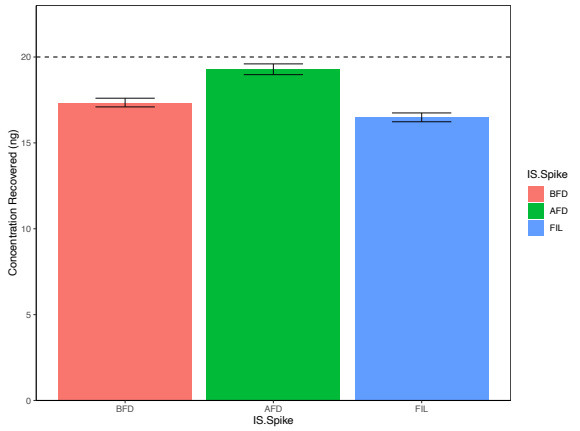

Figure 8.118 Buprofezin internal standard recovery before freeze-drying (BFD), after freeze-drying (AFD), and filter (FIL) stage of extractions. Bars are standard error, dashed line are amount spiked.

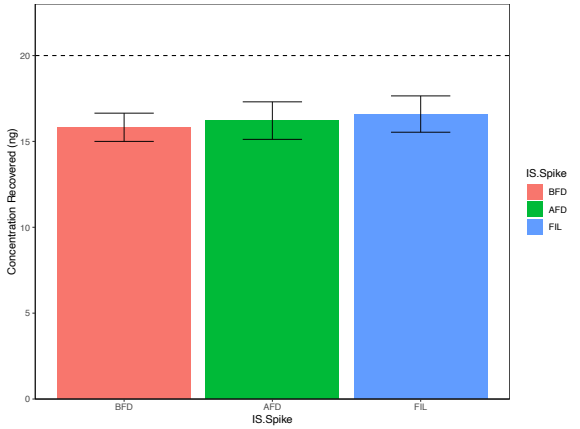

Figure 8.119 Kresoxim-Methyl internal standard recovery before freeze-drying (BFD), after freeze-drying (AFD), and filter (FIL) stage of extractions. Bars are standard error, dashed line are amount spiked.

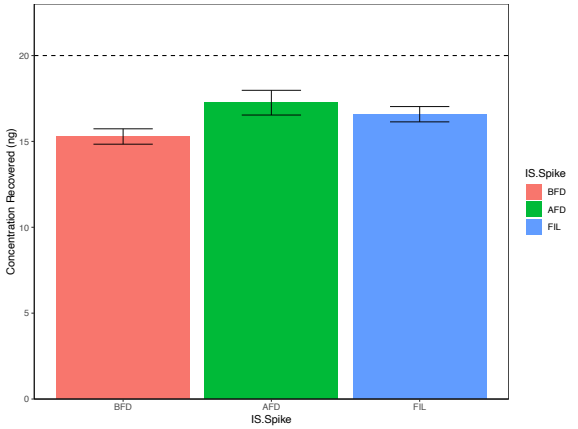

Figure 8.121 Benzodiflupyr internal standard recovery before freeze-drying (BFD), after freeze-drying (AFD), and filter (FIL) stage of extractions. Bars are standard error, dashed line are amount spiked.

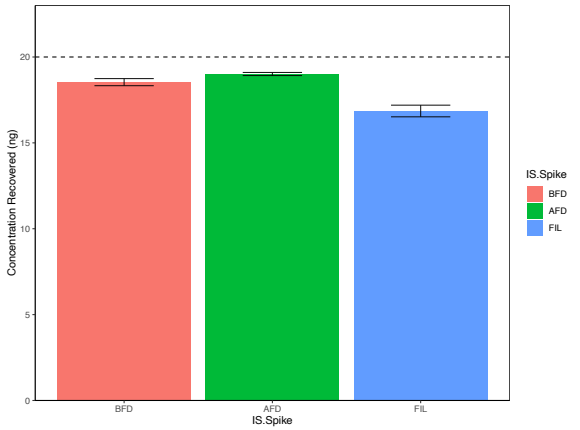

Figure 8.120 Diazinon internal standard recovery before freeze-drying (BFD), after freeze-drying (AFD), and filter (FIL) stage of extractions. Bars are standard error, dashed line are amount spiked.

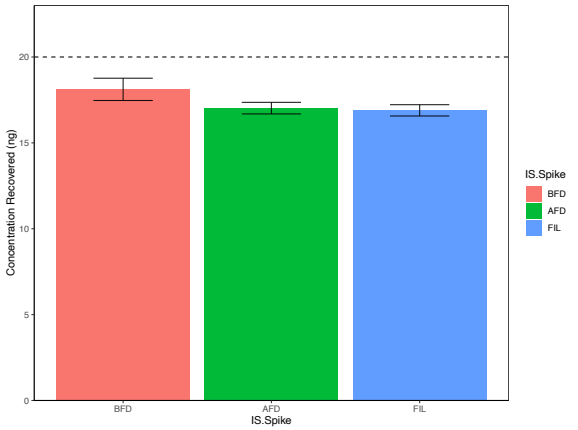

Figure 8.122 Prallethrin internal standard recovery before freeze-drying (BFD), after freeze-drying (AFD), and filter (FIL) stage of extractions. Bars are standard error, dashed line are amount spiked.

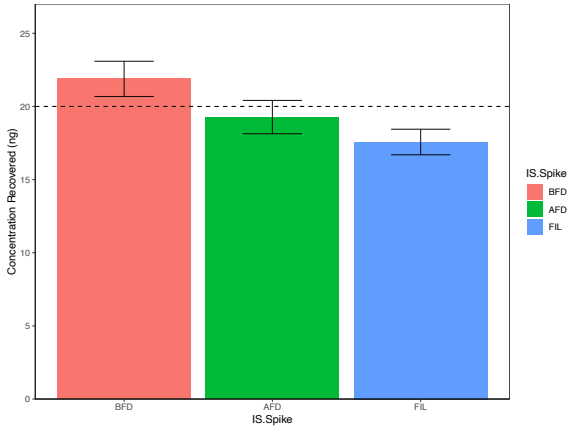

Figure 8.123 Pyrethrin II internal standard recovery before freeze-drying (BFD), after freeze-drying (AFD), and filter (FIL) stage of extractions. Bars are standard error, dashed line are amount spiked.

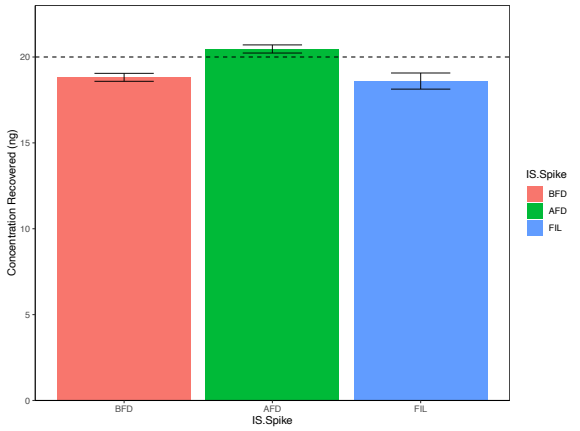

Figure 8.124 Pyraclostrobin internal standard recovery before freeze-drying (BFD), after freeze-drying (AFD), and filter (FIL) stage of extractions. Bars are standard error, dashed line are amount spiked.

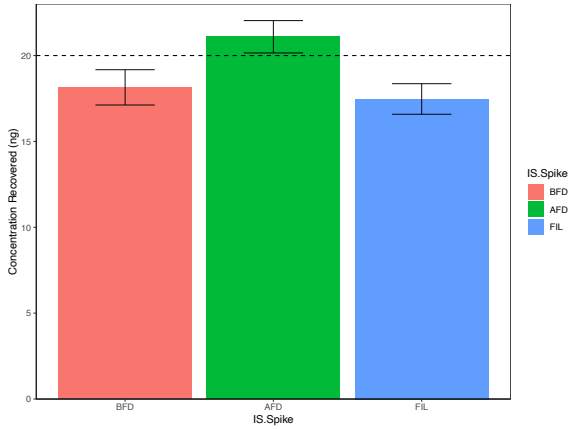

Figure 8.125 Clofentazine internal standard recovery before freeze-drying (BFD), after freeze-drying (AFD), and filter (FIL) stage of extractions. Bars are standard error, dashed line are amount spiked.

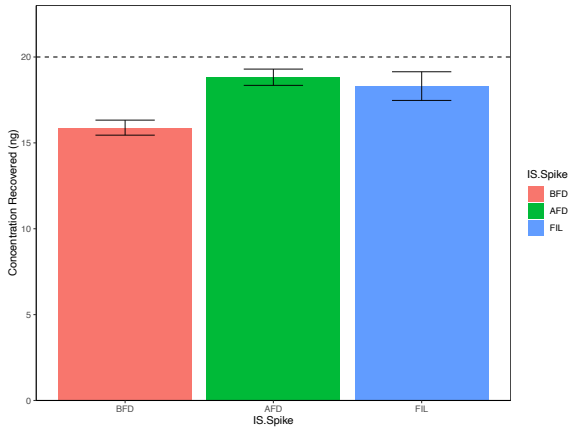

Figure 8.126 MGK 264 internal standard recovery before freeze-drying (BFD), after freeze-drying (AFD), and filter (FIL) stage of extractions. Bars are standard error, dashed line are amount spiked.

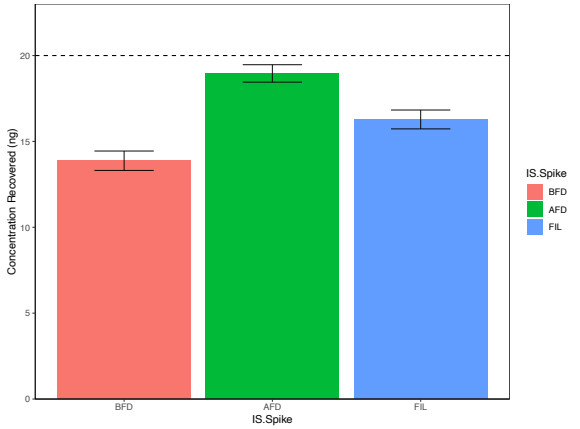

Figure 8.127 Coumaphos internal standard recovery before freeze-drying (BFD), after freeze-drying (AFD), and filter (FIL) stage of extractions. Bars are standard error, dashed line are amount spiked.

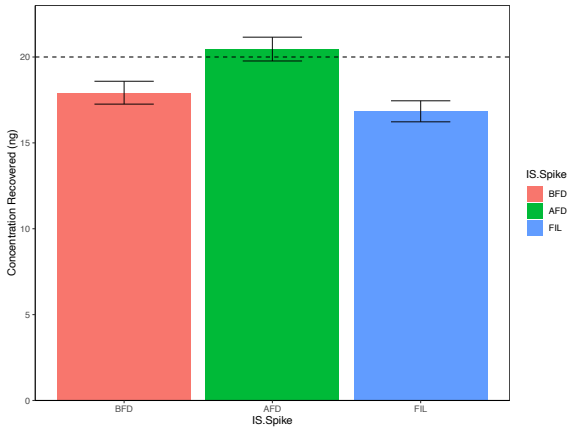

Figure 8.128 Teflubenzuron internal standard recovery before freeze-drying (BFD), after freeze-drying (AFD), and filter (FIL) stage of extractions. Bars are standard error, dashed line are amount spiked.

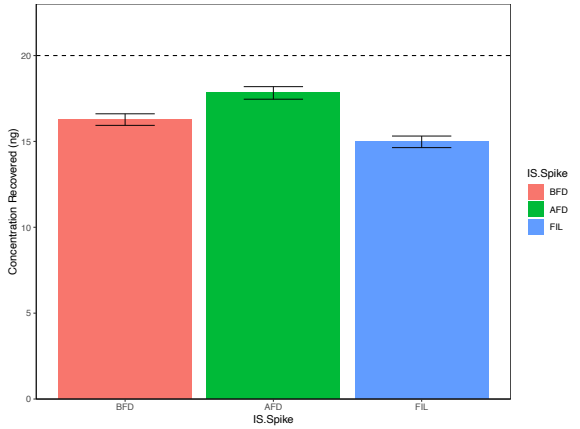

Figure 8.129 Allethrin internal standard recovery before freeze-drying (BFD), after freeze-drying (AFD), and filter (FIL) stage of extractions. Bars are standard error, dashed line are amount spiked.

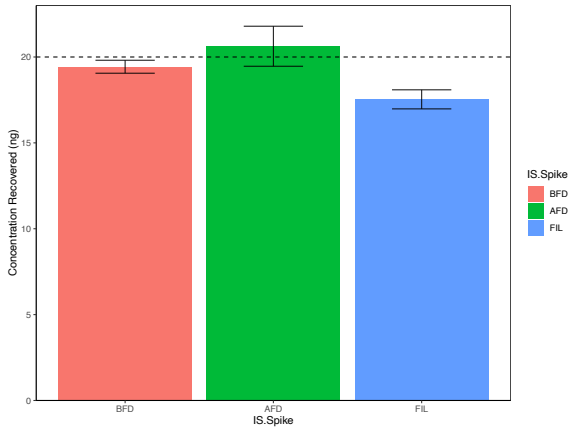

Figure 8.130 Tetramethrin internal standard recovery before freeze-drying (BFD), after freeze-drying (AFD), and filter (FIL) stage of extractions. Bars are standard error, dashed line are amount spiked.

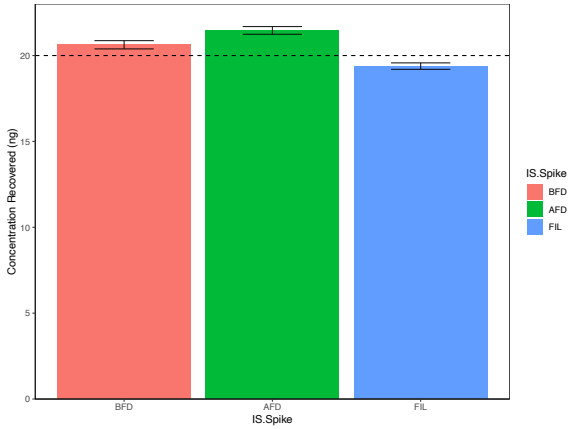

Figure 8.131 Etoxazole internal standard recovery before freeze-drying (BFD), after freeze-drying (AFD), and filter (FIL) stage of extractions. Bars are standard error, dashed line are amount spiked.

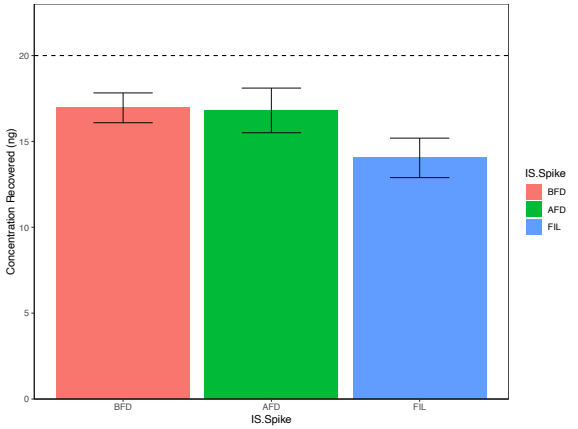

Figure 8.133 Chlorpyrifos internal standard recovery before freeze-drying (BFD), after freeze-drying (AFD), and filter (FIL) stage of extractions. Bars are standard error, dashed line are amount spiked.

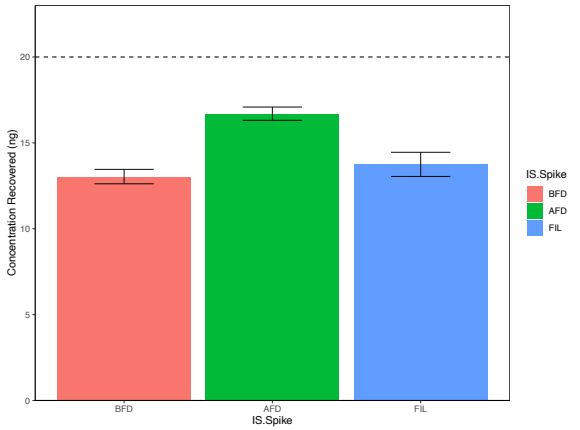

Figure 8.132 Pyrethrin I internal standard recovery before freeze-drying (BFD), after freeze-drying (AFD), and filter (FIL) stage of extractions. Bars are standard error, dashed line are amount spiked.

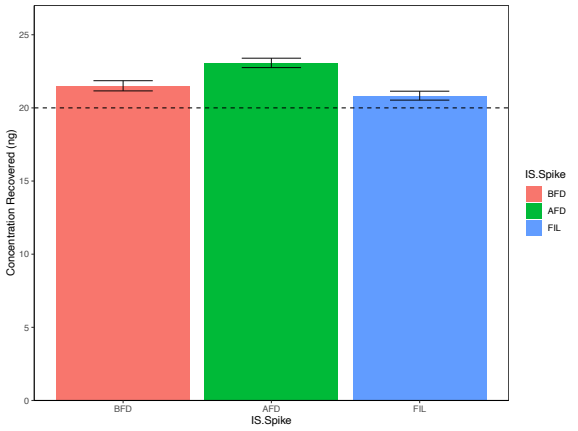

Figure 8.134 Spiromesifen internal standard recovery before freeze-drying (BFD), after freeze-drying (AFD), and filter (FIL) stage of extractions. Bars are standard error, dashed line are amount spiked.

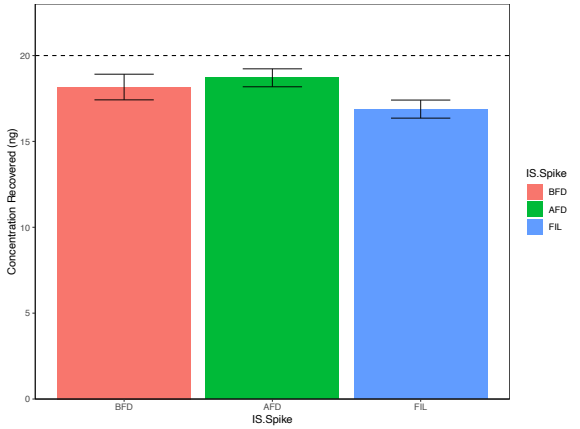

Figure 8.135 Hexythiazox internal standard recovery before freeze-drying (BFD), after freeze-drying (AFD), and filter (FIL) stage of extractions. Bars are standard error, dashed line are amount spiked.

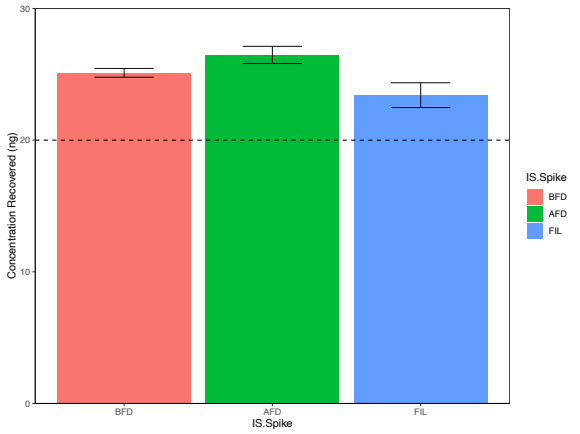

Figure 8.136 Spirodiclofen internal standard recovery before freeze-drying (BFD), after freeze-drying (AFD), and filter (FIL) stage of extractions. Bars are standard error, dashed line are amount spiked.

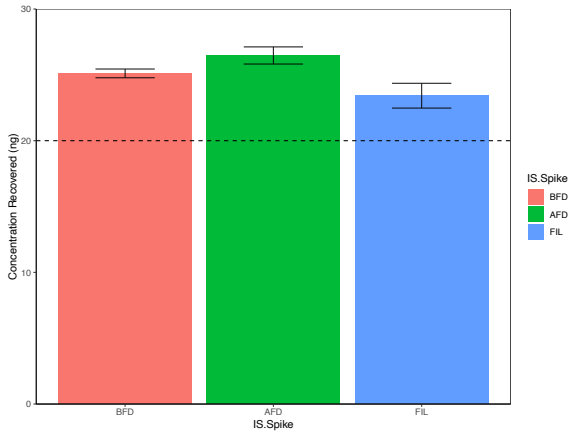

Figure 8.137 Pyridaben internal standard recovery before freeze-drying (BFD), after freeze-drying (AFD), and filter (FIL) stage of extractions. Bars are standard error, dashed line are amount spiked.

9. APPENDIX II: CHAPTER THREE VALIDATION OF QUPPE EXTRACTION

9.1 Chapter 3 QuPPe Method Limits of Detection/Quantification, Accuracy, Precision, and Matrix Effects Validation for Biobeds

Non-extractable pesticides: Acephate, Pirimicarb, Imazalil, Thiophanate-Methyl, Dodemorph, Sprioxamine, Fensulfothion, Cyantraniliprole, Cyprodinil, Fludioxinil, Spinosyn A, Spinosyn D, Phosmet, Spinetoram J, Imazamox, Buprofezin, Pyrethrin II, Clofentazine, Coumaphos, Teflubenzuron, Trifloxystrobin, Piperonyl-Butoxide, Fenpyroximate, Etoxazole, Pyrethrin I, Chlorpyrifos, Pyridaben, Resmethrin, Permethrin, Etofenprox, Bifenthrin, Acequinocyl, Methomyl.

Table 9.1 Method detection and quantification limits (MLD/MLQ), intra- and interday precision, and accuracy for QuPPe extraction method. **Bolded** values represent recoveries greater than 130%, *italicized* values represent recoveries below 70%, and – represent non-extractable pesticides with the method.

Pesticides	QuPPe				
	MLD/MLQ	Precision (Intra, Inter)		Accuracy	
		100 ppb	1,000 ppb	100 ppb	1,000ppb
	ng/g	% CV	% CV	% Rec	% Rec
Acephate	-	-	-	-	-
Oxamyl	2.2 / 7.3	3.9 / 8	5.6 / 7.1	**210**	83
Clopyralid	2.9 / 9.8	11 / 12	12 / 11	120	100
Dinotefuran	0.83 / 2.8	6.1 / 7.5	6.8 / 6.6	120	110
Methomyl	-	-	-	-	-
Thiamethoxam	1.1 / 3.8	5 / 8.3	6.6 / 6	96	100
Flonicamid	1 / 3.3	3.4 / 7.4	6.6 / 9	88	92
Pirimicarb	-	-	-	-	-
Clothianidin	2.1 / 7.1	4.2 / 10	8.7 / 9.1	96	87
Dimethoate	0.76 / 2.5	2.5 / 8.4	7.6 / 9.2	95	90
Imidacloprid	0.96 / 3.2	3.2 / 8.9	6.5 / 8.3	91	85
Mevinphos	0.57 / 1.9	3.5 / 9.2	7.3 / 10	84	80
Acetamiprid	0.43 / 1.4	3.6 / 7.5	8.1 / 8.7	90	89
Imazethapyr	1.2 / 3.9	11 / 10	11 / 10	94	90
Aldicarb	0.72 / 2.4	2.9 / 11	6.9 / 11	86	81
Thiacloprid	0.72 / 2.4	4.3 / 8.8	9.1 / 8.7	79	82
Dicamba	2.7 / 8.9	12 / 9.4	9.7 / 8.4	120	100
Propxur	1.5 / 4.9	2.8 / 5.8	4.8 / 5.7	110	110
Bentazon	1.6 / 5.2	8.7 / 10	9.5 / 7.9	120	110
Imazalil	-	-	-	-	-

Thiophanate-Methyl	-	-	-	-	-
Imazamox	-	-	-	-	-
Carbofuran	0.8 / 2.7	3.8 / 7.3	7 / 8.0	94	93
Atrazine	0.75 / 2.5	8.0 / 6.4	16 / 7.8	92	86
Carbaryl	1.6 / 5.4	4.7 / 6.8	9.9 / 10	79	88
2,4-D	3.0 / 10	8.9 / 17	16 / 12	120	96
Dodemorph	-	-	-	-	-
Fensulfothion	-	-	-	-	-
Cyantraniliprole	-	-	-	-	-
Metalaxyl	1 / 3.4	2.9 / 7.6	4.4 / 9.1	100	91
Spiroxamine	-	-	-	-	-
Paclubutrazol	0.54 / 1.8	2.8 / 8	7.6 / 9.5	79	85
Chlorantraniliprole	2.6 / 8.5	3.7 / 10	1.8 / 14	96	98
Fludioxinil	-	-	-	-	-
Cyprodinil	-	-	-	-	-
Spinosyn A	-	-	-	-	-
Spirotetramat	2.1 / 6.9	3.2 / 8.2	1.7 / 8.6	130	110
Dimetamorph I	1.3 / 4.4	7.8 / 6.0	8.7 / 5.4	85	87
Dimetamorph II	2.5 / 8.3	7.6 / 16	7.6 / 18	110	100
Fenhexamid	2.1 / 7.2	4.2 / 8.3	4.8 / 10	100	99
Ethoprophos	1.1 / 3.8	7.1 / 7.3	7.5 / 8.0	74	100
Myclobutanil	0.97 / 3.2	4.4 / 6.1	6.1 / 6.7	97	100
Spinosyn D	-	-	-	-	-
Phosmet	-	-	-	-	-
Azoxystrobin	1.3 / 4.4	5.5 / 9.2	10 / 6.6	95	100
Fluopyram	0.93 / 3.1	4.3 / 6.4	9.4 / 5.4	85	100
Metolachlor	1.9 / 6.3	5.4 / 7.5	6.6 / 9.2	110	110
Spinetoram J	-	-	-	-	-
Boscalid	9 / 30	8.1 / 8.2	14 / 9.1	110	99
Tebuconazole	2.5 / 8.4	4.7 / 7.6	5.8 / 5.3	100	97
Malathion	2.4 / 8.1	7.5 / 9.2	8.3 / 9.2	110	120
Fenoxycarb	1.8 / 6.1	7 / 9.1	6.5 / 5.3	77	100
Tebufenozide	1.6 / 5.4	8.4 / 5.6	11 / 6.3	110	120
Fipronil	1.4 / 4.7	9.5 / 4.6	9.3 / 7.4	96	110
Propiconazole	1.4 / 4.5	5.5 / 5.8	6.9 / 5.2	110	100
Tetrachlorvinphos	3.6 / 12	8.8 / 6.4	10 / 7.1	95	100
Benzovindiflupyr	2 / 6.6	9.7 / 7.4	12 / 7.8	110	100

Kresoxim-Methyl	3.5 / 12	7.2 / 22	5.8 / 21	110	96
Diazinon	0.55 / 1.8	10 / 6.5	9.2 / 7.7	110	74
Buprofenzin	-	-	-	-	-
Teflubenzuron	-	-	-	-	-
Pyrethin II	-	-	-	-	-
Pyraclostrobin	1.2 / 4	8.9 / 6	8 / 7.8	87	84
MGK-264	3.4 / 11	9.8 / 17	12 / 13	90	90
Piperonyl Butoxide	-	-	-	-	-
Clofentazine	-	-	-	-	-
Allethrin	1.2 / 4.1	6.9 / 8.2	7.5 / 5.3	92	98
Prallethrin	3.5 / 12	14 / 14	9.9 / 12	93	100
Trifloxystrobin	-	-	-	-	-
Tetramethrin	1.7 / 5.7	4.7 / 7.3	3.2 / 8.1	100	88
Etoxazole	-	-	-	-	-
Pyrethrin I	-	-	-	-	-
Chlorpyrifos	-	-	-	-	-
Hexythiazox	1.2 / 4.1	8.5 / 8.4	8.6 / 7.3	86	70
Spriomesifen	1.1 / 3.7	5 / 9.5	11 / 9.3	110	93
Spriodiclofen	1.9 / 6.3	9.1 / 7.9	8.9 / 6.4	99	92
Pyridaben	-	-	-	-	-
Resmethrin	-	-	-	-	-
Coumaphos	-	-	-	-	-
Permethrin [M+NH4]	-	-	-	-	-
Etofenprox	-	-	-	-	-
Bifenthrin	-	-	-	-	-
Acequinocyl	-	-	-	-	-
Fenpyroximate	-	-	-	-	-

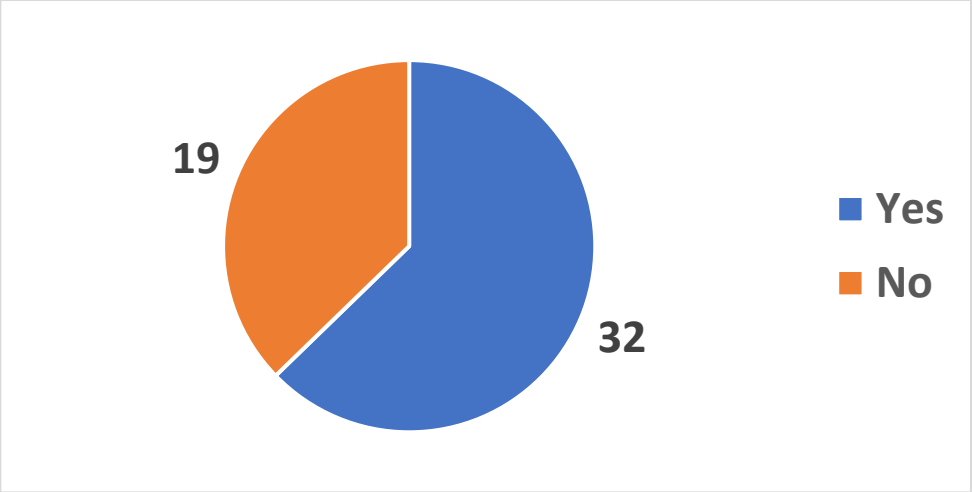

Figure 9.1 ANCOVA's conducted that were found to have a significant matrix effect vs. no effect.

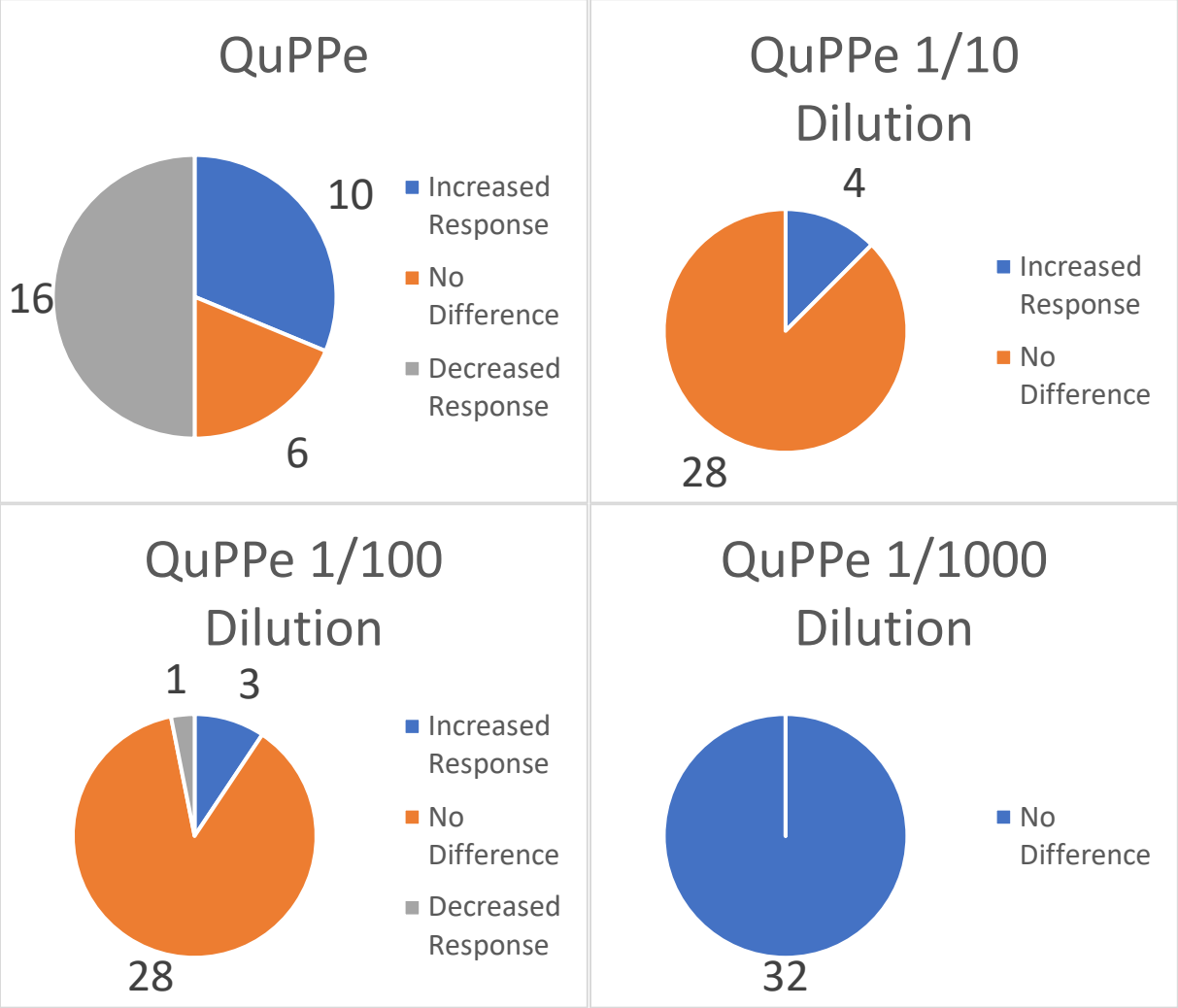

Figure 9.2 Summary of molecule responses from matrix effect found to be significant in an ANOVA and analyzed through Dunnett's test (control vs. matrix) for QuPPe.

Table 9.2 Table of ANOVA "Matrix" significance and *p*-values (*P*) and responses (R) from Dunnett's Post Hoc Test for QuPPe. + = increased molecule response, - = decreased molecule response, and 0 = molecule response did not change. Green highlights represent a significant matrix effect in the ANOVA *but* no significant differences found in Dunnett's test.

QuPPe Matrix vs Control Solutions	ANOVA "Matrix" Significance	Undiluted		1/10 Dilution		1/100 Dilution		1/1,000 Dilution	
		P	R	*P*	R	*P*	R	*P*	R
Dinotefuran	**<0.001**	**<0.0001**	+	**<0.0001**	+	**<0.0001**	+	0.6521	0
Oxamyl	**<0.001**	**<0.0001**	+	**<0.0001**	+	**<0.0001**	+	0.9767	0
Clopyralid	**<0.01**	*0.0013*	-	1	0	0.9616	0	0.9122	0
Thiamethoxam	**<0.001**	**<0.0001**	+	0.2635	0	0.9055	0	0.8698	0
Flonicamid	**<0.001**	*<0.0001*	-	0.9936	0	0.9606	0	1	0
Clothianidin	**<0.05**	0.3521	0	0.7053	0	0.1374	0	0.9658	0
Dimethoate	**<0.01**	**0.0003**	+	0.2018	0	0.617	0	0.6273	0
Imidacloprid	>0.05	NA	NA	NA	NA	NA	NA	NA	NA
Mevinphos	**<0.01**	**0.0003**	+	0.2018	0	0.617	0	0.6273	0
Acetamiprid	>0.05	NA	NA	NA	NA	NA	NA	NA	NA
Imazethapyr	>0.05	NA	NA	NA	NA	NA	NA	NA	NA
Aldicarb	**<0.05**	0.1345	0	0.0194	+	0.4175	0	0.9866	0
Thiacloprid	>0.05	NA	NA	NA	NA	NA	NA	NA	NA
Dicamba	>0.05	NA	NA	NA	NA	NA	NA	NA	NA
Propoxur	>0.05	NA	NA	NA	NA	NA	NA	NA	NA
Carbofuran	>0.05	NA	NA	NA	NA	NA	NA	NA	NA
Bentazon	**<0.01**	*0.0048*	-	0.5184	0	0.1097	0	0.604	0
Atrazine	>0.05	NA	NA	NA	NA	NA	NA	NA	NA
Carbaryl	**<0.001**	*0.0001*	-	0.8026	0	0.4206	0	0.947	0
Metalaxyl	**<0.01**	0.144	0	0.5366	0	0.9479	0	0.4604	0
2,4-D	>0.05	NA	NA	NA	NA	NA	NA	NA	NA
Paclobutrazol	**<0.001**	*0.0001*	-	0.9694	0	0.9998	0	0.9989	0
Chlorantraniliprole	>0.05	NA	NA	NA	NA	NA	NA	NA	NA

Dimetamorph II	>0.05	NA	NA	NA	NA	NA	NA	NA	NA
Spirotetramat	**<0.001**	**<0.0001**	+	**<0.0001**	+	**0.0116**	+	0.2582	0
Dimetamorph I	**<0.05**	0.9992	0	0.2825	0	0.0587	0	0.9985	0
Fenhexamid	**<0.05**	0.0704	0	0.9763	0	0.1585	0	0.9999	0
Ethoprophos	**<0.001**	*0.0002*	-	0.726	0	0.9169	0	0.6979	0
Myclobutanil	**<0.001**	*0.0003*	-	0.9819	0	0.9993	0	1	0
Tebuconazole	**<0.05**	**0.0413**	+	0.6347	0	0.9977	0	0.957	0
Azoxystrobin	**<0.05**	**0.0399**	+	0.3655	0	0.1494	0	0.9471	0
Fluopyram	**<0.001**	*0.0105*	-	0.55	0	0.5409	0	0.76	0
Boscalid	**<0.001**	**<0.0001**	+	0.9994	0	0.9972	0	0.9558	0
Metolachlor	>0.05	NA	NA	NA	NA	NA	NA	NA	NA
Malathion	**<0.01**	*0.0098*	-	0.9995	0	0.965	0	0.8728	0
Fenoxycarb	**<0.001**	*0.0008*	-	0.512	0	0.9806	0	0.7241	0
Tebufenozide	**<0.001**	*0.0001*	-	0.2429	0	0.9671	0	0.51	0
Fipronil	**<0.01**	*0.0202*	-	0.5948	0	0.6255	0	0.7882	0
Tetrachlorvinphos	**<0.01**	*0.0001*	-	0.3556	0	0.9672	0	0.9936	0
Propiconazole	>0.05	NA	NA	NA	NA	NA	NA	NA	NA
Kresoxim Methyl	>0.05	NA	NA	NA	NA	NA	NA	NA	NA
Diazinon	>0.05	NA	NA	NA	NA	NA	NA	NA	NA
Benzovindiflupyr	**<0.01**	*0.0001*	-	0.5209	0	0.8657	0	0.7988	0
Prallethrin	>0.05	NA	NA	NA	NA	NA	NA	NA	NA
Pyraclostrobin	>0.05	NA	NA	NA	NA	NA	NA	NA	NA
MGK-264	**<0.05**	*0.0068*	-	0.8933	0	0.9919	-	0.4237	0
Allethrin	**<0.05**	0.0707	0	0.9934	0	0.9031	0	0.975	0
Tetramethrin	>0.05	NA	NA	NA	NA	NA	NA	NA	NA
Spiromesifen	>0.05	NA	NA	NA	NA	NA	NA	NA	NA
Hexythiazox	**<0.001**	*<0.0001*	-	0.8383	0	0.3881	0	0.9604	0
Spirodiclofen	**<0.001**	**0.0041**	+	0.7878	0	0.4188	0	0.9537	0

Table 9.3 Transformation method, Shapiro-Wilk Test for normality, Bresuch-Pagan Test for homoscedascity, and addition vs. interaction model ANOVA test on model residuals; notes for all compounds extractable with the QuPPe extraction method. Blue highlights represent a need to separate matrices due to non-normality of residuals. *Italicized* values only had detects at 20 ppb, so were proceeded with an ANOVA model in Table. 9.4. NA = not applicable.

Compound	Transformation	Normality	Homoscedascity	Slope Homogeneity	Notes
Dinotefuran	Cube Root	0.2638	0.9685	0.05747	5 ppb removed (Heteroscedascity)
Oxamyl	Log10	0.2393	0.955	0.1275	
Clopyralid	Square Root	0.7937	0.9122	0.9035	
Thiamethoxam	Log10	0.5839	0.2322	0.6734	
Flonicamid	Square Root	0.6504	0.2083	0.3625	
Clothianidin	Log10	0.1917	0.6913	0.3288	
Dimethoate	Square Root	0.6894	0.3324	0.4979	
Imidacloprid	Square Root	0.834	0.5259	0.7112	
Mevinphos	Cube Root	0.6909	0.5447	0.9453	
Acetamiprid	Cube Root	0.09122	0.9182	0.8658	
Imazethapyr	Log10	0.1557	0.2318	0.9177	
Aldicarb	Square Root	0.8216	0.9986	0.6403	
Thiacloprid	Square Root	0.3563	0.8658	0.9893	
Dicamba	Square Root	0.1906	0.2863	0.7136	
Propoxur	Square Root	0.9432	0.403	0.9684	
Carbuforuan	Square Root	0.6932	0.4641	0.6672	
Bentazon	Square Root	0.1504	0.949	0.7359	
Atrazine	Cube Root	0.3354	0.379	0.5901	
Carbaryl	Log10	0.1758	0.1447	0.4177	5 ppb removed (Heteroscedascity)
Metalaxyl	Square Root	0.6495	0.3619	0.2135	
2,4-D	Square Root	0.1171	0.1095	0.7441	

Paclobutrazol	Cube Root	0.09082	0.9453	0.7963	
Chlorantraniliprole	Square Root	0.2868	0.5313	0.9771	5 ppb removed (Heteroscedascity)
Dimetamorph II	Square Root	0.2343	0.1553	0.6787	5 ppb removed (No Response)
Spirotetramat	Square Root	0.4614	0.9012	0.2239	
Dimetamorph I	Square Root	0.2045	0.4405	0.8678	
Fenhexamid	Square Root	0.7702	0.9071	0.4372	
Ethoprophos	Cube Root	0.1742	0.2912	0.6288	
Myclobutanil	Square Root	0.7221	0.4479	0.6034	
Tebuconazole	Square Root	0.9352	0.6311	0.4567	
Azoxystrobin	Log10	0.7038	0.1299	0.1495	
Fluopyram	Square Root	0.3128	0.6221	0.4548	
Boscalid	Square Root	0.6676	0.07423	0.2918	
Metolachlor	Log10	0.1266	0.09417	0.1241	
Malathion	Cube Root	0.6417	0.6666	0.49	
Fenoxycarb	Square Root	0.4105	0.9689	0.7966	
Tebufenozide	Square Root	0.5372	0.1739	0.4449	
Fipronil	Square Root	0.9286	0.5978	0.1228	
Tetrachlorvinphos	Square Root	0.796	0.755	0.8365	
Propiconazole	Log10	0.232	0.6513	0.7118	
Kresoxim-Methyl	*Cube Root*	*NA*	*NA*	*NA*	*Response at 20 ppb*
Diazinon	Cube Root	0.2185	0.98	0.6672	
Benzodiflupyr	Cube Root	0.7285	0.9451	0.2498	
Prallethrin	Cube Root	0.3709	0.7951	0.3009	
Pyraclostrobin	Cube Root	0.2245	0.7216	0.6628	
MGK-264	Cube Root	0.6442	0.4054	0.1299	
Allethrin	Cube Root	0.6125	0.1576	0.3346	

Tetramethrin	Cube Root	0.2722	0.3781	0.2357	5 ppb removed (No Response)
Spiromesifen	Cube Root	0.606	0.948	0.7812	
Hexythiazox	Log10	0.06024	0.8808	0.6251	
Spirodiclofen	Cube Root	0.2427	0.19486	0.8414	5 ppb removed (No Response)

Table 9.4 Transformation method, Shapiro-Wilk Test for normality, and Bartlett's Test for homogeneity of variance for compounds extractable with the QuPPe extraction method and detected at 20 ppb only.

Compound	Transformation	Normality					Homogeneity of Variance
		Methanol/ Water	QuPPer Extract				
		Control	0 Dil	10 Dil	100 Dil	1,000 Dil	
Kresoxim-Methyl	Cube Root	0.2273	0.3485	0.7962	0.6411	0.7558	0.05255

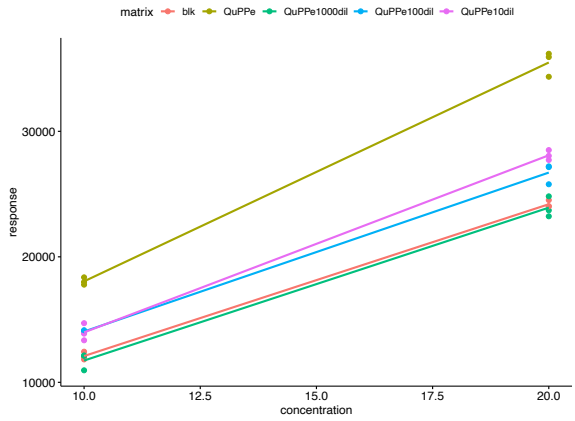

Figure 9.3 Dinotefuran response across concentrations in a 1:1 methanol/water vs QuPPe extracts.

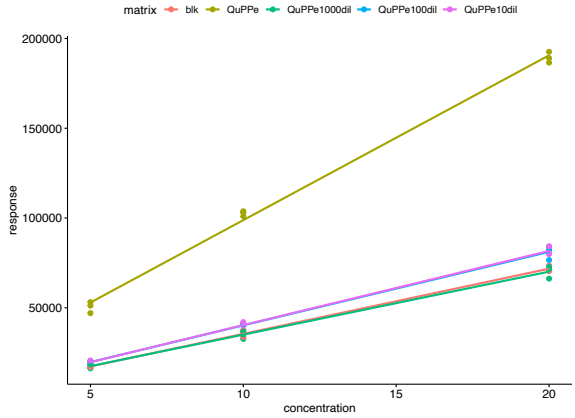

Figure 9.4 Oxamyl response across concentrations in a 1:1 methanol/water vs QuPPe extracts.

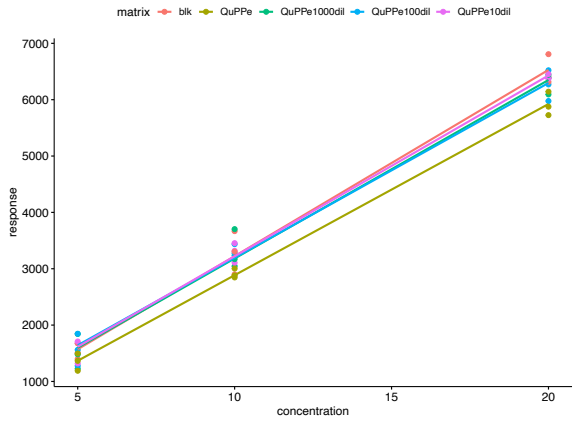

Figure 9.5 Clopyralid response across concentrations in a 1:1 methanol/water vs QuPPe extracts.

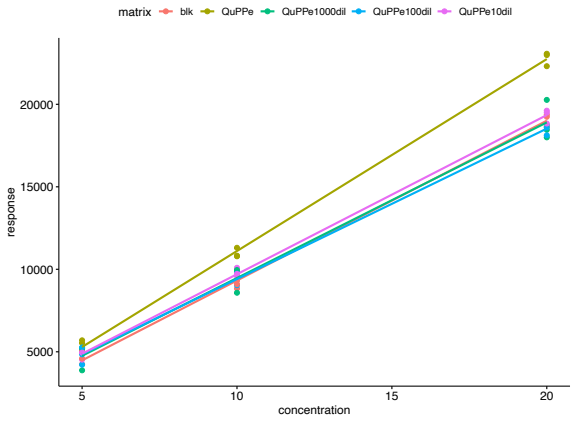

Figure 9.6 Thiamethoxam response across concentrations in a 1:1 methanol/water vs QuPPe extracts.

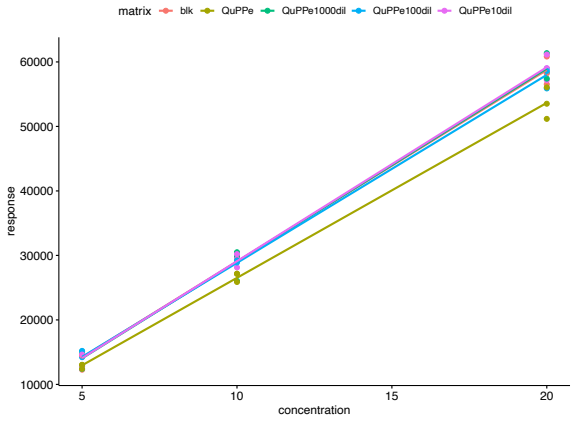

Figure 9.7 Flonicamid response across concentrations in a 1:1 methanol/water vs QuPPe extracts.

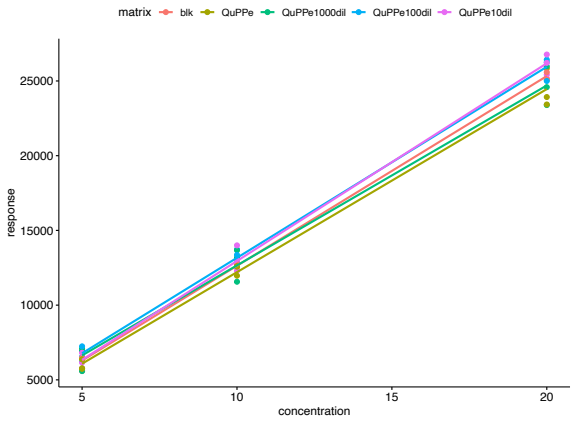

Figure 9.8 Clothianidin response across concentrations in a 1:1 methanol/water vs QuPPe extracts.

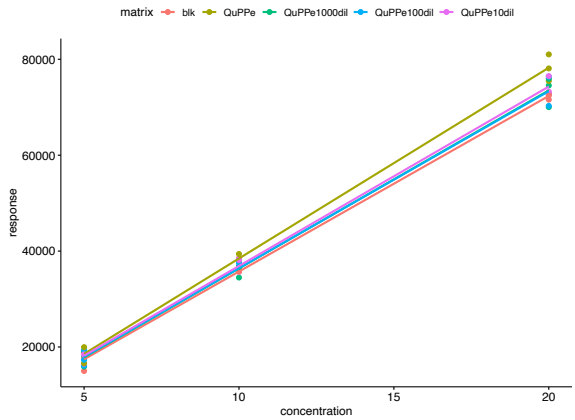

Figure 9.9 Dimethoate response across concentrations in a 1:1 methanol/water vs QuPPe extracts.

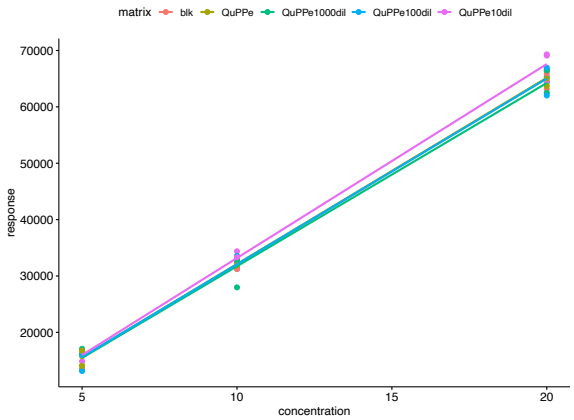

Figure 9.12 Acetamiprid response across concentrations in a 1:1 methanol/water vs QuPPe extracts.

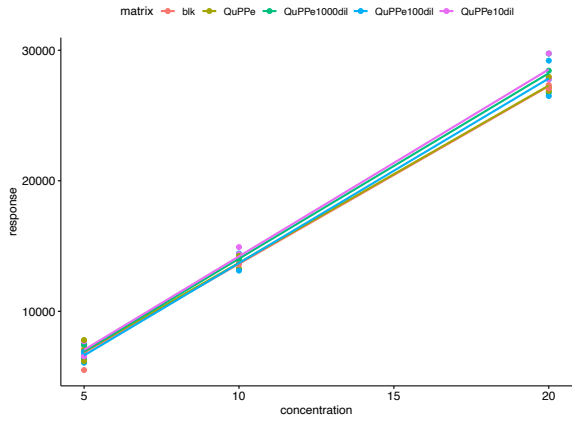

Figure 9.10 Imidacloprid response across concentrations in a 1:1 methanol/water vs QuPPe extracts.

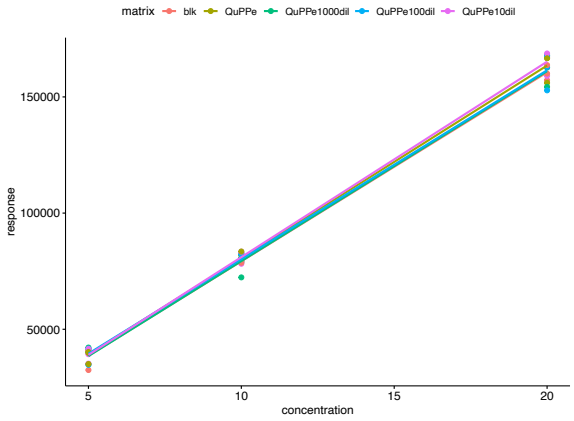

Figure 9.13 Imazethapyr response across concentrations in a 1:1 methanol/water vs QuPPe extracts.

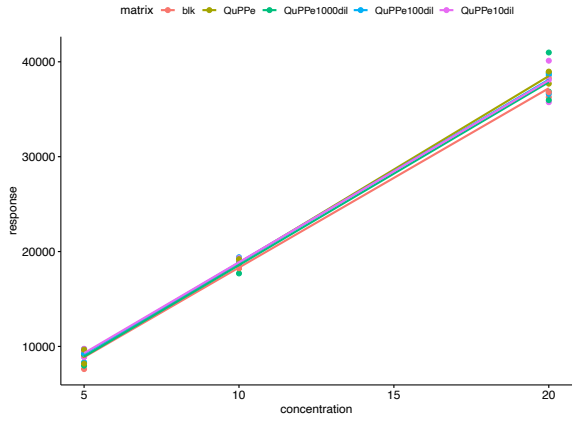

Figure 9.11 Mevinphos response across concentrations in a 1:1 methanol/water vs QuPPe extracts.

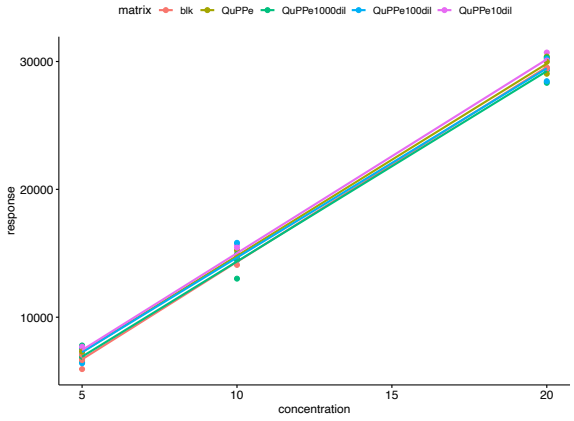

Figure 9.14 Aldicarb response across concentrations in a 1:1 methanol/water vs QuPPe extracts.

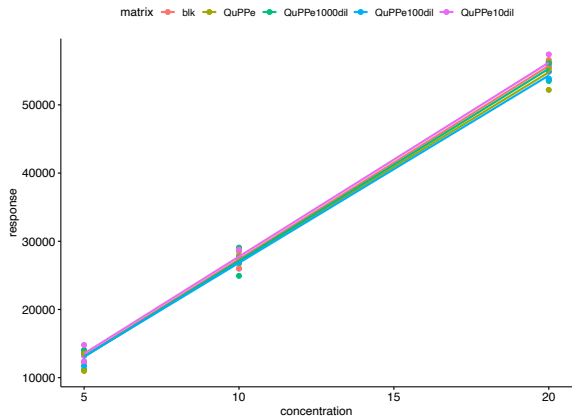

Figure 9.15 Thiacloprid response across concentrations in a 1:1 methanol/water vs QuPPe extracts.

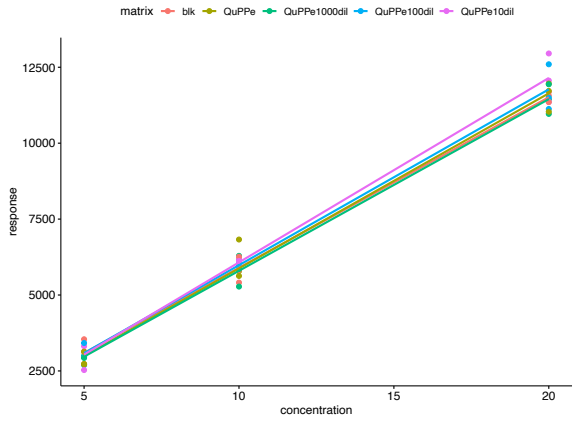

Figure 9.16 Dicamba response across concentrations in a 1:1 methanol/water vs QuPPe extracts.

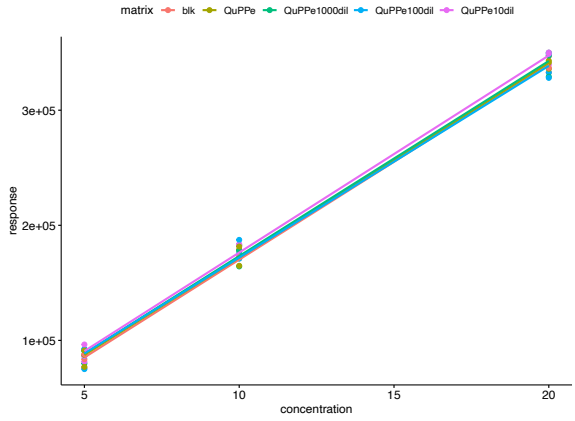

Figure 9.17 Propoxur response across concentrations in a 1:1 methanol/water vs QuPPe extracts.

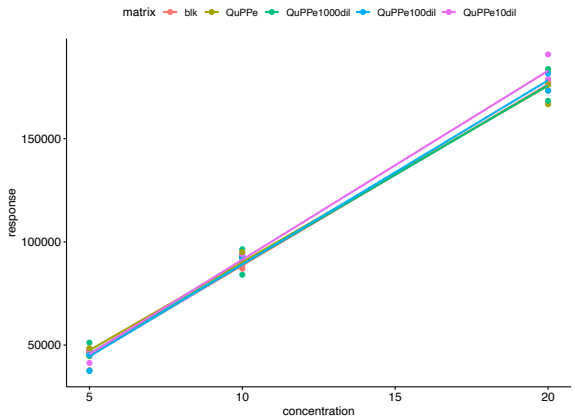

Figure 9.18 Carbofuran response across concentrations in a 1:1 methanol/water vs QuPPe extracts.

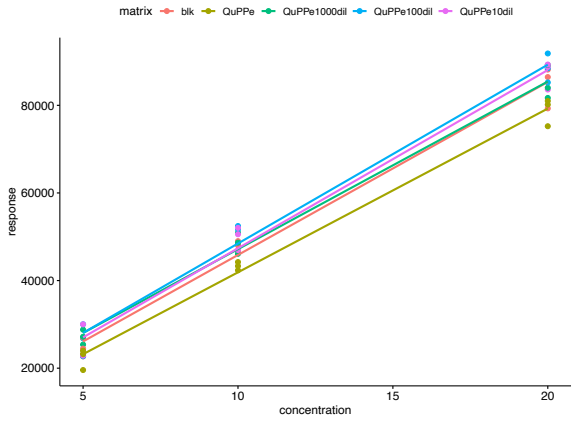

Figure 9.19 Bentazon response across concentrations in a 1:1 methanol/water vs QuPPe extracts.

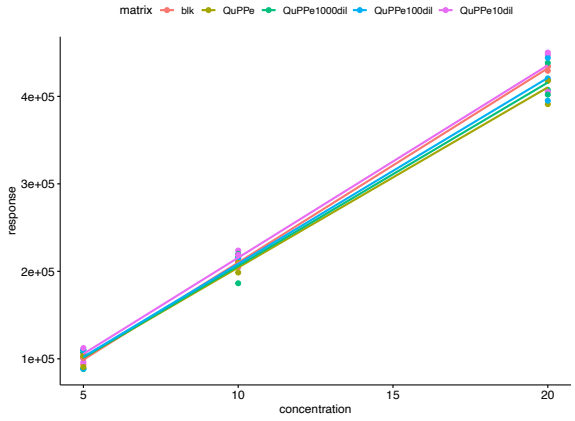

Figure 9.20 Atrazine response across concentrations in a 1:1 methanol/water vs QuPPe extracts.

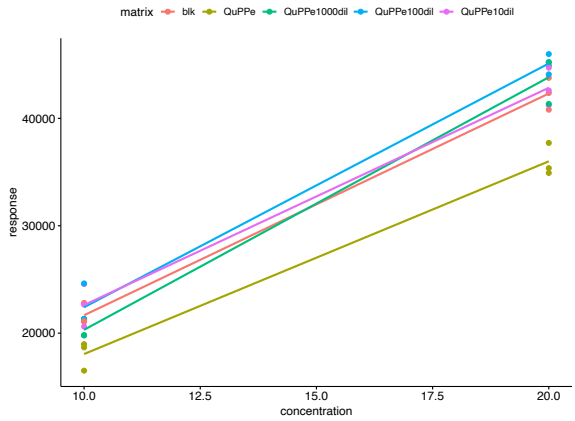

Figure 9.21 Carbaryl response across concentrations in a 1:1 methanol/water vs QuPPe extracts.

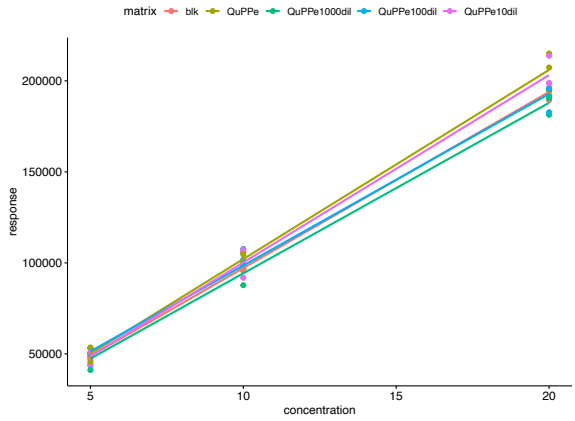

Figure 9.22 Metalaxyl response across concentrations in a 1:1 methanol/water vs QuPPe extracts.

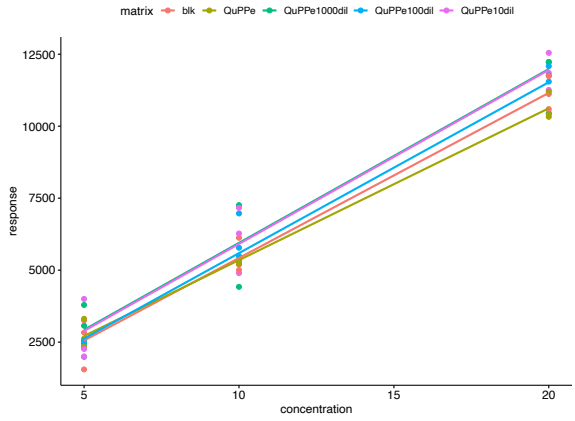

Figure 9.23 2,4-D response across concentrations in a 1:1 methanol/water vs QuPPe extracts.

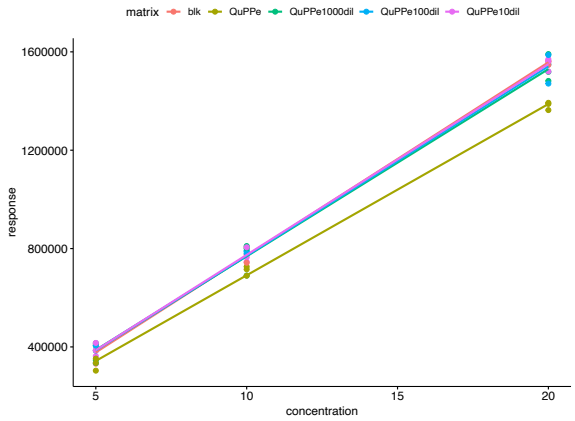

Figure 9.24 Paclobutrazol response across concentrations in a 1:1 methanol/water vs QuPPe extracts.

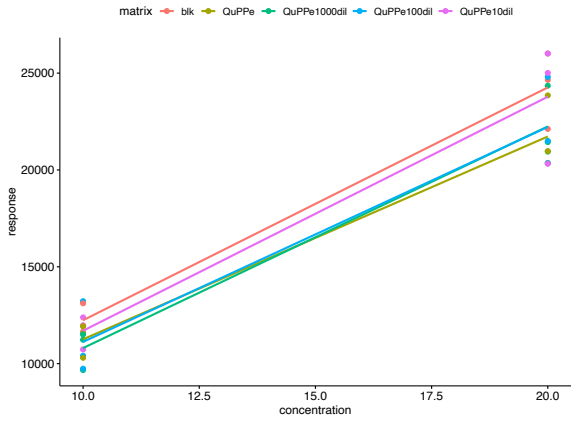

Figure 9.25 Chlorantraniliprole response across concentrations in a 1:1 methanol/water vs QuPPe extracts.

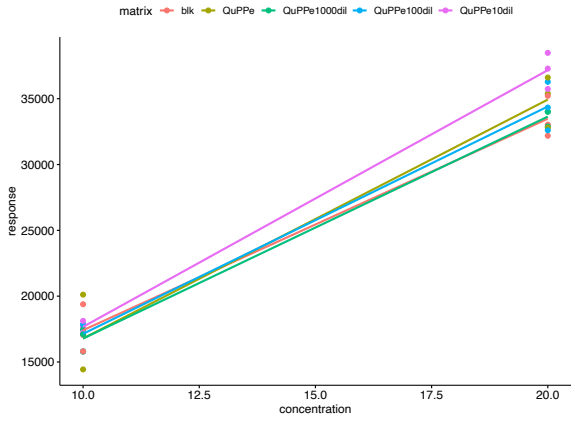

Figure 9.26 Dimethomorph II response across concentrations in a 1:1 methanol/water vs QuPPe extracts.

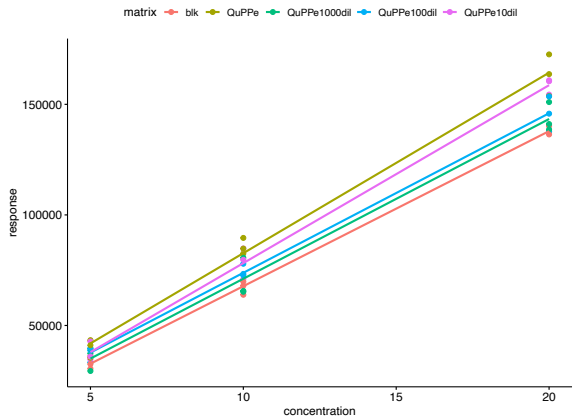

Figure 9.27 Spirotetramat response across concentrations in a 1:1 methanol/water vs QuPPe extracts.

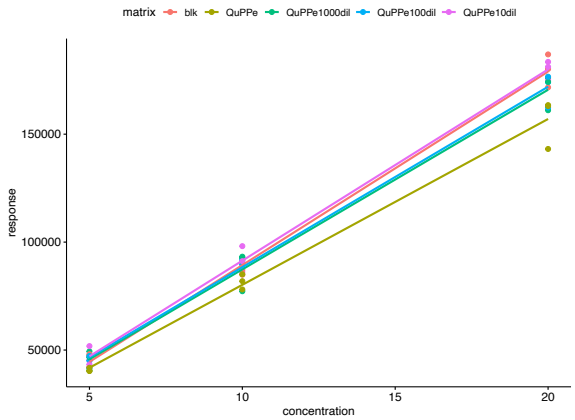

Figure 9.30 Ethoprophos response across concentrations in a 1:1 methanol/water vs QuPPe extracts.

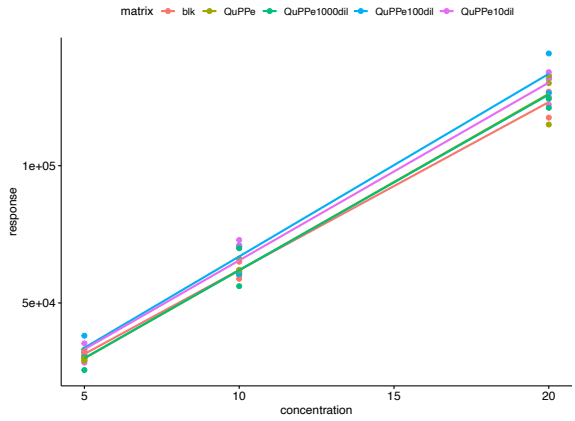

Figure 9.28 Dimethomorph I response across concentrations in a 1:1 methanol/water vs QuPPe extracts.

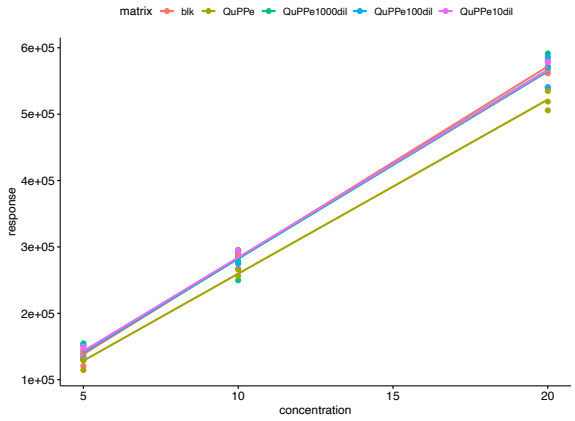

Figure 9.31 Myclobutanil response across concentrations in a 1:1 methanol/water vs QuPPe extracts.

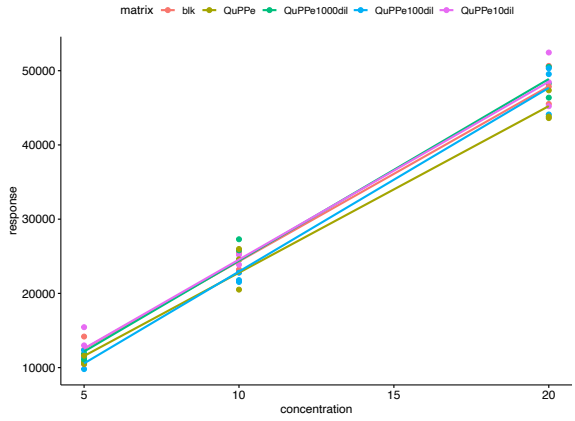

Figure 9.29 Fenhexamid response across concentrations in a 1:1 methanol/water vs QuPPe extracts.

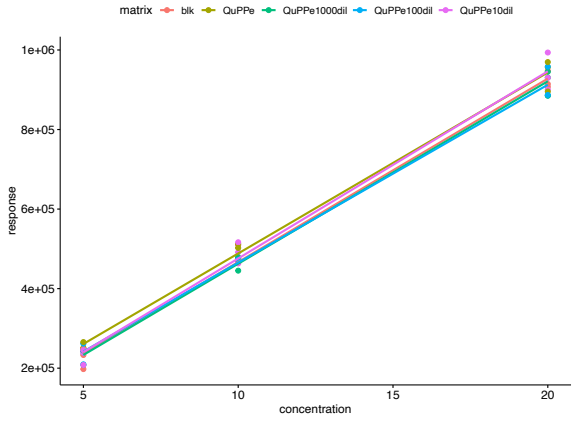

Figure 9.32 Tebuconazole response across concentrations in a 1:1 methanol/water vs QuPPe extracts.

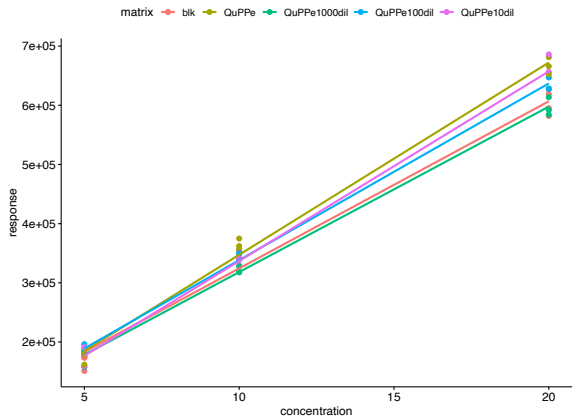

Figure 9.33 Azoxystrobin response across concentrations in a 1:1 methanol/water vs QuPPe extracts.

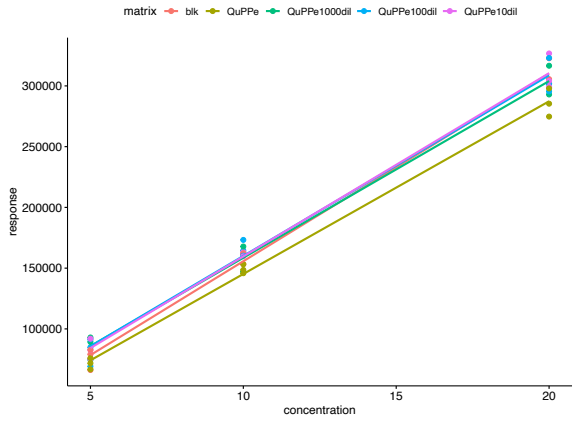

Figure 9.34 Fluopyram response across concentrations in a 1:1 methanol/water vs QuPPe extracts.

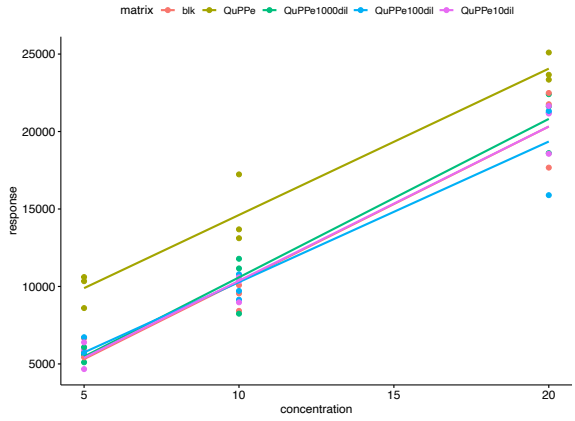

Figure 9.35 Boscalid response across concentrations in a 1:1 methanol/water vs QuPPe extracts.

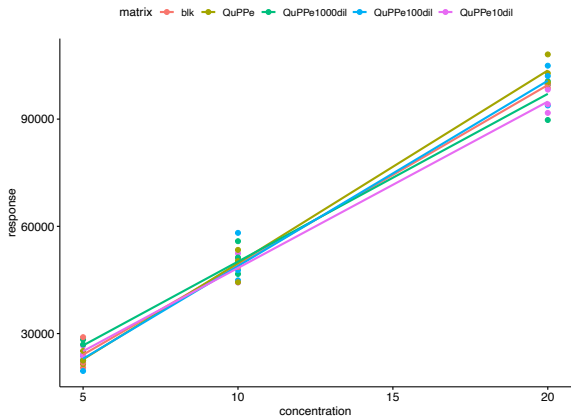

Figure 9.36 Metolachlor response across concentrations in a 1:1 methanol/water vs QuPPe extracts.

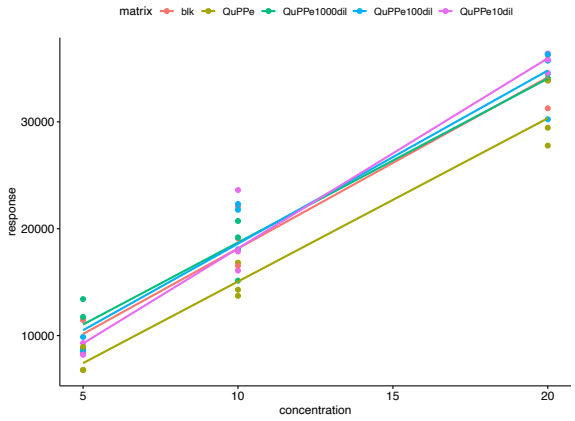

Figure 9.37 Malathion response across concentrations in a 1:1 methanol/water vs QuPPe extracts.

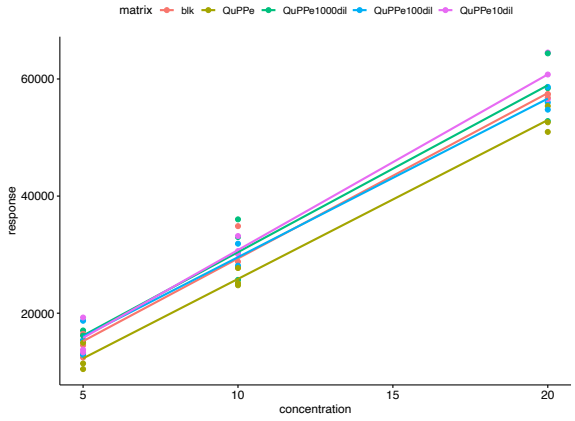

Figure 9.38 Fenoxycarb response across concentrations in a 1:1 methanol/water vs QuPPe extracts.

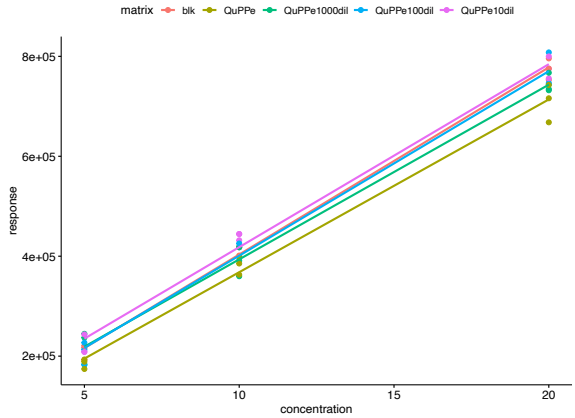

Figure 9.39 Tebufenozide response across concentrations in a 1:1 methanol/water vs QuPPe extracts.

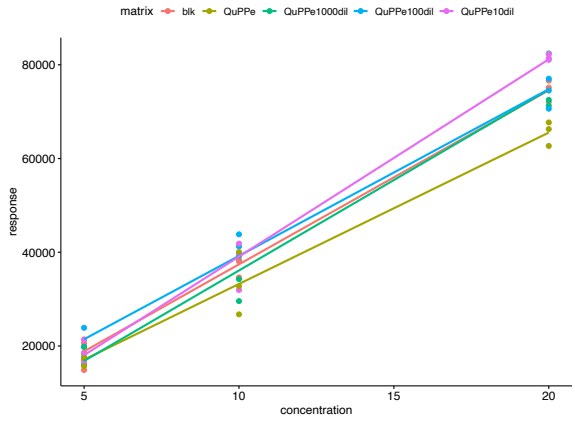

Figure 9.40 Fipronil response across concentrations in a 1:1 methanol/water vs QuPPe extracts.

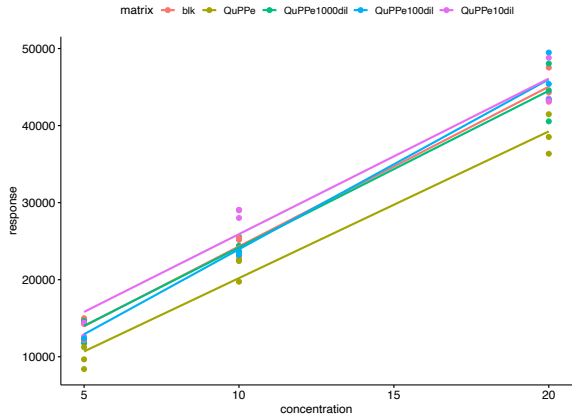

Figure 9.41 Tetrachlorvinphos response across concentrations in a 1:1 methanol/water vs QuPPe extracts.

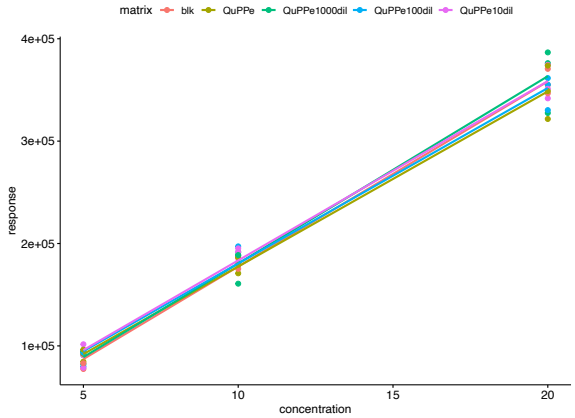

Figure 9.42 Propiconazole response across concentrations in a 1:1 methanol/water vs QuPPe extracts.

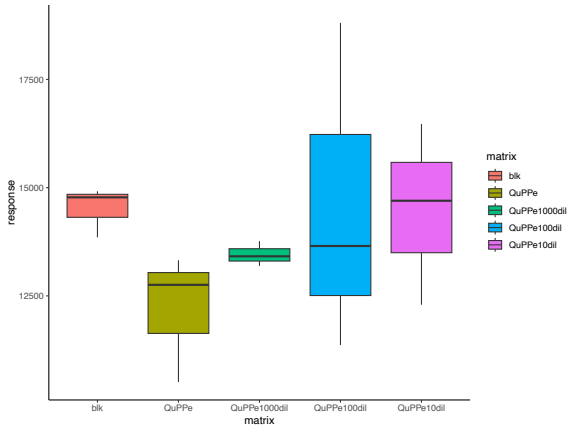

Figure 9.43 Kresoxim-Methyl response at 20 ppb in a 1:1 methanol/water vs QuPPe extracts.

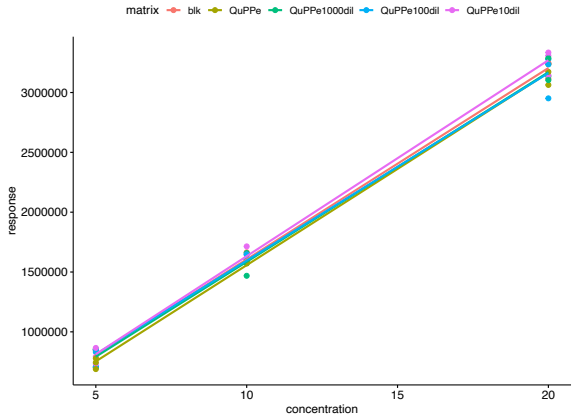

Figure 9.44 Diazinon response across concentrations in a 1:1 methanol/water vs QuPPe extracts.

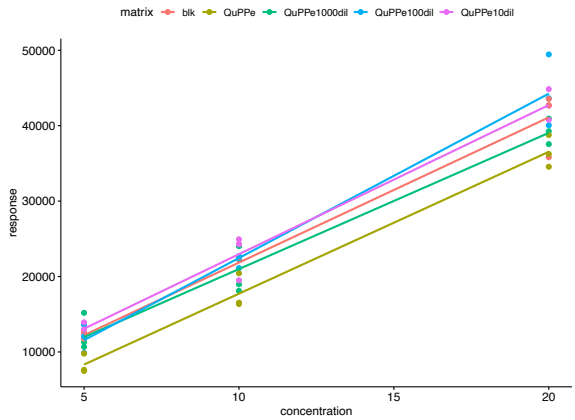

Figure 9.45 Benzovindiflupyr response across concentrations in a 1:1 methanol/water vs QuPPe extracts.

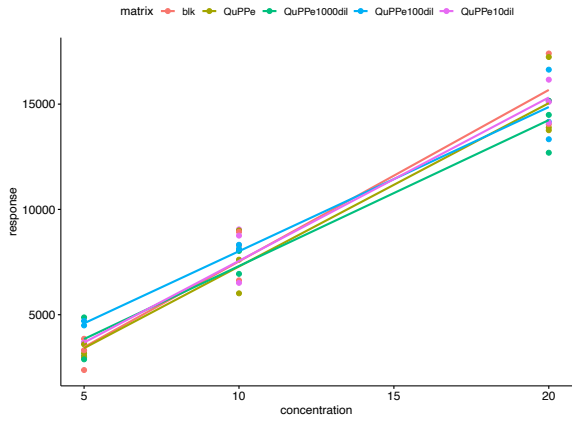

Figure 9.46 Prallethrin response across concentrations in a 1:1 methanol/water vs QuPPe extracts.

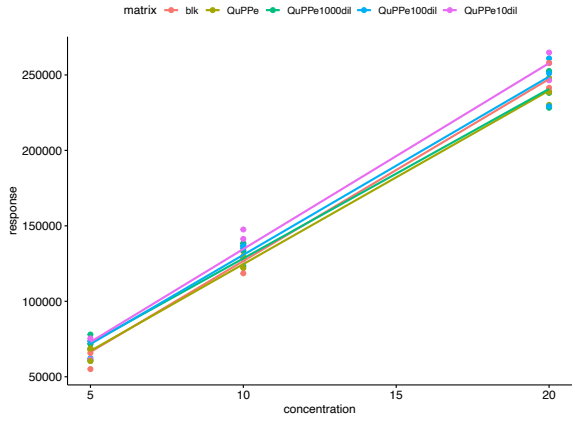

Figure 9.47 Pyraclostrobin response across concentrations in a 1:1 methanol/water vs QuPPe extracts.

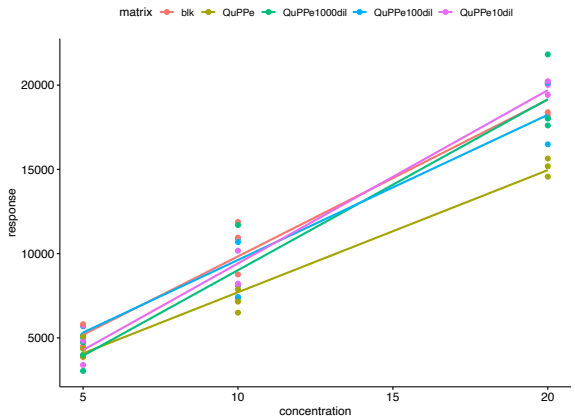

Figure 9.48 MGK 264 response across concentrations in a 1:1 methanol/water vs QuPPe extracts.

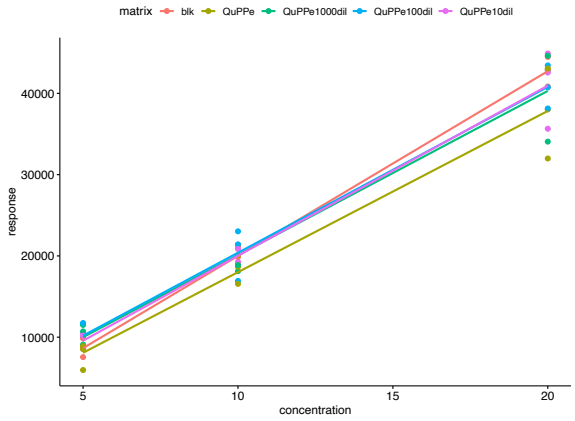

Figure 9.49 Allethrin response across concentrations in a 1:1 methanol/water vs QuPPe extracts.

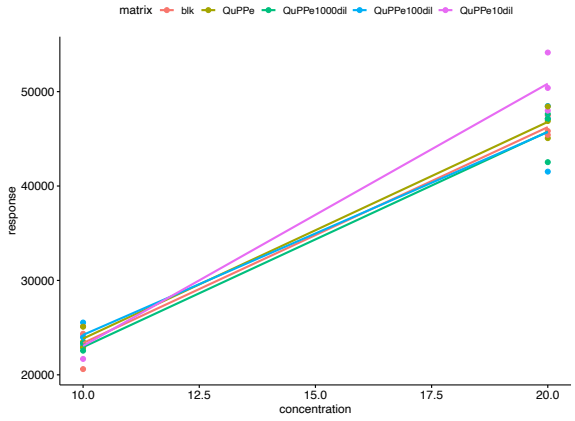

Figure 9.50 Tetramethrin response across concentrations in a 1:1 methanol/water vs QuPPe extracts.

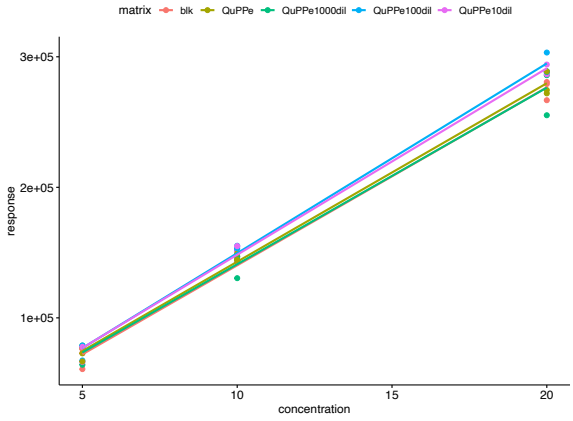

Figure 9.51 Spiromesifen response across concentrations in a 1:1 methanol/water vs QuPPe extracts.

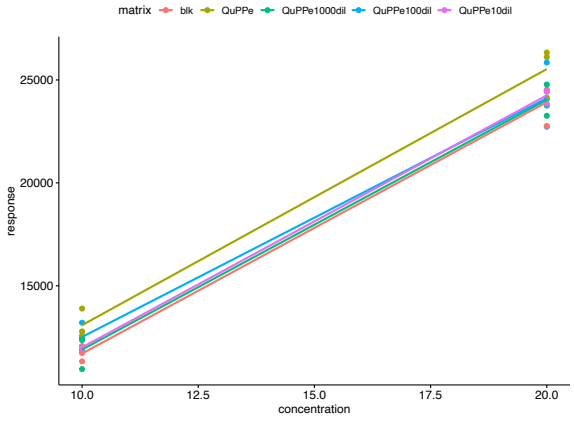

Figure 9.53 Spirodiclofen response across concentrations in a 1:1 methanol/water vs QuPPe extracts.

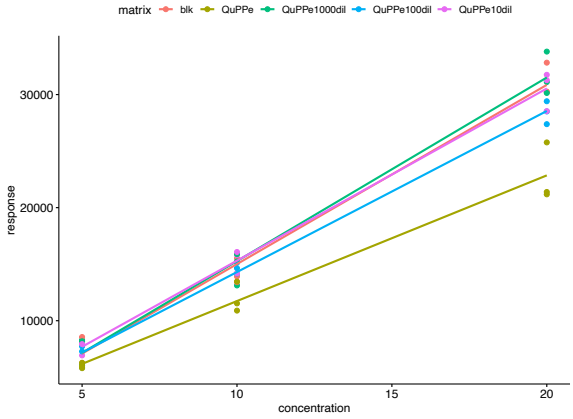

Figure 9.52 Hexythiazox response across concentrations in a 1:1 methanol/water vs QuPPe extracts.

9.2 Chapter 3 QuPPe Internal Standard Losses for Biobeds

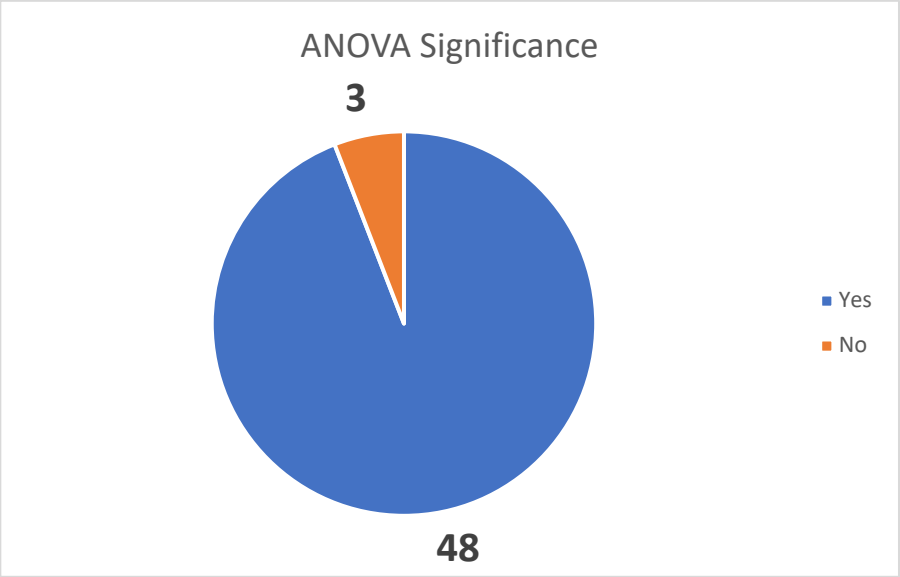

Figure 9.54 Quick Summary of freeze-drying losses detected by an ANOVA for QuPPe.

Table 9.5 Table of internal standard loss ANOVA *p*-values (*P*) and *p*-values from the Tukey's Post Hoc Test for QuPPe.

Compound	ANOVA	BFD v AFD	AFD v FIL	BFD v FIL
Dinotefuran	0.000104	0.6818	0.0002	0.00006
Oxamyl	0.0224	0.9457	0.0519	0.0295
Clopyralid	0.000145	0.9448	0.0005	0.0003
Thiamethoxam	0.000531	0.9286	0.0017	0.0009
Flonicamid	<0.0001	0.7742	0.0001	0.0002
Clothianidin	<0.0001	0.4796	<0.0001	0.0001
Dimethoate	<0.0001	0.9741	<0.0001	0.0001
Imidacloprid	0.000206	0.973	0.0004	0.0006
Mevinphos	<0.0001	0.9203	<0.0001	<0.0001
Acetamiprid	0.000161	0.4272	0.0002	0.0014
Imazethapyr	0.00055	0.8336	0.0008	0.0022
Aldicarb	0.00098	0.4925	0.001	0.0076
Thiacloprid	0.000145	0.4973	0.0002	0.0011
Dicamba	0.00389	0.731	0.0045	0.0174
Propoxur	<0.0001	0.383	<0.0001	<0.0001
Carbuforuan	<0.0001	0.9972	<0.0001	<0.0001
Bentazon	0.00021	0.6385	0.0003	0.0012
Atrazine	<0.0001	0.0331	<0.0001	0.0033
Carbaryl	0.189	NA	NA	NA

Metalaxyl	0.000205	0.9964	0.0005	0.0005
2,4-D	0.00361	0.8857	0.005	0.0117
Paclobutrazol	<0.0001	0.536	<0.0001	<0.0001
Chlorantraniliprole	0.000109	0.0104	0.041	0.0001
Dimetamorph II	0.115	NA	NA	NA
Spirotetramat	<0.0001	0.6846	<0.0001	<0.0001
Dimetamorph I	0.00456	0.152	0.0034	0.1177
Fenhexamid	0.0839	0.987	0.0139	0.0183
Ethoprophos	0.000179	0.7546	0.0009	0.0003
Myclobutanil	<0.0001	0.9516	<0.0001	<0.0001
Tebuconazole	<0.0001	0.7526	<0.0001	<0.0001
Azoxystrobin	0.000632	0.9209	0.0011	0.0021
Fluopyram	0.00135	0.5349	0.0014	0.0095
Boscalid	0.0896	NA	NA	NA
Metolachlor	0.00232	0.9904	0.0044	0.0056
Malathion	<0.0001	0.9988	0.0002	0.0002
Fenoxycarb	<0.0001	0.3262	0.0009	0.0001
Tebufenozide	<0.0001	0.7466	<0.0001	<0.0001
Fipronil	<0.0001	0.2696	<0.0001	<0.0001
Tetrachlorvinphos	0.000377	0.9616	0.0011	0.0007
Propiconazole	<0.0001	0.3893	<0.0001	<0.0001
Kresoxim-Methyl	0.000807	0.0436	0.0006	0.0693
Diazinon	0.000109	0.653	0.0002	0.0004
Benzodiflupyr	0.0165	0.8857	0.02	0.0464
Prallethrin	0.00312	0.1885	0.006	0.0003
Pyraclostrobin	<0.0001	0.0532	<0.0001	<0.0001
MGK-264	0.00382	0.7213	0.0043	0.0175
Allethrin	<0.0001	0.9807	<0.0001	<0.0001
Tetramethrin	0.0156	0.1789	0.012	0.3024
Spiromesifen	<0.0001	0.9737	<0.0001	<0.0001
Hexythiazox	0.015	0.4949	0.0128	0.1
Spirodiclofen	<0.0001	0.4581	<0.0001	<0.0001

Table 9.6 Table of Shaprio-Wilk Test and Bartlett's Test Results for ANOVA assumptions of QuPPe internal standard loss. **Bold** values were significantly different from normal, but boxplots demonstrated a normal distribution.

Compound	Normality			Homogeneity of Variance
	BFD	AFD	FIL	
Dinotefuran	0.1009	**0.03215**	**0.02376**	0.8631
Oxamyl	0.05351	0.2565	0.0995	0.3581
Clopyralid	0.1502	0.9222	0.8768	0.8344
Thiamethoxam	0.6098	0.3787	0.7872	0.1766
Flonicamid	**0.01371**	0.4341	0.9006	0.9416
Clothianidin	0.2206	0.09476	0.2202	0.2871
Dimethoate	0.4115	0.9853	0.2849	0.6154
Imidacloprid	0.8294	0.2048	0.2114	0.3336
Mevinphos	0.9171	0.3306	0.1115	0.2651
Acetamiprid	0.833	0.9999	0.219	0.7253
Imazethapyr	0.9442	0.3165	0.7065	0.9917
Aldicarb	0.1324	0.4961	0.285	0.3921
Thiacloprid	**0.04106**	0.2955	0.1337	0.05507
Dicamba	0.2208	0.7271	0.718	0.5035
Propoxur	0.09388	0.168	0.5601	0.06507
Carbuforuan	0.2835	0.406	**0.0468**	0.9266
Bentazon	0.0944	0.7527	0.1049	0.09883
Atrazine	0.9844	0.1025	0.9454	0.2472
Carbaryl	0.7822	0.5431	0.2726	0.5676
Metalaxyl	0.4072	0.8659	0.1295	0.3536
2,4-D	0.7742	0.8283	0.1367	0.9347
Paclobutrazol	0.1807	0.09482	0.3539	0.3322
Chlorantraniliprole	0.375	0.05783	0.4117	0.9766
Dimetamorph II	0.727	0.9862	0.9127	0.1391
Spirotetramat	0.6933	0.604	0.893	0.3984
Dimetamorph I	0.4741	0.49	0.7062	0.554
Fenhexamid	0.4126	**0.02773**	0.4618	0.8123
Ethoprophos	0.248	0.2712	0.5123	0.191
Myclobutanil	0.07866	0.06054	0.2354	0.334
Tebuconazole	0.5672	-0.1787	0.4856	0.582
Azoxystrobin	0.3825	0.735	0.1	0.5373
Fluopyram	0.7617	0.4429	0.1125	0.2673
Boscalid	0.3934	0.9961	0.9777	0.4833
Metolachlor	0.8441	0.6982	0.2835	0.09145
Malathion	0.1142	0.7839	0.6677	0.7347

Fenoxycarb	**0.03968**	0.4327	0.2385	0.2511
Tebufenozide	0.5049	0.7549	0.4902	0.4406
Fipronil	0.174	**0.04967**	0.2878	0.2936
Tetrachlorvinphos	0.9429	0.3604	0.901	0.6665
Propiconazole	0.6939	0.58	0.5112	0.07561
Kresoxim-Methyl	0.5952	0.8921	0.8058	0.1861
Diazinon	0.9693	0.06791	0.3585	0.6419
Benzodiflupyr	0.1593	0.3597	0.05056	0.9867
Prallethrin	**0.0285**	0.5018	0.9474	0.3721
Pyraclostrobin	**0.03598**	0.7786	0.09519	0.3944
MGK-264	0.177	0.1097	0.6799	0.7603
Allethrin	0.6177	0.5581	0.5115	0.0528
Tetramethrin	0.9042	0.2001	0.7544	0.8228
Spiromesifen	0.344	0.2194	0.8066	0.2987
Hexythiazox	0.7483	0.3739	0.884	9243
Spirodiclofen	0.7898	0.8911	0.2957	0.4519

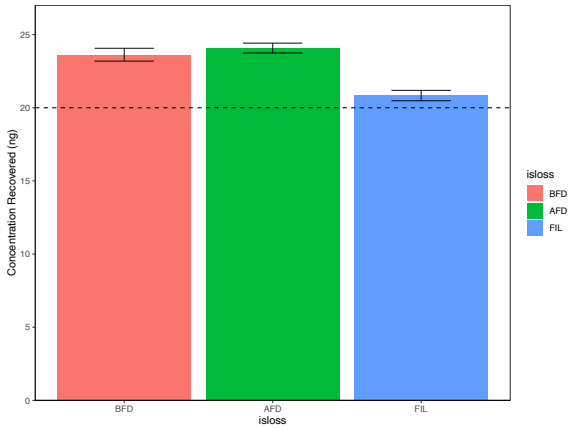

Figure 9.55 Dinotefuran internal standard recovery before freeze-drying (BFD), after freeze-drying (AFD), and filter (FIL) stage of extractions. Bars are standard error, dashed line are amount spiked.

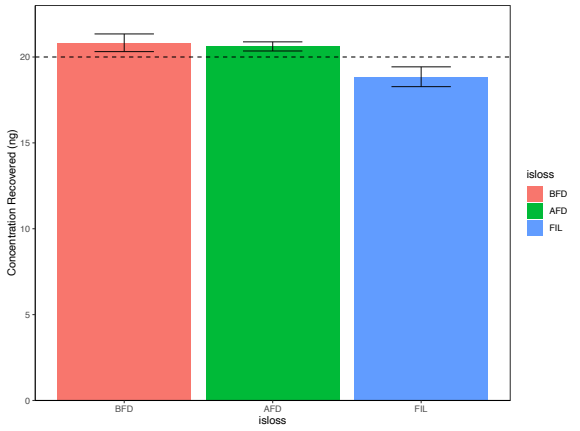

Figure 9.56 Oxamyl internal standard recovery before freeze-drying (BFD), after freeze-drying (AFD), and filter (FIL) stage of extractions. Bars are standard error, dashed line are amount spiked.

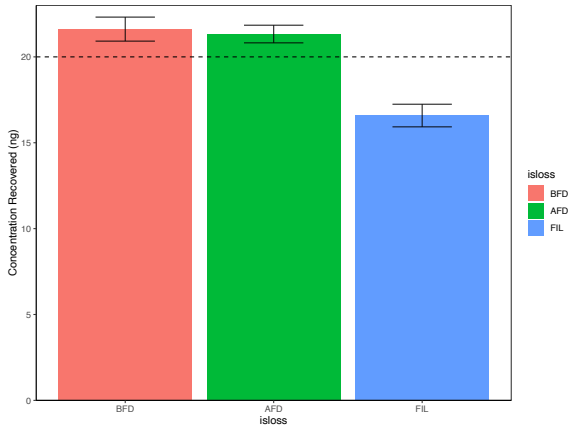

Figure 9.57 Clopyralid internal standard recovery before freeze-drying (BFD), after freeze-drying (AFD), and filter (FIL) stage of extractions. Bars are standard error, dashed line are amount spiked.

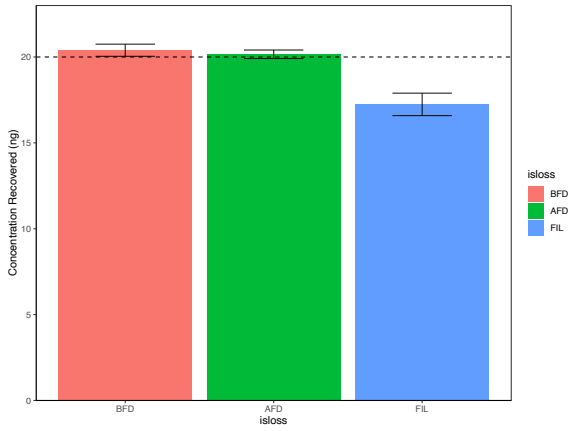

Figure 9.58 Thiamethoxam internal standard recovery before freeze-drying (BFD), after freeze-drying (AFD), and filter (FIL) stage of extractions. Bars are standard error, dashed line are amount spiked.

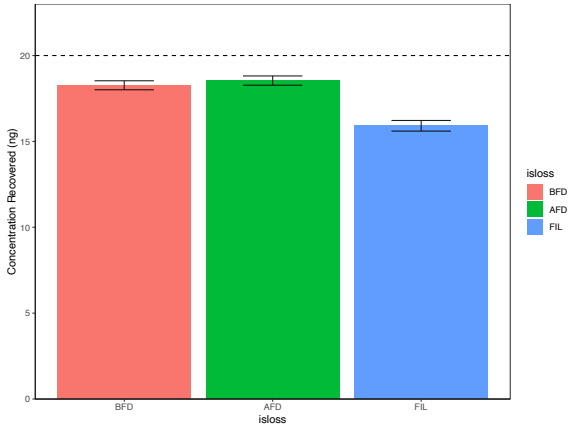

Figure 9.59 Flonicamid internal standard recovery before freeze-drying (BFD), after freeze-drying (AFD), and filter (FIL) stage of extractions. Bars are standard error, dashed line are amount spiked.

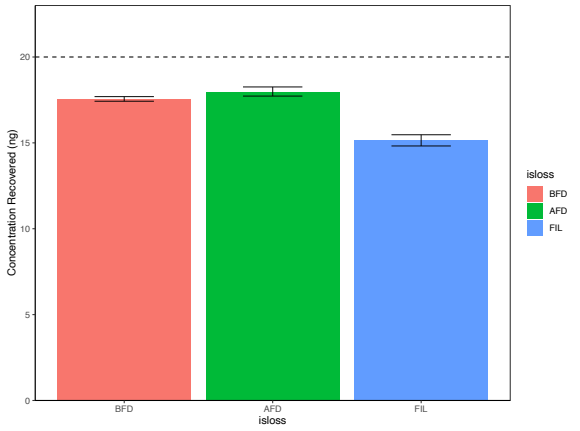

Figure 9.60 Clothianidin internal standard recovery before freeze-drying (BFD), after freeze-drying (AFD), and filter (FIL) stage of extractions. Bars are standard error, dashed line are amount spiked.

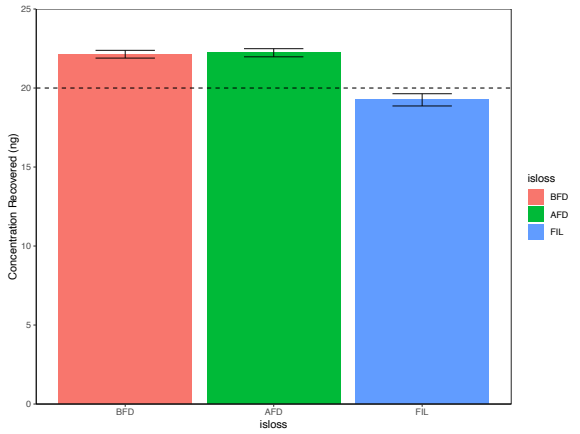

Figure 9.61 Dimethoate internal standard recovery before freeze-drying (BFD), after freeze-drying (AFD), and filter (FIL) stage of extractions. Bars are standard error, dashed line are amount spiked.

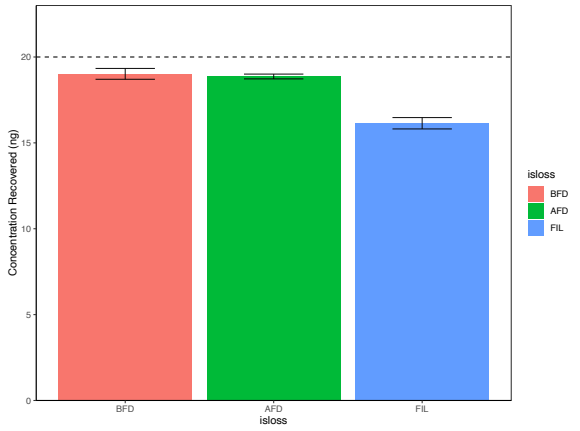

Figure 9.62 Mevinphos internal standard recovery before freeze-drying (BFD), after freeze-drying (AFD), and filter (FIL) stage of extractions. Bars are standard error, dashed line are amount spiked.

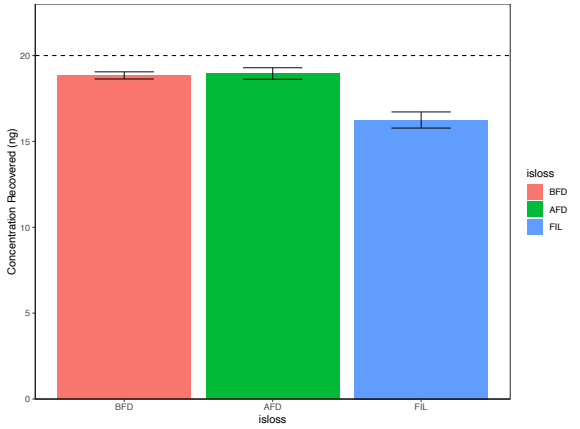

Figure 9.63 Imidacloprid internal standard recovery before freeze-drying (BFD), after freeze-drying (AFD), and filter (FIL) stage of extractions. Bars are standard error, dashed line are amount spiked.

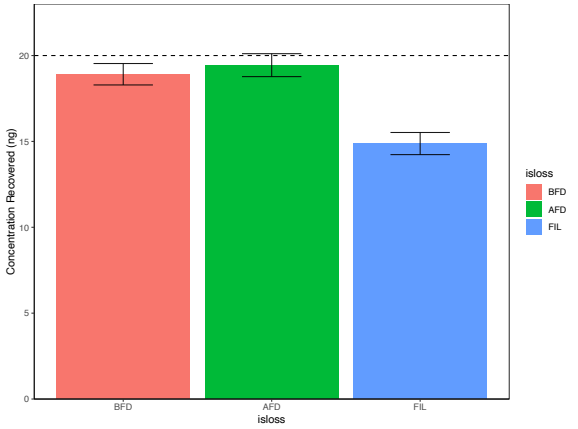

Figure 9.65 Imazethapyr internal standard recovery before freeze-drying (BFD), after freeze-drying (AFD), and filter (FIL) stage of extractions. Bars are standard error, dashed line are amount spiked.

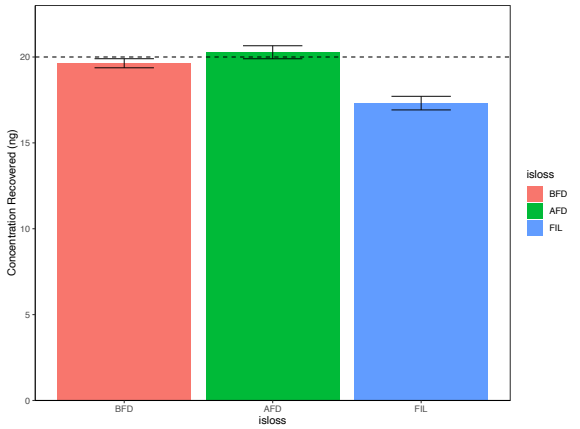

Figure 9.64 Acetamiprid internal standard recovery before freeze-drying (BFD), after freeze-drying (AFD), and filter (FIL) stage of extractions. Bars are standard error, dashed line are amount spiked.

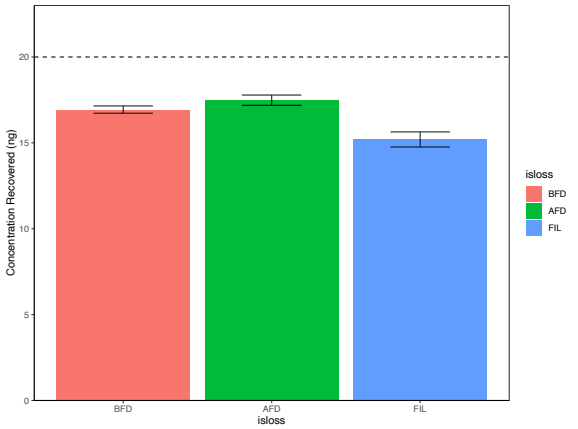

Figure 9.66 Aldicarb internal standard recovery before freeze-drying (BFD), after freeze-drying (AFD), and filter (FIL) stage of extractions. Bars are standard error, dashed line are amount spiked.

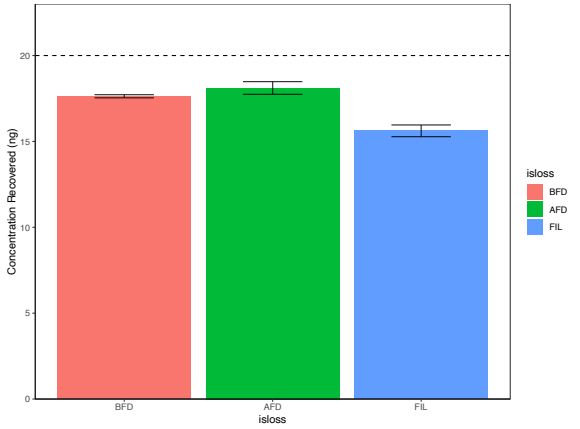

Figure 9.67 Thiacloprid internal standard recovery before freeze-drying (BFD), after freeze-drying (AFD), and filter (FIL) stage of extractions. Bars are standard error, dashed line are amount spiked.

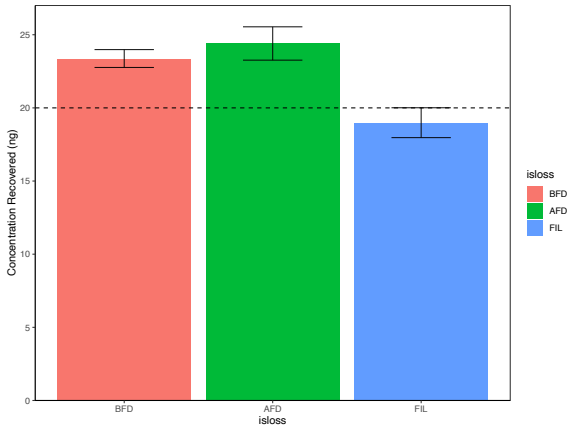

Figure 9.68 Dicamba internal standard recovery before freeze-drying (BFD), after freeze-drying (AFD), and filter (FIL) stage of extractions. Bars are standard error, dashed line are amount spiked.

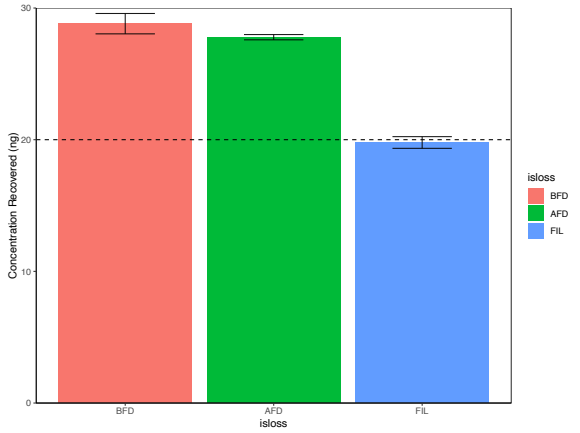

Figure 9.69 Propoxur internal standard recovery before freeze-drying (BFD), after freeze-drying (AFD), and filter (FIL) stage of extractions. Bars are standard error, dashed line are amount spiked.

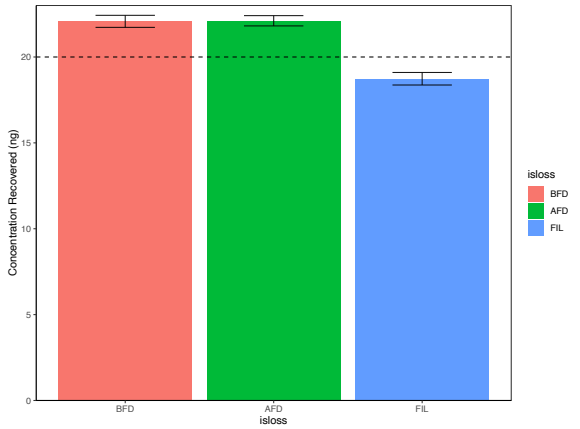

Figure 9.70 Carbofuran internal standard recovery before freeze-drying (BFD), after freeze-drying (AFD), and filter (FIL) stage of extractions. Bars are standard error, dashed line are amount spiked.

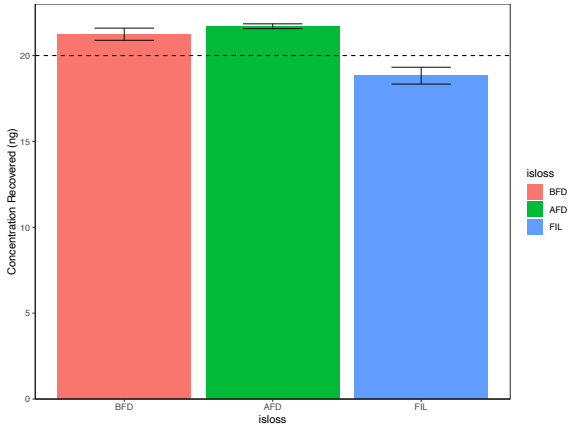

Figure 9.71 Bentazon internal standard recovery before freeze-drying (BFD), after freeze-drying (AFD), and filter (FIL) stage of extractions. Bars are standard error, dashed line are amount spiked.

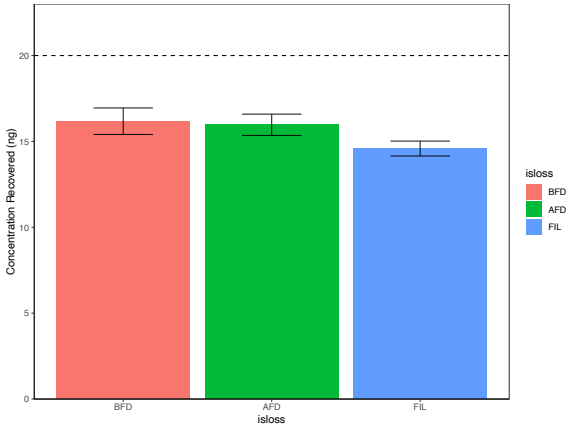

Figure 9.73 Carbaryl internal standard recovery before freeze-drying (BFD), after freeze-drying (AFD), and filter (FIL) stage of extractions. Bars are standard error, dashed line are amount spiked.

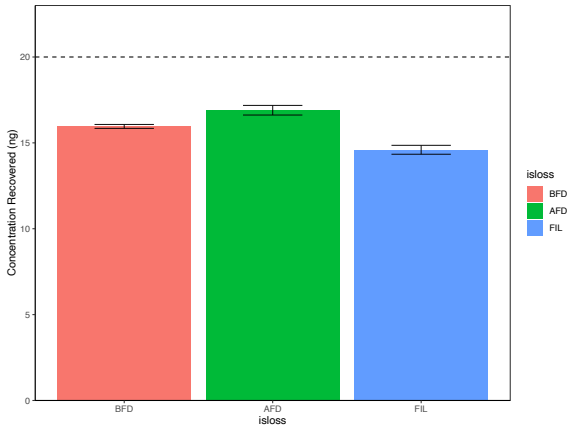

Figure 9.72 Atrazine internal standard recovery before freeze-drying (BFD), after freeze-drying (AFD), and filter (FIL) stage of extractions. Bars are standard error, dashed line are amount spiked.

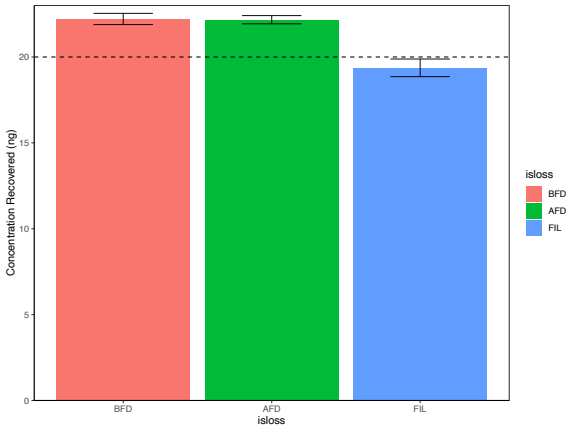

Figure 9.74 Metalaxyl internal standard recovery before freeze-drying (BFD), after freeze-drying (AFD), and filter (FIL) stage of extractions. Bars are standard error, dashed line are amount spiked.

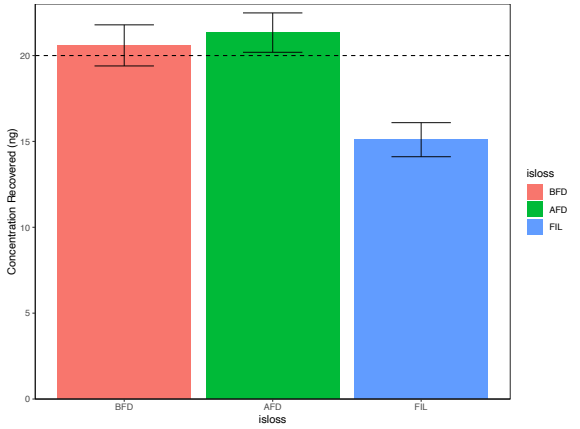

Figure 9.75 2,4-D internal internal standard recovery before freeze-drying (BFD), after freeze-drying (AFD), and filter (FIL) stage of extractions. Bars are standard error, dashed line are amount spiked.

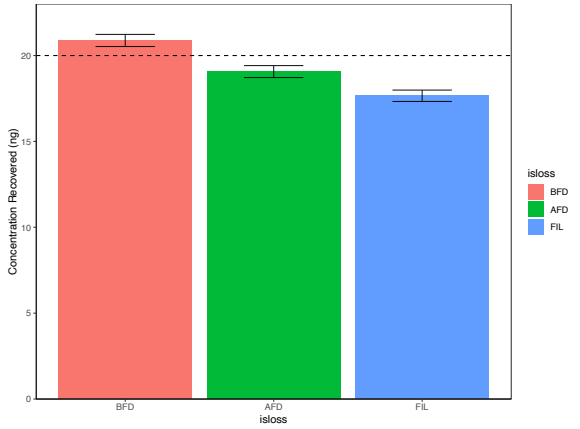

Figure 9.77 Chlorantraniliprole internal standard recovery before freeze-drying (BFD), after freeze-drying (AFD), and filter (FIL) stage of extractions. Bars are standard error, dashed line are amount spiked.

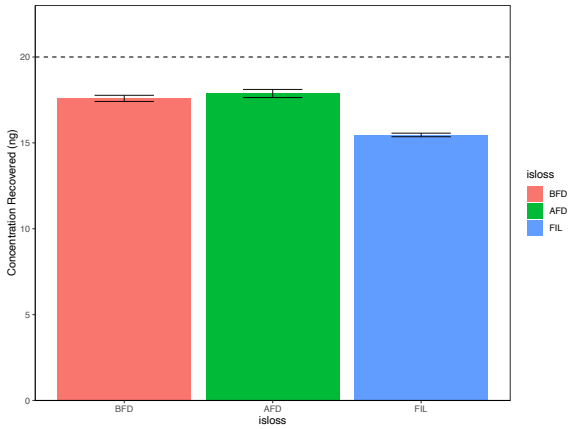

Figure 9.76 Paclobutrazol internal standard recovery before freeze-drying (BFD), after freeze-drying (AFD), and filter (FIL) stage of extractions. Bars are standard error, dashed line are amount spiked.

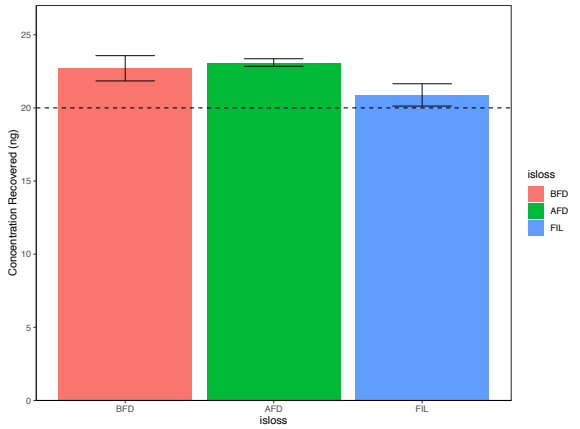

Figure 9.78 Dimethomorph II internal standard recovery before freeze-drying (BFD), after freeze-drying (AFD), and filter (FIL) stage of extractions. Bars are standard error, dashed line are amount spiked.

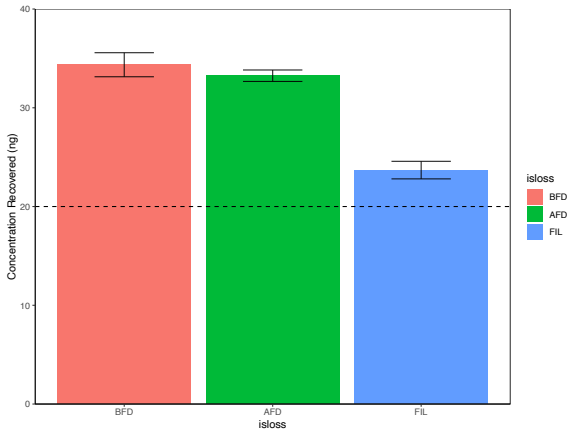

Figure 9.79 Spirotetramat internal standard recovery before freeze-drying (BFD), after freeze-drying (AFD), and filter (FIL) stage of extractions. Bars are standard error, dashed line are amount spiked.

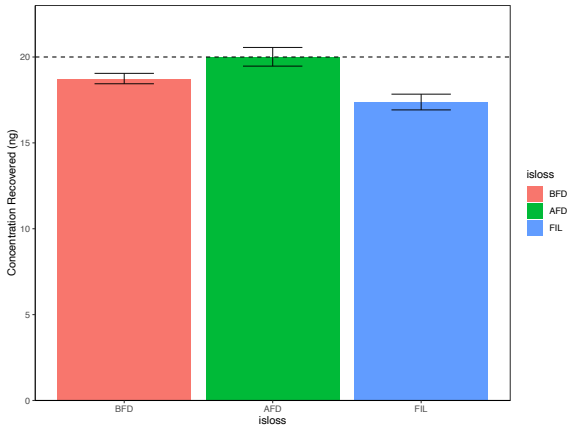

Figure 9.80 Dimethomorph I internal standard recovery before freeze-drying (BFD), after freeze-drying (AFD), and filter (FIL) stage of extractions. Bars are standard error, dashed line are amount spiked.

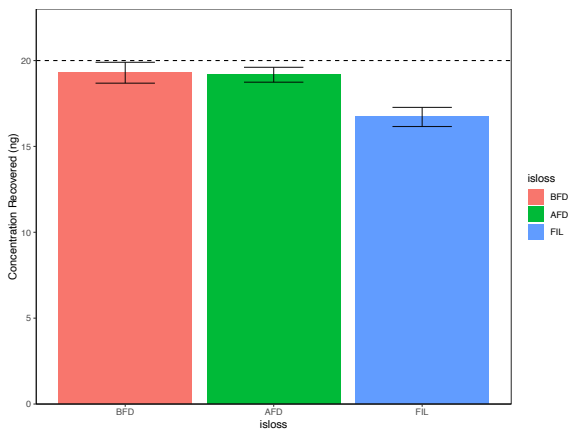

Figure 9.81 Fenhexamid internal standard recovery before freeze-drying (BFD), after freeze-drying (AFD), and filter (FIL) stage of extractions. Bars are standard error, dashed line are amount spiked.

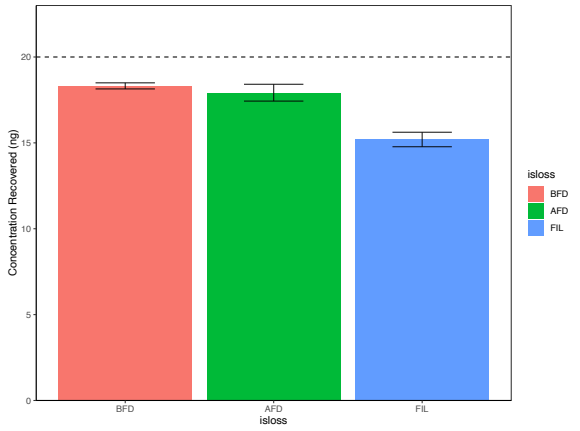

Figure 9.82 Ethoprophos internal standard recovery before freeze-drying (BFD), after freeze-drying (AFD), and filter (FIL) stage of extractions. Bars are standard error, dashed line are amount spiked.

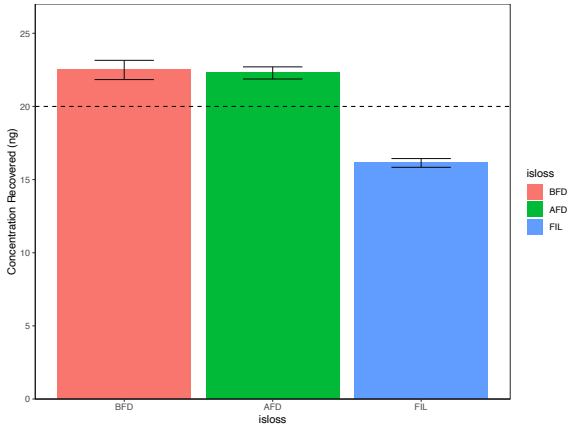

Figure 9.83 Myclobutanil internal standard recovery before freeze-drying (BFD), after freeze-drying (AFD), and filter (FIL) stage of extractions. Bars are standard error, dashed line are amount spiked.

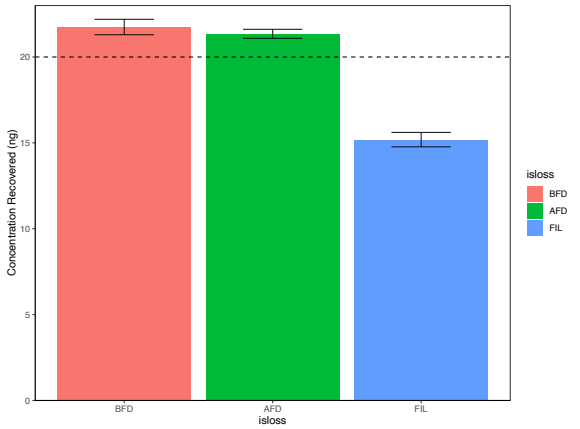

Figure 9.84 Tebuconazole internal standard recovery before freeze-drying (BFD), after freeze-drying (AFD), and filter (FIL) stage of extractions. Bars are standard error, dashed line are amount spiked.

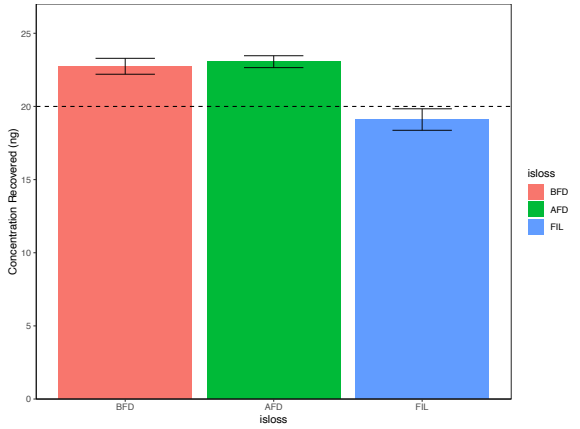

Figure 9.85 Azoxystrobin internal standard recovery before freeze-drying (BFD), after freeze-drying (AFD), and filter (FIL) stage of extractions. Bars are standard error, dashed line are amount spiked.

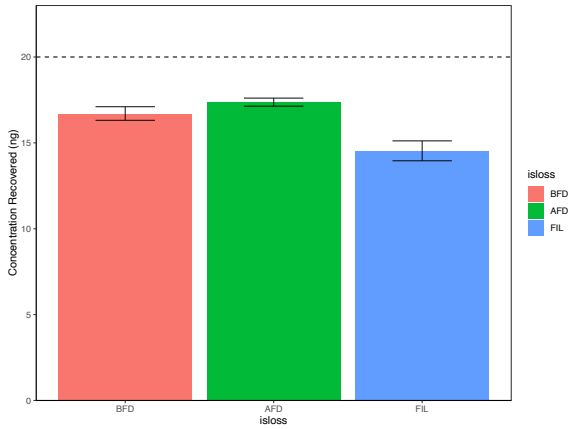

Figure 9.86 Fluopyram internal standard recovery before freeze-drying (BFD), after freeze-drying (AFD), and filter (FIL) stage of extractions. Bars are standard error, dashed line are amount spiked.

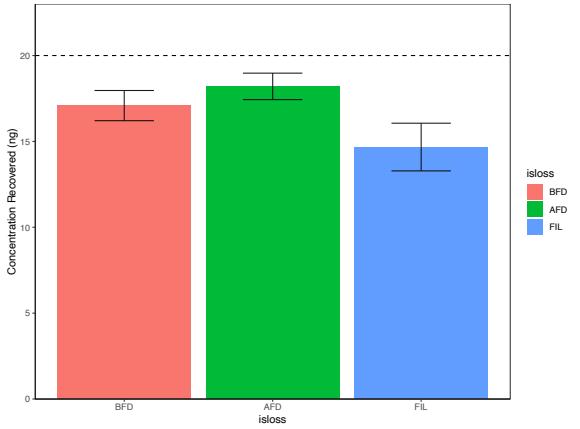

Figure 9.87 Boscalid internal standard recovery before freeze-drying (BFD), after freeze-drying (AFD), and filter (FIL) stage of extractions. Bars are standard error, dashed line are amount spiked.

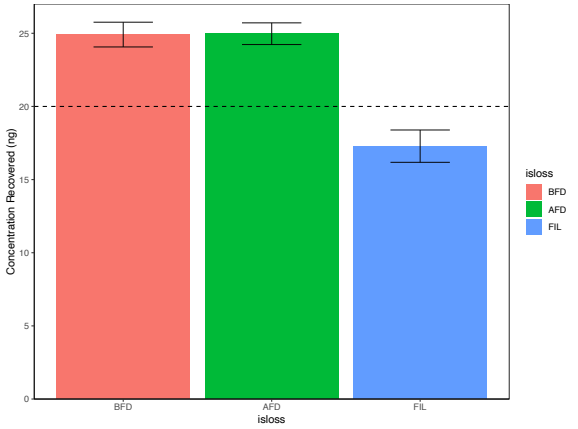

Figure 9.89 Malathion internal standard recovery before freeze-drying (BFD), after freeze-drying (AFD), and filter (FIL) stage of extractions. Bars are standard error, dashed line are amount spiked.

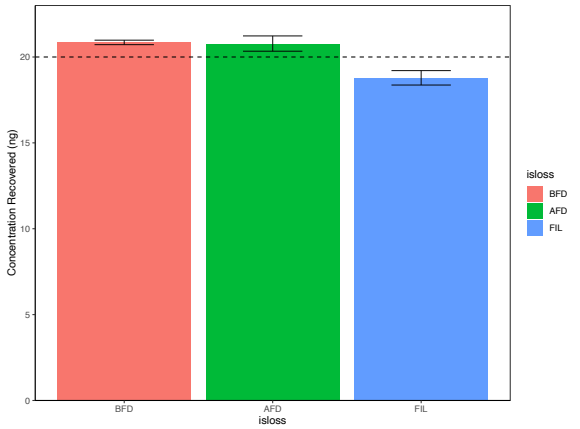

Figure 9.88 Metolachlor internal standard recovery before freeze-drying (BFD), after freeze-drying (AFD), and filter (FIL) stage of extractions. Bars are standard error, dashed line are amount spiked.

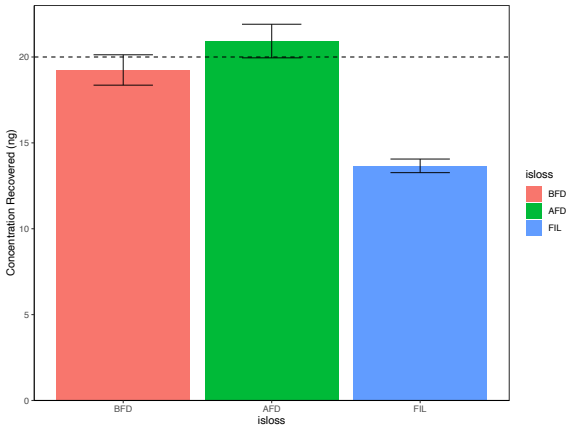

Figure 9.90 Fenoxycarb internal standard recovery before freeze-drying (BFD), after freeze-drying (AFD), and filter (FIL) stage of extractions. Bars are standard error, dashed line are amount spiked.

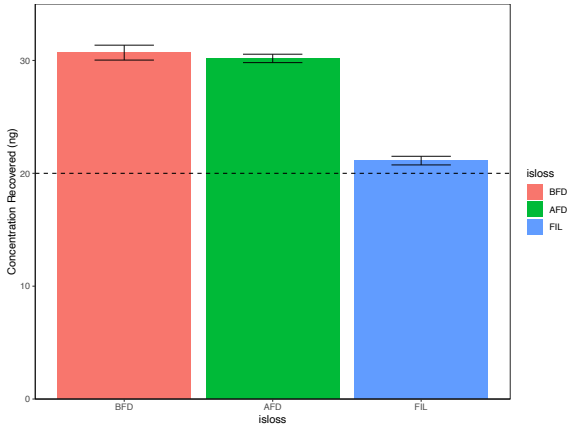

Figure 9.91 Tebufenozide internal standard recovery before freeze-drying (BFD), after freeze-drying (AFD), and filter (FIL) stage of extractions. Bars are standard error, dashed line are amount spiked.

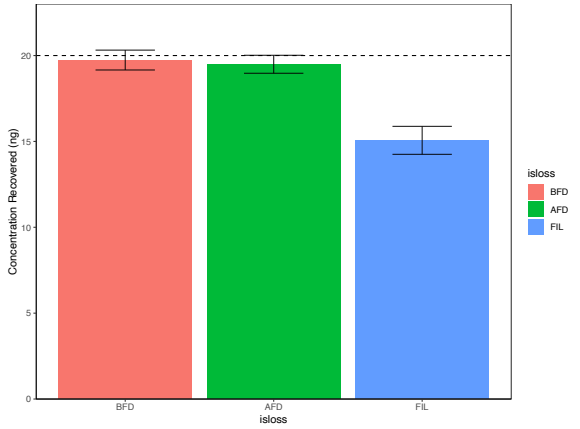

Figure 9.93 Tetrachlorvinphos internal standard recovery before freeze-drying (BFD), after freeze-drying (AFD), and filter (FIL) stage of extractions. Bars are standard error, dashed line are amount spiked.

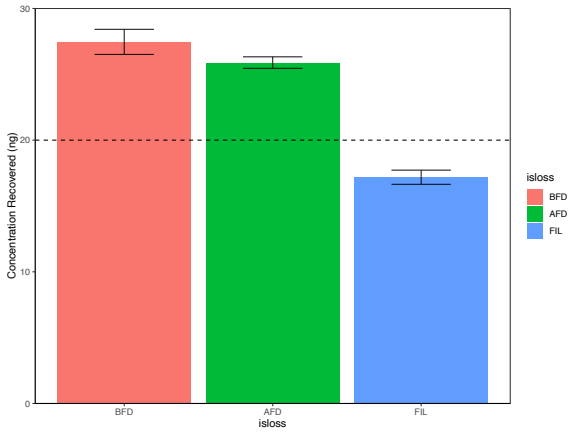

Figure 9.92 Friponil internal standard recovery before freeze-drying (BFD), after freeze-drying (AFD), and filter (FIL) stage of extractions. Bars are standard error, dashed line are amount spiked.

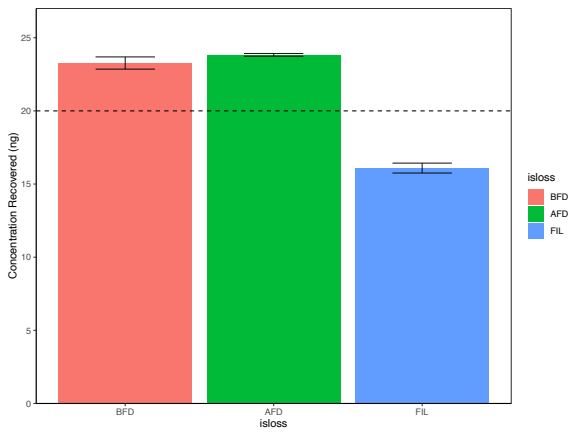

Figure 9.94 Propiconazole internal standard recovery before freeze-drying (BFD), after freeze-drying (AFD), and filter (FIL) stage of extractions. Bars are standard error, dashed line are amount spiked.

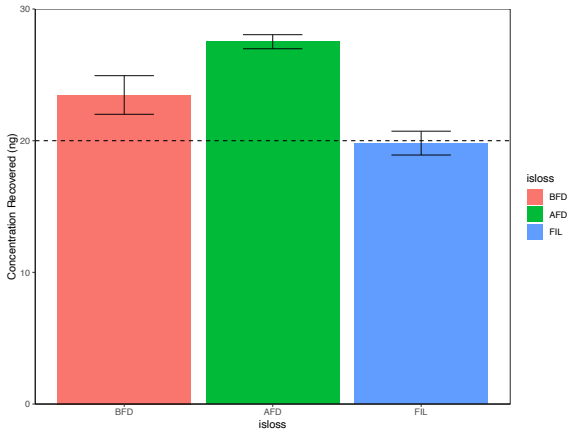

Figure 9.95 Kresoxim-Methyl internal standard recovery before freeze-drying (BFD), after freeze-drying (AFD), and filter (FIL) stage of extractions. Bars are standard error, dashed line are amount spiked.

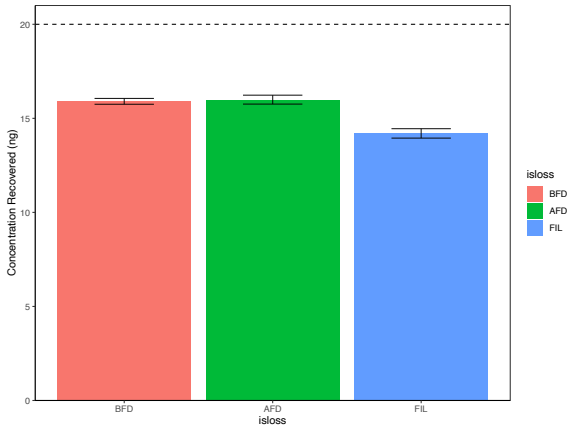

Figure 9.96 Diazinon internal standard recovery before freeze-drying (BFD), after freeze-drying (AFD), and filter (FIL) stage of extractions. Bars are standard error, dashed line are amount spiked.

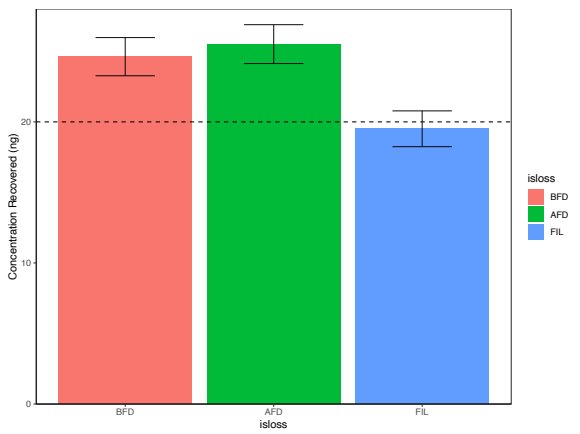

Figure 9.97 Benzovindiflupyr internal standard recovery before freeze-drying (BFD), after freeze-drying (AFD), and filter (FIL) stage of extractions. Bars are standard error, dashed line are amount spiked.

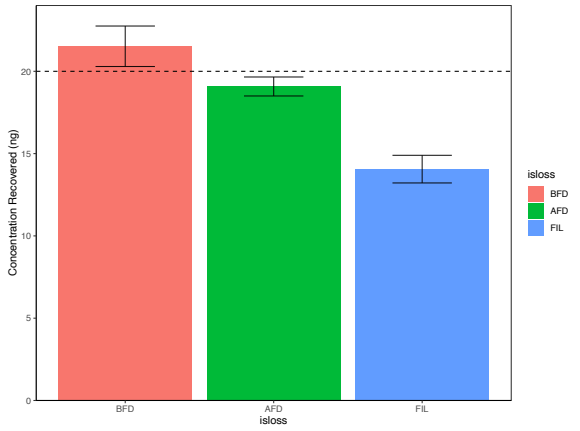

Figure 9.98 Prallethrin internal standard recovery before freeze-drying (BFD), after freeze-drying (AFD), and filter (FIL) stage of extractions. Bars are standard error, dashed line are amount spiked.

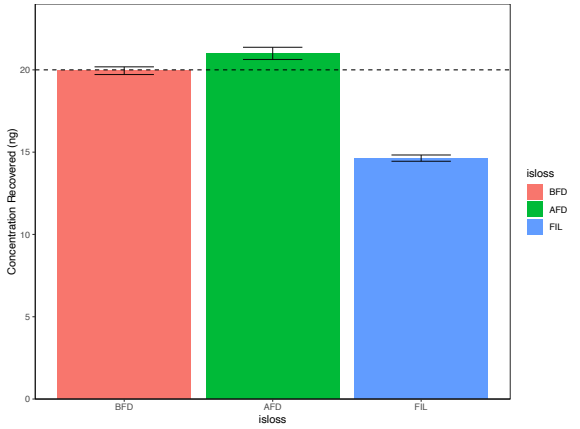

Figure 9.99 Pyraclostrobin internal standard recovery before freeze-drying (BFD), after freeze-drying (AFD), and filter (FIL) stage of extractions. Bars are standard error, dashed line are amount spiked.

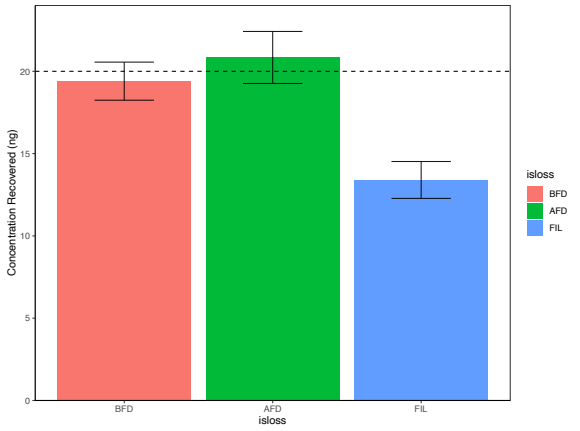

Figure 9.100 MGK 264 internal standard recovery before freeze-drying (BFD), after freeze-drying (AFD), and filter (FIL) stage of extractions. Bars are standard error, dashed line are amount spiked.

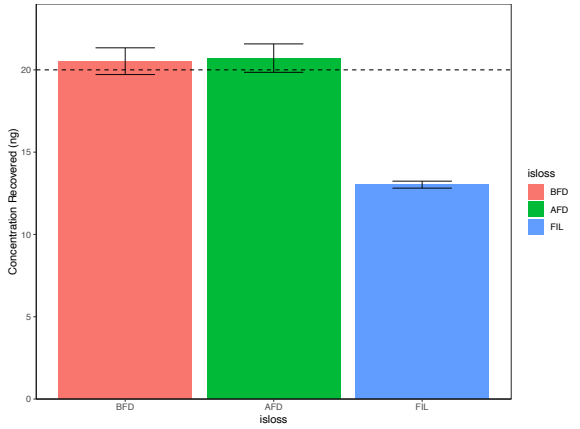

Figure 9.101 Allethrin internal standard recovery before freeze-drying (BFD), after freeze-drying (AFD), and filter (FIL) stage of extractions. Bars are standard error, dashed line are amount spiked.

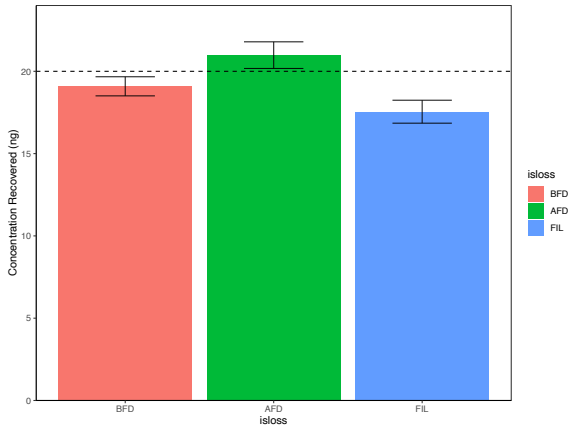

Figure 9.102 Tetramethrin internal standard recovery before freeze-drying (BFD), after freeze-drying (AFD), and filter (FIL) stage of extractions. Bars are standard error, dashed line are amount spiked.

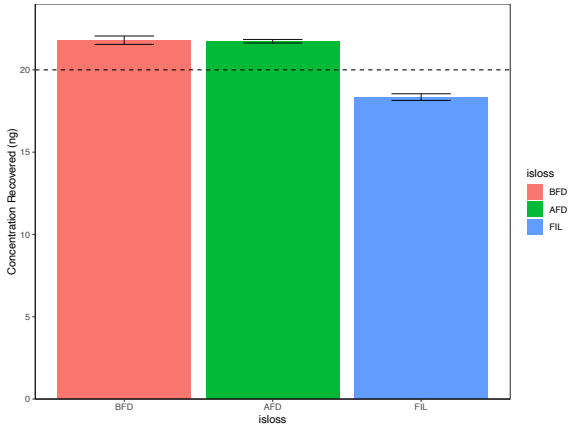

Figure 9.103 Spiromesifen internal standard recovery before freeze-drying (BFD), after freeze-drying (AFD), and filter (FIL) stage of extractions. Bars are standard error, dashed line are amount spiked.

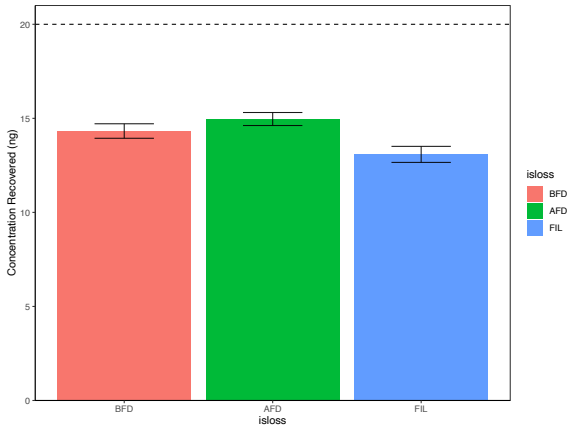

Figure 9.104 Hexythiazox internal standard recovery before freeze-drying (BFD), after freeze-drying (AFD), and filter (FIL) stage of extractions. Bars are standard error, dashed line are amount spiked.

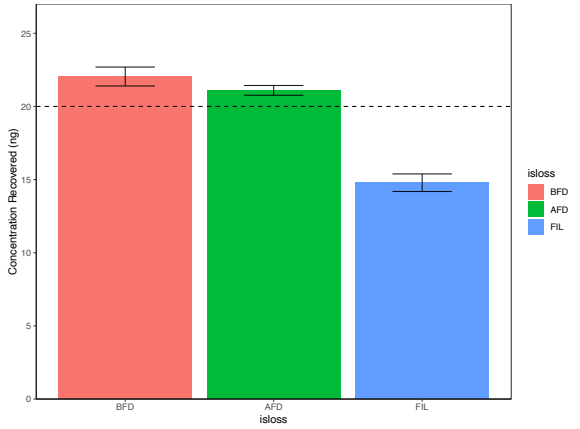

Figure 9.105 Spirodiclofen internal standard recovery before freeze-drying (BFD), after freeze-drying (AFD), and filter (FIL) stage of extractions. Bars are standard error, dashed line are amount spiked.

10. APPENDIX II: CHAPTER THREE IN-SITU DATA FOR 2022 (BIOMIXUTRE) AND 2023 (WATER AND BIOMIXUTRE)

10.1 Chapter 3 Water Statistical Analysis

Table 10.1 Results from the Shapiro-Wilk Test for normality, Welch's ANOVA, and Games-Howell Post-Hoc Tests for biobed water data in 2023. Bold values represent non-normal distribution.

Compound	Shapiro-Wilk Test			Welch's ANOVA		Games-Howell Post-Hoc Test		
	Rinsate	Primary Effluent	Final Effluent	*F-value*	*p-value*	RIN v PEF	RIN v FEF	PEF v FEF
Clopyralid	0.3959	0.1695	0.2517	0.37155	0.6958	NA	NA	NA
Imazethapyr	0.1863	0.3956	0.6131	10.083	0.001945	0.466	0.221	0.0002
Bentazon	0.4356	0.4586	0.6942	1.4735	0.2618	NA	NA	NA
Atrazine	0.1481	0.8955	0.5052	16.971	0.0004944	0.007	0.01	0.005
Metolachlor[a]	0.3402	**0.01602**	0.3096	16.811	0.0002603	0.039	0.002	0.013
Dicamba[b]	0.245	0.4983	0.1428	13.51	0.0003998	0.025	0.000341	0.021
Chlorantraniliprole[c]	0.1003	0.2994	0.04461	43.264	0.000004	0.048	0.028	0.00001
Imazamox[d]	0.1964	0.1275	0.6421	30.723	0.000006	0.009	0.00001	0.018

[a]Square Root transformed values, [b]Log Transformation; rinsate (8) and final effluent (4) imputed with MLE, [c]Log Transformation; final effluent (7) imputed with MLE, [d]Log Transformation; primary (7) and final (3) effluent imputed with MLE

10.2 Chapter 3 Biomixture Statistical Analysis

Table 10.2 Repeated Measures ANOVA Table for all compounds detected within biomixtures for both 2022 and 2023. Acronyms for compounds are as follows: IMZ = Imazethapyr, DIC = Dicamba, ATR = Atrazine, BEN = Bentazon, CHL = Chlorantraniliprole, MET = Metolachlor, CLP = Clopyralid, PYR = Pyraclostrobin, TEB = Tebuconazole, and BOS = Boscalid. Factor acronyms are as follows: (I) = Model Intercept, Y = Year of Operation, C = Biobed Cell, D = Depth Sampled, and T = Time of Sampling. Other Acronyms as follows: DF_n = Degrees of Freedom (Numerator), DF_d = Degrees of Freedom (Denominator), SS_n = Sum of Squares (Numerator), SS_d = Sum of Squares (Denominator), F = F-statistic, and p = p-value.

		(I)	Y	C	D	T	C:Y	C:D	Y:D	C:T	Y:T	D:T	Y:C:D	Y:C:T	Y:D:T	C:D:T	Y:C:D:T
	DF_n	1	1	1	2	1	1	2	2	1	1	2	2	1	2	2	2
	DF_d	8	8	8	16	8	8	16	16	8	8	16	16	8	16	16	16
IMZ	SS_n	**102.323**	**15.642**	0.013	**0.293**	**26.211**	0.000303	0.218	0.033	**1.334**	0.014	0.119	0.118	**0.23**	**2.291**	0.035	0.273
	SS_d	**0.47**	**0.47**	0.47	**0.602**	**0.169**	0.47	0.602	0.602	**0.169**	0.169	1.634	0.602	**0.169**	**1.634**	1.634	1.634
	F	**1742.346**	**266.354**	0.225	**3.887**	**1238.127**	0.005	2.899	0.441	**63.034**	0.674	0.582	1.573	**10.879**	**11.217**	0.169	1.337
	p	**1.20E-10**	**2.00E-07**	6.48E-01	**4.20E-02**	**4.66E-10**	9.44E-01	8.40E-02	6.51E-01	**4.61E-05**	4.35E-01	5.70E-01	2.38E-01	**1.10E-02**	**9.02E-04**	8.46E-01	2.91E-01
DIC	SS_n	**949.263**	0.263	2.1	**38.014**	**73.006**	5.334	**8.778**	**11.601**	0.529	0.007	**21.44**	**10.582**	7.127	8.469	10.769	3.889
	SS_d	**59.748**	59.748	59.748	**18.883**	**43.53**	59.748	**18.883**	**18.883**	43.53	43.53	**25.979**	**18.883**	43.53	25.979	25.979	25.979
	F	**127.101**	0.035	0.281	**16.105**	**13.417**	0.714	**3.719**	**4.915**	0.097	0.001	**6.602**	**4.483**	1.31	2.608	3.316	1.198
	p	**3.44E-06**	8.56E-01	6.10E-01	**1.47E-04**	**6.00E-03**	4.23E-01	**4.70E-02**	**2.20E-02**	7.63E-01	9.73E-01	**8.00E-03**	**2.80E-02**	2.86E-01	1.05E-01	6.20E-02	3.28E-01
ATR	SS_n	**690.353**	**35.595**	**22.543**	0.209	**118.322**	1.333	0.911	**19.439**	**19.78**	**53.721**	**3.083**	**2.825**	0.574	1.326	**5.966**	1.997
	SS_d	**4.176**	**4.176**	**4.176**	4.778	**8.798**	4.176	4.778	**4.778**	**8.798**	**8.798**	**5.379**	**4.778**	8.798	5.379	**5.379**	5.379
	F	**1322.572**	**68.192**	**43.187**	0.35	**107.588**	2.553	1.526	**32.546**	**17.985**	**48.848**	**4.585**	**4.73**	0.522	1.972	**8.873**	2.971
	p	**3.58E-10**	**3.47E-05**	**1.74E-04**	7.10E-01	**6.46E-06**	1.49E-01	2.48E-01	**2.30E-06**	**3.00E-03**	**1.14E-04**	**2.70E-02**	**2.40E-02**	4.91E-01	1.72E-01	**3.00E-03**	8.00E-02
BEN	SS_n	**1613.615**	**18.902**	**216.801**	9.654	**547.267**	0.226	8.583	0.393	0.059	**178.433**	**19.736**	2.714	9.388	5.709	2.038	3.764
	SS_d	**22.333**	**22.333**	**22.333**	35.962	**23.876**	22.333	35.962	35.962	23.876	**23.876**	**19.13**	35.962	23.876	19.13	19.13	19.13
	F	**578.028**	**6.771**	**77.662**	2.148	**183.369**	0.081	1.909	0.087	0.02	**59.786**	**8.253**	0.604	3.145	2.388	0.852	1.574
	p	**9.55E-09**	**3.20E-02**	**2.16E-05**	1.49E-01	**8.49E-07**	7.83E-01	1.80E-01	9.17E-01	8.92E-01	**5.58E-05**	**3.00E-03**	5.59E-01	1.14E-01	1.24E-01	4.45E-01	2.38E-01

CHL	SS_n	**1396.699**	**296.706**	**36.135**	**44.159**	**107.882**	**8.057**	**13.773**	**12.559**	9.226	**30.517**	**65.758**	**21.39**	0.129	6.724	4.931	0.824
	SS_d	**9.762**	**9.762**	**9.762**	**9.97**	**20.86**	**9.762**	**9.97**	**9.97**	20.86	**20.86**	**20.579**	**9.97**	20.86	20.579	20.579	20.579
	F	**1144.543**	**243.139**	**29.611**	**35.434**	**41.373**	**6.603**	**11.051**	**10.077**	3.538	**11.703**	**25.563**	**17.163**	0.049	2.614	1.917	0.32
	p	**6.37E-10**	**2.85E-07**	**6.15E-04**	**1.32E-06**	**2.02E-04**	**3.30E-02**	**9.67E-04**	**1.00E-03**	9.70E-02	**9.00E-03**	**1.04E-05**	**1.04E-04**	8.30E-01	1.04E-01	1.79E-01	7.30E-01
MET	SS_n	**2286.239**	**110.26**	**249.059**	**29.761**	**535.581**	0.027	10.037	**27.17**	5.323	**33.154**	**52.734**	**23.166**	3.527	0.059	6.432	7.294
	SS_d	**7.467**	**7.467**	**7.467**	**32.822**	**10.729**	7.467	32.822	**32.822**	10.729	**10.729**	**22.272**	**32.822**	10.729	22.272	22.272	22.272
	F	**2449.399**	**118.129**	**266.833**	**7.254**	**399.337**	0.028	2.446	**6.623**	3.969	**24.72**	**18.942**	**5.646**	2.63	0.021	2.31	2.62
	p	**3.08E-11**	**4.54E-06**	**1.99E-07**	**6.00E-03**	**4.10E-08**	8.70E-01	1.18E-01	**8.00E-03**	8.20E-02	**1.00E-03**	**6.04E-05**	**1.40E-02**	1.44E-01	9.79E-01	1.31E-01	1.04E-01
CLP	SS_n	**1519.276**	16.454	**161.518**	7.956	**412.748**	0.188	3.121	6.604	1.873	**126.348**	**17.653**	1.32	0.286	3.783	2.692	7.632
	SS_d	**26.262**	26.262	**26.262**	18.271	**14.843**	26.262	18.271	18.271	14.843	**14.843**	**17.38**	18.271	14.843	17.38	17.38	17.38
	F	**462.803**	5.012	**49.202**	3.484	**222.461**	0.057	1.366	2.892	1.01	**68.098**	**8.126**	0.578	0.154	1.741	1.239	3.513
	p	**2.30E-08**	5.60E-02	**1.11E-04**	5.50E-02	**4.03E-07**	8.17E-01	2.83E-01	8.50E-02	3.44E-01	**3.49E-05**	**4.00E-03**	5.72E-01	7.05E-01	2.07E-01	3.16E-01	5.40E-02
PYR	SS_n	**393.959**	**75.209**	**89.395**	**240.164**	**641.101**	2.754	3.916	**79.952**	67.801	**160.799**	**280.713**	11.754	30.173	4.247	36.709	1.83
	SS_d	**41.103**	**41.103**	**41.103**	**110.237**	**138.146**	41.103	110.237	**110.237**	138.146	**138.146**	**129.466**	110.237	138.146	129.466	129.466	129.466
	F	**76.678**	**14.638**	**17.399**	**17.429**	**37.126**	0.536	0.284	**5.802**	3.926	**9.312**	**17.346**	0.853	1.747	0.262	2.268	0.113
	p	**2.27E-05**	**5.00E-03**	**3.00E-03**	**9.60E-05**	**2.92E-04**	4.85E-01	7.56E-01	**1.30E-02**	8.30E-02	**1.60E-02**	**9.85E-05**	4.45E-01	2.23E-01	7.72E-01	1.36E-01	8.94E-01
TEB	SS_n	**278.767**	**5.782**	**23.644**	0.06	1.093	**3.147**	**1.478**	**2.244**	0.071	0.175	**1.851**	0.059	0.112	1.354	0.765	0.93
	SS_d	**3.968**	**3.968**	**3.968**	1.013	5.34	**3.968**	**1.013**	**1.013**	5.34	5.34	**3.205**	1.013	5.34	3.205	3.205	3.205
	F	**562.068**	**11.657**	**47.672**	0.474	1.638	**6.345**	**11.673**	**17.721**	0.106	0.263	**4.619**	0.463	0.168	3.378	1.91	2.322
	p	**1.07E-08**	**9.00E-03**	**1.24E-04**	6.31E-01	2.36E-01	**3.60E-02**	**7.48E-04**	**8.76E-05**	7.53E-01	6.22E-01	**2.60E-02**	6.38E-01	6.93E-01	6.00E-02	1.80E-01	1.30E-01
BOS	SS_n	**371.685**	**8.636**	0.027	**0.628**	**5.885**	0.201	0.401	**1.642**	**1.402**	**11.6**	**1.388**	0.07	**5.159**	0.261	0.169	**0.688**
	SS_d	**0.411**	**0.411**	0.411	**0.987**	**0.354**	0.411	0.987	**0.987**	**0.354**	**0.354**	**0.752**	0.987	**0.354**	0.752	0.752	**0.752**
	F	**7243.145**	**168.289**	0.528	**5.085**	**132.863**	3.91	3.252	**13.307**	**31.659**	**261.914**	**14.768**	0.564	**116.48**	2.775	1.798	**7.324**
	p	**4.05E-13**	**1.18E-06**	4.88E-01	**2.00E-02**	**2.91E-06**	8.30E-02	6.50E-02	**3.95E-04**	**4.95E-04**	**2.14E-07**	**2.32E-04**	5.80E-01	**4.79E-06**	9.20E-02	1.98E-01	**6.00E-03**

Table 10.3 Testing of sphericity assumption for each RM ANOVA run; acronyms same as Table 10.2. Bolded values indicate Greenhouse-Geisser adjustment due to violation of sphericity.

Compound	Effect	*W*	*p*
IMZ	D	0.958	0.861
	Y:D	0.958	0.861
	C:D	0.958	0.861
	Y:C:D	0.958	0.861
	D:T	0.792	0.442
	Y:D:T	0.792	0.442
	C:D:T	0.792	0.442
	Y:C:D:T	0.792	0.442
DIC	D	0.965	0.883
	Y:D	0.965	0.883
	C:D	0.965	0.883
	Y:C:D	0.965	0.883
	D:T	0.879	0.636
	Y:D:T	0.879	0.636
	C:D:T	0.879	0.636
	Y:C:D:T	0.879	0.636
ATR	D	0.636	0.205
	Y:D	0.636	0.205
	C:D	0.636	0.205
	Y:C:D	0.636	0.205
	D:T	0.827	0.515
	Y:D:T	0.827	0.515
	C:D:T	0.827	0.515
	Y:C:D:T	0.827	0.515
BEN	D	0.916	0.736
	Y:D	0.916	0.736
	C:D	0.916	0.736
	Y:C:D	0.916	0.736
	D:T	0.862	0.594
	Y:D:T	0.862	0.594
	C:D:T	0.862	0.594
	Y:C:D:T	0.862	0.594
CHL	D	0.977	0.923
	Y:D	0.977	0.923
	C:D	0.977	0.923
	Y:C:D	0.977	0.923

	D:T	0.806	0.47
	Y:D:T	0.806	0.47
	C:D:T	0.806	0.47
	Y:C:D:T	0.806	0.47
MET	**D**	**0.562**	**0.022**
	Y:D	**0.562**	**0.152**
	C:D	**0.562**	**0.028**
	Y:C:D	**0.562**	**0.039**
	D:T	0.88	0.639
	Y:D:T	0.88	0.639
	C:D:T	0.88	0.639
	Y:C:D:T	0.88	0.639
CLP	D	0.932	0.783
	Y:D	0.932	0.783
	C:D	0.932	0.783
	Y:C:D	0.932	0.783
	D:T	0.475	0.074
	Y:D:T	0.475	0.074
	C:D:T	0.475	0.074
	Y:C:D:T	0.475	0.074
PYR	**D**	**0.579**	**0.002**
	Y:D	**0.579**	**0.64**
	C:D	**0.579**	**0.035**
	Y:C:D	**0.579**	**0.396**
	D:T	0.65	0.221
	Y:D:T	0.65	0.221
	C:D:T	0.65	0.221
	Y:C:D:T	0.65	0.221
TEB	D	0.982	0.938
	Y:D	0.982	0.938
	C:D	0.982	0.938
	Y:C:D	0.982	0.938
	D:T	0.558	0.13
	Y:D:T	0.558	0.13
	C:D:T	0.558	0.13
	Y:C:D:T	0.558	0.13
BOS	D	0.961	0.871
	Y:D	0.961	0.871
	C:D	0.961	0.871
	Y:C:D	0.961	0.871

D:T	0.912	0.725
Y:D:T	0.912	0.725
C:D:T	0.912	0.725
Y:C:D:T	0.912	0.725

Table 10.4 Summary of Levene's Test for homogeneity of variance across cell years grouped into depth and time categories. Acronyms are the same as Table 10.2.

Depth		0-5 cm	0-5 cm	5-15 cm	5-15 cm	15-30 cm	15-30 cm
Time		pre	post	pre	post	pre	post
IMZ	*W*	0.277	0.278	0.863	0.902	0.326	0.443
	p	0.841	0.84	0.499	0.481	0.807	0.729
DIC	*W*	0.502	1.01	0.294	0.234	0.333	0.64
	p	0.691	0.439	0.829	0.871	0.802	0.61
ATR	*W*	0.871	0.613	0.876	1.17	0.476	0.284
	p	0.495	0.625	0.493	0.38	0.708	0.836
BEN	*W*	0.564	0.295	0.447	0.357	0.533	0.218
	p	0.654	0.828	0.726	0.786	0.672	0.881
CHL	*W*	1.16	0.26	0.912	0.854	1	0.0751
	p	0.383	0.852	0.477	0.503	0.441	0.972
MET	*W*	0.239	0.814	0.602	0.634	0.637	0.772
	p	0.867	0.521	0.632	0.614	0.612	0.542
CLP	*W*	0.767	1.02	0.171	0.445	0.85	0.676
	p	0.544	0.434	0.913	0.727	0.505	0.591
PYR	*W*	1.45	0.59	1.18	0.509	0.508	0.356
	p	0.3	0.639	0.376	0.687	0.688	0.786
TEB	*W*	0.859	1.22	0.409	1.98	1.39	0.955
	p	0.501	0.363	0.751	0.196	0.314	0.459
BOS	*W*	0.757	0.374	1.13	0.816	1.79	0.992
	p	0.549	0.774	0.393	0.52	0.226	0.444

Table 10.5 Summary of Shapiro-Wilk tests for normality of each grouping of cell, year, depth, and time. Acronyms for compounds and factors (bolded) same as Table 10.2. Additional acronyms are: 1_22 = Cell One, 2022; 1_23 = Cell One, 2023; 2_22 = Cell Two, 2022; 2_23 = Cell Two, 2023; T = Top 0-5 cm; M = Middle 5-15 cm; O = Bottom 15-30 cm; B = Pre-Operation; A = After Operation; *W* = Wilks Statistics, and; *p* = *p*-value.

C:YDT		1_22 T B	1_22 T A	1_22 M B	1_22 M A	1_22 O B	1_22 O A	1_23 T B	1_23 T A	1_23 M B	1_23 M A	1_23 O B	1_23 O A
IMZ	*W*	0.976	0.792	0.984	1	**0.756**	0.997	0.774	0.873	0.945	0.998	0.802	0.98
	p	0.704	0.0948	0.756	0.978	**0.0143**	0.897	0.0527	0.304	0.547	0.92	0.119	0.728
DIC	*W*	0.978	0.952	0.996	0.794	0.819	0.955	0.888	0.991	0.997	0.804	0.974	0.989
	p	0.718	0.579	0.878	0.0997	0.16	0.592	0.349	0.82	0.892	0.125	0.693	0.803
ATR	*W*	0.977	0.889	0.984	1	**0.756**	0.997	0.802	0.908	0.84	0.941	0.998	0.871
	p	0.708	0.352	0.758	0.997	**0.0144**	0.892	0.12	0.41	0.215	0.532	0.924	0.298
BEN	*W*	0.978	0.846	0.954	0.889	**0.756**	0.935	0.774	0.99	0.979	0.884	0.912	0.936
	p	0.718	0.229	0.587	0.351	**0.0144**	0.508	0.0531	0.807	0.722	0.337	0.424	0.513
CHL	*W*	0.979	0.844	**0.758**	1	0.97	0.886	0.992	0.865	0.776	0.914	0.999	0.78
	p	0.72	0.224	**0.0169**	0.968	0.665	0.343	0.832	0.282	0.0591	0.432	0.934	0.0674
MET	*W*	0.977	**0.75**	0.773	0.802	0.925	0.906	**0.75**	1	0.802	0.905	**0.75**	0.832
	p	0.707	**0**	0.0519	0.12	0.47	0.405	**0**	0.973	0.118	0.401	**0**	0.194
CLP	*W*	0.979	0.954	0.886	0.813	0.999	1	0.986	0.919	0.788	0.998	0.921	0.977
	p	0.719	0.588	0.342	0.146	0.954	0.958	0.772	0.449	0.0863	0.913	0.457	0.711
PYR	*W*	0.981	0.836	0.782	0.867	0.858	0.822	0.997	0.813	0.846	0.774	0.841	0.985
	p	0.734	0.203	0.0717	0.287	0.261	0.167	0.904	0.145	0.231	0.0533	0.217	0.768
TEB	*W*	0.818	0.875	0.812	0.944	0.936	0.967	0.791	0.985	0.974	0.99	0.973	0.896
	p	0.158	0.309	0.143	0.544	0.51	0.651	0.0927	0.765	0.693	0.812	0.684	0.372
BOS	*W*	0.995	0.876	**0.75**	0.96	0.999	0.894	0.791	0.999	0.974	0.93	0.973	0.951
	p	0.866	0.314	**0**	0.615	0.952	0.367	0.0927	0.942	0.693	0.49	0.684	0.574

C:YDT		2_22TB	2_22TA	2_22MB	2_22MA	2_22OB	2_22OA	2_23TB	2_23TA	2_23MB	2_23MA	2_23OB	2_23OA
IMZ	*W*	0.972	0.792	0.976	0.919	0.939	**0.75**	0.879	0.873	0.864	0.998	0.995	**0.75**
	p	0.676	0.0948	0.703	0.447	0.522	**0**	0.32	0.304	0.279	0.917	0.868	**0**
DIC	*W*	0.824	0.89	0.995	0.873	0.986	0.836	0.999	0.936	0.92	0.844	0.989	0.999
	p	0.173	0.354	0.861	0.305	0.776	0.205	0.954	0.512	0.453	0.225	0.799	0.937
ATR	*W*	0.972	0.81	0.976	0.876	0.939	**0.75**	0.969	0.938	0.811	0.846	0.778	0.982
	p	0.676	0.137	0.703	0.312	0.522	**0**	0.66	0.519	0.142	0.229	0.0633	0.74
BEN	*W*	0.972	0.899	0.982	0.928	0.831	0.847	0.86	0.948	1	0.884	0.979	0.975
	p	0.677	0.382	0.746	0.479	0.19	0.233	0.267	0.559	0.984	0.337	0.72	0.694
CHL	*W*	**0.756**	0.997	0.931	0.944	0.977	0.951	0.975	0.815	0.845	0.918	0.952	0.809
	p	**0.0137**	0.899	0.491	0.545	0.706	0.575	0.697	0.151	0.226	0.445	0.579	0.136
MET	*W*	0.971	0.99	0.98	0.92	0.827	**0.75**	**0.752**	0.81	**0.75**	0.994	0.874	1
	p	0.675	0.805	0.732	0.451	0.18	**0**	**0.00435**	0.138	**0**	0.851	0.306	0.967
CLP	*W*	0.827	0.997	0.963	0.862	0.92	0.937	0.943	0.947	0.788	0.835	0.977	**0.771**
	p	0.18	0.901	0.63	0.273	0.453	0.515	0.538	0.556	0.0863	0.2	0.711	**0.0481**
PYR	*W*	0.782	0.979	0.937	0.956	0.969	0.984	0.837	1	0.804	**0.75**	0.993	0.909
	p	0.0726	0.723	0.517	0.594	0.662	0.758	0.206	0.978	0.125	**0**	0.839	0.416
TEB	*W*	0.999	0.889	0.834	0.778	0.998	0.898	0.994	**0.75**	0.774	**0.75**	0.997	0.983
	p	0.955	0.353	0.199	0.0622	0.909	0.38	0.855	**0**	0.0549	**0**	0.904	0.751
BOS	*W*	0.896	0.867	0.864	0.984	0.99	0.961	0.994	0.938	0.774	**0.75**	0.997	0.881
	p	0.374	0.286	0.279	0.757	0.813	0.618	0.855	0.521	0.0549	**0**	0.904	0.328

Table 10.6 Pairwise comparisons for the significant Depth*Time interaction for bentazon from Table 10.2. White "=" values were insignificant, magenta ">" values indicate column value was greater than the row value, and yellow "<" values indicate column value was lesser than the row value. Pre = Pre-operation, Pos = Post-operation, 0-5 = 0-5 cm, 5-15 = 5-15 cm, and 15-30 = 15-30 cm.

Row Labels	Conc	0-5 Pre	0-5 Pos	5-15 Pre	5-15 Pos	15-30 Pre
		0.347 (0.19)	14.426 (11)	1.143 (0.5)	1.87 (2.4)	0.109 (0.093)
0-5 Pos	14.426 (11)	>				
5-15 Pre	1.143 (0.5)	=	<			
5-15 Pos	1.87 (2.4)	>	<	>		
15-30 Pre	0.109 (0.093)	=	<	=	>	
15-30 Pos	1.101 (1.2)	>	<	<	=	>

Table 10.7 Pairwise comparisons for the significant Year*Time interaction for bentazon from Table 10.2. White "=" values were insignificant, magenta ">" values indicate column value was greater than the row value, and yellow "<" values indicate column value was lesser than the row value. '22 = 2022, '23 = 2023, Pre = Pre-operation, Pos = Post-operation.

Row Labels	Conc	'22 Pre	'22 Pos	'23 Pre
		0.00224 (0.0011)	12.089 (5.5)	0.924 (0.52)
'22 Pos	12.089 (5.5)	>		
'23 Pre	0.924 (0.52)	>	<	
'23 Pos	5.78 (4.3)	>	=	>

Table 10.8 Pairwise comparisons for the significant Depth*Time interaction for clopyralid from Table 10.2. White "=" values were insignificant, magenta ">" values indicate column value was greater than the row value, and yellow "<" values indicate column value was lesser than the row value. Pre = Pre-operation, Pos = Post-operation, 0-5 = 0-5 cm, 5-15 = 5-15 cm, and 15-30 = 15-30 cm.

Row Labels	Conc	0-5 Pre	0-5 Pos	5-15 Pre	5-15 Pos	15-30 Pre
		0.246 (0.14)	3.135 (4.1)	0.357 (0.25)	2.032 (2.4)	0.0733 (0.067)
0-5 Pos	3.135 (4.1)	>				
5-15 Pre	0.357 (0.25)	=	<			
5-15 Pos	2.032 (2.4)	>	<	>		
15-30 Pre	0.0733 (0.067)	=	<	=	<	
15-30 Pos	0.484 (0.57)	>	<	>	<	>

Table 10.9 Pairwise comparisons for the significant Year*Time interaction for clopyralid from Table 10.2. White "=" values were insignificant, magenta ">" values indicate column value was greater than the row value, and yellow "<" values indicate column value was lesser than the row value.'22 = 2022, '23 = 2023, Pre = Pre-operation, Pos = Post-operation.

Row Labels	Conc	'22 Pre	'22 Pos	'23 Pre
		0.000896 (0.00096)	1.606 (1.8)	0.297 (0.31)
'22 Pos	1.606 (1.8)	>		
'23 Pre	0.297 (0.31)	>	<	
'23 Pos	3.22 (2.9)	>	=	>

Table 10.10 Pairwise comparisons for the significant Depth*Time interaction for tebuconazole from Table 10.2. White "=" values were insignificant, magenta ">" values indicate column value was greater than the row value, and yellow "<" values indicate column value was lesser than the row value. Pre = Pre-operation, Pos = Post-operation, 0-5 = 0-5 cm, 5-15 = 5-15 cm, and 15-30 = 15-30 cm.

Row Labels	Conc	0-5 Pre	0-5 Pos	5-15 Pre	5-15 Pos	15-30 Pre
		0.0894 (0.067)	5.42 (2.1)	1.329 (0.63)	5.446 (1.7)	0.665 (0.44)
0-5 Pos	5.42 (2.1)	=				
5-15 Pre	1.329 (0.63)	=	=			
5-15 Pos	5.446 (1.7)	=	=	=		
15-30 Pre	0.665 (0.44)	=	=	=	=	
15-30 Pos	4.538 (1.9)	=	=	=	=	=

Table 10.11 Pairwise comparisons for the significant Cell*Depth interaction for tebuconazole from Table 10.2. White "=" values were insignificant, magenta ">" values indicate column value was greater than the row value, and yellow "<" values indicate column value was lesser than the row value. C1 = Cell 1, C2 = Cell 2, 0-5 = 0-5 cm, 5-15 = 5-15 cm, and 15-30 = 15-30 cm.

Row Labels	Conc	C1 0-5	C1 5-15	C1 15-30	C2 0-5	C2 5-15
		5.444 (1.9)	5.432 (2.3)	4.426 (2.2)	0.791 (0.29)	0.0864 (0.093)
C1 5-15	5.432 (2.3)	=				
C1 15-30	4.426 (2.2)	=	=			
C2 0-5	0.791 (0.29)	=	=	=		
C2 5-15	0.0864 (0.093)	=	=	<	=	
C2 15-30	0.0868 (0.074)	=	<	<	=	=

Table 10.12 Pairwise comparisons for the significant Year*Depth interaction for tebuconazole from Table 10.2. White "=" values were insignificant, magenta ">" values indicate column value was greater than the row value, and yellow "<" values indicate column value was lesser than the row value. '22 = 2022, '23 = 2023, 0-5 = 0-5 cm, 5-15 = 5-15 cm, and 15-30 = 15-30 cm.

Row Labels	Conc	'22 0-5	'22 5-15	'22 15-30	'23 0-5	'23 5-15
		0.797 (0.27)	0.0288 (0.029)	0.0606 (0.042)	5.437 (1.9)	5.404 (2.3)
'22 5-15	0.0288 (0.029)	=				
'22 15-30	0.0606 (0.042)	=	=			
'23 0-5	5.437 (1.9)	=	>	>		
'23 5-15	5.404 (2.3)	>	>	>	=	
'23 15-30	4.409 (2.3)	>	>	>	<	=

Table 10.13 Pairwise comparisons for the significant Cell*Year interaction for tebuconazole from Table 10.2. White "=" values were insignificant, magenta ">" values indicate column value was greater than the row value, and yellow "<" values indicate column value was lesser than the row value. C1 = Cell 1, C2 = Cell 2, '22 = 2022, '23 = 2023,.

Row Labels	Conc	C1 '22	C1 '23	C2 '22
		0.0538 (0.05)	6.474 (4.2)	0.655 (0.18)
C1 '23	6.474 (4.2)	>		
C2 '22	0.655 (0.18)	=	<	
C2 '23	0.0688 (0.13)	>	<	<

Table 10.14 Pairwise comparisons for the significant Year*Depth interaction for pyraclostrobin from Table 10.2. White "=" values were insignificant, magenta ">" values indicate column value was greater than the row value, and yellow "<" values indicate column value was lesser than the row value.'22 = 2022, '23 = 2023, 0-5 = 0-5 cm, 5-15 = 5-15 cm, and 15-30 = 15-30 cm.

Row Labels	Conc	'22 0-5	'22 5-15	'22 15-30	'23 0-5	'23 5-15
		5.51 (2.4)	7.662 (3.5)	3.743 (1.1)	0.598 (0.28)	2.968 (1.4)
'22 5-15	7.662 (3.5)	=				
'22 15-30	3.743 (1.1)	=	=			
'23 0-5	0.598 (0.28)	=	=	=		
'23 5-15	2.968 (1.4)	=	=	<	=	
'23 15-30	1.35 (0.72)	=	=	=	=	=

Table 10.15 Pairwise comparisons for the significant Depth*Time interaction for pyraclostrobin from Table 10.2. White "=" values were insignificant, magenta ">" values indicate column value was greater than the row value, and yellow "<" values indicate column value was lesser than the row value. Pre = Pre-operation, Pos = Post-operation, 0-5 = 0-5 cm, 5-15 = 5-15 cm, and 15-30 = 15-30 cm.

Row Labels	Conc	0-5 Pre	0-5 Pos	5-15 Pre	5-15 Pos	15-30 Pre
		0.147 (0.043)	5.431 (2.6)	1.244 (0.47)	7.744 (4.4)	0.515 (0.26)
0-5 Pos	5.431 (2.6)	>				
5-15 Pre	1.244 (0.47)	>	=			
5-15 Pos	7.744 (4.4)	>	=	=		
15-30 Pre	0.515 (0.26)	>	=	=	=	
15-30 Pos	3.835 (1.6)	>	=	=	=	=

Table 10.16 Pairwise comparisons for the significant Year*Time interaction for pyraclostrobin from Table 10.2. White "=" values were insignificant, magenta ">" values indicate column value was greater than the row value, and yellow "<" values indicate column value was lesser than the row value.'22 = 2022, '23 = 2023, Pre = Pre-operation, Pos = Post-operation.

Row Labels	Conc	'22 Pre	'22 Pos	'23 Pre
		0.000953 (0.00056)	7.565 (4.6)	1.055 (0.51)
'22 Pos	7.565 (4.6)	>		
'23 Pre	1.055 (0.51)	>	=	
'23 Pos	2.504 (1.1)	>	=	=

Table 10.17 Pairwise comparisons for the significant Cell*Depth interaction for dicamba from Table 10.2. White "=" values were insignificant, magenta ">" values indicate column value was greater than the row value, and yellow "<" values indicate column value was lesser than the row value. C1 = Cell 1, C2 = Cell 2, 0-5 = 0-5 cm, 5-15 = 5-15 cm, and 15-30 = 15-30 cm.

Row Labels	Conc	C1 0-5	C1 5-15	C1 15-30	C2 0-5	C2 5-15
		1.683 (0.79)	0.262 (0.25)	0.0412 (0.038)	0.945 (0.51)	0.452 (0.26)
C1 5-15	0.262 (0.25)	=				
C1 15-30	0.0412 (0.038)	=	=			
C2 0-5	0.945 (0.51)	=	=	=		
C2 5-15	0.452 (0.26)	=	=	=	=	
C2 15-30	0.034 (0.026)	=	>	=	>	>

Table 10.18 Pairwise comparisons for the significant Year*Depth interaction for dicamba from Table 10.2. White "=" values were insignificant, magenta ">" values indicate column value was greater than the row value, and yellow "<" values indicate column value was lesser than the row value.'22 = 2022, '23 = 2023, 0-5 = 0-5 cm, 5-15 = 5-15 cm, and 15-30 = 15-30 cm.

Row Labels	Conc	'22 0-5	'22 5-15	'22 15-30	'23 0-5	'23 5-15
		0.379 (0.28)	0.37 (0.25)	0.0427 (0.04)	1.823 (1)	0.369 (0.25)
'22 5-15	0.37 (0.25)	=				
'22 15-30	0.0427 (0.04)	=	=			
'23 0-5	1.823 (1)	=	=	>		
'23 5-15	0.369 (0.25)	=	=	>	=	
'23 15-30	0.0315 (0.024)	=	=	=	<	<

Table 10.19 Pairwise comparisons for the significant Depth*Time interaction for dicamba from Table 10.2. White "=" values were insignificant, magenta ">" values indicate column value was greater than the row value, and yellow "<" values indicate column value was lesser than the row value. Pre = Pre-operation, Pos = Post-operation, 0-5 = 0-5 cm, 5-15 = 5-15 cm, and 15-30 = 15-30 cm.

Row Labels	Conc	0-5 Pre	0-5 Pos	5-15 Pre	5-15 Pos	15-30 Pre
		0.0629 (0.037)	1.715 (1.3)	0.15 (0.11)	0.454 (0.4)	0.0144 (0.013)
0-5 Pos	1.715 (1.3)	>				
5-15 Pre	0.15 (0.11)	=	=			
5-15 Pos	0.454 (0.4)	>	=	=		
15-30 Pre	0.0144 (0.013)	=	<	<	<	
15-30 Pos	0.0442 (0.051)	=	<	=	=	=

Table 10.20 Pairwise comparisons for the significant Cell*Year*Time interaction for imazethapyr from Table 10.2 White "=" values were insignificant, magenta ">" values indicate column value was greater than the row value, and yellow "<" values indicate column value was lesser than the row value. C1 = Cell 1, C2 = Cell 2, '22 = 2022, '23 = 2023, Pre = Pre-operation, Pos = Post-operation.

Row Labels	Conc	C1 '22 Pre	C1 '22 Pos	C1 '23 Pre	C1 '23 Pos	C2 '22 Pre	C2 '22 Pos	C2 '23 Pre
		0.0013 (0.00075)	0.027 (0.014)	0.016 (0.011)	0.19 (0.16)	0.0013 (0.001)	0.039 (0.017)	0.021 (0.012)
C1 '22 Pos	0.027 (0.014)	>						
C1 '23 Pre	0.016 (0.011)	>	=					
C1 '23 Pos	0.19 (0.16)	>	>	>				
C2 '22 Pre	0.0013 (0.001)	=	<	<	<			
C2 '22 Pos	0.039 (0.017)	>	=	>	<	>		
C2 '23 Pre	0.021 (0.012)	>	=	=	<	>	<	
C2 '23 Pos	0.17 (0.17)	>	>	>	=	>	>	>

Table 10.21 Pairwise comparisons for the significant Year*Depth*Time interaction for imazethapyr from Table 10.2. White "=" values were insignificant, magenta ">" values indicate column value was greater than the row value, and yellow "<" values indicate column value was lesser than the row value.'22 = 2022, '23 = 2023, Pre = Pre-operation, Pos = Post-operation, 0-5 = 0-5 cm, 5-15 = 5-15 cm, and 15-30 = 15-30 cm.

Row Labels	Conc	'22 0-5 Pre	'22 0-5 Pos	'22 5-15 Pre	'22 5-15 Pos	'22 15-30 Pre	'22 15-30 Pos	'23 0-5 Pre	'23 0-5 Pos	'23 5-15 Pre	'23 5-15 Pos	'23 15-30 Pre
		0.0022 (0.00037)	0.028 (0.007)	0.00087 (0.00072)	0.04 (0.021)	0.00081 (0.00052)	0.03 (0.018)	0.0079 (0.0016)	0.32 (0.21)	0.026 (0.01)	0.11 (0.071)	0.023 (0.011)
'22 0-5 Pos	0.028 (0.007)	>										
'22 5-15 Pre	0.00087 (0.00072)	<	<									
'22 5-15 Pos	0.04 (0.021)	>	=	>								
'22 15-30 Pre	0.00081 (0.00052)	<	<	=	<							
'22 15-30 Pos	0.03 (0.018)	>	=	>	=	>						
'23 0-5 Pre	0.0079 (0.0016)	>	>	>	>	>	>					
'23 0-5 Pos	0.32 (0.21)	>	>	>	>	>	>	>				
'23 5-15 Pre	0.026 (0.01)	>	=	>	<	>	=	>	<			
'23 5-15 Pos	0.11 (0.071)	>	>	>	=	>	=	>	<	>		
'23 15-30 Pre	0.023 (0.011)	>	=	>	=	>	=	>	<	=	<	
'23 15-30 Pos	0.1 (0.043)	>	>	>	>	>	>	>	<	>	=	>

Table 10.22 Pairwise comparisons for the significant Cell*Year*Depth interaction for metolachlor from Table 10.2. White "=" values were insignificant, magenta ">" values indicate column value was greater than the row value, and yellow "<" values indicate column value was lesser than the row value. C1 = Cell 1, C2 = Cell 2, '22 = 2022, '23 = 2023, 0-5 = 0-5 cm, 5-15 = 5-15 cm, and 15-30 = 15-30 cm.

Row Labels	Conc	C1 '22 0-5	C1 '22 5-15	C1 '22 15-30	C2 '22 0-5	C2 '22 5-15	C2 '22 15-30	C1 '23 0-5	C1 '23 5-15	C1 '23 15-30	C2 '23 0-5	C2 '23 5-15
		2.6 (2.9)	2.5 (3.1)	2.3 (2.8)	0.73 (0.91)	0.31 (0.41)	0.085 (0.18)	67 (120)	53 (85)	72 (88)	1.7 (2.5)	2.6 (3.6)
C1 '22 5-15	2.5 (3.1)	=										
C1 '22 15-30	2.3 (2.8)	=	=									
C2 '22 0-5	0.73 (0.91)	=	<	<								
C2 '22 5-15	0.31 (0.41)	=	<	<	=							
C2 '22 15-30	0.085 (0.18)	=	<	<	=	=						
C1 '23 0-5	67 (120)	>	=	=	>	>	>					
C1 '23 5-15	53 (85)	>	>	>	>	>	>	=				
C1 '23 15-30	72 (88)	>	>	>	>	>	>	=	=			
C2 '23 0-5	1.7 (2.5)	=	=	=	=	=	>	<	<	<		
C2 '23 5-15	2.6 (3.6)	=	=	=	=	>	>	=	=	=	=	
C2 '23 15-30	4.5 (8.2)	=	=	=	=	=	>	=	=	=	=	=

Table 10.23 Pairwise comparisons for the significant Cell*Year*Depth interaction for chlorantraniliprole from Table 10.2. White "=" values were insignificant, magenta ">" values indicate column value was greater than the row value, and yellow "<" values indicate column value was lesser than the row value. C1 = Cell 1, C2 = Cell 2, '22 = 2022, '23 = 2023, 0-5 = 0-5 cm, 5-15 = 5-15 cm, and 15-30 = 15-30 cm.

Row Labels	Conc	C1 '22 0-5	C1 '22 5-15	C1 '22 15-30	C2 '22 0-5	C2 '22 5-15	C2 '22 15-30	C1 '23 0-5	C1 '23 5-15	C1 '23 15-30	C2 '23 0-5	C2 '23 5-15
		2.5 (2.9)	2.7 (2.6)	2.2 (1.9)	0.06 (0.077)	0.018 (0.027)	0.0026 (0.0023)	1.6 (2.7)	2.2 (2)	2.8 (1.6)	0.0097 (0.011)	0.098 (0.065)
C1 '22 5-15	2.7 (2.6)	=										
C1 '22 15-30	2.2 (1.9)	=	=									
C2 '22 0-5	0.06 (0.077)	=	<	<								
C2 '22 5-15	0.018 (0.027)	=	<	<	=							
C2 '22 15-30	0.0026 (0.0023)	=	<	<	=	=						
C1 '23 0-5	1.6 (2.7)	=	=	=	>	=	>					
C1 '23 5-15	2.2 (2)	=	=	=	>	>	>	=				
C1 '23 15-30	2.8 (1.6)	=	=	=	>	>	>	=	=			
C2 '23 0-5	0.0097 (0.011)	=	<	<	=	=	=	<	<	<		
C2 '23 5-15	0.098 (0.065)	=	=	=	=	=	>	=	<	<	<	
C2 '23 15-30	0.094 (0.068)	=	<	<	=	=	>	=	<	<	<	=

Table 10.24 Pairwise comparisons for the significant Year*Depth*Time interaction for atrazine from Table 10.2. White "=" values were insignificant, magenta ">" values indicate column value was greater than the row value, and yellow "<" values indicate column value was lesser than the row value.'22 = 2022, '23 = 2023, Pre = Pre-operation, Pos = Post-operation, 0-5 = 0-5 cm, 5-15 = 5-15 cm, and 15-30 = 15-30 cm.

Row Labels	Conc	'22 0-5 Pre	'22 0-5 Pos	'22 5-15 Pre	'22 5-15 Pos	'22 15-30 Pre	'22 15-30 Pos	'23 0-5 Pre	'23 0-5 Pos	'23 5-15 Pre	'23 5-15 Pos	'23 15-30 Pre
		0.0029 (0.00072)	0.24 (0.12)	0.00068 (0.00069)	0.16 (0.15)	0.00067 (0.00049)	0.17 (0.21)	0.0075 (0.0037)	0.18 (0.27)	0.065 (0.043)	0.2 (0.3)	0.047 (0.022)
'22 0-5 Pos	0.24 (0.12)	>										
'22 5-15 Pre	0.00068 (0.00069)	<	<									
'22 5-15 Pos	0.16 (0.15)	>	=	>								
'22 15-30 Pre	0.00067 (0.00049)	<	<	=	<							
'22 15-30 Pos	0.17 (0.21)	>	=	>	=	<						
'23 0-5 Pre	0.0075 (0.0037)	>	<	>	<	<	<					
'23 0-5 Pos	0.18 (0.27)	>	=	>	=	<	=	=				
'23 5-15 Pre	0.065 (0.043)	>	<	>	=	<	=	>	=			
'23 5-15 Pos	0.2 (0.3)	>	=	>	=	<	=	>	=	=		
'23 15-30 Pre	0.047 (0.022)	>	<	>	=	<	=	>	=	=	=	
'23 15-30 Pos	0.23 (0.33)	>	=	>	=	<	=	>	=	=	=	=

If you have made it here, congratulations! Thank you so much for reading, checking, and the interest in all of the statistics and work! This was a long time to make, so anyone reading this, I want you to know that I appreciate you and thank you; I hope you enjoyed it!

Table 10.25 Pairwise comparisons for the significant Cell*Year*Depth*Time interaction for boscalid from Table 10.2. Due to its size, the table is split into multiple parts, in order of: within cell one, 2022; within cell two, 2022; within cell one, 2023; within cell two, 2023; between cell comparisons, 2022; between cell comparisons, 2023; between year comparisons, cell one; between years comparisons, cell two; cell one, 2022 compared with cell two, 2023, and; cell one, 2023 compared with cell two, 2022. White "=" values were insignificant, magenta ">" values indicate column value was greater than the row value, and yellow "<" values indicate column value was lesser than the row value. C1 = Cell 1, C2 = Cell 2, '22 = 2022, '23 = 2023, Pre = Pre-operation, Pos = Post-operation, 0-5 = 0-5 cm, 5-15 = 5-15 cm, and 15-30 = 15-30 cm.

Row Labels	Conc	C1 '22 0-5 Pre	C1 '22 0-5 Pos	C1 '22 5-15 Pre	C1 '22 5-15 Pos	C1 '22 15-30 Pre	-
		0.047 (0.019)	8.8 (2.8)	0.042 (0.00058)	9.4 (4.9)	0.033 (0.0045)	-
C1 '22 0-5 Pos	8.8 (2.8)	>	-	-	-	-	-
C1 '22 5-15 Pre	0.042 (0.00058)	=	<	-	-	-	-
C1 '22 5-15 Pos	9.4 (4.9)	>	=	>	-	-	-
C1 '22 15-30 Pre	0.033 (0.0045)	=	<	=	<	-	-
C1 '22 15-30 Pos	4.8 (5.4)	=	=	=	=	=	-

Row Labels	Conc	C2 '22 0-5 Pre	C2 '22 0-5 Pos	C2 '22 5-15 Pre	C2 '22 5-15 Pos	C2 '22 15-30 Pre	-
		0.045 (0.0047)	0.48 (0.29)	0.041 (0.0032)	0.11 (0.041)	0.038 (0.0045)	-
C2 '22 0-5 Pos	0.48 (0.29)	=	-	-	-	-	-
C2 '22 5-15 Pre	0.041 (0.0032)	=	=	-	-	-	-
C2 '22	0.11 (0.041)	=	=	=	-	-	-

5-15 Pos							
C2 '22 15-30 Pre	0.038 (0.0045)	=	=	=	=	-	-
C2 '22 15-30 Pos	0.084 (0.0067)	=	=	<	=	<	-

Row Labels	Conc	C1 '23 0-5 Pre	C1 '23 0-5 Pos	C1 '23 5-15 Pre	C1 '23 5-15 Pos	C1 '23 15-30 Pre	-
		0.14 (0.17)	0.26 (0.13)	2.3 (2)	0.35 (0.18)	1.5 (0.15)	-
C1 '23 0-5 Pos	0.26 (0.13)	=	-	-	-	-	-
C1 '23 5-15 Pre	2.3 (2)	=	=	-	-	-	-
C1 '23 5-15 Pos	0.35 (0.18)	=	=	=	-	-	-
C1 '23 15-30 Pre	1.5 (0.15)	=	=	=	=	-	-
C1 '23 15-30 Pos	0.11 (0.049)	=	=	=	=	<	-

Row Labels	Conc	C2 '23 0-5 Pre	C2 '23 0-5 Pos	C2 '23 5-15 Pre	C2 '23 5-15 Pos	C2 '23 15-30 Pre	-
		0.06 (0.0095)	0.083 (0.033)	0.17 (0.096)	0.14 (0.0058)	0.087 (0.04)	-
C2 '23 0-5 Pos	0.083 (0.033)	=	-	-	-	-	-
C2 '23 5-15 Pre	0.17 (0.096)	=	=	-	-	-	-
C2 '23 5-15 Pos	0.14 (0.0058)	=	=	=	-	-	-
C2 '23 15-30 Pre	0.087 (0.04)	=	=	=	=	-	-
C2 '23 15-30 Pos	0.079 (0.027)	=	=	=	=	=	-

Row Labels	Conc	C1 '22 0-5 Pre	C1 '22 0-5 Pos	C1 '22 5-15 Pre	C1 '22 5-15 Pos	C1 '22 15-30 Pre	C1 '22 15-30 Pos
		0.047 (0.019)	8.8 (2.8)	0.042 (0.00058)	9.4 (4.9)	0.033 (0.0045)	4.8 (5.4)
C2 '22 0-5 Pre	0.045 (0.0047)	=	<	=	<	=	=
C2 '22 0-5 Pos	0.48 (0.29)	=	=	=	=	=	=
C2 '22 5-15 Pre	0.041 (0.0032)	=	<	=	<	=	=
C2 '22 5-15 Pos	0.11 (0.041)	=	<	=	<	=	=
C2 '22 15-30 Pre	0.038 (0.0045)	=	<	=	<	=	=
C2 '22 15-30 Pos	0.084 (0.0067)	=	<	0.027	<	0.018	=
Row Labels	Conc	C1 '23 0-5 Pre	C1 '23 0-5 Pos	C1 '23 5-15 Pre	C1 '23 5-15 Pos	C1 '23 15-30 Pre	C1 '23 15-30 Pos
		0.14 (0.17)	0.26 (0.13)	2.3 (2)	0.35 (0.18)	1.5 (0.15)	0.11 (0.049)
C2 '23 0-5 Pre	0.06 (0.0095)	=	=	=	=	<	=
C2 '23 0-5 Pos	0.083 (0.033)	=	=	=	=	<	=
C2 '23 5-15 Pre	0.17 (0.096)	=	=	=	=	=	=
C2 '23 5-15 Pos	0.14 (0.0058)	=	=	=	=	<	=
C2 '23 15-30 Pre	0.087 (0.04)	=	=	=	=	<	=
C2 '23 15-30 Pos	0.079 (0.027)	=	=	=	=	<	=

Row Labels	Conc	C1 '22 0-5 Pre	C1 '22 0-5 Pos	C1 '22 5-15 Pre	C1 '22 5-15 Pos	C1 '22 15-30 Pre	C1 '22 15-30 Pos
		0.047 (0.019)	8.8 (2.8)	0.042 (0.00058)	9.4 (4.9)	0.033 (0.0045)	4.8 (5.4)
C1 '23 0-5 Pre	0.14 (0.17)	=	=	=	=	=	=
C1 '23 0-5 Pos	0.26 (0.13)	>	<	=	<	=	=
C1 '23 5-15 Pre	2.3 (2)	>	=	=	=	=	=
C1 '23 5-15 Pos	0.35 (0.18)	=	<	=	<	=	=
C1 '23 15-30 Pre	1.5 (0.15)	>	=	>	=	>	=
C1 '23 15-30 Pos	0.11 (0.049)	=	=	=	=	=	=

Row Labels	Conc	C2 '22 0-5 Pre	C2 '22 0-5 Pos	C2 '22 5-15 Pre	C2 '22 5-15 Pos	C2 '22 15-30 Pre	C2 '22 15-30 Pos
		0.045 (0.0047)	0.48 (0.29)	0.041 (0.0032)	0.11 (0.041)	0.038 (0.0045)	0.084 (0.0067)
C2 '23 0-5 Pre	0.06 (0.0095)	=	=	=	=	=	=
C2 '23 0-5 Pos	0.083 (0.033)	=	=	=	=	=	=
C2 '23 5-15 Pre	0.17 (0.096)	=	=	=	=	=	=
C2 '23 5-15 Pos	0.14 (0.0058)	>	=	>	=	>	>
C2 '23 15-30 Pre	0.087 (0.04)	=	=	=	=	=	=
C2 '23 15-30 Pos	0.079 (0.027)	=	=	=	=	=	=

Row Labels	Conc	C1 '22 0-5 Pre	C1 '22 0-5 Pos	C1 '22 5-15 Pre	C1 '22 5-15 Pos	C1 '22 15-30 Pre	C1 '22 15-30 Pos
		0.047 (0.019)	8.8 (2.8)	0.042 (0.00058)	9.4 (4.9)	0.033 (0.0045)	4.8 (5.4)
C2 '23 0-5 Pre	0.06 (0.0095)	=	<	=	<	=	=
C2 '23 0-5 Pos	0.083 (0.033)	=	<	=	=	=	=
C2 '23 5-15 Pre	0.17 (0.096)	=	=	=	=	=	=
C2 '23 5-15 Pos	0.14 (0.0058)	=	<	>	<	>	=
C2 '23 15-30 Pre	0.087 (0.04)	=	<	=	<	=	=
C2 '23 15-30 Pos	0.079 (0.027)	=	<	=	<	=	=

Row Labels	Conc	C2 '22 0-5 Pre	C2 '22 0-5 Pos	C2 '22 5-15 Pre	C2 '22 5-15 Pos	C2 '22 15-30 Pre	C2 '22 15-30 Pos
		0.045 (0.0047)	0.48 (0.29)	0.041 (0.0032)	0.11 (0.041)	0.038 (0.0045)	0.084 (0.0067)
C1 '23 0-5 Pre	0.14 (0.17)	=	=	=	=	=	=
C1 '23 0-5 Pos	0.26 (0.13)	=	=	=	=	=	=
C1 '23 5-15 Pre	2.3 (2)	=	=	=	=	=	=
C1 '23 5-15 Pos	0.35 (0.18)	=	=	=	>	=	=
C1 '23 15-30 Pre	1.5 (0.15)	>	=	>	>	>	>
C1 '23 15-30 Pos	0.11 (0.049)	=	=	=	=	=	=